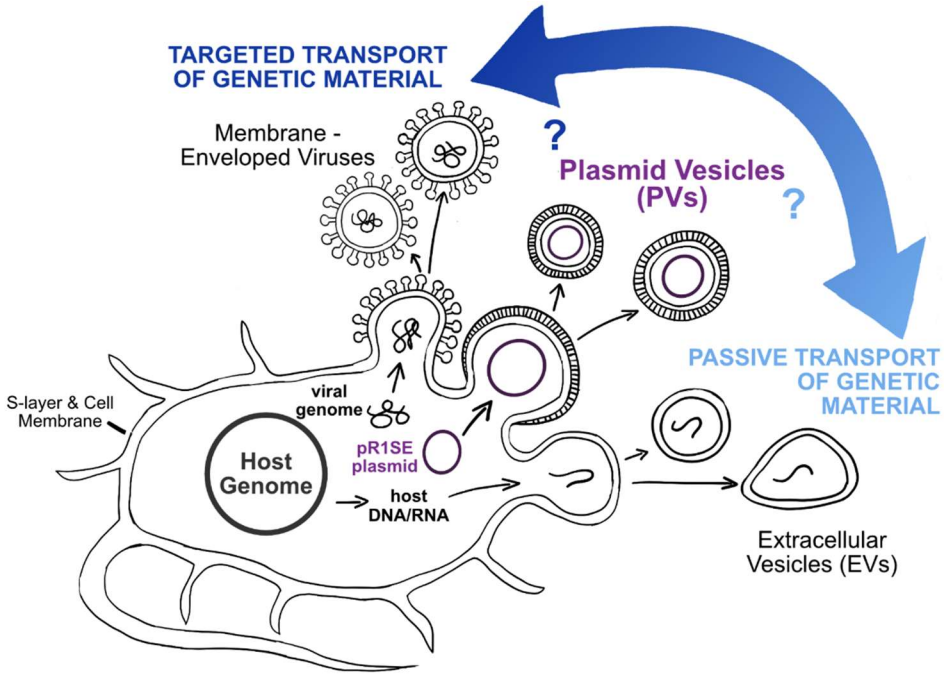

© L. Johanna Gebhard

MAX PLANCK INSTITUTE
FOR MARINE MICROBIOLOGY

Universität
Bremen

Genetic and Biochemical Characterisation of Plasmid Vesicles & Other Virus-Like Elements in Archaea

Dissertation zur Erlangung des Grades eines
Doktors der Naturwissenschaften
– Dr. rer. nat. –

dem Fachbereich Biologie/Chemie der
Universität Bremen vorgelegt von

L. Johanna Gebhard

Bremen, August 2023

“The only thing that makes life possible is permanent, intolerable uncertainty: not knowing what comes next.”

— Ursula K. Le Guin, *The Left Hand of Darkness*

Die vorliegende Arbeit wurde in der Zeit von Mai 2019 bis August 2023 in der Arbeitsgruppe Archaea Virologie am Max-Planck-Institut für Marine Mikrobiologie unter der Leitung von Dr. Susanne Erdmann durchgeführt. Sie wurde weiterhin im Rahmen der International Max Planck Research School of Marine Microbiology (MarMic) angefertigt.

The research that forms the basis for this thesis was conducted from May 2019 to August 2023 in the Archaeal Virology Group at the Max Planck Institute for Marine Microbiology under the super-vision of Dr. Susanne Erdmann. The thesis was prepared under the framework of the International Max Planck Research School of Marine Microbiology (MarMic)

Gutachter*innen / Reviewers

Dr. Susanne Erdmann

Prof. Dr. Andreas Dotzauer

Prüfer*innen / Examiners

Prof. Dr. Michael Friedrich

Dr. Susanne Erdmann

Prof. Dr. Andreas Dotzauer

Dr. Elina Roine

Datum des Promotionskolloquiums / Date of the doctoral defense

18.10.2023

Cover © Dr. Coraline Mercier

Summary

Plasmid vesicles (PVs) are a novel class of vesicles that cross the divide between horizontal gene transfer in extracellular vesicles and targeted transfer of nucleic acids by selfishly replicating viruses. The archaeal plasmid pR1SE is enclosed and propagated through PVs containing both host-derived and plasmid-encoded proteins. PVs thus display a distinct morphology compared to the extracellular vesicles produced concurrently by the host. Infection of plasmid-free host cells occurs without direct cell-to-cell contact. Dissemination by PVs has only been described for the pR1SE plasmid to date. Its unique characteristics separate it from previously described dissemination mechanisms of other non-viral mobile genetic elements. This virus-like lifestyle supports the evolutionary connections between viruses and plasmids and marks PVs out as potential evolutionary precursors to viruses.

This dissertation is part of a continued effort to characterize pR1SE and PVs to better understand this unique interaction between cells and mobile genetic elements. In **Chapter I,** I describe our successful improvement of the genetic system in *Halorubrum lacusprofundi*, the only currently known producer of PVs. This system allowed detailed investigations into the PV life cycle by the deletion of targeted genes in the host, as demonstrated in the following chapters. We showed that PV stability is negatively affected (**Chapter II**) when the host machinery responsible for the posttranslational modification of proteins with polysaccharides is impaired. Detailed tracking of intracellular pR1SE replication and PV production after infection of a new host revealed strong similarities between the infection cycles of pR1SE and actively replicating viruses infecting the same host. This research was expanded to the analysis of the lipid composition of vesicles produced by *Hrr. lacusprofundi*, and comparison to a related organism *Haloferax volcanii* (**Chapter III**).

We showed that the vesicles of both organisms are selectively enriched in specific lipid species. This suggests common patterns of physical processes at the cell membrane during the formation of vesicles and membrane-enveloped viruses in halophilic archaea. Chapter III also includes a description of the archaeal vesiculating GTPase enzyme, which is a critical component of the vesicle formation machinery in *H. volcanii.* Based on this work, we could show that deletion of this gene also alters the extracellular vesicle formation in *Hrr. lacusprofundi* (**Chapter IV**). Finally, we also confirmed that PV production is independent of the machinery of GTPase-driven production of extracellular vesicles by the host.

The results presented in this dissertation provide valuable new insights into the life cycle and host dependency of PVs and set them into a broader context with the vesicles that are produced with PVs, and the viruses that infect the same organism. This allows us to better consider the position pR1SE occupies within the total diversity of mobile genetic elements and provides a potential template for future research into unique mobile genetic elements in archaea.

Zusammenfassung

Plasmidvesikel (PVs) sind eine neue Klasse von Vesikeln, die die Grenze zwischen dem horizontalen Gentransfer in extrazellulären Vesikeln und dem gezielten Transfer von Nukleinsäuren durch egoistisch replizierende Viren überschreiten. Das archaeelle pR1SE Plasmid verbreitet sich eingeschlossen in PVs, die sowohl vom Wirt stammende als auch vom Plasmid kodierte Proteine enthalten. PVs unterschieden sich daher morphologisch von den extrazellulären Vesikeln, die oft zur gleichen Zeit vom Wirt produziert werden. Die Infektion von pR1SE freien Wirtszellen erfolgt ohne direkten Zell-zu-Zell-Kontakt. Eine solche Verbreitungsart ist bisher nur vom pR1SE Plasmid bekannt. Auch im Kontext zu anderen nicht-viralen mobilen genetischen Elemente ist diese Verbreitung einzigartig. Die virusähnliche Lebensweise von PVs unterstützt die evolutionären Verbindungen zwischen Viren und Plasmiden und weist PVs als mögliche evolutionäre Vorläufer von Viren aus.

Diese Dissertation ist ein Teil der fortlaufenden Charakterisierung von pR1SE und PVs, und dient dazu unser Wissen um diese einzigartige Interaktion zwischen Zellen und mobilen genetischen Elementen zu erweitern. **Kapitel I** beschreibt die erfolgreiche Verbesserung des genetischen Systems *in Halorubrum lacusprofundi*, dem einzigen derzeit bekannten Wirtsorganismus von PVs. Wie in den folgenden Kapiteln gezeigt wird, ermöglichte dieses System detaillierte Untersuchungen des PV-Lebenszykluses durch die Deletion von gezielten Genen im Wirt. Wir konnten zeigen, dass die Stabilität von PVs negativ beeinflusst wird (**Kapitel II**), wenn der Prozess, der für die posttranslationale Modifikation von Proteinen mit Polysacchariden verantwortlich ist, im Wirt beeinträchtigt wird. Detaillierte Beobachtungen der intrazellulären Replikation von pR1SE und der Produktion von PVs nach der Infektion eines neuen Wirts zeigten starke

Ähnlichkeiten zwischen den Infektionszyklen von pR1SE und aktiv replizierenden Viren auf, die denselben Wirt infizieren. Die Analyse wurde weiterhin auf die Betrachtung der Lipidzusammensetzung der von *Hrr. lacusprofundi* produzierten Vesikel im Vergleich mit einem verwandten Organismus, *Haloferax volcanii*, ausgeweitet (**Kapitel III**). Wir konnten zeigen, dass die Vesikel in beiden Organismen selektiv mit bestimmten Lipidarten angereichert sind. Dies deutet auf gemeinsame Muster von physikalischen Prozessen an der Zellmembran hin, die während der Entstehung von Vesikeln und membranumhüllten Viren an der Zellmembran von halophilen Archaeen geschehen. Kapitel III enthält auch eine Beschreibung des archaeellen vesikulierenden GTPase-Enzyms, welches eine entscheidende Komponente in der Bildung von extrazellulären Vesikeln in *H. volcanii* ist. Auf dieser Grundlage konnten wir zeigen, dass die Deletion dieses Gens auch die Bildung von extrazellulären Vesikeln in *Hrr. lacusprofundi* verändert (**Kapitel IV**). Schließlich konnten wir auch bestätigen, dass die Produktion von PVs unabhängig von der GTPase-gesteuerten Produktion extrazellulärer Vesikel durch den Wirt ist.

Die in dieser Dissertation vorgestellten Ergebnisse liefern wertvolle neue Einblicke in den Lebenszyklus von PVs und deren Abhängigkeit vom Wirtsorganismus. Diese Erkenntnisse stellen PVs in einen breiteren Kontext mit Vesikeln, die oft gleichzeitig zu PVs produziert werden, und den Viren, die denselben Organismus infizieren. Auf diese Weise können wir die Position von pR1SE innerhalb der gesamten Vielfalt mobiler genetischer Elemente besser einschätzen und eine mögliche Vorlage für künftige Forschungen zu einzigartigen mobilen genetischen Elementen in Archaeen liefern.

List of original publications

This thesis is based on the following scientific articles; each manuscript corresponds to an individual chapter as indicated

Gebhard, L. J., Duggin, I. G., & Erdmann, S. (2023a). Improving the genetic system for *Halorubrum lacusprofundi* to allow in-frame deletions. *Frontiers in Microbiology*, 14. doi:10.3389/fmicb.2023.1095621 (Chapter I)

Gebhard, L. J.*, Vershinin, Z.*, Alarcón-Schumacher, T., Eichler, J., & Erdmann, S. (2023b). Influence of N-Glycosylation on Virus-Host Interactions in *Halorubrum lacusprofundi*. *Viruses*, 15(7), 1469. doi:10.3390/v15071469 (Chapter II)

* These authors contributed equally to this work

Gebhard, L. J., Queiss, L., Mills, J. & Erdmann, S. Plasmid vesicle formation is independent of the archaeal small vesiculating GTPase (ArcV) driven extracellular vesicle formation.

Manuscript in preparation (Chapter IV)

Co-authored manuscripts

Mills, J., **Gebhard, L. J.**, Schubotz, F., Shevchenko, A., Speth, D. R., Liao, Y., Duggin, I. G., Marchfelder, A., & Erdmann, S. (2023). Extracellular vesicles of Euryarchaeida: precursor to eukaryotic membrane trafficking. *bioRxiv*. doi:10.1101/2023.03.03.530948

Manuscript under review at *PNAS*; preprint available on *bioRxiv* and this preprint version is included in the thesis as Chapter III in order to provide context for the extended data assembled in this addendum:

> **Gebhard, L.J.**, Schubotz, F., Mills, J. & Erdmann, S. (2023). Extended Data: Selective enrichment of intact polar lipids in extracellular vesicles of halophilic *Euryarchaeota.*
>
> Manuscript in preparation (Chapter IV)

Table of Contents

Introduction

1.1 What is a virus? The search for an unambiguous definition

What is a virus? This is a question that seems intuitively easy to answer; after all everyone knows what a virus is. Yet, a clear definition of what exactly is or is not considered to be a virus has been difficult to establish. Therefore, a short excursion into historical concepts and the current scientific consensus about 'virus-like' elements and viruses in a strict sense appears necessary in order to establish a common ground at the outset for terms and concepts that will be used frequently in this dissertation.

The first definitions of viruses were mainly based on size [Koonin *et al*. (2021), and references therein], viruses were any infectious agents that passed through a filter with small enough pore sizes to exclude cells of any size. In the first half of the 20th century, a scientific consensus started to form. As summarized by the microbiologist André Lwoff (1957); viruses were considered to be '…*strictly intracellular and potentially pathogenic entities . . . possessing only one type of nucleic acid . . . unable to grow and to undergo binary fission '* (Lwoff, 1957). The following decades saw the discoveries of several new categories of 'virus-like' mobile genetic elements (MGEs) that complicated previous assertions of what could be classified as a virus. These included among others, virioids, 'un-protected' infectious circular RNAs that rely on host replication (Diener, 1971; Diener & Raymer, 1967), virusoids (Forster & Symons, 1987), satellites (Briddon *et al.*, 2011), and virioforms (Kogay *et al.*, 2022a; Kuhn & Koonin, 2023). Further refinement of definitions over many iterations (Van Regenmortel, 1989; Pringle, 1991; Raoult & Forterre, 2008; Claverie & Abergel, 2016; Nasir *et al.*, 2020), have led to the

current definition of the International Committee on Taxonomy of Viruses (ICTV):

> *'1. Viruses sensu stricto are defined operationally by the ICTV as a type of [mobile genetic element] MGEs that encode at least one protein that is a major component of the virion encasing the nucleic acid of the respective MGE and therefore the gene encoding the major virion protein itself; or MGEs that are clearly demonstrable to be members of a line of evolutionary descent of such major virion protein-encoding entities. Any monophyletic group of MGEs that originates from a virion protein-encoding ancestor should be classified as a group of viruses.' (ICTV, 2021; Kuhn et al., 2021).*

This will also be the definition underlying any reference to 'viruses' in the following dissertation. The definition is mainly operational following the pattern established by previous definitions, thus avoiding controversial topics such as whether or not viruses can be considered as being 'alive'. The term 'virosphere' then encompasses both viruses and virus-like elements. Koonin *et al.*, (2021) divided the 'virosphere' into a 'orthovirosphere' core, containing 'real viruses', surrounded by an outer 'perivirosphere'. A hazy boundary separates the core from the perivirosphere of replicating elements that share some but not all virus characteristics included in defining the core. The total virosphere is separated from the other replicating elements, such as genomes and plasmids (Koonin *et al.*, 2021). These definitions will be used in this dissertation when discussing the virosphere concept, viruses and virus-like elements, in general, and plasmid vesicles, in particular.

1.2 The enigmatic origin of viruses, as explained by three hypotheses and one chimeric scenario

After establishing common ground on virus definitions, looking into the origin and evolution of viruses will help us determine why and how the virosphere could have separated from the broader space of replicating entities including cellular organisms. The origin of viral genomes and virus particles remains a fundamental, yet controversial scientific question. Genetic mutation is the basis of evolution and viruses mutate at rates that make real-time observations of their 'microevolution' possible. Several factors are thought to cause the high mutation rates presented by viruses, including polymerase-induced error, environmental mutagens (e.g. UV irradiation) and host immune responses (Duffy *et al.*, 2008). However, the rapid evolution and general genome plasticity of viruses and virus-like elements can complicate conclusions about viral evolution. Current evidence suggests that viruses likely evolved in multiple separate events over life's history [see Koonin *et al.* (2006); Krupovič and Koonin (2017b); Nasir *et al.* (2020); Koonin *et al.* (2023), and references therein].

1.2.1 The virus first hypothesis

The 'virus first' or 'virus early' hypothesis (Figure 1a) assumes that virus-like entities evolved from proto-replicators, i.e., self-replicating entities. This may have occurred concurrently with, or preceding cellular life (Koonin *et al.*, 2006; Koonin & Dolja, 2013). Modern viruses exhibit a diversity of genome types that is not found in cellular organisms such as, single-stranded RNA or DNA, double-stranded RNA or DNA or hybrid forms. Moreover, viral replication genes are shared between viruses infecting all three domains and show an unmatched diversity, as compared to their counterparts in cellular organisms (Kazlauskas *et al.*, 2016). The proteins encoded by these genes likely represent a virus-specific core-set of ancestral proteins that could be pre-

cellular and were never acquired by proto-cellular replicators (Koonin *et al.*, 2006). For instance, early emergence of the RNA-recognition motif could have enabled the evolution of diverse RNA replication function enzymes, that are exclusively found in viruses today (Krupovič *et al.*, 2019a). However, not all modern viruses encode a full set of replication proteins and have optimized recruitment cellular replication genes for their own gain instead [see e.g. Kazlauskas *et al.* (2016), and references therein].

A pre-cellular origin of viruses is paradoxical, considering that all modern viruses are obligate parasites that replicate within cells. Yet, modelling of potential pre-cellular replicator spaces shows that genomic parasites could have evolved quickly in order to maintain balance in the system (Iranzo *et al.*, 2016; Koonin *et al*., 2017b; Conrad *et al*., 2023). On a larger scale, this could then lead to our current world where there are no known cellular organisms without virus(es) that can infect them.

Nevertheless, there are restrictions to infection. If the origin of viruses predated the Last Universal Cellular Ancestor (LUCA), we would expect modern viruses to be broadly distributed across the three domains of cellular life. However, the three domains are infected by specific groups of viruses. For instance, RNA viruses for eukaryotes are very common, rare for bacteria and currently unknown for archaea (Nasir *et al.,* 2014; Nasir & Caetano-Anollés, 2015). None of the currently known modern viruses is able bridge the gap between the three domains. Some virus classes are shared between archaea and bacteria [e.g. *Caudoviricetes,* see Y. Liu *et al.* (2021)], although individual virus species inside the phylum are only able to infect hosts within one domain. The evolution of the three cellular domains may have diverged too far to enable such a fossil from the genesis of viruses to survive and to be experimentally validated.

a 'virus first' hypothesis

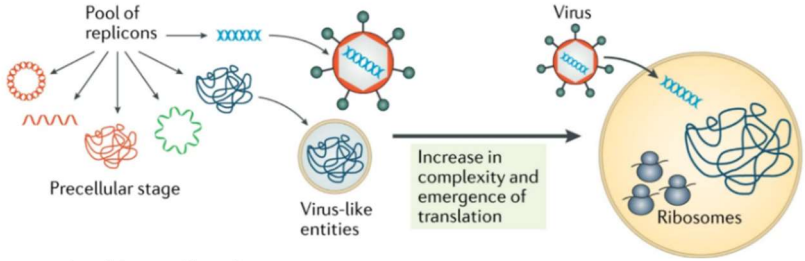

b 'regression' hypothesis

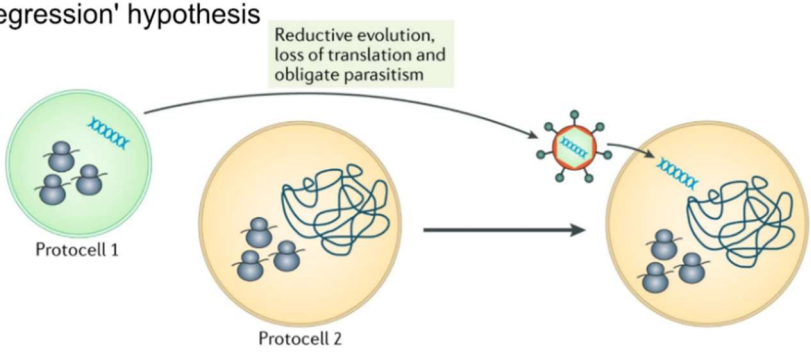

c 'escape' hypothesis

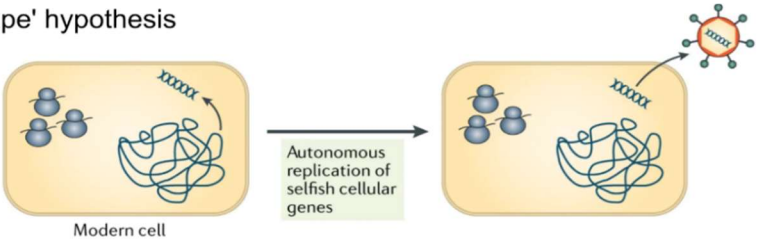

d chimeric scenario

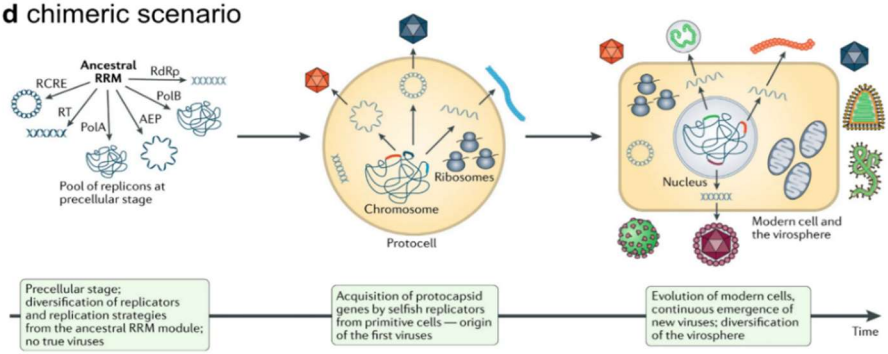

Figure 1: Schematic representation of the four currently prevalent theories on the evolutionary origin of viruses. (a) The 'virus first' hypothesis postulates that viruses evolved from proto-replicators either simultaneously or before the first cells emerged. (b) The 'regression' hypothesis assumes that parasitic cells became viruses over consecutive degeneration and loss of cellular functions. (c) According to the 'escape' hypothesis virus genomes evolved from cellular nucleic acids, with their capsids originating from extracellular vesicle and cell wall material. These precursors acquired 'selfish' replication and dissemination abilities. Finally, (d) the chimeric scenario combines aspects of the 'virus first' and 'escape' hypotheses. Graphs modified from Krupovič *et al.* (2019a).

1.2.2 The 'regression' hypothesis

The 'regression' hypothesis (Figure 1b) assumes that viruses originated from parasitic cells that degenerated into viruses as obligate intracellular parasites (Abergel *et al.*, 2015; Koonin *et al.*, 2015; Nasir & Caetano-Anollés, 2015). The theory re-gained popularity in the 2000s after the discovery of giant viruses infecting single-celled eukaryotes (La Scola *et al.*, 2003; Raoult & Forterre, 2008). These viruses called for a re-evaluation of previously established norms about virus size, genome size, and complexity (La Scola *et al.*, 2003; Schulz *et al.*, 2022). Giant virus genomes encode the most complete translation machineries found in modern viruses, including e.g., tRNAs and ribosomes (Philippe *et al.*, 2013; Abrahão *et al.*, 2017; Abrahão *et al.*, 2018; Legendre *et al.*, 2018). Moreover, giant viruses are infected by their own specialized viruses and MGEs (La Scola *et al.*, 2008; Desnues *et al*., 2012; Jeudy *et al*., 2020; Tokarz-Deptuła *et al*., 2023). These findings led to fiercely debated proposals to classify giant viruses as a fourth domain of life e.g. (Nasir *et al.*, 2012), and to consider giant virus as models for the regression of cellular organisms into modern viruses.

However, growing evidence shows that at least some giant viruses evolved from much smaller viruses. Successive acquisition of genes from cellular organisms inflated their genomes to their current size and complexity (T. A. Williams *et al.*, 2011; Koonin *et al.*, 2015; Schulz *et al*., 2017; Krupovič *et al.*, 2020; Schulz *et al*., 2022). The genomes of numerous smaller-sized bacteri-

ophages also encode ribosomal genes, that were likely acquired by horizontal gene transfer and have continued evolution over time (Mizuno *et al.*, 2019), thus removing one distinction of giant viruses. Therefore, it seems unlikely that giant viruses indeed evolved out of degenerated cells. Modern parasitic cells such as the intracellular eukaryotic parasites microsporidia (Wadi & Reinke, 2020), for instance, have retained some key cellular characteristics (e.g., ribosomes) and their origins can be clearly traced back to cells within in the three domains of life (Forterre, 2006). No other potential intermediates between cells and viruses are currently known that could lend additional support to the regression hypothesis.

1.2.3 The 'escape' hypothesis

The 'escape hypothesis' (Figure 1c) proposes that viral entities evolved from genomic fragments which escaped from their respective host genomes, developed autonomous replication and subsequently became infectious agents of their hosts (Forterre & Krupovič, 2012). Viral capsids may have developed from the nucleoprotein complexes or membrane vesicles of host cells (Forterre & Krupovič, 2012).

The acquisition of cellular genes likely occurred on multiple independent occasions and is not limited to viruses infecting a singular domain of life [Krupovič and Koonin (2017b), and references therein]. The ancestry of viral replication proteins of certain lineages can be traced back to the rolling-circle replication initiation proteins of bacterial plasmids (Krupovič, 2013; Koonin *et al*., 2015). However, cellular ancestors cannot be identified for every conserved virus gene (Koonin *et al*., 2006; Krupovič *et al.*, 2019a). As such, these genes could be derived from yet unknown proteins or were generated *de novo*. Individual selection pressures and gene exchange between viruses can further conceal potential cellular ancestors of viral proteins [see Krupovič (2013); Kazlauskas *et al.* (2017); Munke *et al.* (2022), and references therein].

The question remains as to at which point in the evolution of cellular life the first viruses emerged as independent, selfish replicators. A straightforward evolutionary connection between genes of modern viruses and the genes of their respective hosts cannot be established in most cases, and no gene is shared between all modern viruses (E. C. Holmes, 2011). The ubiquity of the jelly roll fold in the capsid proteins of viruses infecting every domain of life (Krupovič & Koonin, 2017b; Krupovič *et al.*, 2019a; Krupovič *et al*., 2022), points to a likely acquisition event before LUCA or only shortly after the divergence of domains. The later diversification of viruses could then be tied to individual events. For instance, the homologous capsid proteins of reverse-transcribing viruses exclusive to eukaryotes were likely acquired during early eukaryogenesis (Krupovič & Koonin, 2017a). This may explain the diversity of viruses infecting archaea, which consist of both cosmopolitan viruses with a potentially ancient origin, and archaea-specific viruses that could have emerged more recently from archaeal mobile genetic elements [Krupovič *et al.* (2018), and references therein].

Recently Krupovič, Koonin and colleagues (2019a) proposed a chimeric origin for viruses by combining aspects of the virus-first and escape hypotheses (Figure 1d). At least some classes of viruses likely emerged from the replication modules of primitive selfish genetic elements before LUCA, but other viruses may have evolved more recently from non-viral mobile genetic elements (Krupovič & Koonin, 2017b; Krupovič *et al.*, 2019a; Koonin *et al.*, 2021). The capsid proteins of modern viruses probably evolved from cellular proteins over multiple independent acquisitions.

Finally, it should be noted that each hypothesis is necessarily influenced by our understanding of modern viruses and applies similar characteristics to ancient viruses. It is also not a given that all modern viruses evolved via the same route.

1.3 Viruses and other mobile genetic elements of archaea

1.3.1 Archaea the third domain of life

Archaea represent an interesting system for studying virus-host interactions in prokaryotes as they share some of their characteristics with either bacteria or eukarya, but also have a distinct set of characteristics that separates them from the two other cellular domains [see van Wolferen *et al.* (2022), and references therein]. Even more than forty years since the discovery and description of archaea by Carl Woese and George Fox (1977), knowledge about archaea and their viruses is limited as compared to what is known about bacteria and bacteriophages. Particularly since the official declaration of archaea as the third domain of life (Woese *et al.*, 1990), it is clear that we cannot simply assume that characteristics of viruses infecting bacteria also apply to viruses infecting archaea.

Archaea are globally distributed, and reach abundances up to or exceeding bacteria in some environments (Lloyd *et al.*, 2013; Crowther *et al.*, 2019; Hoshino *et al.*, 2020). They are important contributors to the global cycling of carbon and nitrogen (Spang *et al.*, 2017; B. J. Baker *et al.*, 2020). The global abundance of archaea suggests that their viruses are also important factors in nutrient cycling and microbial community composition, as shown for phages and eukaryotic viruses in aquatic environments [see Zimmerman *et al.* (2020), and references therein]. Indeed, large-scale metagenomics studies and mesocosm experiments suggest a potential global importance of archaeal viruses for carbon cycling in the pelagic (Roux *et al.*, 2016; Philosof *et al.*, 2017) and deep-sea benthos (Danovaro *et al.*, 2016).

The majority of isolated archaeal species are extremophiles, since the lower abundance of bacteria in extreme environments (e.g., at high temperatures, low pH or hypersalinity) has traditionally been beneficial for the isolation and

cultivation of slower-growing archaea. Thus, cultured representatives are currently available for only a minority of the archaeal phyla (Figure 2), even as the phylogenetic tree of archaea expands with new additions almost daily (Spang *et al*., 2017; B. J. Baker *et al*., 2020). Most of our knowledge on archaeal cell biology comes from a limited set composed of hyperthermophilic *Thermoproteota* [formerly known as *Crenarchaeota* (Oren & Garrity, 2021)], hyperthermophilic *Euryarchaeota*, halophilic *Euryarchaeota* (haloarchaea) or methanogenic *Euryarchaeota*.

The lipid composition of archaea is unique among cells (Jain *et al*., 2014; Caforio & Driessen, 2017). Unlike bacterial or eukaryotic lipids, archaeal phospholipids are composed of highly methylated isoprenoid chains linked to a glycerol-1-phosphate backbone via ether bonds. This composition likely confers high membrane stability that is essential in the extreme environments that many archaea inhabit. The diversity of archaeal lipids is based on two fundamental building blocks: a C_{20} sn-2,3-dyacilglycerol diether lipid (archaeol) or a C_{40} glycerol-dialkylglycerol tetraether lipid (GDGTs or tetaether lipids) (Caforio & Driessen, 2017). The former is often found in the bilayer membranes of halophilic *Euryarchaeota* and can include modifications, such as e.g. elongated isoprenoid chains (C_{25}) or double bonds in the isoprenoid chains as adaptations to extreme environments (Kellermann *et al*., 2016). The tetraether-based lipids isolated from both hyperthermophilic and mesophilic archaea form monolayers instead of typical phospholipid bilayers. Modifications of tetraether lipids via the formation of carbon rings in the isoprenoid chains or variable chain length are likely adaptations to hyperthermophilic conditions (Caforio & Driessen, 2017). Additional modifications of the polar head group further contributes to the remarkable diversity of archaeal lipids (Jain *et al*., 2014; Caforio & Driessen, 2017).

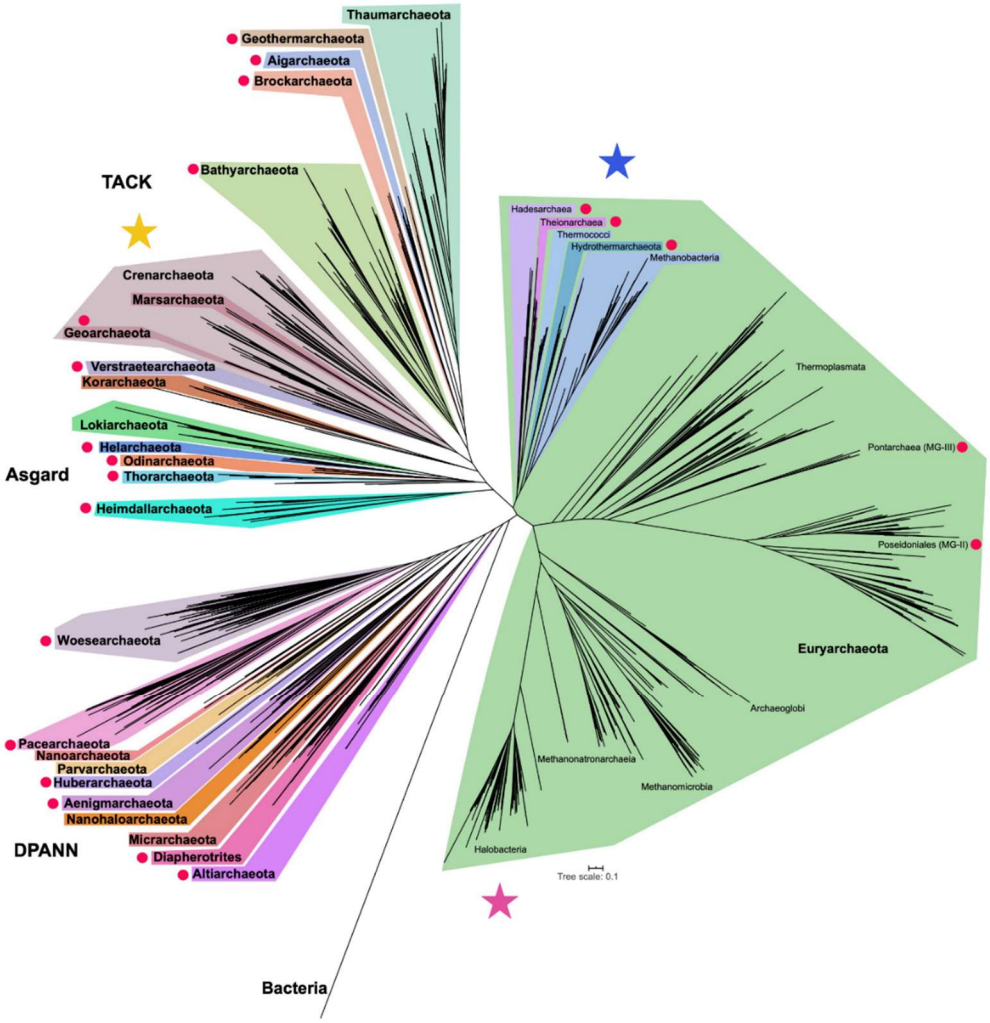

Figure 2: A current version of the archaeal tree of life based on 36 conserved marker proteins. Phyla marked with red dots do not have any cultured representatives. Particularly after the initial descriptions of the DPANN and Asgard archaeal phyla the archaeal tree has been subject to constant re-organization as more phyla are added and established phyla are shifted. Nevertheless, the major well-established archaeal phyla have remained apart from the *Crenarchaeota* which have been renamed to *Thermoproteota* (Oren & Garrity, 2021). The three groups marked with stars, *Crenarchaeota/Thermoproteota* (yellow), *Thermococci* (blue) and *Halobacteria* (pink) will be the archaeal groups most often referred to in this dissertation. Modified from B. J. Baker *et al*. (2020).

Archaea contain many homologues of eukaryotic proteins, thus providing the opportunity to more easily study mechanisms involving these protein homologues. This list includes proteins involved in DNA replication (Pisani *et al.*, 1992; Kazlauskas *et al.*, 2020), transcription (Huet *et al.*, 1983; Hirata *et al.*, 2008; Blombach *et al.*, 2019) and chromatin organisation (Sandman *et al.*, 1990; Sanders *et al.*, 2019; Laursen *et al*., 2021). Other archaeal homologues or eukaryotic-like proteins participate in cell division (Ellen *et* al., 2009; Tarrason Risa *et al.*, 2020; Hurtig *et al*., 2023), vesicle formation (J. Liu *et al.*, 2021b; Mills *et al.*, 2023) and fusion (Moi *et al.*, 2022). Finally, the enigmatic Asgard archaea appear to contain the closest living prokaryotic relatives of eukaryotes (Spang *et al*., 2015; Y. Liu *et al*., 2021; Eme *et al.*, 2023). Continued isolation and cultivation of Asgard archaea (Imachi *et al.*, 2020; Rodrigues-Oliveira *et al.*, 2023) will give us the opportunity to study their cell biology and help us determine what separates the Asgards from other archaea, and thus provide valuable information to enhance hypotheses about eukaryogenesis [e.g. Krupovič *et al.* (2023)].

1.3.2 Viruses of archaea

The viruses of archaea present an interesting conundrum in that cultured hosts are difficult to obtain and have mainly been limited to extremophiles, despite the fact that archaea and their viruses are also present in mesophilic environments. The genomes of archaeal viruses encode many unique genes with no apparent relationship to genes of their hosts or those of other viruses (Krupovič *et al.*, 2018). Nevertheless, archaeal viruses also share characteristics with the viruses infecting other domains of life and archaeal hosts share many immune defence systems with bacteria (Koonin *et al.*, 2017a; Dimitriu *et al.*, 2020; Gao *et al.*, 2020), suggesting that similar arms races occur between viruses and hosts in both domains.

To date, all identified archaeal viruses have circular of linear DNA-based genomes in form of either single-stranded DNA, double-stranded DNA, or

ssDNA-dsDNA hybrids. No RNA viruses have been identified so far, which could have evolutionary explanations or simply mean that such viruses were not yet identified because of their presumably high sequence divergence from any known virus (Prangishvili *et al.*, 2017). Like other MGEs, archaeal viruses can be inserted into the genomes of their hosts via site-specific integrases. Many of the identified integrases found in archaeal viruses and non-viral MGEs thus far are suicidal. Upon insertion, these integrase genes split into two fragments that flank the integrated MGE in the host chromosome, with excision involving recombination of both ends into a functional gene (Muskhelishvili *et al.*, 1993; She *et al.*, 2001; She *et al.*, 2004; Badel *et al.*, 2021).

Most characterized archaeal viruses infect extremophilic archaea within the *Euryarchaeota* and *Thermoproteota* phyla (formerly known as *Crenarchaeota*), with a few notable exceptions, such as viruses infecting anaerobic methanogens [e.g. Weidenbach *et al.* (2017); Wolf *et al.* (2019)] or marine *Thaumarchaeota* (Kim *et al.*, 2019). Hence, the described viruses are extremophiles themselves, with specific adaptations to the extreme environments of their host organisms, such as hypersalinity (halophilic *Euryarchaeota*), high temperatures (hyperthermophilic *Euryarchaeota* and *Thermoproteota*) and extremes in pH (*Euryarchaeota* and *Thermoproteota*). The few isolates available have served to define comparatively many taxonomic families, suggesting the existence of an enormous wealth of unexplored diversity that is ready to be discovered.

Viruses that infect archaea viruses can divided into two main categories: archaea-specific viruses (Figure 3a) and cosmopolitan viruses (Figure 3b). This split has been suggested to point to the polyphyletic origin of archaeal viruses with a mixture of cosmopolitan viruses of ancient origin and archaea-

specific viruses that emerged later from non-viral mobile genetic elements (MGEs) [Krupovič *et al.* (2018), and references therein]. The cosmopolitan archaeal viruses (Figure 3b) are divided between five virus families and likely share common ancestry with viruses that infect other domains of life. The basic morphology of their virions, of icosahedral (20 sided) capsids with or without tails, is similar to bacteriophages. Most cosmopolitan archaeal viruses fall into the *Caudoviricetes* class (Y. Liu *et al.*, 2021). Further subdivision into the *Myoviridae*, *Siphovirida* or *Podoviridae* families is based on the morphology of the proteinaceous tail (Senčilo & Roine, 2014; Krupovič *et al.*, 2018). While the core gene set of the *Caudoviricetes* genes appears to be shared between viruses infecting bacteria and archaea (Krupovič *et al.*, 2010; Krupovič *et al.*, 2018), network analyses suggest that the divergence of viruses infecting the two domains is very ancient (Y. Liu *et al.*, 2021).

Other cosmopolitan archaeal viruses fall into the *Sphaerolipoviridae* and *Turriviridae* families that also contain bacterial viruses. Their virions are spherical with an internal membrane envelope that is surrounded by capsid proteins with either single-jelly-roll (*Sphaerolipoviridae*) or double-jelly-roll folds (*Turriviridae*) (Krupovič *et al.*, 2018). The presence of cosmopolitan virus families in archaea strengthens the connection between archaeal viruses and the broader virosphere. The archaea-specific viruses are very diverse in morphology, including several unique virion shapes not found in any other viruses and only present in a few characterized isolates (Figure 3a). Archaea-specific viruses are currently distributed into 12 families: the bottle-shaped *Ampullaviridae* (Häring *et al*., 2005), spindle-shaped *Bicaudaviridae* and *Fuselloviridae* (Krupovič *et al*., 2014b), club-shaped *Clavaviridae* (Mochizuki *et al*., 2010), spherical *Globuloviridae* (Häring *et al.*, 2004), ovoid-shaped *Guttaviridae* (Arnold *et al*., 2000), flexible filamentous *Lipothrixviridae* (Bettstetter *et al.*, 2003), pleomorphic *Pleolipoviridae* (Bamford *et al.*, 2017), polyhedral *Portogloboviridae* (Liu *et al.*, 2017),

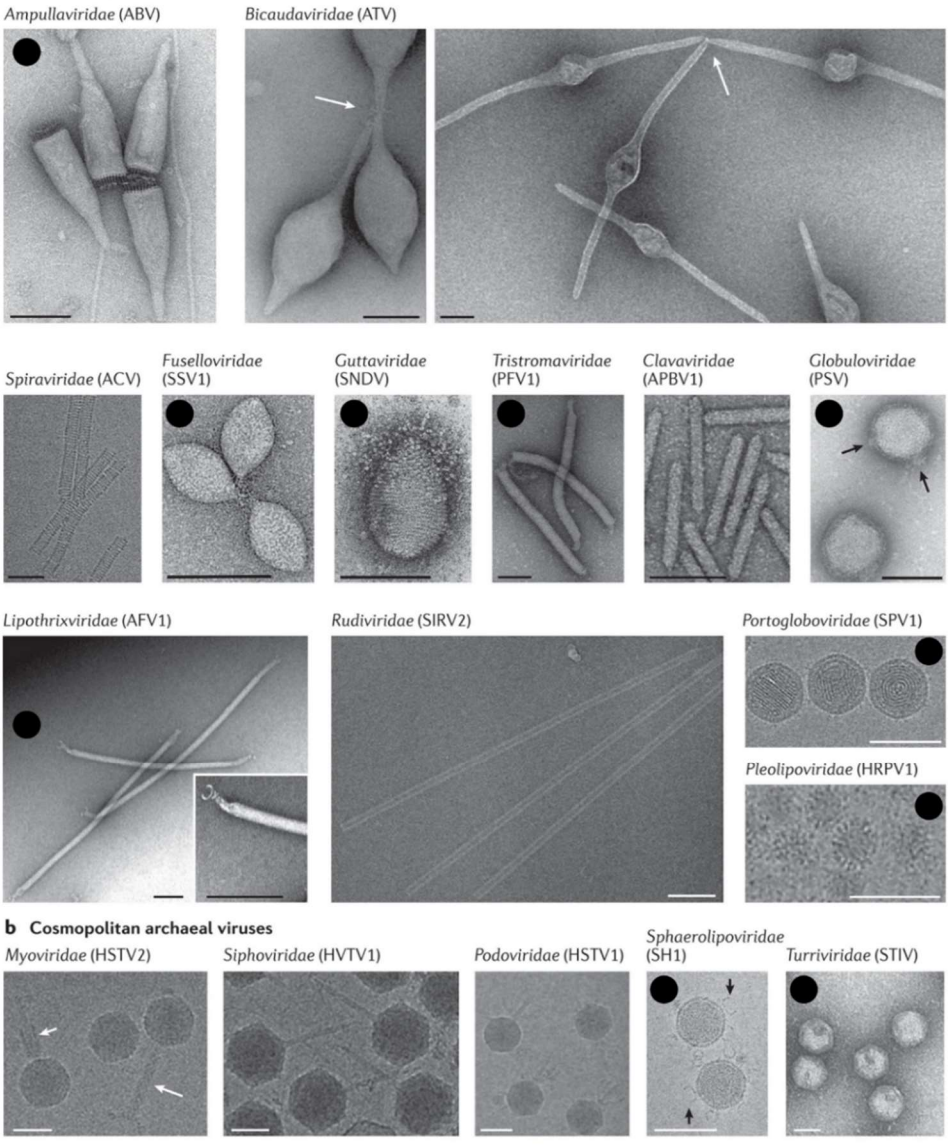
a Archaea-specific viruses
Ampullaviridae (ABV)
Bicaudaviridae (ATV)
Spiraviridae (ACV)
Fuselloviridae (SSV1)
Guttaviridae (SNDV)
Tristromaviridae (PFV1)
Clavaviridae (APBV1)
Globuloviridae (PSV)
Lipothrixviridae (AFV1)
Rudiviridae (SIRV2)
Portogloboviridae (SPV1)
Pleolipoviridae (HRPV1)
b Cosmopolitan archaeal viruses
Myoviridae (HSTV2)
Siphoviridae (HVTV1)
Podoviridae (HSTV1)
Sphaerolipoviridae (SH1)
Turriviridae (STIV)

Figure 3: Electron micrographs of archaeal viruses. Archaea-specific (a) and cosmopolitan viruses shared between bacteria and archaea (b), modified from Prangishvili *et al.* (2017) wherein the original sources of the images are indicated. Groups that have been reported to contain lipids either inside or at the outside enveloping their virions are marked with black dots. Virus families are named and represented by their type species. All scale bars represent 100 nm. First row: Acidianus bottle-shaped virus; (ABV) and Acidianus two-tailed virus (ATV). Second row: Aeropyrum coil-shaped virus (ACV), Sulfolobus spindle-shaped virus 1 (SSV1), Sulfolobus neozealandicus droplet-shaped virus (SNDV), Pyrobaculum filamentous virus 1 (PFV1), Aeropyrum pernix bacilliform virus 1 (APBV1) and Pyrobaculum spherical virus (PSV). Third row: Acidianus filamentous virus 1 (AFV1), Sulfolobus islandicus rod-shaped virus 2 (SIRV2), Sulfolobus polyhedral virus 1 (SPV1) and Halorubrum pleomorphic virus 1 (HRPV1). Last row: Halorubrum sodomense tailed virus 2 (HSTV2), Haloarcula vallismortis tailed virus 1 (HVTV1), Haloarcula sinaiiensis tailed virus 1 (HSTV1), Haloarcula hispanica virus (SH1) and Sulfolobus turreted icosahedral virus (STIV).

rod-shaped *Rudiviridae* (Prangishvili *et al.*, 1999), coiled fibres *Spiraviridae* (Mochizuki *et al.*, 2012) and the layered filamentous *Tristromaviridae* (Rensen *et al.*, 2016). Several unique features of virion organisation are also so far specific for individual archaeal viruses, such as tight packaging of DNA in the A-form within the capsid (DiMaio *et al.*, 2015), virion envelopes containing tetraether lipids orientated in a horseshoe shape (Kasson *et al.*, 2017), and special proteinaceous structures for virion release (Brumfield *et al.*, 2009; Quax *et al.*, 2011).

Since the emergence of metagenomics more and more virus metagenome assembled genomes (MAGs) from mesophilic archaea (Philosof *et al.*, 2017; Ahlgren *et al.*, 2019), methanotrophs (Laso-Pérez *et al.*, 2023) and Asgard archaea have been presented (Medvedeva *et al.*, 2022; Rambo *et al.*, 2022; Tamarit *et al.*, 2022). Presumably, a large pool of potential viruses is waiting to be identified and characterized.

1.3.3 Fusion and budding of membrane-enveloped viruses from the host membrane

In general, it is not known how most archaeal viruses pass the physical barriers surrounding archaeal cells in order to deliver their genomes for replication inside new hosts. Tailed archaeal viruses likely employ similar

mechanisms of DNA injection to bacteriophages. No virus-encoded enzymes capable of degrading the archaeal surface (S)-layer are currently known (Quemin & Quax, 2015). This poses a particular enigma for membrane-enveloped virions that would conceivably need to interact directly with the host cell membrane for fusion or budding to occur, similarly to eukaryotic viruses (Prangishvili *et al.*, 2017). Many archaeal viruses release their virions in chronic or persistent infections and cannot rely on cell lysis for release (Pina *et al.*, 2011; Mäntynen *et al.*, 2021). The virus particles of archaeal viruses may contain either external (Bettstetter *et al.*, 2003; Häring *et al.*, 2004; Pietilä *et al.*, 2009) or internal membranes (Bamford *et al.*, 2005; Porter *et al.*, 2005; Quax & Daum, 2018), composed of host-derived lipids (Figure 3).

Archaeal viruses appear to have developed multiple unique mechanisms to overcome the barriers presented by the archaeal cell envelope. Specialized proteinaceous egress structures have been described for lytic viruses (Quax & Daum, 2018; H. Wang *et al.*, 2018; Baquero *et al.*, 2021a), and the fusion and budding mechanisms of individual archaeal viruses have been characterized. For instance, SSV1 (*Fuselloviridae*) virion emerges as a protrusion out of the host cell membrane through a constricted neck in an elongated form, only to later mature into the final spindle-shape while still attached to the cell (Quemin *et al.*, 2016). This process strongly resembles the budding of eukaryotic viruses but also raises the question of how the monolayer-forming lipids of the cell membrane of *Sulfolobus* (Řezanka *et al.*, 2023) could be divided in this process. The scission mechanism has yet to be shown experimentally but may involve cellular proteins of the endosomal sorting complexes required for transport (ESCRT) cell division machinery (Quemin *et al.*, 2016), given how the eukaryotic homologues of these proteins are commonly exploited by eukaryotic viruses (Votteler & Sundquist, 2013). In contrast, another *Sulfolobus* virus, STSV2, down-regulates the ESCRT cell division machinery of its host, likely in order to facilitate budding via asymmetric cell

division of the host (J. Liu *et al.*, 2021a). Other archaeal viruses are also predicted to exit their hosts via budding, although experimental evidence remains lacking in many cases (Baquero *et al.*, 2021b), including for the archaea-specific family of *Pleolipoviridae* (Bamford *et al.*, 2017; Liu *et al.*, 2022).

Pleolipoviridae virions consist of an external membrane envelope surrounding the virus genome, and two major capsid proteins, namely, the internal small membrane proteins and the external spike proteins (Bamford *et al.*, 2017; Liu *et al.*, 2022). The spike protein of HRPV-6 has been identified as its fusion protein (El Omari *et al.*, 2019), and fusion activity is specifically triggered by the S-layer protein of the native host organism (Bignon *et al.*, 2022). The spike protein likely adopts an elongated conformation upon binding to the S-layer protein, bridging the gap to the cell membrane to initiate membrane fusion (El Omari *et al.*, 2019). The molecular mechanism of membrane fusion still needs to be determined for this virus-receptor system.

1.3.4 Plasmids and other mobile genetic elements of archaea

While archaeal viruses are in many ways quite distinct from the viruses infecting other cellular domains, there seems to be more overlap and exchange between the non-viral MGEs of archaea and bacteria. The majority of characterized non-viral MGEs in archaea are restricted to the *Sulfolobales* and *Halobacteriales* as a consequence of the availability of culturable hosts from these taxonomic groups. Other MGEs have been reconstructed from metagenomic sequence information.

The first archaeal plasmids were identified in the 1970s in *Halobacterium salinarium* (Simon, 1978; Pfeifer *et al.*, 1981), followed by discoveries of plasmids in other archaeal lineages (Zillig *et al.*, 1985; Charlebois *et al.*, 1987; Nölling & Vos, 1992). Systematic screening of archaeal populations has revealed that plasmids are widespread (Prangishvili *et al.*, 1998;

Prieur *et al.*, 2006), particularly among haloarchaea (S. DasSarma *et al.*, 2009; Wu *et al.*, 2012). Plasmids can also integrate specifically at tRNA sites in the genome using tyrosine recombinase superfamily integrases (She *et al.*, 2004; Hawkins *et al.*, 2013; Anderson *et al.*, 2017; Badel *et al.*, 2021). Archaeal plasmids have been suggested to play roles in horizontal gene transfer (see Section *1.4.1*), although the functions of most archaeal plasmids or their genes remain to be determined.

Archaeal plasmids share two basic replication mechanisms with bacterial plasmids, namely, rolling-circle-replication (RCR) and theta-replication (θ-). However, archaeal plasmids appear to be more diverse in terms of replication strategies than their bacterial counterparts. In many cases, their putative replication proteins are not homologues to known bacterial proteins. Some archaeal plasmids encode homologues of the host replication initiation proteins (H. Wang *et al.*, 2015; Erdmann *et al.*, 2017; Contreras *et al.*, 2022), which are themselves homologues to the eukaryotic Cdc6/Orc1 replication initiation proteins (Myllykallio *et al.*, 2000; Dueber *et al.*, 2011). This diversity points to convergent evolution of archaeal plasmids, indicating that the replication proteins in individual lineages evolved from diverse mixtures of host-derived DNA replication proteins (H. Wang *et al.*, 2015).

Rolling-circle replication involves a plasmid-encoded replication initiation protein (Rep) that binds to the double-stranded origin of replication and creates a nick, i.e., a discontinuity in one DNA strand, thus initiating DNA replication of the leading strand (Ruiz-Masó *et al.*, 2015).The host RNA polymerase binds to the single-stranded origin of the lagging strand and synthesizes primers for the DNA replication machinery to finish template replication.

Both the conjugative plasmids and the pRN1 family non-conjugative plasmids of the *Sulfolobales* (Peng *et al.,* 2000; Garrett *et al.*, 2004;

H. Wang *et al.*, 2015) encode putative replication initiation RepA proteins (Solar *et al*., 1998). The pRN1-family RepA is a multifunctional enzyme that combines both a C-terminal helicase and an unusual N-terminal domain with both DNA polymerase and primase activity, (Lipps *et al.*, 2003; Lipps *et al.*, 2004). Yet, other characteristics of RCR Rep proteins are lacking in pRN1-family RepA proteins, such as clear target origins of replication, or nicking-closing activity (H. Wang *et al.*, 2015). Rolling-circle replication proteins have also been identified in plasmids of hyperthermophilic *Euryarchaeota* (Erauso *et al.*, 1996; Marsin & Forterre, 1998; Soler *et al.*, 2007) and experimentally characterized in methanogenic *Euryarchaeota* (Thomsen & Schmitz, 2022). A putative haloarchaea-specific replication protein RepH (W. L. Ng & DasSarma, 1993) with a conserved RCR Rep motif (Ilyina & Koonin, 1992) has been identified, suggesting RCR-like mechanisms for many haloarchaeal plasmids (Hall & Hackett, 1989; Holmes & Dyall-Smith, 1990; H. Wang *et al.*, 2015). RepH proteins are very distinct from the archaeal RepA replication initiation proteins and are highly divergent across haloarchaeal lineages (Ilyina & Koonin, 1992; H. Wang *et al.*, 2015). RC-like replication was subsequently experimentally characterized for two plasmids of haloalkalophilic archaea (M. Zhou *et al.*, 2004; L. Zhou *et al.*, 2008).

The other basic plasmid replication mechanism, θ-replication (Lilly & Camps, 2015), involves binding of a replication initiator protein (also called Rep) to a specific DNA-binding motif upstream of an AT-rich genomic region where the replication bubble is formed. In contrast to RC-replication, the lagging strand is synthesized discontinuously. To date, θ-replication has only been experimentally verified for one haloarchaeal plasmid (Sun *et al*., 2006). Other plasmids from hyperthermophilic *Euryarchaeota* encode helicases or primases as their replication proteins and likely employ θ-like replication (Soler *et al.*, 2010; Gonnet *et al.*, 2011; Béguin *et al*., 2014; Gill *et al.*, 2014; Kazlauskas

et al., 2018). Members of the pT26-2 plasmid family (Soler *et al.*, 2010), predicted to replicate with a θ-like mechanism, appear to be spread across marine archaea with distinct lineages in the hyper-thermophilic *Thermococcales* and in the *Methanococcales* order of methanogenic *Euryarchaeota* (Badel *et al.,* 2019).

Many plasmids ensure their maintenance in the host by encoding toxin-antitoxin (TA) systems. Removal of the plasmids or damage to the TA system kills the host through the loss of instable antitoxins (protein or RNA) and accumulation of stable proteins or RNAs that act as toxins (Jurėnas *et al*., 2022), although the mechanism depends on the specific TA system family [see Jurėnas *et al.* (2022), and references therein]. Our knowledge about the diversity and function of TA systems on archaeal plasmids is limited. Currently only systems located on chromosomes have been experimentally characterized in *Sulfolobus* (Maezato *et al.*, 2011; Cooper *et al.*, 2023) and in haloarchaea (Li *et al*., 2021). Screening of plasmids of methanogenic and hyperthermophilic *Euryarchaeota* has revealed several putative TA systems (Krupovič *et al.*, 2013), yet our identification of TA systems is clearly primed by examples from bacteria and, thus, may miss any novel archaea-specific systems.

Recently, new archaeal MGEs that have resisted categorization as viruses, plasmids or minichromosomes have been described. These 'Borgs' are large (≤ 1 Mb) linear dsDNA MGEs associated with the *Methanoperedens,* uncultivated anaerobic methane oxidizing archaea (Al-Shayeb *et al.*, 2022). The Borgs described thus far share ancestry, but their specificity to particular *Methanoperedens* hosts is still unclear (Al-Shayeb *et al*., 2022; Schoelmerich *et al.*, 2023). No canonical archaeal plasmid genes have been identified in the published Borg sequences so far, although many genes appeared to have viral homologues (Schoelmerich *et al.*, 2023). Borgs also carry genes encoding components of key processes in their hosts, such as anaerobic

methane oxidation and nitrogen fixation (Al-Shayeb *et al.*, 2022; Schoelmerich *et al.*, 2023). Previously, other archaeal megaplasmids (> 1 Mb) were shown to carry essential genes, thus blurring the line between plasmids carrying auxiliary genes and host chromosomes that encode core genes (W. V. Ng *et al.*, 1998; S. DasSarma *et al.*, 2009).

In addition to plasmids, archaeal MGEs also include transposons, casposons and inteins, among others. Transposons are short DNA segments integrated into genomes able to re-locate into different positions in the genome by way of a translocating enzyme, the transposase. Transposons can be categorized into insertion sequences (ISs) that self-encode a transposase, miniature inverted-repeat transposable elements (MITEs) that do not encode a functional transposase, or composite transposons, where a DNA segment is flanked by two copies of an IS (Filée *et al.*, 2007). Other self-replicating MGEs include the casposons that gave rise to the prokaryotic CRISPR-Cas immune system. These casposons encode a Cas1 endonucelase homologue and use mechanisms similar to the acquisition of new CRISPR spacers for their own integration and excision from the genome (Krupovič *et al.*, 2014a; Krupovič *et al.*, 2017; Béguin *et al.*, 2019).

Finally, the inteins, which are integrated within protein-coding genes, catalyse their own excision from the protein after translation, leaving a functional protein behind. Inteins are able to invade intein-free new hosts with a self-encoded homing endonuclease that generates double strand breaks in the DNA sequence of the same gene that does not contain an intein (Barzel *et al.*, 2011; Belfort, 2017; Gophna & Altman-Price, 2022). Inteins generally invade house-keeping genes of their host and are widespread among archaea, in particular among *Euryarchaeota* (Novikova *et al.*, 2015). They may also promote horizontal gene transfer to other gene loci when invading a new host (Naor *et al.*, 2016). The diversity of non-viral MGEs described here is not

exclusive to archaea and strongly suggests shared connections and gene exchange across the boundaries of the virosphere proper into the broader MGE space.

1.4 Vesicles and their role in horizontal gene transfer between archaea

1.4.1 Mechanisms of horizontal gene transfer

Horizontal gene transfer between cells is one of the main drivers of evolution and likely responsible for the emergence of several lineages in the archaeal domain (Nelson-Sathi *et al.*, 2012; Nelson-Sathi *et al.*, 2015; Gophna & Altman-Price, 2022). The general mechanisms of horizontal gene transfer described for bacteria are also found in archaea. These include natural transformation, transduction, cell fusion and mating, chromosome exchange, and vesicle mediated transport (Wagner *et al.*, 2017; Gophna & Altman-Price, 2022). However, not all mechanisms have been described for every phylum for which cultured representatives are available, such that our knowledge about shared mechanisms for specific modes of horizontal gene transfer is limited.

Populations of archaea frequently exchange DNA through transfer mechanisms and homologous recombination between close relatives (Papke *et al.*, 2004; Whitaker *et al.*, 2005; Cadillo-Quiroz *et al.*, 2012; DeMaere *et al.*, 2013). This high exchange rate appears to be crucial for the formation of archaeal species (Wagner *et al.*, 2017; Gophna & Altman-Price, 2022) and for DNA repair in intra-species exchanges (Wagner *et al.*, 2017). Genomic evidence suggests that large-scale horizontal gene transfer of key metabolic functions from bacteria to archaea played a key role in several instances during archaeal evolution (Nelson-Sathi *et al.,* 2012; Nelson-Sathi *et al.*, 2015). Incorporation and usage of ‘foreign’ DNA could theoretically be associated with fewer fitness disadvantages in archaea, although no mechanisms are currently known that could explain this effect (Deschamps *et al.*, 2014).

Natural transformation, namely, uptake of unprotected environmental DNA, has been observed in several methanogenic and hyperthermophilic archaea (Bertani & Baresi, 1987; Worrell *et al.*, 1988; Lipscomb *et al.*, 2011; Fonseca *et al.*, 2020; Song *et al.*, 2021). Natural competence has not yet been demonstrated for haloarchaea (Chimileski *et al.*, 2014; Gophna & Altman-Price, 2022). However, uptake of extracellular DNA may be increased under low-salt conditions and increased S-layer permeability (Chen *et al.*, 2012; Chen *et al.*, 2019), when cell mating is inhibited under low-salt conditions (Shalev *et al.*, 2017).

Transduction, or the transfer of host genetic material by viruses via mature virions, can be non-specific or linked to distinct regions of the host chromosome. No archaeal viruses are currently known to perform true non-specific transduction, however, the *Sulfolobus* viruses SSV1 and SSV2 can transfer the pSSVx and pSSVi satellite viruses in their virions (Arnold *et al.*, 1999; Y. Wang *et al.*, 2007; Contursi *et al.*, 2014). Gene-transfer-agents (GTAs) are non-functional phage/virus particles (Lang *et al.*, 2012; Lang *et al.*, 2017; Kogay *et al.*, 2022b). They do not transport a viral genome, but instead transport pieces of the host genome that are released by cell lysis and are injected into new hosts by the virion structures. Only one GTA has been described for the archaeal domain to date (Bertani, 1999).

Conjugation, or the unidirectional self-transmission of plasmids via direct cell-to-cell contact mediated by type IV secretion systems, has only been described for a limited number of lineages, namely, the *Sulfolobales* of the *Thermoproteota* phylum (Schleper *et al.*, 1995; Grogan, 1996; Prangishvili *et al.*, 1998; Wagner *et al.*, 2017). Conjugation is mediated by type IV pili and inducible by UV radiation (Fröls *et al.*, 2007; Schmidt *et al.*, 1999; Ajon *et al.*, 2011; van Wolferen *et al.*, 2016). The first archaeal conjugative plasmid outside the *Sulfolobales* was only described very recently for hyperthermophilic *Euryarchaeota* (Catchpole *et al.*, 2023). However, the spread of genes encoding for homologues of the bacterial conjugation machinery indicates that

conjugative plasmids may be more widespread in archaea, (Krupovič *et al.*, 2019b; Catchpole *et al.*, 2023). Archaea likely acquired conjugative plasmids via inter-domain transfer in multiple instances (Guglielmini *et al.*, 2012).

Halophilic *Euryarchaeota* (haloarchaea) frequently perform large-scale gene exchanges between individuals of the same species and across species boundaries (Papke *et al*., 2004; Naor *et al.*, 2012; DeMaere *et al*., 2013). Conjugative plasmids have not been identified in haloarchaea to date, but mating of cells leads to bi-directional gene exchange (≤ 500 kB) of plasmids and chromosomes via direct recombination (Mevarech & Werczberger, 1985; Tchelet & Mevarech, 1993, Naor *et al.*, 2012; Makkay *et al*., 2020). Cell-to-cell bridges enable DNA exchange by connecting the cytoplasm of mating cells (Rosenshine *et al*., 1989; Sivabalasarma *et al.*, 2021). Recognition of suitable mating partners *in Haloferax volcanii* relies on recognition of the specific N-glycosylation (a post-translational modification by polysaccharides) pattern of the proteinaceous S-layer (Tripepi *et al*., 2010; Shalev *et al.*, 2017). There are indications that this behaviour could be more widespread across haloarchaea beyond *H. volcanii* (Kuwabara *et al*., 2005; Kuwabara *et al*., 2007; Comolli & Banfield, 2014).

Vesicle-mediated transport, or vesiduction (Soler & Forterre, 2020), shows similarities to transduction, where nucleic acids are packaged and delivered by a protective structure. In vesiduction, extracellular vesicles (EVs) produced by the cell serve this role. EVs are formed by budding from the cell membrane in all three domains of life (Gill *et al*., 2019). Soler *et al.* (2008) first described vesiduction for *Thermococcus kodakarensis* with the detection of extracellular and plasmid DNA within spherical EVs produced by the host. Transformation of the host with a shuttle plasmid led to packaging of the recombinant plasmid into EVs and EV preparations could be used to 'infect' plasmid-free strains of *T. kodakarensis* (Gaudin *et al.*, 2013).

Moreover, *Thermococcus nautilus* selectively packages some of its native plasmids into EVs, including a defective viral genome in plasmid form that is not able to form virions (Gaudin *et al.*, 2014). The authors suggested that packaging in EVs could be a way for the virus to forgo formation of its own virion, given how; the EVs that package the virus are not distinct from the other EVs produced by the host.

1.4.2 Two major cell division machineries suggest at least two distinct mechanisms of vesicle formation in archaea

Bacteria, Eukarya and Archaea all produce EVs (Deatherage & Cookson, 2012). EVs can contain cellular components and nucleic acids and, therefore, act as vectors for horizontal gene transfer in bacteria and archaea, as described above. In addition to horizontal gene transfer by vesiduction, EVs have been linked to anti-viral defence mechanisms in prokaryotes (Manning & Kuehn, 2011), and are thought to mediate interactions of bacteria with multicellular organisms (Koeppen *et al.*, 2016; Moriano-Gutierrez *et al.*, 2020).

The major archaeal clades likely encode different mechanisms of EV formation, based on their very different systems of cell division. The split separates the cell division machineries of *Thermoproteota* and Asgard archaea (ESCRT homologues) from the *Euryarchaeota*, the DPANN superphylum, *Thaumarchaeota* and *Korarchaeota* (FtsZ homologues) [van Wolferen *et al.* (2022), and references therein]. However, some members of the *Thaumarchaeota* and Asgard archaea appear to encode both systems (Pelve *et al.*, 2011; Pende *et al.*, 2021).

The cell division machinery of the *Sulfolobales* in the *Thermoproteota* phylum is homologous to the eukaryotic ESCRT system, which facilitates vesicle formation orientated away from the cytosol including to the extracellular environment (McCullough *et al.,* 2018; Vietri *et al.,* 2020). *Sulfolobales* ESCRTs (Lindås *et al.*, 2008; Caspi & Dekker, 2018; Tarrason Risa *et al.,* 2020;

Hurtig *et al.*, 2023), also appear to be involved both in EV formation and in the budding of viruses (J. Liu *et al.*, 2021a; J. Liu *et al.*, 2021b). The other main archaeal cell division machinery is based on homologues of bacterial FtsZs (Bisson-Filho *et al.*, 2017) and other cell division proteins (van Wolferen *et al.*, 2022), as well as CetZs, which are tubulin-like proteins that control cell shape, motility and have cell surface-related functions (Duggin *et al.*, 2015; Brown & Duggin, 2023). The mechanisms and components of FtsZ-based cell division have been extensively studied in *H. volcanii*, where cell division proteins are consecutively assembled in rings at the division plane (Duggin *et al.*, 2015; Liao *et al.*, 2018; Liao *et al.*, 2021; Nußbaum *et al.*, 2021). Homo-logues of the main FtsZ-based cell division proteins were also found in other haloarchaea (Baumann & Jackson, 1996; Margolin *et al.*, 1996; Ozawa *et al.*, 2005; T. J. Williams *et al.*, 2017; Liao *et al.*, 2021).

No homologues of proteins involved in vesicle formation in the *Thermoproteota* have been identified thus far in *Euryarchaeota* (Pende *et al.*, 2021). Mass spectrometry analysis of EVs from the halophile *Halorubrum lacusprofundi* (*Euryarchaeota*) did not detect any ESCRT homologues but identified other cellular proteins that were enriched in the EV fraction (Erdmann *et al.*, 2017). Notable among them were a CetZ-like tubulin protein (Brown & Duggin, 2023), and a bacterial outer membrane protein BamB-like protein which could be involved in the insertion of membrane-bound proteins into the vesicle (Gunasinghe *et al.*, 2018). A putative vesicle coat protein with structural similarities to the γ-subunit of the COPI complex which is one of the protein coats of eukaryotic intracellular vesicles (Faini *et al.*, 2013), was also identified. Moreover, a small GTPase assigned to the same family of small GTPases that initiate COPI vesicle coat protein assembly and vesicle budding in eukaryotes (Nielsen *et al.*, 2008) was also enriched in EV preparations (Erdmann *et al.*, 2017). The fact that proteins showing homology to eukaryotic intracellular trafficking such as COPI vesicles were identified in

vesicle preparations of *Euryarchaeota* suggests that vesicle production in this phylum could involve a COPI-like mechanism, possibly with the involvement of cell division proteins. Indeed, recent results from another haloarchaeon, *H. volcanii* , suggest that *Euryarchaeota* require a small GTPase to initiate vesicle formation similar to intracellular vesicle trafficking in eukaryotes [see Mills *et al.* (2023) in Chapter III].

1.4.3 Plasmid vesicles could represent an intermediate step in viral evolution between vesiduction and enveloped viruses

Plasmid vesicles (PVs) are a novel class of vesicles that blur the boundaries between EVs and virions (Erdmann *et al.*, 2017). PVs, sometimes also called plasmidions, were first identified in a halophilic archaeon from Antarctica (Erdmann *et al.,* 2017; Forterre *et al.*, 2017). The pR1SE plasmid is packaged inside PVs, which infect plasmid-free strains of the host without direct cell-to-cell contact (Erdmann *et al.*, 2017).

PVs were originally isolated from *Halorubrum lacusprofundi* strain R1S1, containing low level of host-derived DNA and a circular plasmid of 50 kb size (Figure 4). The plasmid encodes hallmark plasmid genes in the conserved region 1, such as a putative RepH replication protein (Erdmann *et al.*, 2017), indicating possible rolling-circle replication (Ilyina & Koonin, 1992; W. L. Ng & DasSarma, 1993), and a putative toxin gene of a toxin-antitoxin system (ORF3). Region 2 (Figure 4) contains a Cdc6/Orc1 replication initiation protein homologue (ORF29) next to a putative origin of replication and several pR1SE-specific proteins (Erdmann *et al.*, 2017). Mass spectrometry analysis of proteins in PVs, as compared to cell membrane proteins of the host, showed that some pR1SE-specific proteins were only found in PV preparations whereas four others were found in both PVs and the host membrane (Erdmann *et al*., 2017). Such incorporation of plasmid-encoded proteins into the vesicle structure had not been described before

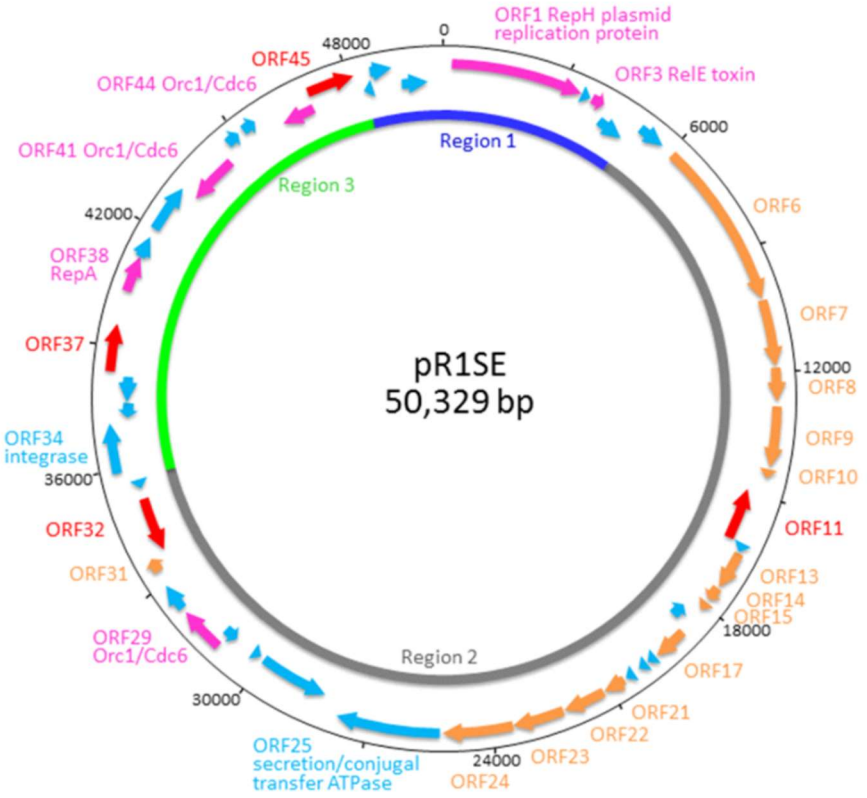

Figure 4: Plasmid map of the pR1SE plasmid originally isolated from *Hrr. lacusprofundi* R1S1. The positions and gene annotations are indicated on the outermost ring. The positions of the ORFs are indicated in the second ring and their predicted functions are indicated in colour: plasmid replication/stability genes (pink), other (light blue), proteins detected in PV preparations (orange) and transposases (red). The innermost ring shows the distribution of pR1SE into core conserved plasmid regions 1 (dark blue) and 2 (grey), and region 3 (green) which is likely directly host-derived and highly variable between different versions of pR1SE. Modified from Erdmann *et al.* (2017).

and suggests that similarly to a virus, pR1SE encodes proteins necessary for its own dissemination. The pR1SE-specific genes show the highest similarity to other haloarchaeal proteins and, therefore, appear to be originally host-derived but have likely evolved since over continuous interactions between pR1SE and its host (Erdmann *et al.*, 2017).

The most abundant pR1SE proteins found in PVs include a putative kinase or chaperone protein (ORF8), a transmembrane protein that could serve as a scaffold for protein interactions (ORF6), coat complex proteins (ORF10, 22, 23 and 24) and a subtilisin-like serine protease (ORF7) (Erdmann *et al.*, 2017). The latter contains a TAT signal peptide (Ruiz *et al.*, 2012), predicting its export to the extracellular space and represents the first protease identified in a virus-like archaeal MGE. Thereby providing insight into how membrane-enveloped archaeal viruses could overcome the S-layer barrier during infection and egress (Quemin & Quax, 2015). PV preparations also contained a number of host proteins which may be involved in EV formation as they were also identified in EV preparations from non-infected *Hrr. lacusprofundi* cells [Erdmann *et al.* (2017), see Section *1.4.2* for more details].

Region 3 of the plasmid is identical to host *Hrr. lacusprofundi* genomic DNA and was likely incorporated into the plasmid by the transposases flanking the region (Erdmann *et al.,* 2017). Subsequently alternate versions of the complete pR1SE plasmid including the conserved core regions 1 and 2 and variable region 3s were identified in other *Hrr. lacusprofundi* strains from the same environment. PVs could be obtained from HLS1 and DL18 strains, in the latter of which the plasmid is integrated into the primary chromosome but can also be isolated from PVs as a smaller (ca. 38 kb) excised version (Erdmann *et al.*, 2017). In both strains, region 3 shared high identity with genomic DNA of other haloarchaea from Deep Lake and other *Halorubrum* species and was highly variable in size (DeMaere *et al.*, 2013; Erdmann *et al.*, 2017). Therefore, pR1SE appears to be capable of large-scale uptake of host-derived DNA and could represent an important vector for horizontal gene transfer in the hypersaline lakes of Antarctica, although infection of other potential hosts with PVs could not be replicated in the laboratory (Erdmann *et al.*, 2017).

No canonical virus genes or proteins were identified on the pR1SE plasmid or the PV particles. The only exception was a virus-like integrase (ORF34), which are frequently found on archaeal plasmids (H. Wang *et al.*, 2015; Erdmann *et al.*, 2017; Badel *et al.*, 2021). The PV life cycle appears to go beyond what has been described for vesiduction in other archaea. PVs transfer pR1SE DNA with only low levels of free host DNA and have a distinct protein composition compared to the EVs that *Hrr. lacusprofundi* produces concurrently. Therefore, pR1SE could represent a potential intermediate form in virus evolution, supporting the escape hypothesis (see Section *1.2.3*). The association of pR1SE with at least one culturable host enables us to characterize these novel MGEs in the laboratory. Important questions remain to be answered, including the host-dependency of PV formation, which would determine functional proximity to true viruses, in-depth characterization of the pR1SE infection cycle and identification of the spread of pR1SE homologues beyond the hypersaline lakes of Antarctica.

1.5 Haloarchaea as model systems to study virus-host interactions

1.5.1 Haloarchaea, obligate halophilic archaea

Halophilic *Euryarchaeota,* i.e., haloarchaea are among the best studied archaeal phyla due to their comparatively easy isolation from hypersaline environments (> 1.5 M NaCl), where they can be the predominant members of the community (Ventosa *et al.*, 2015). As a consequence of their description before the discovery of the archaea as a distinct domain of life they are officially assigned to the *Halobacteria* class of *Euryarchaeota* phylum (P. DasSarma & S. DasSarma, 2008). The viruses, plasmids and other MGEs of halophilic archaea have been studied since the 1970s [see H. Wang *et al.* (2015), and references therein] and show remarkable diversity, similar to the MGEs of other archaeal phyla, such as the *Thermococcales* and *Sulfolobales*.

Haloarchaea likely evolved from moderately halophilic, i.e., 'salt-loving', methanogenic *Euryarchaeota* into obligate halophiles (Nelson-Sathi *et al.*, 2012). Other halophilic lineages of the *Euryarchaeota* include the extremely halophilic, methanogenic *Methanonatronarchaeia* (Sorokin *et al.*, 2017), acidophilic *Haloplasmatales* within the *Thermoplasmatota* (H. Zhou *et al.*, 2022), and the small symbiotic *Nanohaloarchaeota* included in the DPANN superphylum (Narasingarao *et al.*, 2012; B. A. Baker *et al.,* 2023). Adaptation to hypersaline environments probably occurred in multiple instances across *Euryarchaeota* and DPANN evolution (B. A. Baker *et al.*, 2023).

Haloarchaea are primarily heterotrophs that live in hypersaline environments where salinity can approach saturation (> 30% w/v), such as the Dead Sea, Great Salt Lake, artificial salterns, soda lakes and salt flats (Ventosa *et al.*, 2015; S. DasSarma & P. DasSarma, 2017;). While a sizable portion of haloarchaea are mesophilic, some species are poly-extremophilic and are able to deal with low temperatures (DeMaere *et al.*, 2013; T. J. Williams *et al.*, 2017), low pH (Minegishi *et al.*, 2010), high pH (Sorokin *et al.*, 2018) or any combination thereof (Harrison *et al.*, 2013). Adaptations to the harsh environmental conditions include osmotic regulation either by high intracellular concentrations of organic solutes which appears to be a bacterial solution, or a 'salt-in' strategy of accumulating high intracellular potassium concentrations (~ 4 M) that haloarchaea employ (Oren, 2013). The latter requires the development of a highly acidic and, therefore, negatively charged proteome, with accumulation of glutamic and aspartic acid residues ensuring protein stability and activity (Oren, 2013; B. A. Baker *et al.,* 2023). Other adaptations to high salinity include changes to membrane permeability by unsaturation of the isoprenoid chains of bilayer-forming lipids and accumulation of non-bilayer forming lipids as permeability barriers (Kellermann *et al.*, 2016) and GC-rich genomes (S. DasSarma & P. DasSarma, 2017).

The cell surface proteins of haloarchaea are extensively modified with polysaccharides linked to asparagine residues after translation, i.e., N-glycosylated. This ensures proper folding, stability and function of proteins under hypersaline conditions (Yurist-Doutsch *et al.*, 2010; Tamir & Eichler, 2017; Vershinin *et al.*, 2021a; Eichler, 2020). N-glycosylation also appears to play additional roles in cell-cell recognition (Shalev *et al.*, 2017; Shalev *et al.*, 2018) and cell-virus interactions (Kandiba *et al.,* 2012; Shalev *et al.*, 2018; Zaretsky *et al.*, 2018).

The individual composition of N-linked glycans attached the S-layer glycoproteins and other cell appendages creates a unique recognition motif on the cell surface that can differ even on a strain level (Kaminski *et al.*, 2013; Shalev *et al.*, 2018; Pfeiffer *et al.*, 2020). The universal marker genes of the N-glycosylation pathway are broadly distributed across archaea (Magidovich & Eichler, 2009; Kaminski *et al.*, 2013; Eichler, 2020), but our knowledge of the components of N-glycosylation pathway in haloarchaea is mainly based on studies performed with *H. volcanii* (Figure 5). Here, soluble monosaccharides are first sequentially assembled on the cytoplasmic side of the membrane onto a dolichol phosphate carrier, by the glycosyltransferases AglJ, AglG, AglI and AglE (Abu-Qarn *et al.*, 2008; Yurist-Doutsch *et al.*, 2008; Guan *et al.*, 2010; Kaminski & Eichler, 2010). The tetrasaccharide chain is then flipped onto the extracellular side and the key enzyme of the pathway, the oligosaccharyltransferase AglB, attaches the glycan to the asparagine residues Asn-13 and Asn-83 of the S-layer proteins (Abu-Qarn *et al.*, 2007; Kandiba *et al.*, 2016). The fifth and final sugar residue is attached to AglD on the cytoplasmic side, delivered across the membrane by AglR and finally added to the glycan by AglS (Guan *et al.*, 2010; Cohen-Rosenzweig *et al.*, 2012; Kaminski *et al.*, 2012).

Although we now know the N-glycosylation pathway of *H. volcanii* fairly well (Figure 5), characterization of the N-glycosylation pathways of other

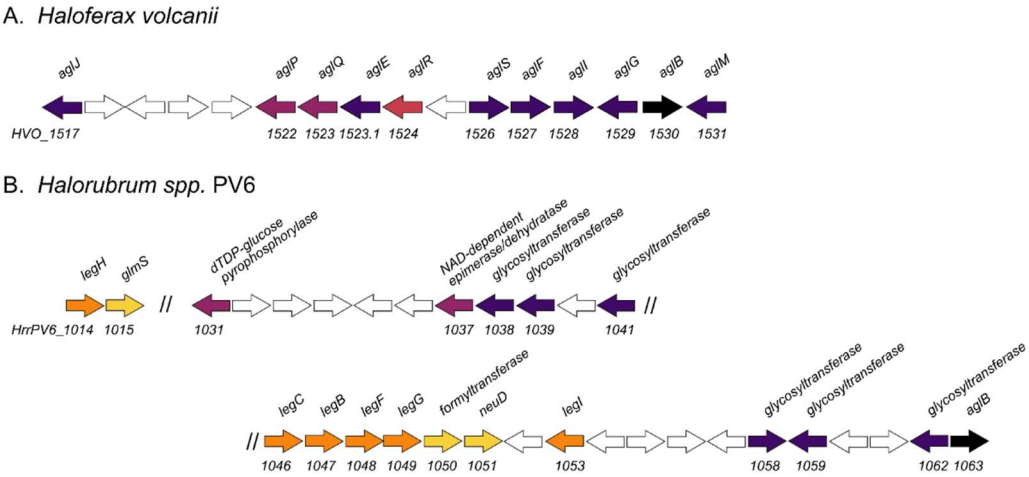

Figure 5: Genome comparison of the archaeal glycosylation (*agl*) clusters of *H. volcanii* and *Halorubrum* sp. PV6. Published gene annotations for *agl* cluster genes in *H. volcanii* (a) after Abu-Qarn *et al.* (2007); Abu-Qarn *et al.* (2008); Yurist-Doutsch *et al.* (2008); Guan *et al.* (2010); Kaminski and Eichler (2010); Kandiba *et al.* (2016) and *Halorubrum* spp. PV6 (b) after Zaretsky *et al.* (2018). The oligosacharyltransferases (*aglBs*) are shown in black, glycosyltransferases and glycosylation related genes are in dark and light purple respectively. Flippases or flippase-related genes are in red, legionaminic acid biosynthesis genes are in orange and biosynthesis related genes are in yellow.

haloarchaea is ongoing (Zaretsky *et al.*, 2018; Zaretsky *et al.*, 2019; Vershinin *et al.*, 2021a; Vershinin *et al.*, 2021b), and will likely reveal new glycan modifications and novel pathway components in the future.

The genomes of haloarchaea are also characterized by extreme polyploidy (Soppa, 2013; Zerulla *et al.*, 2014; Ludt & Soppa, 2019), which is tied to growth stage and could maintain low mutation rates and provide resistance against desiccation (Zerulla & Soppa, 2014). In addition to the chromosome, haloarchaeal genomes also contain various small plasmids and megaplasmids (S. DasSarma *et al.*, 2009; Wu *et al.*, 2012). Multiple origins of replication are necessary to maintain and coordinate these multi-replicon genomes (Breuert *et al.*, 2006; Norais *et al.*, 2007; Hawkins *et al.*, 2013).

Plasmid replication origins may also be able to override chromosomal origins by preferential binding of replication initiation proteins as shown in *Haloferax volcanii* (Norais *et al.*, 2007).

1.5.2 *Haloferax volcanii* and *Halorubrum lacusprofundi*

H. volcanii (*Haloferacales)* is the model organism for the haloarchaea. First isolated from Dead Sea sediment (Mullakhanbhai & Larsen, 1975), subsequent efforts have led to the development of a wide arsenal of tools to study its cell biology. These include plasmid-mediated gene deletion (Bitan-Banin *et al*., 2003; Allers *et al*., 2004;), inducible promotors (Allers *et al.*, 2010; Rados *et al*., 2023), recombinant protein labels (Reuter & Maupin-Furlow, 2004; Davis *et al*., 2020) and a characterized CRISPR-Cas system (Maier *et al.*, 2019).

These tools have led to new insights into the cellular processes of archaea, including motility (Nußbaum *et al.*, 2020), cell division (Liao *et al.*, 2021; Nußbaum *et al.*, 2021), cell shape (Brown & Duggin, 2023), extracellular vesicle (Mills *et al.*, 2023) and gas vesicle formation (Winter *et al.*, 2018), mating (Makkay *et al.*, 2020), small proteomes (Hadjeras *et al*., 2023), stress responses (Mondragon *et al.*, 2022), post-translational modification [Eichler (2020), and references therein], ribosome function (Jüttner *et al.*, 2019) and DNA replication and repair [Pérez-Arnaiz *et al.* (2020), and references therein]. However, *H. volcanii* appears to be uniquely unsusceptible to viral infection, even within the *Haloferax* genus (Aguirre Sourrouille *et al.*, 2022) and is, therefore, not very well suited as a model organism to study virus-host interactions in haloarchaea. To date, only the Haloferax Pleomorphic Virus 1 (HFPV-1) of the archaea-specific *Pleolipoviridae* family (Bamford *et al.*, 2017; Alarcón-Schumacher *et al.*, 2022) is able to infect *H. volcanii* where it causes growth retardation instead of host lysis in a productive chronic infection (Mäntynen *et al.*, 2021).

In contrast, *Halorubrum lacusprofundi* (*Haloferacales*) has proven itself a useful host organism for studying a diverse range of viruses, virus-like elements, and symbiotic Nanohaloarchaea (Hamm *et al*., 2019; Hamm *et al.*, 2023). An archaeal tailed virus isolated from Deep Lake is able to induce lysis in a laboratory strain of *Hrr. lacusprofundi* ACAM34 that has lost its main immune system (Tschitschko *et al.,* 2018; Mercier *et al*., 2022). Several *Hrr. lacusprofundi* strains are susceptible to infection by the pleomorphic HFPV-1 virus that exhibits an unusually broad range (Alarcón-Schumacher *et al*., 2022). Moreover, *Hrr. lacusprofundi* is currently the only known host that the pR1SE plasmid is able to infect, and in which PVs are produced [see Erdmann *et al.* (2017), and Section *1.4.3*].

Hrr. lacusprofundi was the first cold-adapted archaeon to be isolated and cultivated in the laboratory (Franzmann *et al*., 1988) and has become a model organism to study cold-adaptation in archaea (S. DasSarma *et al*., 2013; P. DasSarma *et al*., 2017; T. J. Williams *et al*., 2017). The original isolate strains ACAM32 and ACAM34 were obtained from Deep Lake but other strains are spread among other hypersaline lakes in eastern Antarctica (Erdmann *et al*., 2017; Tschitschko *et al*., 2018). These lakes were separated from the Southern Ocean around 3,500 years ago (Zwartz *et al*., 1998; Gibson, 1999; Hodgson *et al*., 2001) and are highly hypersaline [> 30% w/v, Ferris and Burton (1988)] with differing concentrations of the major cations (Hodgson *et al.,* 2001).

The microbial community of Deep Lake has been characterized extensively (DeMaere *et al*., 2013; T. J. Williams *et al*., 2014; Tschitschko *et al*., 2015) and consists in essence of one green algae and four genera of heterotrophic archaea. *Hrr. lacusprofundi* represents approx. 10% of the total microbial community (DeMaere *et al*., 2013). All known strains of *Hrr. lacusprofundi* share the main chromosome, but the secondary chromosome (≥ 500 Mb) and the megaplasmid pHLAC01 (≥ 400 Mb) are highly variable between

strains (Tschitschko *et al.*, 2018), and can be lost or incorporated under laboratory conditions (Mercier *et al.*, 2022). This genomic variability and the high ploidy of haloarchaea in general, raises some challenges to the use of *Hrr. lacusprofundi* as a model organism. Although a genetic system on the basis of antibiotic resistance has been described (Liao *et al.*, 2016), many genetic tools have not yet been established.

1.5.3 Genetic manipulation of Haloarchaea

In-depth characterization of virus-host interactions in prokaryotes requires a culturable and characterized host organism and ideally molecular biology and genetic tools to manipulate the host organism. While many such tools exist for *H. volcanii*, possibilities are currently limited for many other haloarchaea, such as *Hrr. lacusprofundi*. In contrast to other haloarchaea, the main chromosome of *H. volcanii* appears to be comparatively stable, as insertion sequences are mainly found in the megaplasmids (Harrison & Allers, 2022), which is, of course, beneficial for the stability of genomic tools.

The first genetic systems in the haloarchaea were established in *H. volcanii* on the basis of amino acid auxotrophic mutants generated by induced mutagenesis (Mevarech & Werczberger, 1985). This was followed by establishment of transformation protocols (Cline *et al.*, 1989) and shuttle vectors derived from the native pHV2 plasmid (Charlebois *et al.*, 1987). Subsequently, uracil auxotrophic strains of *H. volcanii* (Bitan-Banin *et al.*, 2003) were generated by mutagenesis of the orotate phosphoribosyl-transferase gene (*pyrE2*). In *H. volcanii,* targeted gene deletion of *pyrE2* was achieved with a non-functional gene construct carried on a non-replicate shuttle vector. Recombination at the *pyrE2* gene locus was induced based on a halobacterial novobiocin resistance gene (*gyrB*) (Bitan-Banin *et al.,* 2003). Novobiocin and statins, including menviolin and pravastatin, are effective antibiotics against archaea, whereas many bacterial antibiotics that act on the peptidoglycan

layer are ineffective in archaea (Harrison & Allers, 2022). Overexpression of the cellular proteins GyrB and HmgA confers antibiotic resistance in archaea (Blaseio & Pfeifer, 1990; Holmes & Dyall-Smith, 1991; Lam & Doolittle, 1992; Wendoloski *et al.*, 2001; Harrison & Allers, 2022). Excision of the vector plasmid is forced by the addition of 5-fluoroorotic acid (5-FOA) as a counter-selectable marker, which is converted by functional pyrE2 genes into the cytotoxic 5-fluoro-UMP (Boeke *et al.*, 1984; Bitan-Banin *et al.*, 2003; Redder & Linder, 2012). Subsequent gene deletions no longer require the initial selection step with antibiotics. Further refinement of this 'pop-in pop-out' system has led to a well-established genetic system (Allers *et al.*, 2004; Dattani *et al.*, 2022) for targeted gene deletions. Inducible promotors also enable manipulation of gene expression (Allers, 2010; Rados *et al.,* 2023).

Generation of uracil auxotrophic mutants in *Hrr. lacusprofundi* has been unsuccessful so far. Instead, Liao and colleagues (2016) established a genetic system for *Hrr. lacusprofundi* based on pravastatin resistance. However, the lack of a strong counter-selection marker means that the pravastatin resistance gene *hmgA* remains inserted in the genome, thus necessitating very high pravastatin concentrations to facilitate additional gene deletions in the same strain (Liao *et al.*, 2016). This has already proven to be impractical for further genetic manipulation of *Hrr. lacusprofundi* as copies of *hmgA* can be duplicated and spread among replicons, making the strain functionally resistant. Moreover, transposase-mediated disruption of genes can render shuttle vectors non-functional (Liao *et al.*, 2016; Hamm *et al.*, 2019;). Other methods are thus needed to establish a genetic system that allows for multiple gene deletions in the same strain to allow us to study the interactions between PVs and their host in more depth under controlled conditions.

1.6 Aims of the dissertation

Plasmid vesicles (PVs) represent a novel type of vesicle containing a specific plasmid (pR1SE) which cross the divide between viruses and plasmids. The pR1SE plasmid encodes plasmid-specific proteins that are found in the PVs, and PVs have a very distinct morphology compared to the morphologically diverse EVs. Dissemination of the pR1SE plasmid occurs without direct cell-to-cell contact or exposure of the plasmid DNA to the extracellular environment and the infection of plasmid-free host cells occurs rapidly.

This behaviour goes beyond what has been described for the dissemination of plasmids in extracellular vesicles and has clear virus-like characteristics regarding the transmission in virion-like structures. The evolutionary origin of pR1SE and PVs is still unknown, however, this system shows clear parallels to one of the proposed theories on the origin of viruses from selfish genetic elements and cellular components. The origin of some modern viruses has been traced back to prokaryotic plasmids and pR1SE could represent one such plasmid caught at an evolutionary snapshot on its way to evolve into a genuine virus.

The aim of this work was to provide more insights into this novel extrachromosomal element and its interactions with the host *Halorubrum lacusprofundi*. The specific aims were as follows:

- To establish a genetic system for *Hrr. lacusprofundi*. To enable us to perform in-frame gene deletions and multiple mutations in a strain, allowing in-depth study of the effect of targeted host genes on plasmid vesicles.

- To characterize the intracellular replication and particle production of PVs during infection in comparison to viruses infecting the same host organism

- To determine the effect of post-translational modification of PV coat proteins on particle stability after disruption of the N-glycosylation machinery of the host by targeted gene deletion.

- To characterize the lipid content of PVs and extracellular vesicles to identify possible patterns of selective uptake of lipid species. Selective enrichment was previously identified for some enveloped viruses which infect archaea.

- To determine if PV formation is independent of host proteins involved with vesicle formation by targeted gene deletion of the small GTPase which drives extracellular vesicle formation in a related haloarchaeon, *Haloferax volcanii*

1.7 References

Abergel, C., Legendre, M., & Claverie, J.-M. (2015). The rapidly expanding universe of giant viruses: Mimivirus, Pandoravirus, Pithovirus and Mollivirus. *FEMS microbiology reviews, 39*(6), 779-796. doi:10.1093/femsre/fuv037

Abrahão, J. S., Araújo, R., Colson, P., & La Scola, B. (2017). The analysis of translation-related gene set boosts debates around origin and evolution of mimiviruses. *PLoS Genet, 13*(2), e1006532. doi:10.1371/journal.pgen.1006532

Abrahão, J. S., Silva, L., Silva, L. S., Khalil, J. Y. B., Rodrigues, R., Arantes, T., Assis, F., Boratto, P., Andrade, M., & Kroon, E. G. (2018). Tailed giant Tupanvirus possesses the most complete translational apparatus of the known virosphere. *Nature communications, 9*(1), 1-12. doi:10.1038/s41467-018-03168-1

Abu-Qarn, M., Giordano, A., Battaglia, F., Trauner, A., Hitchen, P. G., Morris, H. R., Dell, A., & Eichler, J. (2008). Identification of AglE, a Second Glycosyltransferase Involved in N Glycosylation of the *Haloferax volcanii* S-Layer Glycoprotein. *Journal of bacteriology, 190*(9), 3140-3146. doi:doi:10.1128/JB.00056-08

Abu-Qarn, M., Yurist-Doutsch, S., Giordano, A., Trauner, A., Morris, H. R., Hitchen, P., Medalia, O., Dell, A., & Eichler, J. (2007). *Haloferax volcanii* AglB and AglD are Involved in N-glycosylation of the S-layer Glycoprotein and Proper Assembly of the Surface Layer. *Journal of Molecular Biology, 374*(5), 1224-1236. doi:10.1016/j.jmb.2007.10.042

Aguirre Sourrouille, Z., Schwarzer, S., Lequime, S., Oksanen, H. M., & Quax, T. E. F. (2022). The Viral Susceptibility of the *Haloferax* Species. *Viruses, 14*(6), 1344. doi:10.3390/v14061344

Ahlgren, N. A., Fuchsman, C. A., Rocap, G., & Fuhrman, J. A. (2019). Discovery of several novel, widespread, and ecologically distinct marine *Thaumarchaeota* viruses that encode *amoC* nitrification genes. *The ISME journal, 13*(3), 618-631. doi:10.1038/s41396-018-0289-4

Ajon, M., Fröls, S., van Wolferen, M., Stoecker, K., Teichmann, D., Driessen, A. J. M., Grogan, D. W., Albers, S.-V., & Schleper, C. (2011). UV-inducible DNA exchange in hyperthermophilic archaea mediated by type IV pili. *Molecular Microbiology, 82*(4), 807-817. doi:10.1111/j.1365-2958.2011.07861.x

Al-Shayeb, B., Schoelmerich, M. C., West-Roberts, J., Valentin-Alvarado, L. E., Sachdeva, R., Mullen, S., Crits-Christoph, A., Wilkins, M. J., Williams, K. H., Doudna, J. A., & Banfield, J. F. (2022). Borgs are giant genetic elements with potential to expand metabolic capacity. *Nature, 610*(7933), 731-736. doi:10.1038/s41586-022-05256-1

Alarcón-Schumacher, T., Naor, A., Gophna, U., & Erdmann, S. (2022). Isolation of a virus causing a chronic infection in the archaeal model organism *Haloferax volcanii* reveals antiviral activities of a provirus. *Proceedings of the National Academy of Sciences, 119*(35), e2205037119. doi:10.1073/pnas.2205037119

Allers, T. (2010). Overexpression and purification of halophilic proteins in *Haloferax volcanii*. *Bioengineered bugs, 1*(4), 290-292. doi:10.4161/bbug.1.4.11794

Allers, T., Barak, S., Liddell, S., Wardell, K., & Mevarech, M. (2010). Improved strains and plasmid vectors for conditional overexpression of His-tagged proteins in Haloferax volcanii. *J Appl. Environ. Microbiol., 76*(6), 1759-1769. doi:10.1128/AEM.02670-09

Allers, T., Ngo, H.-P., Mevarech, M., & Lloyd, R. G. (2004). Development of Additional Selectable Markers for the Halophilic Archaeon *Haloferax volcanii* Based on the *leuB* and *trpA* Genes. *Applied and Environmental Microbiology, 70*(2), 943-953. doi:10.1128/aem.70.2.943-953.2004

Anderson, R. E., Kouris, A., Seward, C. H., Campbell, K. M., & Whitaker, R. J. (2017). Structured Populations of *Sulfolobus acidocaldarius* with Susceptibility to Mobile Genetic Elements. *Genome biology and evolution, 9*(6), 1699-1710. doi:10.1093/gbe/evx104

Arnold, H. P., She, Q., Phan, H., Stedman, K., Prangishvili, D., Holz, I., Kristjansson, J. K., Garrett, R., & Zillig, W. (1999). The genetic element pSSVx of the extremely thermophilic crenarchaeon *Sulfolobus* is a hybrid between a plasmid and a virus. *Molecular Microbiology, 34*(2), 217-226. doi:10.1046/j.1365-2958.1999.01573.x

Arnold, H. P., Ziese, U., & Zillig, W. (2000). SNDV, a Novel Virus of the Extremely Thermophilic and Acidophilic Archaeon *Sulfolobus*. *Virology, 272*(2), 409-416. doi:10.1006/viro.2000.0375

Badel, C., Da Cunha, V., & Oberto, J. (2021). Archaeal tyrosine recombinases. *FEMS microbiology reviews, 45*(4). doi:10.1093/femsre/fuab004

Badel, C., Erauso, G., Gomez, A., Catchpole, R., Gonnet, M., Oberto, J., Forterre, P., & Da Cunha, V. (2019). The global distribution and evolutionary history of the pT26-2 archaeal plasmid family. *Environmental microbiology, 21*(12), 4685-4705. doi:10.1111/1462-2920.14800

Baker, B. A., Gutiérrez-Preciado, A., Rodríguez del Río, Á., McCarthy, C. G. P., López-García, P., Huerta-Cepas, J., Susko, E., Roger, A. J., Eme, L., & Moreira, D. (2023). Several independent adaptations of archaea to hypersaline environments. *bioRxiv*. doi:10.1101/2023.07.03.547478

Baker, B. J., De Anda, V., Seitz, K. W., Dombrowski, N., Santoro, A. E., & Lloyd, K. G. (2020). Diversity, ecology and evolution of Archaea. *Nature microbiology, 5*(7), 887-900. doi:10.1038/s41564-020-0715-z

Bamford, D. H., Pietilä, M. K., Roine, E., Atanasova, N. S., Dienstbier, A., & Oksanen, H. M. (2017). ICTV virus taxonomy profile: *Pleolipoviridae*. *Journal of General Virology, 98*(12), 2916-2917. doi:10.1099/jgv.0.000972

Bamford, D. H., Ravantti, J. J., Rönnholm, G., Laurinavicius, S., Kukkaro, P., Dyall-Smith, M., Somerharju, P., Kalkkinen, N., & Bamford, J. K. (2005). Constituents of SH1, a novel lipid-containing virus infecting the halophilic euryarchaeon Haloarcula hispanica. *J Virol, 79*(14), 9097-9107. doi:10.1128/jvi.79.14.9097-9107.2005

Baquero, D. P., Gazi, A. D., Sachse, M., Liu, J., Schmitt, C., Moya-Nilges, M., Schouten, S., Prangishvili, D., & Krupovic, M. (2021a). A filamentous archaeal virus is enveloped inside the cell and released through pyramidal portals. *Proceedings of the National Academy of Sciences, 118*(32), e2105540118. doi:10.1073/pnas.2105540118

Baquero, D. P., Liu, J., & Prangishvili, D. (2021b). Egress of archaeal viruses. *Cellular Microbiology, 23*(12), e13394. doi:10.1111/cmi.13394

Barzel, A., Naor, A., Privman, E., Kupiec, M., & Gophna, U. (2011). Homing endonucleases residing within inteins: evolutionary puzzles awaiting genetic solutions. *Biochemical Society Transactions, 39*(1), 169-173. doi:10.1042/bst0390169

Baumann, P., & Jackson, S. P. (1996). An archaebacterial homologue of the essential eubacterial cell division protein FtsZ. *Proceedings of the National Academy of Sciences, 93*(13), 6726-6730. doi:10.1073/pnas.93.13.6726

Béguin, P., Baron, B., Gill, S., Charpin, N., & Forterre, P. (2014). The SF1 helicase encoded by the archaeal plasmid pTN2 of *Thermococcus nautili*. *Extremophiles, 18*(4), 779-787. doi:10.1007/s00792-014-0658-5

Béguin, P., Chekli, Y., Sezonov, G., Forterre, P., & Krupovič, M. (2019). Sequence motifs recognized by the casposon integrase of *Aciduliprofundum boonei*. *Nucleic acids research, 47*(12), 6386-6395. doi:10.1093/nar/gkz447

Belfort, M. (2017). Mobile self-splicing introns and inteins as environmental sensors. *Current opinion in microbiology, 38*, 51-58. doi:10.1016/j.mib.2017.04.003

Bertani, G. (1999). Transduction-Like Gene Transfer in the Methanogen *Methanococcus voltae*. *Journal of bacteriology, 181*(10), 2992-3002. doi:10.1128/jb.181.10.2992-3002.1999

Bertani, G., & Baresi, L. (1987). Genetic transformation in the methanogen *Methanococcus voltae* PS. *Journal of bacteriology, 169*(6), 2730-2738. doi:10.1128/jb.169.6.2730-2738.1987

Bettstetter, M., Peng, X., Garrett, R. A., & Prangishvili, D. (2003). AFV1, a novel virus infecting hyperthermophilic archaea of the genus acidianus. *Virology, 315*(1), 68-79. doi:10.1016/S0042-6822(03)00481-1

Bignon, E. A., Chou, K. R., Roine, E., & Tischler, N. D. (2022). Halorubrum pleomorphic virus-6 Membrane Fusion Is Triggered by an S-Layer Component of Its Haloarchaeal Host. *Viruses, 14*(2), 254. doi:10.3390/v14020254

Bisson-Filho, A. W., Hsu, Y.-P., Squyres, G. R., Kuru, E., Wu, F., Jukes, C., Sun, Y., Dekker, C., Holden, S., VanNieuwenhze, M. S., Brun, Y. V., & Garner, E. C. (2017). Treadmilling by FtsZ filaments drives peptidoglycan synthesis and bacterial cell division. *Science, 355*(6326), 739-743. doi:10.1126/science.aak9973

Bitan-Banin, G., Ortenberg, R., & Mevarech, M. (2003). Development of a Gene Knockout System for the Halophilic Archaeon *Haloferax volcanii* by Use of the *pyrE* Gene. *Journal of bacteriology, 185*(3), 772-778. doi:10.1128/jb.185.3.772-778.2003

Blaseio, U., & Pfeifer, F. (1990). Transformation of *Halobacterium halobium*: development of vectors and investigation of gas vesicle synthesis. *Proceedings of the National Academy of Sciences, 87*(17), 6772-6776. doi:10.1073/pnas.87.17.6772

Blombach, F., Matelska, D., Fouqueau, T., Cackett, G., & Werner, F. (2019). Key Concepts and Challenges in Archaeal Transcription. *Journal of Molecular Biology, 431*(20), 4184-4201. doi:10.1016/j.jmb.2019.06.020

Boeke, J. D., LaCroute, F., & Fink, G. R. (1984). A positive selection for mutants lacking orotidine-5'-phosphate decarboxylase activity in yeast: 5-fluoro-orotic acid resistance. *Mol Gen Genet, 197*(2), 345-346. doi:10.1007/bf00330984

Breuert, S., Allers, T., Spohn, G., & Soppa, J. (2006). Regulated polyploidy in halophilic archaea. *PLOS ONE, 1*(1), e92. doi:10.1371/journal.pone.0000092

Briddon, R., Ghabrial, S., Lin, N., Palukaitis, P., Scholthof, K., & Vetten, H. (2011). *Satellites and Other Virus-dependent Nucleic Acids*. Retrieved from London, United Kingdom: https://ictv.global/report_9th/subviral/Satellites-introduction

Brown, H. J., & Duggin, I. G. (2023). Diversity and Potential Multifunctionality of Archaeal CetZ Tubulin-like Cytoskeletal Proteins. *Biomolecules, 13*(1), 134. doi:10.3390/biom13010134

Brumfield, S. K., Ortmann, A. C., Ruigrok, V., Suci, P., Douglas, T., & Young, M. J. (2009). Particle assembly and ultrastructural features associated with replication of the lytic archaeal virus *Sulfolobus* turreted icosahedral virus. *J Virol, 83*(12), 5964-5970. doi:10.1128/jvi.02668-08

Cadillo-Quiroz, H., Didelot, X., Held, N. L., Herrera, A., Darling, A., Reno, M. L., Krause, D. J., & Whitaker, R. J. (2012). Patterns of Gene Flow Define Species of Thermophilic Archaea. *PLOS Biology, 10*(2), e1001265. doi:10.1371/journal.pbio.1001265

Caforio, A., & Driessen, A. J. M. (2017). Archaeal phospholipids: Structural properties and biosynthesis. *Biochimica et Biophysica Acta (BBA) - Molecular and Cell Biology of Lipids, 1862*(11), 1325-1339. doi:10.1016/j.bbalip.2016.12.006

Caspi, Y., & Dekker, C. (2018). Dividing the Archaeal Way: The Ancient Cdv Cell-Division Machinery. *Frontiers in microbiology, 9*. doi:10.3389/fmicb.2018.00174

Catchpole, R. J., Barbe, V., Magdelenat, G., Marguet, E., Terns, M., Oberto, J., Forterre, P., & Da Cunha, V. (2023). A self-transmissible plasmid from a hyperthermophile that facilitates genetic modification of diverse Archaea. *Nature microbiology*. doi:10.1038/s41564-023-01387-x

Charlebois, R. L., Lam, W. L., Cline, S. W., & Doolittle, W. F. (1987). Characterization of pHV2 from *Halobacterium volcanii* and its use in demonstrating transformation of an archaebacterium. *Proceedings of the National Academy of Sciences, 84*(23), 8530-8534. doi:10.1073/pnas.84.23.8530

Chen, S., Sun, S., Korfanty, G. A., Liu, J., & Xiang, H. (2019). A Halocin Promotes DNA Uptake in *Haloferax mediterranei*. *Frontiers in microbiology, 10*. doi:10.3389/fmicb.2019.01960

Chen, S., Tulloss, R. E., Liu, Y., Feng, B., Zhao, Z., & Yang, Z. L. (2012). Lateral gene transfer occurring in haloarchaea: an interpretative imitation study. *World Journal of Microbiology and Biotechnology, 28*(9), 2913-2918. doi:10.1007/s11274-012-1101-7

Chimileski, S., Dolas, K., Naor, A., Gophna, U., & Papke, R. T. (2014). Extracellular DNA metabolism in *Haloferax volcanii*. *Frontiers in microbiology, 5*. doi:10.3389/fmicb.2014.00057

Claverie, J.-M., & Abergel, C. (2016). Giant viruses: The difficult breaking of multiple epistemological barriers. *Studies in History and Philosophy of Science Part C: Studies*

in History and Philosophy of Biological and Biomedical Sciences, 59, 89-99. doi:10.1016/j.shpsc.2016.02.015

Cline, S. W., Lam, W. L., Charlebois, R. L., Schalkwyk, L. C., & Doolittle, W. F. (1989). Transformation methods for halophilic archaebacteria. *Canadian Journal of Microbiology, 35*(1), 148-152. doi:10.1139/m89-022 %M 2497937

Cohen-Rosenzweig, C., Yurist-Doutsch, S., & Eichler, J. (2012). AglS, a Novel Component of the *Haloferax volcanii* N-Glycosylation Pathway, Is a Dolichol Phosphate-Mannose Mannosyltransferase. *Journal of bacteriology, 194*(24), 6909-6916. doi:10.1128/JB.01716-12

Comolli, L. R., & Banfield, J. F. (2014). Inter-species interconnections in acid mine drainage microbial communities. *Frontiers in microbiology, 5*. doi:10.3389/fmicb.2014.00367

Conrad, B., Iseli, C., & Pirovino, M. (2023). Energy-harnessing problem solving of primordial life: Modeling the emergence of catalytic host-nested parasite life cycles. *PLOS ONE, 18*(3), e0281661. doi:10.1371/journal.pone.0281661

Contreras, G., Thomsen, J., Pfitzer, M., Hafenbradl, D., Kostner, D., Holtmann, D., Schmitz, R. A., Rother, M., & Molitor, B. (2022). New perspectives for biotechnological applications of methanogens. *Current Research in Biotechnology, 4*, 468-474. doi:10.1016/j.crbiot.2022.10.001

Contursi, P., Fusco, S., Cannio, R., & She, Q. (2014). Molecular biology of fuselloviruses and their satellites. *Extremophiles, 18*(3), 473-489. doi:10.1007/s00792-014-0634-0

Cooper, C. R., Lewis, A. M., Notey, J. S., Mukherjee, A., Willard, D. J., Blum, P. H., & Kelly, R. M. (2023). Interplay between transcriptional regulators and VapBC toxin–antitoxin loci during thermal stress response in extremely thermoacidophilic archaea. *Environmental microbiology, 25*(6), 1200-1215. doi:10.1111/1462-2920.16350

Crowther, T. W., van den Hoogen, J., Wan, J., Mayes, M. A., Keiser, A. D., Mo, L., Averill, C., & Maynard, D. S. (2019). The global soil community and its influence on biogeochemistry. *Science, 365*(6455), eaav0550. doi:10.1126/science.aav0550

Danovaro, R., Dell'Anno, A., Corinaldesi, C., Rastelli, E., Cavicchioli, R., Krupovič, M., Noble, R. T., Nunoura, T., & Prangishvili, D. (2016). Virus-mediated archaeal hecatomb in the deep seafloor. *Science advances, 2*(10), e1600492. doi:10.1126/sciadv.1600492

DasSarma, P., & DasSarma, S. (2008). On the origin of prokaryotic "species": the taxonomy of halophilic Archaea. *Saline Systems, 4*, 5. doi:10.1186/1746-1448-4-5

DasSarma, P., Laye, V. J., Harvey, J., Reid, C., Shultz, J., Yarborough, A., Lamb, A., Koske-Phillips, A., Herbst, A., Molina, F., Grah, O., Phillips, T., & DasSarma, S. (2017). Survival of halophilic Archaea in Earth's cold stratosphere. *International Journal of Astrobiology, 16*(4), 321-327. doi:10.1017/S1473550416000410

DasSarma, S., Capes, M., & DasSarma, P. (2009). Haloarchaeal Megaplasmids. In E. Schwartz (Ed.), *Microbial Megaplasmids* (pp. 3-30). Berlin, Heidelberg: Springer Berlin Heidelberg.

DasSarma, S., Capes, M. D., Karan, R., & DasSarma, P. (2013). Amino Acid Substitutions in Cold-Adapted Proteins from *Halorubrum lacusprofundi,* an Extremely Halophilic Microbe from Antarctica. *PLOS ONE, 8*(3), e58587. doi:10.1371/journal.pone.0058587

DasSarma, S., & DasSarma, P. (2017). Halophiles. In *Encyclopedia of Life Sciences* (pp. 1-13): John Wiley & Sons, Ltd.

Dattani, A., Harrison, C., & Allers, T. (2022). Genetic Manipulation of *Haloferax* Species. In S. Ferreira-Cerca (Ed.), *Archaea: Methods and Protocols* (pp. 33-56). New York, NY: Springer US.

Davis, C. R., Johnson, C. H., & Robertson, J. B. (2020). A bioluminescent reporter for the halophilic archaeon *Haloferax volcanii*. *Extremophiles, 24*(5), 773-785. doi:10.1007/s00792-020-01193-x

Deatherage, B. L., & Cookson, B. T. (2012). Membrane vesicle release in bacteria, eukaryotes, and archaea: a conserved yet underappreciated aspect of microbial life. *Infection and immunity, 80*(6), 1948-1957. doi:10.1128/iai.06014-11

DeMaere, M. Z., Williams, T. J., Allen, M. A., Brown, M. V., Gibson, J. A., Rich, J., Lauro, F. M., Dyall-Smith, M., Davenport, K. W., & Woyke, T. (2013). High level of intergenera gene exchange shapes the evolution of haloarchaea in an isolated Antarctic lake. *Proceedings of the National Academy of Sciences, 110*(42), 16939-16944. doi:10.1073/pnas.1307090110

Deschamps, P., Zivanovic, Y., Moreira, D., Rodriguez-Valera, F., & López-García, P. (2014). Pangenome evidence for extensive interdomain horizontal transfer affecting lineage core and shell genes in uncultured planktonic thaumarchaeota and euryarchaeota. *Genome biology and evolution, 6*(7), 1549-1563. doi:10.1093/gbe/evu127

Desnues, C., La Scola, B., Yutin, N., Fournous, G., Robert, C., Azza, S., Jardot, P., Monteil, S., Campocasso, A., Koonin, E. V., & Raoult, D. (2012). Provirophages and transpovirons as the diverse mobilome of giant viruses. *Proceedings of the National Academy of Sciences, 109*(44), 18078-18083. doi:10.1073/pnas.1208835109

Diener, T. O. (1971). Potato spindle tuber "virus": IV. A replicating, low molecular weight RNA. *Virology, 45*(2), 411-428. doi:10.1016/0042-6822(71)90342-4

Diener, T. O., & Raymer, W. B. (1967). Potato Spindle Tuber Virus: A Plant Virus with Properties of a Free Nucleic Acid. *Science, 158*(3799), 378-381. doi:10.1126/science.158.3799.378

DiMaio, F., Yu, X., Rensen, E., Krupovič, M., Prangishvili, D., & Egelman, E. H. (2015). A virus that infects a hyperthermophile encapsidates A-form DNA. *Science, 348*(6237), 914-917. doi:10.1126/science.aaa4181

Dimitriu, T., Szczelkun, M. D., & Westra, E. R. (2020). Evolutionary Ecology and Interplay of Prokaryotic Innate and Adaptive Immune Systems. *Current Biology, 30*(19), R1189-R1202. doi:10.1016/j.cub.2020.08.028

Dueber, E. C., Costa, A., Corn, J. E., Bell, S. D., & Berger, J. M. (2011). Molecular determinants of origin discrimination by Orc1 initiators in archaea. *Nucleic Acids Res, 39*(9), 3621-3631. doi:10.1093/nar/gkq1308

Duffy, S., Shackelton, L. A., & Holmes, E. C. (2008). Rates of evolutionary change in viruses: patterns and determinants. *Nature Reviews Genetics, 9*(4), 267-276. doi:10.1038/nrg2323

Duggin, I. G., Aylett, C. H., Walsh, J. C., Michie, K. A., Wang, Q., Turnbull, L., Dawson, E. M., Harry, E. J., Whitchurch, C. B., & Amos, L. A. (2015). CetZ tubulin-like proteins control archaeal cell shape. *Nature, 519*(7543), 362. doi:10.1038/nature13983

Eichler, J. (2020). N-glycosylation in Archaea—New roles for an ancient posttranslational modification. *Molecular Microbiology, 114*(5), 735-741. doi:10.1111/mmi.14569

El Omari, K., Li, S., Kotecha, A., Walter, T. S., Bignon, E. A., Harlos, K., Somerharju, P., De Haas, F., Clare, D. K., Molin, M., Hurtado, F., Li, M., Grimes, J. M., Bamford, D. H., Tischler, N. D., Huiskonen, J. T., Stuart, D. I., & Roine, E. (2019). The structure of a prokaryotic viral envelope protein expands the landscape of membrane fusion proteins. *Nature communications, 10*(1), 846. doi:10.1038/s41467-019-08728-7

Ellen, A. F., Albers, S.-V., Huibers, W., Pitcher, A., Hobel, C. F., Schwarz, H., Folea, M., Schouten, S., Boekema, E. J., & Poolman, B. (2009). Proteomic analysis of secreted membrane vesicles of archaeal *Sulfolobus* species reveals the presence of endosome sorting complex components. *Extremophiles, 13*(1), 67. doi:10.1007/s00792-008-0199-x

Eme, L., Tamarit, D., Caceres, E. F., Stairs, C. W., De Anda, V., Schön, M. E., Seitz, K. W., Dombrowski, N., Lewis, W. H., Homa, F., Saw, J. H., Lombard, J., Nunoura, T., Li, W.-J., Hua, Z.-S., Chen, L.-X., Banfield, J. F., John, E. S., Reysenbach, A.-L., Stott, M. B., Schramm, A., Kjeldsen, K. U., Teske, A. P., Baker, B. J., & Ettema, T. J. G. (2023). Inference and reconstruction of the heimdallarchaeial ancestry of eukaryotes. *Nature*. doi:10.1038/s41586-023-06186-2

Erauso, G., Marsin, S., Benbouzid-Rollet, N., Baucher, M. F., Barbeyron, T., Zivanovic, Y., Prieur, D., & Forterre, P. (1996). Sequence of plasmid pGT5 from the archaeon *Pyrococcus abyssi:* evidence for rolling-circle replication in a hyperthermophile. *J Bacteriol, 178*(11), 3232-3237. doi:10.1128/jb.178.11.3232-3237.1996

Erdmann, S., Tschitschko, B., Zhong, L., Raftery, M. J., & Cavicchioli, R. (2017). A plasmid from an Antarctic haloarchaeon uses specialized membrane vesicles to disseminate and infect plasmid-free cells. *Nature microbiology, 2*(10), 1446. doi:10.1038/s41564-017-0009-2

Faini, M., Beck, R., Wieland, F. T., & Briggs, J. A. (2013). Vesicle coats: structure, function, and general principles of assembly. *Trends in cell biology, 23*(6), 279-288. doi:10.1016/j.tcb.2013.01.005

Ferris, J. M., & Burton, H. R. (1988). The annual cycle of heat content and mechanical stability of hypersaline Deep Lake, Vestfold Hills, Antarctica. *Hydrobiologia, 165*(1), 115-128. doi:10.1007/BF00025579

Filée, J., Siguier, P., & Chandler, M. (2007). Insertion sequence diversity in archaea. *Microbiol Mol Biol Rev, 71*(1), 121-157. doi:10.1128/mmbr.00031-06

Fonseca, D. R., Halim, M. F. A., Holten, M. P., & Costa, K. C. (2020). Type IV-Like Pili Facilitate Transformation in Naturally Competent Archaea. *Journal of bacteriology, 202*(21), 10.1128/jb.00355-00320. doi:10.1128/jb.00355-20

Forster, A. C., & Symons, R. H. (1987). Self-cleavage of plus and minus RNAs of a virusoid and a structural model for the active sites. *Cell, 49*(2), 211-220. doi:10.1016/0092-8674(87)90562-9

Forterre, P. (2006). The origin of viruses and their possible roles in major evolutionary transitions. *Virus research, 117*(1), 5-16. doi:10.1016/j.virusres.2006.01.010

Forterre, P., Da Cunha, V., & Catchpole, R. (2017). Plasmid vesicles mimicking virions. *Nature microbiology, 2*(10), 1340. doi:10.1038/s41564-017-0032-

Forterre, P., & Krupovič, M. (2012). The Origin of Virions and Virocells: The Escape Hypothesis Revisited. In G. Witzany (Ed.), *Viruses: Essential Agents of Life* (pp. 43-60). Dordrecht: Springer Netherlands.

Franzmann, P., Stackebrandt, E., Sanderson, K., Volkman, J., Cameron, D., Stevenson, P., McMeekin, T., & Burton, H. (1988). *Halobacterium lacusprofundi* sp. nov., a halophilic bacterium isolated from Deep Lake, Antarctica. *Systematic and Applied Microbiology, 11*(1), 20-27. doi:10.1016/S0723-2020(88)80044-4

Fröls, S., Gordon, P. M. K., Panlilio, M. A., Duggin, I. G., Bell, S. D., Sensen, C. W., & Schleper, C. (2007). Response of the Hyperthermophilic Archaeon *Sulfolobus solfataricus* to UV Damage. *Journal of bacteriology, 189*(23), 8708-8718. doi:10.1128/jb.01016-07

Gao, L., Altae-Tran, H., Böhning, F., Makarova, K. S., Segel, M., Schmid-Burgk, J. L., Koob, J., Wolf, Y. I., Koonin, E. V., & Zhang, F. (2020). Diverse enzymatic activities mediate antiviral immunity in prokaryotes. *Science, 369*(6507), 1077-1084. doi:10.1126/science.aba0372

Garrett, R. A., Redder, P., Greve, B., Brügger, K., Chen, L., & She, Q. (2004). Archaeal Plasmids. In B. E. P. Funnell, Gregory J. (Ed.), *Plasmid Biology* (pp. 377-392).

Gaudin, M., Gauliard, E., Schouten, S., Houel-Renault, L., Lenormand, P., Marguet, E., & Forterre, P. (2013). Hyperthermophilic archaea produce membrane vesicles that can transfer DNA. *Environmental Microbiology Reports, 5*(1), 109-116. doi:10.1111/j.1758-2229.2012.00348.x

Gaudin, M., Krupovič, M., Marguet, E., Gauliard, E., Cvirkaite-Krupovič, V., Le Cam, E., Oberto, J., & Forterre, P. (2014). Extracellular membrane vesicles harbouring viral genomes. *Environmental microbiology, 16*(4), 1167-1175. doi:10.1111/1462-2920.12235

Gibson, J. A. E. (1999). The meromictic lakes and stratified marine basins of the Vestfold Hills, East Antarctica. *Antarctic Science, 11*(2), 175-192. doi:10.1017/S0954102099000243

Gill, S., Catchpole, R., & Forterre, P. (2019). Extracellular membrane vesicles in the three domains of life and beyond. *FEMS microbiology reviews, 43*(3), 273-303. doi:10.1093/femsre/fuy042

Gill, S., Krupovič , M., Desnoues, N., Béguin, P., Sezonov, G., & Forterre, P. (2014). A highly divergent archaeo-eukaryotic primase from the *Thermococcus nautilus* plasmid, pTN2. *Nucleic acids research, 42*(6), 3707-3719. doi:10.1093/nar/gkt1385

Gonnet, M., Erauso, G., Prieur, D., & Le Romancer, M. (2011). pAMT11, a novel plasmid isolated from a Thermococcus sp. strain closely related to the virus-like integrated element TKV1 of the *Thermococcus kodakaraensis* genome. *Research in Microbiology, 162*(2), 132-143. doi:10.1016/j.resmic.2010.11.003

Gophna, U., & Altman-Price, N. (2022). Horizontal Gene Transfer in Archaea—From Mechanisms to Genome Evolution. *Annual Review of Microbiology, 76*(1), 481-502. doi:10.1146/annurev-micro-040820-124627

Grogan, D. (1996). Exchange of genetic markers at extremely high temperatures in the archaeon *Sulfolobus acidocaldarius*. *Journal of bacteriology, 178*(11), 3207-3211. doi:10.1128/jb.178.11.3207-3211.1996

Guan, Z., Naparstek, S., Kaminski, L., Konrad, Z., & Eichler, J. (2010). Distinct glycan-charged phosphodolichol carriers are required for the assembly of the pentasaccharide N-linked to the *Haloferax volcanii* S-layer glycoprotein. *Molecular Microbiology, 78*(5), 1294-1303. doi:10.1111/j.1365-2958.2010.07405.x

Guglielmini, J., de la Cruz, F., & Rocha, E. P. C. (2012). Evolution of Conjugation and Type IV Secretion Systems. *Molecular biology and evolution, 30*(2), 315-331. doi:10.1093/molbev/mss221

Gunasinghe, S. D., Shiota, T., Stubenrauch, C. J., Schulze, K. E., Webb, C. T., Fulcher, A. J., Dunstan, R. A., Hay, I. D., Naderer, T., Whelan, D. R., Bell, T. D. M., Elgass, K. D., Strugnell, R. A., & Lithgow, T. (2018). The WD40 Protein BamB Mediates Coupling of BAM Complexes into Assembly Precincts in the Bacterial Outer Membrane. *Cell Reports, 23*(9), 2782-2794. doi:10.1016/j.celrep.2018.04.093

Hadjeras, L., Bartel, J., Maier, L.-K., Maaß, S., Vogel, V., Svensson, S. L., Eggenhofer, F., Gelhausen, R., Müller, T., Alkhnbashi, O. S., Backofen, R., Becher, D., Sharma, C. M., & Marchfelder, A. (2023). Revealing the small proteome of *Haloferax volcanii* by combining ribosome profiling and small-protein optimized mass spectrometry. *microLife, 4*, uqad001. doi:10.1093/femsml/uqad001

Hall, M. J., & Hackett, N. R. (1989). DNA sequence of a small plasmid from *Halobacterium strain* GN101. *Nucleic Acids Res, 17*(24), 10501. doi:10.1093/nar/17.24.10501

Hamm, J. N., Erdmann, S., Eloe-Fadrosh, E. A., Angeloni, A., Zhong, L., Brownlee, C., Williams, T. J., Barton, K., Carswell, S., Smith, M. A., Brazendale, S., Hancock, A. M., Allen, M. A., Raftery, M. J., & Cavicchioli, R. (2019). Unexpected host dependency of Antarctic Nanohaloarchaeota. *Proceedings of the National Academy of Sciences*, 201905179. doi:10.1073/pnas.1905179116

Hamm, J. N., Liao, Y., von Kügelgen, A., Dombrowski, N., Landers, E., Brownlee, C., Johansson, E. M. V., Whan, R. M., Baker, M. A. B., Baum, B., Bharat, T. A. M., Duggin, I. G., Spang, A., & Cavicchioli, R. (2023). The intracellular lifestyle of an archaeal symbiont. *bioRxiv*, 2023.2002.2024.529834. doi:10.1101/2023.02.24.529834

Häring, M., Peng, X., Brügger, K., Rachel, R., Stetter, K. O., Garrett, R. A., & Prangishvili, D. (2004). Morphology and genome organization of the virus PSV of the hyperthermophilic archaeal genera *Pyrobaculum* and *Thermoproteus*: a novel virus family, the *Globuloviridae*. *Virology, 323*(2), 233-242. doi:10.1016/j.virol.2004.03.002

Häring, M., Rachel, R., Peng, X., Garrett, R. A., & Prangishvili, D. (2005). Viral diversity in hot springs of Pozzuoli, Italy, and characterization of a unique archaeal virus, Acidianus bottle-shaped virus, from a new family, the Ampullaviridae. *J Virol, 79*(15), 9904-9911. doi:10.1128/jvi.79.15.9904-9911.2005

Harrison, C., & Allers, T. (2022). Progress and Challenges in Archaeal Genetic Manipulation. In S. Ferreira-Cerca (Ed.), *Archaea: Methods and Protocols* (pp. 25-31). New York, NY: Springer US.

Harrison, J. P., Gheeraert, N., Tsigelnitskiy, D., & Cockell, C. S. (2013). The limits for life under multiple extremes. *Trends in Microbiology, 21*(4), 204-212. doi:10.1016/j.tim.2013.01.006

Hawkins, M., Malla, S., Blythe, M. J., Nieduszynski, C. A., & Allers, T. (2013). Accelerated growth in the absence of DNA replication origins. *Nature, 503*(7477), 544-547. doi:10.1038/nature12650

Hirata, A., Klein, B. J., & Murakami, K. S. (2008). The X-ray crystal structure of RNA polymerase from Archaea. *Nature, 451*(7180), 851-854. doi:10.1038/nature06530

Hodgson, D., Vyverman, W., & Sabbe, K. (2001). Limnology and biology of saline lakes in the Rauer Islands, eastern Antarctica. *Antarctic Science, 13*(3), 255-270. doi:10.1017/S0954102001000372

Holmes, E. C. (2011). What does virus evolution tell us about virus origins? *Journal of virology, 85*(11), 5247-5251. doi:10.1128/jvi.02203-10

Holmes, M. L., & Dyall-Smith, M. L. (1990). A plasmid vector with a selectable marker for halophilic archaebacteria. *Journal of bacteriology, 172*(2), 756-761. doi:10.1128/jb.172.2.756-761.1990

Holmes, M. L., & Dyall-Smith, M. L. (1991). Mutations in DNA gyrase result in novobiocin resistance in halophilic archaebacteria. *Journal of bacteriology, 173*(2), 642-648. doi:10.1128/jb.173.2.642-648.1991

Hoshino, T., Doi, H., Uramoto, G.-I., Wörmer, L., Adhikari, R. R., Xiao, N., Morono, Y., D'Hondt, S., Hinrichs, K.-U., & Inagaki, F. (2020). Global diversity of microbial communities in marine sediment. *Proceedings of the National Academy of Sciences, 117*(44), 27587-27597. doi:10.1073/pnas.1919139117

Huet, J., Schnabel, R., Sentenac, A., & Zillig, W. (1983). Archaebacteria and eukaryotes possess DNA-dependent RNA polymerases of a common type. *The EMBO Journal, 2*(8), 1291-1294. doi:10.1002/j.1460-2075.1983.tb01583.x

Hurtig, F., Burgers, T. C. Q., Cezanne, A., Jiang, X., Mol, F. N., Traparić, J., Pulschen, A. A., Nierhaus, T., Tarrason-Risa, G., Harker-Kirschneck, L., Löwe, J., Šarić, A., Vlijm, R., & Baum, B. (2023). The patterned assembly and stepwise Vps4-mediated disassembly of composite ESCRT-III polymers drives archaeal cell division. *Science advances, 9*(11), eade5224. doi:10.1126/sciadv.ade5224

ICTV. (2021). *The International Code of Virus Classification and Nomenclature (ICVCN)*. Retrieved from https://ictv.global/about/code (°accessed on°07.07.2023).

Ilyina, T. V., & Koonin, E. V. (1992). Conserved sequence motifs in the initiator proteins for rolling circle DNA replication encoded by diverse replicons from eubacteria, eucaryotes and archaebacteria. *Nucleic acids research, 20*(13), 3279-3285. doi:10.1093/nar/20.13.3279

Imachi, H., Nobu, M. K., Nakahara, N., Morono, Y., Ogawara, M., Takaki, Y., Takano, Y., Uematsu, K., Ikuta, T., Ito, M., Matsui, Y., Miyazaki, M., Murata, K., Saito, Y., Sakai, S., Song, C., Tasumi, E., Yamanaka, Y., Yamaguchi, T., Kamagata, Y., Tamaki, H., & Takai, K. (2020). Isolation of an archaeon at the prokaryote–eukaryote interface. *Nature, 577*(7791), 519-525. doi:10.1038/s41586-019-1916-6

Iranzo, J., Puigbò, P., Lobkovsky, A. E., Wolf, Y. I., & Koonin, E. V. (2016). Inevitability of Genetic Parasites. *Genome biology and evolution, 8*(9), 2856-2869. doi:10.1093/gbe/evw193

Jain, S., Caforio, A., & Driessen, A. J. M. (2014). Biosynthesis of archaeal membrane ether lipids. *Frontiers in microbiology, 5*. doi:10.3389/fmicb.2014.00641

Jeudy, S., Bertaux, L., Alempic, J. M., Lartigue, A., Legendre, M., Belmudes, L., Santini, S., Philippe, N., Beucher, L., Biondi, E. G., Juul, S., Turner, D. J., Couté, Y., Claverie, J. M., & Abergel, C. (2020). Exploration of the propagation of transpovirons within Mimiviridae reveals a unique example of commensalism in the viral world. *Isme j, 14*(3), 727-739. doi:10.1038/s41396-019-0565-y

Jurėnas, D., Fraikin, N., Goormaghtigh, F., & Van Melderen, L. (2022). Biology and evolution of bacterial toxin–antitoxin systems. *Nature Reviews Microbiology, 20*(6), 335-350. doi:10.1038/s41579-021-00661-1

Jüttner, M., Weiß, M., Ostheimer, N., Reglin, C., Kern, M., Knüppel, R., & Ferreira-Cerca, S. (2019). A versatile cis-acting element reporter system to study the function,

maturation and stability of ribosomal RNA mutants in archaea. *Nucleic acids research, 48*(4), 2073-2090. doi:10.1093/nar/gkz1156
Kaminski, L., & Eichler, J. (2010). Identification of Residues Important for the Activity of *Haloferax volcanii* AglD, a Component of the Archaeal N-Glycosylation Pathway. *Archaea, 2010*, 315108. doi:10.1155/2010/315108
Kaminski, L., Guan, Z., Abu-Qarn, M., Konrad, Z., & Eichler, J. (2012). AglR is required for addition of the final mannose residue of the N-linked glycan decorating the *Haloferax volcanii* S-layer glycoprotein. *Biochimica et Biophysica Acta (BBA) - General Subjects, 1820*(10), 1664-1670. doi:10.1016/j.bbagen.2012.06.014
Kaminski, L., Lurie-Weinberger, M. N., Allers, T., Gophna, U., & Eichler, J. (2013). Phylogenetic- and genome-derived insight into the evolution of N-glycosylation in Archaea. *Molecular Phylogenetics and Evolution, 68*(2), 327-339. doi:10.1016/j.ympev.2013.03.024
Kandiba, L., Aitio, O., Helin, J., Guan, Z., Permi, P., Bamford, D. H., Eichler, J., & Roine, E. (2012). Diversity in prokaryotic glycosylation: an archaeal-derived N-linked glycan contains legionaminic acid. *Molecular Microbiology, 84*(3), 578-593. doi:10.1111/j.1365-2958.2012.08045.x
Kandiba, L., Lin, C. W., Aebi, M., Eichler, J., & Guerardel, Y. (2016). Structural characterization of the N-linked pentasaccharide decorating glycoproteins of the halophilic archaeon *Haloferax volcanii*. *Glycobiology, 26*(7), 745-756. doi:10.1093/glycob/cww014
Kasson, P., DiMaio, F., Yu, X., Lucas-Staat, S., Krupovič, M., Schouten, S., Prangishvili, D., & Egelman, E. H. (2017). Model for a novel membrane envelope in a filamentous hyperthermophilic virus. *eLife, 6*, e26268. doi:10.7554/eLife.26268
Kazlauskas, D., Dayaram, A., Kraberger, S., Goldstien, S., Varsani, A., & Krupovič, M. (2017). Evolutionary history of ssDNA bacilladnaviruses features horizontal acquisition of the capsid gene from ssRNA nodaviruses. *Virology, 504*, 114-121. doi:10.1016/j.virol.2017.02.001
Kazlauskas, D., Krupovič, M., Guglielmini, J., Forterre, P., & Venclovas, Č. (2020). Diversity and evolution of B-family DNA polymerases. *Nucleic acids research, 48*(18), 10142-10156. doi:10.1093/nar/gkaa760
Kazlauskas, D., Krupovic, M., & Venclovas, Č. (2016). The logic of DNA replication in double-stranded DNA viruses: insights from global analysis of viral genomes. *Nucleic acids research, 44*(10), 4551-4564. doi:10.1093/nar/gkw322
Kazlauskas, D., Sezonov, G., Charpin, N., Venclovas, Č., Forterre, P., & Krupovič, M. (2018). Novel Families of Archaeo-Eukaryotic Primases Associated with Mobile Genetic Elements of Bacteria and Archaea. *Journal of Molecular Biology, 430*(5), 737-750. doi:10.1016/j.jmb.2017.11.014
Kellermann, M. Y., Yoshinaga, M. Y., Valentine, R. C., Wörmer, L., & Valentine, D. L. (2016). Important roles for membrane lipids in haloarchaeal bioenergetics. *Biochimica et Biophysica Acta (BBA)-Biomembranes, 1858*(11), 2940-2956. doi:10.1016/j.bbamem.2016.08.010
Kim, J.-G., Kim, S.-J., Cvirkaite-Krupovič, V., Yu, W.-J., Gwak, J.-H., López-Pérez, M., Rodriguez-Valera, F., Krupovič, M., Cho, J.-C., & Rhee, S.-K. (2019). Spindle-shaped viruses infect marine ammonia-oxidizing thaumarchaea. *Proceedings of the National Academy of Sciences*, 201905682. doi:10.1073/pnas.1905682116
Koeppen, K., Hampton, T. H., Jarek, M., Scharfe, M., Gerber, S. A., Mielcarz, D. W., Demers, E. G., Dolben, E. L., Hammond, J. H., Hogan, D. A., & Stanton, B. A. (2016). A Novel Mechanism of Host-Pathogen Interaction through sRNA in Bacterial Outer Membrane Vesicles. *PLoS pathogens, 12*(6), e1005672. doi:10.1371/journal.ppat.1005672
Kogay, R., Koppenhöfer, S., Beatty, J. T., Kuhn, J., Lang, A. S., & Zhaxybayeva, O. (2022a). Formal recognition and classification of gene transfer agents as viriforms. *Virus Evolution, 8*(2), veac100. doi:10.1093/ve/veac100
Kogay, R., Koppenhöfer, S., Beatty, J. T., Kuhn, J. H., Lang, A. S., & Zhaxybayeva, O. (2022b). Formal recognition and classification of gene transfer agents as viriforms. *Virus Evolution, 8*(2). doi:10.1093/ve/veac100

Koonin, E. V., & Dolja, V. V. (2013). A virocentric perspective on the evolution of life. *Current opinion in virology, 3*(5), 546-557. doi:10.1016/j.coviro.2013.06.008
Koonin, E. V., Dolja, V. V., Krupovič, M., & Kuhn, J. H. (2021). Viruses Defined by the Position of the Virosphere within the Replicator Space. *Microbiology and Molecular Biology Reviews, 85*(4), e00193-00120. doi:10.1128/MMBR.00193-20
Koonin, E. V., Krupovič, M., & Dolja, V. V. (2023). The global virome: How much diversity and how many independent origins? *Environmental microbiology, 25*(1), 40-44. doi:10.1111/1462-2920.16207
Koonin, E. V., Krupovič, M., & Yutin, N. (2015). Evolution of double-stranded DNA viruses of eukaryotes: from bacteriophages to transposons to giant viruses. *Annals of the New York Academy of Sciences, 1341*(1), 10-24. doi:10.1111/nyas.12728
Koonin, E. V., Makarova, K. S., & Wolf, Y. I. (2017a). Evolutionary Genomics of Defense Systems in Archaea and Bacteria. *Annual Review of Microbiology, 71*(1), 233-261. doi:10.1146/annurev-micro-090816-093830
Koonin, E. V., Senkevich, T. G., & Dolja, V. V. (2006). The ancient Virus World and evolution of cells. *Biology direct, 1*(1), 29. doi:10.1186/1745-6150-1-29
Koonin, E. V., Wolf, Y. I., & Katsnelson, M. I. (2017b). Inevitability of the emergence and persistence of genetic parasites caused by evolutionary instability of parasite-free states. *Biol Direct, 12*(1), 31. doi:10.1186/s13062-017-0202-5
Krupovič, M. (2013). Networks of evolutionary interactions underlying the polyphyletic origin of ssDNA viruses. *Curr Opin Virol, 3*(5), 578-586. doi:10.1016/j.coviro.2013.06.010
Krupovič, M., Béguin, P., & Koonin, E. V. (2017). Casposons: mobile genetic elements that gave rise to the CRISPR-Cas adaptation machinery. *Current opinion in microbiology, 38*, 36-43. doi:10.1016/j.mib.2017.04.004
Krupovič, M., Cvirkaite-Krupovič, V., Iranzo, J., Prangishvili, D., & Koonin, E. V. (2018). Viruses of archaea: Structural, functional, environmental and evolutionary genomics. *Virus research, 244*, 181-193. doi:10.1016/j.virusres.2017.11.025
Krupovič, M., Dolja, V. V., & Koonin, E. V. (2019a). Origin of viruses: primordial replicators recruiting capsids from hosts. *Nature Reviews Microbiology, 17*(7), 449-458. doi:10.1038/s41579-019-0205-6
Krupovič, M., Dolja, V. V., & Koonin, E. V. (2023). The virome of the last eukaryotic common ancestor and eukaryogenesis. *Nature microbiology, 8*(6), 1008-1017. doi:10.1038/s41564-023-01378-y
Krupovič, M., Forterre, P., & Bamford, D. H. (2010). Comparative Analysis of the Mosaic Genomes of Tailed Archaeal Viruses and Proviruses Suggests Common Themes for Virion Architecture and Assembly with Tailed Viruses of Bacteria. *Journal of Molecular Biology, 397*(1), 144-160. doi:10.1016/j.jmb.2010.01.037
Krupovič, M., Gonnet, M., Hania, W. B., Forterre, P., & Erauso, G. (2013). Insights into Dynamics of Mobile Genetic Elements in Hyperthermophilic Environments from Five New *Thermococcus* Plasmids. *PLOS ONE, 8*(1), e49044. doi:10.1371/journal.pone.0049044
Krupovič, M., & Koonin, E. V. (2017a). Homologous Capsid Proteins Testify to the Common Ancestry of Retroviruses, Caulimoviruses, Pseudoviruses, and Metaviruses. *Journal of virology, 91*(12). doi:10.1128/jvi.00210-17
Krupovič, M., & Koonin, E. V. (2017b). Multiple origins of viral capsid proteins from cellular ancestors. *Proceedings of the National Academy of Sciences, 114*(12), E2401-E2410. doi:10.1073/pnas.1621061114
Krupovič, M., Makarova, K. S., Forterre, P., Prangishvili, D., & Koonin, E. V. (2014a). Casposons: a new superfamily of self-synthesizing DNA transposons at the origin of prokaryotic CRISPR-Cas immunity. *BMC Biology, 12*(1), 36. doi:10.1186/1741-7007-12-36
Krupovič, M., Makarova, K. S., & Koonin, E. V. (2022). Cellular homologs of the double jelly-roll major capsid proteins clarify the origins of an ancient virus kingdom. *Proceedings of the National Academy of Sciences, 119*(5), e2120620119. doi:10.1073/pnas.2120620119

Krupovič, M., Makarova, K. S., Wolf, Y. I., Medvedeva, S., Prangishvili, D., Forterre, P., & Koonin, E. V. (2019b). Integrated mobile genetic elements in Thaumarchaeota. *Environmental microbiology, 21*(6), 2056-2078. doi:10.1111/1462-2920.14564

Krupovič, M., Quemin, E. R., Bamford, D. H., Forterre, P., & Prangishvili, D. (2014b). Unification of the globally distributed spindle-shaped viruses of the Archaea. *J Virol, 88*(4), 2354-2358. doi:10.1128/jvi.02941-13

Krupovič, M., Yutin, N., & Koonin, E. V. (2020). Evolution of a major virion protein of the giant pandoraviruses from an inactivated bacterial glycoside hydrolase. *Virus Evolution, 6*(2), veaa059. doi:10.1093/ve/veaa059

Kuhn, J., Dolja, V., Krupovič, M., Adriaenssens, E., Di Serio, F., Dutilh, B., Flores, R., Harrach, B., Mushegian, A., Owens, B., Randles, J., Rubino, L., Sabanadzovic, S., Simmonds, P., Varsani, A., Zerbini, F., & Koonin, E. V. (2021). *Expand, amend, and emend the International Code of Virus Classification and Nomenclature (ICVCN; "the Code") and the Statutes to clearly define the remit of the ICTV*.

Kuhn, J., & Koonin, E. V. (2023). Viriforms — A New Category of Classifiable Virus-Derived Genetic Elements. *Biomolecules, 13*(2). doi:10.3390/biom13020289

Kuwabara, T., Minaba, M., Iwayama, Y., Inouye, I., Nakashima, M., Marumo, K., Maruyama, A., Sugai, A., Itoh, T., Ishibashi, J.-i., Urabe, T., & Kamekura, M. (2005). *Thermococcus coalescens* sp. nov., a cell-fusing hyperthermophilic archaeon from Suiyo Seamount. *International Journal of Systematic and Evolutionary Microbiology, 55*(6), 2507-2514. doi:10.1099/ijs.0.63432-0

Kuwabara, T., Minaba, M., Ogi, N., & Kamekura, M. (2007). *Thermococcus celericrescens* sp. nov., a fast-growing and cell-fusing hyperthermophilic archaeon from a deep-sea hydrothermal vent. *International Journal of Systematic and Evolutionary Microbiology, 57*(3), 437-443. doi:10.1099/ijs.0.64597-0

La Scola, B., Audic, S., Robert, C., Jungang, L., de Lamballerie, X., Drancourt, M., Birtles, R., Claverie, J.-M., & Raoult, D. (2003). A Giant Virus in Amoebae. *Science, 299*(5615), 2033-2033. doi:10.1126/science.1081867

La Scola, B., Desnues, C., Pagnier, I., Robert, C., Barrassi, L., Fournous, G., Merchat, M., Suzan-Monti, M., Forterre, P., Koonin, E. V., & Raoult, D. (2008). The virophage as a unique parasite of the giant mimivirus. *Nature, 455*(7209), 100-104. doi:10.1038/nature07218

Lam, W. L., & Doolittle, W. F. (1992). Mevinolin-resistant mutations identify a promoter and the gene for a eukaryote-like 3-hydroxy-3-methylglutaryl-coenzyme A reductase in the archaebacterium *Haloferax volcanii*. *Journal of Biological Chemistry, 267*(9), 5829-5834.

Lang, A. S., Westbye, A. B., & Beatty, J. T. (2017). The Distribution, Evolution, and Roles of Gene Transfer Agents in Prokaryotic Genetic Exchange. *Annual review of virology, 4*(1), 87-104. doi:10.1146/annurev-virology-101416-041624

Lang, A. S., Zhaxybayeva, O., & Beatty, J. T. (2012). Gene transfer agents: phage-like elements of genetic exchange. *Nature Reviews Microbiology, 10*(7), 472-482. doi:10.1038/nrmicro2802

Laso-Pérez, R., Wu, F., Crémière, A., Speth, D. R., Magyar, J. S., Zhao, K., Krupovic, M., & Orphan, V. J. (2023). Evolutionary diversification of methanotrophic ANME-1 archaea and their expansive virome. *Nature microbiology*. doi:10.1038/s41564-022-01297-4

Laursen, S. P., Bowerman, S., & Luger, K. (2021). Archaea: The Final Frontier of Chromatin. *Journal of Molecular Biology, 433*(6), 166791. doi:10.1016/j.jmb.2020.166791

Legendre, M., Fabre, E., Poirot, O., Jeudy, S., Lartigue, A., Alempic, J.-M., Beucher, L., Philippe, N., Bertaux, L., Christo-Foroux, E., Labadie, K., Couté, Y., Abergel, C., & Claverie, J.-M. (2018). Diversity and evolution of the emerging Pandoraviridae family. *Nature communications, 9*(1), 2285. doi:10.1038/s41467-018-04698-4

Li, M., Gong, L., Cheng, F., Yu, H., Zhao, D., Wang, R., Wang, T., Zhang, S., Zhou, J., Shmakov, S. A., Koonin, E. V., & Xiang, H. (2021). Toxin-antitoxin RNA pairs safeguard CRISPR-Cas systems. *Science, 372*(6541), eabe5601. doi:10.1126/science.abe5601

Liao, Y., Ithurbide, S., de Silva, R. T., Erdmann, S., & Duggin, I. G. (2018). Archaeal cell biology: diverse functions of tubulin-like cytoskeletal proteins at the cell envelope. *Emerging Topics in Life Sciences, 2*(4), 547-559. doi:10.1042/etls20180026

Liao, Y., Ithurbide, S., Evenhuis, C., Löwe, J., & Duggin, I. G. (2021). Cell division in the archaeon *Haloferax volcanii* relies on two FtsZ proteins with distinct functions in division ring assembly and constriction. *Nature microbiology, 6*(5), 594-605. doi:10.1038/s41564-021-00894-z

Liao, Y., Williams, T. J., Walsh, J. C., Ji, M., Poljak, A., Curmi, P. M. G., Duggin, I. G., & Cavicchioli, R. (2016). Developing a genetic manipulation system for the Antarctic archaeon, *Halorubrum lacusprofundi*: investigating acetamidase gene function. *Scientific Reports, 6*, 34639. doi:10.1038/srep34639

Lilly, J., & Camps, M. (2015). Mechanisms of Theta Plasmid Replication. In M. E. Tomalsky & J. C. Alonso (Eds.), *Plasmids* (pp. 33-44).

Lindås, A.-C., Karlsson, E. A., Lindgren, M. T., Ettema, T. J. G., & Bernander, R. (2008). A unique cell division machinery in the Archaea. *Proceedings of the National Academy of Sciences, 105*(48), 18942-18946. doi:10.1073/pnas.0809467105

Lipps, G., Röther, S., Hart, C., & Krauss, G. (2003). A novel type of replicative enzyme harbouring ATPase, primase and DNA polymerase activity. *The EMBO Journal, 22*(10), 2516-2525. doi:10.1093/emboj/cdg246

Lipps, G., Weinzierl, A. O., von Scheven, G., Buchen, C., & Cramer, P. (2004). Structure of a bifunctional DNA primase-polymerase. *Nature Structural & Molecular Biology, 11*(2), 157-162. doi:10.1038/nsmb723

Lipscomb, G. L., Stirrett, K., Schut, G. J., Yang, F., Jenney, F. E., Scott, R. A., Adams, M. W. W., & Westpheling, J. (2011). Natural Competence in the Hyperthermophilic Archaeon *Pyrococcus furiosus* Facilitates Genetic Manipulation: Construction of Markerless Deletions of Genes Encoding the Two Cytoplasmic Hydrogenases. *Applied and Environmental Microbiology, 77*(7), 2232-2238. doi:10.1128/AEM.02624-10

Liu, J., Cvirkaite-Krupovič, V., Baquero, D. P., Yang, Y., Zhang, Q., Shen, Y., & Krupovič, M. (2021a). Virus-induced cell gigantism and asymmetric cell division in archaea. *Proceedings of the National Academy of Sciences, 118*(15), e2022578118. doi:10.1073/pnas.2022578118

Liu, J., Cvirkaite-Krupovič, V., Commere, P.-H., Yang, Y., Zhou, F., Forterre, P., Shen, Y., & Krupovič, M. (2021b). Archaeal extracellular vesicles are produced in an ESCRT-dependent manner and promote gene transfer and nutrient cycling in extreme environments. *The ISME journal, 15*(10), 2892-2905. doi:10.1038/s41396-021-00984-0

Liu, Y., Demina, T. A., Roux, S., Aiewsakun, P., Kazlauskas, D., Simmonds, P., Prangishvili, D., Oksanen, H. M., & Krupovič, M. (2021). Diversity, taxonomy, and evolution of archaeal viruses of the class *Caudoviricetes*. *PLOS Biology, 19*(11), e3001442. doi:10.1371/journal.pbio.3001442

Liu, Y., Dyall-Smith, M., & Oksanen, H. M. (2022). ICTV Virus Taxonomy Profile: Pleolipoviridae 2022. *Journal of General Virology, 103*(11). doi:10.1099/jgv.0.001793

Liu, Y., Ishino, S., Ishino, Y., Pehau-Arnaudet, G., Krupovič, M., & Prangishvili, D. (2017). A Novel Type of Polyhedral Viruses Infecting Hyperthermophilic Archaea. *Journal of virology, 91*(13), 10.1128/jvi.00589-00517. doi:10.1128/jvi.00589-17

Liu, Y., Makarova, K. S., Huang, W.-C., Wolf, Y. I., Nikolskaya, A. N., Zhang, X., Cai, M., Zhang, C.-J., Xu, W., Luo, Z., Cheng, L., Koonin, E. V., & Li, M. (2021). Expanded diversity of Asgard archaea and their relationships with eukaryotes. *Nature, 593*(7860), 553-557. doi:10.1038/s41586-021-03494-3

Lloyd, K. G., May, M. K., Kevorkian, R. T., & Steen, A. D. (2013). Meta-analysis of quantification methods shows that archaea and bacteria have similar abundances in the subseafloor. *Appl Environ Microbiol, 79*(24), 7790-7799. doi:10.1128/aem.02090-13

Ludt, K., & Soppa, J. (2019). Polyploidy in halophilic archaea: regulation, evolutionary advantages, and gene conversion. *Biochemical Society Transactions, 47*(3), 933-944. doi:10.1042/bst20190256

Lwoff, A. (1957). The concept of virus. *Microbiology, 17*(2), 239-253. Retrieved from https://citeseerx.ist.psu.edu/document?repid=rep1&type=pdf&doi=a4a6929fbcd9494bf9e02ac81b23fe8b26cc8874

Maezato, Y., Daugherty, A., Dana, K., Soo, E., Cooper, C., Tachdjian, S., Kelly, R. M., & Blum, P. (2011). VapC6, a ribonucleolytic toxin regulates thermophilicity in the crenarchaeote *Sulfolobus solfataricus*. *Rna, 17*(7), 1381-1392. doi:10.1261/rna.2679911

Magidovich, H., & Eichler, J. (2009). Glycosyltransferases and oligosaccharyltransferases in Archaea: putative components of the N-glycosylation pathway in the third domain of life. *FEMS microbiology letters, 300*(1), 122-130. doi:10.1111/j.1574-6968.2009.01775.x

Maier, L.-K., Stachler, A.-E., Brendel, J., Stoll, B., Fischer, S., Haas, K. A., Schwarz, T. S., Alkhnbashi, O. S., Sharma, K., Urlaub, H., Backofen, R., Gophna, U., & Marchfelder, A. (2019). The nuts and bolts of the Haloferax CRISPR-Cas system I-B. *RNA biology, 16*(4), 469-480. doi:10.1080/15476286.2018.1460994

Makkay, A. M., Louyakis, A. S., Ram-Mohan, N., Gophna, U., Gogarten, J. P., & Papke, R. T. (2020). Insights into gene expression changes under conditions that facilitate horizontal gene transfer (mating) of a model archaeon. *Scientific Reports, 10*(1), 22297. doi:10.1038/s41598-020-79296-w

Manning, A. J., & Kuehn, M. J. (2011). Contribution of bacterial outer membrane vesicles to innate bacterial defense. *BMC microbiology, 11*(1), 258. doi:10.1186/1471-2180-11-258

Mäntynen, S., Laanto, E., Oksanen, H. M., Poranen, M. M., & Díaz-Muñoz, S. L. (2021). Black box of phage–bacterium interactions: exploring alternative phage infection strategies. *Open Biology, 11*(9), 210188. doi:10.1098/rsob.210188

Margolin, W., Wang, R., & Kumar, M. (1996). Isolation of an ftsZ homolog from the archaebacterium *Halobacterium salinarium*: implications for the evolution of FtsZ and tubulin. *Journal of bacteriology, 178*(5), 1320-1327. doi:10.1128/jb.178.5.1320-1327.1996

Marsin, S., & Forterre, P. (1998). A rolling circle replication initiator protein with a nucleotidyl-transferase activity encoded by the plasmid pGT5 from the hyperthermophilic archaeon *Pyrococcus abyssi*. *Molecular Microbiology, 27*(6), 1183-1192. doi:10.1046/j.1365-2958.1998.00759.x

McCullough, J., Frost, A., & Sundquist, W. I. (2018). Structures, Functions, and Dynamics of ESCRT-III/Vps4 Membrane Remodeling and Fission Complexes. *Annual Review of Cell and Developmental Biology, 34*(1), 85-109. doi:10.1146/annurev-cellbio-100616-060600

Medvedeva, S., Sun, J., Yutin, N., Koonin, E. V., Nunoura, T., Rinke, C., & Krupovič, M. (2022). Three families of Asgard archaeal viruses identified in metagenome-assembled genomes. *Nature microbiology, 7*(7), 962-973. doi:10.1038/s41564-022-01144-6

Mercier, C., Thies, D., Zhong, L., Raftery, M. J., Cavicchioli, R., & Erdmann, S. (2022). In depth characterization of an archaeal virus-host system reveals numerous virus exclusion mechanisms. *bioRxiv*. doi:10.1101/2022.10.18.512658

Mevarech, M., & Werczberger, R. (1985). Genetic transfer in *Halobacterium volcanii*. *J Bacteriol, 162*(1), 461-462. doi:10.1128/jb.162.1.461-462.1985

Mills, J., Gebhard, L. J., Schubotz, F., Shevchenko, A., Speth, D. R., Liao, Y., Duggin, I. G., Marchfelder, A., & Erdmann, S. (2023). Extracellular vesicles of *Euryarchaeida*: precursor to eukaryotic membrane trafficking. *bioRxiv*. doi:10.1101/2023.03.03.530948

Minegishi, H., Echigo, A., Nagaoka, S., Kamekura, M., & Usami, R. (2010). *Halarchaeum acidiphilum gen. nov., sp. nov.,* a moderately acidophilic haloarchaeon isolated from

commercial solar salt. *International Journal of Systematic and Evolutionary Microbiology, 60*(11), 2513-2516. doi:10.1099/ijs.0.013722-0

Mizuno, C. M., Guyomar, C., Roux, S., Lavigne, R., Rodriguez-Valera, F., Sullivan, M. B., Gillet, R., Forterre, P., & Krupovič, M. (2019). Numerous cultivated and uncultivated viruses encode ribosomal proteins. *Nat Communications, 10*(1), 752. doi:10.1038/s41467-019-08672-6

Mochizuki, T., Krupovič, M., Pehau-Arnaudet, G., Sako, Y., Forterre, P., & Prangishvili, D. (2012). Archaeal virus with exceptional virion architecture and the largest single-stranded DNA genome. *Proceedings of the National Academy of Sciences, 109*(33), 13386-13391. doi:10.1073/pnas.1203668109

Mochizuki, T., Yoshida, T., Tanaka, R., Forterre, P., Sako, Y., & Prangishvili, D. (2010). Diversity of viruses of the hyperthermophilic archaeal genus *Aeropyrum*, and isolation of the *Aeropyrum pernix* bacilliform virus 1, APBV1, the first representative of the family *Clavaviridae*. *Virology, 402*(2), 347-354. doi:10.1016/j.virol.2010.03.046

Moi, D., Nishio, S., Li, X., Valansi, C., Langleib, M., Brukman, N. G., Flyak, K., Dessimoz, C., de Sanctis, D., Tunyasuvunakool, K., Jumper, J., Graña, M., Romero, H., Aguilar, P. S., Jovine, L., & Podbilewicz, B. (2022). Discovery of archaeal fusexins homologous to eukaryotic HAP2/GCS1 gamete fusion proteins. *Nature communications, 13*(1), 3880. doi:10.1038/s41467-022-31564-1

Mondragon, P., Hwang, S., Kasirajan, L., Oyetoro, R., Nasthas, A., Winters, E., Couto-Rodriguez, R. L., Schmid, A., & Maupin-Furlow, J. A. (2022). TrmB Family Transcription Factor as a Thiol-Based Regulator of Oxidative Stress Response. *MBio, 13*(4), e00633-00622. doi:10.1128/mbio.00633-22

Moriano-Gutierrez, S., Bongrand, C., Essock-Burns, T., Wu, L., McFall-Ngai, M. J., & Ruby, E. G. (2020). The noncoding small RNA SsrA is released by *Vibrio fischeri* and modulates critical host responses. *PLOS Biology, 18*(11), e3000934. doi:10.1371/journal.pbio.3000934

Mullakhanbhai, M. F., & Larsen, H. (1975). *Halobacterium volcanii* spec. nov., a Dead Sea halobacterium with a moderate salt requirement. *Archives of Microbiology, 104*(1), 207-214. doi:10.1007/BF00447326

Munke, A., Kimura, K., Tomaru, Y., Wang, H., Yoshida, K., Mito, S., Hongo, Y., & Okamoto, K. (2022). Primordial Capsid and Spooled ssDNA Genome Structures Unravel Ancestral Events of Eukaryotic Viruses. *MBio, 13*(4), e00156-00122. doi:10.1128/mbio.00156-22

Muskhelishvili, G., Palm, P., & Zillig, W. (1993). SSV1-encoded site-specific recombination system in *Sulfolobus shibatae*. *Molecular and General Genetics MGG, 237*(3), 334-342. doi:10.1007/BF00279436

Myllykallio, H., Lopez, P., López-García, P., Heilig, R., Saurin, W., Zivanovic, Y., Philippe, H., & Forterre, P. (2000). Bacterial Mode of Replication with Eukaryotic-Like Machinery in a Hyperthermophilic Archaeon. *Science, 288*(5474), 2212-2215. doi:10.1126/science.288.5474.2212

Naor, A., Altman-Price, N., Soucy, S. M., Green, A. G., Mitiagin, Y., Turgeman-Grott, I., Davidovich, N., Gogarten, J. P., & Gophna, U. (2016). Impact of a homing intein on recombination frequency and organismal fitness. *Proceedings of the National Academy of Sciences, 113*(32), E4654-E4661. doi:10.1073/pnas.1606416113

Naor, A., Lapierre, P., Mevarech, M., Papke, R. T., & Gophna, U. (2012). Low Species Barriers in Halophilic Archaea and the Formation of Recombinant Hybrids. *Current Biology, 22*(15), 1444-1448. doi:10.1016/j.cub.2012.05.056

Narasingarao, P., Podell, S., Ugalde, J. A., Brochier-Armanet, C., Emerson, J. B., Brocks, J. J., Heidelberg, K. B., Banfield, J. F., & Allen, E. E. (2012). De novo metagenomic assembly reveals abundant novel major lineage of Archaea in hypersaline microbial communities. *The ISME journal, 6*(1), 81-93. doi:10.1038/ismej.2011.78

Nasir, A., & Caetano-Anollés, G. (2015). A phylogenomic data-driven exploration of viral origins and evolution. *Science advances, 1*(8), e1500527. doi:10.1126/sciadv.1500527

Nasir, A., Forterre, P., Kim, K. M., & Caetano-Anollés, G. (2014). The distribution and impact of viral lineages in domains of life. *Frontiers in microbiology, 5*. doi:10.3389/fmicb.2014.00194

Nasir, A., Kim, K. M., & Caetano-Anolles, G. (2012). Giant viruses coexisted with the cellular ancestors and represent a distinct supergroup along with superkingdoms Archaea, Bacteria and Eukarya. *BMC evolutionary biology, 12*(1), 156. doi:10.1186/1471-2148-12-156

Nasir, A., Romero-Severson, E., & Claverie, J.-M. (2020). Investigating the Concept and Origin of Viruses. *Trends in Microbiology, 28*(12), 959-967. doi:10.1016/j.tim.2020.08.003

Nelson-Sathi, S., Dagan, T., Landan, G., Janssen, A., Steel, M., McInerney, J. O., Deppenmeier, U., & Martin, W. F. (2012). Acquisition of 1,000 eubacterial genes physiologically transformed a methanogen at the origin of Haloarchaea. *Proceedings of the National Academy of Sciences, 109*(50), 20537-20542. doi:10.1073/pnas.1209119109

Nelson-Sathi, S., Sousa, F. L., Roettger, M., Lozada-Chávez, N., Thiergart, T., Janssen, A., Bryant, D., Landan, G., Schönheit, P., Siebers, B., McInerney, J. O., & Martin, W. F. (2015). Origins of major archaeal clades correspond to gene acquisitions from bacteria. *Nature, 517*(7532), 77-80. doi:10.1038/nature13805

Ng, W. L., & DasSarma, S. (1993). Minimal replication origin of the 200-kilobase *Halobacterium* plasmid pNRC100. *Journal of bacteriology, 175*(15), 4584-4596. doi:10.1128/jb.175.15.4584-4596.1993

Ng, W. V., Ciufo, S. A., Smith, T. M., Bumgarner, R. E., Baskin, D., Faust, J., Hall, B., Loretz, C., Seto, J., Slagel, J., Hood, L., & DasSarma, S. (1998). Snapshot of a large dynamic replicon in a halophilic archaeon: megaplasmid or minichromosome? *Genome Research, 8*(11), 1131-1141. doi:10.1101/gr.8.11.1131

Nielsen, E., Cheung, A. Y., & Ueda, T. (2008). The Regulatory RAB and ARF GTPases for Vesicular Trafficking *Plant Physiology, 147*(4), 1516-1526. doi:10.1104/pp.108.121798

Nölling, J., & Vos, W. M. d. (1992). Identification of the CTAG-recognizing restriction-modification systems Mth ZI and Mth FI from *Methanobacterium thermoformicicum* and characterization of the plasmid-encoded mthZIM gene. *Nucleic acids research, 20*(19), 5047-5052. doi:10.1093/nar/20.19.5047

Norais, C., Hawkins, M., Hartman, A. L., Eisen, J. A., Myllykallio, H., & Allers, T. (2007). Genetic and Physical Mapping of DNA Replication Origins in *Haloferax volcanii*. *PLoS Genet, 3*(5), e77. doi:10.1371/journal.pgen.0030077

Novikova, O., Jayachandran, P., Kelley, D. S., Morton, Z., Merwin, S., Topilina, N. I., & Belfort, M. (2015). Intein Clustering Suggests Functional Importance in Different Domains of Life. *Molecular biology and evolution, 33*(3), 783-799. doi:10.1093/molbev/msv271

Nußbaum, P., Gerstner, M., Dingethal, M., Erb, C., & Albers, S.-V. (2021). The archaeal protein SepF is essential for cell division in *Haloferax volcanii*. *Nature communications, 12*(1), 3469. doi:10.1038/s41467-021-23686-9

Nußbaum, P., Ithurbide, S., Walsh, J. C., Patro, M., Delpech, F., Rodriguez-Franco, M., Curmi, P. M. G., Duggin, I. G., Quax, T. E. F., & Albers, S.-V. (2020). An Oscillating MinD Protein Determines the Cellular Positioning of the Motility Machinery in Archaea. *Current Biology*. doi:10.1016/j.cub.2020.09.073

Oren, A. (2013). Life at high salt concentrations, intracellular KCl concentrations, and acidic proteomes. *Frontiers in microbiology, 4*(315). doi:10.3389/fmicb.2013.00315

Oren, A., & Garrity, G. M. (2021). Valid publication of the names of forty-two phyla of prokaryotes. *International Journal of Systematic and Evolutionary Microbiology, 71*(10). doi:10.1099/ijsem.0.005056

Ozawa, K., Harashina, T., Yatsunami, R., & Nakamura, S. (2005). Gene cloning, expression and partial characterization of cell division protein FtsZ1 from extremely halophilic archaeon *Haloarcula japonica* strain TR-1. *Extremophiles, 9*(4), 281-288. doi:10.1007/s00792-005-0443-6

Papke, R. T., Koenig, J. E., Rodríguez-Valera, F., & Doolittle, W. F. (2004). Frequent Recombination in a Saltern Population of Halorubrum. *Science, 306*(5703), 1928-1929. doi:10.1126/science.1103289

Pelve, E. A., Lindås, A.-C., Martens-Habbena, W., de la Torre, J. R., Stahl, D. A., & Bernander, R. (2011). Cdv-based cell division and cell cycle organization in the thaumarchaeon *Nitrosopumilus maritimus*. *Molecular Microbiology, 82*(3), 555-566. doi:10.1111/j.1365-2958.2011.07834.x

Pende, N., Sogues, A., Megrian, D., Sartori-Rupp, A., England, P., Palabikyan, H., Rittmann, S. K. M. R., Graña, M., Wehenkel, A. M., Alzari, P. M., & Gribaldo, S. (2021). SepF is the FtsZ anchor in archaea, with features of an ancestral cell division system. *Nature communications, 12*(1), 3214. doi:10.1038/s41467-021-23099-8

Peng, X., Holz, I., Zillig, W., Garrett, R. A., & She, Q. (2000). Evolution of the family of pRN plasmids and their integrase-mediated insertion into the chromosome of the crenarchaeon *Sulfolobus solfataricus*. *Journal of Molecular Biology, 303*(4), 449-454. doi:10.1006/jmbi.2000.4160

Pérez-Arnaiz, P., Dattani, A., Smith, V., & Allers, T. (2020). *Haloferax volcanii* a model archaeon for studying DNA replication and repair. *Open Biology, 10*(12), 200293. doi:10.1098/rsob.200293

Pfeifer, F., Weidinger, G., & W., G. (1981). Characterization of plasmids in halobacteria. *Journal of bacteriology, 145*(1), 369-374. doi:10.1128/jb.145.1.369-374.1981

Pfeiffer, F., Losensky, G., Marchfelder, A., Habermann, B., & Dyall-Smith, M. (2020). Whole-genome comparison between the type strain of *Halobacterium salinarum* (DSM 3754T) and the laboratory strains R1 and NRC-1. *MicrobiologyOpen, 9*(2), e974. doi:10.1002/mbo3.974

Philippe, N., Legendre, M., Doutre, G., Couté, Y., Poirot, O., Lescot, M., Arslan, D., Seltzer, V., Bertaux, L., Bruley, C., Garin, J., Claverie, J.-M., & Abergel, C. (2013). Pandoraviruses: Amoeba Viruses with Genomes Up to 2.5 Mb Reaching That of Parasitic Eukaryotes. *Science, 341*(6143), 281-286. doi:10.1126/science.1239181

Philosof, A., Yutin, N., Flores-Uribe, J., Sharon, I., Koonin, E. V., & Béjà, O. (2017). Novel Abundant Oceanic Viruses of Uncultured Marine Group II Euryarchaeota. *Current Biology, 27*(9), 1362-1368. doi:10.1016/j.cub.2017.03.052

Pietilä, M. K., Roine, E., Paulin, L., Kalkkinen, N., & Bamford, D. H. (2009). An ssDNA virus infecting archaea: a new lineage of viruses with a membrane envelope. *Molecular Microbiology, 72*(2), 307-319. doi:10.1111/j.1365-2958.2009.06642.x

Pina, M., Bize, A., Forterre, P., & Prangishvili, D. (2011). The archeoviruses. *FEMS microbiology reviews, 35*(6), 1035-1054. doi:10.1111/j.1574-6976.2011.00280.x

Pisani, F. M., Martino, C. D., & Rossi, M. (1992). A DNA polymerase from the archaeon *Sulfolobus solfataricus* shows sequence similarity to family B DNA polymerases. *Nucleic acids research, 20*(11), 2711-2716. doi:10.1093/nar/20.11.2711

Porter, K., Kukkaro, P., Bamford, J. K. H., Bath, C., Kivelä, H. M., Dyall-Smith, M. L., & Bamford, D. H. (2005). SH1: A novel, spherical halovirus isolated from an Australian hypersaline lake. *Virology, 335*(1), 22-33. doi:10.1016/j.virol.2005.01.043

Prangishvili, D., Albers, S.-V., Holz, I., Arnold, H. P., Stedman, K., Klein, T., Singh, H., Hiort, J., Schweier, A., Kristjansson, J. K., & Zillig, W. (1998). Conjugation in Archaea: Frequent Occurrence of Conjugative Plasmids in *Sulfolobus*. *Plasmid, 40*(3), 190-202. doi:10.1006/plas.1998.1363

Prangishvili, D., Arnold, H. P., Götz, D., Ziese, U., Holz, I., Kristjansson, J. K., & Zillig, W. (1999). A Novel Virus Family, the *Rudiviridae*: Structure, Virus-Host Interactions and Genome Variability of the Sulfolobus Viruses SIRV1 and SIRV2. *Genetics, 152*(4), 1387-1396. doi:10.1093/genetics/152.4.1387

Prangishvili, D., Bamford, D. H., Forterre, P., Iranzo, J., Koonin, E. V., & Krupovič, M. (2017). The enigmatic archaeal virosphere. *Nature Reviews Microbiology, 15*, 724. doi:10.1038/nrmicro.2017.125

Prieur, D., Erauso, G., Flament, D., Gaillard, M., Geslin, C., Gonnet, M., Romancer, M. L., Lucas, S., & Forterrre, P. (2006). 11 Deep-sea Thermococcales and their Genetic Elements:

Plasmids and Viruses. In *Methods in Microbiology* (Vol. 35, pp. 253-278): Academic Press.
Pringle, C. R. (1991). The 20th meeting of the executive committee of the international committee on virus taxonomy. *Archives of Virology, 119*(3), 303-304. doi:10.1007/BF01310680
Quax, T. E., & Daum, B. (2018). Structure and assembly mechanism of virus-associated pyramids. *Biophysical Reviews, 10*(2), 551-557. doi:10.1007/s12551-017-0357-4
Quax, T. E., Lucas, S., Reimann, J., Pehau-Arnaudet, G., Prevost, M.-C., Forterre, P., Albers, S.-V., & Prangishvili, D. (2011). Simple and elegant design of a virion egress structure in Archaea. *Proceedings of the National Academy of Sciences, 108*(8), 3354-3359. doi:10.1073/pnas.1018052108
Quemin, E. R. J., Chlanda, P., Sachse, M., Forterre, P., Prangishvili, D., & Krupovič, M. (2016). Eukaryotic-Like Virus Budding in Archaea. *MBio, 7*(5), e01439-01416. doi:10.1128/mBio.01439-16
Quemin, E. R. J., & Quax, T. E. F. (2015). Archaeal viruses at the cell envelope: entry and egress. *Frontiers in microbiology, 6*. doi:10.3389/fmicb.2015.00552
Rados, T., Andre, K., Cerletti, M., & Bisson, A. (2023). A sweet new set of inducible and constitutive promoters in *Haloferax volcanii*. *Frontiers in microbiology, 14*. doi:10.3389/fmicb.2023.1204876
Rambo, I. M., Langwig, M. V., Leão, P., De Anda, V., & Baker, B. J. (2022). Genomes of six viruses that infect Asgard archaea from deep-sea sediments. *Nature microbiology, 7*(7), 953-961. doi:10.1038/s41564-022-01150-8
Raoult, D., & Forterre, P. (2008). Redefining viruses: lessons from Mimivirus. *Nature Reviews Microbiology, 6*(4), 315-319. doi:10.1038/nrmicro1858
Redder, P., & Linder, P. (2012). New Range of Vectors with a Stringent 5-Fluoroorotic Acid-Based Counterselection System for Generating Mutants by Allelic Replacement in *Staphylococcus aureus*. *Applied and Environmental Microbiology, 78*(11), 3846-3854. doi:10.1128/AEM.00202-12
Rensen, E. I., Mochizuki, T., Quemin, E., Schouten, S., Krupovič, M., & Prangishvili, D. (2016). A virus of hyperthermophilic archaea with a unique architecture among DNA viruses. *Proceedings of the National Academy of Sciences, 113*(9), 2478-2483. doi:10.1073/pnas.1518929113
Reuter, C. J., & Maupin-Furlow, J. A. (2004). Analysis of Proteasome-Dependent Proteolysis in *Haloferax volcanii* Cells, Using Short-Lived Green Fluorescent Proteins. *Applied and Environmental Microbiology, 70*(12), 7530-7538. doi:10.1128/AEM.70.12.7530-7538.2004
Řezanka, T., Kyselová, L., & Murphy, D. J. (2023). Archaeal lipids. *Progress in Lipid Research, 91*, 101237. doi:10.1016/j.plipres.2023.101237
Rodrigues-Oliveira, T., Wollweber, F., Ponce-Toledo, R. I., Xu, J., Rittmann, S. K. M. R., Klingl, A., Pilhofer, M., & Schleper, C. (2023). Actin cytoskeleton and complex cell architecture in an Asgard archaeon. *Nature, 613*(7943), 332-339. doi:10.1038/s41586-022-05550-y
Rosenshine, I., Tchelet, R., & Mevarech, M. (1989). The Mechanism of DNA Transfer in the Mating System of an Archaebacterium. *Science, 245*(4924), 1387-1389. doi:10.1126/science.2818746
Roux, S., Brum, J. R., Dutilh, B. E., Sunagawa, S., Duhaime, M. B., Loy, A., Poulos, B. T., Solonenko, N., Lara, E., Poulain, J., Pesant, S., Kandels-Lewis, S., Dimier, C., Picheral, M., Searson, S., Cruaud, C., Alberti, A., Duarte, C. M., Gasol, J. M., Vaqué, D., Bork, P., Acinas, S. G., Wincker, P., Sullivan, M. B., & Tara Oceans, C. (2016). Ecogenomics and potential biogeochemical impacts of globally abundant ocean viruses. *Nature, 537*(7622), 689-693. doi:10.1038/nature19366
Ruiz-Masó, J. A., Machón, C., Bordanaba-Ruiseco, L., Espinosa, M., Coll, M., & del Solar, G. (2015). Plasmid Rolling-Circle Replication. In M. E. A. Tolmasky, Juan C. (Ed.), *Plasmids* (pp. 45-69).

Ruiz, D. M., Paggi, R. A., Giménez, M. I., & Castro, R. E. D. (2012). Autocatalytic Maturation of the Tat-Dependent Halophilic Subtilase Nep Produced by the Archaeon Natrialba magadii. *Journal of bacteriology, 194*(14), 3700-3707. doi:10.1128/JB.06792-11

Sanders, T. J., Marshall, C. J., & Santangelo, T. J. (2019). The Role of Archaeal Chromatin in Transcription. *Journal of Molecular Biology, 431*(20), 4103-4115. doi:10.1016/j.jmb.2019.05.006

Sandman, K., Krzycki, J. A., Dobrinski, B., Lurz, R., & Reeve, J. N. (1990). HMf, a DNA-binding protein isolated from the hyperthermophilic archaeon Methanothermus fervidus, is most closely related to histones. *Proceedings of the National Academy of Sciences, 87*(15), 5788-5791. doi:10.1073/pnas.87.15.5788

Schleper, C., Holz, I., Janekovic, D., Murphy, J., & Zillig, W. (1995). A multicopy plasmid of the extremely thermophilic archaeon *Sulfolobus* effects its transfer to recipients by mating. *Journal of bacteriology, 177*(15), 4417-4426. doi:10.1128/jb.177.15.4417-4426.1995

Schmidt, K. J., Beck, K. E., & Grogan, D. W. (1999). UV Stimulation of Chromosomal Marker Exchange in Sulfolobus acidocaldarius: Implications for DNA Repair, Conjugation and Homologous Recombination at Extremely High Temperatures. *Genetics, 152*(4), 1407-1415. doi:10.1093/genetics/152.4.1407

Schoelmerich, M. C., Ly, L., West-Roberts, J., Shi, L.-D., Shen, C., Malvankar, N., Taib, N., Gribaldo, S., Woodcroft, B. J., Al-Shayeb, B., Dai, X., Mozsary, C., Hickey, S., He, C., Beaulaurier, J. A., Juul, S., Sachdeva, R., & Banfield, J. (2023). Borg extrachromosomal elements of methane-oxidizing archaea have conserved and expressed genetic repertoires. *bioRxiv*. doi:10.1101/2023.08.01.549754

Schulz, F., Abergel, C., & Woyke, T. (2022). Giant virus biology and diversity in the era of genome-resolved metagenomics. *Nature Reviews Microbiology, 20*(12), 721-736. doi:10.1038/s41579-022-00754-5

Schulz, F., Yutin, N., Ivanova, N. N., Ortega, D. R., Lee, T. K., Vierheilig, J., Daims, H., Horn, M., Wagner, M., Jensen, G. J., Kyrpides, N. C., Koonin, E. V., & Woyke, T. (2017). Giant viruses with an expanded complement of translation system components. *Science, 356*(6333), 82-85. doi:10.1126/science.aal4657

Senčilo, A., & Roine, E. (2014). A Glimpse of the genomic diversity of haloarchaeal tailed viruses. *Frontiers in microbiology, 5*. doi:10.3389/fmicb.2014.00084

Shalev, Y., Soucy, S. M., Papke, R. T., Gogarten, J. P., Eichler, J., & Gophna, U. (2018). Comparative Analysis of Surface Layer Glycoproteins and Genes Involved in Protein Glycosylation in the Genus *Haloferax*. *Genes, 9*(3), 172. doi:10.3390/genes9030172

Shalev, Y., Turgeman-Grott, I., Tamir, A., Eichler, J., & Gophna, U. (2017). Cell Surface Glycosylation Is Required for Efficient Mating of *Haloferax volcanii*. *Frontiers in microbiology, 8*(1253). doi:10.3389/fmicb.2017.01253

She, Q., Peng, X., Zillig, W., & Garrett, R. A. (2001). Gene capture in archaeal chromosomes. *Nature, 409*(6819), 478-478. doi:10.1038/35054138

She, Q., Shen, B., & Chen, L. (2004). Archaeal integrases and mechanisms of gene capture. *Biochemical Society Transactions, 32*(2), 222-226. doi:10.1042/bst0320222

Simon, R. D. (1978). *Halobacterium* strain 5 contains a plasmid which is correlated with the presence of gas vacuoles. *Nature, 273*(5660), 314-317. doi:10.1038/273314a0

Sivabalasarma, S., Wetzel, H., Nußbaum, P., van der Does, C., Beeby, M., & Albers, S.-V. (2021). Analysis of Cell-Cell Bridges in *Haloferax volcanii* Using Electron Cryo-Tomography Reveal a Continuous Cytoplasm and S-Layer. *Frontiers in microbiology, 11*, 612239-612239. doi:10.3389/fmicb.2020.612239

Solar, G. d., Giraldo, R., Ruiz-Echevarría, M. J., Espinosa, M., & Díaz-Orejas, R. (1998). Replication and Control of Circular Bacterial Plasmids. *Microbiology and Molecular Biology Reviews, 62*(2), 434-464. doi:10.1128/mmbr.62.2.434-464.1998

Soler, N., & Forterre, P. (2020). Vesiduction: the fourth way of HGT. *Environmental microbiology, 22*(7), 2457-2460. doi:10.1111/1462-2920.15056

Soler, N., Justome, A., Quevillon-Cheruel, S., Lorieux, F., Le Cam, E., Marguet, E., & Forterre, P. (2007). The rolling-circle plasmid pTN1 from the hyperthermophilic archaeon

Thermococcus nautilus. *Molecular Microbiology, 66*(2), 357-370. doi:10.1111/j.1365-2958.2007.05912.x

Soler, N., Marguet, E., Cortez, D., Desnoues, N., Keller, J., van Tilbeurgh, H., Sezonov, G., & Forterre, P. (2010). Two novel families of plasmids from hyperthermophilic archaea encoding new families of replication proteins. *Nucleic acids research, 38*(15), 5088-5104. doi:10.1093/nar/gkq236

Soler, N., Marguet, E., Verbavatz, J.-M., & Forterre, P. (2008). Virus-like vesicles and extracellular DNA produced by hyperthermophilic archaea of the order *Thermococcales*. *Research in Microbiology, 159*(5), 390-399. doi:10.1016/j.resmic.2008.04.015

Song, Y., Zhu, Z., Zhou, W., & Zhang, Y.-H. P. J. (2021). High-efficiency transformation of archaea by direct PCR products with its application to directed evolution of a thermostable enzyme. *Microbial Biotechnology, 14*(2), 453-464. doi:10.1111/1751-7915.13613

Soppa, J. (2013). Evolutionary advantages of polyploidy in halophilic archaea. *Biochemical Society Transactions, 41*(1), 339-343. doi:10.1042/bst20120315

Sorokin, D. Y., Khijniak, T. V., Kostrikina, N. A., Elcheninov, A. G., Toshchakov, S. V., Bale, N. J., Damsté, J. S. S., & Kublanov, I. V. (2018). *Natronobiforma cellulositropha* gen. nov., sp. nov., a novel haloalkaliphilic member of the family *Natrialbaceae* (class *Halobacteria*) from hypersaline alkaline lakes. *Systematic and Applied Microbiology, 41*(4), 355-362. doi:10.1016/j.syapm.2018.04.002

Sorokin, D. Y., Makarova, K. S., Abbas, B., Ferrer, M., Golyshin, P. N., Galinski, E. A., Ciordia, S., Mena, M. C., Merkel, A. Y., Wolf, Y. I., van Loosdrecht, M. C. M., & Koonin, E. V. (2017). Discovery of extremely halophilic, methyl-reducing euryarchaea provides insights into the evolutionary origin of methanogenesis. *Nature microbiology, 2*(8), 17081. doi:10.1038/nmicrobiol.2017.81

Spang, A., Caceres, E. F., & Ettema, T. J. G. (2017). Genomic exploration of the diversity, ecology, and evolution of the archaeal domain of life. *Science, 357*(6351), eaaf3883. doi:10.1126/science.aaf3883

Spang, A., Saw, J. H., Jørgensen, S. L., Zaremba-Niedzwiedzka, K., Martijn, J., Lind, A. E., van Eijk, R., Schleper, C., Guy, L., & Ettema, T. J. G. (2015). Complex archaea that bridge the gap between prokaryotes and eukaryotes. *Nature, 521*(7551), 173-179. doi:10.1038/nature14447

Sun, C., Zhou, M., Li, Y., & Xiang, H. (2006). Molecular Characterization of the Minimal Replicon and the Unidirectional Theta Replication of pSCM201 in Extremely Halophilic Archaea. *Journal of bacteriology, 188*(23), 8136-8144. doi:10.1128/jb.00988-06

Tamarit, D., Caceres, E. F., Krupovič, M., Nijland, R., Eme, L., Robinson, N. P., & Ettema, T. J. G. (2022). A closed *Candidatus* Odinarchaeum chromosome exposes Asgard archaeal viruses. *Nature microbiology, 7*(7), 948-952. doi:10.1038/s41564-022-01122-y

Tamir, A., & Eichler, J. (2017). N-Glycosylation Is Important for Proper *Haloferax volcanii* S-Layer Stability and Function. *Applied and Environmental Microbiology, 83*(6), e03152-03116. doi:10.1128/AEM.03152-16

Tarrason Risa, G., Hurtig, F., Bray, S., Hafner, A. E., Harker-Kirschneck, L., Faull, P., Davis, C., Papatziamou, D., Mutavchiev, D. R., Fan, C., Meneguello, L., Arashiro Pulschen, A., Dey, G., Culley, S., Kilkenny, M., Souza, D. P., Pellegrini, L., de Bruin, R. A. M., Henriques, R., Snijders, A. P., Šarić, A., Lindås, A.-C., Robinson, N. P., & Baum, B. (2020). The proteasome controls ESCRT-III–mediated cell division in an archaeon. *Science, 369*(6504), eaaz2532. doi:10.1126/science.aaz2532

Tchelet, R., & Mevarech, M. (1993). Interspecies Genetic Transfer in Halophilic Archaebacteria. *Systematic and Applied Microbiology, 16*(4), 578-581. doi:10.1016/S0723-2020(11)80328-0

Thomsen, J., & Schmitz, R. A. (2022). Generating a Small Shuttle Vector for Effective Genetic Engineering of *Methanosarcina mazei* Allowed First Insights in Plasmid Replication

Mechanism in the Methanoarchaeon. *International Journal of Molecular Sciences, 23*(19), 11910. doi:10.3390/ijms231911910
Tokarz-Deptuła, B., Chrzanowska, S., Gurgacz, N., Stosik, M., & Deptuła, W. (2023). Virophages - Known and Unknown Facts. *Viruses, 15*(6), 1321. doi:10.3390/v15061321
Tripepi, M., Imam, S., & Pohlschröder, M. (2010). *Haloferax volcanii* flagella are required for motility but are not involved in *PibD*-dependent surface adhesion. *Journal of bacteriology, 192*(12), 3093-3102. doi:10.1128/JB.00133
Tschitschko, B., Erdmann, S., DeMaere, M. Z., Roux, S., Panwar, P., Allen, M. A., Williams, T. J., Brazendale, S., Hancock, A. M., Eloe-Fadrosh, E. A., & Cavicchioli, R. (2018). Genomic variation and biogeography of Antarctic haloarchaea. *Microbiome, 6*(1), 113. doi:10.1186/s40168-018-0495-3
Tschitschko, B., Williams, T. J., Allen, M. A., Páez-Espino, D., Kyrpides, N., Zhong, L., Raftery, M. J., & Cavicchioli, R. (2015). Antarctic archaea–virus interactions: metaproteome-led analysis of invasion, evasion and adaptation. *The ISME journal, 9*(9), 2094-2107. doi:10.1038/ismej.2015.110
Van Regenmortel, M. H. V. (1989). Applying the species concept to plant viruses. *Archives of Virology, 104*(1), 1-17. doi:10.1007/BF01313804
van Wolferen, M., Pulschen, A. A., Baum, B., Gribaldo, S., & Albers, S. V. (2022). The cell biology of archaea. *Nat Microbiol, 7*(11), 1744-1755. doi:10.1038/s41564-022-01215-8
van Wolferen, M., Wagner, A., van der Does, C., & Albers, S.-V. (2016). The archaeal Ced system imports DNA. *Proceedings of the National Academy of Sciences, 113*(9), 2496-2501. doi:10.1073/pnas.1513740113
Ventosa, A., de la Haba, R. R., Sánchez-Porro, C., & Papke, R. T. (2015). Microbial diversity of hypersaline environments: a metagenomic approach. *Current opinion in microbiology, 25*, 80-87. doi:10.1016/j.mib.2015.05.002
Vershinin, Z., Zaretsky, M., Guan, Z., & Eichler, J. (2021a). Identifying Components of a *Halobacterium salinarum* N-Glycosylation Pathway. *Front Microbiol, 12*, 779599. doi:10.3389/fmicb.2021.779599
Vershinin, Z., Zaretsky, M., Guan, Z., & Eichler, J. (2021b). Revisiting N-glycosylation in *Halobacterium salinarum:* Characterizing a dolichol phosphate- and glycoprotein-bound tetrasaccharide. *Glycobiology, 31*(12), 1645-1654. doi:10.1093/glycob/cwab080
Vietri, M., Radulovic, M., & Stenmark, H. (2020). The many functions of ESCRTs. *Nature Reviews Molecular Cell Biology, 21*(1), 25-42. doi:10.1038/s41580-019-0177-4
Votteler, J., & Sundquist, Wesley I. (2013). Virus Budding and the ESCRT Pathway. *Cell Host & Microbe, 14*(3), 232-241. doi:10.1016/j.chom.2013.08.012
Wadi, L., & Reinke, A. W. (2020). Evolution of microsporidia: An extremely successful group of eukaryotic intracellular parasites. *PLoS pathogens, 16*(2), e1008276. doi:10.1371/journal.ppat.1008276
Wagner, A., Whitaker, R. J., Krause, D. J., Heilers, J.-H., van Wolferen, M., van der Does, C., & Albers, S.-V. (2017). Mechanisms of gene flow in archaea. *Nature Reviews Microbiology, 15*(8), 492-501. doi:10.1038/nrmicro.2017.41
Wang, H., Guo, Z., Feng, H., Chen, Y., Chen, X., Li, Z., Hernández-Ascencio, W., Dai, X., Zhang, Z., Zheng, X., Mora-López, M., Fu, Y., Zhang, C., Zhu, P., & Huang, L. (2018). Novel Sulfolobus Virus with an Exceptional Capsid Architecture. *Journal of virology, 92*(5), 10.1128/jvi.01727-01717. doi:10.1128/jvi.01727-17
Wang, H., Peng, N., Shah, S. A., Huang, L., & She, Q. (2015). Archaeal extrachromosomal genetic elements. *Microbiol. Mol. Biol. Rev., 79*(1), 117-152. doi:10.1128/mmbr.00042-14
Wang, Y., Duan, Z., Zhu, H., Guo, X., Wang, Z., Zhou, J., She, Q., & Huang, L. (2007). A novel *Sulfolobus* non-conjugative extrachromosomal genetic element capable of integration into the host genome and spreading in the presence of a fusellovirus. *Virology, 363*(1), 124-133. doi:10.1016/j.virol.2007.01.035

Weidenbach, K., Nickel, L., Neve, H., Alkhnbashi Omer, S., Künzel, S., Kupczok, A., Bauersachs, T., Cassidy, L., Tholey, A., Backofen, R., & Schmitz Ruth, A. (2017). Methanosarcina Spherical Virus, a Novel Archaeal Lytic Virus Targeting *Methanosarcina* Strains. *Journal of virology, 91*(22), e00955-00917. doi:10.1128/JVI.00955-17

Wendoloski, D., Ferrer, C., & Dyall-Smith, M. (2001). A new simvastatin (mevinolin)-resistance marker from *Haloarcula hispanica* and a new *Haloferax volcanii* strain cured of plasmid pHV2. . *Microbiology, 147*(4), 959-964. doi:10.1099/00221287-147-4-959

Whitaker, R. J., Grogan, D. W., & Taylor, J. W. (2005). Recombination Shapes the Natural Population Structure of the Hyperthermophilic Archaeon *Sulfolobus islandicus*. *Molecular biology and evolution, 22*(12), 2354-2361. doi:10.1093/molbev/msi233

Williams, T. A., Embley, T. M., & Heinz, E. (2011). Informational Gene Phylogenies Do Not Support a Fourth Domain of Life for Nucleocytoplasmic Large DNA Viruses. *PLOS ONE, 6*(6), e21080. doi:10.1371/journal.pone.0021080

Williams, T. J., Allen, M. A., DeMaere, M. Z., Kyrpides, N. C., Tringe, S. G., Woyke, T., & Cavicchioli, R. (2014). Microbial ecology of an Antarctic hypersaline lake: genomic assessment of ecophysiology among dominant haloarchaea. *The ISME journal, 8*(8), 1645. doi:10.1038/ismej.2014.18

Williams, T. J., Liao, Y., Ye, J., Kuchel, R. P., Poljak, A., Raftery, M. J., & Cavicchioli, R. (2017). Cold adaptation of the Antarctic haloarchaea *Halohasta litchfieldiae* and *Halorubrum lacusprofundi*. *Environmental microbiology, 19*(6), 2210-2227. doi:10.1111/1462-2920.13705

Winter, K., Born, J., & Pfeifer, F. (2018). Interaction of Haloarchaeal Gas Vesicle Proteins Determined by Split-GFP. *Frontiers in microbiology, 9*. doi:10.3389/fmicb.2018.01897

Woese, C. R., & Fox, G. E. (1977). Phylogenetic structure of the prokaryotic domain: the primary kingdoms. *Proceedings of the National Academy of Sciences, 74*(11), 5088-5090. doi:10.1073/pnas.74.11.5088

Woese, C. R., Kandler, O., & Wheelis, M. L. (1990). Towards a natural system of organisms: proposal for the domains Archaea, Bacteria, and Eucarya. *Proceedings of the National Academy of Sciences, 87*(12), 4576-4579. doi:10.1073/pnas.87.12.4576

Wolf, S., Fischer, M. A., Kupczok, A., Reetz, J., Kern, T., Schmitz, R. A., & Rother, M. (2019). Characterization of the lytic archaeal virus Drs3 infecting *Methanobacterium formicicum*. *Archives of Virology, 164*(3), 667-674. doi:10.1007/s00705-018-04120-w

Worrell, V. E., Nagle, D. P., McCarthy, D., & Eisenbraun, A. (1988). Genetic transformation system in the archaebacterium *Methanobacterium thermoautotrophicum* Marburg. *Journal of bacteriology, 170*(2), 653-656. doi:10.1128/jb.170.2.653-656.1988

Wu, Z., Liu, H., Liu, J., Liu, X., & Xiang, H. (2012). Diversity and evolution of multiple orc/cdc6-adjacent replication origins in haloarchaea. *BMC genomics, 13*(1), 478. doi:10.1186/1471-2164-13-478

Yurist-Doutsch, S., Abu-Qarn, M., Battaglia, F., Morris, H. R., Hitchen, P. G., Dell, A., & Eichler, J. (2008). aglF, aglG and aglI, novel members of a gene island involved in the N-glycosylation of the *Haloferax volcanii* S-layer glycoprotein. *Molecular Microbiology, 69*(5), 1234-1245. doi:10.1111/j.1365-2958.2008.06352.x

Yurist-Doutsch, S., Magidovich, H., Ventura, V. V., Hitchen, P. G., Dell, A., & Eichler, J. (2010). N-glycosylation in Archaea: on the coordinated actions of *Haloferax volcanii* AglF and AglM. *Molecular Microbiology, 75*(4), 1047-1058. doi:10.1111/j.1365-2958.2009.07045.x

Zaretsky, M., Darnell, C. L., Schmid, A. K., & Eichler, J. (2019). N-Glycosylation Is Important for *Halobacterium salinarum* Archaellin Expression, Archaellum Assembly and Cell Motility. *Frontiers in microbiology, 10*. doi:10.3389/fmicb.2019.01367

Zaretsky, M., Roine, E., & Eichler, J. (2018). Sialic Acid-Like Sugars in Archaea: Legionaminic Acid Biosynthesis in the Halophile *Halorubrum* sp. PV6. *Frontiers in microbiology, 9*. doi:10.3389/fmicb.2018.02133

Zerulla, K., Chimileski, S., Näther, D., Gophna, U., Papke, R. T., & Soppa, J. (2014). DNA as a Phosphate Storage Polymer and the Alternative Advantages of Polyploidy for Growth or Survival. *PLOS ONE, 9*(4), e94819. doi:10.1371/journal.pone.0094819

Zerulla, K., & Soppa, J. (2014). Polyploidy in haloarchaea: advantages for growth and survival. *Frontiers in microbiology, 5*. doi:10.3389/fmicb.2014.00274

Zhou, H., Zhao, D., Zhang, S., Xue, Q., Zhang, M., Yu, H., Zhou, J., Li, M., Kumar, S., & Xiang, H. (2022). Metagenomic insights into the environmental adaptation and metabolism of Candidatus Haloplasmatales, one archaeal order thriving in saline lakes. *Environmental microbiology, 24*(5), 2239-2258. doi:10.1111/1462-2920.15899

Zhou, L., Zhou, M., Sun, C., Han, J., Lu, Q., Zhou, J., & Xiang, H. (2008). Precise Determination, Cross-Recognition, and Functional Analysis of the Double-Strand Origins of the Rolling-Circle Replication Plasmids in Haloarchaea. *Journal of bacteriology, 190*(16), 5710-5719. doi:10.1128/jb.00596-08

Zhou, M., Xiang, H., Sun, C., Li, Y., Liu, J., & Tan, H. (2004). Complete sequence and molecular characterization of pNB101, a rolling-circle replicating plasmid from the haloalkaliphilic archaeon *Natronobacterium* sp. strain AS7091. *Extremophiles, 8*(2), 91-98. doi:10.1007/s00792-003-0366-z

Zillig, W., Yeats, S., Holz, I., Böck, A., Gropp, F., Rettenberger, M., & Lutz, S. (1985). Plasmid-related anaerobic autotrophy of the novel archaebacterium *Sulfolobus ambivalens*. *Nature, 313*(6005), 789-791. doi:10.1038/313789a0

Zimmerman, A. E., Howard-Varona, C., Needham, D. M., John, S. G., Worden, A. Z., Sullivan, M. B., Waldbauer, J. R., & Coleman, M. L. (2020). Metabolic and biogeochemical consequences of viral infection in aquatic ecosystems. *Nature Reviews Microbiology, 18*(1), 21-34. doi:10.1038/s41579-019-0270-x

Zwartz, D., Bird, M., Stone, J., & Lambeck, K. (1998). Holocene sea-level change and ice-sheet history in the Vestfold Hills, East Antarctica. *Earth and Planetary Science Letters, 155*(1-2), 131-145.

Chapter I

Improving the genetic system for *Halorubrum lacusprofundi* to allow in-frame deletions

Improving the genetic system for *Halorubrum lacusprofundi* to allow in-frame deletions

L. Johanna Gebhard, Iain G. Duggin & Susanne Erdmann

* Manuscript published in *Frontiers in Microbiology*

Author contributions: L.J.G. performed the majority of the experimental work. S.E. performed some of the experiments, conceived and led the study, and L.J.G and S.E. performed the primary writing of the manuscript. I.D. led the initial phase of the study. All authors participated in the analysis and interpretation of the data and contributed to the writing of the manuscript.

frontiers | Frontiers in Microbiology

TYPE Original Research
PUBLISHED 31 March 2023
DOI 10.3389/fmicb.2023.1095621

Check for updates

OPEN ACCESS

EDITED BY
Marleen van Wolferen,
University of Freiburg,
Germany

REVIEWED BY
Changyi Zhang,
University of Illinois Urbana-Champaign,
United States
Jörg Soppa,
Goethe University Frankfurt,
Germany

*CORRESPONDENCE
Susanne Erdmann
serdmann@mpi-bremen.de

SPECIALTY SECTION
This article was submitted to
Biology of Archaea,
a section of the journal
Frontiers in Microbiology

RECEIVED 11 November 2022
ACCEPTED 13 March 2023
PUBLISHED 31 March 2023

CITATION
Gebhard LJ, Duggin IG and Erdmann S (2023) Improving the genetic system for *Halorubrum lacusprofundi* to allow in-frame deletions. *Front. Microbiol.* 14:1095621. doi: 10.3389/fmicb.2023.1095621

COPYRIGHT
© 2023 Gebhard, Duggin and Erdmann. This is an open-access article distributed under the terms of the Creative Commons Attribution License (CC BY). The use, distribution or reproduction in other forums is permitted, provided the original author(s) and the copyright owner(s) are credited and that the original publication in this journal is cited, in accordance with accepted academic practice. No use, distribution or reproduction is permitted which does not comply with these terms.

Improving the genetic system for *Halorubrum lacusprofundi* to allow in-frame deletions

L. Johanna Gebhard[1], Iain G. Duggin[2] and Susanne Erdmann[1]*

[1]Archaeal Virology, Max Planck Institute for Marine Microbiology, Bremen, Germany, [2]The Australian Institute for Microbiology and Infection, University of Technology Sydney, Sydney, NSW, Australia

Halorubrum lacusprofundi is a cold-adapted halophilic archaeon isolated from Deep Lake, Antarctica. *Hrr. lacusprofundi* is commonly used to study adaptation to cold environments and thereby a potential source for biotechnological products. Additionally, in contrast to other haloarchaeal model organisms, *Hrr. lacusprofundi* is also susceptible to a range of different viruses and virus-like elements, making it a great model to study virus-host interactions in a cold-adapted organism. A genetic system has previously been reported for *Hrr. lacusprofundi*; however, it does not allow in-frame deletions and multiple gene knockouts. Here, we report the successful generation of uracil auxotrophic (*pyrE2*) mutants of two strains of *Hrr. lacusprofundi*. Subsequently, we attempted to generate knockout mutants using the auxotrophic marker for selection. However, surprisingly, only the combination of the auxotrophic marker and antibiotic selection allowed the timely and clean in-frame deletion of a target gene. Finally, we show that vectors established for the model organism *Haloferax volcanii* are deployable for genetic manipulation of *Hrr. lacusprofundi*, allowing the use of the portfolio of genetic tools available for *H. volcanii* in *Hrr. lacusprofundi*.

KEYWORDS

***Halorubrum lacusprofundi*, archaea, genetic system, cold adaptation, haloarchaea, auxotrophic mutant**

Introduction

Halophilic archaea (haloarchaea) are established as commonly used model systems to study archaeal cell biology and virus-host interactions in archaea (Luk et al., 2014; van Wolferen et al., 2022). Additionally, they are of great interest for their potential use in biotechnological applications (Litchfield, 2011; Javier et al., 2017; Singh and Singh, 2017; Correa and Abreu, 2020; Li et al., 2022). They are easy to culture and genetic systems have already been developed for some members, with *Haloferax volcanii* currently being the most studied model organism (Hartman et al., 2010; Pohlschroder and Schulze, 2019). However, only one virus has been isolated for *H. volcanii* so far (Alarcón-Schumacher et al., 2022), while the majority of hosts for haloarchaeal viruses remain genetically inaccessible. In contrast to *Haloferax* species, that have been shown to be rather unsusceptible to virus infection (Aguirre Sourrouille et al., 2022), a great number of haloarchaeal viruses have been isolated on *Halorubrum* species (Atanasova et al., 2015; Pietilä et al., 2016; Liu et al., 2021). *Halorubrum lacusprofundi* ATCC 49239 (ACAM34) (Franzmann et al., 1988; McGenity and Grant, 1995), a model organism to study cold adaptation in archaea (DasSarma et al., 2013, 2017; Williams et al., 2017), has previously been shown to be genetically accessible (Liao et al., 2016). Several different viruses were shown

to infect *Hrr. lacusprofundi* (Nuttall and Dyall-Smith, 1993; Dyall-Smith, 2009d; Krupovič et al., 2010; Atanasova et al., 2012; Porter et al., 2013; Li et al., 2014; Tschitschko et al., 2015; Alarcón-Schumacher et al., 2022; Mercier et al., 2022). Additionally, the formation of plasmid vesicles (PVs), proposed to be an evolutionary precursor of viruses, has only been reported for *Hrr. lacusprofundi* (Erdmann et al., 2017). This makes *Hrr. lacusprofundi* a great model for studying virus-host relationships in archaea, in particular under low temperature, and to investigate the origin and evolution of viruses. A stable genetic system would allow for more in depth studies.

A genetic system, based on an auxotrophic selection marker, that allows in-frame deletions using the pop-in pop-out method has been developed in *H. volcanii* on the basis of the orotate phosphoribosyltransferase gene (*pyrE2*) (Lam and Doolittle, 1992; Wendoloski et al., 2001; Bitan-Banin et al., 2003; Allers et al., 2004; Liao et al., 2021). The Δ*pyrE2* deletion in *H. volcanii* was generated with a non-replicative plasmid containing a non-functional gene construct, created by fusing upstream and downstream flanking regions of the wild-type Δ*pyrE2* gene, and selection with the halobacterial novobiocin resistance gene (*gyrB*) (Bitan-Banin et al., 2003). Pop-in refers to the homologous recombination of plasmid and host chromosome caused by selection pressure applied with novobiocin in the culture media. Excision of the plasmid (pop-out) can either result in the wild-type or the mutated gene remaining in the chromosome; therefore, a fraction of the resulting clones is expected to be mutants with a non-functional target gene. The pop-out can either be initiated by removing the original selection pressure (e.g., novobiocin) or with an additional selection pressure using 5-fluoroorotic acid (5-FOA) and uracil (Bitan-Banin et al., 2003). The practicality of 5-FOA as counter-selectable marker was first described in yeast (Boeke et al., 1984) but has since been widely used for both bacteria and archaea (Liu et al., 2011; Redder and Linder, 2012; Liao et al., 2021; Matsuda et al., 2022; Piatek et al., 2022). In prokaryotes, orotate phosphoribosyltransferase (*pyrE*) and orotidine 5-phosphate decarboxylase (*pyrF*) catalyze the final steps in the pyrimidine biosynthesis pathway. The two enzymes convert 5-FOA to the toxic 5-fluoro-UMP leading to cell death (Redder and Linder, 2012).

However, generating spontaneous *pyrE2* mutants by subjecting the cells to 5-FOA and uracil, has not been successful for *Hrr. lacusprofundi* so far (Liao et al., 2016). Liao et al. (2016) described a method for knocking out the acetamidase *amd3* in *Hrr. lacusprofundi* with a suicide plasmid containing *hmgA* (pJWID1), conferring resistance to pravastatin. The 3-hydroxy-3-methylglutaryl coenzyme A reductase gene (*hmgA*) is involved in the isoprenoid lipid synthesis pathway in archaea. Overexpression of *hmgA* leads to mevinolin, fluvastatin, simvastatin, and pravastatin resistance in haloarchaea (Blaseio and Pfeifer, 1990; Lam and Doolittle, 1992; Wendoloski et al., 2001). However, in practice, pravastatin has proven to be the most reliable selection marker for *Hrr. lacusprofundi* (Liao et al., 2016). Liao et al. (2016) were able to show that the *hmgA* gene was inserted between flanking regions of *amd3*. After double recombination, *hmgA* replaced the target gene on the genome resulting in a successful deletion of the target gene. However, the *hmgA* gene remains in the genome and can interfere with the expression of genes in the same operon. The pravastatin resistance conferred by the permanent insertion into the genome also makes it nearly impossible to use the strain for the knockout of additional genes except when using very high pravastatin concentrations, e.g., 150 μg/mL (Liao et al., 2016). However, consecutive culturing of *Hrr. lacusprofundi* in pravastatin concentrations of 10 μg/mL and low concentrations of mevinolin and simvastatin led to multiple insertions and duplications of the *hmgA* gene into all three chromosomes of the strain (Hamm et al., 2019). Additionally, *Hrr. lacusprofundi* transposases also disrupted genes of the vector used, rendering them non-functional.

The aim of the study was to develop a stable system for the genetic manipulation of *Hrr. lacusprofundi* ACAM34 that uses the pop-in pop-out method and allows for in-frame deletions without leaving the antibiotic resistance gene in the genome. We successfully generated Δ*pyrE2* mutants for two *Hrr. lacusprofundi* ACAM34 strains. Subsequently, we demonstrate that the auxotrophic mutants can be used for in-frame deletions of genes using vectors that have been designed for *H. volcanii*, eliminating the necessity to design entirely new vectors.

Methods

Strains and cultivation conditions

Unless otherwise specified, strains that are referred to only by their strain name are all strains of *Halorubrum lacusprofundi ACAM34* (ATCC 49239). *Hrr. lacusprofundi* ACAM34_DSMZ was obtained from the DSMZ (German Collection of Microorganisms and Cell Cultures). *Hrr. lacusprofundi* ACAM34_UNSW is a variant with a reduced genome, derived from an original ACAM34 strain, and has been described in Mercier et al. (2022). The standard medium for cultivation was DBCM2 (Dyall-Smith, 2009b), with slight modifications. Standard DBCM2 medium contained 180 g/L NaCl, 25 g/L MgCl, 29 g/L $MgSO_4{\cdot}7H_2O$, 5.8 g/L KCl (all Merck, Germany) as well as 0.3 g/L peptone and 0.05 g/L yeast extract (both by Oxoid, Thermo Fisher Scientific, United States), dissolved in ddH_2O, and adjusted to pH 7.5 with 1 M Tris–HCl pH 8.0 prior to autoclaving. After autoclaving, supplements were added 6 mL/L 1 M $CaCl_2$, 2 mL/L K_2HPO_4 buffer (Dyall-Smith, 2009b), 4.4 mL/L 25% sodium pyruvate, 5 mL/L 1 M NH_4Cl, 1 mL/L SL10 trace elements solution (Dyall-Smith, 2009c), and 3 mL/L vitamin 10 solution (Dyall-Smith, 2009c). Initially, agar plates were prepared with ddH_2O and 18 g/L Oxoid™ agar. However, tap water was found to be best suited to support growth of ACAM34 on agar plates. Starting with the plating of pTA131_*hmgA*_Δ*trpA* transformants from liquid onto agar plates, the components for agar plates were dissolved in tap water and supplemented with 18 g/L Difco™ agar (BD, United States). We are aware that tap water is prone to contaminations and changes in composition, and indeed, we observed slight growth of auxotrophic mutants on selection plates in some seasons of the year. However, using tap water allowed for growth of ACAM34 colonies on plates in a reasonable time, while ddH_2O often did not result in colonies. For the rich medium DBCM2+, peptone and yeast extract concentrations were adjusted to 1 g/L and 0.5 g/L, respectively. Medium DBCM2 contained 5 g/L casamino acids (Oxoid) instead. For the generation of ACAM34_UNSWΔ*pyrE2*, the strain was plated on Hv-Cab solid agar as described in de Silva et al. (2021). Liquid cultures were inoculated at 28°C, because biofilm formation was often observed at 37°C (published optimal growth temperature) in liquid; however, plates were incubated at 37°C leading to a timely (7–10 days) formation of colonies. For light microscopy images, cells in mid-exponential

growth were fixed for 1 h at room temperature (RT) with 1% glutaraldehyde, immobilized on 4% agar slides, and imaged on a Zeiss AxioPhot microscope with AxioCam MRm.

Escherichia coli strains (DH5alpha and C2925) were grown at 37°C, either in liquid lysogeny broth (LB) medium (10 g/L tryptone, 5 g/L yeast extract, 10 g/L $NaCl_2$) (AppliChem, Germany and by Merck) in ddH_2O at pH 7.0 or on LB plates with 15 g/L Bacto™ agar (BD). Ampicillin was used as a selection agent at a final concentration of 100 μg/mL.

Molecular cloning procedures

DNA extractions were performed with the Bioline Isolate II Genomic DNA Kit (Meridian Bioscience, Cincinnati, United States). Plasmid extractions were performed using the Bioline Isolate II Plasmid Mini Kit, and DNA purification (from PCR or gel electrophoresis) was performed using the Bioline Isolate II PCR and Gel Clean-Up Kit. All extractions were performed following the manufacturer's instructions. Plasmids used in this study are summarized in Supplementary Table 1. The primers are listed with their respective annealing temperatures and targets in Supplementary Table 2. Amplification of archaeal genes was performed with Q5 Polymerase (NEB) as follows: Approximately 100 ng of template DNA was added to PCR master mix (per 100 μL; 1x reaction buffer (NEB, Ipswich, United States), 1x high GC enhancer (NEB), 40 μM dNTPS (NEB), 100 μM of forward and reverse primer each (biomers.net, Ulm, Germany), and 1 μL Q5 polymerase (NEB) and PCR was performed with the following program: Initial denaturation at 96°C for 1 min, 30x cycles at denaturation 96°C for 30 s, annealing (temperature in Supplementary Table 2) for 30 s, elongation at 72°C (1 min/kb), a final elongation at 72°C for 10 min, and storage at 12°C. When generating PCR fragments for cloning (with restriction sides included), a two-step PCR was performed with 10 cycles using the annealing temperature for the part of the primer that binds the template and 30 cycles with the annealing temperature calculated for the entire length of the primer, including additional bases (e.g., the restriction side). Overlapping PCRs were performed with Phusion Polymerase (NEB) according to the manufacturer's instructions with 5% DMSO in the reaction in two steps: 24 cycles without primers and 35 cycles with fresh dNTPs, Phusion Polymerase, and the outermost primers added to the PCR mix (forward primer used to generate the upstream fragment and reverse primer used to generate the downstream fragment). Restriction digest was performed in 30 μl reactions with 1 μL enzyme (as specified for individual cloning reactions), 3 μL 10x reaction buffer, and 1–3 μg of DNA for 2 h at 37°C with an inactivation step of 20 min at 70°C. Ligation reactions were performed in 20 μl volume with 1 μL T4 Ligase (NEB), 2 μL 10x reaction buffer approximately 100 ng of vector and 300 ng of insert for 2 h at RT.

Ligated constructs were transformed into *E. coli* DH5alpha, *via* heat-shock for 1 min at 42°C and plated on LB medium agar plates amended with 100 μg/mL ampicillin, followed by transformation into *E. coli* C2925 (NEB) for demethylation (Liao et al., 2021). Both *E. coli* and *Hrr. lacusprofundi* colonies were screened *via* colony PCR after transformation. Scratched cell material from each colony was spread on a fresh agar plate and the remaining cell material on the sterile pipet tip was either directly swirled in Q5 PCR master mix aliquots (for *E. coli*) or in 10 μL of sterile ddH_2O (for *Hrr. lacusprofundi*), from which 1 μL was used per colony as the PCR template as described above. Plasmid constructs were verified by Sanger sequencing in-house on the ABI 3130xl Sequence Analyzer (Applied Biosystems, Foster City, United States).

Plasmid construction

The PCR construct to attempt knockout of the *pyrE2* gene by homologous recombination in *Hrr. lacusprofundi* was generated by PCR amplification of the upstream fragment using Pyr_USF and Pyr_USR, the downstream fragment using Pyr_DSF and Pyr_DSR and subsequent fusion of the two fragments by overlapping PCR (as described previously, e.g., Dattani et al., 2022; Supplementary Table 2). The PCR construct was either used directly in a transformation or cloned into the pTA131 vector (Allers et al., 2004) using *Hind*III and *BamH*I restriction sites. For pTA131_*ΔpyrE2_hmgA*, the *hmgA* gene was amplified from pJWID1 (Wendoloski et al., 2001; Liao et al., 2016) using prav_F and prav_R in a two-step PCR. The resulting product was then cloned into pTA131 using *Xba*I and *Not*I restriction sites.

For pTA131_*hmgA*_Δ*trpA*, the *hmgA* gene was cloned into pTA131 as described for pTA131_*ΔpyrE2_hmgA*. Subsequently, upstream (1273UF and 1273UR) and downstream (1273DF and 1273DR) flanking regions of the *trpA* gene Hlac_1273 were amplified separately and fused together in consecutive PCR reactions (as described above). The primers included restriction sites for *Hind*III and *BamH*I, through which the PCR product was cloned into the pTA131_*hmgA* vector. The pTA131_*hmgA*_*ΔHlac_2746* and pTA132_*ΔHlac_2746* vectors were constructed the same way, *via* amplification and fusion of flanking regions of the putative GTPase gene Hlac_2746 (Hlac_2746UF, Hlac_2746UR, Hlac_2746DF, and Hlac_2746DR), followed by insertion into the plasmids (see Supplementary Table 1) with *HindIII* and *BamHI* as described above.

Genetic manipulation of *Hrr. lacusprofundi*

All plasmids were transformed into *E. coli* C2925 (NEB) for demethylation before transformation into *Hrr. lacusprofundi* strains. Transformation of *Hrr. lacusprofundi* was performed as described earlier (Liao et al., 2016) following a PEG_{600}-based protocol with slight modifications. The incubation of the cells with DNA after the addition of PEG_{600} lasted 70 min. Incubation in regeneration buffer was performed overnight at 30°C. For the transformation with pTA132_*ΔHlac_2746*, the *Hrr. lacusprofundi* ACAM34_UNSWΔ*pyrE2*Δ*trpA* transformants were resuspended in regeneration solution containing 10x casamino acids replacing 10x YPC with trace elements and vitamins added in the ratio common for DBCM2 medium (Dyall-Smith, 2009a). Transformants were plated on selective media and liquid cultures were inoculated as well. For *pyrE2* deletions, both ACAM34_UNSW and ACAM34_DSMZ were directly plated on plates containing 150 μg/mL 5-fluoroorotic acid (5-FOA) and 50 μg/mL uracil. For *trpA* deletions, ACAM34_UNSW and ACAM34_UNSWΔ*pyrE2* were grown in DBCM2- media with pravastatin at concentrations indicated. Pop-out was performed on plates containing 150 μg/mL 5-FOA and 50 μg/mL uracil. ACAM34_UNSWΔ*pyrE2*Δ*trpA* mutants S1 and S2 were plated on

DBCM2-media with uracil (50 μg/mL) selecting for pTA132_*ΔHlac_2746* which includes a functional *trpA* gene. The deletion mutant of *Hlac_2746* in ACAM34_UNSWΔ*pyrE2* was subsequently generated by transformation with the pTA131_*hmgA*_*ΔHlac_2746* plasmid and a two-step selection as described above for the *trpA* deletion mutants. We screened liquid cultures and single colonies for the correct insert by colony PCRs and Sanger sequencing as described above.

Genome sequencing and analysis of *trpA* mutants

Library preparation (FS DNA Library, NEBNext® Ultra™) and sequencing (Illumina HiSeq3000, 2 × 150 bp, 1 Gigabase per sample) was performed at the Max Planck-Genome-Centre Cologne (Cologne, Germany). For genome analysis, reads were mapped to ACAM34_UNSW genome using "geneious mapper" (Geneious Prime® 2022.2.1) with medium-low sensitivity and default settings. No reads could be recruited for the described gene deletion.

Results

Attempts to generate uracil auxotroph mutants by directed double crossover resulted in spontaneous mutants with unexpected deletions

Orotate *phosphoribosyltransferase* (*pyrE2)* is an ideal target to generate auxotrophic strains for genetic manipulation. Previous attempts to generate spontaneous *ΔpyrE2* mutants of *Hrr. lacusprofundi* with uracil (U) and 5-fluoroorotic acid (5-FOA) treatments (Bitan-Banin et al., 2003) have been unsuccessful (Liao et al., 2016). Therefore, we attempted to generate *pyrE2* deletions by transforming *Hrr. lacusprofundi* strain ACAM34_UNSW with a knockout (KO) PCR product composed of the fused up- and downstream flanks of the *pyrE2* gene of ACAM34, followed by selection on U/5-FOA plates (Figure 1C). In a successful double-crossover homologous recombination, the construct would be inserted into the genome and mutation of wild-type (WT) genes would be induced by 5-FOA. However, none of the obtained cultures tested showed the expected deletion in the *pyrE2* gene (Supplementary Figure 1), even though single-nucleotide polymorphisms (SNPs) and small insertions or deletions cannot be ruled out. Next, we cloned the KO PCR product into pTA131, a non-replicating vector designed for *H. volcanii* (Allers et al., 2004). We then transformed pTA131_Δ*pyrE2* and pTA131 as control into *Hrr. lacusprofundi* ACAM34_UNSW and ACAM34_DSMZ followed by selection on U/5-FOA plates. Similar growth was detected for both strains, and for both the control and pTA131_Δ*pyrE2*. The majority of colonies tested for ACAM34_UNSW revealed either wild-type size of the gene (approximately 60%) or an increased size of the gene, indicating the insertion of a transposase (approximately 40%) (Supplementary Figure 2) that was confirmed for one representative clone by sequencing. One out of 64 tested colonies revealed a PCR product indicative of a gene deletion; however, wild-type gene copies could still be detected. Haloarchaea are known for being polyploid (Maurer et al., 2018; Ludt and Soppa, 2019) and the mixture of wild-type gene and mutant gene is likely the result of the heterozygous genome of this particular clone. After re-streaking, we obtained a clone (ACAM34_UNSWΔ*pyrE2* S1) with a clean PCR signal for a gene deletion without any apparent background levels of wild-type genes present (Figure 1A; Supplementary Figure 2B). The strain was unable to grow in absence of uracil, confirming the inactivation of the *pyrE2* gene. Surprisingly, sequencing of the genomic region revealed a deletion of 628 base pairs (bp) including the C-terminus of *pyrE2* [amino acids (aa) 73–191] and the C-terminus (last 84 aa) of a downstream gene, Hlac_0585, an ATPase associated with various cellular activities encoded on the opposite strand (Figure 1C). We conclude that this deletion is a spontaneous deletion, because it does not reflect the region we targeted with pTA131_Δ*pyrE2*.

In a third attempt to obtain a clean *pyrE2* deletion in ACAM34_UNSW, we cloned the *hmgA* gene from pJWID1, conferring resistance against pravastatin (Liao et al., 2016), into pTA131_Δ*pyrE2*. Pravastatin selection was used to force the insertion of the KO construct into the genome (pop-in) and then U/5-FOA to force the vector to excise again (pop-out). The construct was transformed into ACAM34_UNSW and two colonies that were positive in PCR screens for the *hmgA* gene were chosen for pop-out after two successive dilutions in 2.5 μg/mL pravastatin. As with previous attempts, a double-crossover homologous recombination could not be achieved (Supplementary Figure 3). Out of 32 screened colonies one clone with a deletion was identified (Supplementary Figure 2C), hereafter referred to as ACAM34_UNSWΔ*pyrE2*_S2 (Figure 1A). Sequencing of the genomic region also showed a deletion identical to ACAM34_UNSWΔ*pyrE2*_S1 that we conclude to be a spontaneous mutation. We are aware that this mutation also affects a second gene. However, we did not detect any major defects in neither growth (Figure 2C) nor morphology (Figure 2D and Supplementary Figure 4). The mutants are furthermore unable to grow on medium without uracil (Figure 1A). Since an in-frame deletion could not be achieved, we selected this auxotrophic mutant for further studies.

A similar phenomenon occurred in ACAM34_DSMZ. None of 40 tested colonies from the transformation with pTA131_Δ*pyrE2*, showed a change in size of the target region. However, out of eight colonies screened from a control transformation with water, two showed increased size and one a reduced size (ACAM34_DSMZΔ*pyrE2*) (Figure 1B; Supplementary Figure 5). Sequencing of the PCR product revealed a short deletion that expands over the promotor region of the gene and the first 16 aa (Figure 1C). After re-streaking of the strain, we were able to isolate a colony that had a clean PCR result for the gene deletion and was not able to grow without uracil (Figure 1B).

Successful in-frame deletion of the *trpA* gene in uracil auxotrophic strains required a double selection

To test whether the newly generated auxotrophic *pyrE2* mutant ACAM34_UNSWΔ*pyrE2*, is stable and suitable to be used for genetic manipulation, we targeted the alpha subunit of the tryptophan synthase (*trpA*, Hlac_1273) that is also commonly used in *H. volcanii* as a second auxotrophic marker (Allers et al., 2004).

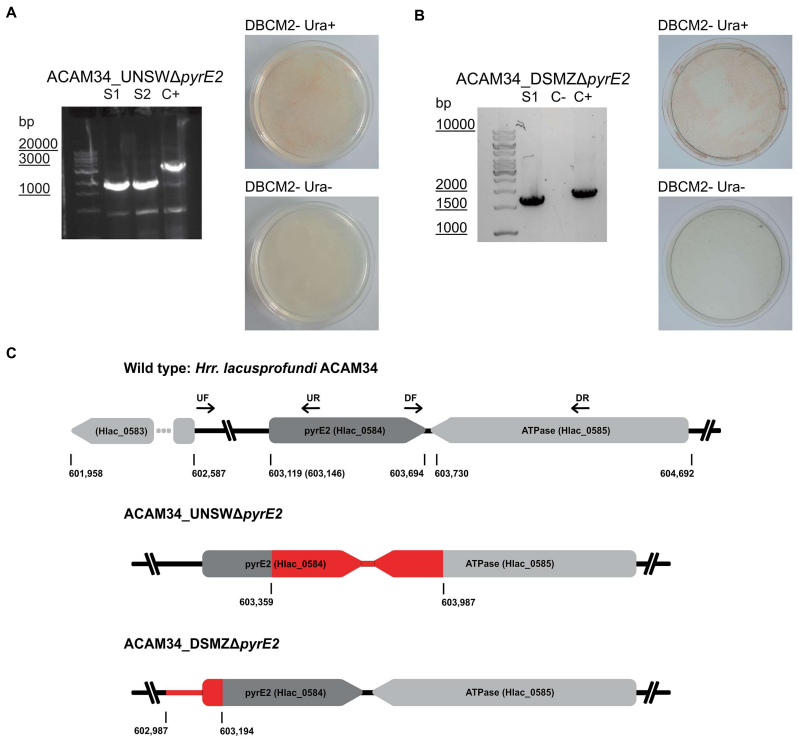

FIGURE 1
Successful *pyrE2* knockout in *Hrr. lacusprofundi* ACAM34 strains. **(A)** Characterization of ACAM34_UNSWΔ*pyrE2* mutants. Left: PCR on the *pyrE2* locus of the two knockout strains S1 and S2 (see also Supplementary Figure 2) and a wild-type ACAM34_UNSW control (C+). Right: Growth of ACAM34_UNSWΔ*pyrE2* on DBCM2- supplemented with uracil (top), and growth defect on DBCM2– without uracil (bottom). **(B)** Characterization of ACAM34_DSMZΔ*pyrE2*. Left: PCR on the *pyrE2* locus of the knockout mutant, ACAM34_DSMZ wild-type DNA served as the positive control (+C) (see also Supplementary Figure 5). Right: Growth of ACAM34_DSMZΔ*pyrE2* on DBCM2- supplemented with uracil (top), and growth defect on DBCM2- without uracil (bottom). **(C)** Schematic representation of the genomes including the wild-type strain ACAM34_UNSW with the position (bp) of *pyrE2* and neighboring genes. ACAM34_DSMZ and ACAM34_UNSW deviate in the length of the annotated *pyrE2* gene, the different position is marked in brackets for ACAM34_DSMZ. The primer binding sites for upstream (UF, UR) and downstream (DF, DR) flanking regions are represented as arrows. The deletion in the ACAM34_UNSWΔ*pyrE2* S1 and S2 clones is identical and highlighted in red. The deletion in ACAM34_DSMZΔ*pyrE2* is also highlighted in red.

Both ACAM34_UNSW and ACAM34_UNSWΔ*pyrE2*_S2 were transformed with pTA131_*hmgA*_Δ*trpA* containing a non-functional *trpA* construct (Figure 3A). While selection of ACAM34_UNSW transformants was only based on pravastatin resistance (2.5 μg/mL) conferred by *hmgA*, ACAM34_UNSWΔ*pyrE2* transformants were selected for the presence of the plasmid with both pravastatin (*hmgA*) and uracil depletion, forcing the uptake of the plasmid with the *H. volcanii pyrE2* gene (83% amino acid identity to ACAM34_UNSW). Growth of transformants was only achieved in liquid cultures and not on solid agar plates. However, while both ACAM34_UNSW and ACAM34_UNSWΔ*pyrE2* were growing in selective media, the presence of the plasmid could only be detected in ACAM34_UNSWΔ*pyrE2* (Supplementary Figure 6). Since ACAM34_UNSW controls transformed with an empty vector (pTA131) or water also showed growth in liquid, we conclude that 2.5 μg/mL pravastatin was not sufficient for selection (Supplementary Figure 6). The slight growth of ACAM34_UNSWΔ*pyrE2* in liquid without uracil was only observed shortly after transformation and we assume that contaminations with uracil in the regeneration buffer could have supported the growth. The ACAM34_UNSWΔ*pyrE2* culture transformed with pTA131_*hmgA*_Δ*trpA* was plated on selective media (2.5 μg/mL pravastatin, DBCM2-) and single colonies were screened by PCR. While the presence of the *hmgA* gene was detectable in all clones, PCR with primers targeting the *trpA* gene on the genome

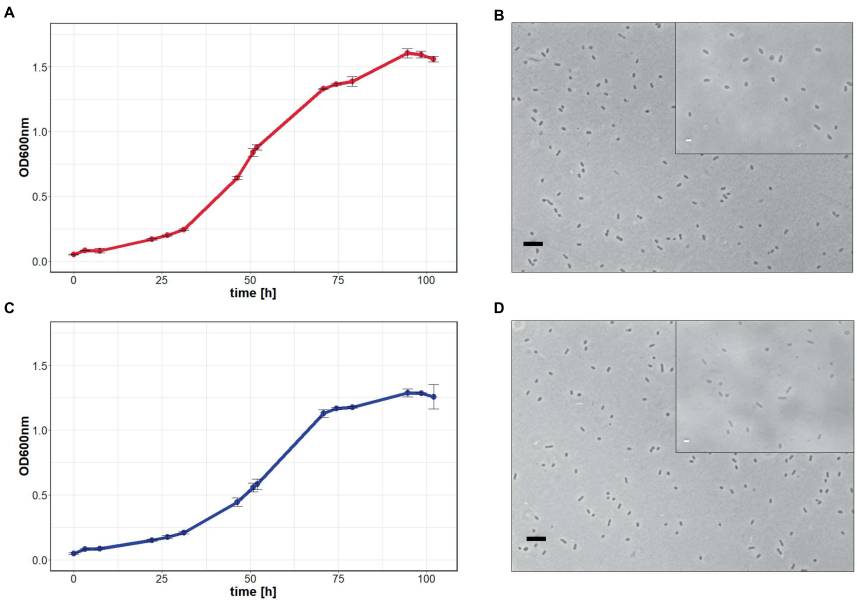

FIGURE 2
Growth comparison of *Hrr. lacusprofundi* ACAM34_UNSW and ACAM34_UNSW*ΔpyrE2*. The growth of wild-type **(A)** and mutant cells **(C)** in rich medium was observed by optical density measurements at 600nm ($OD_{600\ nm}$) over 102h. Points represent the average values and each time point measured, including the standard deviation represented by error bars (n=3). Light microscopy images of wild-type **(B)** and mutant cells **(D)** represent one of the three biological replicates (Supplementary Figure 4). Larger image at 400× magnification, black scale bar indicates 10μm, inlet at 1,000× magnification, white scale bar indicates 2μm.

revealed mixed signal of both WT and mutated *trpA* genes in all samples (Supplementary Figure 7). We concluded that, similar to other haloarchaea (Maurer et al., 2018), *Hrr. lacusprofundi* exhibits several copies of its genome within one cell. The PCR signals from the targeted genomic region suggested that some chromosome copies had already excluded the plasmid, resulting in either a mutated or a wild-type *trpA*, and some wild-type copies might have not taken up the plasmid. To force the cell to exclude chromosome copies without the inserted plasmid before pop-out, we selected three colonies for culturing in increased (7.5 μg/mL) pravastatin concentrations in liquid culture; however, after four generations (G4), no changes were detected by PCR. The following generations were grown in increasing pravastatin concentrations of 10, 15, 20, and 40 μg/mL (G8) and both G4 and G8 were selected for pop-out on U/5-FOA plates. Colonies of G4 and G8 on pop-out plates were screened with genomic primers for the *trpA* gene. G4 colonies, with a PCR signal, all showed the wild-type gene with one exception that resulted in a mixture of wild-type and mutant *trpA* (Supplementary Figure 8). The majority of G8 pop-out clones showed a mixture of wild-type and mutant *trpA*, and five clones with a clean *trpA* deletion were identified (Supplementary Figure 9). These five clones were transferred into both full media (containing tryptophan and uracil) and selective media (with uracil only) to test for tryptophan auxotrophy. Four clones reverted back to WT and were able to grow in selective media, but one clone referred to as ACAM34_UNSW*ΔpyrE2ΔtrpA* was unable to grow without tryptophan (Figure 3D) and PCR confirmed a corrupted *trpA* gene (Figure 3B; Supplementary Figure 10).

After replating, we selected two clones ACAM34_UNSW*ΔpyrE2ΔtrpA* (S1 and S2) for genome sequencing. For both ACAM34_UNSW*ΔpyrE2ΔtrpA* S1 and S2, no reads could be detected for the target region, between the upstream and downstream flanking regions of the non-functional *trpA* construct in pTA131_*hmgA*_*ΔtrpA* (Figure 3C). The gap extends from aa63 to aa265, creating a clean 202aa deletion in both deletion strains without affecting any other genes or non-coding regions (Figure 3C).

A vector designed for *trpA* selection in *H. volcanii* can be used for selection in the tryptophan auxotrophic mutant ACAM34_UNSW*ΔpyrE2ΔtrpA*

All the plasmids created in this study were derived from plasmids originally created for the haloarchaeal model organism *H. volcanii*. For convenience in future experiments, we decided to test whether other plasmids designed for *H. volcanii* could be effectively used in

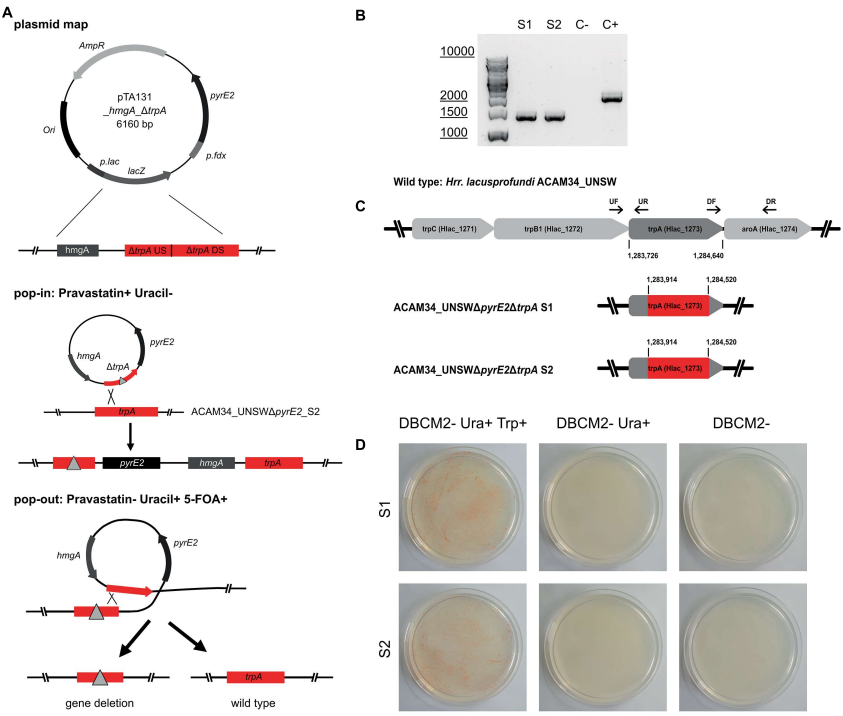

FIGURE 3
Successful *trpA* knockout in *Hrr. lacusprofundi* ACAM34_UNSWΔ*pyrE2*. **(A)** Recombination strategy used to generate ACAM34_UNSWΔ*pyrE2* Δ*trpA via* double selection. A vector based on pTA131 (Allers et al., 2004) (with *pyrE2* for uracil synthesis), was used to insert a pravastatin resistance gene (*hmgA*), as well as a non-functional copy of the *trpA* gene created by the fusion of upstream (US) and downstream (DS) fragments of the gene. Both the non-functional gene (represented by a triangle) and the functional wild-type *trpA* gene are marked in red. Crossover at the *trpA* genes leads to the integration of the plasmid into the genome (pop-in) using uracil depletion and the addition of pravastatin as selection pressure. Excision of the plasmid (pop-out) is enforced by the addition of 5-FOA and uracil, through which either the non-functional construct (left) or the wild-type gene (right) remains in the genome. **(B)** PCR on the *trpA* locus of the two knockout strains S1 and S2, with a wild-type ACAM34_UNSW control (C+) and a negative control (C−). **(C)** Operon encoding genes for tryptophan synthesis in the wild-type strain ACAM34_UNSW including the position (bp) of *trpA* and the primer binding sites for upstream (UF, UR) and downstream (DF, DR) flanking regions amplified for the deletion construct. Deletion in ACAM34_UNSWΔ*pyrE2*Δ*trpA* S1 and in ACAM34_UNSWΔ*pyrE2*Δ*trpA* S2 highlighted in red. **(D)** Growth of ACAM34_UNSWΔ*pyrE2*Δ*trpA* S1 (top) and S2 (bottom) on DBCM2 supplemented with uracil and tryptophan (left), growth defect on DBCM2 with uracil but without tryptophan (middle), growth defect on DBCM2 (right).

Hrr. lacusprofundi without modifications. For this purpose, we selected a putative SAR1 family GTPase (Hlac_2746, Erdmann et al., 2017) as a target gene for a gene knockout. We chose pTA132 (Allers et al., 2004), a non-replicating vector including a functional *H. volcanii trpA* gene. In this case, plasmid uptake would be solely dependent on the *trpA* selection, allowing us to assess the efficiency of *trpA* selection in the newly generated ACAM34_UNSWΔ*pyrE2*Δ*trpA* strain.

We transformed both ACAM34_UNSWΔ*pyrE2*Δ*trpA* strains (S1 and S2) with pTA132_ Δ*Hlac_2746* containing a non-functional Hlac_2746 construct, followed by selection with media lacking tryptophan [DBCM2- and uracil (50 μg/mL)]. Growth was only detected in liquid cultures of S2 transformants that went through regeneration in 10x casamino acids derived medium instead of 10x YPC as in previous transformations (see Methods). No growth was detected for transformants of S1 neither on plates nor in liquid culture.

Without an additional antibiotic selection with pravastatin, we expected a lower selection efficiency and cultivated the transformants over successive generations before pop-out in selective media. After four generations (G4) we screened 34 colonies for plasmid insertion with primers binding in the region outside of Hlac_2746 and a long elongation time (6 min) to detect inserted plasmids (Supplementary Figure 11). Most colonies showed a mixture of both wild-type gene and inserted plasmid (approximately 95%), including two liquid cultures that represented the fifth generation (G5). We concluded that several copies of the genome are present in these cells some with an insertion and some without, as we observed

earlier. We conclude that pTA132 designed for *trpA*-mediated selection in *H. volcanii* was also effective for *trpA*-mediated selection in *Hrr. lacusprofundi*. However, *trpA* selection alone does not seem to be sufficient to force the cells to include the plasmid into all chromosome copies.

We plated G5 on rich medium (DBCM2+ 50 μg/mL uracil and tryptophan) to allow pop-out. After three successive passages (G6-G8) in rich medium, colonies ($n = 22$) screened in G9 either still retained the plasmid (41%), showed a mixture of wild-type Hlac_2746 and mutated Hlac_2746 (18%), a mixture of plasmid insertion and wild type (9%), a mixture of plasmid insertion, wild-type and mutated Hlac_2746 (23%), or no signal at all (9%) (Supplementary Figure 12). Since the insertion of the plasmid into all chromosome copies was already inefficient, it is not surprising that we could not identify any deletion mutants without background signal.

Subsequently, we attempted the knockout of *Hlac_2746* in ACAM34_UNSWΔ*pyrE2* by double selection, using uracil depletion and pravastatin selection as described above. After transformation with pTA131_*hmgA*_Δ*Hlac_2746*, colonies that had successfully taken up the plasmid were subjected to increasing pravastatin concentrations over 8 generations in liquid culture (DBCM2-) followed by pop-out on U/5-FOA plates. Out of 62 colonies, 6 showed a PCR product smaller than wild-type *Hlac_2746* (Supplementary Figure 13), and three of them were confirmed to contain the target deletion by sequencing.

Discussion

The previously reported genetic system for *Hrr. lacusprofundi* that is based on antibiotic selection, inserting the *hmgA* gene into the target gene (Liao et al., 2016), does not exclude effects on gene expression downstream of the deletion. Additionally, it was shown later that *hmgA* can be incorporated from a plasmid into the genome of *Hrr. lacusprofundi*, making it a volatile selection marker (Hamm et al., 2019). In this study, we aimed to generate a uracil auxotrophic mutant for robust selection and for the development of a genetic system allowing us to perform in-frame deletions.

Since generation of spontaneous *pyrE2* mutants on U/5-FOA plates was unsuccessful in a previous study (Liao et al., 2016), we attempted to generate *pyrE2* mutants by double crossover. All three attempts, using either a pure PCR product of the deletion construct or a vector including the deletion construct, with and without antibiotic selection, failed to produce the target deletion. However, we obtained spontaneous *pyrE2* mutants from these experiments for two strains of *Hrr. lacusprofundi* (ACAM34_UNSW and ACAM34_DSMZ). Two auxotrophic mutants of ACAM34_UNSW experienced the exact same deletion in two independent experiments (Figure 1B), suggesting that this deletion, including the 5′-part of a downstream gene, is not random. The strain does not show significant growth defects (Figure 2); therefore, ACAM34_UNSWΔ*pyrE2* was chosen as suitable candidate for further genetic manipulation.

To attempt the generation of an in-frame gene deletion, we chose the *trpA* gene as a target. We tested both wild-type ACAM34_UNSW and the uracil auxotroph ACAM34_UNSWΔ*pyrE2*. Antibiotics selection alone was not sufficient to achieve the uptake of the plasmid in ACAM34_UNSW wild type. However, double selection of the auxotrophic mutant with antibiotic and uracil depletion in ACAM34_UNSWΔ*pyrE2* resulted in a successful uptake. A clean deletion mutant was only isolated from an ACAM34_UNSWΔ*pyrE2* transformant that was subjected to increasing concentrations of pravastatin (up to 40 μg/mL) before pop-out.

We subsequently tested the newly generated ACAM34_UNSWΔ*pyrE2*Δ*trpA* auxotrophic mutant for the efficiency of *trpA*-mediated selection without the additional selection markers *hmgA* and *pyrE2*. The plasmid, including a functional *trpA* gene derived from *H. volcanii*, was successfully taken up under tryptophan depleted conditions. However, an insertion into all chromosome copies could not be achieved without additional selection. Subsequently, we were not able to obtain clean deletion mutants. Haloarchaea are known for polyploidy (Maurer et al., 2018; Ludt and Soppa, 2019). Therefore, successive cultivation under selective conditions is essential to remove any remaining wild-type copies of the gene and selection for auxotrophic markers alone was not efficient in *Hrr. lacusprofundi* over four generations. Extending the selection over more generations might be sufficient, however, is also very time consuming. Alternatively, phosphate starvation, to reduce the number of genome copies (Maurer et al., 2018), could be used to add additional selection pressure. Nevertheless, the double selection with pravastatin and U/5-FOA yielded several clean deletion mutants that were not obtained with *trpA*-mediated selection when targeting the same gene. Both the selection with antibiotics alone and the auxotrophic marker alone proved to be unsuccessful. We conclude that the combination of an auxotrophic selection marker together with antibiotics selection is the most time efficient strategy to achieve clean deletion mutants in *Hrr. lacusprofundi*. Indeed, we and other collaborating laboratories have successfully generated several knockout mutants in *Hrr. lacusprofundi* ACAM34_UNSW using this strategy (unpublished results).

We successfully used plasmids originally designed for the haloarchaeal model organism *H. volcanii* for the genetic manipulation of *Hrr. lacusprofundi*. This opens up the possibility to use the entire genetic tool box available for *H. volcanii* (Dattani et al., 2022; Harrison and Allers, 2022) in *Hrr. lacusprofundi*. In addition to derivatives of the pTA131/132 used for gene knockouts (Liao et al., 2021), vectors for protein overexpression (Allers, 2010), recombinant luciferase (Davis et al., 2020), and fluorescent proteins (Reuter and Maupin-Furlow, 2004) are available to visually track gene expression (Duggin et al., 2015), protein interactions (Winter et al., 2018), and protein location inside of cells (Lestini et al., 2015; Liao et al., 2021; Nußbaum et al., 2021).

In conclusion, we successfully generated uracil and tryptophan auxotrophic mutants of *Hrr. lacusprofundi* ACAM34 and demonstrate that uracil auxotrophic mutants can be genetically manipulated using well-established plasmids designed for the model organism *H. volcanii*.

Data availability statement

The datasets presented in this study can be found in online repositories. Raw data from genome sequencing are available in the NCBI repository (https://www.ncbi.nlm.nih.gov) under BioProjectID: PRJNA894865.

Author contributions

LJG performed the majority of the experimental work. SE performed some of the experiments, conceived, and led the study. LJG and SE performed the primary writing of the manuscript. ID led the initial phase of the study. All authors participated in the analysis and interpretation of the data and contributed to the writing of the manuscript.

Funding

Funding was provided by the Volkswagen Foundation (reference 98 190), Germany, and the Max Planck Society (Munich, Germany). Part of this work was supported by the Australian Research Council Future fellowship to ID (FT160100010).

Acknowledgments

We thank the Max Planck-Genome-Centre Cologne (Cologne, Germany) for assistance with DNA sequencing. We thank Daniela Thies (MPI for Marine Microbiology, Bremen, Germany) for assistance with the experiments. We thank Thorsten Allers and Anita Marchfelder for providing *H. volcanii* plasmids. Finally, we want to thank the Max-Planck-Institute for Marine Microbiology and the Max-Planck-Society for continuous support.

Conflict of interest

The authors declare that the research was conducted in the absence of any commercial or financial relationships that could be construed as a potential conflict of interest.

Publisher's note

All claims expressed in this article are solely those of the authors and do not necessarily represent those of their affiliated organizations, or those of the publisher, the editors and the reviewers. Any product that may be evaluated in this article, or claim that may be made by its manufacturer, is not guaranteed or endorsed by the publisher.

Supplementary material

The Supplementary material for this article can be found online at: https://www.frontiersin.org/articles/10.3389/fmicb.2023.1095621/full#supplementary-material

References

Aguirre Sourrouille, Z., Schwarzer, S., Lequime, S., Oksanen, H. M., and Quax, T. E. F. (2022). The viral susceptibility of the *Haloferax* species. *Viruses* 14:1344. doi: 10.3390/v14061344

Alarcón-Schumacher, T., Naor, A., Gophna, U., and Erdmann, S. (2022). Isolation of a virus causing a chronic infection in the archaeal model organism *Haloferax volcanii* reveals antiviral activities of a provirus. *Proc. Natl. Acad. Sci. U. S. A.* 119:e2205037119. doi: 10.1073/pnas.2205037119

Allers, T. (2010). Overexpression and purification of halophilic proteins in *Haloferax volcanii*. *Bioeng. Bugs* 1, 290–292. doi: 10.4161/bbug.1.4.11794

Allers, T., Ngo, H.-P., Mevarech, M., and Lloyd, R. G. (2004). Development of additional selectable markers for the halophilic archaeon *Haloferax volcanii* based on the *leuB* and *trpA* genes. *Appl. Environ. Microbiol.* 70, 943–953. doi: 10.1128/aem.70.2.943-953.2004

Atanasova, N. S., Demina, T. A., Buivydas, A., Bamford, D. H., and Oksanen, H. M. (2015). Archaeal viruses multiply: Temporal screening in a solar saltern. *Viruses* 7, 1902–1926. doi: 10.3390/v7041902

Atanasova, N. S., Roine, E., Oren, A., Bamford, D. H., and Oksanen, H. M. (2012). Global network of specific virus–host interactions in hypersaline environments. *Environ. Microbiol.* 14, 426–440. doi: 10.1111/j.1462-2920.2011.02603.x

Bitan-Banin, G., Ortenberg, R., and Mevarech, M. (2003). Development of a gene knockout system for the halophilic archaeon *Haloferax volcanii* by use of the *pyrE* gene. *J. Bacteriol.* 185, 772–778. doi: 10.1128/jb.185.3.772-778.2003

Blaseio, U., and Pfeifer, F. (1990). Transformation of *Halobacterium halobium*: Development of vectors and investigation of gas vesicle synthesis. *Proc. Natl. Acad. Sci. U. S. A.* 87, 6772–6776. doi: 10.1073/pnas.87.17.6772

Boeke, J. D., LaCroute, F., and Fink, G. R. (1984). A positive selection for mutants lacking orotidine-5′-phosphate decarboxylase activity in yeast: 5-fluoro-orotic acid resistance. *Mol. Gen. Genet.* 197, 345–346. doi: 10.1007/bf00330984

Correa, T., and Abreu, F. (2020). "Chapter 20 – Antarctic microorganisms as sources of biotechnological products" in *Physiological and biotechnological aspects of extremophiles*. eds. R. Salwan and V. Sharma (Cambridge: Academic Press), 269–284.

DasSarma, S., Capes, M. D., Karan, R., and DasSarma, P. (2013). Amino acid substitutions in cold-adapted proteins from *Halorubrum lacusprofundi*, an extremely halophilic microbe from Antarctica. *PLoS One* 8:e58587. doi: 10.1371/journal.pone.0058587

DasSarma, P., Laye, V. J., Harvey, J., Reid, C., Shultz, J., Yarborough, A., et al. (2017). Survival of halophilic archaea in Earth's cold stratosphere. *Int. J. Astrobiol.* 16, 321–327. doi: 10.1017/S1473550416000410

Dattani, A., Harrison, C., and Allers, T. (2022). "Genetic manipulation of *Haloferax* species" in *Archaea: Methods and protocols*. ed. S. Ferreira-Cerca (New York, NY: Springer US), 33–56.

Davis, C. R., Johnson, C. H., and Robertson, J. B. (2020). A bioluminescent reporter for the halophilic archaeon *Haloferax volcanii*. *Extremophiles* 24, 773–785. doi: 10.1007/s00792-020-01193-x

de Silva, R. T., Abdul-Halim, M. F., Pittrich, D. A., Brown, H. J., Pohlschroder, M., and Duggin, I. G. (2021). Improved growth and morphological plasticity of *Haloferax volcanii*. *Microbiology* 167:001012. doi: 10.1099/mic.0.001012

Duggin, I. G., Aylett, C. H., Walsh, J. C., Michie, K. A., Wang, Q., Turnbull, L., et al. (2015). CetZ tubulin-like proteins control archaeal cell shape. *Nature* 519, 362–365. doi: 10.1038/nature13983

Dyall-Smith, M. (2009a). "Media recipes from the Thorsten Allers lab" in *The halohandbook: Protocols for halobacterial genetics*. ed. M. Dyall-Smith Available at: https://haloarchaea.com/wp-content/uploads/2018/10/Halohandbook_2009_v7.3mds.pdf

Dyall-Smith, M. (2009b). "Medium DBCM2, for square haloarchaea of Walsby ("*Haloquadratum walsbyi*")" in *The halohandbook: Protocols for halobacterial genetics*. ed. M. Dyall-Smith Available at: https://haloarchaea.com/wp-content/uploads/2018/10/Halohandbook_2009_v7.3mds.pdf

Dyall-Smith, M. (2009c). "Trace element solution SL10" in *The halohandbook: Protocols for halobacterial genetics*. ed. M. Dyall-Smith Available at: https://haloarchaea.com/wp-content/uploads/2018/10/Halohandbook_2009_v7.3mds.pdf

Dyall-Smith, M. (2009d). "HF1 and HF2 - examples of lytic, head-tail haloviruses" in *The halohandbook: Protocols for halobacterial genetics*. ed. M. Dyall-Smith Available at: https://haloarchaea.com/wp-content/uploads/2018/10/Halohandbook_2009_v7.3mds.pdf

Erdmann, S., Tschitschko, B., Zhong, L., Raftery, M. J., and Cavicchioli, R. (2017). A plasmid from an Antarctic haloarchaeon uses specialized membrane vesicles to disseminate and infect plasmid-free cells. *Nat. Microbiol.* 2, 1446–1455. doi: 10.1038/s41564-017-0009-2

Franzmann, P., Stackebrandt, E., Sanderson, K., Volkman, J., Cameron, D., Stevenson, P., et al. (1988). *Halobacterium lacusprofundi* sp. nov., a halophilic bacterium isolated from deep Lake, Antarctica. *Syst. Appl. Microbiol.* 11, 20–27. doi: 10.1016/S0723-2020(88)80044-4

Hamm, J. N., Erdmann, S., Eloe-Fadrosh, E. A., Angeloni, A., Zhong, L., Brownlee, C., et al. (2019). Unexpected host dependency of Antarctic nanohaloarchaeota. *Proc. Natl. Acad. Sci. U. S. A.* 116, 14661–14670. doi: 10.1073/pnas.1905179116

Harrison, C., and Allers, T. (2022). "Progress and challenges in archaeal genetic manipulation" in *Archaea: Methods and protocols*. ed. S. Ferreira-Cerca (New York, NY: Springer US), 25–31.

Hartman, A. L., Norais, C., Badger, J. H., Delmas, S., Haldenby, S., Madupu, R., et al. (2010). The complete genome sequence of *Haloferax volcanii* DS2, a model archaeon. *PLoS One* 5:e9605. doi: 10.1371/journal.pone.0009605

Javier, T.-C., Carmen Pire, G., and Rosa María, M.-E. (2017). "Biocompounds from haloarchaea and their uses in biotechnology" in *Archaea, Ch. 4*. eds. S. Haitham, N. Afef and G. Kais (Rijeka: IntechOpen)

Krupovič, M., Forterre, P., and Bamford, D. H. (2010). Comparative analysis of the mosaic genomes of tailed archaeal viruses and proviruses suggests common themes for virion architecture and assembly with tailed viruses of bacteria. *J. Mol. Biol.* 397, 144–160. doi: 10.1016/j.jmb.2010.01.037

Lam, W. L., and Doolittle, W. F. (1992). Mevinolin-resistant mutations identify a promoter and the gene for a eukaryote-like 3-hydroxy-3-methylglutaryl-coenzyme a reductase in the archaebacterium *Haloferax volcanii*. *J. Biol. Chem.* 267, 5829–5834. doi: 10.1016/S0021-9258(18)42628-2

Lestini, R., Delpech, F., and Myllykallio, H. (2015). DNA replication restart and cellular dynamics of Hef helicase/nuclease protein in *Haloferax volcanii*. *Biochimie* 118, 254–263. doi: 10.1016/j.biochi.2015.07.022

Li, J., Gao, Y., Dong, H., and Sheng, G.-P. (2022). Haloarchaea, excellent candidates for removing pollutants from hypersaline wastewater. *Trends Biotechnol.* 40, 226–239. doi: 10.1016/j.tibtech.2021.06.006

Li, M., Wang, R., Zhao, D., and Xiang, H. (2014). Adaptation of the *Haloarcula hispanica* CRISPR-Cas system to a purified virus strictly requires a priming process. *Nucleic Acids Res.* 42, 2483–2492. doi: 10.1093/nar/gkt1154

Liao, Y., Ithurbide, S., Evenhuis, C., Löwe, J., and Duggin, I. G. (2021). Cell division in the archaeon *Haloferax volcanii* relies on two FtsZ proteins with distinct functions in division ring assembly and constriction. *Nat. Microbiol.* 6, 594–605. doi: 10.1038/s41564-021-00894-z

Liao, Y., Williams, T. J., Walsh, J. C., Ji, M., Poljak, A., Curmi, P. M. G., et al. (2016). Developing a genetic manipulation system for the Antarctic archaeon, *Halorubrum lacusprofundi*: Investigating acetamidase gene function. *Sci. Rep.* 6:34639. doi: 10.1038/srep34639

Litchfield, C. D. (2011). Potential for industrial products from the halophilic archaea. *J. Ind. Microbiol. Biotechnol.* 38, 1635–1647. doi: 10.1007/s10295-011-1021-9

Liu, Y., Demina, T. A., Roux, S., Aiewsakun, P., Kazlauskas, D., Simmonds, P., et al. (2021). Diversity, taxonomy, and evolution of archaeal viruses of the class Caudoviricetes. *PLoS Biol.* 19:e3001442. doi: 10.1371/journal.pbio.3001442

Liu, H., Han, J., Liu, X., Zhou, J., and Xiang, H. (2011). Development of *pyrF*-based gene knockout systems for genome-wide manipulation of the archaea *Haloferax mediterranei* and *Haloarcula hispanica*. *J. Genet. Genomics* 38, 261–269. doi: 10.1016/j.jgg.2011.05.003

Ludt, K., and Soppa, J. (2019). Polyploidy in halophilic archaea: Regulation, evolutionary advantages, and gene conversion. *Biochem. Soc. Trans.* 47, 933–944. doi: 10.1042/bst20190256

Luk, A. W., Williams, T. J., Erdmann, S., Papke, R. T., and Cavicchioli, R. (2014). Viruses of haloarchaea. *Life* 4, 681–715. doi: 10.3390/life4040681

Matsuda, R., Suzuki, S., and Kurosawa, N. (2022). Genetic study of four candidate holliday junction processing proteins in the thermophilic crenarchaeon *Sulfolobus acidocaldarius*. *Int. J. Mol. Sci.* 23:707. doi: 10.3390/ijms23020707

Maurer, S., Ludt, K., and Soppa, J. (2018). Characterization of copy number control of two *Haloferax volcanii* replication origins using deletion mutants and haloarchaeal artificial chromosomes. *J. Bacteriol.* 200. doi: 10.1128/jb.00517-17

McGenity, T. J., and Grant, W. D. (1995). Transfer of *Halobacterium saccharovorum*, *Halobacterium sodomense*, *Halobacterium trapanicum* NRC 34021 and *Halobacterium lacusprofundi* to the genus *Halorubrum* gen. Nov., as *Halorubrum saccharovorum* comb. nov., *Halorubrum sodomense* comb. nov., *Halorubrum trapanicum* comb. nov., and *Halorubrum lacusprofundi* comb. nov. *Syst. Appl. Microbiol.* 18, 237–243. doi: 10.1016/S0723-2020(11)80394-2

Mercier, C., Thies, D., Zhong, L., Raftery, M. J., Cavicchioli, R., and Erdmann, S. (2022). In depth characterization of an archaeal virus-host system reveals numerous virus exclusion mechanisms. *bioRxiv*. doi: 10.1101/2022.10.18.512658

Nußbaum, P., Gerstner, M., Dingethal, M., Erb, C., and Albers, S.-V. (2021). The archaeal protein SepF is essential for cell division in *Haloferax volcanii*. *Nat. Commun.* 12:3469. doi: 10.1038/s41467-021-23686-9

Nuttall, S. D., and Dyall-Smith, M. L. (1993). HF1 and HF2: Novel bacteriophages of halophilic archaea. *Virology* 197, 678–684. doi: 10.1006/viro.1993.1643

Piatek, P., Humphreys, C., Raut, M. P., Wright, P. C., Simpson, S., Köpke, M., et al. (2022). Agr Quorum Sensing influences the Wood-Ljungdahl pathway in *Clostridium autoethanogenum*. *Sci. Rep.* 12:411. doi: 10.1038/s41598-021-03999-x

Pietilä, M. K., Roine, E., Sencilo, A., Bamford, D. H., and Oksanen, H. M. (2016). *Pleolipoviridae*, a newly proposed family comprising archaeal pleomorphic viruses with single-stranded or double-stranded DNA genomes. *Arch. Virol.* 161, 249–256. doi: 10.1007/s00705-015-2613-x

Pohlschroder, M., and Schulze, S. (2019). Haloferax volcanii. *Trends Microbiol.* 27, 86–87. doi: 10.1016/j.tim.2018.10.004

Porter, K., Tang, S.-L., Chen, C.-P., Chiang, P.-W., Hong, M.-J., and Dyall-Smith, M. (2013). PH1: An archaeovirus of *Haloarcula hispanica* related to SH1 and HHIV-2. *Archaea* 2013:456318. doi: 10.1155/2013/456318

Redder, P., and Linder, P. (2012). New range of vectors with a stringent 5-fluoroorotic acid-based counterselection system for generating mutants by allelic replacement in *Staphylococcus aureus*. *Appl. Environ. Microbiol.* 78, 3846–3854. doi: 10.1128/AEM.00202-12

Reuter, C. J., and Maupin-Furlow, J. A. (2004). Analysis of proteasome-dependent proteolysis in *Haloferax volcanii* cells, using short-lived green fluorescent proteins. *Appl. Environ. Microbiol.* 70, 7530–7538. doi: 10.1128/AEM.70.12.7530-7538.2004

Singh, A., and Singh, A. K. (2017). Haloarchaea: Worth exploring for their biotechnological potential. *Biotechnol. Lett.* 39, 1793–1800. doi: 10.1007/s10529-017-2434-y

Tschitschko, B., Williams, T. J., Allen, M. A., Páez-Espino, D., Kyrpides, N., Zhong, L., et al. (2015). Antarctic archaea–virus interactions: Metaproteome-led analysis of invasion, evasion and adaptation. *ISME J.* 9, 2094–2107. doi: 10.1038/ismej.2015.110

van Wolferen, M., Pulschen, A. A., Baum, B., Gribaldo, S., and Albers, S. V. (2022). The cell biology of archaea. *Nat. Microbiol.* 7, 1744–1755. doi: 10.1038/s41564-022-01215-8

Wendoloski, D., Ferrer, C., and Dyall-Smith, M. (2001). A new simvastatin (mevinolin)-resistance marker from *Haloarcula hispanica* and a new *Haloferax volcanii* strain cured of plasmid pHV2. The GenBank accession number for the sequence reported in this paper is AF123438. *Microbiology* 147, 959–964. doi: 10.1099/00221287-147-4-959

Williams, T. J., Liao, Y., Ye, J., Kuchel, R. P., Poljak, A., Raftery, M. J., et al. (2017). Cold adaptation of the antarctic haloarchaea *Halohasta litchfieldiae* and *Halorubrum lacusprofundi*. *Environ. Microbiol.* 19, 2210–2227. doi: 10.1111/1462-2920.13705

Winter, K., Born, J., and Pfeifer, F. (2018). Interaction of haloarchaeal gas vesicle proteins determined by Split-GFP. *Front. Microbiol.* 9:1897. doi: 10.3389/fmicb.2018.01897

Supplementary Material

Improving the genetic system for *Halorubrum lacusprofundi* to allow in-frame deletions

L. Johanna Gebhard[1], Iain G. Duggin[2] &
Susanne Erdmann[1]*

[1]Max Planck Institute for Marine Microbiology, Archaeal Virology, Celsiusstrasse 1, 28359, Bremen, Germany.

[2]The Australian Institute for Microbiology and Infection, University of Technology Sydney, Sydney, New South Wales, Australia

Supplementary Material

Table of Contents

Supplementary Figures

Supplementary Figure 6: Transformation of pTA131_*hmgA*_Δ*trpA* into ACAM34_UNSW strains.

Supplementary Figure 7: PCR using genomic primers targeting *trpA* on ACAM34_UNSWΔ*pyrE2* transformants positive for pTA131_*hmgA*_Δ*trpA.*

Supplementary Figure 8: Pop-out of G4 of ACAM34_UNSWΔ*pyrE2* transformants positive for pTA131_*hmgA*_Δ*trpA.*

Supplementary Figure 9: Pop-out of G8 of ACAM34_UNSWΔ*pyrE2* transformants positive for pTA131_*hmgA*_Δ*trpA.*

Supplementary Figure 10: Test for tryptophan auxotrophy of ACAM34_UNSWΔ*pyrE2*Δ*trpA* strains.

Supplementary Figure 11: PCR using primers targeting *Hlac_2746* in ACAM34_UNSWΔ*pyrE2*Δ*trpA* S2 transformants**.**

Supplementary Figure 12: Screening of G9 of pTA132_Δ*Hlac_2746* transformants of ACAM34_UNSW*ΔpyrE2*Δ*trpA* S2 for successful pop-out.

Supplementary Figure 13: Screening of G8 of pTA131_hmgA_Δ*Hlac_2746* transformants of ACAM34_UNSWΔ*pyrE2* for successful pop-out.

Supplementary Tables

Supplementary Table 1: Plasmids used in this study

Supplementary Table 2: Primers used in this study

Supplementary References

1. Allers, T., Ngo, H.-P., Mevarech, M., & Lloyd, R. G. (2004). Development of Additional Selectable Markers for the Halophilic Archaeon Haloferax volcanii Based on the leuB and trpA Genes. Applied and Environmental Microbiology, 70(2), 943-953. doi:10.1128/aem.70.2.943-953.2004

2. Liao, Y., Williams, T. J., Walsh, J. C., Ji, M., Poljak, A., Curmi, P. M. G., Duggin, I. G., Cavicchioli, R. (2016). Developing a genetic manipulation system for the Antarctic archaeon, Halorubrum lacusprofundi: investigating acetamidase gene function. Scientific Reports, 6, 34639. doi:10.1038/srep34639

Supplementary Figures

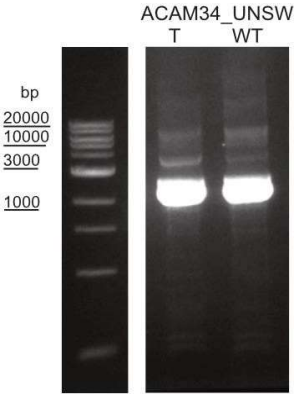

Supplementary Figure 1. Attempt of a Δ*pyrE2* deletion in *Hrr. lacusprofundi* ACAM34_UNSW using a PCR product of the Δ*pyrE2* construct. PCR with primers targeting the *pyrE2* gene region, on a liquid culture of cell material scratched from plates with a lawn of transformants. Samples from left to right: DNA Ladder (GeneRuler 1 kb Plus DNA Ladder, Thermo Scientific™)), (T) ACAM34_UNSW transformant culture and (WT) ACAM34_UNSW wild type control. DNA was separated on 1% agarose gels and stained with SYBR™ Safe.

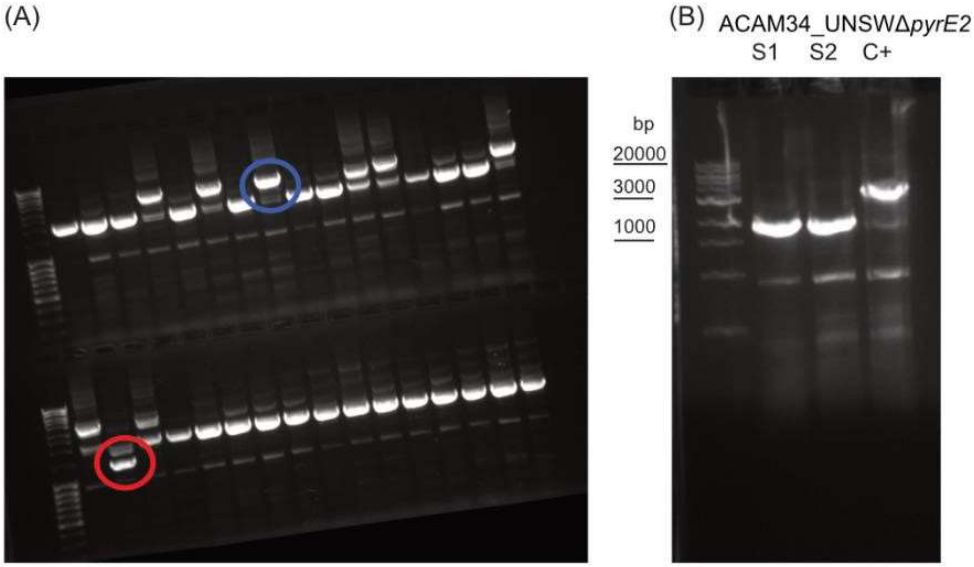

Supplementary Figure 2. Δ*pyrE2* deletion in ACAM34_UNSW using pTA131_Δ*pyrE2*.

Colony PCR with primers for the *pyrE2* gene region. (A) an exemplary colony with a transposon insertion is marked with a blue circle and the only colony with a deletion (ACAM34_UNSW_Δ*pyrE2*) is marked with a red circle. (B) two clones (S1 and S2 (for S2 see Supplementary Figure 3)) of ACAM34_UNSWΔ*pyrE2* after re-streaking together with a wild type ACAM_UNSW control (C+). First lane from the left in all panels: DNA marker (GeneRuler 1 kb Plus DNA Ladder, Thermo Scientific™). DNA was separated on 1% agarose gels and stained with SYBR™ Safe.

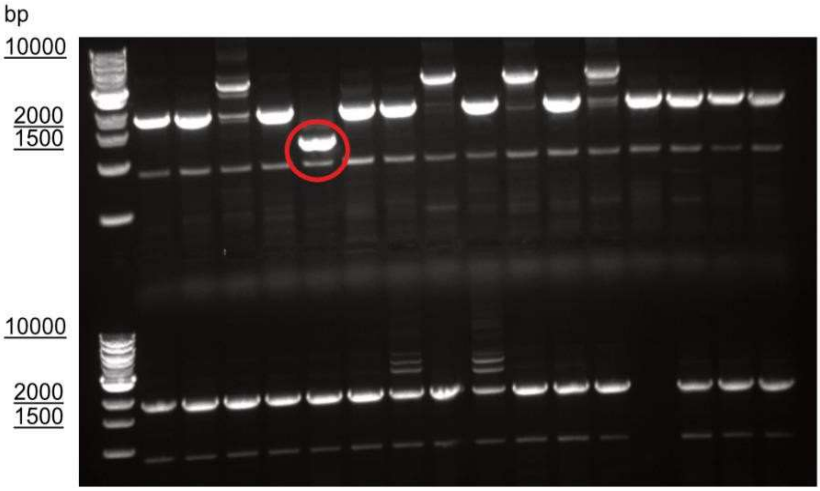

Supplementary Figure 3. Δ*pyrE2* deletion in ACAM34_UNSW using pTA131_Δ*pyrE2_hmgA*. Colony PCR with primers targeting the *pyrE2* gene on pTA131_Δ*pyrE2_hmgA* transformants. One colony showed a *pyrE2* gene of reduced size (labelled with a red circle) and was subsequently sequenced (ACAM34_UNSWΔ*pyrE2* S2). First lane from the left in all panels: DNA marker (GeneRuler 1 kb Plus DNA Ladder, Thermo Scientific™). DNA was separated on 1% agarose gels and stained with SYBR™ Safe.

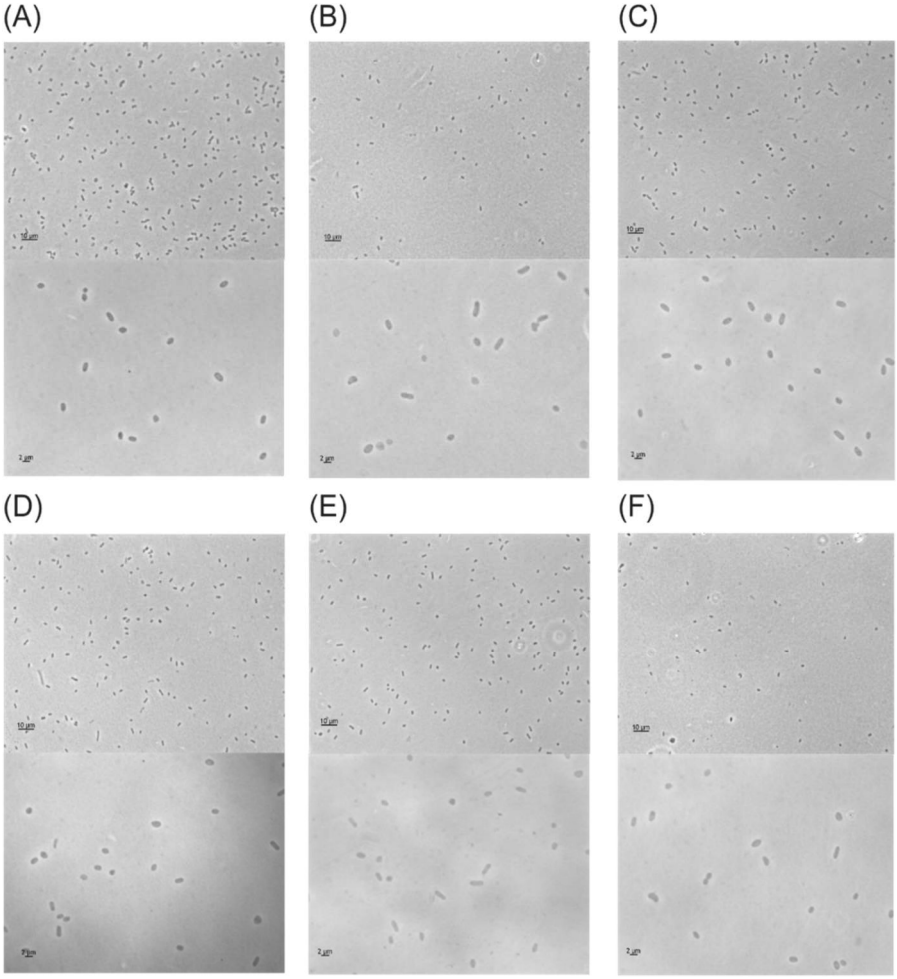

Supplementary Figure 4: Light microscopy images from wild type and mutant *Hrr. lacusprofundi* cultures. Cells imaged during mid-exponential growth (OD_{600}: 0.55-0.65) on agar coated slides (4%). (A- C) three biological replicates of ACAM34_UNSW cultures, (D-F) three biological replicates of ACAM34_UNSWΔ*pyrE2* cultures. Top images at 400x magnification, scale bars represent 10 µm. Bottom images at 1000x magnification, scale bars represent 2 µm.

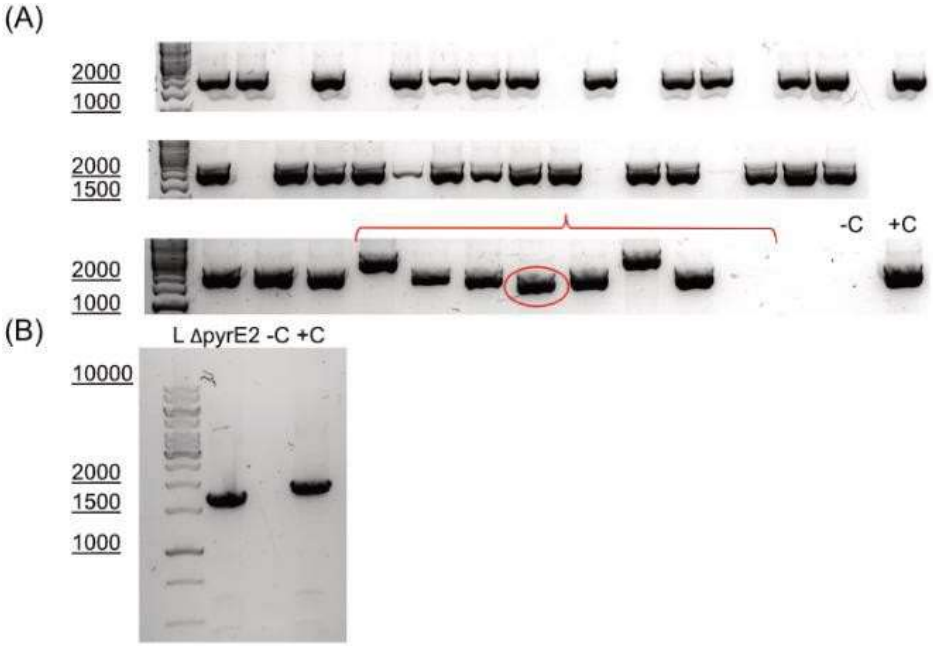

Supplementary Figure 5: Δ*pyrE2* deletion using pTA131_Δ*pyrE2* in ACAM34_DSMZ. (A) Colony PCR with primers targeting the *pyrE2* gene on pTA131_Δ*pyrE2* transformants and on colonies from a H_2O control transformation (marked with a red bracket). A colony with a PCR product that was slightly reduced in size (labelled with a red circle) was chosen for further characterization (ACAM_DSMZΔ*pyrE2*). (B) PCR with primers targeting the *pyrE2* gene on ACAM34_DSMZΔ*pyrE2* after propagation of the colony in liquid media. ACAM34_DSMZ wild type served as control (+C). First lane from the left in all panels: DNA marker (GeneRuler 1 kb Plus DNA Ladder, Thermo Scientific™). DNA was separated on 1% agarose gels and stained with SYBR™ Safe.

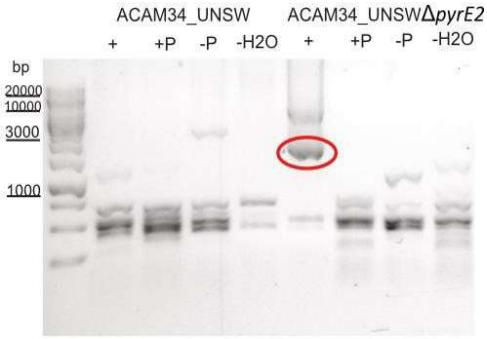

Supplementary Figure 6: Transformation of pTA131_*hmgA*_Δ*trpA* into ACAM34_UNSW strains. PCR with primers targeting the *hmgA* gene on pTA131_*hmgA*_Δ*trpA* on liquid cultures of transformants of ACAM34_UNSW and ACAM34_UNSWΔ*pyrE2*. (+) pTA131_*hmgA*_Δ*trpA*, (+P) pTA131_*hmgA* control, (- P) pTA131 control, (-H_2O) H_2O control. pTA131_*hmgA*_Δ*trpA* could only be detected in ACAM34_UNSWΔ*pyrE2* (red circle). Remaining bands are products of unspecific primer binding. First lane from the left: DNA marker (GeneRuler 1 kb Plus DNA Ladder, Thermo Scientific™). DNA was separated on 1% agarose gels and stained with SYBR™ Safe.

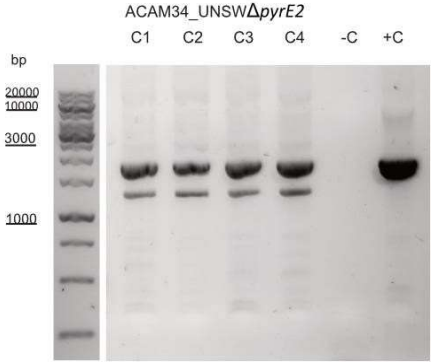

Supplementary Figure 7: PCR using genomic primers targeting *trpA* on ACAM34_UNSWΔ*pyrE2* transformants positive for pTA131_*hmgA*_Δ*trpA*. PCR with primers targeting the *trpA* gene on pTA131_*hmgA*_Δ*trpA* transformants of ACAM34_UNSWΔ*pyrE2*. (C1-C4) Colonies 1-4, (-C) negative control, (+C) positive control. All transformants show a mixture of wild type and mutant *trpA*. First lane from the left: DNA marker (GeneRuler 1 kb Plus DNA Ladder, Thermo Scientific™). DNA was separated on 1% agarose gels and stained with SYBR™ Safe.

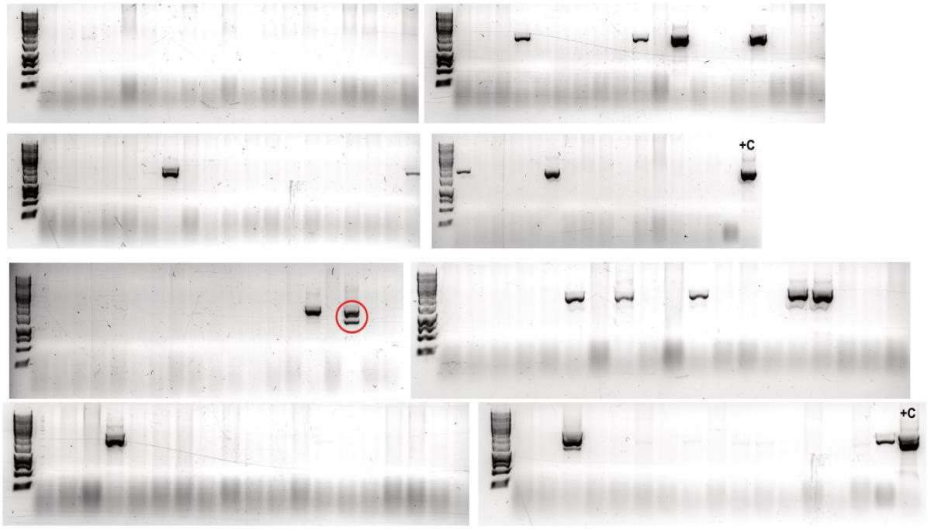

Supplementary Figure 8: Pop-out of G4 of ACAM34_UNSWΔ*pyrE2* transformants positive for pTA131_*hmgA*_Δ*trpA*. PCR using genomic primers targeting *trpA* on colonies of pTA131_*hmgA*_Δ*trpA* transformant ACAM34_UNSWΔ*pyrE2* after pop-out of G4. (+C) positive control. Lanes with no signal are colonies that still include the plasmid where the pop-out was not successful. Only one colony showed a mixture of wild type and mutant *trpA* (red circle). First lane from the left in all panels: DNA marker (GeneRuler 1 kb Plus DNA Ladder, Thermo Scientific™). DNA was separated on 1% agarose gels and stained with SYBR™ Safe.

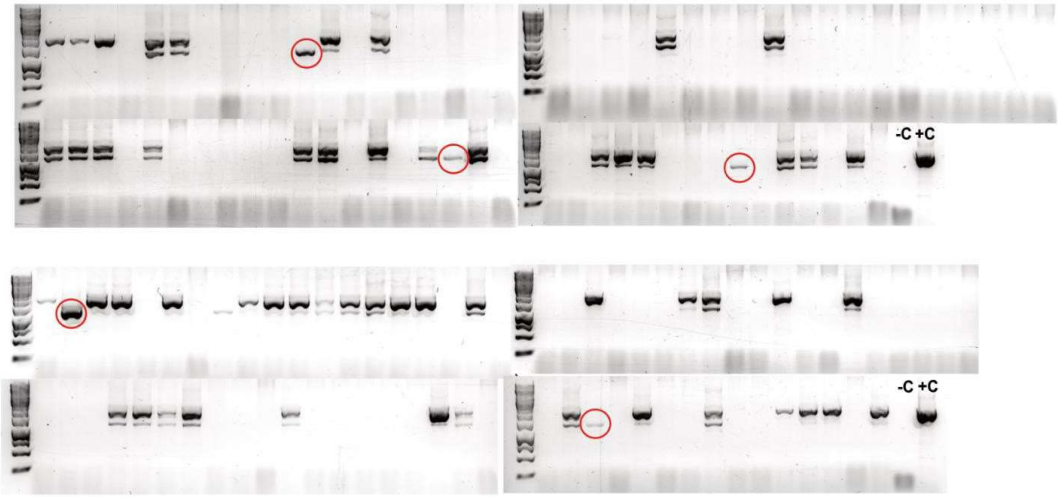

Supplementary Figure 9: Pop-out of G4 of ACAM34_UNSWΔ*pyrE2* transformants positive for pTA131_*hmgA*_Δ*trpA*. PCR using genomic primers targeting *trpA* on colonies of pTA131_*hmgA*_Δ*trpA* transformant ACAM34_UNSWΔ*pyrE2* after pop-out of G8. (+C) positive control, (-C) negative control. Lanes with no signal are colonies that still include the plasmid where the pop-out was not successful. The majority of colonies showed a mixture of wild type and mutant *trpA,* only five appeared to have a clean deletion (red circles). First lane from the left in all panels: DNA marker (GeneRuler 1 kb Plus DNA Ladder, Thermo Scientific™). DNA was separated on 1% agarose gels and stained with SYBR™ Safe.

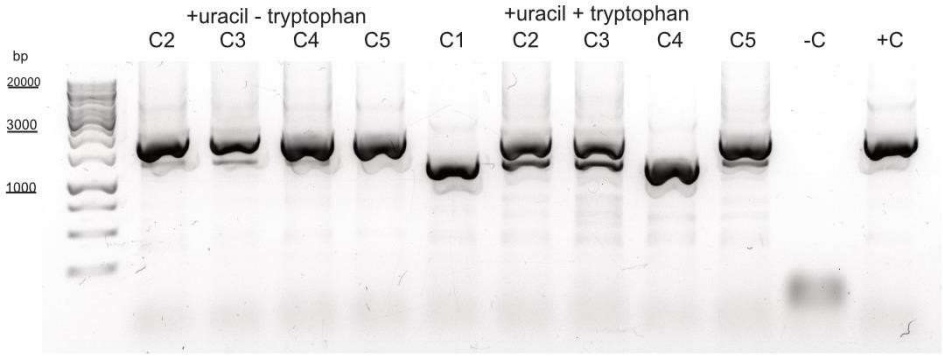

Supplementary Figure 10: Test for tryptophan auxotrophy of ACAM34_UNSWΔ*pyrE2*Δ*trpA* strains. PCR using genomic primers targeting *trpA* on 5 potential ACAM34_UNSWΔ*pyrE2*Δ*trpA* clones (+C) positive control, (-C) negative control. (C1-C5) Colonies 1-5. C2-5 converted to wild type in media without tryptophan, indicating that they had some remaining wild type copies of *trpA*. C1 was not able to grow in in media without tryptophan and shows a clean deletion in the *trpA* gene. First lane from the left: DNA marker (GeneRuler 1 kb Plus DNA Ladder, Thermo Scientific™). DNA was separated on 1% agarose gels and stained with SYBR™ Safe.

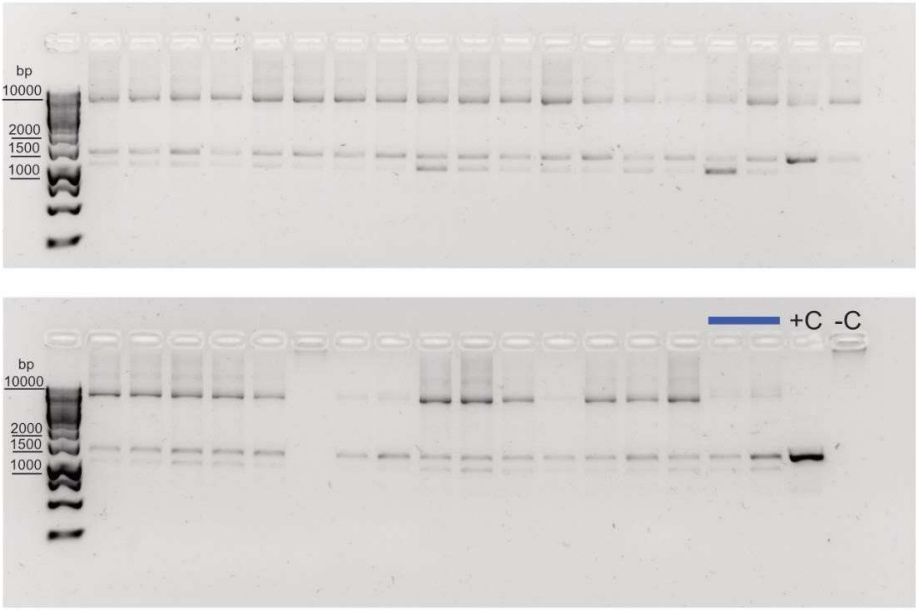

Supplementary Figure 11: PCR using primers targeting *Hlac_2746* in ACAM34_UNSWΔ*pyrE2*Δ*trpA* S2 transformants. PCR using genomic primers targeting the predicted GTPase (*Hlac_2746*) on 36 potential ACAM34_UNSWΔ*pyrE2*Δ*trpA* pTA132_*ΔHlac_2746* transformants with 6 min elongation (+C) positive control wild type ACAM_UNSW genomic DNA, (-C) negative control (H_2O). (C1-C34) colonies from G4 after successive culturing in selective media. (C35-36, marked with blue bar) liquid cultures (G5) after cell material was scratched from G4 plates. Bands at around 1500 bp indicate wild type Hlac_2746 presence, larger bands near 10,000 bp indicate the presence of the knockout plasmid integrated into the genome (successful pop-in). Smaller than WT bands could indicate already mutated *Hlac_2746*. First lane from the left in both gels: DNA marker (GeneRuler 1 kb Plus DNA Ladder, Thermo Scientific™). DNA was separated on 1% agarose gels and stained with SYBR™ Safe.

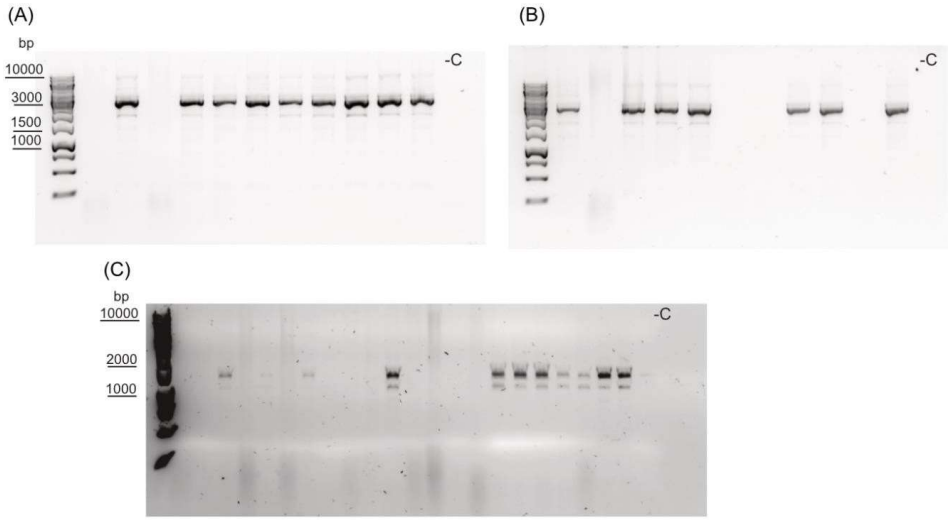

Supplementary Figure 12: Screening of G9 of pTA132_Δ*Hlac_2746* transformants of ACAM34_UNSWΔ*pyrE2* Δ*trpA* S2 for successful pop-out. PCRs targeting the predicted GTPase (Hlac_2746) on 22 potential ACAM34_UNSWΔ*pyrE2*Δ*trpA*Δ*Hlac_2746* clones. (A-B) PCR with forward primer binding the genome outside of *Hlac_2746* and the reverse primer binding pTA132. (-C) negative controls (H_2O), (A) C1-11 and (B) C12-22 colonies picked from G9 plates. Amplified bands indicate plasmid presence in the genome and an unsuccessful pop-out. (C) PCR using genomic primers targeting *Hlac_2746* on C1-22, (-C) negative control (H_2O). Amplified fragments indicate either wild type or mutated *Hlac_2746*, while no amplification indicates plasmid presence (unsuccessful pop-out). First lane from the left: DNA marker (GeneRuler 1 kb Plus DNA Ladder, Thermo Scientific™). DNA was separated on 1% agarose gels and stained with SYBR™ Safe.

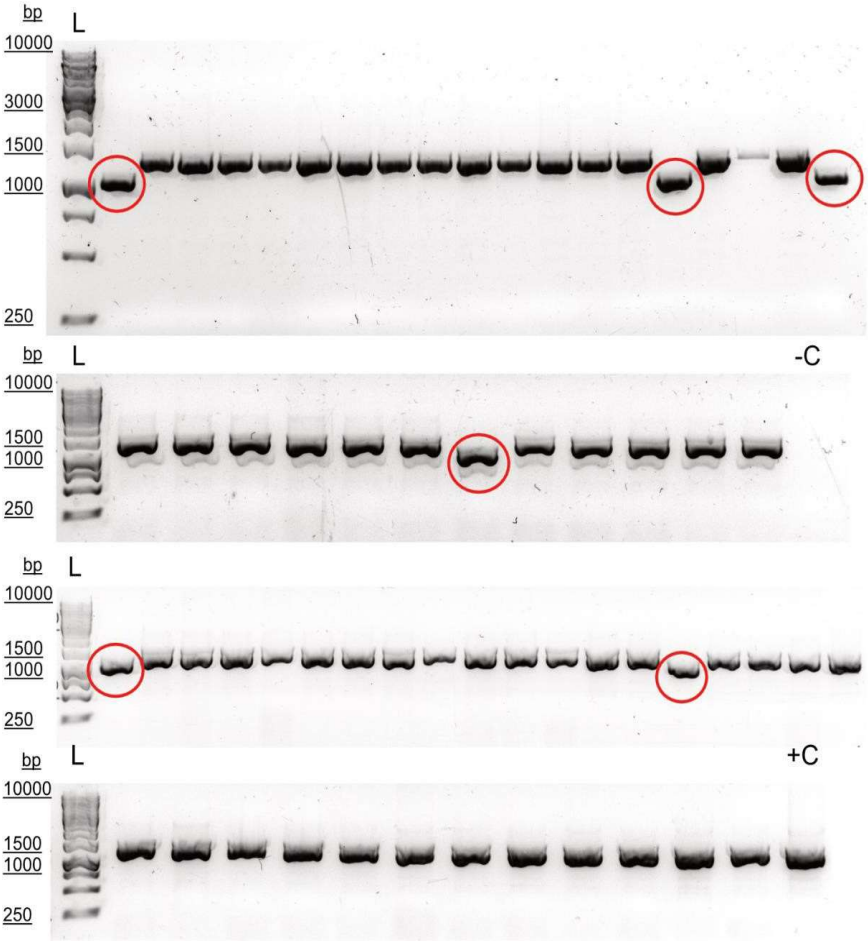

Supplementary Figure 13: Screening of G8 of pTA131_*hmgA*_Δ*Hlac_2746* transformants of ACAM34_UNSW Δ*pyrE2* for successful pop-out. PCR targeting the predicted GTPase (*Hlac_2746*) on 62 potential ACAM34_UNSWΔ*pyrE2*Δ*Hlac_2746* clones. Clones with PCR signals for mutated *Hlac_2746* are marked with red circles. (-C) negative control with ddH_2O, (+C) positive control with wild type ACAM34_UNSW genomic DNA. First lane from the left: DNA marker (GeneRuler 1 kb Plus DNA Ladder, Thermo Scientific™). DNA was separated on 1% agarose gels and stained with SYBR™ Safe.

Supplementary Tables

Supplementary Table 1: Plasmids used in this study

plasmid	Relevant properties	Reference or source
pTA131	pBluescript II derived, non-replicative *H. volcanii* plasmid containing *pyrE2*	[1]
pTA131_Δ*pyrE2*	pTA131 with *Hind*III and *Bam*HI fragment containing *pyrE2* nonfunctional construct for gene inactivation	This study
pTA131_*hmgA*	pTA131 with *hmgA* from pJWID1 inserted with *Xba*I and *Not*I to confer pravastatin resistance	This study
pTA131_*ΔpyrE2_ hmgA*	pTA131_Δ*pyrE2* with *hmgA* from pJWID1 inserted with *Xba*I and *Not*I to confer pravastatin resistance	This study
pTA131_*hmgA_ ΔtrpA*	pTA131_*hmgA* with *Hind*III and *Bam*HI fragment containing *trpA* nonfunctional construct for gene inactivation and a functional *pyrE2* gene for complementation	This study
pTA131_*hmgA_ ΔHlac_2746*	pTA131_*hmgA* with *Hind*III and *Bam*HI fragment containing Hlac_2746 (GTPase) nonfunctional construct for gene inactivation and a functional *pyrE2* gene for complementation	This study
pTA132	pBluescript II derived, non-replicative *H. volcanii* plasmid containing *trpA*	[1]
pTA132_ *ΔHlac_2746*	pTA132 with *Hind*III and *Bam*HI fragment containing GTPase (Hlac_2746) nonfunctional construct for gene inactivation	This study
pJWID1	*H.volcanii* shuttle vector containing *pyrE2*, *hdrB*, *hmgA*, *bla*, SmRS-GFP and pHV2 origin of replication	[2]

Supplementary Table 2: Primers used in this study

Name	Sequence 5' -> 3'	Description	product length (bp)	annealing temperature Q5 polymerase (°C)	Restriction Sites (if applicable)
Pyr_USF	CCGGCCAAGCTTGTGAATAT GTTGATCCGAGCGTG	Forward primer to amplify upstream region of *Hrr. lacusprofundi pyrE2* gene *Hlac_0584* for knock out	686	58 -> 72	*Hind*III
Pyr_USR	GAATTCGCCGCCCGAAGATC TGTACTTGTCGACGTAGTAGT CGC	Reverse primer to amplify upstream region of *Hrr. lacusprofundi pyrE2* gene *Hlac_0584* for knock out	686	58 -> 72	*Eco*RI & *Bgl*II
Pyr_DSF	AGATCTTCGGGCGGCGAATT CGACGGAATTGCTGGCGGAA CGC	Forward primer to amplify downstream region of *Hrr. lacusprofundi pyrE2* gene *Hlac_0584* for knock out	637	58 -> 72	*Eco*RI & *Bgl*II
Pyr_DSR	CCGGCCGGATCCCTACGTCA TCGCGACGCAGAAC	Reverse primer to amplify downstream region of *Hrr. lacusprofundi pyrE2* gene *Hlac_0584* for knock out	637	58 -> 72	*Bam*HI
Seq_PyrF	GATGAACGTGCGCCGAGAGA C	Forward genomic sequencing primer binding upstream of *Hrr. lacusprofundi pyrE2* gene *Hlac_0584*	1923 (WT)	70	

Seq_PyrR	CGACCTCCTTCCCAGCGACG TG	Reverse genomic sequencing primer binding downstream of *Hrr. lacusprofundi pyrE2* gene *Hlac_0584*	1923 (WT)	70	
prav_F	CTCATCTAGAGTGCCTAATGA GTGAGCTAAC	Forward primer for cloning of *hmgA* gene (*Haloferax*) into pTA131	1550	58 -> 72	*Xba*I
prav_R	CTCAGCGGCCGCACTCTGAA CCTATGAATCGAG	Reverse primer for cloning of *hmgA* gene (*Haloferax*) into pTA131	1550	58 -> 72	*Not*I
1273UPF	CCGGCCAAGCTTGGAAGAGT TCCACGAGGAAC	Forward primer to amplify upstream region of *Hrr. lacusprofundi trpA* gene *Hlac_1273* for knock out	330	64 -> 72	*Hind*III
1273UPR	GAATTCGCCGCCCGAAGATC TCGAGAACGGGAGTCCGAGT	Reverse primer to amplify upstream region of *Hrr. lacusprofundi trpA* gene *Hlac_1273*	330	64 -> 72	*Eco*RI & *Bgl*II
1273DSF	AGATCTTCGGGCGGCGAATT CGTCGAGGACGACCTCTCGA C	Forward primer to amplify downstream region of *Hrr. lacusprofundi trpA* gene *Hlac_1273*	650	66 -> 72	*Eco*RI & *Bgl*II
1273DSR	CCGGCCGGATCCGTCCGAGC GATTCAGGATCTG	Forward primer to amplify downstream region of *Hrr. lacusprofundi trpA* gene *Hlac_1273*	650	66 -> 72	*Bam*HI
1273seqF_v2	CAGATCATGGAGAGCCACTC G	Forward genomic sequencing primer binding upstream of *Hrr. lacusprofundi trpA* gene *Hlac_1273*	1870 (WT)	69	
1273seqR_v2	GTAGCCGGTTTTCACCACGT C	Reverse genomic sequencing primer binding downstream of *Hrr. lacusprofundi trpA* gene *Hlac_1273*	1870 (WT)	69	

Hlac_2746UF	CCGGCCAAGCTTCTGACGCA GTTCTTAAGTG	Forward primer to amplify upstream region of *Hrr. lacusprofundi GTPase* gene *Hlac_2746* for knock out	321	61 -> 72	*Hind*III
Hlac_2746UR	GAATTCGCCGCCCGAAGATC TCGAGTTTCGTGTGGAATGTG	Reverse primer to amplify upstream region of *Hrr. lacusprofundi GTPase* gene *Hlac_2746* for knock out	321	61 -> 72	*Eco*RI & *Bgl*II
Hlac_2746DF	AGATCTTCGGGCGGCGAATT CGATGCTCATCGGGATCATC	Forward primer to amplify downstream region of *Hrr. lacusprofundi GTPase* gene *Hlac_2746* for knock out	525	66 -> 72	*Eco*RI & *Bgl*II
Hlac_2746DR	CCGGCCGGATCCGAGCTTCT GGGTCGAGTTG	Reverse primer to amplify downstream region of *Hrr. lacusprofundi GTPase* gene *Hlac_2746* for knock out	525	66 -> 72	*Bam*HI
Hlac_2746KO F	CGAATAAGTAAACAACCGATA TC	Forward genomic sequencing primer binding upstream of *Hrr. lacusprofundi GTPase* gene *Hlac_2746*	1270	59	
Hlac_2746KO R	GGTGTGGCATTTACTTACG	Reverse genomic sequencing primer binding downstream of *Hrr. lacusprofundi GTPase* gene *Hlac_2746*	1270	59	
M13/pUC_R	AGCGGATAACAATTTCACACA GG	Reverse plasmid screening primer for pUC/pTA plasmids	ca. 200	66	

Chapter II

Influence of N-Glycosylation on Virus-Host Interactions in *Halorubrum lacusprofundi*

Influence of N-Glycosylation on Virus-Host Interactions in *Halorubrum lacusprofundi*

L. Johanna Gebhard[#], Zlata Vershinin[#], Tomás Alarcón-Schumacher, Jerry Eichler & Susanne Erdmann

# These authors contributed equally to this work

* Manuscript published in *Viruses*

Author contributions: L.J.G. performed experiments with HRTV-DL1 and PVs, and performed strain characterization. Z.V. generated the Δ*aglB* mutant strain and performed strain characterization. T.A.S. performed experiments with HFPV-1. S.E. and J.E. conceived and led the study, and L.J.G and S.E. performed the primary writing of the manuscript. All authors participated in the analysis and interpretation of the data and contributed to the writing of the manuscript.

viruses

MDPI

Article

Influence of N-Glycosylation on Virus–Host Interactions in *Halorubrum lacusprofundi*

L. Johanna Gebhard [1,†], Zlata Vershinin [2,†], Tomás Alarcón-Schumacher [1], Jerry Eichler [2,*] and Susanne Erdmann [1,*]

[1] Max Planck Institute for Marine Microbiology, Archaeal Virology, 28359 Bremen, Germany
[2] Department of Life Sciences, Ben-Gurion University of the Negev, Beersheva 84105, Israel
* Correspondence: jeichler@bgu.ac.il (J.E.); serdmann@mpi-bremen.de (S.E.)
† These authors contributed equally to this work.

Abstract: N-glycosylation is a post-translational modification of proteins that occurs across all three domains of life. In Archaea, N-glycosylation is crucial for cell stability and motility, but importantly also has significant implications for virus–host interactions. While some archaeal viruses present glycosylated proteins or interact with glycosylated host proteins, the direct influence of N-glycosylation on archaeal virus–host interactions remains to be elucidated. In this study, we generated an N-glycosylation-deficient mutant of *Halorubrum lacusprofundi*, a halophilic archaeon commonly used to study cold adaptation, and examined the impact of compromised N-glycosylation on the infection dynamics of two very diverse viruses. While compromised N-glycosylation had no influence on the life cycle of the head-tailed virus HRTV-DL1, we observed a significant effect on membrane-containing virus HFPV-1. Both intracellular genome numbers and extracellular virus particle numbers of HFPV-1 were increased in the mutant strain, which we attribute to instability of the surface-layer which builds the protein envelope of the cell. When testing the impact of compromised N-glycosylation on the life cycle of plasmid vesicles, specialized membrane vesicles that transfer a plasmid between host cells, we determined that plasmid vesicle stability is strongly dependent on the host glycosylation machinery. Our study thus provides important insight into the role of N-glycosylation in virus–host interactions in Archaea, while pointing to how this influence strongly differs amongst various viruses and virus-like elements.

Keywords: archaea; archaeal virus; haloarchaea; protein glycosylation; virus

check for updates

Citation: Gebhard, L.J.; Vershinin, Z.; Alarcón-Schumacher, T.; Eichler, J.; Erdmann, S. Influence of N-Glycosylation on Virus–Host Interactions in *Halorubrum lacusprofundi*. *Viruses* **2023**, *15*, 1469. https://doi.org/10.3390/v15071469

Academic Editor: Mikael Skurnik

Received: 30 April 2023
Revised: 23 June 2023
Accepted: 26 June 2023
Published: 28 June 2023

Copyright: © 2023 by the authors. Licensee MDPI, Basel, Switzerland. This article is an open access article distributed under the terms and conditions of the Creative Commons Attribution (CC BY) license (https://creativecommons.org/licenses/by/4.0/).

1. Introduction

Protein glycosylation is a post-translational modification involving the attachment of sugar multimers, or glycans, to specific amino acid residues within a protein. N-glycosylation refers to the attachment of glycans to the nitrogen atom of the amino acid asparagine (Asn), while O-glycosylation involves the attachment of glycans to the oxygen atom of the amino acid serine or threonine. Long thought to be restricted to Eukarya, it is now clear that Archaea are also capable of protein glycosylation. Detailed understanding of N-glycosylation pathways has been obtained for some archaeal species [1], and genome analysis suggests that N-glycosylation is an almost universal trait of Archaea [2–6]. In contrast, O-glycosylation has so far only been observed in a few species, and very little is known of how Archaea perform this modification [1].

In halophilic Archaea (haloarchaea), Archaea that thrive in environments characterized by high salt concentrations, N-glycosylation is important for protein folding, stability, and function [2,7–9]. For example, N-glycosylation of the surface (S)-layer glycoprotein, comprising the protein envelope of haloarchaeal cells, is important for cell stability. Additionally, glycan-based modification of haloarchaeal proteins was shown to provide unique markers for pair recognition of mating cells [10,11], for virus–host recognition [12,13] and for virus evasion [11].

In haloarchaea, the N-glycosylation pathway has been extensively studied in the model organism *Haloferax volcanii*. Here, four glycosyltransferases sequentially add four soluble monosaccharides onto a dolichol phosphate carrier on the cytoplasmic side of the plasma membrane [14–17]. The lipid-linked tetrasaccharide is then flipped to face the extracellular environment, at which point the oligosaccharyltransferase AglB transfers the glycan to selected Asn residues of target proteins [18,19]. Therefore, AglB, with homologues in Eukaryotes and Bacteria (i.e., Stt3 and PglB), can be considered the central enzyme of archaeal N-glycosylation pathways [20]. The fifth and final sugar residue of the pentasaccharide N-linked to *Hfx. volcanii* glycoproteins is attached to a distinct dolichol phosphate carrier on the cytoplasmic side of the membrane. This sugar-charged lipid is translocated across the membrane, and the sugar is added to the glycoprotein-bound tetrasaccharide [16,21,22].

While the general mechanism of N-glycosylation is shared across Archaea, the composition of the N-linked glycans generated is highly diverse, even among species or strains of the same genus [4,11,23]. Such diversity in glycans N-linked to proteins comprising the S-layer and cell appendages has long been considered to play a major role in host-recognition by archaeal viruses.

Accordingly, numerous studies have described interactions of archaeal viruses with highly glycosylated S-layer glycoproteins both in haloarchaea and other archaeal groups. The S-layer of *Halorubrum* sp. SS7-4 was found to trigger fusion of the membrane enveloped Halorubrum Pleomorphic Virus-6 (HRPV-6) with the host cell via the virus spike protein, an interaction that is dependent on the specific host S-layer [24]. The S-layer protein has also been identified as a potential receptor for several archaeal head-tailed viruses [25–27] infecting haloarchaea. Archaeal head-tailed viruses do not contain membrane lipids and exit host cells by lysis. Furthermore, partial removal of the highly N-glycosylated S-layer decreased the efficiency of viral infection of the thermophilic archaeon *Sulfolobus solfataricus* (Thermoproteota) by the lipid enveloped Sulfolobus Spindle-shaped Virus 1 (SSV1) [28], that has been shown to exit host cells by budding [29]. Nevertheless, the influence of S-layer protein glycosylation on these interactions is not yet understood.

Conversely, a number of archaeal viruses contain glycosylated proteins. Three of the capsid proteins of SSV1 were found to be glycosylated [30] and are likely required for host attachment and particle stability in the face of high temperatures and acidity. The tail architecture of SSV19, another *Sulfolobus*-targeting virus containing host lipids, includes two highly glycosylated proteins (VP4 and B210). VP4 exhibits a putative glycoside hydrolase core that has been proposed to degrade host S-layer glycans upon binding [31]. The virions of another membrane-enveloped virus infecting hyperthermophilic *Thermoproteota*, Thermoproteus Spherical Piliferous Virus 1 (TSPV1) possess unusual filaments, and glycosylation is thought to contribute to both filament stability at high temperatures and host recognition [32]. Proteins of the lipid-enveloped haloarchaeal virus Halorubrum Pleomorphic Virus 1 (HRPV-1), were shown to be modified by the same glycan as cell surface proteins of its host *Halorubrum* sp. PV6 [12,13]. However, for the majority of archaeal viruses, it remains unknown whether viruses utilize the host N-glycosylation machinery for glycosylation of their proteins. At the same time, a few archaeal viruses encode putative glycosyltransferases [33–38], suggesting that there are viruses that could, at least partially, circumvent the host glycosylation machinery. Thus, in most cases, disruption of the N-glycosylation machinery of the host should also affect viral glycosylation, leading to severe effects on virus–host interactions.

To investigate the effect of N-glycosylation on the infection dynamics of archaeal viruses, we generated a *Halorubrum lacusprofundi* mutant strain lacking *Hlac_1062*, annotated as encoding the oligosaccharyltransferase AglB [4,6]. While the composition of glycans decorating *Hrr. lacusprofundi* glycoproteins is currently unknown, cells lacking AglB are expected to be compromised in terms of their ability to perform N-glycosylation. Accordingly, the life cycle of two different viruses and a virus-like element was analyzed and compared between *Hrr. lacusprofundi* parent and N-glycosylation-deficient mutant

strains. Furthermore, we tested the impact of N-glycosylation on virus particle stability at different NaCl concentrations. Halorubrum Tailed Virus DL1 (HRTV-DL1) is an archaeal head-tailed virus that was shown to use the S-layer glycoprotein as its primary receptor [26]. Haloferax Pleomorphic Virus 1 (HFPV-1), a membrane-enveloped pleolipovirus [39,40], exhibits a glycosylated spike protein similar to HRPV-1 [12,13]. Finally, plasmid vesicles (PVs), also referred to as plasmidions [41,42], are vesicle-like structures that are morphologically distinct from extracellular vesicles (EVs) [41,43]. PVs contain unique plasmid-encoded proteins which form part of the vesicle coat and disseminate an enclosed plasmid. As such, PVs have been proposed to represent potential evolutionary precursors of some viruses. Hence, comparing the importance of N-glycosylation for host-interactions of true viruses and PVs could help determine the position of PVs within or in proximity to the virosphere [44].

2. Materials and Methods

2.1. Strains and Cultivation Conditions

All strains solely referred to by their strain name belong to the species *Halorubrum lacusprofundi*. ACAM34_UNSWΔ*pyrE2* was grown in modified DBCM2 medium, as previously described [45,46] (180 g/L NaCl, 25 g/L $MgCl_2$, 29 g/L $MgSO_4{\cdot}7\ H_2O$, 5.8 g/L KCl, 0.3 g/L peptone, 0.05 g/L yeast extract, 0.006 M $CaCl_2$, 2 mL/L K_2HPO_4 buffer [47], 0.11% (*w*/*v*) sodium pyruvate, 0.005 M NH_4Cl, 1 mL/L SL10 trace elements solution [47] and 3 mL/L vitamin 10 solution [47]), supplemented with 50 µg/mL uracil. Selection medium (DBCM2−) [46] was supplemented with 50 µg/mL uracil, 50 µg/mL 5-fluoroorotic acid (5′-FOA) or with indicated concentrations of pravastatin when needed. To assess the sensitivity of the strains to changing salt concentrations, biological triplicates of cultures were grown in DBCM2+ (DBCM2 with 1 g/L peptone and 0.5 g/L yeast extract), supplemented with 50 µg/mL uracil, and varying NaCl concentrations (100 g/L = 1.7 M, 120 g/L = 2.05 M, 240 g/L = 4.1 M and 250 g/L = 4.3 M, compared to 180 g/L = 3.1 M). During infection experiments and particle stability assays, wild-type ACAM34_UNSW, ACAM34_UNSWΔ*pyrE2* and ACAM34_UNSWΔ*pyrE2*Δ*aglB* were each grown in DBCM2+ medium supplemented with 50 µg/mL uracil. All liquid cultures were grown at 28 °C, with shaking at 120 rpm, rather than at the optimal growth temperature (37 °C, [48]) so as to delay biofilm formation during the stationary phase. Growth on solid media was at 37 °C.

2.2. Deletion of Hlac_1062 (aglB)

We targeted *Hlac_1062*, annotated as encoding the oligosaccharyltransferase AglB [4], for gene deletion. The ACAM34_UNSWΔ*pyrE2* strain [46] was used to generate the Δ*pyrE2*Δ*aglB* deletion strain, using a pop-in/pop-out approach, as described previously [46]. Briefly, approximately 500 bp-long upstream and downstream flanking regions of the *aglB* gene were PCR-amplified (primers used are listed in Supplementary Table S1) and inserted into plasmid pTA131_*hmgA* [46,49] using *Eco*RI and *Hind*III restriction sites. The ACAM34_UNSWΔ*pyrE2* strain was transformed with the generated plasmid and selected on DBCM2− plates, prepared with DBCM2− medium containing 7.5 µg/mL pravastatin, together with 15 g/L bacteriological agar (OxoidLtd, Basingstoke, United Kingdom). Pravastatin-resistant colonies were re-plated for additional selection on DBCM2− plates with increasing concentrations of pravastatin (10, 15, 15, 30, 45 and 60 µg/mL) over several generations. For the pop-out step, colonies that grew on 60 µg/mL pravastatin plates were selected on plates containing 50 µg/mL 5′-FOA and 50 µg/mL uracil. Finally, selected colonies were screened for *aglB* deletion by PCR and validated by qPCR (primers indicated in Supplementary Table S1).

2.3. Proteinase K Digestion of the S-Layer Glycoprotein

The effect of *aglB* deletion on the stability of the S-layer was measured by susceptibility to protease treatment compared to the parent strain. Aliquots of *Hrr. lacusprofundi* cul-

tures (three biological replicates per strain) in late exponential growth ($OD_{600} \geq 0.8$) were harvested and resuspended in DBCM2 salt solution to an adjusted OD_{600} of 1.0 in 1.2 mL in replicates for both the parent and deletion strains. Proteinase K was added to a final concentration of 0.2 mg/mL and samples were incubated at 37 °C. Aliquots (150 µL) were removed immediately after the addition of proteinase K (0 min) and at several time points until 120 min of incubation. Trichloroacetic acid was added directly to each aliquot (final concentration 15 %), after which samples were incubated at 4 °C for 30 min, centrifuged at 10,000× *g* and 4 °C for 15 min and washed with 1 mL of ice-cold acetone. Acetone was removed from the samples and dried pellets were resuspended in 30 µL (Δ*aglB*) or 38 µL (parent) of a mixture containing 1 part sample buffer (0.2 g SDS, 1 mg Bromphenol Blue, 0.78 mL glycerol, 0.2 mL 0.5 M Tris pH 6.8 and 0.155 g DTT per 10 mL) and 5 parts 125 mM Tris-HCl pH 8.0. This difference in volume was chosen to correct for the difference in protein concentration between strains of approx. 0.8:1.0 (Δ*aglB*:parent), as determined using Pierce BCA Protein Assay Kit (Thermo Fisher Scientific, Waltham, MA, USA) following the manufacturer's instructions. Finally, 30 µL portions of each sample were separated by SDS-PAGE (8% acrylamide, Tris-HCl pH 8.8), and stained with Coomassie blue.

2.4. Quantification of Extracellular Vesicles

Extracellular vesicles (EVs) were quantified based on a protocol described by Mills et al. [43]. In brief, EVs were isolated from the culture supernatant ($n = 3$ for each strain) via centrifugation (45 min, 4500× *g*) and precipitated from the culture supernatant with PEG_{6000}. Precipitated vesicles were resuspended in DBCM2 salt solution [26], filtered through syringe-top filters (0.8, 0.45 and 2 × 0.2 µm in sequence) and stained with 500 nM MitoTracker Green FM (Invitrogen) for 30 min. Subsequently, EVs were precipitated after overnight incubation with PEG_{6000} (final concentration of 10%) via centrifugation at 20,000× *g* for 40 min. After removal of the supernatant, the precipitates were resuspended in 200 µL DBCM2 salt solution and fluorescence was measured in a DeNovix, DS-11 FX+ spectrophotometer at emission wavelengths between 514–567 nm, with blue excitation at 470 nm. For transmission electron microscopy (TEM), purified EVs were adsorbed onto carbon-coated copper grids for 5 min, stained with 2% (*w*/*v* in ddH_2O) uranyl acetate for 1 min and imaged with a JEM2100 Plus TEM at 200 kV acceleration voltage.

2.5. Isolation of PVs and Viruses, Infection and Growth Experiments

Infection experiments were performed in biological triplicates using the ACAM34_UNSWΔ*pyrE2* (parent) and Δ*pyrE2*Δ*aglB* (Δ*aglB* mutant) strains. The head-tailed virus HRTV-DL1 was obtained from infected *Hrr. lacusprofundi* ACAM34_UNSW cultures [26]. *Hrr. lacusprofundi* cultures were infected with a multiplicity of infection (MOI) of 10 from a $1.64 * 10^{12}$ plaque-forming units/mL stock in DBCM2 salt solution. Fresh HFPV-1 stocks were obtained from infected *Hfx. volcanii* cultures following the protocol described by Alarcón-Schumacher et al. [39]. PVs containing the pR1SE plasmid were isolated from *Hrr. lacusprofundi* DL18 [41]. Liquid cultures were inoculated from glycerol stocks, grown until OD_{600} reached approx. 0.8 and subsequently diluted into fresh DBCM2+ medium to OD_{600} 0.05. This process was repeated three times, at which point the cultures were diluted to OD_{600} 0.05 and supplemented with 30 mL of 10× YPC solution [47] to induce increased PV production [41]. Cells were harvested in early stationary phase (OD_{600} $1.3 - 1.6$) at 4500× *g* for 45 min at room temperature (RT). PVs were precipitated with 10% PEG_{6000} (final concentration) overnight at 4 °C, harvested at 30,000× *g* for 45 min at 4 °C (JA-14, Beckman-Coulter) and the precipitate was resuspended in 7 mL of DBCM2 salt solution. The PV preparation was centrifuged for 10 min at 10,000× *g*, and the supernatant was filtered once through a 0.45 µm syringe filter and three times through 0.2 µm filters to remove remaining cells. Since the number of plasmids per PV has not yet been determined and because PVs do not induce plaque formation, precise quantification of PVs in suspension is not possible. Infection was, therefore, performed with a plasmid copy number:host cell ratio of approximately 75:1.

Infection of ACAM34_UNSWΔ*pyrE2* and Δ*pyrE2*Δ*aglB* was performed as described by Alarcón-Schumacher et al. [39]. Briefly, cultures were diluted three times from mid-exponential growth to OD_{600} 0.05, harvested at mid-exponential phase by centrifugation (4500× *g* for 45 min at RT), resuspended in 1 mL medium and subsequently incubated with the virus or PV stock in DBCM2 salt solution, followed by removal of unbound particles by washing after 2 h. For HRTV-DL1, free virus particles were not removed from infected cell suspensions after the 2 h infection step, with the mixture being directly transferred into the cultures, as described [26]. Each strain (n = 2) was infected in biological triplicates for each infectious element (n = 3); biological triplicates of uninfected controls (n = 3) were performed for each infectious agent (total n = 36). All cultures were incubated at 28 °C and 120 rpm, and growth was monitored by measuring OD_{600}. Aliquots for quantification by qPCR were removed at the time points indicated, covering early infection, exponential growth and the late exponential phase. Two milliliters of culture from each biological replicate was centrifuged at 18,000× *g* for 10 min at RT. The cell pellet was washed twice with DBCM2+ medium, snap frozen with liquid N_2 and stored at −80 °C until DNA extraction. Virus particles and PVs were precipitated from 1.5 mL (HRTV-DL1 and PVs) or 1 mL (HFPV-1) supernatant with 10% final concentration of PEG_{6000} (as described above) and the resulting pellets were snap-frozen with liquid N_2 and stored at −80 °C until DNA extraction. For PV infection, extended cultivation was performed by diluting (to OD_{600} 0.05) aliquots into fresh DBCM2+ medium (150 mL) at late exponential growth phase after the final aliquot was removed during the initial cultivation.

2.6. Virus and PV Quantification

All DNA extractions were performed with an Isolate II Genomic DNA Kit (Bioline, London. United Kingdom) according to the manufacturer's instructions. Host, virus, and plasmid genome copy numbers were quantified by qPCR as described previously in technical triplicates for each biological replicate [26,39]. Primer sequences, annealing temperatures and primer concentrations are listed in Supplementary Table S1. Genome copy numbers in all samples were quantified with a CFX96 Touch Real-Time PCR machine (Bio-Rad Laboratories, Hercules, CA, USA) and CFX Manager Software in 10 µL reactions with SsoAdvanced Universal SYBR Green Supermix (Bio-Rad, Hercules, CA, USA). The qPCR program consisted of 5 min at 95 °C and 30 s at 95 °C, 30 s at X °C for 35–40 cycles (X, corresponding to the annealing temperature of the respective primer sets, is indicated in Supplementary Table S1), with measurements being taken between each cycle. Assays were only considered for quantification when efficiencies were between 95–105% and $R^2 \geq 0.98$. Prior to statistical analysis, normal distribution and homogeneity of variances in sample sets separated by virus and time point were confirmed based on the consensus of a Shapiro–Wilk Test, F-Test, Bartlett's Test [50], Levene's Test [51] and a Fligner–Killeen's Test [52]. The means from parent and Δ*aglB* samples were compared with two-sided, unpaired Student's *t*-tests. All analysis was performed with R version 4.1.2 [53] and RStudio version 2023.3.0.386 [54].

2.7. Glycostaining of Cells and Particles

Periodic acid-Schiff staining following the protocol of Dubray and Bezard [55] was performed on aliquots of *Hrr. lacusprofundi* cells that were separated by SDS-PAGE (8% acrylamide, Tris-HCl pH 8.8). HRTV-DL1 virions and PVs were obtained from the supernatant of infected *Hrr. lacusprofundi* cultures, HFPV-1 from *Hfx. volcanii*, and purified as described above. Aliquots of each infectious agent were separated by SDS-PAGE (8% acrylamide, Tris-HCl pH 8.8) and glycosylated proteins were stained with the Pro-Q Emerald 300 glycoprotein gel and blot stain kit (Invitrogen, Waltham, MA, USA), using periodate-based oxidation of carbohydrate groups according to the manufacturer's instructions. Total protein content was visualized with Coomassie blue.

2.8. Determination of Virus Stability

Cultures of the ACAM34_UNSWΔ*pyrE2* and Δ*pyrE2*Δ*aglB* strains were each infected with HRTV-DL1 or HFPV-1 in separate experiments. Virions were harvested from the culture supernatants and purified according to the protocols described above. Purified preparations from each strain were precipitated again into three aliquots with PEG_{6000} and resuspended in 0.075 mL DBCM2+ medium prepared with 120 g/L (2.05 M), 180 g/L (3.1 M), or 240 g/L (4.1 M) NaCl. After overnight incubation at room temperature, 1 mL aliquots of the wild type ACAM34_UNSW strain (OD_{600} = 1.0) [26] were infected with viral preparations (biological triplicates per virus), with sterile medium (biological triplicates per virus) serving as the negative control. MOIs were 5 (for Δ*aglB*-strain-produced virions) or 1 (for parent-strain-produced virions) for HRTV-DL1 and 3.5 (for Δ*aglB*-strain-produced virions) or 5.3 (for parent-strain-produced virions) for HFPV-1, respectively. Differences in MOI were caused by disparate yields of viral preparations from infected strains. After incubation (2 h), cells were washed twice with sterile medium and subsequently snap-frozen in liquid nitrogen. Viral copy numbers in DNA extracts of cell pellets were determined via qPCR as described above and compared to copy numbers of the *Hrr. lacusprofundi* chromosome. The infection efficiency was calculated as a percentage. Intracellular viral genome copy numbers per ng of DNA from each biological replicate were multiplied by the total DNA content (in ng) of the respective sample and subsequently divided by the total number of viral genome copy numbers added to each replicate during infection. Homogeneity of variances was confirmed based on the consensus of Shapiro–Wilk, Bartlett's [50], Levene's [51] and Fligner–Killeen's tests [52]. The effect of NaCl concentration on infection efficiency was determined with two-sided, unpaired student's *t*-tests, per virus and per strain. All analysis was performed with R version 4.1.2 [53] and RStudio version 2023.3.0.386 [54].

3. Results

3.1. Deletion of Hrr. lacusprofundi aglB Leads to Growth Deficiencies at Varying Salt Concentrations and S-Layer Instability

A putative glycosylation cluster was previously identified in *Hrr. lacusprofundi* (*Hlac_1062* to *_1075* [4]), including the archaeal oligosaccharyltransferase *aglB* within the vicinity of several genes annotated as encoding predicted glycosyltransferases, putative sugar epimerases and one putative flippase. In order to manipulate the *Hrr. lacusprofundi* N-glycosylation pathway, we generated a knockout strain for *Hlac_1062* (*aglB*). Deletion of *aglB* was confirmed by qPCR (Figure 1A), while glycoprotein staining confirmed strongly decreased glycosylation of the S-layer glycoprotein in the mutant strain (Supplementary Figure S1). In *Hfx. volcanii*, deletion of *aglB* leads to instability and increased release of the S-layer glycoprotein [18]. Accordingly, protease treatment of *Hrr. lacusprofundi* parent and mutant cells revealed increased protease sensitivity of the mutants' S-layer glycoprotein, reflecting a change in S-layer glycoprotein conformation and subsequently, increased instability of the S-layer in the *aglB*-deletion strain (Figure 1B). The Δ*aglB* strain (ACAM34_UNSWΔ*pyrE2*Δ*aglB*) either grew to the same or to a slightly higher optical density (600 nm) than the parent strain (ACAM34_UNSWΔ*pyrE2*) in standard DBCM2 media containing a NaCl concentration of 180 g/L (3.1 M) (Figure 1C, Supplementary Figure S2). However, growth of the Δ*aglB* strain was negatively impacted both at a high NaCl concentration of 240 g/L (4.1 M) and in low-salt medium containing 120 g/L NaCl (2.05 M) (Figure 1B). Unlike the parent strain, the mutant strain was unable to grow in 250 g/L NaCl medium (4.3 M) and both strains struggled at 100 g/L NaCl (1.7 M) (Supplementary Figure S2). These observations mirror findings previously reported for *Hfx. volcanii* Δ*aglB* cells [18].

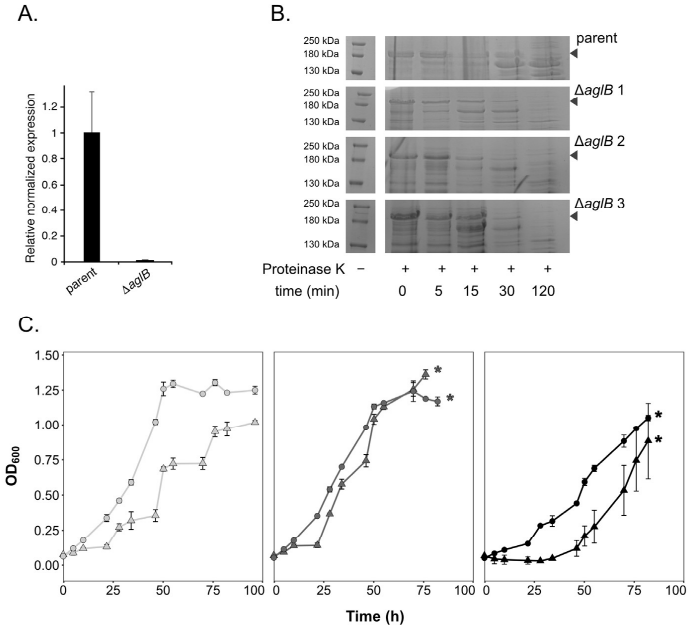

Figure 1. The *Hrr. lacusprofundi* Δ*aglB* strain shows altered growth and increased protease sensitivity of the S-layer. (**A**) Validation of *aglB* deletion by qPCR. The relative mRNA expression of *aglB* (*Hlac_1062*) was normalized to that of a housekeeping gene (*16S rRNA*). The values presented are the average of four technical repeats ± standard error of the mean. (**B**) Parent and Δ*aglB* cells were challenged with 0.2 mg/mL proteinase K at 37 °C for the indicated times (min). Precipitated cellular proteins are visualized on 8% acrylamide SDS-PAGE gels for one representative replicate (out of three biological replicates) from the parent strain and three biological replicates from the Δ*aglB* strain. The position of the S-layer glycoprotein is indicated with an arrow. (**C**) The growth of parent (circles) and Δ*aglB* (triangles) strains was monitored in media with NaCl concentrations of 120 g/L (2.05 M, light grey), 180 g/L (3.1 M, dark grey) or 240 g/L (4.1 M, black). Each point represents the average of three biological replicates ± standard deviation of the mean. The data were generated simultaneously for both strains across NaCl concentrations in a separate experiment to the data shown in Supplementary Figure S2. Asterisks indicate when cultures went into biofilm and OD_{600} could no longer be accurately measured.

S-layer instability was suggested to be responsible for the rise of extracellular vesicle (EV, [56–58]) production in *Hfx. volcanii* [43]. We, therefore, assessed EV production in the *Hrr. lacusprofundi* parent and Δ*aglB* mutant strain. EVs could be isolated from both strains (Figure 2A,B). Quantification of EVs using a fluorescence-based assay (see Methods) revealed increased vesicle production by the Δ*aglB* stain, relative to the parent strain (Figure 2C), confirming reduced stability of the S-layer.

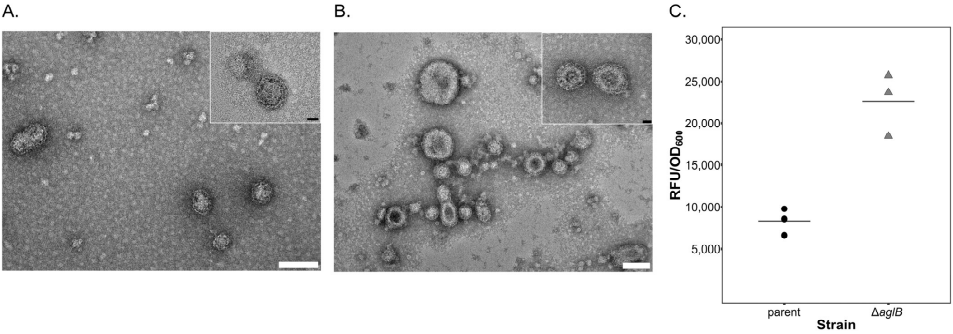

Figure 2. Extracellular vesicle production is increased upon *aglB* deletion. Electron micrographs of EVs isolated from the supernatant of the parent strain (**A**) and the Δ*aglB* mutant (**B**). The white scale bars represent 100 nm and the black scale bars in the inserts represent 20 nm. (**C**) EVs in the culture supernatant were quantified by fluorescent labelling (relative fluorescent units, RFUs, normalized to OD_{600}) of the parent and Δ*aglB* strains. Individual measurements from three biological replicates are presented, and the average value for each strain is indicated by the horizontal line.

3.2. The Life cycle of the Lytic Virus HRTV-DL1 Is not Influenced by Changes in Host N-Glycosylation

HRTV-DL1 is an archaeal tailed virus that causes a lytic infection in ACAM34_UNSW and was shown to use the host cell S-layer for attachment [26] (Table 1). The major capsid protein that builds the virus particle presents three N-glycosylation motifs or sequons (i.e., NXS/T, where X is any residue but Pro [59]), while some of the other structural proteins that form the neck or tail of the virion also contain (<5) sequons. The protein encoded by ORF24, suggested to play a role in host attachment, presents nine such motifs and may thus be N-glycosylated [26]. Glycoprotein staining of viral proteins revealed two faint bands >72 kDa, possibly including the ORF24 protein, and one band <72 kDa, that could represent the major capsid protein encoded by ORF12 (Supplementary Figure S1C).

Infection with HRTV-DL1 led to the characteristic lysis of both the parent strain and Δ*aglB* mutant cells about 23 h post infection (h.p.i.) (Figure 3A). Viral titers in the culture supernatants strongly increased after lysis, reaching similar maximal values for both strains ($3.2*10^{+11} \pm 9.7*10^{+10}$ per mL, $n = 3$, for the parent strain versus $1.35*10^{+11} \pm 1.2*10^{+11}$ per mL, $n = 3$, for the Δ*aglB* mutant) at approximately 40 h.p.i. The intracellular virus genome copy numbers (Supplementary Figure S3A), as well as the virus:host genome ratio (Figure 3B), were not significantly different between the two strains (p-values < 0.05). This led us to conclude that the deletion of *aglB* did not have a significant effect on the life cycle of HRTV-DL1.

Table 1. Summary of the characteristics and the effect of *aglB* deletion on the three infectious agents used in this study.

	HRTV-DL1	HFPV-1	PVs (pR1SE)
Genome size	37.7 kb	8 kb	37.8 kb (pR1SEDL18 = 109 kb)
Particle	head-tailed virus, non-contractile tail	pleomorphic, membrane enveloped	undescribed morphology, membrane enveloped
Life cycle	lytic	chronic	chronic
Predicted glycosylated virus/plasmid proteins	ORF12 (major capsid protein) ORF24 (host attachment) [26]	ORF4 (spike protein) [39]	ORF6 (structural protein), ORF9 (structural protein) [41]
S-layer interactions	binds S-layer as primary receptor [26]	not known	not known
Glycosylation-related genes on genome	ORF26 (predicted glycosyl hydrolase [26])	none	ORF89 (predicted glycosyltransferase/glycogen phosphorylase), ORF90 (predicted glycosyltransferase) [41] from plasmid pR1SEDL18
Effect of host N-glycosylation on life cycle of infectious agent	not significant	significant increase in HFPV-1 extracellular titers and intracellular virus:host genome ratios in Δ*aglB* cells	significant decrease in extracellular pR1SE/PV titers in Δ*aglB* cells
Effect of N-glycosylation of particles on particle stability in varying NaCl concentrations	changes in stability in varying NaCl concentrations are similar to parent strain	particle stability of Δ*aglB*-produced particles does not increase when comparing low-salt to physiological salt conditions, as observed for particles produced in the parent strain, indicating altered particle stability	not tested

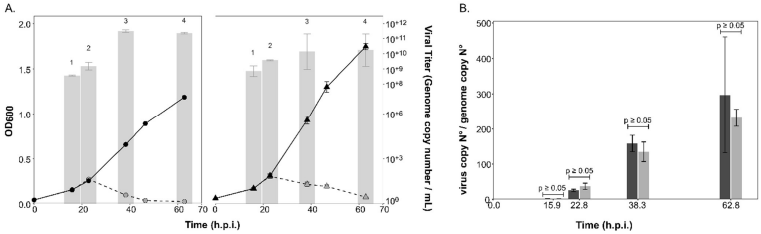

Figure 3. Growth of the parent and Δ*aglB* strains and virus titers during infection with HRTV-DL1. (**A**) Growth of uninfected (black, solid line) and infected (grey, dashed line) cultures of *Hrr. lacusprofundi* parent (circles) and Δ*aglB* (triangles) strains over time (h.p.i.). Virus titers in the culture supernatant (genome copy number/mL) are shown as bar graphs in logarithmic scale (log base 10). Data points and bars represent the average of three biological replicates ($n = 3$) ± standard deviation of the mean. Samples were compared with two-sided, unpaired Student's *t*-tests per time point (1–4), which did not reveal a significant difference between strains (1: $p = 0.4$, 2: $p = 0.11$, 3: $p = 0.10$ and 4: $p = 0.3$). (**B**) HRTV-DL1 genome copy numbers normalized to the level of the host chromosome within cells. Bars represent the average of three biological replicates ($n = 3$) ± standard deviation of the mean for the parent (dark grey) and Δ*aglB* strain (light grey). Samples were compared with two-sided, unpaired Student's *t*-tests per time point, which did not reveal a significant difference between strains (as indicated above the bars with $p \geq 0.05$).

3.3. Intracellular and Extracellular Virus Numbers of the Chronic Virus HFPV-1 Are Significantly Increased in the ΔaglB Mutant

Proteins comprising the HFPV-1 virus particle contain N-glycosylation sequons and protein glycosylation was confirmed by glycostaining of the SDS-PAGE-separated proteins from purified particles (Supplementary Figure S1B). Additionally, no glycosylation-related genes that could compensate for compromised host N-glycosylation were identified on the genome of HFPV-1 (Table 1), suggesting that the impairment of N-glycosylation due to *aglB* deletion would have an effect on the life cycle of HFPV-1.

Infection with the HFPV-1 virus led to a slight growth retardation during early exponential growth (ca. 25 h.p.i.) of both the parent and Δ*aglB* strains (Figure 4A). HFPV-1 causes a productive chronic infection, in which viral particles are released by extrusion or by budding through the cell membrane without lysis of the host [39,60]. Viral titers in the culture supernatant did not show a sharp increase, as observed after lysis of HRTV-DL1-infected cultures, but rather remained within similar orders of magnitude (10^{+7}–10^{+8}) throughout growth, although titer values did decline over time. Interestingly, we detected significant differences in viral titer between strains, with consistently higher titers being recorded for the Δ*aglB* strain. Maximal viral genome copy numbers per ml were three times higher (p = 0.0001; Figure 4A) for the mutant strain ($6.42*10^{+8} \pm 4.8*10^{+7}$, n = 3) at 44 h.p.i than in the parent strain ($1.89*10^{+8} \pm 2.4*10^{+7}$, n = 3). Intracellular virus:host genome ratios remained consistently below one for both strains (Figure 4B, Supplementary Figure S3B), yet were higher in the mutant strain with a statistically significant difference (e.g., p = 0.0009 at 44 h.p.i), except at the last time point, displaying a consistent pattern with the viral titers in the culture supernatants.

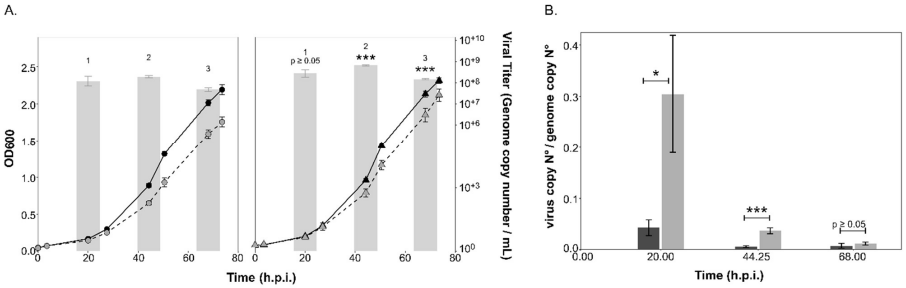

Figure 4. Growth of the parent and Δ*aglB* strains and virus titers during infection with HFPV-1. (**A**) Growth of uninfected (black, solid line) and infected (grey, dashed line) cultures of *Hrr. lacusprofundi* parent (circles) and Δ*aglB* (triangles) strains over time (h.p.i.). Virus titers in the culture supernatant (genome copy number/mL) are shown as bar graphs in logarithmic scale (log base 10). Data points and bars represent the average of three biological replicates (n = 3) ± standard deviation of the mean. Statistical significance is indicated in the graph for the Δ*aglB* strain, with the following significance codes: '***' for $p < 0.001$, '*' for $p \leq 0.05$ and $p \geq 0.05$. (**B**) HFPV-1 genome copy numbers normalized to the level of host chromosome within cells. Bars represent the average of three biological replicates (n = 3) ± standard deviation of the mean for the parent (dark grey) and Δ*aglB* strains (light grey). Statistical significance is indicated in the graph using the same significance codes as described above for (**A**).

3.4. PV Production Is Reduced in the aglB Deletion Strain

PV plasmid-encoded proteins contain N-glycosylation sequons. Protein glycosylation was confirmed by glycostaining of the SDS-PAGE-separated proteins from purified particles (Supplementary Figure S1D). Interestingly, the pR1SEDL18 plasmid (produced by *Hrr. lacusprofundi* strain DL18 [41], used in this study) encodes two predicted glycosyltransferases that have been identified in PVs and host cell membrane preparations ([41],

Table 1). These could potentially impact the glycosylation of PVs, yet are unlikely to fully compensate for the lack of host *aglB*.

Infection with PVs (containing plasmid pR1SE) did not result in any major changes in the growth rate of either the parent or Δ*aglB* strains (Figure 5). Infection efficiency of PVs was the same for the Δ*aglB* mutant and the parent strain (average of 6.83% ± 1.4% for Δ*aglB* strain and 3.45% ± 1.92% for parent strain), indicating that infection is independent of N-glycosylation of the host cell envelope proteins and S-layer stability. The plasmid could be detected at 20.25 h.p.i., with the titer reaching a maximum value of $7.31*10^{+8}$ (± $1.5*10^{+8}$, $n = 3$) in culture supernatants of the parent strain, confirming production of PVs. Maximum plasmid titers per ml reached higher values in parent cultures ($7.87*10^{+8}$ ± $3.15*10^{+8}$, $n = 3$; at 43 h.p.i than in the Δ*aglB* strain (Figure 5A). Intracellular copy numbers of the infectious plasmid pR1SE reached a maximum of $9.8*10^{+5}$*ng DNA^{-1} (± $6.9*10^{+4}$, $n = 3$) at 20.25 h.p.i. for the parent strain and $7.3*10^{+5}$*ng DNA^{-1} (± $1.54*10^{+5}$, $n = 3$) at 20.25 h.p.i. for the Δ*aglB* strain (Supplementary Figure S3C). Plasmid:host ratios reached up to 7.6 (20.25 h.p.i.) and 3.6 (20.25 h.p.i) in the mutant and parent strains, respectively, with statistically significant differences between strains being noted during early infection (20.25 h.p.i., $p = 0.0002$) and exponential growth (43 h.p.i., $p = 0.03$*). Interestingly, despite higher plasmid:host ratios in the Δ*aglB* mutant at 20.25 h.p.i., the extracellular titer remained significantly lower relative to the parent strain. However, reduction of PV titers in the Δ*aglB* mutant was at most only fourfold, suggesting that the impacted N-glycosylation of PV proteins did not prevent the formation of PVs. Additionally, the release of both extracellular vesicles and enveloped virus HFPV-1 was increased in the Δ*aglB* mutant, demonstrating that release of membranous structures was not hindered. Therefore, we suggest that the reduction of extracellular plasmid numbers is due to reduced stability of PV particles produced by the Δ*aglB* mutant.

To test whether PV production was consistent over longer-term infections, we extended the growth of the plasmid pR1SE-infected cultures. Interestingly, while plasmid: host ratios increased over time in both strains, extracellular plasmid numbers did not increase accordingly (Figure 5B,C), indicating that PV production is not coupled to intracellular plasmid copy numbers. Extracellular plasmid copy numbers remained consistently lower in the Δ*aglB* mutant, confirming the negative effect of N-glycosylation deficiency on PV stability.

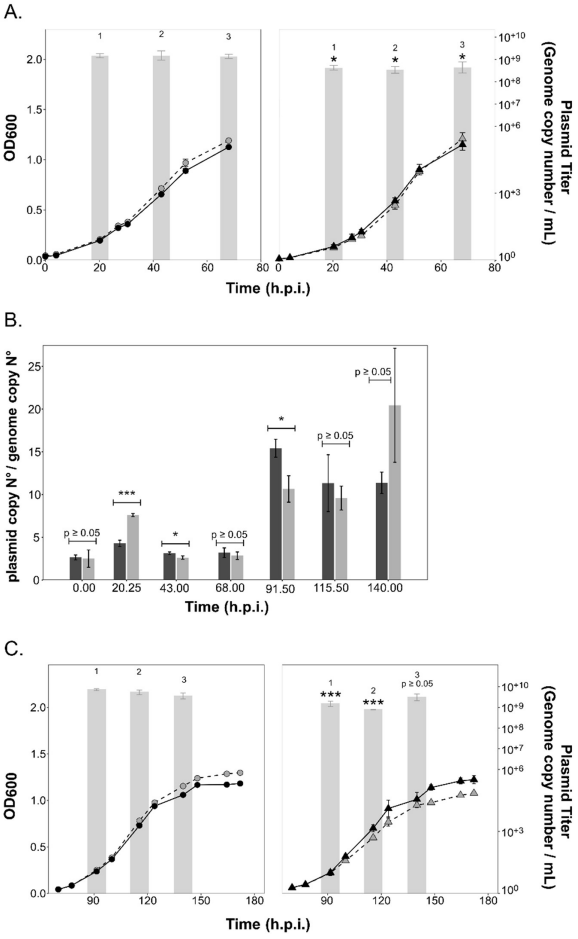

Figure 5. Growth of the parent and Δ*aglB* strains and plasmid titers during infection with plasmid pR1SE. (**A**) Growth of uninfected (black, solid line) and infected (grey, dashed line) cultures of *Hrr. lacusprofundi* parent (circles) and Δ*aglB* (triangles) strains over time (0–68 h.p.i.) Plasmid titer of pR1SE in the culture supernatant (genome copy number/mL) are shown as bar graphs in logarithmic scale (log base 10). Data points and bars represent the average of three biological replicates ($n = 3$) ± standard deviation of the mean. Statistical significance is indicated in the graph above the values for the Δ*aglB* strain, with the following significance codes: '***' for $p < 0.001$, '*' for $p \leq 0.05$ and $p \geq 0.05$. (**B**) Plasmid pR1SE genome copy numbers normalized to the level of the main host chromosome within cells. Bars represent the average of three biological replicates ($n = 3$) ± standard deviation of the mean for parent (dark grey) and Δ*aglB* (light grey) strains. Statistical significance is indicated in the graph using the same significance codes described above for (**A**). (**C**) Continued growth of cultures after dilution of the cultures shown in (**A**) with the same graphical representation and statistical analysis.

3.5. Impaired Glycosylation has an Impact on the Stability of HFPV-1

Since PV production was reduced in the Δ*aglB* mutant, we concluded that PVs produced in the Δ*aglB* mutant are likely less stable, and that the same could possibly apply to virus particles. We had previously determined that the Δ*aglB* mutant is sensitive to changes in NaCl concentration (Figure 1C). Therefore, we exposed virus particles produced in the parent and Δ*aglB* strains to different salt concentrations to test particle stability. We calculated infection efficiency of the particles at 2 h.p.i as a measure of particle stability.

For HRTV-DL1 particles (Figure 6A), the salt concentration had a significant effect on the infectivity of particles produced in both strains, with high salt promoting particle stability (Figure 6). However, no significant difference was observed when comparing the effect between strains. Varying salt concentration also had a statistically significant effect on HFPV-1 particles when produced in the parent strain (Figure 6B). Particles appeared to be more stable in physiological and high-salt conditions when compared to low-salt conditions ($p = 0.039$ and $p = 0.017$ respectively). In contrast, particles produced in the Δ*aglB* strain only showed increased stability in high-salt conditions when compared to low-salt conditions. This indicates that HFPV-1 particle stability is altered when N-glycosylation is impaired.

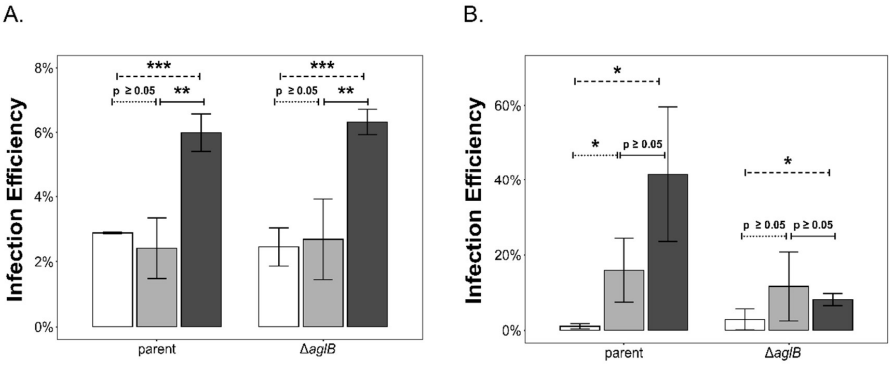

Figure 6. Deletion of *aglB* negatively affects particle stability of HFPV-1. Infection efficiency of HRTV-DL1 (**A**) and HFPV-1 (**B**) particles after overnight incubation in medium containing 120 (2.05 M, white), 180 (3.1 M, light grey) or 240 g/L (4.1 M, dark grey) NaCl was tested on wild type *Hrr. lacusprofundi* cells, as a measure of particle stability. Infection efficiency (within 2 h) is given as the percentage of viral genome copy numbers inside the cells divided by total viral copy numbers used for infection per replicate. Bars represent the average of three independent biological replicates ($n = 3$) ± standard deviation of the mean for viruses produced in the parent and Δ*aglB* strains. Infection efficiencies were compared in pairs separately for each strain and virus as indicated in the graph (dotted line = 120 g/L against 180 g/L, dashed line = 120 g/L against 240 g/L, solid line = 180 g/L against 240 g/L). Statistical significance is indicated in the graph with the following significance codes: '***' for $p < 0.001$, '**' for $p < 0.01$, '*' for $p \leq 0.05$ and $p \geq 0.05$.

4. Discussion

In this study, we generated an in-frame deletion mutant of *Hlac_1062*, corresponding to the archaeal oligosaccharyltransferase-encoding *aglB* gene in *Hrr. lacusprofundi*. The oligosaccharyltransferase is considered to be the central enzyme of N-glycosylation pathways in Eukaryotes, Bacteria and Archaea [20]. To date, every archaeal species with *aglB* deleted has shown a loss of N-glycosylation [1,18,61,62], except for *Sulfolobus acidocaldarius*, where *aglB* is essential and could not be deleted [1]. Yet, in *Hfx. volcanii*, evidence for the existence of a second N-linked glycan generated in low-salt conditions and added to pro-

tein targets in an AglB-independent manner has been presented [63,64]. *Hrr. lacusprofundi* proteins may be additionally modified by O-linked glycans, as previously described for other haloarchaea [65–68], although genes involved in the assembly of this glycan have not yet been identified. Thus while, deletion of *Hrr. lacusprofundi aglB* could theoretically not lead to a complete loss of N-glycosylation, we nonetheless showed that N-glycosylation was strongly impacted by such deletion (Supplementary Figure S1). Moreover, the *Hrr. lacusprofundi aglB* mutant showed growth deficiencies in medium containing salt levels below and above the optimum concentration, confirming that N-glycosylation is important for cell stability and adaptability to changing extracellular salt concentrations. Given the increased susceptibility of the S-layer glycoprotein to proteinase K treatment (Figure 1B) and the increased production of extracellular vesicles (Figure 2C) [10,43] in the deletion strain, we concluded that a reduced stability of the S-layer resulted in compromised N-glycosylation, suggesting that such post-translational modification is very important for the function of the *Hrr. lacusprofundi* S-layer [41,69], as previously shown for both *Hfx. volcanii* [15] and *Halobacterium salinarum* [9]. To gain insight into the relationship between N-glycosylation and viral infection, we used the Δ*aglB* mutant to analyze the importance of this post-translational modification on the life cycle of PVs and two viruses with different lifestyles infecting this species (Table 1).

HRTV-DL1 is a head-tailed virus that exhibits a lytic life cycle, with virus particles being released via cell lysis without incorporating host membrane lipids. Glycosylation was shown for some of the structural proteins, possibly including the major capsid protein. Infection with HRTV-DL1 was not impacted by impaired N-glycosylation, and neither HRTV-DL1 intracellular replication nor virus particle production were affected in the Δ*aglB* mutant. While changes in salt concentrations had strong effects on HRTV-DL1 particle stability in general, with high-salt conditions preserving virion infectivity, there was no evidence for an impact of N-glycosylation on particle stability. The N-glycosylation status of the host receptor, the S-layer glycoprotein [26], does not affect the life cycle of HRTV-DL1 which indicates that neither host recognition nor virus adsorption is dependent on sugar residues on the host cell surface, as has been shown for a number of bacterial tailed viruses. Carbohydrate-binding domains have been widely identified as playing a role in host recognition and attachment of siphophages infecting Gram-positive bacteria [70–73], where the thick peptidoglycan layer can be considered analogous to the archaeal S-layer. The host ranges of archaeal tailed viruses of the *Caudoviricetes* class vary greatly, even among members of the same family [25]. HRTV-DL1 exhibits a very narrow host range, infecting only a laboratory strain of *Hrr. lacusprofundi*, whereas other archaeal tailed viruses can infect hosts across haloarchaeal genera [25,74–76]. Therefore, host recognition and attachment via binding to glycan groups exposed on the host S-layer might well play a crucial role for other archaeal tailed viruses.

In contrast to HRTV-DL1, deletion of *aglB* affected the reproduction of HFPV-1 and plasmid pR1SE. Both infectious agents most likely release particles by budding from the host membrane and probably rely on the host machinery to glycosylate their structural proteins. HFPV-1 was detected at comparatively low copy numbers both within host cells and in the supernatant of the tested strains, which we attribute to the fact that *Hrr. lacusprofundi* is not the optimal host for this virus [39]. Nevertheless, we did detect a significant difference in both intracellular and extracellular virus genome copy numbers, numbers that were significantly higher in the Δ*aglB* mutant. We conclude that HFPV-1 does not rely on host N-glycosylation for interactions with the host cell, similar to HRTV-DL1 [39]. At the same time, destabilization of the S-layer caused by incorporation of non- or incompletely N-glycosylated S-layer glycoproteins may have improved accessibility of the host cell envelope during both virus entry and exit. In a similar way to the increased EV production seen in the Δ*aglB* mutant, the destabilized S-layer seems to allow for increased virus budding.

Interestingly, while a less rigid S-layer appears to be beneficial for continuous virion release through budding, it does not have a significant effect on HRTV-DL1 virion release

via cell lysis. This indicates that the mechanism of HRTV-DL1-induced lysis is entirely driven by the virus and is either independent of the condition of the S-layer or includes S-layer destabilization. It has been suggested that HRTV-DL1 uses a glycosyl hydrolase (ORF26) to degrade surface glycans and destabilize the S-layer, while a holin-like protein disrupts membrane integrity and leads to lysis. In contrast, HFPV-1 release seems to benefit from partial instability of the cell envelope. No protease encoded in the genomes of membrane-containing archaeal viruses has been detected to date [77], suggesting that enveloped viruses may either target S-layer stability by other means, such as attacking glycosylation or blocking assembly of the S-layer. Alternatively, they might entirely depend on partial S-layer instability where it naturally occurs, for example, at sites of cell division, when S-layer glycoproteins are naturally released during growth of the host [18], or during C-terminal post-translational modifications of the S-layer glycoprotein at the cell surface, specifically lipid attachment and proteolytic cleavage that could introduce temporary S-layer disruption [5,78–80].

While extracellular copy numbers of plasmid pR1SE were significantly reduced in the Δ*aglB* strain, the difference in infection efficiencies between strains was not statistically relevant. Therefore, we conclude that recognition of the host cell and contact of PVs with the host cell are not dependent on interactions with host glycans, as for HRTV-DL1 and HFPV-1. However, extracellular PV numbers appeared to be strongly impacted by the host glycosylation deficiency, an effect we suggest results from reduced particle stability.

We also confirmed the altered stability of HFPV-1 particles produced by the Δ*aglB* mutant upon exposing particles to different salt concentrations. The spike protein of HFPV-1 and the putative vesicle coat protein of PVs are both in all likelihood N-glycosylated [39,41] (Supplementary Figure S1). Considering the altered particle stability of PVs and HFPV-1, we conclude that both are reliant on the host glycosylation machinery for adding glycans to their structural surface proteins, and that N-glycosylation is crucial for their stability. We assume that reduced stability might mask any potential increase in PV titers caused by instability of the cell envelope that we detect for HFPV-1. Similarly, while we did see a statistically significant increase in HFPV-1 titers in the mutant strain, these are not very high. We suggest that the reduced particle stability of HFPV-1 negatively affected the final titers observed. We conclude that, for both HFPV-1 and PVs, impairment of N-glycosylation has two major effects, namely reduced particle stability and increased particle release due to S-layer instability, while the impact of each effect differs for each of the two elements at the conditions tested.

Finally, this study provided new insight into the nature of the PV life cycle. PV production was already detected 20 h post-infection, similarly to the production of HFPV-1 and HRTV-DL1 particles. The plasmid:host ratio of plasmid pR1SE (up to 15.4) was significantly lower than that of the two viruses (virus:host ratio up to 10^3 for HFPV-1 in its preferred host *Hfx. volcanii* [39], and up to 297 for HRTV-DL1). However, this ratio was significantly higher than those of haloarchaeal mini-chromosomes or mega-plasmids (>100 kb, copy numbers ≤2) [81,82] and smaller archaeal plasmids (≤10 kb, copy numbers ranging from 6–15) [50,83,84]. Furthermore, plasmid:host ratios of pR1SE increased over time during prolonged infection, in contrast to previously reported data on the dissemination of large conjugative plasmids (~25–45 kb) in the *Sulfolobaceae*, where copy numbers declined over time to reach stable low copy numbers in the long-term [85–87]. We suggest that this difference is caused by the dissemination mechanism of plasmid pR1SE, which is more similar to the transmission of viruses rather than the transmission of conjugative plasmids. Thus, this mobile genetic element behaves more similarly to an actively replicating virus than to a conventional plasmid. The rapid replication and dissemination of plasmid pR1SE do not have any apparent negative effect on host fitness, posing further questions as to the nature of the interaction between the host and these plasmid vesicles at the edge of the virosphere [44].

5. Conclusions

This study revealed that N-glycosylation is not only crucial for *Hrr. lacusprofundi* cells to adapt to changing environmental conditions, but also for the stability of some viruses and virus-like particles that include glycosylated proteins. At the same time, N-glycosylation does not play a role in host cell recognition and attachment for HRTV-DL1, HFPV-1 and PVs. We propose that destabilization of the S-layer leads to increased entry and exit of membrane-enveloped HFPV-1, indicating that HFPV-1 might depend on naturally occurring gaps in the S-layer for exit and entry. Finally, our study revealed that plasmid pR1SE copy numbers range between those of viruses and similarly sized plasmids, supporting the hypothesis that PVs are an intermediate between plasmids and viruses, potentially representing evolutionary precursors of viruses.

Supplementary Materials: The following supporting information can be downloaded at: https://www.mdpi.com/article/10.3390/v15071469/s1; Supplementary Figures S1–S3 and Supplementary Table S1 are available as combined pdf file.

Author Contributions: L.J.G. performed experiments with HRTV-DL1 and PVs, and performed strain characterization. Z.V. generated the Δ*aglB* mutant strain and performed strain characterization. T.A.-S. performed experiments with HFPV-1. S.E. and J.E. conceived and led the study, and L.J.G. and S.E. performed the primary writing of the manuscript. All authors have read and agreed to the published version of the manuscript.

Funding: Funding was provided by the Volkswagen Foundation (reference 98 190) to J.E. and S.E. and the Max Planck Society (Munich, Germany) to S.E.

Institutional Review Board Statement: Not applicable.

Informed Consent Statement: Not applicable.

Data Availability Statement: Not applicable.

Acknowledgments: We thank Elina Roine and Kirsi Laukkanen, University of Helsinki, for providing the qPCR primer sequences for plasmid pR1SE. We thank Daniela Thies (MPI for Marine Microbiology, Bremen, Germany) for assistance with the experiments. Finally, we want to thank the Max-Planck-Institute for Marine Microbiology and the Max-Planck-Society for continuous support.

Conflicts of Interest: The authors declare no conflict of interest.

References

1. Jarrell, K.F.; Ding, Y.; Meyer, B.H.; Albers, S.-V.; Kaminski, L.; Eichler, J. N-Linked Glycosylation in *Archaea*: A Structural, Functional, and Genetic Analysis. *Microbiol. Mol. Biol. Rev.* **2014**, *78*, 304–341. [CrossRef] [PubMed]
2. Eichler, J. *N*-glycosylation in Archaea—New roles for an ancient posttranslational modification. *Mol. Microbiol.* **2020**, *114*, 735–741. [CrossRef] [PubMed]
3. Magidovich, H.; Eichler, J. Glycosyltransferases and oligosaccharyltransferases in *Archaea*: Putative components of the *N*-glycosylation pathway in the third domain of life. *FEMS Microbiol. Lett.* **2009**, *300*, 122–130. [CrossRef] [PubMed]
4. Kaminski, L.; Lurie-Weinberger, M.N.; Allers, T.; Gophna, U.; Eichler, J. Phylogenetic- and genome-derived insight into the evolution of *N*-glycosylation in Archaea. *Mol. Phylogenet. Evol.* **2013**, *68*, 327–339. [CrossRef]
5. Abdul Halim, M.F.; Karch, K.R.; Zhou, Y.; Haft, D.H.; Garcia, B.A.; Pohlschroder, M. Permuting the PGF Signature Motif Blocks both Archaeosortase-Dependent C-Terminal Cleavage and Prenyl Lipid Attachment for the *Haloferax volcanii* S-Layer Glycoprotein. *J. Bacteriol.* **2015**, *198*, 808–815. [CrossRef] [PubMed]
6. Nikolayev, S.; Cohen-Rosenzweig, C.; Eichler, J. Evolutionary considerations of the oligosaccharyltransferase AglB and other aspects of *N*-glycosylation across *Archaea*. *Mol. Phylogenetics Evol.* **2020**, *153*, 106951. [CrossRef]
7. Yurist-Doutsch, S.; Magidovich, H.; Ventura, V.V.; Hitchen, P.G.; Dell, A.; Eichler, J. *N*-glycosylation in Archaea: On the coordinated actions of *Haloferax volcanii* AglF and AglM. *Mol. Microbiol.* **2010**, *75*, 1047–1058. [CrossRef]
8. Tamir, A.; Eichler, J. *N*-glycosylation Is Important for Proper *Haloferax volcanii* S-Layer Stability and Function. *Appl. Environ. Microbiol.* **2017**, *83*, e03152-16. [CrossRef]
9. Vershinin, Z.; Zaretsky, M.; Guan, Z.; Eichler, J. Identifying Components of a *Halobacterium salinarum N*-glycosylation Pathway. *Front. Microbiol.* **2021**, *12*, 779599. [CrossRef]
10. Shalev, Y.; Turgeman-Grott, I.; Tamir, A.; Eichler, J.; Gophna, U. Cell Surface Glycosylation Is Required for Efficient Mating of *Haloferax volcanii*. *Front. Microbiol.* **2017**, *8*, 1253. [CrossRef]

11. Shalev, Y.; Soucy, S.M.; Papke, R.T.; Gogarten, J.P.; Eichler, J.; Gophna, U. Comparative Analysis of Surface Layer Glycoproteins and Genes Involved in Protein Glycosylation in the Genus *Haloferax*. *Genes* **2018**, *9*, 172. [CrossRef] [PubMed]
12. Kandiba, L.; Aitio, O.; Helin, J.; Guan, Z.; Permi, P.; Bamford, D.H.; Eichler, J.; Roine, E. Diversity in prokaryotic glycosylation: An archaeal-derived N-linked glycan contains legionaminic acid. *Mol. Microbiol.* **2012**, *84*, 578–593. [CrossRef] [PubMed]
13. Zaretsky, M.; Roine, E.; Eichler, J. Sialic Acid-Like Sugars in *Archaea*: Legionaminic Acid Biosynthesis in the Halophile *Halorubrum* sp. PV6. *Front. Microbiol.* **2018**, *9*, 2133. [CrossRef]
14. Abu-Qarn, M.; Giordano, A.; Battaglia, F.; Trauner, A.; Hitchen, P.G.; Morris, H.R.; Dell, A.; Eichler, J. Identification of AglE, a Second Glycosyltransferase Involved in N Glycosylation of the *Haloferax volcanii* S-Layer Glycoprotein. *J. Bacteriol.* **2008**, *190*, 3140–3146. [CrossRef]
15. Yurist-Doutsch, S.; Abu-Qarn, M.; Battaglia, F.; Morris, H.R.; Hitchen, P.G.; Dell, A.; Eichler, J. aglF, aglG and aglI, novel members of a gene island involved in the *N*-glycosylation of the *Haloferax volcanii* S-layer glycoprotein. *Mol. Microbiol.* **2008**, *69*, 1234–1245. [CrossRef] [PubMed]
16. Guan, Z.; Naparstek, S.; Kaminski, L.; Konrad, Z.; Eichler, J. Distinct glycan-charged phosphodolichol carriers are required for the assembly of the pentasaccharide N-linked to the *Haloferax volcanii* S-layer glycoprotein. *Mol. Microbiol.* **2010**, *78*, 1294–1303. [CrossRef]
17. Kaminski, L.; Eichler, J. Identification of Residues Important for the Activity of *Haloferax volcanii* AglD, a Component of the Archaeal *N*-glycosylation Pathway. *Archaea* **2010**, *2010*, 315108. [CrossRef]
18. Abu-Qarn, M.; Yurist-Doutsch, S.; Giordano, A.; Trauner, A.; Morris, H.R.; Hitchen, P.; Medalia, O.; Dell, A.; Eichler, J. *Haloferax volcanii* AglB and AglD are Involved in *N*-glycosylation of the S-layer Glycoprotein and Proper Assembly of the Surface Layer. *J. Mol. Biol.* **2007**, *374*, 1224–1236. [CrossRef]
19. Kandiba, L.; Lin, C.W.; Aebi, M.; Eichler, J.; Guerardel, Y. Structural characterization of the N-linked pentasaccharide decorating glycoproteins of the halophilic archaeon *Haloferax volcanii*. *Glycobiology* **2016**, *26*, 745–756. [CrossRef]
20. Kohda, D. Structural Basis of Protein Asn-Glycosylation by Oligosaccharyltransferases. In *Glycobiophysics*; Yamaguchi, Y., Kato, K., Eds.; Springer: Singapore, 2018; pp. 171–199. [CrossRef]
21. Cohen-Rosenzweig, C.; Yurist-Doutsch, S.; Eichler, J. AglS, a Novel Component of the *Haloferax volcanii N*-glycosylation Pathway, Is a Dolichol Phosphate-Mannose Mannosyltransferase. *J. Bacteriol.* **2012**, *194*, 6909–6916. [CrossRef]
22. Kaminski, L.; Guan, Z.; Abu-Qarn, M.; Konrad, Z.; Eichler, J. AglR is required for addition of the final mannose residue of the N-linked glycan decorating the *Haloferax volcanii* S-layer glycoprotein. *Biochim. Et Biophys. Acta (BBA) Gen. Subj.* **2012**, *1820*, 1664–1670. [CrossRef] [PubMed]
23. Pfeiffer, F.; Losensky, G.; Marchfelder, A.; Habermann, B.; Dyall-Smith, M. Whole-genome comparison between the type strain of *Halobacterium salinarum* (DSM 3754T) and the laboratory strains R1 and NRC-1. *Microbiologyopen* **2020**, *9*, e974. [CrossRef] [PubMed]
24. Bignon, E.A.; Chou, K.R.; Roine, E.; Tischler, N.D. Halorubrum pleomorphic virus-6 Membrane Fusion Is Triggered by an S-Layer Component of Its Haloarchaeal Host. *Viruses* **2022**, *14*, 254. [CrossRef] [PubMed]
25. Liu, Y.; Demina, T.A.; Roux, S.; Aiewsakun, P.; Kazlauskas, D.; Simmonds, P.; Prangishvili, D.; Oksanen, H.M.; Krupovic, M. Diversity, taxonomy, and evolution of archaeal viruses of the class *Caudoviricetes*. *PLoS Biol.* **2021**, *19*, e3001442. [CrossRef]
26. Mercier, C.; Thies, D.; Zhong, L.; Raftery, M.J.; Cavicchioli, R.; Erdmann, S. In depth characterization of an archaeal virus-host system reveals numerous virus exclusion mechanisms. *bioRxiv* **2022**. [CrossRef]
27. Schwarzer, S.; Hackl, T.; Oksanen Hanna, M.; Quax Tessa, E.F. Archaeal Host Cell Recognition and Viral Binding of HFTV1 to Its *Haloferax* Host. *mBio* **2023**, *14*, e01833-22. [CrossRef]
28. Zink, I.A.; Pfeifer, K.; Wimmer, E.; Sleytr, U.B.; Schuster, B.; Schleper, C. CRISPR-mediated gene silencing reveals involvement of the archaeal S-layer in cell division and virus infection. *Nat. Commun.* **2019**, *10*, 4797. [CrossRef]
29. Quemin, E.R.J.; Chlanda, P.; Sachse, M.; Forterre, P.; Prangishvili, D.; Krupovic, M. Eukaryotic-Like Virus Budding in *Archaea*. *mBio* **2016**, *7*, e01439-16. [CrossRef]
30. Quemin, E.R.J.; Pietilä, M.K.; Oksanen, H.M.; Forterre, P.; Rijpstra, W.I.C.; Schouten, S.; Bamford, D.H.; Prangishvili, D.; Krupovic, M. *Sulfolobus* Spindle-Shaped Virus 1 Contains Glycosylated Capsid Proteins, a Cellular Chromatin Protein, and Host-Derived Lipids. *J. Virol.* **2015**, *89*, 11681–11691. [CrossRef]
31. Han, Z.; Yuan, W.; Xiao, H.; Wang, L.; Zhang, J.; Peng, Y.; Cheng, L.; Liu, H.; Huang, L. Structural insights into a spindle-shaped archaeal virus with a sevenfold symmetrical tail. *Proc. Natl. Acad. Sci. USA* **2022**, *119*, e2119439119. [CrossRef]
32. Hartman, R.; Biewenga, L.; Munson-McGee, J.; Refai, M.; Boyd, E.S.; Bothner, B.; Lawrence, C.M.; Young, M. Discovery and Characterization of Thermoproteus Spherical Piliferous Virus 1: A Spherical Archaeal Virus Decorated with Unusual Filaments. *J. Virol.* **2020**, *94*, e00036-20. [CrossRef] [PubMed]
33. Kim, J.-G.; Kim, S.-J.; Cvirkaite-Krupovic, V.; Yu, W.-J.; Gwak, J.-H.; López-Pérez, M.; Rodriguez-Valera, F.; Krupovic, M.; Cho, J.-C.; Rhee, S.-K. Spindle-shaped viruses infect marine ammonia-oxidizing thaumarchaea. *Proc. Natl. Acad. Sci. USA* **2019**, *116*, 15645–15650. [CrossRef] [PubMed]
34. Larson, E.T.; Reiter, D.; Young, M.; Lawrence, C.M. Structure of A197 from *Sulfolobus* Turreted Icosahedral Virus: A Crenarchaeal Viral Glycosyltransferase Exhibiting the GT-A Fold. *J. Virol.* **2006**, *80*, 7636–7644. [CrossRef]
35. Bath, C.; Cukalac, T.; Porter, K.; Dyall-Smith, M.L. His1 and His2 are distantly related, spindle-shaped haloviruses belonging to the novel virus group, *Salterprovirus*. *Virology* **2006**, *350*, 228–239. [CrossRef]

36. Iranzo, J.; Koonin Eugene, V.; Prangishvili, D.; Krupovic, M. Bipartite Network Analysis of the Archaeal Virosphere: Evolutionary Connections between Viruses and Capsidless Mobile Elements. *J. Virol.* **2016**, *90*, 11043–11055. [CrossRef] [PubMed]
37. Munson-McGee, J.H.; Rooney, C.; Young, M.J. An Uncultivated Virus Infecting a Nanoarchaeal Parasite in the Hot Springs of Yellowstone National Park. *J. Virol.* **2020**, *94*, e01213-19. [CrossRef]
38. Rambo, I.M.; Langwig, M.V.; Leão, P.; De Anda, V.; Baker, B.J. Genomes of six viruses that infect Asgard archaea from deep-sea sediments. *Nat. Microbiol.* **2022**, *7*, 953–961. [CrossRef]
39. Alarcón-Schumacher, T.; Naor, A.; Gophna, U.; Erdmann, S. Isolation of a virus causing a chronic infection in the archaeal model organism *Haloferax volcanii* reveals antiviral activities of a provirus. *Proc. Natl. Acad. Sci. USA* **2022**, *119*, e2205037119. [CrossRef] [PubMed]
40. Pietilä, M.K.; Roine, E.; Sencilo, A.; Bamford, D.H.; Oksanen, H.M. *Pleolipoviridae*, a newly proposed family comprising archaeal pleomorphic viruses with single-stranded or double-stranded DNA genomes. *Arch. Virol.* **2016**, *161*, 249–256. [CrossRef]
41. Erdmann, S.; Tschitschko, B.; Zhong, L.; Raftery, M.J.; Cavicchioli, R. A plasmid from an Antarctic haloarchaeon uses specialized membrane vesicles to disseminate and infect plasmid-free cells. *Nat. Microbiol.* **2017**, *2*, 1446. [CrossRef]
42. Forterre, P.; Da Cunha, V.; Catchpole, R. Plasmid vesicles mimicking virions. *Nat. Microbiol.* **2017**, *2*, 1340. [CrossRef]
43. Mills, J.; Gebhard, L.J.; Schubotz, F.; Shevchenko, A.; Speth, D.R.; Liao, Y.; Duggin, I.G.; Marchfelder, A.; Erdmann, S. Extracellular vesicles of *Euryarchaeida*: Precursor to eukaryotic membrane trafficking. *bioRxiv* **2023**. [CrossRef]
44. Koonin, E.V.; Dolja, V.V.; Krupovic, M.; Kuhn, J.H. Viruses Defined by the Position of the Virosphere within the Replicator Space. *Microbiol. Mol. Biol. Rev.* **2021**, *85*, e00193-20. [CrossRef] [PubMed]
45. Burns, D.; Dyall-Smith, M. 22 Cultivation of haloarchaea. In *Methods in Microbiology*; Elsevier: Amsterdam, The Netherlands, 2006; Volume 35, pp. 535–552.
46. Gebhard, L.J.; Duggin, I.G.; Erdmann, S. Improving the genetic system for *Halorubrum lacusprofundi* to allow in-frame deletions. *Front. Microbiol.* **2023**, *14*, 5621. [CrossRef] [PubMed]
47. Dyall-Smith, M. *The Halohandbook: Protocols for Halobacterial Genetics*, Version 7.3. 2009. Available online: https://haloarchaea.com/wp-content/uploads/2018/10/Halohandbook_2009_v7.3mds.pdf(accessed on 1 November 2022).
48. Franzmann, P.; Stackebrandt, E.; Sanderson, K.; Volkman, J.; Cameron, D.; Stevenson, P.; McMeekin, T.; Burton, H. *Halobacterium lacusprofundi* sp. nov., a halophilic bacterium isolated from Deep Lake, Antarctica. *Syst. Appl. Microbiol.* **1988**, *11*, 20–27. [CrossRef]
49. Allers, T.; Ngo, H.-P.; Mevarech, M.; Lloyd, R.G. Development of Additional Selectable Markers for the Halophilic Archaeon *Haloferax volcanii* Based on the *leuB* and *trpA* Genes. *Appl. Environ. Microbiol.* **2004**, *70*, 943–953. [CrossRef]
50. Snedecor, G.; Cochran, W. *Statistical Methods*, 7th ed.; The Iowa State University: Ames, IA, USA, 1989.
51. Levene, H. Robust tests for equality of variances. In *Contributions to Probability and Statistics*; Olkin, I., Ed.; Stanford University Press: Palo Alto, CA, USA, 1960; pp. 278–292.
52. Fligner, M.A.; Killeen, T.J. Distribution-Free Two-Sample Tests for Scale. *J. Am. Stat. Assoc.* **1976**, *71*, 210–213. [CrossRef]
53. R Core Team. *R: A Language and Environment for Statistical Computing*, Version 4.1.2; R Foundation for Statistical Computing: Vienna, Austria, 2021.
54. *RStudio TeamRStudio: Integrated Development Environment for R*, Version 2023.3.0.386; Posit Software, PBC: Boston, MA, USA, 2023. Available online: http://www.rstudio.com/(accessed on 1 November 2022).
55. Dubray, G.; Bezard, G. A highly sensitive periodic acid-silver stain for 1,2-diol groups of glycoproteins and polysaccharides in polyacrylamide gels. *Anal. Biochem.* **1982**, *119*, 325–329. [CrossRef]
56. Deatherage, B.L.; Cookson, B.T. Membrane vesicle release in bacteria, eukaryotes, and archaea: A conserved yet underappreciated aspect of microbial life. *Infect. Immun.* **2012**, *80*, 1948–1957. [CrossRef]
57. Schatz, D.; Vardi, A. Extracellular vesicles—New players in cell–cell communication in aquatic environments. *Curr. Opin. Microbiol.* **2018**, *43*, 148–154. [CrossRef]
58. Gill, S.; Catchpole, R.; Forterre, P. Extracellular membrane vesicles in the three domains of life and beyond. *FEMS Microbiol. Rev.* **2019**, *43*, 273–303. [CrossRef] [PubMed]
59. Gavel, Y.; von Heijne, G. Sequence differences between glycosylated and non-glycosylated Asn-X-Thr/Ser acceptor sites: Implications for protein engineering. *Protein Eng.* **1990**, *3*, 433–442. [CrossRef]
60. Mäntynen, S.; Laanto, E.; Oksanen, H.M.; Poranen, M.M.; Díaz-Muñoz, S.L. Black box of phage–bacterium interactions: Exploring alternative phage infection strategies. *Open Biol.* **2021**, *11*, 210188. [CrossRef] [PubMed]
61. Zaretsky, M.; Darnell, C.L.; Schmid, A.K.; Eichler, J. *N*-glycosylation Is Important for *Halobacterium salinarum* Archaellin Expression, Archaellum Assembly and Cell Motility. *Front. Microbiol.* **2019**, *10*, 1367. [CrossRef] [PubMed]
62. Chaban, B.; Voisin, S.; Kelly, J.; Logan, S.M.; Jarrell, K.F. Identification of genes involved in the biosynthesis and attachment of *Methanococcus voltae* N-linked glycans: Insight into N-linked glycosylation pathways in *Archaea*. *Mol. Microbiol.* **2006**, *61*, 259–268. [CrossRef]
63. Guan, Z.; Naparstek, S.; Calo, D.; Eichler, J. Protein glycosylation as an adaptive response in *Archaea*: Growth at different salt concentrations leads to alterations in *Haloferax volcanii* S-layer glycoprotein *N*-glycosylation. *Environ. Microbiol.* **2012**, *14*, 743–753. [CrossRef]
64. Kaminski, L.; Guan, Z.; Yurist-Doutsch, S.; Eichler, J. Two Distinct *N*-glycosylation Pathways Process the *Haloferax volcanii* S-Layer Glycoprotein upon Changes in Environmental Salinity. *mBio* **2013**, *4*, e00716-13. [CrossRef]

65. Mescher, M.F.; Strominger, J.L. Purification and characterization of a prokaryotic glycoprotein from the cell envelope of *Halobacterium salinarium*. *J. Biol. Chem.* **1976**, *251*, 2005–2014. [CrossRef]
66. Sumper, M.; Berg, E.; Mengele, R.; Strobel, I. Primary structure and glycosylation of the S-layer protein of *Haloferax volcanii*. *J. Bacteriol.* **1990**, *172*, 7111–7118. [CrossRef]
67. Lu, H.; Pei, C.; Zhou, H.; Lü, Y.; He, Y.; Li, Y.; Han, J.; Xiang, H.; Eichler, J.; Jin, C. Agl22 and Agl23 are involved in the synthesis and utilization of the lipid-linked intermediates in the glycosylation pathways of the halophilic archaeaon *Haloarcula hispanica*. *Mol. Microbiol.* **2020**, *114*, 762–774. [CrossRef]
68. Kelly, J.; Vinogradov, E.; Robotham, A.; Tessier, L.; Logan, S.M.; Jarrell, K.F. Characterizing the N- and O-linked glycans of the PGF-CTERM sorting domain-containing S-layer protein of *Methanoculleus marisnigri*. *Glycobiology* **2022**, *32*, 629–644. [CrossRef] [PubMed]
69. Tschitschko, B.; Williams, T.J.; Allen, M.A.; Páez-Espino, D.; Kyrpides, N.; Zhong, L.; Raftery, M.J.; Cavicchioli, R. Antarctic archaea–virus interactions: Metaproteome-led analysis of invasion, evasion and adaptation. *ISME J.* **2015**, *9*, 2094–2107. [CrossRef] [PubMed]
70. Legrand, P.; Collins, B.; Blangy, S.; Murphy, J.; Spinelli, S.; Gutierrez, C.; Richet, N.; Kellenberger, C.; Desmyter, A.; Mahony, J.; et al. The Atomic Structure of the Phage Tuc2009 Baseplate Tripod Suggests that Host Recognition Involves Two Different Carbohydrate Binding Modules. *mBio* **2016**, *7*, e01781-15. [CrossRef]
71. Hayes, S.; Vincentelli, R.; Mahony, J.; Nauta, A.; Ramond, L.; Lugli, G.A.; Ventura, M.; van Sinderen, D.; Cambillau, C. Functional carbohydrate binding modules identified in evolved dits from siphophages infecting various Gram-positive bacteria. *Mol. Microbiol.* **2018**, *110*, 777–795. [CrossRef] [PubMed]
72. Lavelle, K.; Goulet, A.; McDonnell, B.; Spinelli, S.; van Sinderen, D.; Mahony, J.; Cambillau, C. Revisiting the host adhesion determinants of *Streptococcus thermophilus* siphophages. *Microb. Biotechnol.* **2020**, *13*, 1765–1779. [CrossRef] [PubMed]
73. Beamud, B.; García-González, N.; Gómez-Ortega, M.; González-Candelas, F.; Domingo-Calap, P.; Sanjuan, R. Genetic determinants of host tropism in *Klebsiella* phages. *Cell Rep.* **2023**, *42*, 112048. [CrossRef]
74. Atanasova, N.S.; Roine, E.; Oren, A.; Bamford, D.H.; Oksanen, H.M. Global network of specific virus–host interactions in hypersaline environments. *Environ. Microbiol.* **2012**, *14*, 426–440. [CrossRef]
75. Atanasova, N.S.; Demina, T.A.; Buivydas, A.; Bamford, D.H.; Oksanen, H.M. Archaeal viruses multiply: Temporal screening in a solar saltern. *Viruses* **2015**, *7*, 1902–1926. [CrossRef]
76. Mizuno, C.M.; Prajapati, B.; Lucas-Staat, S.; Sime-Ngando, T.; Forterre, P.; Bamford, D.H.; Prangishvili, D.; Krupovic, M.; Oksanen, H.M. Novel haloarchaeal viruses from Lake Retba infecting *Haloferax* and *Halorubrum* species. *Environ. Microbiol.* **2019**, *21*, 2129–2147. [CrossRef]
77. Quemin, E.R.J.; Quax, T.E.F. Archaeal viruses at the cell envelope: Entry and egress. *Front. Microbiol.* **2015**, *6*, 552. [CrossRef]
78. Konrad, Z.; Eichler, J. Lipid modification of proteins in Archaea: Attachment of a mevalonic acid-based lipid moiety to the surface-layer glycoprotein of *Haloferax volcanii* follows protein translocation. *Biochem. J.* **2002**, *366*, 959–964. [CrossRef] [PubMed]
79. Abdul Halim, M.F.; Pfeiffer, F.; Zou, J.; Frisch, A.; Haft, D.; Wu, S.; Tolić, N.; Brewer, H.; Payne, S.H.; Paša-Tolić, L.; et al. *Haloferax volcanii* archaeosortase is required for motility, mating, and C-terminal processing of the S-layer glycoprotein. *Mol. Microbiol.* **2013**, *88*, 1164–1175. [CrossRef] [PubMed]
80. Kandiba, L.; Guan, Z.; Eichler, J. Lipid modification gives rise to two distinct *Haloferax volcanii* S-layer glycoprotein populations. *Biochim. Biophys. Acta* **2013**, *1828*, 938–943. [CrossRef] [PubMed]
81. Hawkins, M.; Malla, S.; Blythe, M.J.; Nieduszynski, C.A.; Allers, T. Accelerated growth in the absence of DNA replication origins. *Nature* **2013**, *503*, 544–547. [CrossRef]
82. Liu, X.; Miao, D.; Zhang, F.; Wu, Z.; Liu, J.; Xiang, H. Characterization of the minimal replicon of pHM300 and independent copy number control of major and minor chromosomes of *Haloferax mediterranei*. *FEMS Microbiol. Lett.* **2013**, *339*, 66–74. [CrossRef]
83. Chen, S.; Wang, C.; Xiang, H. Sequence analysis and minimal replicon determination of a new haloarchaeal plasmid pHF2 isolated from *Haloferax* sp. strain Q22. *Plasmid* **2016**, *83*, 1–7. [CrossRef]
84. Charlebois, R.L.; Lam, W.L.; Cline, S.W.; Doolittle, W.F. Characterization of pHV2 from *Halobacterium volcanii* and its use in demonstrating transformation of an archaebacterium. *Proc. Natl. Acad. Sci. USA* **1987**, *84*, 8530–8534. [CrossRef]
85. Schleper, C.; Holz, I.; Janekovic, D.; Murphy, J.; Zillig, W. A multicopy plasmid of the extremely thermophilic archaeon *Sulfolobus* effects its transfer to recipients by mating. *J. Bacteriol.* **1995**, *177*, 4417–4426. [CrossRef]
86. Prangishvili, D.; Albers, S.-V.; Holz, I.; Arnold, H.P.; Stedman, K.; Klein, T.; Singh, H.; Hiort, J.; Schweier, A.; Kristjansson, J.K.; et al. Conjugation in Archaea: Frequent Occurrence of Conjugative Plasmids in *Sulfolobus*. *Plasmid* **1998**, *40*, 190–202. [CrossRef]
87. Erauso, G.; Stedman, K.M.; van de Werken, H.J.G.; Zillig, W.; van der Oost, J. Two novel conjugative plasmids from a single strain of *Sulfolobus*. *Microbiology* **2006**, *152*, 1951–1968. [CrossRef]

Disclaimer/Publisher's Note: The statements, opinions and data contained in all publications are solely those of the individual author(s) and contributor(s) and not of MDPI and/or the editor(s). MDPI and/or the editor(s) disclaim responsibility for any injury to people or property resulting from any ideas, methods, instructions or products referred to in the content.

Supplementary Material

Influence of N-Glycosylation on Virus-Host Interactions in *Halorubrum lacusprofundi*

Table of contents

Supplementary Figures

Supplementary Tables

Supplementary Figures

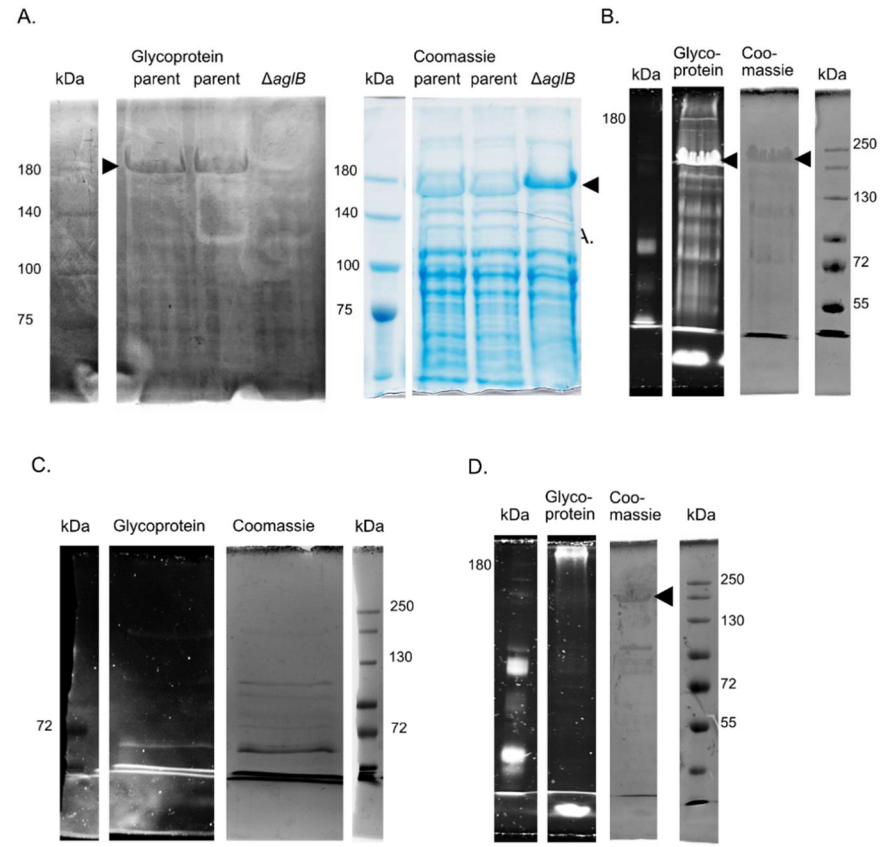

Supplementary Figure 1: Glycoprotein staining of cells and infectious agents. Cell preparations from parent and Δ*aglB* strains **(A)** were separated via SDS-PAGE (8% Acrylamide) and stained with either periodic acid-Schiff staining or Coomassie dye to visualize all proteins. ExcelBand 3-color Regular Range Protein Marker (Bio Lab) was added a as a size standard (kDa), the position of the S-layer glycoprotein is marked with black arrows in this and all following graphs. Purified preparations of HFPV-1 **(B),** HRTV-DL1 **(C)** and PVs **(D),** produced in their native host organisms, were separated via SDS-PAGE (8% Acrylamide). Glycoproteins were visualized with the Pro-Q Emerald 300 Glycoprotein Kit (Invitrogen) after which gels were stained with Coomassie Dye to visualize all proteins. CandyCane Glycoprotein Standard (Invitrogen, left) and broad Range Color Prestained Protein Standard (NEB, right) were added as size markers (kDa).

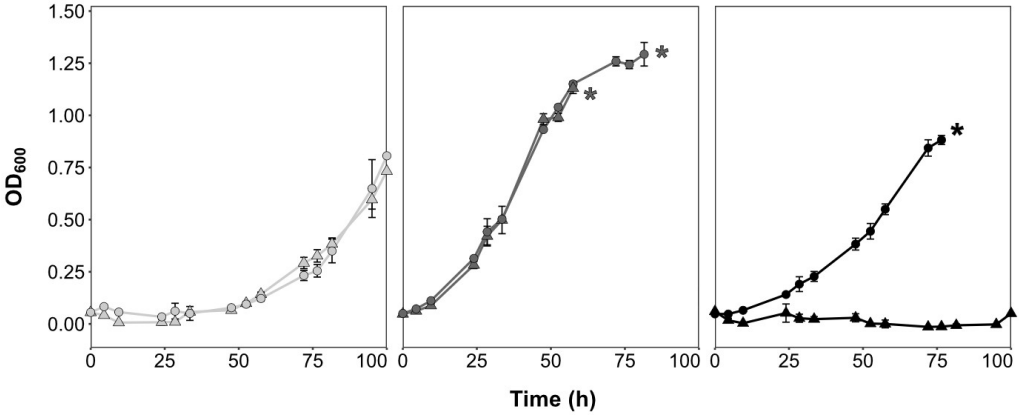

Supplementary Figure 2: The Δ*aglB* mutant shows decreased adaptability to changes in sodium chloride concentrations, as compared to the parent strain.

The growth of the parent (Δ*pyrE2,* circles) and Δ*aglB* (triangles) strains was monitored in media containing NaCl concentrations of 100 g/l = 1.7 M (light grey), 180 g/l = 3.1 M (dark grey) or 250 g/l = 4.3 M (black). The growth data for 180 g/l was generated in a separate experiment to the data shown in Figure 1B, simultaneously with the 100 g/l and 250 g/l cultures. Each point represents the average of three biological replicates ± standard deviation of the mean. Asterisks indicate when cultures went into biofilm and OD_{600} could no longer be accurately measured.

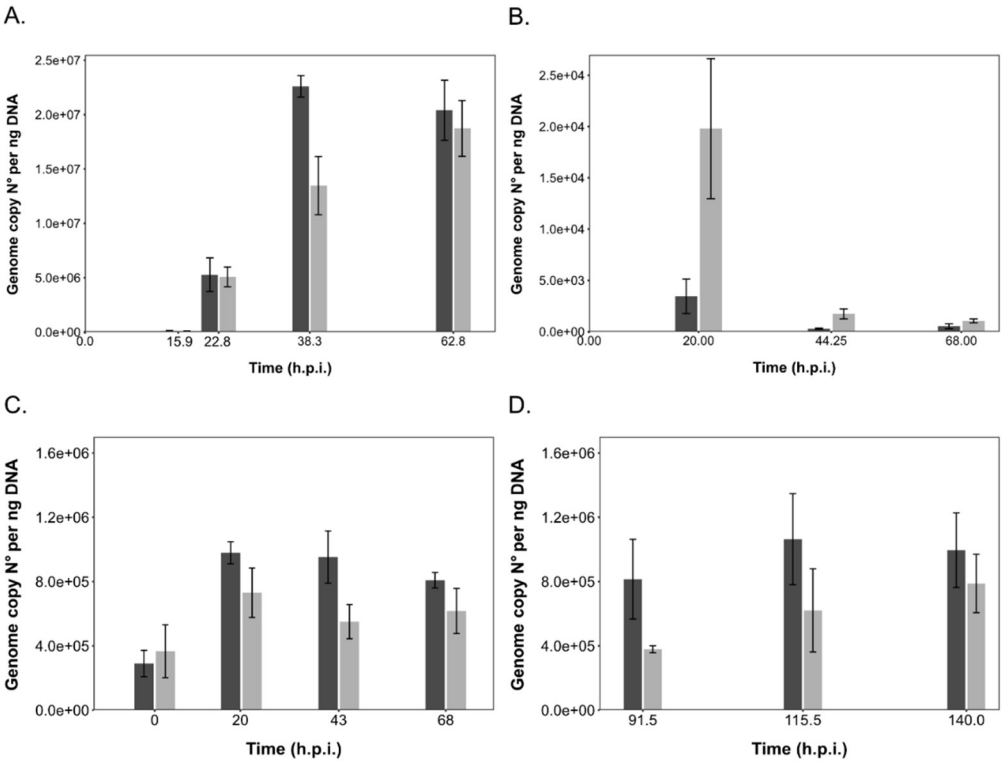

Supplementary Figure 3: Viral and plasmid genome copy numbers in cell pellets for the three infectious agents.

Viral or plasmid gcns per ng of DNA within cells upon infection with HRTV-DL1 **(A)** (Figure 3), HFPV-1 **(B)** (Figure 4), initial **(C)** and extended infection **(D)** with plasmid pR1SE (Figure 5). Bars represent the average of three biological replicates ± standard deviation of the mean for the parental strain (dark grey) and the Δ*aglB* mutant (light grey).

Supplementary Tables

Supplementary Table 1: Primers (PCR and qPCR) used in this study. Nucleotides in lowercase correspond to the exon-flanking regions of the *Hlac_1062* (*aglB*) gene.

Name	Target	Sequence 5' -> 3'	qPCR conditions: Annealing temperature, primer concentration
Hlac_1062-up FW	*Hrr. lacusprofundi Hlac_1062* (*aglB*) upstream fragment, including *EcoRI* restriction site (forward)	CTAGTGGATCCCCCGGGCTGCAGGAATTCcgaatccgcgatgcgtcacg	Not applicable
Hlac_1062-up REV	*Hrr. lacusprofundi Hlac_1062* (*aglB*) upstream fragment (reverse)	gatcaggcggcgggcgggaTCAGGCGCTCAttacgtgaagacgactgtc	Not applicable
Hlac_1062-down FW	*Hrr. lacusprofundi Hlac_1062* (*aglB*) downstream fragment (forward)	gttttgacagtcgtcttcacgtaATGAGCGCCTGatcccgcccgcc	Not applicable
Hlac_1062-down REV	*Hrr. lacusprofundi Hlac_1062* (*aglB*) downstream fragment, including *Hind*III restriction site (reverse)	CCCCTCGAGGTCGACGGTATCGATAAGCTTggaccggcggcgagctcgaaag	Not applicable
Hlac_1062 KO FW	PCR screening primer for *Hrr. lacusprofundi Hlac_1062* (forward)	CGAATCCGCGATGCGTCACG	Not applicable
Hlac_1062-2 FW	PCR screening primer for *Hrr. lacusprofundi Hlac_1062* (forward)	CGTTCCGACGACGCGAACC	Not applicable
Hlac_1062 KO REV	PCR screening primer for *Hrr. lacusprofundi Hlac_1062* (reverse)	GAGCTCGAAAGCGCCGTCG	Not applicable
16S rRNA FW	*Hrr. lacusprofundi* 16S rRNA for quantification (forward)	CGTGGCGAATAGCTCAGTAA	
16S rRNA REV	*Hrr. lacusprofundi* 16S rRNA for quantification (reverse)	TTCCAGGTGGATTGTGGTATG	
Hlac_1062 FW	*Hrr. lacusprofundi Hlac_1062* for quantification (forward)	CATCATGGAGAACTACCCGAATC	

Hlac_1062 REV	*Hrr. lacusprofundi Hlac_1062* for quantification (reverse)	CATGATGTGGTCCCAGAGTG	
TyrVUF	HFPV-1 infection detection	ACGAACGAGAACACCGACC	Not applicable
TyrVUR	HFPV-1 infection detection	TGATGACGAATCCAACGAGCAG	Not applicable
FVP3	VP3 of HFPV-1 for quantification (forward)	TTGCGTACGCGGTATCTGTC	68°C , 0.13 µM
RVP3	VP3 of HFPV-1 for quantification (reverse)	AGCTTCTCCGCATCGTCTTT	68°C , 0.13 µM
qPMC2 F	CH1 of all *Hrr. lacusprofundi* strains for quantification (forward)	GAGTTAGTGAAGTATCTTCG	61°C, 0.15 µM
qPMC2 R	CH1 of all *Hrr. lacusprofundi* strains for quantification (reverse)	GCTCTACATCCTCATAATAC	61°C, 0.15 µM
HRTV-DLF	HRTV-DL1 genome test for infection (forward)	CTAACAGCACGCCAAGAGGA	Not applicable
HRTV-DLR	HRTV-DL1 genome test for infection (reverse)	CACCACTGGTTTGCTTTCCG	Not applicable
BV37VPF	HRTV-DL1 genome for quantification (forward)	CACGCTCTCGGAAGCAAACC	71°C, 0.2 µM
BV37VPR	HRTV-DL1 genome for quantification (reverse)	CTCGGAGTCGCCATACTGGG	71°C, 0.2 µM
ORF6_seq1F	ORF6 of pR1SE to test for infection (forward)	CAATCATTTTCTGATTCGGAAGC	Not applicable
ORF6_seq1R	ORF6 of pR1SE to test for infection (reverse)	GAGGGTTGTGAGTCGTTGTAG	Not applicable
qORF6F	ORF6 of pR1SE for quantification (forward)	ATCGACGACGCAGCCAACAC	67.8°C, 0.125 µM
qORF6R	ORF6 of pR1SE for quantification (reverse)	GTGATTGCGTCCGGGTTGAG	67.8°C, 0.125 µM

Chapter III

Extracellular vesicles of Euryarchaeida: precursor to eukaryotic membrane trafficking

Extracellular vesicles of Euryarchaeida: precursor to eukaryotic membrane trafficking

Joshua Mills[1], L. Johanna Gebhard[1], Florence Schubotz[2], Anna Shevchenko[3], Daan R. Speth[4], Yan Liao[5], Iain G. Duggin[5], Anita Marchfelder[6] & Susanne Erdmann[1*]

[1]Archaeal Virology, Max Planck Institute for Marine Microbiology, Celsiusstrasse 1, 28359, Bremen, Germany

[2]MARUM Center for Marine Environmental Sciences, University of Bremen, Bremen 28359, Germany

[3]Max Planck Institute of Molecular Cell Biology and Genetics, Pfotenhauerstrasse 108, 01307, Dresden, Germany

[4]Department of Biogeochemistry, Max Planck Institute for Marine Microbiology, Celsiusstrasse 1, 28359, Bremen, Germany

[5]The Australian Institute for Microbiology and Infection, University of Technology Sydney, Sydney, New South Wales, Australia

[6]Biology II, Ulm University, Ulm, Germany

* Manuscript under review at *PNAS*, this preprint version is available on *bioRxiv*

Author contributions: J.M. performed the majority of the experimental work. L.J.G. and F.C. performed the lipid analysis. A.S. performed proteomics. Y.L. generated the AglB mutant. D.S. performed oapA phylogeny analysis. S.E. discovered the presence of RNA in EVs, conceived and led the study. I.D. and A.M. led the initial phase of the study. Some of the experiments were performed in A.M. laboratory. J.M. and S.E. performed the primary writing of the manuscript. All authors participated in the analysis and interpretation of the data and contributed to the writing of the manuscript

Abstract

Since their discovery, extracellular vesicles (EVs) have changed our view on how organisms interact with their extracellular world. EVs are able to traffic a diverse array of molecules across different species and even domains, facilitating numerous functions. In this study, we investigate EV production in *Haloferax volcanii*, as representative for Euryarchaeida. We uncover that EVs enclose RNA, with specific transcripts preferentially enriched, including those with regulatory potential, and conclude that EVs can act as an RNA communication system between haloarchaea. We demonstrate the key role of an EV-associated Ras superfamily GTPase for EV formation in *H. volcanii* that is also present across other diverse evolutionary branches of Archaea. Ras superfamily GTPases are key players in eukaryotic intracellular vesicle formation and trafficking mechanisms that have been crucial for the emergence of Eukaryotes. Therefore, we propose that archaeal EV formation could reveal insights into the origin of the compartmentalized eukaryotic cell.

Introduction

Extracellular vesicles (EVs) (also referred to as outer membrane vesicles, membrane vesicles, or exosomes) are small membrane bound structures that bud off from the cellular envelope, and are produced by living cells across all domains of life [1–3]. They are able to enclose a wide range of cargo, including proteins, nucleic acids, and signaling molecules, facilitating a mechanism of interaction with the extracellular world. Communication mediated through EVs provides specific advantages for the cell, such as protection of the cargo from environmental stressors and degradation, the concentration of specific molecules into a self-contained structure, and the potential for selective delivery to designated targets [4, 5]. With the diversity of

EV composition and the advantages of EV-based communication, prokaryotic EV trafficking has been connected to a wide range of cellular functions. EVs have been discovered to act as defense against viral infection and antibiotic stress [6], mediating Bacteria-host interactions through the trafficking of regulatory RNA [7, 8], and facilitating the transfer of genetic material between cells [9, 10]. Both their ubiquity amongst organisms and cellular functions make EVs an exciting new field for exploring intercellular communication and expand our view of the dynamics driving microbial environments.

EVs are known to be present in marine and aquatic samples [11, 12], and they likely play important roles in regulating environmental microbial populations. However, while there is a growing amount of research focusing on EVs deriving from pathogenic Bacteria and their role in Bacteria-host interactions, fewer studies have investigated the role that EVs play in microbial ecology, and even less investigate EVs in Archaea. Within the archaeal domain, EVs from only a few organisms have been studied. For the *Thermoproteota* (formerly *Crenarchaeota*) genus, *Sulfolobus*, vesicles were found to enclose proteinaceous toxins [13] as well as fragmented genomic DNA [14]. Members of the Euryarchaeida have also been found to produce EVs enriched with DNA such as *Thermococcus* [15]. *Halorubrum lacusprofundi* [16] was found to produce specialized EVs including plasmid-encoded proteins and plasmid DNA (named plasmid vesicles, PVs). These studies demonstrate the ability of archaeal EVs to transport DNA between cells, which suggests that EV production may play an important role in horizontal gene transfer in Archaea. This route of genetic exchange may be especially beneficial for organisms in extreme environments to counteract various common stressors.

EV production in *Sulfolobus* has been linked to its ESCRT (endosomal sorting complex required for transport)-like cell division machinery [14]. The ESCRT system is well studied in Eukaryotes, and is responsible for the sorting and production of exosomes and the budding of various viruses [17],

suggesting an evolutionary linkage between EV formation in *Thermoproteota* and exosome production in Eukaryotes. However, ESCRT-like proteins are not present in most currently annotated Euryarchaeida genomes [18], suggesting that a different mechanism is responsible for EV production. Proteins homologous to eukaryotic intracellular vesicle trafficking system were identified in PVs from *Hrr. lacusprofundi*, a member of the Euryarchaeida, implying that multiple mechanisms of vesicle production exist among the archaeal domain [16].

In order to understand EV production in Euryarchaeida, and in particular halophilic Archaea (haloarchaea), we used the model organism, *Haloferax volcanii*, to investigate the composition of EVs as well as their capacity to transfer their cargo to other organisms. We observe for the first time particular RNAs being enriched in EVs of various haloarchaea, and demonstrate that the RNA cargo can be transferred between cells of the same species. We also investigated the roles of various genes in EV production, suggesting a mechanism for EV generation in halophilic Archaea that is related to intracellular vesicle trafficking in Eukaryotes. From our findings, we hypothesize that halophilic Archaea utilize EVs to communicate and potentially regulate the microbial community in hypersaline environments.

Methods

Strains and media

Haloferax volcanii strains and other haloarchaea used in this study are summarized in Supplementary Table 1. *H. volcanii* was either grown in minimal media HV-Ca supplemented with the SL10 trace elements and vitamins as described for DBCM2 [66] (HV-Cab), or nutrient rich media HV-YPC supplemented with the same trace elements and vitamins [66]. Cultures were grown in glass flasks aerobically at 120 rpm at the temperatures indicated. For auxotrophic strains that required additional nutrients, media was supplemented

with uracil (50 µg/mL) and tryptophan (50 µg/mL), depending on the strain (Supplementary Table 1). *Hbt. salinarum* was grown in media described in [67], aerobically at 45 °C and 120 rpm. *Halorubrum lacusprofundi* was grown in DBCM2 media [66] aerobically at 28 °C (120 rpm). UV treatment was performed by pouring the culture into a petri dish that was then placed into a UV crosslinker from Biometra™ and exposed to 0.05 J of UV radiation. Infection of *H. volcanii* cultures with the virus, HFPV-1, was performed as described in [22], and infection was confirmed by PCR as previously described in [22].

Generation of knock out strains

To construct plasmids for the deletion of *aglB* gene, PCR fragments of the upstream and downstream flanking sequences (~ 530 bp) were amplified (primers listed in Supplementary Table 2). The upstream and downstream fragments were joined by Gibson assembly and the products were digested with BamHI and HindIII (restriction sites located on the outer primers) and ligated to pTA131 digested with BamHI and HindIII. The resulting plasmid was demethylated and then used to transform *H. volcanii* H26 using the two-step procedure (pop-in and pop-out) [68]. The expected mutations were verified by allele-specific PCR to detect the absence of the *aglB* gene on genome, yielding strain ∆*aglB*.

Isolation and purification of EVs

For isolation of EVs from *H. volcanii*, cultures were grown at 45 °C in minimal media with serial dilution (two times in exponential growth to OD_{600} = 0.05) before being transferred into nutrient rich media and grown at 28 °C (unless otherwise specified). EVs were isolated and purified as described in [69]. Briefly, cells were removed at late stationary (~ 144 hours growth) by centrifugation (4,500 x *g*, 40 min), and EVs were precipitated with the addition of polyethylene glycol (PEG) 6000 and incubation at 4 °C. EVs were subse-

quently pelleted by centrifugation (14,000 x *g*¸ 50 min, 4 °C) and after resuspending the pellet, remaining cell contaminations were removed by an additional centrifugation (14,000 x *g*, 10 min) and filtration (1 x 0.45 µm filter, 1 x 0.2 µm filter). Extracellular nucleic acids were removed with DNase I (New England Biolabs, 20 U/mL) and RNase A (New England Biolabs, 20 U/mL) [70]. The samples were further purified through an OptiPrep™ density gradient, yielding two bands containing EVs.

EVs from *H. lacusprofundi* were isolated and purified following methods in [16]. EVs from *Hbt. salinarum* were isolated as described for *H. volcanii*¸ but temperature for synchronization and final growth were 45 °C in media described above.

Transmission electron microscopy

Samples were adsorbed onto a copper grid (FCF200-Cu) for 3 min and negatively stained with 2% uranyl acetate for 45 s. Grids were imaged at 200 kV with JEOL JEM-2100 Plus transmission electron microscope.

RNA extraction and transcriptomic analysis

RNA was extracted from cell pellets or EV pellets using TRIzol™ (Thermo Fischer Scientific). 1 mL TRIzol™ reagent was added to the pellet, homogenized by pipetting, and incubated at room temperature for 5 min. 0.2 mL chloroform was added to the sample, gently mixed via inversion, and incubated at room temperature for 10 min. The sample was then centrifuged at 4 °C for 10 min at maximal speed (~20,000 x *g*). Upper phase was transferred to a new tube, and 500 mL isopropanol was added, mixed gently by inversion, and incubated at room temperature for 10 min. The sample was then centrifuged at 4 °C for 15 min at maximal speed. The supernatant was removed and pellets washed twice with ice-cold 75% ethanol. The remaining liquid was removed and the pellet was air-dried for 10 min. Pellets were resuspended in RNase/DNase free water.

Libraries (small RNA libraries) were prepared and sequenced at the Max Planck-Genome-Center (Cologne, Germany). Preliminary RNA sequencing experiments (see Supplementary Results) were conducted with one replicate, while the final RNA sequencing for both untreated and HFPV-1 infected *H. volcanii* were performed in triplicates. RNA sequencing for *H. salinarum* was conducted with one replicate of cellular RNA and two replicates of EV-associated RNA pooled together. Read mapping and calculations of gene expression and differential expression was performed using Geneious Prime® (2021.0.1). Reads were mapped to a compiled version of all genomic elements using the Geneious mapper (including a standard read trimming step) with 99% minimum overlap identity (90% minimum overlap identity for preliminary *H. volcanii* read mapping and *Hbt. salinarum* RNAseq). For samples with 3 or more replicates, differential expression was calculated with DESeq2. For samples with only one replicate, the default Geneious differential expression calculator was used. Transcripts were considered significant if transcripts per million (TPM) was greater than 10, log2 fold change was greater than 1, and p-value was lower than 0.05. Consensus sequences were predicted using MEME [71] with default settings. Sequence alignment and structural alignment among asRNA was predicted using locaRNA [72–74], with the temperature setting set to 28 °C.

Northern blot

The Northern blotting protocol was adapted from [75]. Briefly, RNA was extracted as described above and separated on formaldehyde-MOPS agarose gels, with a final concentration of 2% formaldehyde and 2% NuSieve 3:1 agarose (Lonza). 5 µg RNA was denatured for 10 min at 70 °C with 1 X MOPS buffer (20 mM MOPS, 5 mM NaOAc, 1 mM EDTA, pH 7.0), 3.7% formaldehyde and loading dye (67 nM EDTA pH 8, bromophenol blue and xylene cyanol in deionized formamide). Samples were heat denatured for 10 min at 70 °C then placed on ice for 3 min before loading onto gel. The gel

was run at 125 V for 3 to 4 hours and the RNA was then transferred to a Zeta-Probe GT membrane (Bio-Rad) by capillary action with 20 x SSC buffer (3 M NaCl, 300 mM Sodium Citrate, pH 7.0) and 2 x SSC buffer. The oligonucleotide probe is listed in Supplementary Table 2, and was labelled with [γ-^{32}P] ATP using polynucleotide kinase (Thermo Fisher).

Plasmid construction and expression of OapA

The coding region for *oapA* was amplified by PCR (primers listed in Supplementary Table 2), digested with *Nco*I and *Eco*RI (restriction sites located on primer extensions), and ligated into pTA1852 digested by *Pci*I and *Eco*RI. The plasmid, pTA1852 (provided by Thorsten Allers), is derived from pTA1392 [76] with a replacement of the 112 bp *Nde*I and *Not*I region containing an N-terminal 6 x His tag and a C-terminal 1 x StrepII tag with an N-terminal 7 x His tag and 2 x StrepII tag. Expression of tagged OapA ($OapA_t$) on pTA1852 is controlled by tryptophan-inducible promoter, p.tnaA. The resulting plasmid was demethylated and transformed into *H. volcanii* strain H26, and plated onto HV-cab plates (1% agar).

Expression of $OapA_t$ was adapted from [77]. Cultures were grown in HV-YPC supplemented with 200 µg/mL tryptophan at 28 °C until OD_{600} of approximately 1. Cultures were then supplemented with tryptophan by adding 10% of total volume 18% BSW containing 5 mg/mL tryptophan (final concentration of 450 µg/mL tryptophan) to the culture. Cultures were grown for 2 hrs at 28 °C before EVs were quantified as described below.

Affinity purification of $OapA_t$ was modified from [78]. Cells from 500 mL culture were pelleted (11,000 x *g*, 40 min) and resuspended in 7 mL Binding Buffer (20 mM HEPES pH 7.5, 2 M NaCl, 1 mM PMSF). Cells were lysed by sonication (6 x 30 seconds at 35% amplitude) on ice, and treated with 20 µL DNase I (New England Biolabs, 20 U/mL) for 1 hr at 28 °C. Lysates were centrifuged (20,000 x *g*, 15 min, 4 °C) and filtered through 0.8 µm, 0.45 µm and 0.22 µm pore-size filters. The remaining flow through was incubated

overnight with 1 mL Strep-Tactin® Sepharose® beads (iba-lifesciences) equilibrated with Binding Buffer and applied to a Poly-Prep chromatography column (Bio-Rad). Flow through was run twice on the column, and the column was then washed 5 x with Binding Buffer. The column was then incubated with 3 mL Elution Buffer (Binding buffer with 5 mM D-desthiobiotin) for 30 min, and flow through was concentrated using Vivaspin® 500 centrifugal concentrator (10,000 MWCO, Sartorius). Expression of $OapA_t$ was then confirmed using Western blot (Supplementary Figure 15A).

Protein extraction and analysis

Protein content of EVs was compared with protein content of cell membranes as described previously in Erdmann et al [16]. Proteins were isolated from purified EVs (triplicates of each upper band and lower band in density gradients) and host membranes (in triplicates) from untreated and UV-treated samples as described in [69], resulting in a total of 12 EV samples and 6 cell membrane samples. TCA precipitated protein mixtures were dissolved in 30 µL 1 x Laemmli sample buffer and loaded on Any kD™ Mini-PROTEAN® TGX™ Precast Protein Gels (Bio-Rad Laboratories, Germany). After short 3 cm SDS PAGE separation, the gels were visualized with Coomassie staining and each gel lanes cut into two slabs, which were processed individually. Proteins were in-gel reduced with dithiothreitol, alkylated with iodoacetamide and digested overnight with trypsin (Promega Mannheim, Germany). Resulting peptide mixtures were extracted twice by exchange of 5% of formic acid (FA) and acetonitrile, extracts pooled together and dried down in a vacuum centrifuge. Peptides were then re-suspended in 25 µL of 5% formic acid and a 5 µL aliquot was analyzed by LC-MS/MS on a nano-UPLC system Ultimate3000 series interfaced to a LTQ Orbitrap-Velos mass spectrometer (both Thermo Fisher Scientific, Bremen, Germany). The nano-UPLC was equipped with an Acclaim PepMap100 C18 75 µm i.d. x 20 mm trap column

and a 75 µm x 15 cm analytical column (3 µm/100 Å, Thermo Fisher Scientific, Bremen, Germany). Peptides were separated using 80 min linear gradient; solvent A was 0.1% aqueous formic acid and solvent B was 0.1% formic acid in neat acetonitrile. Spectra were acquired using Data Dependent Acquisition (DDA) method and Top 20 approach; lock mass was set on *m/z* = 445.1200 (polydimethylcyclosiloxane). Three blank runs were performed after each sample analysis to avoid carryover. Acquired spectra were searched against *H. volcanii* proteins in NCBI database (June 2020, 12045 entries) by MaxQuant software (v. 1.6.10.43) using default settings and MBR (Matched Between Runs) option. False Discovery Rate (FDR) was 1%, variable modifications – methionine oxidized, cysteine carbamidomethylated and propionamide; two miscleavages allowed; minimal number of matched peptides – two. Relative quantification was performed using LFQ intensity values calculated by MaxQuant. Proteins were only considered present in EVs if matched with two or more peptides in all EV samples for that condition, and a respective LFQ value was identified in all EV samples for that condition.

Differential expression of proteins was calculated using R package, DEP (differential enrichment analysis of proteomics data) (v. 1.21.0) [79], based on the LFQ intensity values generated by MaxQuant. Differential expression between EV-associated proteins isolated from upper and lower bands of density gradient was calculated using three replicates of EVs from untreated cultures. For comparison of protein abundancies in EVs and cell membrane, upper and lower bands were pooled together for a total of 6 replicates for EV samples and 3 replicates of cell membrane samples. The threshold for significant enrichment in EVs was a log2 fold change greater than 1 and adjusted p-value lower than 0.05.

Identification and phylogenetic analysis of Ras small GTPases across the archaeal domain

Homologs of small GTPase, HVO_3014, were identified in major archaeal clades using BLAST and analyzed with Interpro [31] to confirm the presence of signatures typical for P-loop GTPases and small GTPases belonging to the Ras superfamily. This resulted in 21 sequences from different organisms, including *H. volcanii* and *Hrr. Lacusprofundi*. These 21 sequences were used as a reference database in a DIAMOND [80] search using as query the entire protein content of a non-redundant set of 78,768 archaeal and bacterial genomes comprised of the genome taxonomy database (GTDB) species representatives (r207) [81] and the global catalog of earth's microbiomes (GEM) OTU dataset [82] dereplicated at 95% average nucleotide identity using fastANI [83]. This search resulted in 96,121 hits, and 1,686 true positive hits were subsequently selected using an alignment score ratio approach [40]. This set was further manually curated, removing the only 5 bacterial GTPases based on protein phylogeny using FastTree 2 [84] and MUSCLE [85], as well as removing 15 sequences longer than 250 amino acids. This resulted in a final protein set of 1,666 archaeal GTPase sequences, representing the total diversity of this protein family in sequenced archaeal and bacterial genomes. The final dataset was aligned with MUSCLE and a phylogenetic tree was constructed using IQ-Tree [86] with ultrafast bootstrap analysis [87] using 1000 bootstrap replicates and default settings, auto-selecting the substitution model [88]. The phylogenetic tree was visualized on iTOL (v 6.6) [89] as unrooted, and taxonomy was mapped onto the resulting tree.

Lipid extraction and analysis

For the total cell and cell membrane fraction, cells were harvested from 50 mL of *H. volcanii* liquid cultures in three biological replicates. The pellets

were dissolved in 5 mL DBCM2 salt solution [66] and divided equally into two halves. For lipid analysis from total cells 2.5 mL of each replicate were divided into 300 µL aliquots. For extraction of cell membranes, 2.5 mL dissolved cell pellet from each replicate was diluted (1:1) with DBCM2 salt solution and sonicated with a microtip sonicator (MS 73 Sonoplus, Bandelin electronic, Germany) 3 times for 30 s on ice at 35% output. The lysate was treated with DNase I (30 min at 28°C, 10 µL per mL), and spun down in a table-top centrifuge (8,000 x *g*, 30 min, 4 °C) to remove cell debris. Cell membranes were pelleted by ultracentrifugation (MLS-5 rotor, 248,000 x *g* for 15 min). The pellets were dissolved in 1 mL DBCM2 salt solution and distributed into 4 x 250 µL aliquots. EVs from three biological replicates (200 mL cultures) were treated with DNase and RNase and purified with an Optiprep™ gradient (4 hr at 150,920 x *g*). The resulting EV bands were extracted separately from gradients. Instead of PEG 6000 precipitation, the samples were concentrated using filter columns (Vivaspin 6, 100,000 MWCO PES, Sartorius, Germany) at 4 °C with a maximal speed of 4,000 x *g* and washed twice with DBCM2 salt solution. Each gradient band was concentrated to 900 µL, from which 3 x 300 µL technical replicates were aliquoted. All samples were stored at -20 °C until lipid extraction.

For lipid extraction, samples were sonicated for 1 h in an ice-cooled ultrasonication bath and treated with a protocol based on [90]. Phase separation after the final centrifugation resulted in an upper lipid-containing organic phase, a lower metabolite-containing aqueous phase and a protein-containing pellet. The separate phases were isolated into combusted glass LC-MS vials, dried under constant N_2 flow and stored at -20 °C until further analysis. Three 300 µL aliquots of sterile DBCM2 salt solution were treated with the same protocol as negative controls.

For ultrahigh performance liquid chromatography (UHPLC) coupled to mass spectrometry (MS) analysis, dried samples were resuspended in a solvent mixture of dichloromethane:methanol (1:9) and 0.4% of the total lipid extract

were injected for total cells, cell membrane and negative control samples, 4% for EV samples from replicate 1 and 2% for all remaining EV samples. Measurements were performed on a Dionex Ultimate 3000 RS UHPLC system coupled to a maXis ultrahigh-resolution quadrupole time of flight tandem mass spectrometer (Q-TOF MS, Bruker Daltonics). Separation of archaeal lipids was achieved on a Waters Acquity UHPLC BEH C18 column (1.7 µm, 2.1 x 150 mm) at 65 °C using reverse phase chromatography from [91]. Briefly, a 26 min gradient was run at a flow rate of 400 µL min^{-1} beginning with 100% A (held for 2 min), followed by an increase to 15% B within 0.1 min and ramping to 85% B in 19 min, followed by 8 min re-equilibration with eluent B. Eluent A was MeOH:H_2O (85:15) and eluent B was IPA:MeOH (50:50), both with addition of 0.04% HCO_2H and 0.1% NH_3. Analysis was performed in positive ionization mode, scanning from m/z 100 to 2000. MS2 scans were obtained in data dependent mode.

Output data were analyzed with the manufacturer's software (DataAnalysis 4.4.2, Bruker Daltonics). Lipid compounds were identified based on retention time, fractionation pattern and exact masses [60, 92, 93]. Several technical replicates were measured for each sample type, of which representative replicates were selected for each biological replicate. Since the EV samples showed minimal differences in lipid distribution between bands after ultracentrifugation (Supplementary Figure 17B), gradient bands were pooled for each biological replicate for further analysis. The samples were compared with respect to their relative abundance distributions without absolute quantification as representative standards to correct for response factors for most of the detected compounds are lacking. While the fractions represented measurements of different percentages of their respective TLE, 0.4% for total cells and cell membrane and 4% for EV.1 and 2% for EV.2-3, we chose not to correct for dilution as it would not affect the relative abundance distributions.

The relative abundances were normalized per replicate and averages for each fraction were calculated from three biological replicates (total cells and cell membrane fraction) and from the upper bands after density gradient centrifugation from three biological replicates (EV fraction). Figures were created in R Statistical Software (v4.1.2; R Core Team 2021) with the ggplot2 [94], plyr [95] and dplyr packages [96].

EV quantification

EVs were quantified from 2 mL of culture supernatant after removal of cells through centrifugation at room temperature (~20,000 x *g*, 10 min twice, followed by 30 min). The supernatant was then filtered through a 0.22 µm pore filter. For quantification using fluorescence staining, MitoTracker® Green (Invitrogen) was added to the 2 mL (final concentration 500 nM), inverted to mix, and incubated at room temperature for 30 min. EVs were precipitated overnight at 4 °C using PEG 6000 (final concentration 10%) and pelleted by centrifugation (~20,000 x *g*, 40 min, 4 °C). The EV pellet was resuspended in 200 µL 22% buffered sea water (BSW) [66], and transferred to a 0.5 mL microcentrifuge tube. Fluorescence was measured on a Spectrophotometer (DeNovix, DS-11 FX+) with blue excitation (470 nm) and emission between 514-567 nm. Base fluorescence of 22% BSW was subtracted from each value to remove background noise. For quantification using immunodetection, EVs were pelleted by centrifugation after PEG precipitation (20,000 x *g*, 4 °C, 40 min) and the supernatant was removed completely. The pellet was resuspended in 100 µL of 50 mM Tris-HCl, and stored at 4 °C until further use. 5 µL of the EV preparation was slowly spotted onto a nitrocellulose membrane (BioRad), and left to dry for 1.5 hours. After the membrane was dried, blocking was performed with blocking solution (60 g skimmed milk powder into 20 mL 1X TBS buffer [10X TBS buffer: 24 g/L Tris-HCl, 5.6 g/L Tris, and 88 g/L NaCl, with pH adjusted to pH 7.6 with HCl]) for 30 min, followed by incubation with the primary antibody (against HVO_2204, CetZ1,

that was found to be highly enriched in EVs [16]) 1:1,000 diluted in blocking solution for 1 hr. The membrane was washed twice with 1X TBS-TT (10X TBS-TT is 10X TBS buffer with 5 mL/L Tween 20 and 5 mL/L Triton X) and once with 1X TBS before incubation with the secondary antibody (IgG anti-rabbit HRP conjugate, Promega) 1:1,000 diluted in blocking solution for 1 hr. Washing steps were repeated and chemiluminescence was visualized using Clarity Western ECL Substrate (Bio Rad). Relative chemiluminescence intensity was calculated using ImageJ [97]. Two different quantification methods were used, because each of them proved unsuitable for some conditions tested. We assume that enclosing CetZ1 into EVs can be influenced by particular conditions. Using CetZ1 [29] as a reporter gene for detection of EVs in culture supernatants (immunodetection) was unsuitable when testing temperatures dependencies (Supplementary Figure 2A and B) and did also not reflect results that we obtained for EVs from the *aglB* knockout strain (Supplementary Figure 16D). The fluorescence-based method proved unsuitable for quantification of EVs in virus infected cultures, because viral particles also appeared to be stained with the fluorescent dye (Supplementary Figure 2F). P-values are calculated by unpaired, two-tailed t-test.

Tracking of EV uptake using 2-14C Uracil

To generate EVs containing radiolabeled RNA, uracil auxotrophic parental strain, H26 [68], and uracil auxotrophic deletion mutant Δ*oapA* were inoculated into 50 mL of HV-cab supplemented with a mix of unlabeled uracil and 14C labeled uracil (8.621 µg/mL final concentration, 25 µCi per culture) with an optical density (600 nm) of 0.05, each in triplicates. Cultures were grown at 28 °C for seven days before EVs were harvested. To harvest the EVs, cells were pelleted by centrifugation (4000 x *g*, 1 hr). The supernatant was filtered through a 0.22 µm pore filter to remove the remainder of larger contaminants. EVs in the flow through were then concentrated with Vivaspin® 20 (10,000 MWCO, Sartorius). The filters were washed three times with 22%

BSW to remove residual unincorporated 14C uracil and subsequently concentrated to 500 µL of radiolabeled EVs per replicate. *H. volcanii DS2* was grown in HV-YPC media at 45 °C until OD (600 nm) of 1. 60 mL of culture were harvested by centrifugation (4000 x *g*, 20 min), washed with 6 mL HV-YPC and subsequently resuspended in 6 mL HV-YPC. For each replicate, 500 µL of cell concentrate were incubated with the 500 µL of EV concentrate in a heat block at 28 °C, 300 rpm. After 20 and 90 minutes post incubation, 300 µL were removed for measurement. The cells were pelleted (5 min, 10000 x *g*) and washed 3 times with 22% BSW to remove any residual EVs present. The resulting cell pellet was resuspended in 500 µL 22% BSW, added to 4 mL scintillation fluid (Ultima Gold™ XR, Perkin Elmer) and measured in a scintillation counter (Tri-Carb 4910 TR, Perkin Elmer).

Results

EV production in H. volcanii is dependent on growth conditions

The production of EVs and PVs (specialized EVs in the presence of the plasmid, pR1SE) has been reported for the Haloarchaeon, *Halorubrum lacusprofundi* [16]. Both were characterized, revealing the packaging of the plasmid pR1SE and a number of plasmid proteins for PVs, and a set of EV-associated proteins for EVs in absence of pR1SE. To further investigate the generation and potential function of EVs in Haloarchaea, we chose to use *H. volcanii* because it is a well-established model organism for haloarchaeal cell biology with a number of genetic tools available [19, 20]. The capability of *H. volcanii* to produce EVs was also previously reported under UV irradiation [21]. EVs were isolated from culture supernatants of *H. volcanii* and were observed to be circular with a diameter ranging from 50 to 150 nm (Figure 1). Purification of EVs by iodixanol (OptiPrep™) density-based gradient purification (see Methods) resulted in EVs concentrating into two distinct bands in the gradient (Supplementary Figure 1A and B).

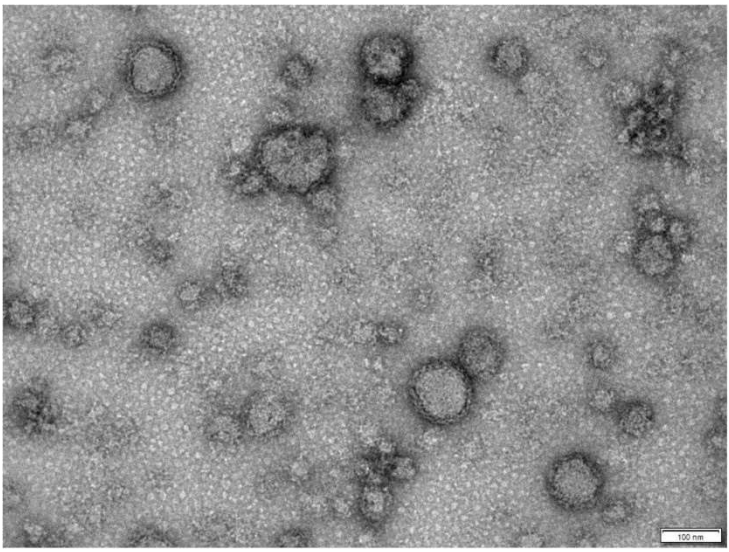

Figure 1. Transmission electron micrograph of EVs from *H. volcanii DS2.* EVs were isolated from culture supernatants and purified by density gradient centrifugation. Size bar represents 100 nm.

No obvious differences distinguishing the two bands could be observed by TEM (Supplementary Figure 1C and D). Initial efforts to isolate EVs close to the documented optimal temperature of *H. volcanii* at 45 °C yielded low amounts of EVs. However, when lowering the temperature of growth to 28 °C, we were able to isolate EVs from culture supernatants, suggesting that EV production is temperature dependent. To determine the optimal conditions for EV production, we tested different growth temperatures using a fluorescence-based method for EV quantification (see methods), and confirmed a temperature-dependent production of EVs reflecting what we observed in large scale purifications (Figure 2A). The abundance of EVs in the supernatant was determined to peak during early stationary phase (Figure 2C, Supplementary Figure 2C), indicating that the rate of EV production versus uptake varies between growth stages.

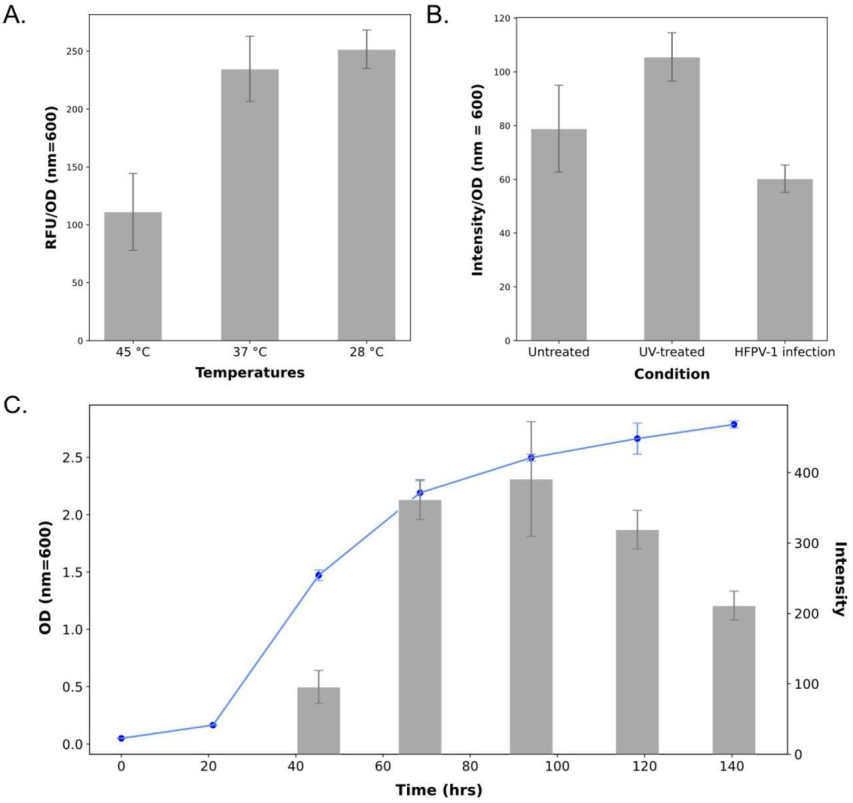

Figure 2. EV abundancies under different conditions and stages of growth. EVs were quantified (gray bars) from culture supernatants of *H. volcanii DS2* grown under different temperatures **(A)**, exposure to UV radiation and viral infection **(B)**, and during different stages of growth **(C)**. Blue line illustrates the OD (nm = 600) of cell cultures averaged over 3 replicates. EV quantities from **(A)** were quantified using fluorescence (see methods) and **(B)** and **(C)** were quantified using immunodetection (see methods). EV quantifications at different temperatures and different conditions **(A and B)** were conducted at stationary phase, and the EV signal was normalized to OD (nm = 600) at the point of measurement. Original spot blots are presented in Supplementary Figure 2. Error bars represent standard deviation over three replicates. RFU = relative fluorescence unit.

Since stress has also been reported to induce EV production, we tested environmental stress conditions such as UV exposure and virus infection using immunodetection-based EV quantification (see methods). Both UV stress (p-value = 0.067) and infection with the chronic infecting virus, HFPV-1 [22]

(p-value = 0.130), did not appear to alter EV production significantly under the conditions tested (Figure 2B).

H. volcanii EVs are associated with RNA

EVs of both *Sulfolobus* (*Thermoproteota*) and *Thermococcus* (Euryarchaeida) were previously shown to enclose DNA [14, 15]. To determine the nucleic acid contents of *H. volcanii* EVs, we attempted to isolate both DNA and RNA from a purified EV preparation. While DNA extraction yielded negligible amounts of DNA associated with the EVs, RNA extraction revealed high yields of EV-associated RNA. Nuclease (DNase and RNase) treatment of the EVs prior to RNA extraction did not eliminate the presence of RNA, confirming that the transcripts are protected and likely enclosed within the vesicles. Analysis of the size distribution of the enclosed RNA revealed differences between EV-associated RNA and intracellular RNA (Figure 3A). While ribosomal subunits were prominent in both EV and cellular preparations, we observed populations of RNAs that are significantly enriched in EVs with a tendency towards smaller transcripts (Supplementary Figure 3).

EV-associated RNA is enriched in tRNAs, rRNAs and ncRNAs

Preliminary sequencing approaches of EV-associated RNA (see Supplementary Results) revealed that using small RNA libraries best reflects the RNA content of EVs. Additionally, we compared the RNA content of upper and lower EV bands in density gradients, revealing that the RNA content alone is unlikely the major factor leading to two subpopulations of EVs. Finally, we deciphered that comparing EV-associated and intracellular RNA is crucial to determining the nature of RNA preferentially associated with EVs.

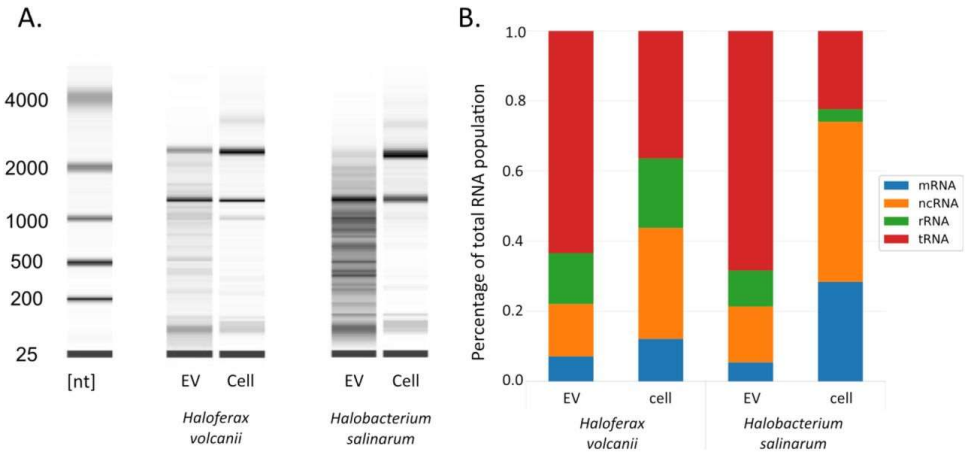

Figure 3. RNA composition of haloarchaeal EVs. (A) Analysis of the size distribution of RNA extracted from purified EVs and whole cells of *H. volcanii* and *Hbt. salinarum*. **(B)** Distributions of RNA subpopulations comparing cellular and EV-associated RNAs for *H. volcanii* and *Hbt. salinarum*.

Using small RNA libraries, we identified around 4,400 genes represented by EV-associated transcripts, comprising the majority of the *H. volcanii* genome with around 79.5% ± 10.5% of genome covered by at least one read (85.2% ± 0.8% for intracellular reads). Though this encompasses nearly all genes in the *H. volcanii* genome, only 474 of the transcripts identified had a TPM (transcript per million) greater than 10, suggesting the majority of identified EV-associated RNA can be considered transcriptional noise. The most abundant of the identified transcripts were tRNAs (68.9 ± 2.1%), followed by non-coding RNAs (ncRNA, transcripts that do not encode a protein, excluding rRNA and tRNA) and rRNAs (16.1 ± 0.9% and 10.4 ± 1.2% respectively) (Figure 3B). The identified ncRNA include intergenic sRNAs [23, 24] and antisense RNAs (asRNA). While we also detected mRNAs in the EV fraction, they only constitute about 4.6 ± 0.1% of the RNA population.

Notably, when we normalized the EV-associated RNA to the intracellular RNA (see Methods), the EV-associated RNA represented a unique subset of transcripts with little variation among replicates (Figure 4A, Supplementary

Table 6). We identified 230 transcripts as highly abundant (TPM > 10) and highly enriched (log2 > 1) in EVs. This population comprised of tRNAs, rRNAs, ncRNAs and mRNAs, with tRNAs being the most dominant group. Surprisingly, while the mRNA fraction was the least represented among EV-associated RNA, the most enriched (242-fold) among all transcripts was the mRNA for the S-layer protein (HVO_2072). A Northern blot analysis probing for the full-length mRNA (gene length 2484 bp) in intracellular and EV-associated RNA revealed only smaller fragments of the transcript associated with EVs (Supplementary Figure 4). Besides HVO_2072, the remainder of highly enriched mRNAs were low in abundance (TPM < 10). We predict that the enrichment of these mRNA relates to their proximity to the cell envelope (transcripts of membrane associated transporters and other transmembrane proteins). Both rRNA and tRNA were previously reported to be associated with EVs from bacterial and eukaryotic organisms [8, 25, 26], and we hypothesize that their presence across RNA-containing EVs is likely due to their structural stability and abundance within cells.

Within the population of ncRNAs associated with EVs, we identified 74 ncRNAs that are both highly abundant and enriched in EVs (Table 1, Supplementary Table 7). This population consists of intergenic RNAs as well as asRNAs. However, no function has been predicted for any of the intergenic ncRNAs so far. We also screened the ncRNAs for consensus sequences or a common secondary structure as specific selection markers for EV packaging; however, no common motif could be identified. Nevertheless, the identified asRNAs (21 asRNAs) appeared to exhibit sequence and structural similarities (Supplementary Figure 5A and B). The average length of these asRNAs was 45.5 nt (± 5.8 nt), and all are associated with the 5' end of ISH3-, ISH5-, ISH8-, ISH9- and ISH11-type transposases from across the genome, overlapping with the predicted start codons of the respective transposase (Supplementary Figure 5C).

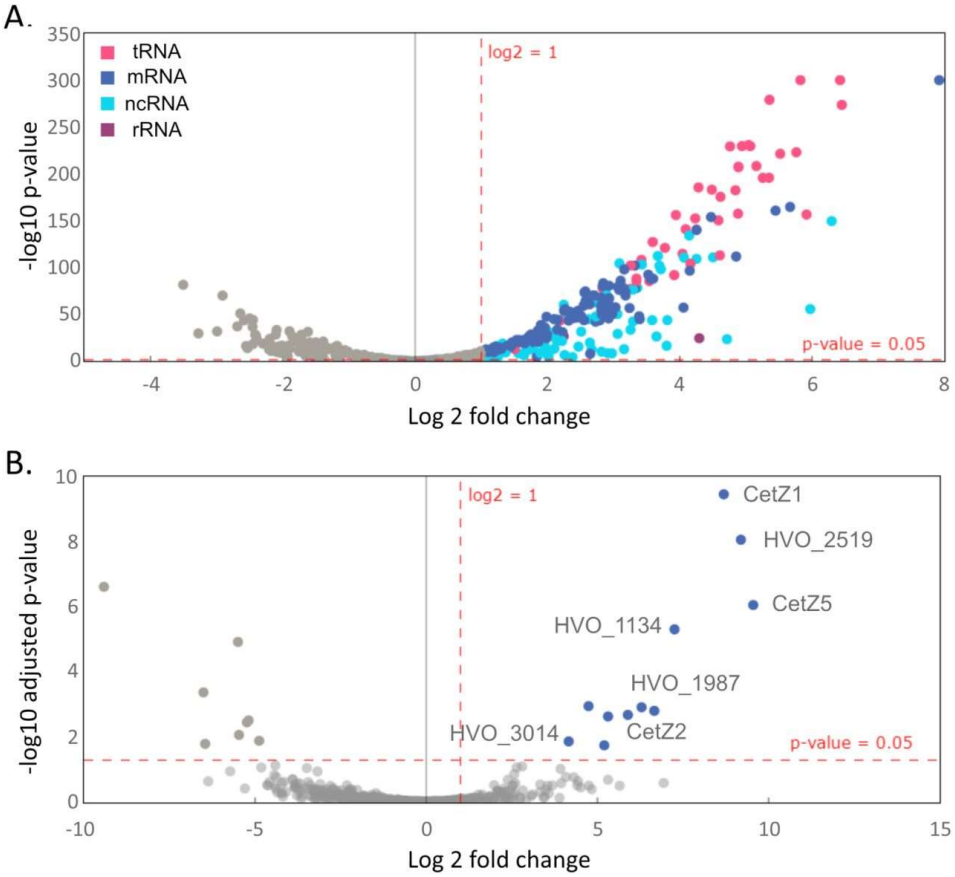

Figure 4. EV associated RNA and proteins. Volcano plots of RNA (**A**) and protein (**B**) abundances in EVs after normalization to cellular RNA abundances and protein abundances from cell membranes. Differential RNA abundancies and p-value calculated using DESeq2. Differential protein abundancies and adjusted p-values calculated by DEP (see methods). Raw data are presented in Supplementary Tables 6 and 10.

Analysis of EV-associated RNA under infection with a virus reveals viral transcripts associated with EVs

Direct interactions between EVs and viruses have been documented, demonstrating the capacity for EVs to act as a viral defense mechanism [6] or facilitate viral propagation [27]. While we did not observe significant

changes to EV quantities under infection with HFPV-1 (Figure 2B), we wanted to test whether infection with HFPV-1 would influence the RNA composition of EVs and thereby possibly indirectly influence virus-host interactions.

Table 1. Top 15 noncoding RNAs enriched in EVs of *H. volcanii*. Full transcriptomic data set in Supplementary Table 6. (IG = intergenic, CHR = Chromosome, pHV1 – pHV4 = plasmids)

Name	Description	Genomic element	Position on genome (bp)	Log2 ratio	p-value
HVO_2488s	HVO_2488-89 IG sRNA of unknown function	CHR	2357769-2357840	6.3	3.00E-150
HVO_1083s	HVO_1083-84 IG sRNA of unknown function	CHR	988804-988820	5.97	3.04E-56
HVO_C0036s	HVO_C0036-37 IG sRNA of unkown function	pHV1	30413-30450	4.71	5.16E-24
HVO_1026_R	7S signal recognition particle RNA	CHR	936055-936360	4.5	1.75E-111
asRNA18	ISH3-Type transposase-associated asRNA	pHV4	131911-131960	4.25	6.98E-110
asRNA20	ISH3-Type transposase-associated asRNA	pHV4	364549-364598	4.14	7.09E-135
asRNA16	ISH14-Type transposase-associated asRNA	pHV1	62764-62815	4.06	2.96E-111
HVO_2565s	HVO_2565-66 IG sRNA of unknown function	CHR	2420311-2420327	3.81	2.35E-44
H62 (Babski et al. 2011)	HVO_1933-4 IG sRNA of unkown function	CHR	1781262-1781347	3.8	5.33E-17
asRNA4	ISH9-Type transposase-associated asRNA	pHV4	115698-115748	3.71	9.34E-99
asRNA21	ISH3-Type transposase-associated asRNA	pHV4	413589-413634	3.69	1.93E-102
asRNA6	ISH8-Type transposase-associated asRNA	CHR	1010936-1010977	3.67	5.36E-113
HVO_2006s	HVO_2006-07 IG sRNA of unkown function	CHR	1852367-1852383	3.65	6.66E-27
H124 (Babski et al. 2011)	HVO_0345-46 IG sRNA of unkown function	CHR	311835-311885	3.58	2.29E-44
asRNA10	ISH3-Type transposase-associated asRNA	pHV1	70152-70197	3.43	8.65E-104

While it was shown that infection with HFPV-1 drastically altered the transcriptomic landscape of the cell during exponential and early stationary growth [22], sRNAseq in late exponential growth revealed a nearly identical transcriptional profile when comparing infected and uninfected cells (Supplementary Fig. 6A). Only two genes showed a significant upregulation (log2 > 1) in the infected cells, HVO_2657 and HVO_0272; however, both are in general rather weakly expressed (TPM < 15). When comparing the RNA content of EVs between infected and uninfected cells, two transcripts were found to be significantly higher in abundance in EVs of infected cells: HVO_A0466 and HVO_0272 (Supplementary Fig. 6A). While HVO_0272 mRNA was about 4-fold upregulated in infected cells (log2 ~ 2), it was about 10-fold upregulated (log2 ~ 5) in EVs of infected cells (Supplementary Fig. 6), indicating that the packaging of this transcript into EVs increases significantly upon infection. Surprisingly, it appeared that the majority of reads mapping to HVO_0272 only map to two short regions of about 30 nt within the coding region of the gene that are identical to a region on the viral genome. Therefore, we conclude that the upregulation of HVO_0272 is due to viral transcripts mapping to the host genome.

Subsequently, when mapping reads to the virus genome, we detected a significant amount of viral transcripts in EVs. While only 1.7 ± 0.07% of intracellular RNA mapped to the HFPV-1 genome, 4.0 ± 0.10% of EV-associated RNA mapped to the viral genome, suggesting a slight enrichment of virus-derived transcripts in EVs. Both cellular and EV-associated RNA mapped the entire HFPV-1 genome, and no enrichment of particular viral RNAs could be detected in EVs (Supplementary Figure 7). However, the detection of viral transcripts within EVs shows that they are also exported in EVs together with host RNA.

Generation of RNA-enriched EVs could be detected in other haloarchaea

We were also interested in whether RNA-enriched EVs are a conserved phenomenon among halophilic Archaea. Therefore, we tested *Halobacterium salinarum* and *Halorubrum lacusprofundi* for EV production and EV-associated RNA content. EVs could be isolated from both organisms (Supplementary Figure 8A and B), and they were likewise found to be enriched in RNA. The size distribution of EV-associated RNA indicates an enrichment for a specific RNA population (Figure 3A and Supplementary Figure 8C). However, we only proceeded with sequence analysis of EV-associated RNA of *Hbt. salinarum*.

RNA sequencing revealed 85.4% of the *Hbt. salinarum* genome was covered by at least one read from EV-associated RNA (94.5% from intracellular RNA library). The distribution of RNA populations were very similar between *H. volcanii* and *Hbt. salinarum* EVs (Figure 3B), with the majority of EV-associated transcripts being tRNAs.

After normalizing EV-associated RNA with intracellular RNA, we identified 228 transcripts as highly abundant and highly enriched in *Hbt. salinarum* EVs (Supplementary Table 8). The transcript for the S-layer subunit was similarly one of the most enriched EV-associated transcripts in *Hbt. salinarum*. The most enriched transcript was a 29 nt asRNA mapping to the coding region of VNG_RS00640, a predicted helix-turn-helix domain protein of unknown function. We also identified 16 highly enriched transposase-associated asRNA that associate with a larger range of transposase families than those from *H. volcanii*, some of which overlap with the respective predicted start codon. In total, 35 ncRNAs were identified as highly enriched and highly abundant in EVs of *Hbt. salinarum*. Of the ncRNA enriched in *Hbt. salinarum* EVs, 6 are sense-overlapping transposase-associated RNA (sotRNA) [28], and 2 are

intergenic sRNAs with high sequence identities to the predicted sRNAs from *H. volcanii*, HVO_2908s and H3.2 [23], that were also found in *H. volcanii* EVs.

EVs are enriched with specific proteins

The protein compositions of *H. volcanii* EVs and their respective cellular membranes were identified by mass spectrometry (LC-MS). Since we determined no difference between the RNA content of upper and lower bands of EV preparations in OptiPrep™ gradients, we analyzed the bands separately for protein content to uncover possible differences in protein composition. We identified 401 proteins associated with EVs deriving from the upper band and 384 proteins from the lower band. However, only 1 protein was found to be more abundant in the upper band and 2 more abundant in the lower band, while the majority of proteins appeared to be consistent between upper and lower bands (Supplementary Figure 9). Therefore, we concluded that protein content alone is most likely not the major factor causing the separation into two bands and pooled the results from both bands for further analysis.

In total, we identified 328 proteins associated with EVs and 668 proteins in the cellular membrane preparations. We compared the abundancies of proteins in EVs with those in cell membranes and obtained 11 proteins significantly enriched in EVs ($\log2 > 1$, adjusted p-value < 0.05) (Supplementary Table 9, Figure 4B), including one protein exclusively detected in EVs (hypothetical protein, HVO_2519, with unknown function and no detectable conserved domains). Several CetZ proteins, including CetZ5 (HVO_2013), CetZ1 (HVO_2204), and CetZ2 (HVO_0745), were also identified to be enriched in EVs. CetZ1 and CetZ2 have been shown to be involved in controlling cell shape and motility in *H. volcanii*, and the CetZ protein family has been predicted to be involved in other cell surface-related functions in Archaea [29, 30].

Other highly enriched, notable proteins include FtsZ2 (cell division protein), HVO_1134 (hypothetical protein), HVO_2985 (hypothetical protein), HVO_1964 (YlmC sporulation protein), and two ABC transporter proteins. Hypothetical protein, HVO_1134, is predicted to contain a rod domain (Interpro) [31], building α-helical coiled coils (Phyre2, I-TASSER) [32, 33], a structure that is also found in viral fusion proteins, representing a candidate gene potentially involved in EV fusion.

Most interesting was the enrichment of the small GTPase, HVO_3014 (OapA), a homolog of the Sar1/Arf1-like GTPase that was also found to be enriched in *Hrr. lacusprofundi* EVs, Hlac_2746 [16] (Figure 4B). OapA was initially thought to have an influence on genome replication due to its association with the origin of replication. However, despite a study characterizing a mutant strain, no distinct function could be assigned to OapA so far [34]. The best homologs for HVO_3014, using a Hidden Markov Model (HMM) based search [35] are Rab-family GTPases (Supplementary Figure 10). Rab-family GTPases belong to the Ras superfamily of small GTPases whose functions include regulating vesicle and membrane trafficking in Eukaryotes[36]. In Eukaryotes, all three types of carrier vesicles (COPI, COP II and clathrin-coated vesicles) require the activation of a small Ras family GTPase to initiate vesicle coat assembly [37]. A COPI-like mechanism of vesicle formation involving a Ras family GTPase was already proposed for *Hrr. lacusprofundi* [16].

We also analyzed the protein composition of EVs from UV-treated cells and compared them with membrane-associated proteins isolated from their respective cells, to determine whether UV treatment would alter protein composition of the EVs. We identified 377 proteins associated with EVs and 668 proteins associated with their respective cell membranes. We identified 11 proteins to be enriched in EVs from UV-treated cells (Supplementary Table 10, Supplementary Figure 11A). All proteins identified as enriched in EVs from untreated cells were also identified as enriched in EVs from UV-treated

cells, except for the small GTPase, HVO_3014, that was calculated as equally enriched but did not pass the E-value threshold. Instead, one additional ABC transport protein (HVO_2399) was identified as enriched.

Differential expression analysis only identifies proteins that are present in higher abundancies in EVs than in cell membranes, leaving out other proteins that could be functionally relevant but are present in equal or lower abundancies when normalized to the cell membrane. For instance, the small GTPase, HVO_3014, was not identified to be enriched in EVs from UV-treated cells using a standard threshold, yet we observe its integral relationship to EV production in *H. volcanii* (see below). Therefore, we also identified the proteins that were found to be present amongst all 12 EV samples analyzed (Supplementary Table 11) and identified 285 proteins present across all samples. All proteins identified as enriched by differential expression analysis were also present in this list, except HVO_2399 identified as enriched in EVs from UV-treated cells, suggesting that the protein composition slightly changes upon UV exposure. The most abundant protein was cytoskeletal protein, CetZ1, followed by the S-layer protein, HVO_2072. Other notable proteins within this list were ribonuclease J (HVO_2724), diadenylate cyclase (HVO_1660), and HVO_1020 (hypothetical protein). RNase J is an exonuclease, and could be relevant to the enrichment of RNAs found associated in the EVs. Diadenylate cyclases are responsible for the production of cyclic-di-AMP, a common secondary messenger among Bacteria and Archaea, including *H. volcanii* [38]. HVO_1020 is a homolog (55% sequence identity) to *H. lacusprofundi* PQQ ß-propeller repeat domain-containing protein, Hlac_2402, that was also identified in *H. lacusprofundi* EVs [16] and has similarities to the gamma subunit of COPI.

Knockout of oapA abolishes EV formation

To investigate the proposed involvement of OapA in EV production in *H. volcanii*, we compared the phenotypes of an OapA knockout strain [34] to the respective parental strain (H26). The OapA knockout strain yielded a dramatically reduced amount of EVs in comparison to the parental strain (about 70% reduction, p-value = 0.007) (Figure 5A, Supplementary Figure 2F).
Gradient purification of concentrated OapA mutant supernatant resulted in either no distinct band or only one band with reduced intensity at about the same height of the upper band in density gradients of the parental strain (Supplementary Figure 12). RNA extracted from this single band yielded very low RNA concentrations and was not detectable on a fragment analyzer. Interestingly, resequencing of the strain revealed the activity of a known proviral region (HVO_1422 – HVO_1434) in the *H. volcanii* genome [39] (Supplementary Figure 13). Therefore, we propose that the remaining particles isolated from supernatants of OapA knockout strain cultures that concentrated in one band of the density gradient could be cell debris and virus particles, and that the strain is unable to produce EVs associated with RNA. Phenotypic changes of the cell shape/morphology were also observed for the knockout strain (Supplementary Fig. 14A). The formation of rod-shaped cells appears to be less frequent when *oapA* is deleted. Interestingly, the OapA mutant also showed a slightly increased growth rate when compared to the parental strain in our laboratory (Supplementary Fig. 14B).

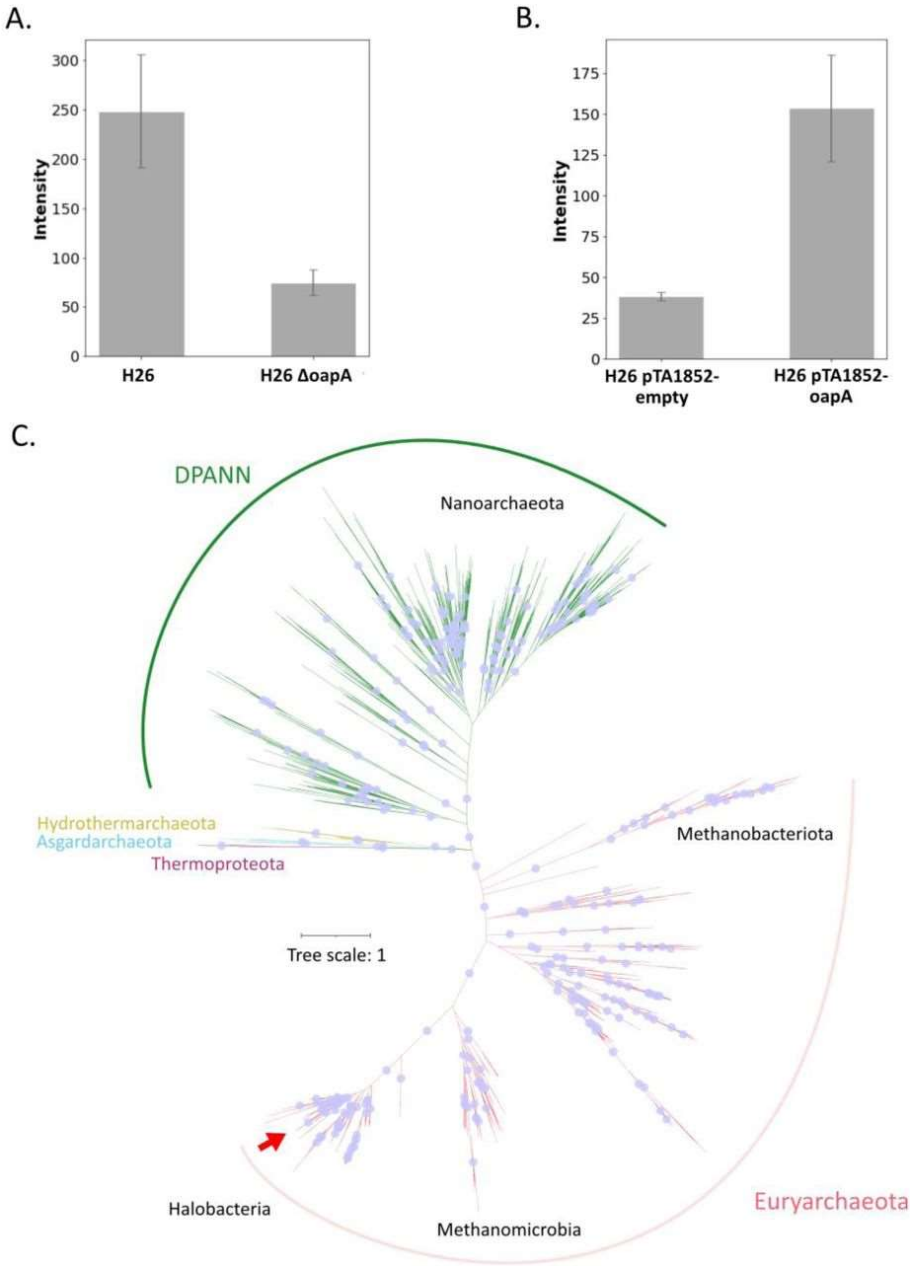
A.
Intensity
300
250
200
150
100
50
0
H26
H26 ΔoapA
B.
Intensity
175
150
125
100
75
50
25
0
H26 pTA1852-empty
H26 pTA1852-oapA
C.
DPANN
Nanoarchaeota
Hydrothermarchaeota
Asgardarchaeota
Thermoproteota
Methanobacteriota
Tree scale: 1
Halobacteria
Methanomicrobia
Euryarchaeota

Figure 5. Analysis of *H. volcanii* EV-associated GTPase, OapA, and homologues in other Archaea. (A) Quantification of EVs in the culture supernatant of the OapA knockout strain and the respective parental strain. **(B)** Quantification of EVs in the culture supernatant of OapA knockout strain and respective parental strain expressing $OapA_t$ under an inducible promotor (pTA1852-$OapA_t$), compared to a control with the empty vector (pTA1852-empty). EVs were quantified using immunodetection (see methods) and were averaged over three replicates with error bars denoting standard deviations. Original spot blots are presented in Supplementary Figures 2D and 16A. **(C)** Unrooted phylogenetic tree of the identified small GTPases across the archaeal domain. Red arrow indicates position of GTPase from *H. volcanii*. Blue dots represent branches with bootstrap value greater than 95.

Further, overexpression of OapA in an OapA wild-type background strain (H26) resulted in increased vesicle production (4-fold, p-value = 0.005) (Figure 5). The hypervesiculation phenotype was confirmed by both quantification and TEM (Figure 5, Supplementary Figure 15B and C), further implicating the crucial role of OapA for EV production.

Ras-superfamily GTPases are conserved amongst various archaeal clades

To get an overview of whether this particular Ras-superfamily GTPase is present in other Archaea, we searched for proteins with high similarity to HVO_3014 against archaeal and bacterial GTDB species representatives using an alignment score ratio approach (see methods) [40]. 1666 archaeal proteins were identified across 14 phyla of Archaea, with an uneven distribution of GTPases across these phyla (Supplementary Figure 16, Supplementary Table 12). The majority of GTPases were identified among the Euryarchaeida, *Halobacteria* and *Methanobacteriota*, as well as in 7 DPANN phyla, including *Nanoarchaeota*, *Nanohaloarchaeota*, and *Altiarchaeota*. Interestingly, only 8 *Korarchaeota* out of 970 *Thermoproteota* genomes analyzed contained a homologous small GTPase. Further, only 8 out of 183 *Asgardarchaeota* were identified to contain a homologous small GTPase. As expected, we were also unable to identify any homologs in two well-studied EV-producing organisms, *Sulfolobus* (*Thermoproteota*), that is known to

generate EVs using ESCRT-like proteins, and *Thermococcus* (*Methanobacteriota_B*), for which other proteins were suggested to be involved in EV formation [14, 41].

A phylogenetic tree was constructed from the alignment of the GTPase database to determine the evolutionary relationships between the GTPases identified and whether they align with taxonomy of the organisms (Figure 5C). Both DPANN and Euryarchaeota appear to have distinct subclades of this family of GTPase that group separately from each other. Within each superphyla, there was also some internal organization. For instance, all of the GTPases of *Halobacteria* and *Methanobacteriota* formed distinct groups, separate from the other Euryarchaeida with mostly small branches, suggesting strong sequence similarity within these groups. Similarly, the nanoarchaeal GTPases also formed a distinct group from the other DPANN organisms. However, the branch lengths were long in relation to the rest of the tree, suggesting a higher variation of sequences within this group. While the bootstrap values of the DPANN and Euryarchaeida branches (100 and 99 respectively) indicate that this division in this family of GTPases based on taxonomy is well supported, the organization of the smaller third branch containing *Asgardarchaeota*, *Thermoproteota*, and *Hydrothermarchaeota* were not as well supported (bootstrap value of 56). However, the GTPases within this cluster form smaller sub-clusters that correlate with their phyla.

Testing other knockout mutants provides further insight into the mechanisms of EV formation

CetZ1 and CetZ2 were amongst the most abundant proteins in EVs; however, we were able to isolate EVs from the supernatant of both CetZ1 and CetZ2 knockout strains. While quantification of EVs by the immunodetection-based method was not possible for the CetZ1 knockout strain, we did not have any indication when purifying EVs that EV production was drastically altered for CetZ1 and CetZ2 knockout strains (Supplementary Figure 17).

RNA could also be isolated from EVs of this strain, and the size distribution of EV-associated RNA was nearly identical when compared to the parental strain (Supplemental Figure 17).

Previous studies in Bacteria have shown that destabilization of the cell envelope results in a 'hypervesiculation' phenotype [42, 43]. To investigate whether changes in cell envelope stability would similarly affect EV production in *H. volcanii*, we assessed EV production in an *aglB* knockout strain. Cells lacking AglB are unable to N-glycosylate the S-layer glycoprotein and absence of AglB results in enhanced release of the S-layer glycoprotein [44]. Thus, deletion of this protein causes a destabilization of the structural integrity of the cell envelope. Indeed, we observed a significant increase in EV production from the *aglB* knockout strain during the purification process as well as by TEM (Supplementary Figure 18A and B). While we could not confirm this result when using the immunodetection-based assay for quantifying EVs (Supplementary Figure 18D), EV quantification by fluorescence staining confirmed an increase in EV production (Supplementary Figure 18E), indicating that CetZ1 incorporation into EVs is altered in this mutant. Interestingly, we observed a drastic change to the morphology of EVs in the mutant. The surface of EVs isolated from the *aglB* knockout strain was significantly different from EVs of the parental strain, appearing very fuzzy (Supplementary Figure 18C), likely due to the instability of the S-layer. Further, while we isolated a significantly larger amount of EVs from the mutant, the RNA yield was slightly lower in EVs (Supplementary Figure 18F), suggesting that a great portion of EVs are likely budding randomly without enclosing RNA.

Lipid analysis reveals differences in the relative abundance of distinct lipids between cells and EVs

To determine whether EVs selectively enclose particular lipids, we analysed the lipid content of EVs and compared the relative abundances of different lipid compounds in EVs to that of cell membranes and total cells of *H. volcanii*. We detected minimal differences in proportions of lipid types between EVs deriving from upper and lower bands of a density gradient (Supplementary Figure 19B), indicating that the lipid content alone is not the differentiating factor between the two subpopulations. We therefore chose to pool samples from different bands of each replicate for comparison.

Lipids with phosphate-based polar head groups were dominant across all samples. Methylated-phosphatidylglycerolphosphate-archaeol (Me-PGP-ARP) both in saturated and unsaturated form (:n) represented the most abundant lipid across samples, with relative abundances of 53.9 ± 2% in whole cells, 66.4 ± 8.81% in cell membranes and 46.8± 1.91% in EVs (Figure 6, Supplementary Figure 19A). The ratio of unsaturated to total Me-PGP-AR abundance was identical in cells and cell membranes (28 ± 1.64% and 29 ± 3.6%), but the comparative amount of unsaturated Me-PGP-AR was lower in the vesicle fraction (11.1 ± 3%) (Supplementary Table 13). Phosphatidylglycerol-archaeol (PG-AR) was the second most abundant lipid in all fractions (18.8 ± 5.3%, 17 ± 3.7% and 32.6 ± 2.9% for cells, cell membranes and EVs respectively) and showed the highest degree of unsaturation (either 4 or 6 double bonds). The ratio of unsaturated to total PG-AR did not show a large variation between cellular (36.1 ± 4.1%), cell membrane (38.9 ± 6.4%) and extracellular fractions (31.3 ± 9%). Sulfated-diglycosyl-archaeol (S-2G-AR) showed relative abundances of 5.75 ± 4.4% (whole cells), 6.8 ± 3.9% (cell membrane) and 12.9 ± 1.5% (EVs) respectively, with negligible amounts of unsaturated lipids detected in the whole cell and cell membrane fraction.

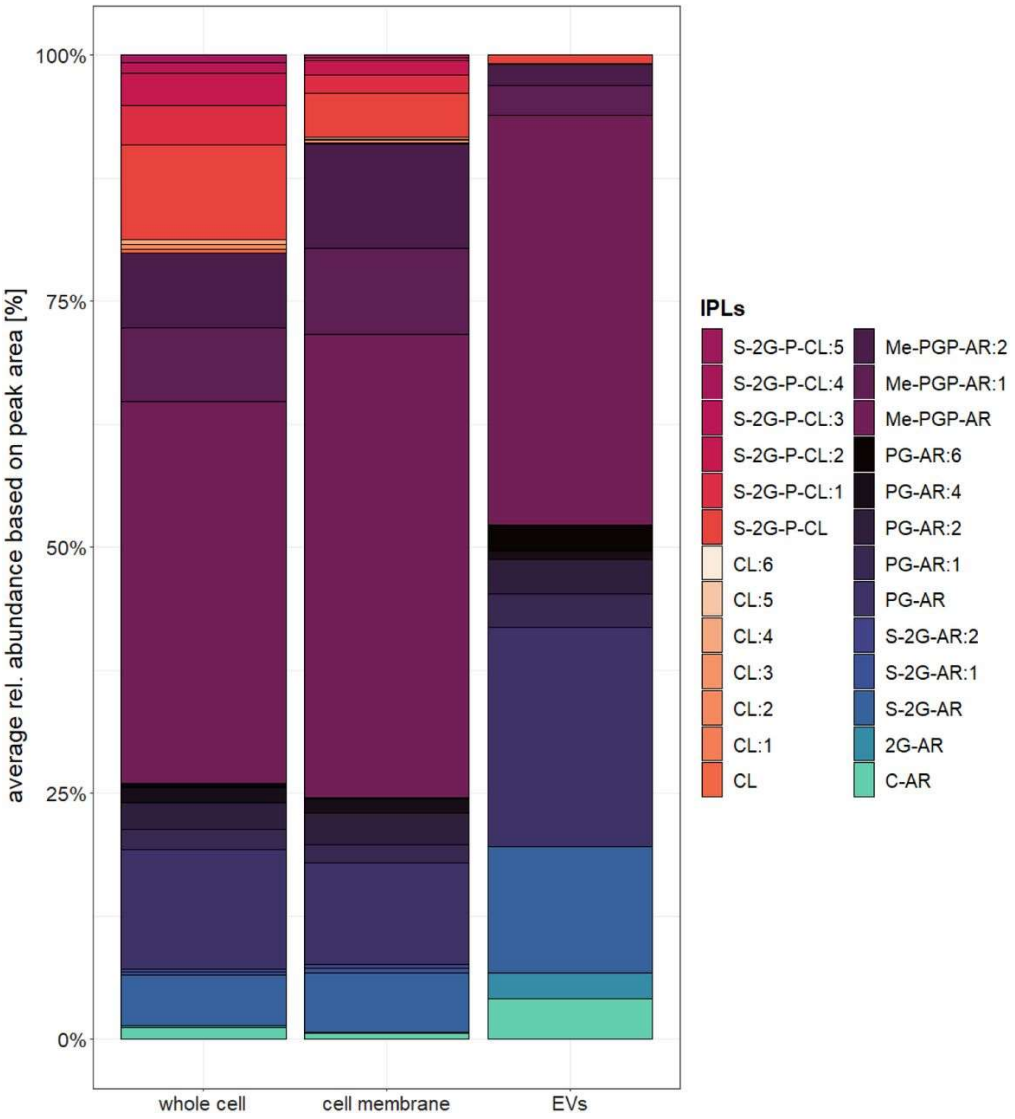

Figure 6. Average distribution of lipid compounds comparing whole cells, cell membranes and EVs of *H. volcanii*. The average (n = 3) relative abundance of lipids was calculated for each preparation; whole cells, cell membrane and extracellular vesicles (EVs) based on the peak area of the most abundant adduct for each compound. The distribution in the individual samples is shown in Supplementary Figure 17A. For the EV fraction, bands after density gradient purification were pooled

together from 3 biological replicates. Lipids were identified based on their retention time, fractionation pattern and exact mass.

Compound abbreviations: AR = archaeol (C_{20}-C_{20} isoprenoidal chains), CL = cardiolipin, :nUS = lipid with n number of unsaturations, UK = unknown compound. Lipids with neutral headgroups: 1G = monoglycosyl, 2G = diglycosyl, C-AR = core-AR. Lipids with anionic headgroups: Me-PGP = phosphatidylglycerophosphate methyl esters, PG = phosphatidylglycerol, S-2G =sulfated diglycosyl, S-GP = sulfoglycophospho, S-2G-P = sulfated diglycosyl-phospho.

Lipids with a neutral headgroup, such as diglycosyl-archaeol (2G-AR) or no head group, such as core-archaeol (C-AR), were detected in all fractions but showed higher relative abundances in the EV samples (2.57 ± 0.19% and 4.1 ± 1%) compared to lipid extracts from cells and cell membranes (<1.2 ± 0.2%). A notable difference was also observed for dimeric phospholipids (or cardiolipins, CL). While they contributed 20.1 ± 9.7% and 9.04 ± 8.1% of the total lipids in whole cells and cell membrane samples respectively, they were almost undetectable in the EV samples (0.91 ± 0.41%). Interestingly, we were not able to detect any extended archaeol lipids (C_{25} instead of C_{20} isoprenoidal chains) with relevant concentrations in any of the samples, despite how common they are among many haloarchaea [45].

As expected, we could not detect any lipid compounds which were only present in the vesicular fraction but not in cells or cell membranes. However, the lipid composition of EVs differed significantly to that of cells and cell membranes when comparing the relative abundance patterns of different lipid groups. The distribution between unsaturated and saturated compounds shifts towards saturated lipids from 67.5 ± 2.7% and 68.7 ± 1.7% in whole cell and cell membrane extracts, to 84.4 ± 4.7% in EVs (Supplementary Table 13). In the vesicle fraction this is likely attributable to the absence of cardiolipins and the lower abundance of unsaturated Me-PGP-ARs.

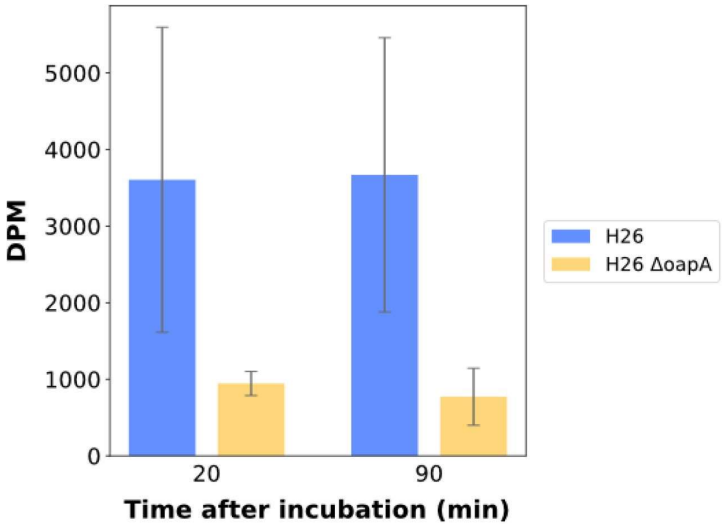

Figure 7. Transfer of radioactively labelled RNA by EVs. EVs were isolated from cells (H26 and H26 ΔoapA) incubated with radiolabeled uracil, resulting in EVs associated with radiolabeled RNA. EVs were then incubated with non-labelled cells and intracellular radioactivity in decays per minute (DPM) was measured 20 and 90 minutes post incubation using a scintillation counter.

EV-associated RNA is taken up by H. volcanii cells

In order to test the ability for EVs to deliver the RNA cargo to a target organism, we used ^{14}C-labelled uracil as a reporter to track the movement of RNA. EV preparations from the EV-deficient OapA knockout strain served as a control.

About 98% of the introduced radioactivity was taken up by both the parental strain and the OapA knockout strain over 6 days of growth. Subsequently, 1.90% of the radioactivity was detected in EV preparations of the parental strain, whereas only 0.11% was detected in EVs of the OapA knockout strain. After 20 min of incubation of the labelled EV preparations with fresh cells, we could detect a transfer of radioactivity into the unlabeled cells, with parental strain EVs transferring significantly more radioactivity than the OapA knockout strain EV preparation (Figure 7). Measurements after 90 min of incubation did not show a change of radioactive uptake from EVs of both strains,

indicating that the transfer was already complete after 20 min. Thereby we confirm that the RNA enclosed in *H. volcanii* EVs can be internalized by *H. volcanii* cells in a short time frame.

Discussion

While more evidence arises that EVs play important roles in mediating important cellular functions in Bacteria and Eukaryota, there is still a disproportionate lack of information regarding the function and cargo of EVs in Archaea. Characterization of archaeal EV production and their biochemical composition can not only provide insights into the interactions between microorganisms in their unique environments, but also allow insights into the evolution of eukaryotic membrane trafficking mechanisms. EV production has been previously reported in haloarchaea [16], and here we used the haloarchaeal model organism, *H. volcanii*, to investigate the nature of these EVs and the mechanisms of EV production.

EV production by *H. volcanii* appeared to be influenced by temperature, while UV exposure and infection with a chronic virus had no significant influence under the conditions tested. EVs are heterogeneous in size, ranging from 50-150 nm. Analysis of the nucleic acid content of EVs produced by *H. volcanii*, as well as other haloarchaea, revealed that EVs are associated with RNA, as it has been described for some bacterial and eukaryotic EVs [46, 47], indicating that RNA associated EVs are conserved among all three domains of life. *Thermococcus onnurineus* (Euryarchaeida) has previously been reported to produce EVs containing RNA [41]; however, no characterization of EV-associated RNA was carried out for this organism. Treatment of EVs with nucleases did not eliminate the presence of EV-associated RNA. Additionally, TEM analysis comparing the wild type and a mutant with a destabilized S-layer, clearly showed that the surface of EVs is covered by the

S-layer without any evidence for nucleic acids (Figure 1, Supplementary Figure 18C), and destabilization of the S-layer did not abolish the RNA cargo. Therefore, we infer that the RNA is internalized within EVs.

During preliminary data acquisition, we realized that a comprehensive picture of the EV composition is only gained when comparing the EV composition with the respective composition of the cell or the cell membrane, an approach that should be more common to studies investigating EVs.

While the RNA composition of *H. volcanii* EVs, both under normal growth conditions and under infection with a virus, appears to reflect intracellular levels to a certain extent, there is a distinct population of transcripts associated with EVs that does not correlate with the respective intracellular abundance, but are instead more enriched within EVs. The majority of highly enriched transcripts encode for tRNAs and rRNA, and we suggest that they are enriched due to both their structural stability and their high intracellular abundance. Both tRNAs and rRNAs have been observed at high abundancies in vesicle-associated transcriptomics in bacterial EVs [8, 25], and could therefore be a commonality among EVs from prokaryotic organisms. Interestingly, the most enriched mRNA that we detected was shown to be non-specifically fragmented in the EV-associated RNA fraction. Since we could not identify a common sequence or structural motif that would allow for a specific selection of particular RNAs to be enclosed into EVs, we suggest that the size, stability or both are a defining factor for packaging. Additionally, the positioning of an mRNA close to the cell envelope, such as the mRNA of the S-layer protein, could play a role in determining the RNA population of EVs. Results we obtained from EVs of viral infected cultures showed that the RNA composition did not change significantly upon infection in both cells and EVs; however, we detected viral RNAs in the cells and subsequently also in EVs, clearly representing the current transcriptional state of the EV-producing cell. When exposing cells to UV radiation, we subsequently observed changes to the

RNA composition in EVs of UV-treated cells when compared to those of untreated cells (Supplementary Results, Supplementary Table 5). However, we did not acquire data to compare EV and intracellular transcriptomes, making it difficult to conclude with confidence whether these changes are due to changes in the cell. Nevertheless, since UV-treatment is known to influence the transcriptional landscape in *H. volcanii* cells [21], we assume that the changes observed in EVs are reflecting changes in the cell. In conclusion, we propose that RNA is taken up randomly into EVs, with transcripts that are highly enriched in the cell as well as transcripts that are translated at the cell envelope being preferably packaged. The respective cargo could be processed within EVs by RNases present in the vesicles (see protein content of EVs), leading to the degradation of mRNAs and a selection towards more stable RNAs (ncRNAs, tRNAs, rRNAs). Alternatively, there could also be a preselection for small-sized RNAs for packaging into EVs. Both scenarios lead to an RNA cargo representing a transcriptomic snapshot of the cell with a particular enrichment in RNAs with a regulatory potential (ncRNAs, tRNAs), as we observe in *H. volcanii* EVs.

The expression of ncRNAs in *H. volcanii* has been observed to shift dramatically under different conditions [48], and we predict that the population of packaged ncRNAs also reflects this shift. There are some notable, studied examples showing EV-packaged ncRNAs regulating gene expression in a receiving organism, such as EV-associated ncRNAs of *Vibrio fischeri* [8] and *Pseudomonas aeruginosa* [7], and we identify ncRNAs with regulatory potential associated with *H. volcanii* EVs. For example, we find a number of asRNAs overlapping with the start codon of various transposases that could potentially modulate the activity of transposases in a receiving organism. Unfortunately, the other identified ncRNAs do not have predicted functions. Currently, the nature of ncRNA-mediated regulation in Archaea is still unknown, with the majority of identified and predicted ncRNAs being uncharacterized.

We have demonstrated that EVs of *H. volcanii* are able to transfer RNA between cells, and that RNA associated EVs are also produced by other haloarchaea. Therefore, we propose that halophilic archaea produce EVs as an intercellular communication mechanism to reflect the current intracellular state of the organism, and possibly influence gene expression in the receiving cell in response to environmental stimuli.

Proteomic analysis of EVs allowed us to draw conclusions about the mechanisms of the formation of EVs in haloarchaea. CetZ proteins were found particularly prominent in EVs of *H. volcanii* and *Hrr. lacusprofundi* [16]. However, EV production could still be observed from knockout strains of the enriched CetZ proteins (Supplementary Figure 17), suggesting that they do not play a significant role in EV formation in *H. volcanii*. CetZ proteins are known to be associated with the cell envelope [29], and we assume that this loose association could lead to enclosing of CetZ proteins during EV formation. Alternatively, the treatment that we used to prepare cell membranes could have also dissociated CetZ proteins from the membrane, leaving the impression that CetZ proteins are enriched in EVs. We also suggest that this could be true for other membrane-associated proteins.

In contrast, the knockout of a small GTPase (OapA), a Ras-superfamily GTPase with homology to a predicted Sar1/Arf1- GTPase that was also detected in PVs and EVs of *Hrr. lacusprofundi* [16], showed a very strong effect on EV formation. While the knockout of OapA results in a EV-deficient strain, overexpression of the small GTPase in the wild-type background leads to overvesiculation, further demonstrating the key role this protein plays in EV formation in haloarchaea. Rab and Arf GTPases, belonging to the Ras superfamily, are integral to the production of various vesicles in eukaryotic cells [49], including COP vesicles. COP vesicles regulate the trafficking of specialized lipids and proteins between the endoplasmic reticulum and Golgi apparatus [37]. The production of these vesicles requires the activation of the

GTPase in order to recruit the coat complex, resulting in deformation of the cell envelope and subsequent budding of the vesicle [50, 51]. Deletion of this protein in Eukaryotes results in the elimination in the production of COP vesicles [52], and we have observed a similar suppression when knocking out the GTPase in *H. volcanii*, demonstrating that a functional Rab/Arf-related GTPase exists in Archaea and is able to regulate vesicle production. Homologous proteins of this new family of archaeal Ras-superfamily small GTPase can be identified across not only haloarchaea and Euryarchaeida, but also within other major branches in the archaeal domain, suggesting that this mechanism of EV production is widespread among specific clades of Archaea, specifically within Euryarchaeida and DPANN. Further, we observed that the archaeal GTPases group in accordance to their phylogeny, implying that these Archaea had acquired the gene early in their evolutionary past. Only a few phyla outside of DPANN and Euryarchaeida were found to contain this family of GTPase, forming a small branch containing *Asgardarchaeota, Thermoprotea, and Hydrothermarchaeota*. Within this branch, only specific clades of each phyla were represented, suggesting that the gene was attained in those clades through horizontal gene transfer events. Small GTPases within the Ras superfamily have been identified previously in Archaea, some of which clustering closely with known eukaryotic Ras GTPases [53]. These specific eukaryotic and eukaryotic-like GTPases contain a conserved aspartate in the G3 region that is also present in the *H. volcanii* GTPase, OapA, suggesting that the family of archaeal small GTPases identified in this study is also closely related to the eukaryotic Ras GTPases. Though homologs were not as widely identified among other clades, this could be due to the fact that some clades are represented by uncultured organisms and their respective MAGs or that the small GTPases present in those organisms are too divergent from the subfamily identified here. We opted for a more stringent search for homologous proteins across the ar-

chaeal domain that could have excluded other novel archaeal protein families more distantly related to the GTPase family identified here, but also still carry out the same function. For instance, only 3% of the surveyed *Asgardarchaeota* contained a homolog to OapA, yet they have been shown to contain small GTPases in close genomic proximity to other coatomer-like proteins, suggesting that they also contain a functionally similar GTPase [54]. Furthermore, we identified one ß-propeller repeat containing protein (WD40 domains) associated with EVs with homologs identified in EVs from *Hrr. lacusprofundi* [16]. Proteins with WD40 domains can also be identified in the coatomer of intracellular vesicles of Eukaryotes [37]. Therefore, we propose that proteins involved in EV formation in haloarchaea, along with other lineages of the archaeal domain, could represent evolutionary precursors to proteins facilitating intracellular vesicle formation in Eukaryotes. *Asgardarchaeota*, the currently known closest relatives to Eukaryotes [55], have been shown to encode homologs to ESCRT machinery proteins, a group of proteins that are involved in EV production in Eukaryotes [56] and have recently been shown to be crucial for EV formation in *Sulfolobus* [14]. *Asgardarchaeota* have also been shown to encode homologs to intracellular membrane trafficking proteins, such as Ras-like GTPases like those identified in this study, and WD40 domain proteins [54]. Provided that the Ras GTPases and ESCRT proteins in *Asgardarchaeota* function in a similar manner to those characterized for *Sulfolobus* and *H. volcanii*, this represents two major mechanisms of eukaryotic vesicle formation potentially combined within one archaeal organism similar to Eukaryotes. Finally, this new family of archaeal Ras-superfamily GTPases appears to be highly conserved among DPANN archaea, implicating that vesicle formation, or a related mechanisms involving the GTPase, could be very crucial for DPANN archaea that are known for their symbiotic lifestyle [57]. The identification of precursors of eukaryotic intracellular vesicle formation in both free-living and symbiotic Archaea could have implications for a revision of the eukaryogenesis hypothesis.

We found other proteins that could also play a role in EV function, such as those with enzymatic functions or transport related proteins. Enzymatic activity was detected for EVs from the abundant marine cyanobacterium, *Prochlorococcus* [58], suggesting that EV-associated proteins can facilitate specific reactions extracellularly. Components of ABC transport systems make up the overall majority of proteins associated with EVs of *H. volcanii*, and were also detected in high abundancies in EVs and PVs of *Hrr. lacusprofundi* [16] as well as other characterized EVs [14]. While this enrichment could be due to their high abundance in the cell envelope, the binding capacity of the EV-associated solute-binding proteins could also allow sequestration of rare nutrients that could be incorporated by the receiving cell [59]. Alternatively, EVs could play a role in the removal of obsolete proteins from the cell envelope, such as components of ABC transporters, allowing the cell to refresh the composition of the envelope to better adapt to their environment. Furthermore, we identified a highly enriched diadenylate-cyclase, an enzyme involved in the formation of cyclic di-AMP. These molecules are known secondary messengers in *H. volcanii* [38] and could be enriched with EVs, providing an additional mechanism of communication.

Analysis of the lipid composition of EVs in comparison to the lipid composition of whole cells and cell membranes revealed some unexpected differences. We were able to detect the major bilayer forming lipids PG-AR, Me-PGP-AR, S-2G-AR, C-AR, 2G-AR and cardiolipins, that were previously described for *H. volcanii* [60, 61] in all samples, albeit in different relative amounts. Me-PGP-AR and PG-AR were the two most abundant lipid species across all samples, while the cardiolipins (CL) contributed to a notable portion of the intact polar lipids (IPLs) in cells and cell membranes and were surprisingly only detected in low abundances in EVs. CLs are considered to be important for membrane curvature [62]; therefore, we expected them to be essential in EVs due to the high degree of bilayer curvature in the vesicles. However, Kellermann et al [60] observed that changing extracellular

Mg^{2+} levels influence CL and Me-PGP ratios in *H. volcanii* and proposed that changes to the ratio of the two compounds are used to control membrane permeability in neutrophilic haloarchaea, in response to extracellular Mg^{2+} levels. As we cultivated *H. volcanii* in medium with a constant high Mg^{2+} concentration (174 mM) it is not surprising that Me-PGP-AR was the most prominent phospholipid species across all samples. This could also explain the absence of CLs in EVs, as Me-PGP-AR may be sufficient to ensure membrane stability in the smaller-sized EVs under high Mg^{2+} concentrations.

C-ARs and 2G-AR showed the opposite trend to cardiolipins, with an increase in their relative abundance in EVs compared to the cellular fraction. EVs of the hyperthermophilic *Sulfolobus solfataricus* were also shown to contain the same lipid species as the respective producing cells with significant shifts in the ratio of particular lipid compounds [63], similar to what we observe in *H. volcanii*. Differences between the lipid composition of cells and EVs could point towards a specific enrichment of particular lipid compounds in the EVs.

In summary, we show that EV production and the enclosing of RNA into EVs is common for multiple haloarchaeal species. We propose that the formation of EVs in haloarchaea is an active and conserved process, considering the conditionality of EV production along with their molecular composition that differs significantly from the originating cell, and the crucial involvement of a GTPase that is conserved among haloarchaea and other archaeal lineages. The enrichment of RNA with regulatory potential in EVs and the conservation of this process among different species lets us propose that halophilic Archaea utilize EVs as a communication mechanism influencing gene expression at a population-wide scale, as it has been proposed for some Bacteria [7, 8]. Finally, we propose that EV formation in haloarchaea, and potentially

a wide range of other Archaea, is related to Ras superfamily GTPase-dependent intracellular vesicle trafficking in Eukaryotes. Together with vesicle formation by *Sulfolobus* species that is dependent on ESCRT-like proteins [14], and related extracellular trafficking facilitated by ESCRT proteins in Eukaryotes, archaeal EV production sheds light on the evolution of both intra- and extracellular vesicle trafficking in Eukaryotes and might help to elucidate the eukaryogenesis puzzle [64].

Data availability

Raw data for resequencing of H26 Δ*oapA* mutant are available at ENA under project number PRJEB58368. Raw data for all RNA sequencing experiments for *H. volcanii* and *Hbt. salinarum* are available at ENA under project numbers PRJEB58342 and PRJEB58367 respectively. The mass spectrometry proteomics data have been deposited to the ProteomeXchange Consortium via the PRIDE [65] partner repository with the dataset identifier PXD038319 and 10.6019/PXD038319. Account details for reviewer: Reviewer account details: Username: reviewer_pxd038319@ebi.ac.uk, Password: KcmThVJF.

Author Contributions

J.M. performed the majority of the experimental work. L.J.G. and F.S. performed the lipid analysis. A.S. performed proteomics. Y.L. generated the AglB mutant. D.R.S. performed oapA phylogeny analysis. S.E. discovered the presence of RNA in EVs, conceived and led the study. I.G.D. and A.M. led the initial phase of the study. Some of the experiments were performed in A.M. laboratory. J.M. and S.E. performed the primary writing of the manuscript. All authors participated in the analysis and interpretation of the data and contributed to the writing of the manuscript.

Competing Interest Statement

The authors declare no competing interests.

Funding

Funding was provided by the Deutsche Forschungsgemeinschaft (SPP 2330, project 465087098), the Volkswagen Foundation, Germany (reference 98 190), and the Max Planck Society (Munich, Germany).

Acknowledgments

We thank the Max Planck-Genome-Centre Cologne (Cologne, Germany) for assistance with DNA and RNA sequencing. We thank Ingrid Kunze (MPI for Marine Microbiology, Bremen, Germany) for assistance with the experiments. We thank Thandi Schwarz (Ulm University) for help with the Northern Blots. We thank Jörg Soppa (Goethe-University Frankfurt) for providing the OapA knockout strain. We thank Thorsten Allers for providing the vector used in this study. We thank José Vicente Gomes-Filho (MPI for Terrestrial Microbiology, Marburg) for assistance with transcriptomic analysis. Finally, we want to thank the Max-Planck-Institute for Marine Microbiology and the Max-Planck-Society for continuous support.

References

1. Deatherage BL, Cookson BT (2012) Membrane vesicle release in bacteria, eukaryotes, and archaea: a conserved yet underappreciated aspect of microbial life. Infect Immun 80:1948–1957. https://doi.org/10.1128/IAI.06014-11
2. Gill S, Catchpole R, Forterre P (2019) Extracellular membrane vesicles in the three domains of life and beyond. FEMS Microbiol Rev 43:273–303. https://doi.org/10.1093/femsre/fuy042
3. Schatz D, Vardi A (2018) Extracellular vesicles - new players in cell-cell communication in aquatic environments. Curr Opin Microbiol 43:148–154. https://doi.org/10.1016/j.mib.2018.01.014

4. Hasegawa Y, Futamata H, Tashiro Y (2015) Complexities of cell-to-cell communication through membrane vesicles: implications for selective interaction of membrane vesicles with microbial cells. Front Microbiol 6:633. https://doi.org/10.3389/fmicb.2015.00633
5. Tashiro Y, Hasegawa Y, Shintani M et al. (2017) Interaction of Bacterial Membrane Vesicles with Specific Species and Their Potential for Delivery to Target Cells. Front Microbiol 8:571. https://doi.org/10.3389/fmicb.2017.00571
6. Manning AJ, Kuehn MJ (2011) Contribution of bacterial outer membrane vesicles to innate bacterial defense. BMC Microbiol 11:258. https://doi.org/10.1186/1471-2180-11-258
7. Koeppen K, Hampton TH, Jarek M et al. (2016) A Novel Mechanism of Host-Pathogen Interaction through sRNA in Bacterial Outer Membrane Vesicles. PLoS Pathog 12:e1005672. https://doi.org/10.1371/journal.ppat.1005672
8. Moriano-Gutierrez S, Bongrand C, Essock-Burns T et al. (2020) The noncoding small RNA SsrA is released by Vibrio fischeri and modulates critical host responses. PLoS Biol 18:e3000934. https://doi.org/10.1371/journal.pbio.3000934
9. Cai J, Wu G, Jose PA et al. (2016) Functional transferred DNA within extracellular vesicles. Exp Cell Res 349:179–183. https://doi.org/10.1016/j.yexcr.2016.10.012
10. Soler N, Forterre P (2020) Vesiduction: the fourth way of HGT. Environ Microbiol 22:2457–2460. https://doi.org/10.1111/1462-2920.15056
11. Toyofuku M, Tashiro Y, Hasegawa Y et al. (2015) Bacterial membrane vesicles, an overlooked environmental colloid: Biology, environmental perspectives and applications. Adv Colloid Interface Sci 226:65–77. https://doi.org/10.1016/j.cis.2015.08.013
12. Biller SJ, Schubotz F, Roggensack SE et al. (2013) Bacterial Vesicles in Marine Ecosystems. Science 343:183–186
13. Prangishvili D, Holz I, Stieger E et al. (2000) Sulfolobicins specific proteinaceous toxins produced by strains of the extremely thermophilic archaeal genus Sulfolobus. Journal of Bacteriology 182:2985–2988
14. Liu J, Cvirkaite-Krupovic V, Commere P-H et al. (2021) Archaeal extracellular vesicles are produced in an ESCRT-dependent manner and promote gene transfer and nutrient cycling in extreme environments. ISME J 15:2892–2905. https://doi.org/10.1038/s41396-021-00984-0
15. Gaudin M, Gauliard E, Schouten S et al. (2013) Hyperthermophilic archaea produce membrane vesicles that can transfer DNA. Environ Microbiol Rep 5:109–116. https://doi.org/10.1111/j.1758-2229.2012.00348.x
16. Erdmann S, Tschitschko B, Zhong L et al. (2017) A plasmid from an Antarctic haloarchaeon uses specialized membrane vesicles to disseminate and infect plasmid-free cells. Nat Microbiol 2:1446–1455. https://doi.org/10.1038/s41564-017-0009-2
17. Henne WM, Buchkovich NJ, Emr SD (2011) The ESCRT pathway. Dev Cell 21:77–91. https://doi.org/10.1016/j.devcel.2011.05.015
18. Makarova KS, Yutin N, Bell SD et al. (2010) Evolution of diverse cell division and vesicle formation systems in Archaea. Nat Rev Microbiol 8:731–741. https://doi.org/10.1038/nrmicro2406
19. Lam WL, Doolitle WF (1989) Shuttle vectors for the archaebacterium halobacterium volcanii. Proc. Natl. Acad. Sci. USA 86:5478–5482
20. Bitan-Banin G, Ortenberg R, Mevarech M (2003) Development of a gene knockout system for the halophilic archaeon Haloferax volcanii by use of the pyrE gene. Journal of Bacteriology 185:772–778. https://doi.org/10.1128/JB.185.3.772-778.2003
21. Delmas S, Duggin IG, Allers T (2013) DNA damage induces nucleoid compaction via the Mre11-Rad50 complex in the archaeon Haloferax volcanii. Mol Microbiol 87:168–179. https://doi.org/10.1111/mmi.12091

22. Alarcón-Schumacher T, Naor A, Gophna U et al. (2022) Isolation of a virus causing a chronic infection in the archaeal model organism Haloferax volcanii reveals antiviral activities of a provirus. Proc Natl Acad Sci U S A 119:e2205037119. https://doi.org/10.1073/pnas.2205037119
23. Babski J, Tjaden B, Voss B et al. (2011) Bioinformatic prediction and experimental verification of sRNAs in the haloarchaeon Haloferax volcanii. RNA Biol 8:806–816. https://doi.org/10.4161/rna.8.5.16039
24. Laass S, Monzon VA, Kliemt J et al. (2019) Characterization of the transcriptome of Haloferax volcanii, grown under four different conditions, with mixed RNA-Seq. PLoS One 14:e0215986. https://doi.org/10.1371/journal.pone.0215986
25. Ghosal A, Upadhyaya BB, Fritz JV et al. (2015) The extracellular RNA complement of Escherichia coli. Microbiologyopen 4:252–266. https://doi.org/10.1002/mbo3.235
26. Turchinovich A, Drapkina O, Tonevitsky A (2019) Transcriptome of Extracellular Vesicles: State-of-the-Art. Front Immunol 10:202. https://doi.org/10.3389/fimmu.2019.00202
27. Martins SdT, Alves LR (2020) Extracellular Vesicles in Viral Infections: Two Sides of the Same Coin? Front Cell Infect Microbiol 10:593170. https://doi.org/10.3389/fcimb.2020.593170
28. Gomes-Filho JV, Zaramela LS, Italiani VCdS et al. (2015) Sense overlapping transcripts in IS1341-type transposase genes are functional non-coding RNAs in archaea. RNA Biol 12:490–500. https://doi.org/10.1080/15476286.2015.1019998
29. Duggin IG, Aylett CHS, Walsh JC et al. (2015) CetZ tubulin-like proteins control archaeal cell shape. Nature 519:362–365. https://doi.org/10.1038/nature13983
30. Brown HJ, Duggin IG (2023) Diversity and Potential Multifunctionality of Archaeal CetZ Tubulin-like Cytoskeletal Proteins. Biomolecules 13. https://doi.org/10.3390/biom13010134
31. Blum M, Chang H-Y, Chuguransky S et al. (2021) The InterPro protein families and domains database: 20 years on. Nucleic Acids Res 49:D344-D354. https://doi.org/10.1093/nar/gkaa977
32. Kelley LA, Mezulis S, Yates CM et al. (2015) The Phyre2 web portal for protein modeling, prediction and analysis. Nat Protoc 10:845–858. https://doi.org/10.1038/nprot.2015.053
33. Jianyi Yang, Renxiang Yan, Ambrish Roy et al. (2015) The I-TASSER Suite: protein structure and function prediction. Nature Methods 12:7–8
34. Wolters M, Borst A, Pfeiffer F et al. (2019) Bioinformatic and genetic characterization of three genes localized adjacent to the major replication origin of Haloferax volcanii. FEMS Microbiol Lett 366. https://doi.org/10.1093/femsle/fnz238
35. Zimmermann L, Stephens A, Nam S-Z et al. (2018) A Completely Reimplemented MPI Bioinformatics Toolkit with a New HHpred Server at its Core. J Mol Biol 430:2237–2243. https://doi.org/10.1016/j.jmb.2017.12.007
36. Stenmark H (2009) Rab GTPases as coordinators of vesicle traffic. Nat Rev Mol Cell Biol 10:513–525. https://doi.org/10.1038/nrm2728
37. Kirchhausen T (2000) Three Ways to Make a Vesicle. Nature 1:187–198
38. Braun F, Thomalla L, van der Does C et al. (2019) Cyclic nucleotides in archaea: Cyclic di-AMP in the archaeon Haloferax volcanii and its putative role. Microbiologyopen 8:e00829. https://doi.org/10.1002/mbo3.829
39. Dyall-Smith M, Pfeiffer F, Chiang P-W et al. (2021) The Novel Halovirus Hardycor1, and the Presence of Active (Induced) Proviruses in Four Haloarchaea. Genes (Basel) 12. https://doi.org/10.3390/genes12020149
40. Speth DR, Orphan VJ (2018) Metabolic marker gene mining provides insight in global mcrA diversity and, coupled with targeted genome reconstruction, sheds further light on

metabolic potential of the Methanomassiliicoccales. PeerJ 6:e5614. https://doi.org/10.7717/peerj.5614
41. Choi DH, Kwon YM, Chiura HX et al. (2015) Extracellular Vesicles of the Hyperthermophilic Archaeon "Thermococcus onnurineus" NA1T. Appl Environ Microbiol 81:4591–4599. https://doi.org/10.1128/AEM.00428-15
42. Bernadac A, Gavioli M, Lazzaroni J-C et al. (1998) Escherichia coli tol-pal Mutants Form Outer Membrane Vesicles. Journal of Bacteriology 180:4872–4878
43. McBroom AJ, Johnson AP, Vemulapalli S et al. (2006) Outer membrane vesicle production by Escherichia coli is independent of membrane instability. Journal of Bacteriology 188:5385–5392. https://doi.org/10.1128/JB.00498-06
44. Abu-Qarn M, Yurist-Doutsch S, Giordano A et al. (2007) Haloferax volcanii AglB and AglD are involved in N-glycosylation of the S-layer glycoprotein and proper assembly of the surface layer. J Mol Biol 374:1224–1236. https://doi.org/10.1016/j.jmb.2007.10.042
45. Dawson KS, Freeman KH, Macalady JL (2012) Molecular characterization of core lipids from halophilic archaea grown under different salinity conditions. Organic Geochemistry 48:1–8. https://doi.org/10.1016/j.orggeochem.2012.04.003
46. Tsatsaronis JA, Franch-Arroyo S, Resch U et al. (2018) Extracellular Vesicle RNA: A Universal Mediator of Microbial Communication? Trends Microbiol 26:401–410. https://doi.org/10.1016/j.tim.2018.02.009
47. O'Brien K, Breyne K, Ughetto S et al. (2020) RNA delivery by extracellular vesicles in mammalian cells and its applications. Nat Rev Mol Cell Biol 21:585–606. https://doi.org/10.1038/s41580-020-0251-y
48. Gelsinger DR, DiRuggiero J (2018) Transcriptional Landscape and Regulatory Roles of Small Noncoding RNAs in the Oxidative Stress Response of the Haloarchaeon Haloferax volcanii. Journal of Bacteriology 200. https://doi.org/10.1128/JB.00779-17
49. Nielsen E, Cheung AY, Ueda T (2008) The regulatory RAB and ARF GTPases for vesicular trafficking. Plant Physiol 147:1516–1526. https://doi.org/10.1104/pp.108.121798
50. Hsu VW, Yang J-S (2009) Mechanisms of COPI vesicle formation. FEBS Letters 583:3758–3763. https://doi.org/10.1016/j.febslet.2009.10.056
51. Szul T, Sztul E (2011) COPII and COPI traffic at the ER-Golgi interface. Physiology (Bethesda) 26:348–364. https://doi.org/10.1152/physiol.00017.2011
52. Beck R, Sun Z, Adolf F et al. (2008) Membrane curvature induced by Arf1-GTPase is essential for MV formation 105:11731–11736. https://doi.org/10.1073/pnas.0805182105
53. Wuichet K, Søgaard-Andersen L (2014) Evolution and diversity of the Ras superfamily of small GTPases in prokaryotes. Genome Biol Evol 7:57–70. https://doi.org/10.1093/gbe/evu264
54. Zaremba-Niedzwiedzka K, Caceres EF, Saw JH et al. (2017) Asgard archaea illuminate the origin of eukaryotic cellular complexity. Nature 541:353–358. https://doi.org/10.1038/nature21031
55. Spang A, Eme L, Saw JH et al. (2018) Asgard archaea are the closest prokaryotic relatives of eukaryotes. PLoS Genet 14:e1007080. https://doi.org/10.1371/journal.pgen.1007080
56. Juan T, Fürthauer M (2018) Biogenesis and function of ESCRT-dependent extracellular vesicles. Semin Cell Dev Biol 74:66–77. https://doi.org/10.1016/j.semcdb.2017.08.022
57. Dombrowski N, Lee J-H, Williams TA et al. (2019) Genomic diversity, lifestyles and evolutionary origins of DPANN archaea. FEMS Microbiol Lett 366. https://doi.org/10.1093/femsle/fnz008
58. Biller SJ, Lundeen RA, Hmelo LR et al. (2022) Prochlorococcus extracellular vesicles: molecular composition and adsorption to diverse microbes. Environ Microbiol 24:420–435. https://doi.org/10.1111/1462-2920.15834

59. Fadeev E, Bastos CC, Hennenfeind J et al. (2022) Characterization of membrane vesicles in Alteromonas macleodii indicates potential roles in their copiotrophic lifestyle
60. Kellermann MY, Yoshinaga MY, Valentine RC et al. (2016) Important roles for membrane lipids in haloarchaeal bioenergetics. Biochim Biophys Acta 1858:2940–2956. https://doi.org/10.1016/j.bbamem.2016.08.010
61. Sprott GD, Larocque S, Cadotte N et al. (2003) Novel polar lipids of halophilic eubacterium Planococcus H8 and archaeon Haloferax volcanii. Biochim Biophys Acta 1633:179–188. https://doi.org/10.1016/j.bbalip.2003.08.001
62. Mileykovskaya E, Dowhan W (2009) Cardiolipin membrane domains in prokaryotes and eukaryotes. Biochim Biophys Acta 1788:2084–2091. https://doi.org/10.1016/j.bbamem.2009.04.003
63. Ellen AF, Albers S-V, Huibers W et al. (2009) Proteomic analysis of secreted membrane vesicles of archaeal Sulfolobus species reveals the presence of endosome sorting complex components. Extremophiles 13:67–79. https://doi.org/10.1007/s00792-008-0199-x
64. Schlacht A, Herman EK, Klute MJ et al. (2014) Missing pieces of an ancient puzzle: evolution of the eukaryotic membrane-trafficking system. Cold Spring Harb Perspect Biol 6:a016048. https://doi.org/10.1101/cshperspect.a016048
65. Perez-Riverol Y, Bai J, Bandla C et al. (2022) The PRIDE database resources in 2022: a hub for mass spectrometry-based proteomics evidences. Nucleic Acids Res 50:D543-D552. https://doi.org/10.1093/nar/gkab1038
66. Dyall-Smith, Michael (2009) The Halohandbook: Protocols for haloarchaeal genetics
67. Pfeiffer F, Losensky G, Marchfelder A et al. (2020) Whole-genome comparison between the type strain of Halobacterium salinarum (DSM 3754T) and the laboratory strains R1 and NRC-1. Microbiologyopen 9:e974. https://doi.org/10.1002/mbo3.974
68. Allers T, Ngo H-P, Mevarech M et al. (2004) Development of additional selectable markers for the halophilic archaeon Haloferax volcanii based on the leuB and trpA genes. Appl Environ Microbiol 70:943–953. https://doi.org/10.1128/AEM.70.2.943-953.2004
69. Mills J, Erdmann S (2022) Isolation, Purification, and Characterization of Membrane Vesicles from Haloarchaea. Methods Mol Biol 2522:435–448. https://doi.org/10.1007/978-1-0716-2445-6_30
70. Witte A, Baranyi U, Klein R et al. (1997) Characterization of Natronobacterium magadii phage ΦCh1, a unique archaeal phage containing DNA and RNA. Mol Microbiol 23:603–616
71. Bailey TL, Elkan C (1994) Fitting a Mixture Model By Expectation Maximization To Discover Motifs In Biopolymer. Proceedings of the Second International Conference on Intelligent Systems for Molecular Biology:28–36
72. Raden M, Ali SM, Alkhnbashi OS et al. (2018) Freiburg RNA tools: a central online resource for RNA-focused research and teaching. Nucleic Acids Res 46:W25-W29. https://doi.org/10.1093/nar/gky329
73. Will S, Joshi T, Hofacker IL et al. (2012) LocARNA-P: accurate boundary prediction and improved detection of structural RNAs. RNA 18:900–914. https://doi.org/10.1261/rna.029041.111
74. Will S, Reiche K, Hofacker IL et al. (2007) Inferring noncoding RNA families and classes by means of genome-scale structure-based clustering. PLoS Comput Biol 3:e65. https://doi.org/10.1371/journal.pcbi.0030065
75. Adams PP, Flores Avile C, Popitsch N et al. (2017) In vivo expression technology and 5' end mapping of the Borrelia burgdorferi transcriptome identify novel RNAs expressed during mammalian infection. Nucleic Acids Res 45:775–792. https://doi.org/10.1093/nar/gkw1180

76. Haque RU, Paradisi F, Allers T (2020) Haloferax volcanii for biotechnology applications: challenges, current state and perspectives. Appl Microbiol Biotechnol 104:1371–1382. https://doi.org/10.1007/s00253-019-10314-2
77. Allers T, Barak S, Liddell S et al. (2010) Improved strains and plasmid vectors for conditional overexpression of His-tagged proteins in Haloferax volcanii. Appl Environ Microbiol 76:1759–1769. https://doi.org/10.1128/AEM.02670-09
78. Gamble-Milner R Genetic analysis of the Hel308 helicase in the archaeon Haloferax volcanii
79. Arne Smits , Wolfgang Huber (2017) DEP. Bioconductor
80. Buchfink B, Reuter K, Drost H-G (2021) Sensitive protein alignments at tree-of-life scale using DIAMOND. Nature Methods 18:366–368. https://doi.org/10.1038/s41592-021-01101-x
81. Parks DH, Chuvochina M, Chaumeil P-A et al. (2020) A complete domain-to-species taxonomy for Bacteria and Archaea. Nat Biotechnol 38:1079–1086. https://doi.org/10.1038/s41587-020-0501-8
82. Nayfach S, Roux S, Seshadri R et al. (2021) A genomic catalog of Earth's microbiomes. Nat Biotechnol 39:499–509. https://doi.org/10.1038/s41587-020-0718-6
83. Jain C, Rodriguez-R LM, Phillippy AM et al. (2018) High throughput ANI analysis of 90K prokaryotic genomes reveals clear species boundaries. Nat Commun 9:5114. https://doi.org/10.1038/s41467-018-07641-9
84. Price MN, Dehal PS, Arkin AP (2010) FastTree 2--approximately maximum-likelihood trees for large alignments. PLoS One 5:e9490. https://doi.org/10.1371/journal.pone.0009490
85. Edgar RC (2004) MUSCLE: multiple sequence alignment with high accuracy and high throughput. Nucleic Acids Res 32:1792–1797. https://doi.org/10.1093/nar/gkh340
86. Trifinopoulos J, Nguyen L-T, Haeseler A von et al. (2016) W-IQ-TREE: a fast online phylogenetic tool for maximum likelihood analysis. Nucleic Acids Res 44:W232-5. https://doi.org/10.1093/nar/gkw256
87. Hoang DT, Chernomor O, Haeseler A von et al. (2018) UFBoot2: Improving the Ultrafast Bootstrap Approximation. Mol Biol Evol 35:518–522. https://doi.org/10.1093/molbev/msx281
88. Kalyaanamoorthy S, Minh BQ, Wong TKF et al. (2017) ModelFinder: fast model selection for accurate phylogenetic estimates. Nature Methods 14:587–589. https://doi.org/10.1038/nmeth.4285
89. Letunic I, Bork P (2021) Interactive Tree Of Life (iTOL) v5: an online tool for phylogenetic tree display and annotation. Nucleic Acids Res 49:W293-W296. https://doi.org/10.1093/nar/gkab301
90. Giavalisco P, Li Y, Matthes A et al. (2011) Elemental formula annotation of polar and lipophilic metabolites using (13) C, (15) N and (34) S isotope labelling, in combination with high-resolution mass spectrometry. Plant J 68:364–376. https://doi.org/10.1111/j.1365-313X.2011.04682.x
91. Wörmer L, Lipp JS, Schröder JM et al. (2013) Application of two new LC–ESI–MS methods for improved detection of intact polar lipids (IPLs) in environmental samples. Organic Geochemistry 59:10–21. https://doi.org/10.1016/j.orggeochem.2013.03.004
92. Bale NJ, Sorokin DY, Hopmans EC et al. (2019) New Insights Into the Polar Lipid Composition of Extremely Halo(alkali)philic Euryarchaea From Hypersaline Lakes. Front Microbiol 10:377. https://doi.org/10.3389/fmicb.2019.00377
93. Yoshinaga MY, Kellermann MY, Rossel PE et al. (2011) Systematic fragmentation patterns of archaeal intact polar lipids by high-performance liquid chromatography/electrospray ionization ion-trap mass spectrometry. Rapid Commun Mass Spectrom 25:3563–3574. https://doi.org/10.1002/rcm.5251

94. Wickham H (2009) ggplot2: Elegant graphics for data analysis / by Hadley Wickham. Use R! Springer, New York, London
95. Wickham H (2011) The Split-Apply-Combine Strategy for Data Analysis. Journal of Statistical Software 40
96. Wickham H, François R, Henry L, Müller K (2022) dplyr: A Grammar of Data Manipulation
97. Schneider CA, Rasband WS, Eliceiri KW (2012) NIH Image to ImageJ: 25 years of image analysis. Nature Methods 9:671–675. https://doi.org/10.1038/nmeth.2089

Extended Data: Selective enrichment of intact polar lipids in extracellular vesicles of halophilic *Euryarchaeota*

L. Johanna Gebhard[1], Florence Schubotz[2], Joshua Mills[1] & Susanne Erdmann[1]

[1]Max Planck Institute for Marine Microbiology, Archaeal Virology, Celsiusstrasse 1, 28359, Bremen, Germany

[2]MARUM Center for Marine Environmental Sciences, University of Bremen, Bremen 28359, Germany

* The manuscript is in preparation and has not been revised by all authors

Author contributions: L.J.G. and S.E conceived the study, L.J.G. prepared the samples and performed lipid extractions, L.J.G. and F.S. measured the samples on the UHPLC QTOF-MS and analyzed the data. J.M. performed the majority of the experimental work in the original manuscript preceding this addendum and assisted with writing, L.J.G drafted the manuscript with support from all authors, S.E. led both the original study and this addendum.

Abstract

Extracellular vesicles (EVs) mediate interactions between microorganisms and the extracellular environment by trafficking a wide variety of cargo. Previous investigation of the lipid composition of the halophilic archaeon *Haloferax volcanii* (Mills *et al.*, 2023) showed high levels of unsaturation in the main bilayer-forming lipids and a selective uptake of intact polar lipids (IPLs) into EVs. In this addendum to Mills *et al.* (2023), we expand the analysis to four strains of a related haloarchaeon, *Halorubrum lacusprofundi.* We compared two pR1SE plasmid infected strains, DL18 and R1S1, which produce specialized plasmid vesicles (PVs) in addition to standard EVs, to two uninfected strains UNSW and DSMZ. The main difference between the four strains was the presence or absence of a pR1SE-infection, however, the effect of the PVs on the total vesicle population could not yet be isolated. Comparison between *H. volcanii* and *Hrr. lacusprofundi* showed shared predominant archaeol (AR) species but differences in enrichment into the vesicle fractions. IPLs with neutral or without head groups were selectively enriched into the *H. volcanii* EV fraction, while cardiolipins and total unsaturated lipids declined. For *Hrr. lacusprofundi*, cardiolipins were not detected at high concentrations and both cellular and vesicle fractions showed a higher level of membrane unsaturation mainly driven by highly (6 double bonds) unsaturated phosphatidylglycerol-ARs and core-ARs. These differences could be caused by shifts in concentrations of individual cations in the growth media of the respective species. Yet, we are able to demonstrate selective enrichment of specific IPLs into the vesicle fraction for two species of haloarchaea. This enrichment mirrors previous observations of membrane enveloped viruses infecting archaea and could be caused by lipid-protein interactions or physical processes during budding of virions or vesicles from the host membrane.

Introduction

In our investigations into the content of the extracellular vesicles (EVs) of *Haloferax volcanii* recounted in Mills *et al.* (2023) in the previous section, the lipid content of their membrane naturally came up as an avenue of investigation. The phospholipids of archaea have a unique composition in which the highly methylated isoprenoid chains are linked to a glycerol-1-phosphate via an ether bond. Bacterial and eukaryotic phospholipids are built out of fatty acids linked to glycerol-3-phosphate with an ester bond in an opposite stereochemistry to archaeal lipids (Jain *et al.*, 2014; Caforio & Driessen, 2017). The lipid chemistry of archaea and the resulting changes to membrane permeability have been identified as one of the major factors in their adaptation to extreme environments where energy conservation is of vital importance (van de Vossenberg *et al.*, 1999; Valentine, 2007; Siliakus *et al.*, 2017). Archaeal lipids can be divided broadly into two categories, tetraether lipids and archaeols, based on their basal units, but additional modifications of the chains and the polar head group lead to a remarkable diversity in archaeal lipids (Jain *et al.*, 2014; Caforio & Driessen, 2017).

Polar lipids that form the monolayer membranes of the hyperthermophilic *Thermoproteota* (Villanueva *et al.*, 2014) and the mainly mesophilic *Thaumarchaeota* (Elling *et al.*, 2017) phyla are characterized by a C_{40} glycerol-dialkylglycerol tetraether lipid (GDGTs or tetraether lipids) with sugar or phosphor-sugar head groups (Schouten *et al.*, 2013; Villanueva *et al.*, 2014; Caforio & Driessen, 2017). The other main class of archaeal lipids are the bilayer-forming C_{20} *sn*-2,3-dyacilglycerol diether lipids (archaeol, AR) with phosphate head groups which are commonly found in *Euryarchaeota* (Villanueva *et al.*, 2014; Kellermann *et al.*, 2016; Caforio & Driessen, 2017). The archaeols can be further modified by e.g., elongated isoprenoid chains (C_{25}) or double bonds in the isoprenoid chains (Dawson *et al.*, 2012;

Kellermann *et al.*, 2016). In addition to the membrane-forming archaeols (Yoshinaga *et al.*, 2011) the membranes of haloarchaea (*Halobacteria, Euryarchaeota*) also contain non-membrane-forming lipid classes that are predicted to fulfil a variety of functions including electron shuttling and membrane permeability regulation (e.g. quinones, carotenoids, squalenes) (Kushwaha *et al.*, 1974; Hauß *et al.*, 2002; Kellermann *et al.*, 2016). Haloarchaeal cell membranes are further distinguished from other archaeal lipids by highly negatively charged head groups (Kellermann *et al.*, 2016), a higher degree of lipid unsaturation, the ability to regulate lipid modifications in response to changes in salinity (Dawson *et al.*, 2012; Kellermann *et al.*, 2016), cation-lipid interactions (Kellermann *et al.*, 2016) and asymmetric configurations (C_{20} – C_{25}) of extended isoprenoid chains (Dawson *et al.*, 2012). Indeed, the tight regulation of membrane permeability appears to be essential for the 'salt-in' strategy of osmoregulation, which haloarchaea employ by accumulating K^+ intracellularly and extruding Na^{2+} cations (Oren, 1999).

The precise molecular basis for the formation and scission of EVs from the cellular membranes of archaea is currently unknown. Nevertheless, analysis of the lipid composition of EVs compared to cell membranes can indicate possible lipid segregation processes during EV budding and scission from the membrane. These could be caused by the three-dimensional shapes of specific lipid species or interactions with vesicle formation machinery proteins. A previous study characterized the lipid content of the EVs obtained from several *Sulfolobus* species (Ellen *et al.*, 2009) and showed reduced abundance of lipids with cyclopentane rings within the EVs but no significant difference to the overall lipid composition of the cell membrane. Direct comparisons are difficult to make, however, since the membrane-forming lipids of *Thermoproteota* and *Euryarchaeota* have fundamentally different structures as described above. We are not currently aware of any published work around the lipid content of haloarchaeal EVs. However, some membrane

containing viruses that infect haloarchaea have shown enrichment of specific lipids compared to their hosts (Bamford *et al.*, 2005; Pietilä *et al.*, 2012; Roine & Bamford, 2012). Roine and Bamford (2012) hypothesized that this effect could be caused by preferential binding of virus proteins to specific lipid species but this has not yet been experimentally verified in archaea.

In this addendum to Mills et al. (2023), we expand the characterization of the lipid composition of EVs produced by *H. volcanii* and examine the lipid composition of a related haloarchaeon, *Halorubrum lacusprofundi* (Franzmann et al., 1988; Gupta et al., 2015). We compare the lipid compositions of both species and identify patterns of selective enrichment into the vesicle fraction of haloarchaea.

In addition to EVs, *Hrr. lacusprofundi* cells infected with the pR1SE plasmid produce specialized plasmid vesicles (PVs), containing the pR1SE plasmid (Erdmann *et al.*, 2017). PVs have a unique protein composition compared to the EVs and show a viral-like lifestyle by infecting new host cells without cell-to-cell contact, leading to the dissemination of the pR1SE plasmid in the population. *Hrr. lacusprofundi* is currently the only known host of pR1SE and producer of PVs, which are produced alongside EVs in infected cells. We are not yet able to physically separate the two vesicle populations. Therefore, we compare the lipid composition of vesicles produced by two pR1SE-infected strains of *Hrr. lacusprofundi*, which produce PVs and EVs, and two uninfected strains of *Hrr. lacusprofundi* that only produce EVs in order to determine possible contributions of PVs to the overall composition of the vesicle fraction.

Methods

Cultivation of Hrr. lacusprofundi cultures and sample preparation

A detailed description of the of *H. volcanii* samples is given in the precious section, Mills *et al.* (2023). For *Hrr. lacusprofundi*, lipids were extracted from whole cells, the cellular membrane and the extracellular vesicles of two pR1SE infected strains of *Hrr. lacusprofundi*, R1S1 and DL18 (Erdmann *et al.*, 2017), and two un-infected strains ACAM34_UNSW and ACAM34_DSMZ (Mercier *et al.*, 2022) in two biological replicates per strain. The individual *Hrr. lacusprofundi* strains will be referred to using only their strain names in the following text, whereas *H. volcanii* samples will be indicated by the species name as only one strain was used for analysis. Infection of *Hrr. lacusprofundi* strains was confirmed prior to extraction with PCR on aliquots of cells obtained from liquid cultures using a pR1SE-specific primer set (5'-GACAGAGACCGGGAAACTGG-3' and reverse: 5'- AGGCGG-TACTTGAGCTTGTC-3') and a Q5-Polymerase (NEB, Ipswich, MA, USA) and with a previously established PCR protocol described in detail in Chapter I (Gebhard *et al.*, 2023).

Liquid cultures of *Hrr. lacusprofundi* were grown at 28 °C and 120 rpm in DBCM2+ medium modified from standard DBCM2 medium by the addition of more organic substrates (Burns & Dyall-Smith, 2006); 180 g/l NaCl, 25 g/l MgCl, 29 g/l $MgSO_4 \cdot 7H_2O$, 5.8 g/l KCl, 1 g/l peptone (Oxoid, Basingstoke, United Kingdom), 0.5 g/l yeast extract (Oxoid), dissolved in ddH_2O with pH adjusted to 7.5. Supplements were added after autoclaving; 6 ml/l 1 M $CaCl_2$, 2 ml/l K_2HPO_4 buffer (Dyall-Smith, 2009), 4.4 ml/l 25 % (w/v) sodium pyruvate, 5 ml/l 1 M NH_4Cl, 1 ml/l SL10 trace elements solution and 3 ml/l vitamin 10 solution (Dyall-Smith, 2009). After five passages through DBCM2 medium, each biological replicate was separated into 3 x 500 ml liquid cultures each supplemented with 30 ml 10x YPC (50 g/l yeast extract, 10 g/l peptone,

10 g/l casamino acids, all Oxoid adjusted to pH 7.4 with KOH Buffer and autoclaved) which were pooled together for each biol. replicate during harvesting.

Sample preparation, lipid extraction and analysis

Harvesting of liquid cultures by centrifugation (45 min, 4500 x *g* at 4 °C) separated cells from the vesicle fraction, which was further purified by PEG_{6000} precipitation (10% [v/v], at 4 °C overnight), followed by centrifugation at 30,000 x g for 45 min at 4 °C (JA-14, Beckman-Coulter). The precipitates were resuspended in DBCM2 salt solution (without organic additives) and filtered through syringe top filters (1x 0.8 µm, 1x 0.45 µm and 2x 0.2 µm pore size in sequence). In contrast to the *H. volcanii* samples, vesicle preparations from the *Hrr. lacusprofundi* strains were further purified in CsCl gradients, 0.45 g/ml CsCl dissolved in DBCM2 salt solution dissolved 1:1 with sterile ddH_2O followed by centrifugation at 247,000 x *g* at 4 °C for 20 h (SW41Ti rotor), instead of OptiPrep™ gradients (Sigma-Aldrich, St. Louis, MO, USA). This arrangement was chosen since *Hrr. lacusprofundi* vesicles can be purified in CsCl gradients, likely due to different density properties compared to *H. volcanii* EVs, and CsCl residues are most likely less contaminating in later mass spectrometry analysis. Gradient bands were extracted separately after ultracentrifugation and concentrated with filter columns (Vivaspin 6, 100,000 MWCO PES (Sartorius, Göttingen, Germany)) at 4 °C and 4000 x *g*, washed twice with DBCM2 salt solution and resuspended to a final volume of 1 ml. From this volume 3 x 200 µl were distributed into three tubes as technical replicates for lipid extraction and stored at -20 °C until further analysis.

For the total cell and cell membrane fraction, aliquots of pellets obtained from each biological replicate equal to approx. 50 ml of liquid culture, were washed twice with DBCM2 salt solution, split into two equal halves and subsequently dissolved in 1.6 ml of DBCM2 salt solution for each extraction.

For the lipid analysis of total cells, 1.6 ml were further aliquoted into 3 x 300 µl technical replicates for lipid extraction. For the cell membranes, 1.6 ml of dissolved cell pellet from each replicate was diluted (1:1) with DBCM2 salt solution and sonicated with a microtip sonicator (MS 73 Sonoplus, Bandelin electronic, Germany) 3 x for 30 s on ice at 35% output. Lysed samples were treated with DNase I (30 min at 28 °C, 10 µl/mL), followed by centrifugation in a table-top centrifuge (8000 x *g*, 30 min at 4 °C). Cell membranes were separated from cell contents by ultracentrifugation (SW41Ti rotor, 247,000 x *g* for 15 min). Subsequently, the pellets were dissolved in 1 ml DBCM2 salt solution and distributed into 4 x 250 µl aliquots as technical replicates for lipid extraction. All samples were stored at -20 °C until further processing.

Lipid extraction was performed with a modified protocol from Giavalisco *et al.* (2011) which is described in detail in the previous section under *Lipid extraction and analysis* in the Methods. After phase separation, the upper lipid-containing phase of each sample was transferred into a combusted glass LC-MS vial, dried under constant N_2 flow and stored at -20 °C until further analysis. The same protocol was also applied to four 300 µl aliquots of sterile DBCM2 salt solution as negative controls.
Dried samples were resuspended and diluted in 1 ml of a solvent mixture of dichloromethane:methanol (1:9) and further diluted to a final concentration of 0.4% of total lipid extract (TLE) for whole cells and cell membrane samples, and 1 % TLE for vesicle samples. Measurements were performed on 10 µl of sample on a Dionex Ultimate 3000 RS UHPLC system coupled to a maXis ultrahigh-resolution quadrupole time of flight tandem mass spectrometer (Q-TOF MS, Bruker Daltonics) using reverse phase chromatography as described in detail in the previous section.

The output was analyzed with the software provided by the manufacturer (DataAnalysis 4.4.2, Bruker Daltonics), intact polar lipids were identified

based on retention time, fractionation pattern and exact mass (Yoshinaga *et al.*, 2011; Kellermann *et al.*, 2016; Bale *et al.*, 2019). Several technical replicates were measured for each sample type, of which representative replicates were selected for each biological replicate for each fraction (see Supplementary Figures 5 & 6 for a breakdown of the samples used for each strain). As for the *H. volcanii* samples, EV samples from different gradient bands in the DL18 and R1S1 strains showed minimal differences in lipid distribution and were therefore pooled for each biological replicate. No distinct bands were observed in the gradients of EV samples from the UNSW and DSMZ strains.

Relative abundances were calculated separately for each replicate and averages for each fraction were first pooled from three technical replicates per biological replicate and subsequently averaged for two biological replicates for each *Hrr. lacusprofundi* strain. For the vesicle fraction, the results from samples obtained from different gradient bands were pooled first for each band, then for each biological replicate and finally averaged for two biological replicates per *Hrr. lacusprofundi* strain. All comparisons between samples were made based on the relative abundance distributions of intact polar lipids without quantification, therefore differences in dilution of total TLE were not considered between sample types. IPLs were identified based on retention time, fractionation pattern and exact masses after Yoshinaga *et al.* (2011); Kellermann *et al.* (2016); Bale *et al.* (2019). Unsaturated IPLs were identified based on the shift of major ions to 2 m/z lower values per double bond and earlier elution times. Figures showing individual mass spectra were created with DataAnalysis (version 4.4.2, Bruker Daltonics, Billerica, MA, USA) which was also the main software used for analysis. Relative abundance figures were created in R (v4.1.2; R Core Team 2021) using the ggplot2 (Wickham, 2016), plyr (Wickham, 2011) and dplyr packages (Wickham *et al.*, 2022).

Results & Discussion

Enrichment of specific lipid compounds in the extracellular vesicles of H. volcanii

Analysis of the lipid content of EVs obtained from *H. volcanii* strain DS2 had shown clear shifts in the relative abundances of certain lipid compounds between cellular fractions and the EV fraction [see Figure 1 and Mills *et al.* (2023)]. Sub-populations of EVs separated by density gradient centrifugation did not show significant differences suggesting that lipid composition is not the factor driving differential separation and were therefore pooled together to reach an overarching comparison of the total EV population (see Supplementary Figure 1 and Supplementary Table 1).

To summarize, intact polar lipids (IPLs) with negatively charged phosphate head groups were the predominant class of lipids across all fractions in *H. volcanii* (Mills *et al.,* 2023). We were able to detect the major bilayer–forming IPLs that have been previously described for *H. volcanii* (Sprott *et al.*, 2003; Kellermann *et al.*, 2016). Methylated-phosphatidyl-glycerolphosphate-archaeol (Me-PGP-AR) and phosphatidylglycerol-archaeol (PG-AR) were the two most abundant IPLs across all samples, followed by sulfated-diglycosyl-archaeol (S-2G-AR). Both Me-PGP-AR and PG-AR were identified in saturated and unsaturated forms, with PG-ARs showing the highest degree of unsaturation of up to 6 double bonds (Figure 1). No IPLs were specific to the EV fraction, but lipids with neutral head groups or no head group, diglycosyl-archaeol (2G-AR) or core-archaeol (C-AR) respectively, were enriched in EVs relative to the cellular fractions. Dimeric phospholipids (or cardiolipins, CL) composed of two pairs of isoprenoid chains, were almost undetectable in the EV samples, but represented a notable portion of the IPLs in the cells and cellular membranes. The low abundance of cardiolipins (CL) in the EV

fraction came as a surprise since they are considered to contribute to membrane curvature (Mileykovskaya & Dowhan, 2009). Our initial hypothesis would have expected them in the vesicle fractions due to the high degree of bilayer curvature in the vesicles. However, it may be that the curvature of EVs is too extreme to be facilitated by CLs. However, the lack of CLs could also come as a result of the increased abundance of Me-PGP-AR. Kellermann *et al.* (2016) showed that the relative abundances of CLs and Me-PGP-AR shifted in response to changes in extracellular Mg^{2+} concentrations and proposed that this shift could be used to control membrane permeability in neutrophilic haloarchaea. At the comparatively high Mg^{2+} concentration (174 mM) in the culture medium used for *H. volcanii* in this study, Me-PGP-AR appears to take over as the predominant IPL as it is able to bind divalent cations (e.g., Mg^{2+}) compared to PGs or CLs.

Kellermann *et al.* (2016) proposed that Mg^{2+} cations bound to Me-PGP-AR could form a protective layer to regulate membrane permeability against Na^{2+}. This shift may potentially interfere with enrichment of CLs into the vesicle fraction if the overall abundance is lower across the cell membrane. Me-PGP-AR might also be sufficient to ensure membrane stability in EVs under constant, high Mg^{2+} concentrations compared to the larger cells. Finally, we observed that the relative amount of unsaturated lipids decreased in the EV fraction of *H. volcanii* by ca. 15% (Figure 1). In contrast to previous work by Kellermann *et al.* (2016), CLs and ME-PGP-AR also contributed significantly to the pool of total unsaturated lipids in addition to PG-AR. These differences in the relative lipid composition of EVs compared to total cells and cell membranes suggested a selective enrichment of specific compounds in the vesicle fraction of *H. volcanii*.

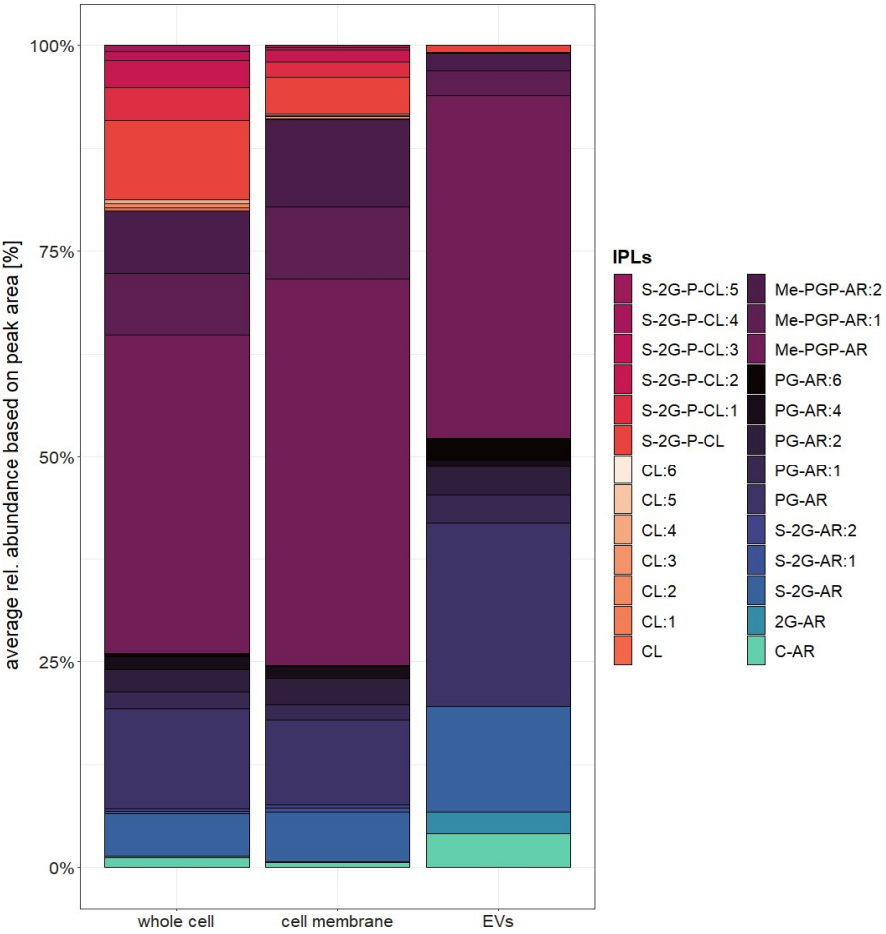

Figure 1: Average distribution of lipid compounds comparing whole cells, cell membranes and EVs of *H. volcanii* reproduced with permission from Mills *et al.* (2023) see previous section. The average (n = 3) relative abundance of lipids was calculated for each preparation; whole cells, cell membrane and extracellular vesicles (EVs) based on the peak area of the most abundant adduct for each compound. The distribution in the individual samples is shown in Supplementary Figure 1. For the EV fraction, bands were pooled together after density gradient purification from 3 biological replicates. Lipids were identified based on their retention time, fractionation pattern and exact mass. Compound abbreviations: AR = archaeol (C_{20}-C_{20} isoprenoidal chains), CL = cardiolipin or dimeric phospholipid, :n = lipid with n number of unsaturations. Lipids with neutral headgroups: 1G = monoglycosyl, 2G = diglycosyl, C-AR = core-AR. Lipids with anionic headgroups: Me-PGP = phosphatidylglycerophosphate methyl esters, PG = phosphatidylglycerol, S-2G = sulfated diglycosyl, S-2G-P = sulfated diglycosyl-phospho.

Hrr. lacusprofundi vesicles are also selectively enriched with specific lipid species, although they are not the same as in H. volcanii.

In order to gather further evidence for selective enrichment, we analysed the cellular and vesicle fractions of a related haloarchaeon, *Hrr. lacusprofundi*. Infection with the pR1SE plasmids leads to production of specialized plasmid vesicles (PVs) in *Hrr. lacusprofundi* alongside regular EVs (Erdmann *et al.*, 2017). Therefore, we compared two pR1SE-infected strains R1S1 and DL18 (Figure 2A & B) to two uninfected control strains ACAM34_UNSW (UNSW) and ACAM34_DSMZ (DSMZ, Figure 3A & B, Supplementary Figure 2). As we are currently unable to physically separate PVs from the total vesicle population, comparison of PVs to uninfected controls allows us to infer effects that the PVs might have on the lipid composition of the total vesicle population. Since we are comparing biologically distinct strains of the same species, final confirmation would require infection of UNSW and DSMZ with the pR1SE plasmid and analysis of the PV and EV fraction in comparison to the pure EV fraction of uninfected cultures. However, this experiment has not yet been performed.

Overall, the four *Hrr. lacusprofundi* strains showed similar relative abundance distributions of IPLs (Table 1). As in *H. volcanii,* the main phospholipids in all fractions across the four Hrr. lacusprofundi strains were Me-PGP-AR (ca. 46-60%), PG-AR with highly variable abundance (ca. 20-40% in total) and S-2G-AR (ca. 3-8%, see Table 1). Unsaturated PG-AR with up to 6 double bonds was detected in all fractions (Supplementary Figure 3), and together with the core-archaeols (Supplementary Figure 4) contributed to the bulk of the total unsaturated IPLs across samples.

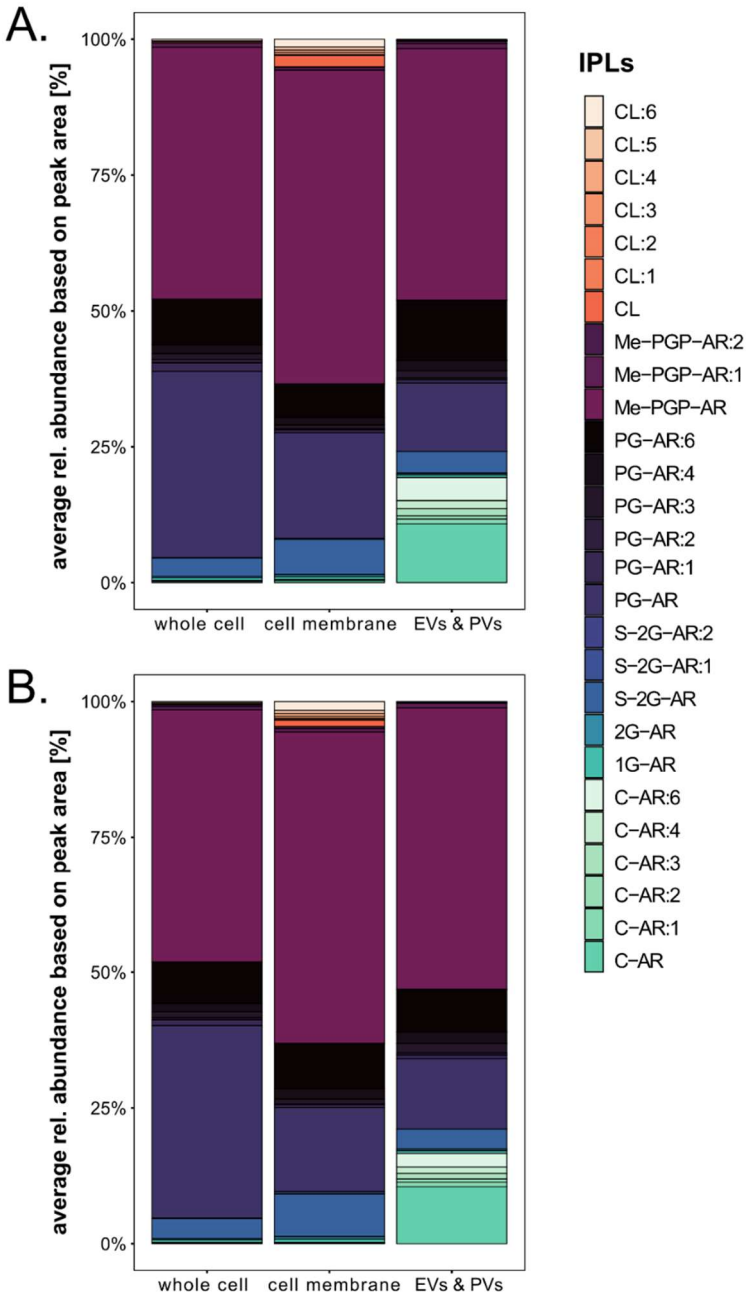
A.
B.
average rel. abundance based on peak area [%]
100%
75%
50%
25%
0%
whole cell
cell membrane
EVs & PVs
IPLs
CL:6
CL:5
CL:4
CL:3
CL:2
CL:1
CL
Me−PGP−AR:2
Me−PGP−AR:1
Me−PGP−AR
PG−AR:6
PG−AR:4
PG−AR:3
PG−AR:2
PG−AR:1
PG−AR
S−2G−AR:2
S−2G−AR:1
S−2G−AR
2G−AR
1G−AR
C−AR:6
C−AR:4
C−AR:3
C−AR:2
C−AR:1
C−AR

Figure 2: Average distribution of lipid compounds comparing whole cells, cell membranes and EVs & PVs of *Hrr. lacusprofundi* strains DL18 and R1S1. The average relative abundance of lipids was calculated for two biological replicates for both DL18 **(A)** and R1S1 **(B)** for whole cells, cell membrane and extracellular and plasmid vesicle (EV & PV) preparations. Averages were calculated based on the peak area of the most abundant adduct for each compound. The distribution in the individual samples is shown in Supplementary Figure 5. For the EV fraction, samples from different bands were pooled together after density gradient purification for each biological replicate. Lipids were identified based on their retention time, fractionation pattern and exact mass. Compound abbreviations: AR = archaeol (C_{20}-C_{20} isoprenoidal chains), :n = lipid with n number of unsaturations. Lipids with neutral headgroups: 1G = monoglycosyl, 2G = diglycosyl, C-AR = core-AR. Lipids with anionic headgroups: CL = cardiolipin or dimeric phospholipid, Me-PGP = phosphatidylglycerophosphate methyl esters, PG = phosphatidylglycerol, S-2G = sulfated diglycosyl.

The contribution of unsaturated (up to 2 double bonds). Me-PGP-AR and cardiolipins (up to 6 double bonds) was low. Both 1G-AR and 2G-AR were present at low (≤ 0.7%) but constant levels across strains and sample types. We were unable to identify enrichment of 2G-AR in the vesicle fraction as was observed in *H. volcanii.*

Interestingly, the relative abundance of total C-ARs increased from below 1% in the cellular fractions to 16-19% in the EV & PV fraction (Table 1) in the DL18 and R1S1 strains (Figure 2, Supplementary Figure 5). This result reflects what we observed in *H volcanii* samples where C-ARs were also enriched in the EV fraction although we detected a higher number of unsaturated C-ARs in *Hrr. lacusprofundi* samples. This effect was less pronounced in the UNSW strain (Figure 3A, Supplementary Figure 6) where the relative abundance of total C-ARs increased by ca. 6% from the whole cell fraction to the EV fraction. For DSMZ, no enrichment could be observed (Figure 3B). C-AR levels were low in the whole cell fraction (ca. 0.5%) but higher in the membrane (ca. 15%) than in the EV fraction (ca. 11%). The strong enrichment of C-ARs appears to be a strong distinction between pR1SE-infected and un-infected strains. However, final confirmation of a possible contribution of PVs and PV formation on this process would require analysis of the lipid composition of pR1SE infected UNSW and DSMZ vesicle preparations.

As with PG-AR, we were able to detect highly unsaturated C-ARs in all fractions from *Hrr. lacusprofundi* strains in all states between 0 and 6 double bonds apart from the compound with 5 double bonds (Supplementary Figure 4).

Another notable difference between the two species is the near absence (≤ 5%) of cardiolipins in the cellular samples of *Hrr. lacusprofundi* strains. In *H. volcanii*, cardiolipins with sulfated diglycosyl-phospho (S-2G-P) headgroups and a minor fraction of CLs without additional headgroups contributed to ca. 20% and 9% of the total cell and cell membrane lipid fractions respectively [see Mills *et al.* (2023)].

Comparison between *Hrr. lacusprofundi* strains shows that CL contribute up to 4-5% of the IPLs in the cell membrane of DL18 and R1S1 (Figure 2), but are almost undetectable (≤ 1%) in the other fractions. For the UNSW and DSMZ strains CL levels stayed constantly below 1% apart from a slight increase (ca. 1.2%) in the EV fraction of the DSMZ strain (Figure 3), which could be explained by random biological variation. We did not quantify IPL concentrations in the samples but it is possible that variation in extraction efficiency between whole cell and cell membrane samples could have led to this observed pattern of CLs across fractions.

Cultivation conditions strongly affect the lipid composition of archaea in culture (Elling *et al.*, 2015; Kellermann *et al.*, 2016; Cobban *et al.*, 2020). While we grew both *H. volcanii* and *Hrr. lacusprofundi* at 28 °C, the growth medium was different, which could contribute to their varying lipid compositions. Other environmental factors or media components might have also played a role. The concentration of Mg^{2+} (174 mM in Hv-YPC, 240 mM in DBCM2+) could explain the lower ratio of cardiolipins to Me-PGP-AR in *Hrr. lacusprofundi* cell samples following the model proposed by Kellermann *et al.* (2016).

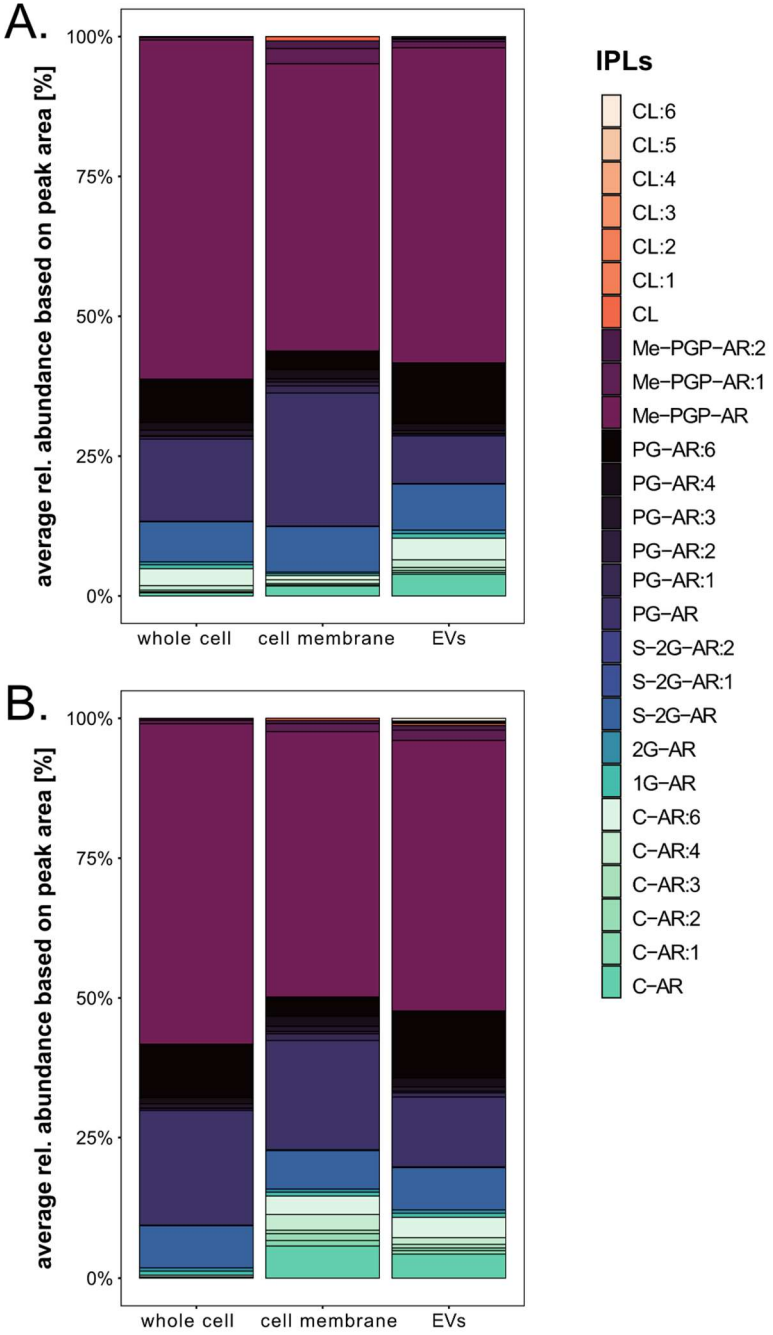
A.
B.
average rel. abundance based on peak area [%]
100%
75%
50%
25%
0%
whole cell
cell membrane
EVs
IPLs
CL:6
CL:5
CL:4
CL:3
CL:2
CL:1
CL
Me−PGP−AR:2
Me−PGP−AR:1
Me−PGP−AR
PG−AR:6
PG−AR:4
PG−AR:3
PG−AR:2
PG−AR:1
PG−AR
S−2G−AR:2
S−2G−AR:1
S−2G−AR
2G−AR
1G−AR
C−AR:6
C−AR:4
C−AR:3
C−AR:2
C−AR:1
C−AR

Figure 3: Average distribution of lipid compounds comparing whole cells, cell membranes and EVs of *Hrr. lacusprofundi* strains UNSW and DSMZ. The average relative abundance of lipids was calculated for two biological replicates for both UNSW **(A)** and DSMZ **(B)** for whole cells, cell membrane and extracellular vesicle (EV) preparations. Averages were calculated based on the peak area of the most abundant adduct for each compound. The distribution in the individual samples is shown in Supplementary Figure 6, no distinct bands were observed for the EV fraction after density gradient centrifugation, therefore technical replicates were pooled for each biological replicate. Lipids were identified based on their retention time, fractionation pattern and exact mass. Compound abbreviations: AR = archaeol (C_{20}-C_{20} isoprenoidal chains), :n = lipid with n number of unsaturations. Lipids with neutral headgroups: 1G = monoglycosyl, 2G = diglycosyl, C-AR = core-AR. Lipids with anionic headgroups: CL = cardiolipin or dimeric phospholipid, Me-PGP = phosphatidylglycerophosphate methyl esters, PG = phosphatidylglycerol, S-2G = sulfated diglycosyl.

However, the overall relative abundance of Me-PGP-AR was not significantly higher in *Hrr. lacusprofundi* compared to *H. volcanii,* thus *Hrr. lacusprofundi* may be employing additional measures to regulate membrane permeability at high extracellular Mg^{2+} concentrations, such as maintaining an increased ratio of unsaturated IPLs.

Choice of lipid extraction protocol has a major influence on which lipid species are recovered from haloarchaea.

An earlier study on the bilayer-forming lipids of *Hrr. lacusprofundi* cells identified PG-AR, Me-PGP-AR, S-2G-AR and phosphatidylglycerylsulfate archaeol (PGS-AR) as the main negatively charged phospholipids, and monoglycosyl (1G)-AR as the main neutral IPL (Gibson *et al*. 2005). Me-PGP-AR has been widely identified as the dominant IPL in the membranes of both neutrophilic and alkali-/acidophilic halorachaea (Kellermann *et al.*, 2016; Bale *et al.*, 2019). Kellermann *et al.* (2016) also detected PG-AR, Me-PGP-AR, S-2G-AR, CLs, neutrally charged archaeols, and C-ARs, but did not identify PGS in *Hrr. lacusprofundi*. We were also not able to identify PGS in our samples, which should have a $[M\text{-}H^+]$ *m/z* of 885.8, despite it being considered a typical IPL of neutrophilic haloarchaea (Oren *et al.*, 2002; Gibson

et al., 2005; Bale *et al.*, 2019). This could because of our specific cultivation conditions or of the lipid extraction protocol used in this study, or a combination of both.

The presence of 1G-AR is distinctive for *Hrr. lacusprofundi* compared to other haloarchaea, as it is generally only found in methanogenic archaea. In contrast, 2G-AR is frequently detected in other haloarchaea but not generally in *Hrr. lacusprofundi* [Gibson *et al.* (2005) and references therein]. We did not detect 1G-AR in the *H. volcanii* samples but detected both 1G-AR and 2G-AR in all four strains of *Hrr. lacusprofundi* at low but approximately equal relative abundances.

The only major class of archaeols not present in the extracted IPLs of either species were the zwitterionic-ARs, such as phosphatidylethanolamine (PE-AR). We were also not able to detect relevant concentrations of extended archaeol lipids, with C_{25} instead of C_{20} isoprenoidal chains, in samples of either species. Alkaliphilic and acidophilic haloarchaea rely on this molecular 'zipper' of extended archaeol lipids with sesterpanyl (C_{25}) isoprenoid chains in asymmetric C_{20} - C_{25} chain configurations for membrane stability (Xu *et al.*, 1999; Minegishi *et al.*, 2010; Dawson *et al.*, 2012; Kellermann *et al.*, 2016; Bale *et al.*, 2019). Which likely explains the lack of extended archaeal IPLs in our *H. volcanii* and *Hrr. lacusprofundi* samples since both are neutrophilic species.

We also did not detect any non-membrane forming lipids in measurable quantities. Kellermann *et al.* (2016) showed that menaquinones, carotenoids and squalenes contributed the majority of extracted lipids (66.1%) compared to bilayer forming lipids (33.9%) in *H. volcanii*, whereas the ratio was 29.6% to 70.4% for the bilayer forming lipids in *Hrr. lacusprofundi* (Kellermann et al., 2016). In general, different haloarchaea species have shown large variability in their respective ratios of membrane-forming archaeols to non-membrane forming lipids (Kellermann *et al.*, 2016).

Table 1: Average relative abundance of intact polar lipids. Averages ± standard deviation of the mean are given as percentage of total population in the whole cell, cell membrane and extracellular (EV) and plasmid vesicle (PV) fraction of four *Hrr. lacusprofundi* strains DL18, R1S1, UNSW and DSMZ. Compound abbreviations are identical to those in Figures 2 & 3.

	DL18			R1S1		
Compound	**whole cell**	**cell membrane**	**EVs & PVs**	**whole cell**	**cell membrane**	**EVs & PVs**
Total unsaturated	14.7% ± 0.7%	12.9% ± 1.4%	25.5% ± 2.0%	13.2% ± 0.6%	16.8% ± 2.2%	20.1% ± 2.3%
Total saturated	85.3% ± 0.7%	87.1% ± 1.4%	74.5% ± 2.0%	86.8% ± 0.6%	83.2% ± 2.2%	79.9% ± 2.3%
PG-AR:US	13.3% ± 0.7%	9.0% ± 0.8%	15.2% ± 1.3%	11.7% ± 0.7%	11.8% ± 3.0%	12.8% ± 1.0%
PG-AR	34.3% ± 1.2%	19.5% ± 1.0%	12.6% ± 1.1%	35.5% ± 0.2%	15.5% ± 2.7%	13.0% ± 0.7%
Me-PGP-AR:US	0.8% ± 0.1%	0.7% ± 0.3%	1.4% ± 0.3%	0.9% ± 0.0%	1.0% ± 0.3%	1.0% ± 0.2%
Me-PGP-AR	46.3% ± 1.7%	57.7% ± 1.2%	46.3% ± 3.2%	46.6% ± 0.7%	57.5% ± 5.5%	52.0% ± 3.1%
S-2G-AR:US	0.1% ± 0.1%	0.2% ± 0.1%	0.0% ± 0.0%	0.0% ± 0.1%	0.4% ± 0.4%	0.0% ± 0.0%
S-2G-AR	3.4% ± 0.1%	6.5% ± 0.2%	4.0% ± 0.3%	3.7% ± 0.2%	7.9% ± 0.6%	3.7% ± 0.5%
2G-AR	0.3% ± 0.0%	0.4% ± 0.2%	0.3% ± 0.0%	0.3% ± 0.0%	0.5% ± 0.2%	0.3% ± 0.0%
1G-AR	0.5% ± 0.0%	0.5% ± 0.1%	0.05% ± 0.0%	0.5% ± 0.0%	0.6% ± 0.2%	0.5% ± 0.1%
C-AR:US	0.1% ± 0.0%	0.2% ± 0.1%	8.5% ± 1.3%	0.1% ± 0.0%	0.1% ± 0.1%	6.1% ± 1.7%
C-AR	0.3% ± 0.0%	0.4% ± 0.5%	10.8% ± 1.8%	0.1% ± 0.0%	0.1% ± 0.0%	10.5% ± 1.7%
CL:US	0.5% ± 0.0%	3.0% ± 0.7%	0.3% ± 0.4%	0.4% ± 0.1%	3.4% ± 0.8%	0.1% ± 0.1%
CL	0.3% ± 0.0%	2.0% ± 0.1%	0.1% ± 0.1%	0.2% ± 0.0%	1.2% ± 0.3%	0.0% ± 0.0%

	UNSW			DSMZ		
Compound	**whole cell**	**cell membrane**	**EVs**	**whole cell**	**cell membrane**	**EVs**
Total unsaturated	15.8% ± 0.9%	13.6% ± 4.0%	21.5% ± 1.2%	13.2% ± 1.3%	19.0% ± 5.2%	25.6% ± 1.2%
Total saturated	84.2% ± 0.9%	86.4% ± 4.0%	78.5% ± 1.2%	86.8% ± 1.3%	81.0% ± 5.2%	74.4% ± 1.2%
PG-AR:US	10.7% ± 0.6%	7.5% ± 2.0%	13.0% ± 0.5%	11.8% ± 1.2%	7.9% ± 1.7%	15.3% ± 0.2%
PG-AR	14.7% ± 0.5%	23.8% ± 0.7%	8.5% ± 0.4%	20.4% ± 1.9%	19.4% ± 1.0%	12.4% ± 0.2%
Me-PGP-AR:US	0.6% ± 0.0%	4.1% ± 1.3%	1.6% ± 0.1%	0.9% ± 0.1%	2.0% ± 1.0%	2.7% ± 0.1%
Me-PGP-AR	60.6% ± 1.4%	51.3% ± 4.1%	56.3% ± 1.8%	57.4% ± 3.1%	47.4% ± 5.1%	48.5% ± 1.9%
S-2G-AR:US	0.1% ± 0.0%	0.1% ± 0.1%	0.1% ± 0.1%	0.1% ± 0.0%	0.2% ± 0.4%	0.1% ± 0.0%
S-2G-AR	7.1% ± 0.1%	8.1% ± 0.4%	8.2% ± 0.2%	7.5% ± 0.1%	6.8% ± 0.4%	7.5% ± 0.2%
2G-AR	0.5% ± 0.0%	0.3% ± 0.3%	0.6% ± 0.0%	0.6% ± 0.0%	0.6% ± 0.3%	0.6% ± 0.0%
1G-AR	0.7% ± 0.0%	0.4% ± 0.4%	0.8% ± 0.1%	0.7% ± 0.0%	0.7% ± 0.3%	0.7% ± 0.0%
C-AR:US	4.3% ± 0.3%	1.9% ± 1.2%	6.4% ± 0.7%	0.4% ± 0.1%	8.9% ± 2.6%	6.5% ± 0.8%
C-AR	0.6% ± 0.1%	1.8% ± 0.3%	3.9% ± 0.4%	0.1% ± 0.0%	5.7% ± 1.2%	4.3% ± 0.7%
CL:US	0.0% ± 0.0%	0.0% ± 0.0%	0.4% ± 0.1%	0.0% ± 0.0%	0.0% ± 0.0%	0.9% ± 0.5%
CL	0.0% ± 0.0%	0.8% ± 0.4%	0.1% ± 0.0%	0.0% ± 0.0%	0.4% ± 0.1%	0.3% ± 0.1%

H. volcanii is one of the species with a stark shift towards non-bilayer forming lipids and towards menaquinones in particular. Kellermann *et al.* (2016) attributed the lower amount of menaquinones in *Hrr. lacusprofundi* compared to *H. volcanii* to the higher number of archaeol unsaturations in *Hrr. lacusprofundi* which increase membrane permeability, therefore lower menaquinone concentrations would be sufficient. The absence of non-membrane forming lipids is likely explained due to the extraction method we used which favours extraction of IPLs compared to other studies (Kellermann *et al.*, 2016). In general, a large amount of archaeal lipids have remained unrecoverable (Huguet *et al.*, 2010; Evans *et al.*, 2022), Archaeols are considered to have relatively high extraction efficiency with the commonly established Bligh and Dyer method yet recently published work has suggested that pre-treatment with freeze-thaw cycles and cetrylimethylammonium bromide treatment could improve yields (Evans *et al.*, 2022). The choice of extraction protocol is necessarily a trade-off between the advantages and biases of each method, our efforts focussed on the analysis of the bilayer-forming lipids of *H. volcanii* and *Hrr. lacusprofundi* and therefore prioritized archaeol extraction.

Both H. volcanii and Hrr. lacusprofundi have highly unsaturated membranes but show opposite trends for the ratios of unsaturated IPLs in vesicles compared to the cells.

Unsaturation of the cell membrane is one of the typical characteristics that haloarchaea use as an adaptation to the hypersaline environment, since it simultaneously increases membrane fluidity and decreases membrane permeability (Gibson *et al.*, 2005; Stiehl *et al.*, 2005; Dawson *et al.*, 2012). Maintaining membrane fluidity is of particular importance to cold-adapted archaea such as *Hrr. lacusprofundi* (Franzmann *et al.*, 1988; Nichols *et al.*, 2004;

Gibson *et al.*, 2005). We observed opposite trends for the ratios of unsaturated to saturated lipids between the two species. In *H. volcanii* unsaturated IPLs contributed to ca. 20% of the total IPLs in the cellular fractions but decreased to ca. 1% in the EV fraction [see Mills *et al.* (2023), Supplementary Table 1]. For the four *Hrr. lacusprofundi* strains, the opposite trend was observed with an increase from the cellular fractions (ca. 13-19%, Table 1) towards the vesicle fraction (20-26%). At this stage, we cannot explain this difference between the two species, but it reaffirms our observations that the enrichment of specific lipid species into the EV fraction follows different patterns for *H. volcanii* and *Hrr. lacusprofundi*.

Kellermann *et al.* (2016) observed changes to the ratio of unsaturated to saturated archaeols in *H. volcanii* as a response to changing Na^{2+} concentrations mainly in PG-AR while the ratios of other IPLs were not as affected. We did not change the Na^{2+} concentrations in our study; nevertheless, PG-AR also showed the highest diversity in saturation states and could likely be the regulator-in-waiting, responding to changes in the extracellular conditions for both *H. volcanii* and *Hrr. lacusprofundi*. We also observed highly unsaturated C-ARs in the latter species, which could potentially be the remaining cores of highly unsaturated PG-AR after head group loss.
Gibson *et al.* (2005) observed significant changes to the unsaturation of the main phospholipids PG, Me-PGP and PGS-AR once *Hrr. lacusprofundi* cultures were grown at 12 °C instead of 25 °C, which was not mirrored by the glycolipids with neutral head groups. While the saturated state was dominant at 25 °C, at colder temperatures unsaturated compounds with up to six double bonds were detected at equal or slightly lower relative abundance than the saturated form. Intermediate states between 0 and 6 double bonds could all be detected by mass spectrometry (Gibson *et al.*, 2005). We have now detected unsaturation of up to six double bonds in the major phospholipid

PG-AR and in the neutral C-ARs without head groups while cells were grown at 28 °C. This temperature is still below the optimal growth temperature of 37 °C recorded for *Hrr. lacusprofundi* (Franzmann *et al.*, 1988), and membrane fluidity is expected to increase as a result of higher temperatures. Therefore, we propose that this level of membrane unsaturation is not likely to be a response to higher temperatures (from 25 °C to 28 °C). The NaCl concentration used by Gibson and colleagues was slightly higher, 200 g/l compared to 180 g/l in DBCM2+ medium but is unlikely to have caused such a big shift in lipid unsaturation. Since Gibson *et al.* (2005) grew their cultures at lower concentrations of Mg^{2+}, ca. 80 mM compared to 240 mM in DBCM2+ medium, the high levels of membrane unsaturation were likely caused by growth in much higher Mg^{2+} concentration.

Membrane-enveloped archaeal viruses serve as a comparison for the selective enrichment of IPLs into budding particles.

As far as we are aware, the lipid content of haloarchaeal EVs has not been previously investigated in detail. However, the lipid content of some membrane-containing viruses infecting haloarchaea has been determined. Viruses with outer membrane layers can presumably bud directly off the host membrane (Garoff *et al.*, 1998), but viruses with internal membranes also need to obtain the lipid compounds from their host organisms (Roine & Bamford, 2012). Budding has not been proven directly for any viruses infecting haloarchaea; however, it remains the most likely scenario for the acquisition of lipids from the host. This similarity in formation mechanism between EVs and enveloped virions allows us to look at the lipid composition of the latter as templates for what selective lipid acquisition could look like for budding particles in archaea.

Bamford *et al.* (2005) detected PG-AR, PGP-Me-AR, and PGS as the major lipids in both *Haloarcula hispanica* and in SH1 virus particles. The virus did not contain detectable amounts of glycolipids, which comprised 20% of total host lipids. SH1 also appears to be able to selectively take up lipids from the host membrane, resulting in a shift in the relative abundance distributions compared to the host cells. Other haloarchaeal viruses appear to not be selective in their lipid uptake from the host membrane (Pietilä *et al.*, 2009; Pietilä *et al.*, 2010; Roine *et al.*, 2010; Atanasova *et al.*, 2018). Other studies have described minor differences, wherein unidentified lipid compounds were present in the host membrane but not in the virions of several pleomorphic viruses (Pietilä *et al.*, 2012). Outside of viruses infecting haloarchaea, selective uptake of lipids has been described for a number of viruses infecting hyperthermophilic archaea [e.g., Quemin *et al.* (2015); Kasson *et al.* (2017)]. In archaea that contain both archaeol and tetraether lipids, but whose membranes are dominated by tetraether lipids (≤ 99%), some virions are selectively enriched in archaeols (Liu *et al.*, 2018; Wang *et al.*, 2019; Baquero *et al.*, 2021) with an extreme shift from 1% to 70% of relative abundance described for one virus (Feng *et al.*, 2023). These examples clearly show that selective enrichment of lipid species from archaeal membranes into small lipid-containing particles is possible and regularly occurs during the formation of virions.

Kasson *et al.* (2017) propose that the selective uptake of lipids into the virion of the AFV1 virus could be caused by local enrichment of lipid species at virus budding sites, by direct binding of lipids to capsid proteins or by physical properties of the viral membrane that would cause lipids to separate during the budding process. The EVs of haloarchaea are formed by budding from the cell membrane and are covered in proteins in like virions whose exit mechanisms are unconfirmed for most archaeal viruses. Similar processes

could cause the enrichment of specific lipid compounds in the EV fraction. Analysis of the EVs of the hyperthermophilic *S. solfataricus* showed that the same lipid species were present in both cells and EVs but with shifts in ratios between the two fractions (Ellen *et al.*, 2009), similar to what we observe for *H. volcanii* and *Hrr. lacusprofundi*. These differences between the lipid composition of cells and EVs point towards a specific enrichment of particular lipid compounds in the EVs, although the underlying causes remain to be determined. While we do observe differences in lipid composition between EVs from pR1SE infected strains and uninfected strains, whether PVs have a specific lipid composition compared to the standard EVs is still currently unknown.

In conclusion, we were able to show selective enrichment of specific lipid compounds into the vesicle fractions of related haloarchaea, *H. volcanii* and *Hrr. lacusprofundi*. EVs of both species showed clear differences in their lipid composition compared the respective cell membranes while sharing the predominant IPL classes. Although the underlying causes still need to be determined, we predict that similarly to enveloped archaeal viruses, archaeal vesicles are likely selectively enriched in specific lipid species during their formation at the cellular membrane.

Author Contributions

Author contributions: L.J.G. and S.E conceived the study, L.J.G. prepared the samples and performed lipid extractions, L.J.G. and F.S. measured the samples on the UHPLC QTOF-MS and analysed the data. J.M. performed the majority of the experimental work in the original manuscript preceding this addendum and assisted with writing, L.J.G drafted the manuscript with support from all authors, S.E. led both the original study and this this addendum.

Data Availability Statement

The raw data from the lipid measurements of *H. volcanii* is available in Supplementary Table 13 of the preprint Mills *et al*., 2023 on *BioRxiv* under the following link: https://doi.org/10.1101/2023.03.03.530948

The raw data from *Hrr. lacusprofundi* measurements will be deposited in an appropriate data repository upon submission of the manuscript for peer-review. It is currently available upon request.

Competing Interest Statement

The authors declare no competing interests.

Funding

Funding was provided by the Volkswagen Foundation (reference 98 190) to SE and the Max Planck Society (Munich, Germany) to SE.

Acknowledgements

We thank Julius Lipp and Julia Cordes (MARUM, University of Bremen, Germany) for assistance during sample processing and QTOF measurements. We thank Ingrid Kunze (MPI for Marine Microbiology, Bremen, Germany) for assistance with the experiments. Finally, we want to thank the Max-Planck-Institute for Marine Microbiology and the Max-Planck-Society for continuous support.

References

Atanasova, N. S., Demina, T. A., Krishnam Rajan Shanthi, S. N. V., Oksanen, H. M., & Bamford, D. H. (2018). Extremely halophilic pleomorphic archaeal virus HRPV9 extends the diversity of pleolipoviruses with integrases. *Research in Microbiology, 169*(9), 500-504. doi:10.1016/j.resmic.2018.04.004

Bale, N. J., Sorokin, D. Y., Hopmans, E. C., Koenen, M., Rijpstra, I. C. W., Villanueva, L., Wienk, H., & Sinninghe Damsté, J. S. (2019). New Insights Into the Polar Lipid Composition of Extremely Halo(alkali)philic Euryarchaea From Hypersaline Lakes. *Frontiers in microbiology, 10*. doi:10.3389/fmicb.2019.00377

Bamford, D. H., Ravantti, J. J., Rönnholm, G., Laurinavicius, S., Kukkaro, P., Dyall-Smith, M., Somerharju, P., Kalkkinen, N., & Bamford, J. K. (2005). Constituents of SH1, a novel lipid-containing virus infecting the halophilic euryarchaeon Haloarcula hispanica. *J Virol, 79*(14), 9097-9107. doi:10.1128/jvi.79.14.9097-9107.2005

Baquero, D. P., Gazi, A. D., Sachse, M., Liu, J., Schmitt, C., Moya-Nilges, M., Schouten, S., Prangishvili, D., & Krupovic, M. (2021). A filamentous archaeal virus is enveloped inside the cell and released through pyramidal portals. *Proceedings of the National Academy of Sciences, 118*(32), e2105540118. doi:10.1073/pnas.2105540118

Burns, D., & Dyall-Smith, M. (2006). 22 Cultivation of haloarchaea. In *Methods in Microbiology* (Vol. 35, pp. 535-552): Elsevier.

Caforio, A., & Driessen, A. J. M. (2017). Archaeal phospholipids: Structural properties and biosynthesis. *Biochimica et Biophysica Acta (BBA) - Molecular and Cell Biology of Lipids, 1862*(11), 1325-1339. doi:10.1016/j.bbalip.2016.12.006

Cobban, A., Zhang, Y., Zhou, A., Weber, Y., Elling, F. J., Pearson, A., & Leavitt, W. D. (2020). Multiple environmental parameters impact lipid cyclization in *Sulfolobus acidocaldarius*. *Environmental microbiology, 22*(9), 4046-4056. doi:10.1111/1462-2920.15194

Dawson, K. S., Freeman, K. H., & Macalady, J. L. (2012). Molecular characterization of core lipids from halophilic archaea grown under different salinity conditions. *Organic Geochemistry, 48*, 1-8. doi:10.1016/j.orggeochem.2012.04.003

Dyall-Smith, M. (2009). The halohandbook: protocols for halobacterial genetics, version 7.3. Retrieved from https://haloarchaea.com/wp-content/uploads/2018/10/Halohandbook_2009_v7.3mds.pdf

Ellen, A. F., Albers, S.-V., Huibers, W., Pitcher, A., Hobel, C. F., Schwarz, H., Folea, M., Schouten, S., Boekema, E. J., & Poolman, B. (2009). Proteomic analysis of secreted membrane vesicles of archaeal *Sulfolobus* species reveals the presence of endosome sorting complex components. *Extremophiles, 13*(1), 67. doi:10.1007/s00792-008-0199-x

Elling, F. J., Könneke, M., Mußmann, M., Greve, A., & Hinrichs, K.-U. (2015). Influence of temperature, pH, and salinity on membrane lipid composition and TEX86 of marine planktonic thaumarchaeal isolates. *Geochimica et Cosmochimica Acta, 171*, 238-255. doi:10.1016/j.gca.2015.09.004

Elling, F. J., Könneke, M., Nicol, G. W., Stieglmeier, M., Bayer, B., Spieck, E., de la Torre, J. R., Becker, K. W., Thomm, M., Prosser, J. I., Herndl, G. J., Schleper, C., & Hinrichs, K.-U. (2017). Chemotaxonomic characterisation of the thaumarchaeal lipidome. *Environmental microbiology, 19*(7), 2681-2700. doi:10.1111/1462-2920.13759

Erdmann, S., Tschitschko, B., Zhong, L., Raftery, M. J., & Cavicchioli, R. (2017). A plasmid from an Antarctic haloarchaeon uses specialized membrane vesicles to disseminate and infect plasmid-free cells. *Nature microbiology, 2*(10), 1446. doi:10.1038/s41564-017-0009-2

Evans, T. W., Elling, F. J., Li, Y., Pearson, A., & Summons, R. E. (2022). A new and improved protocol for extraction of intact polar membrane lipids from archaea. *Organic Geochemistry, 165*, 104353. doi:10.1016/j.orggeochem.2021.104353

Feng, X., Li, Y., Tian, C., Yang, W., Liu, X., Zhang, C., & Zeng, Z. (2023). Isolation of archaeal viruses with lipid membrane from Tengchong acidic hot springs. *Frontiers in microbiology, 14*. doi:10.3389/fmicb.2023.1134935

Franzmann, P., Stackebrandt, E., Sanderson, K., Volkman, J., Cameron, D., Stevenson, P., McMeekin, T., & Burton, H. (1988). *Halobacterium lacusprofundi* sp. nov., a halophilic bacterium isolated from Deep Lake, Antarctica. *Systematic and Applied Microbiology, 11*(1), 20-27. doi:10.1016/S0723-2020(88)80044-4

Garoff, H., Hewson, R., & Opstelten, D.-J. E. (1998). Virus maturation by budding. *Microbiology and Molecular Biology Reviews, 62*(4), 1171-1190.

Gebhard, L. J., Duggin, I. G., & Erdmann, S. (2023). Improving the genetic system for *Halorubrum lacusprofundi* to allow in-frame deletions. *Frontiers in microbiology, 14*. doi:10.3389/fmicb.2023.1095621

Giavalisco, P., Li, Y., Matthes, A., Eckhardt, A., Hubberten, H.-M., Hesse, H., Segu, S., Hummel, J., Köhl, K., & Willmitzer, L. (2011). Elemental formula annotation of polar and lipophilic metabolites using 13C, 15N and 34S isotope labelling, in combination with high-resolution mass spectrometry. *The Plant Journal, 68*(2), 364-376. doi:10.1111/j.1365-313X.2011.04682.x

Gibson, J. A. E., Miller, M. R., Davies, N. W., Neill, G. P., Nichols, D. S., & Volkman, J. K. (2005). Unsaturated diether lipids in the psychrotrophic archaeon *Halorubrum lacusprofundi*. *Systematic and Applied Microbiology, 28*(1), 19-26. doi:10.1016/j.syapm.2004.09.004

Gupta, R. S., Naushad, S., & Baker, S. (2015). Phylogenomic analyses and molecular signatures for the class Halobacteria and its two major clades: a proposal for division of the class Halobacteria into an emended order Halobacteriales and two new orders, Haloferacales ord. nov. and Natrialbales ord. nov., containing the novel families Haloferacaceae fam. nov. and Natrialbaceae fam. nov. *International Journal of Systematic and Evolutionary Microbiology, 65*(Pt_3), 1050-1069. doi:10.1099/ijs.0.070136-0

Hauß, T., Dante, S., Dencher, N. A., & Haines, T. H. (2002). Squalane is in the midplane of the lipid bilayer: implications for its function as a proton permeability barrier. *Biochimica et Biophysica Acta (BBA) - Bioenergetics, 1556*(2), 149-154. doi:10.1016/S0005-2728(02)00346-8

Huguet, C., Martens-Habbena, W., Urakawa, H., Stahl, D. A., & Ingalls, A. E. (2010). Comparison of extraction methods for quantitative analysis of core and intact polar glycerol dialkyl glycerol tetraethers (GDGTs) in environmental samples. *Limnology and Oceanography: Methods, 8*(4), 127-145. doi:10.4319/lom.2010.8.127

Jain, S., Caforio, A., & Driessen, A. J. M. (2014). Biosynthesis of archaeal membrane ether lipids. *Frontiers in microbiology, 5*. doi:10.3389/fmicb.2014.00641

Kasson, P., DiMaio, F., Yu, X., Lucas-Staat, S., Krupovič, M., Schouten, S., Prangishvili, D., & Egelman, E. H. (2017). Model for a novel membrane envelope in a filamentous hyperthermophilic virus. *eLife, 6*, e26268. doi:10.7554/eLife.26268

Kellermann, M. Y., Yoshinaga, M. Y., Valentine, R. C., Wörmer, L., & Valentine, D. L. (2016). Important roles for membrane lipids in haloarchaeal bioenergetics. *Biochimica et Biophysica Acta (BBA)-Biomembranes, 1858*(11), 2940-2956. doi:10.1016/j.bbamem.2016.08.010

Kushwaha, S. C., Gochnauer, M. B., Kushner, D. J., & Kates, M. (1974). Pigments and isoprenoid compounds in extremely and moderately halophilic bacteria. *Canadian Journal of Microbiology, 20*(2), 241-245. doi:10.1139/m74-038

Liu, Y., Osinski, T., Wang, F., Krupovic, M., Schouten, S., Kasson, P., Prangishvili, D., & Egelman, E. H. (2018). Structural conservation in a membrane-enveloped filamentous virus infecting a hyperthermophilic acidophile. *Nature communications, 9*(1), 3360. doi:10.1038/s41467-018-05684-6

Mercier, C., Thies, D., Zhong, L., Raftery, M. J., Cavicchioli, R., & Erdmann, S. (2022). In depth characterization of an archaeal virus-host system reveals numerous virus exclusion mechanisms. *bioRxiv*. doi:10.1101/2022.10.18.512658

Mileykovskaya, E., & Dowhan, W. (2009). Cardiolipin membrane domains in prokaryotes and eukaryotes. *Biochimica et Biophysica Acta (BBA)-Biomembranes, 1788*(10), 2084-2091. doi:10.1016/j.bbamem.2009.04.003

Mills, J., Gebhard, L. J., Schubotz, F., Shevchenko, A., Speth, D. R., Liao, Y., Duggin, I. G., Marchfelder, A., & Erdmann, S. (2023). Extracellular vesicles of *Euryarchaeida*: precursor to eukaryotic membrane trafficking. *bioRxiv*. doi:10.1101/2023.03.03.530948

Minegishi, H., Echigo, A., Nagaoka, S., Kamekura, M., & Usami, R. (2010). *Halarchaeum acidiphilum gen. nov., sp. nov.,* a moderately acidophilic haloarchaeon isolated from commercial solar salt. *International Journal of Systematic and Evolutionary Microbiology, 60*(11), 2513-2516. doi:10.1099/ijs.0.013722-0

Nichols, D. S., Miller, M. R., Davies, N. W., Goodchild, A., Raftery, M., & Cavicchioli, R. (2004). Cold Adaptation in the Antarctic Archaeon *Methanococcoides burtonii* Involves Membrane Lipid Unsaturation. *Journal of bacteriology, 186*(24), 8508-8515. doi:10.1128/jb.186.24.8508-8515.2004

Oren, A. (1999). Bioenergetic Aspects of Halophilism. *Microbiology and Molecular Biology Reviews, 63*(2), 334-348. doi:10.1128/mmbr.63.2.334-348.1999

Oren, A., Elevi, R., Watanabe, S., Ihara, K., & Corcelli, A. (2002). *Halomicrobium mukohataei* gen. nov., comb. nov., and emended description of *Halomicrobium mukohataei*. *International Journal of Systematic and Evolutionary Microbiology, 52*(5), 1831-1835. doi:10.1099/00207713-52-5-1831

Pietilä, M. K., Atanasova, N. S., Manole, V., Liljeroos, L., Butcher, S. J., Oksanen, H. M., & Bamford, D. H. (2012). Virion Architecture Unifies Globally Distributed Pleolipoviruses Infecting Halophilic Archaea. *Journal of virology, 86*(9), 5067-5079. doi:10.1128/jvi.06915-11

Pietilä, M. K., Laurinavicius, S., Sund, J., Roine, E., & Bamford, D. H. (2010). The single-stranded DNA genome of novel archaeal virus halorubrum pleomorphic virus 1 is enclosed in the envelope decorated with glycoprotein spikes. *Journal of virology, 84*(2), 788-798. doi:10.1128/jvi.01347-09

Pietilä, M. K., Roine, E., Paulin, L., Kalkkinen, N., & Bamford, D. H. (2009). An ssDNA virus infecting archaea: a new lineage of viruses with a membrane envelope. *Molecular Microbiology, 72*(2), 307-319. doi:10.1111/j.1365-2958.2009.06642.x

Quemin, E. R. J., Pietilä, M. K., Oksanen, H. M., Forterre, P., Rijpstra, W. I. C., Schouten, S., Bamford, D. H., Prangishvili, D., & Krupovič, M. (2015). *Sulfolobus* Spindle-Shaped Virus 1 Contains Glycosylated Capsid Proteins, a Cellular Chromatin Protein, and Host-Derived Lipids. *Journal of virology, 89*(22), 11681-11691. doi:10.1128/JVI.02270-15

Roine, E., & Bamford, D. H. (2012). Lipids of archaeal viruses. *Archaea, 2012*. doi:10.1155/2012/384919

Roine, E., Kukkaro, P., Paulin, L., Laurinavičius, S., Domanska, A., Somerharju, P., & Bamford, D. H. (2010). New, Closely Related Haloarchaeal Viral Elements with Different Nucleic Acid Types. *Journal of virology, 84*(7), 3682-3689. doi:10.1128/jvi.01879-09

Schouten, S., Hopmans, E. C., & Sinninghe Damsté, J. S. (2013). The organic geochemistry of glycerol dialkyl glycerol tetraether lipids: A review. *Organic Geochemistry, 54*, 19-61. doi:10.1016/j.orggeochem.2012.09.006

Siliakus, M. F., van der Oost, J., & Kengen, S. W. M. (2017). Adaptations of archaeal and bacterial membranes to variations in temperature, pH and pressure. *Extremophiles, 21*(4), 651-670. doi:10.1007/s00792-017-0939-x

Sprott, G. D., Larocque, S., Cadotte, N., Dicaire, C. J., McGee, M., & Brisson, J. R. (2003). Novel polar lipids of halophilic eubacterium *Planococcus* H8 and archaeon *Haloferax volcanii*. *Biochimica et Biophysica Acta (BBA) - Molecular and Cell Biology of Lipids, 1633*(3), 179-188. doi:10.1016/j.bbalip.2003.08.001

Stiehl, T., Rullkötter, J., & Nissenbaum, A. (2005). Molecular and isotopic characterization of lipids in cultured halophilic microorganisms from the Dead Sea and comparison with

the sediment record of this hypersaline lake. *Organic Geochemistry, 36*(9), 1242-1251. doi:10.1016/j.orggeochem.2005.05.002

Valentine, D. L. (2007). Adaptations to energy stress dictate the ecology and evolution of the Archaea. *Nature Reviews Microbiology, 5*(4), 316-323. doi:10.1038/nrmicro1619

van de Vossenberg, J. L. C. M., Driessen, A. J. M., Grant, D., & Konings, W. N. (1999). Lipid membranes from halophilic and alkali-halophilic Archaea have a low H+ and Na+ permeability at high salt concentration. *Extremophiles, 3*(4), 253-257. doi:10.1007/s007920050124

Villanueva, L., Damsté, J. S. S., & Schouten, S. (2014). A re-evaluation of the archaeal membrane lipid biosynthetic pathway. *Nature Reviews Microbiology, 12*(6), 438-448. doi:10.1038/nrmicro3260

Wang, F., Liu, Y., Su, Z., Osinski, T., de Oliveira, G. A. P., Conway, J. F., Schouten, S., Krupovic, M., Prangishvili, D., & Egelman, E. H. (2019). A packing for A-form DNA in an icosahedral virus. *116*(45), 22591-22597. doi:10.1073/pnas.1908242116 %J Proceedings of the National Academy of Sciences

Wickham, H. (2011). The Split-Apply-Combine Strategy for Data Analysis. *Journal of Statistical Software, 40*(1), 1-29. Retrieved from https://www.jstatsoft.org/v40/i01/

Wickham, H. (2016). ggplot2: Elegant Graphics for Data Analysis. In. New York: Springer-Verlag.

Wickham, H., François, R., Henry, L., & Müller, K. (2022). dplyr: A Grammar of Data Manipulation. In *R package version 1.0.8*.

Xu, Y., Zhou, P., & Tian, X. (1999). Characterization of two novel haloalkaliphilic archaea Natronorubrum bangense gen. nov., sp. nov. and Natronorubrum tibetense gen. nov., sp. nov. *International Journal of Systematic and Evolutionary Microbiology, 49*(1), 261-266. doi:10.1099/00207713-49-1-261

Yoshinaga, M. Y., Kellermann, M. Y., Rossel, P. E., Schubotz, F., Lipp, J. S., & Hinrichs, K.-U. (2011). Systematic fragmentation patterns of archaeal intact polar lipids by high-performance liquid chromatography/electrospray ionization ion-trap mass spectrometry. *Rapid Communications in Mass Spectrometry, 25*(23), 3563-3574. doi:10.1002/rcm.5251

Supplementary Material for Main Manuscript

Extracellular vesicles of Euryarchaeida: precursor to eukaryotic membrane trafficking

Supplementary Results

EV-associated RNA is best analyzed when using small RNA libraries and normalizing EV RNA content with host cell RNA content

To determine the nature of the EV enclosed RNA, total RNA and small RNA (enriching for transcripts below 150 nt in length) libraries were prepared from EV-extracted RNA. When comparing sequencing results from both libraries, we observed a drastically different transcriptional profile (Supplementary Table 3). Around 95% of reads from total RNAseq mapped to ribosomal RNA (rRNA) and only 17 transcripts recruited enough reads to reach the threshold (TPM > 10). In contrast, the small RNA library revealed a more diverse array of transcripts with transfer RNA (tRNA) being the most dominant RNA species (around 85% of reads) and 264 transcripts identified within the threshold. Further, over 2000 transcripts were only identified in the small RNA library and not in the total RNA library, the majority of them being tRNAs and non-coding RNAs (ncRNA), indicating that the total RNA library excludes important smaller transcripts. Therefore, we decided to use small RNA libraries for further analysis of EV-associated RNAs, as this seems to yield a more accurate picture of the RNA composition of EVs.

We also compared transcripts from EVs in the upper and lower bands in density gradients to determine whether the bands represented different subpopulations of EVs with respect to RNA content (Supplementary Table 4). Indeed, we identified transcripts that were only present in the upper band (app. 200) or only in the lower band (80). However, the abundance of these transcripts was below the threshold (TPM > 10) and they were disregarded. Overall, the RNA composition between both bands was mostly identical, with few outliers. We concluded that the RNA composition alone is not the differentiating factor between the two subpopulations of EVs in different density gradient bands, and pooling the bands for further sequencing analysis is acceptable.

Since vesicle production could be linked to UV exposure [1], we aimed to determine whether subjecting cultures to UV radiation would alter the RNA composition of EVs. Indeed, 145 transcripts appeared to be present in a higher abundance (log2 fold change > 1) in the UV-treated sample, and 32 transcripts were present in a higher abundance (log 2 fold change < -1) in the untreated sample (Supplementary Table 5). This population of EV-associated RNA from UV-treated cultures included all forms of RNA, including mRNAs, tRNAs, rRNAs and ncRNAs. Nevertheless, we realized that without determining transcriptional changes within the cells, it is difficult to distinguish transcripts that are associated with EVs as a response to UV exposure and transcripts that are present in EVs simply due to changes in intracellular levels. In order to differentiate between random packaging and potentially selective packaging of RNA into EVs, it became clear that sequencing intracellular RNA at the time of EV harvesting was imperative for any kind of analysis.

Supplementary Figures

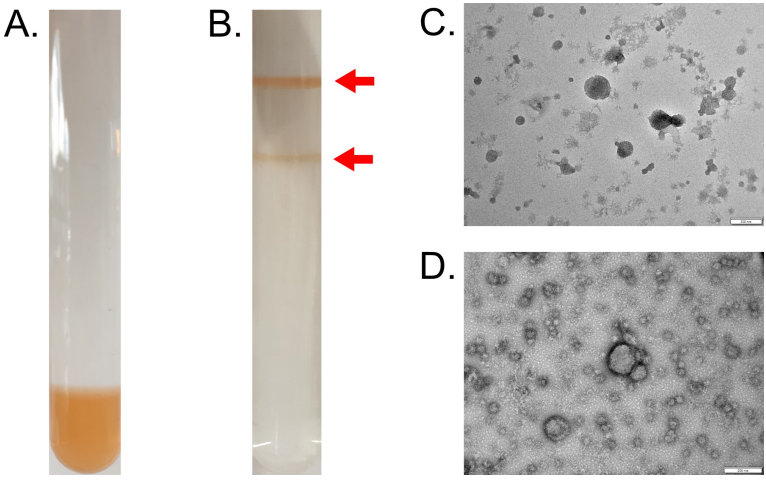

Supplementary Figure 1: Purification of *H. volcanii* H26 EVs by Optiprep™ density gradient purification. Gradient before **(A)** and after **(B)** ultracentrifugation. Red arrows indicate upper and lower band. Transmission electron micrograph of EVs isolated from upper **(C)** and lower **(D)** bands. Size bar: 200 nm.

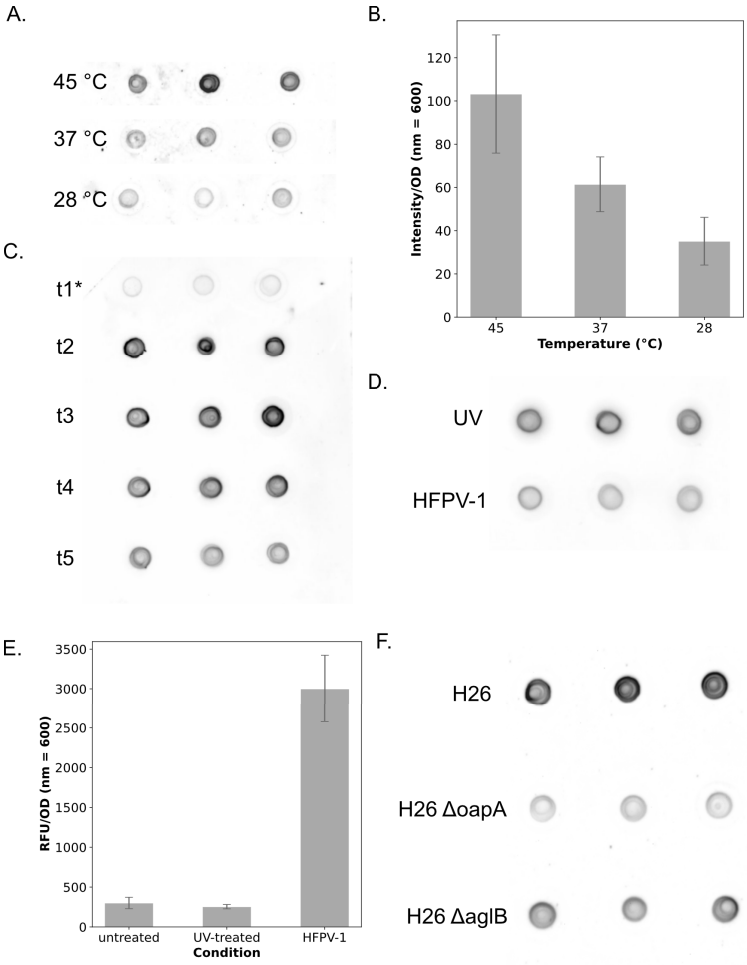

Supplementary Figure 2: EV quantification of *H. volcanii* cultures grown under different conditions, through growth and gene knockouts. **(A)** Spot blot for quantification of EVs in *H. volcanii* culture supernatants grown at 45, 37 and 28 °C. **(B)** Bar plot representing spot blot **(A). (C)** Spot blot for quantification of *H. volcanii* grown at 28 °C with time points taken at 45.3, 68.5, 94, 118.3, and 140.5 hours. Asterisk represents sample diluted by a factor of 2. **(D)** Spot blot for quantification of *H. volcanii* grown with either UV or viral stress. (**E)** Bar plot representing fluorescence-based quantification of EVs of *H. volcanii* grown with either UV or viral stress. **(F)** Spot blot for quantification of *H. volcanii* H26 background strains with knockouts of OapA and AglB.

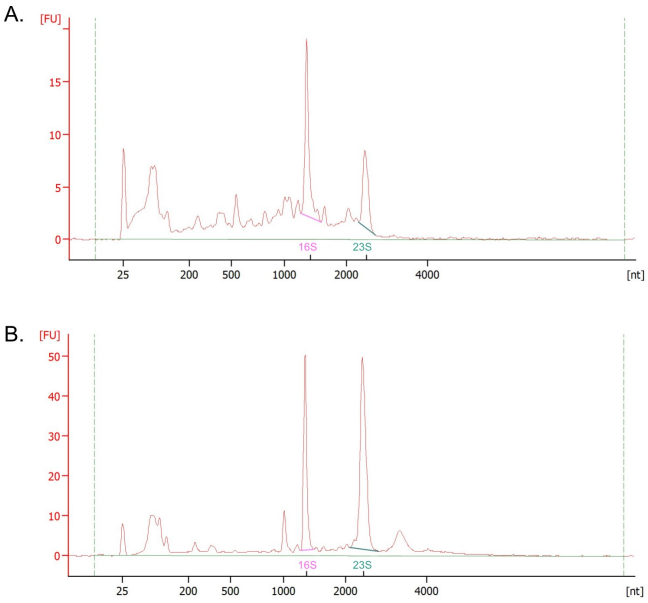

Supplementary Figure 3: Electropherograms of EV-associated RNA (A) and cellular RNA (B). Capillary electrophoresis demonstrates differences in size distribution between RNA isolated from EVs and cells of *H. volcanii*.

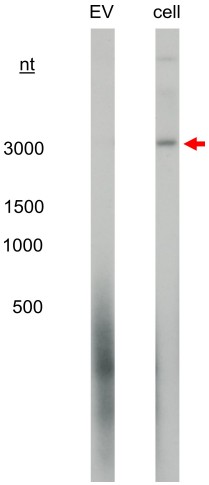

Supplementary Figure 4: Northern blot with EV and cellular RNA probed for HVO_2072. Red arrow indicates full-length transcript. Northern was conducted in duplicates, but only one replicated is presented here.

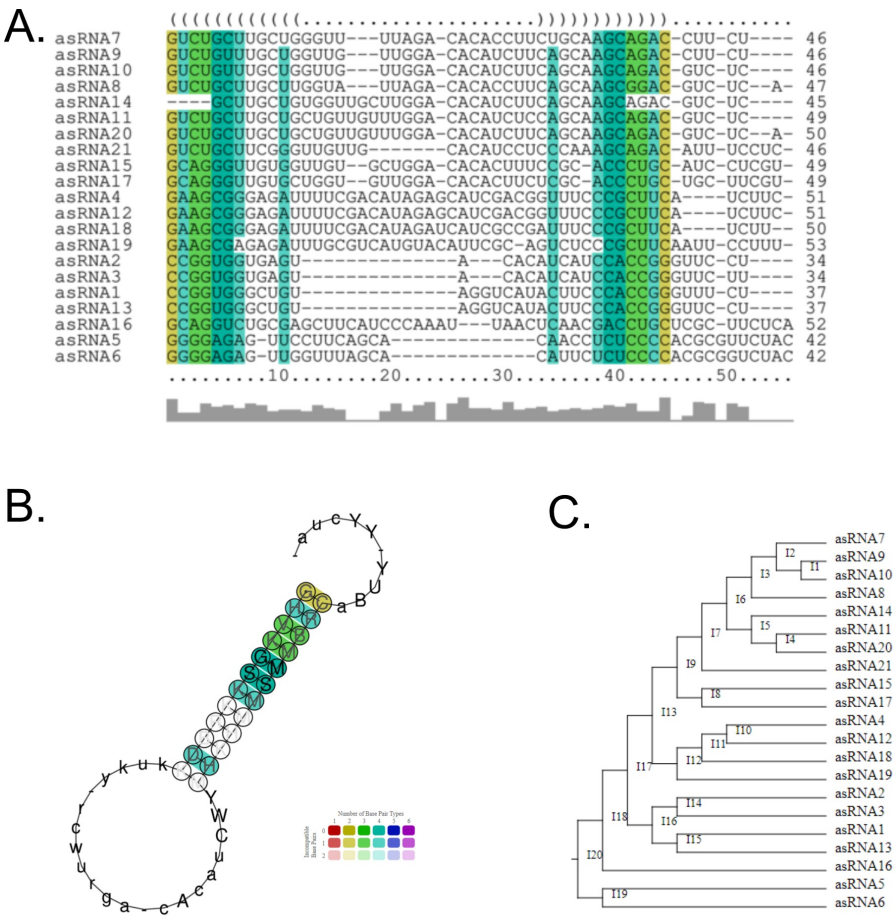

Supplementary Figure 5: Secondary structure alignment prediction of EV-associated asRNA from LocARNA [2–4]. (A) Sequence alignment with RNAalifold consensus structure. **(B)** Predicted consensus secondary structure with legend. **(C)** Hierarchical clustering based on similarities of sequences.

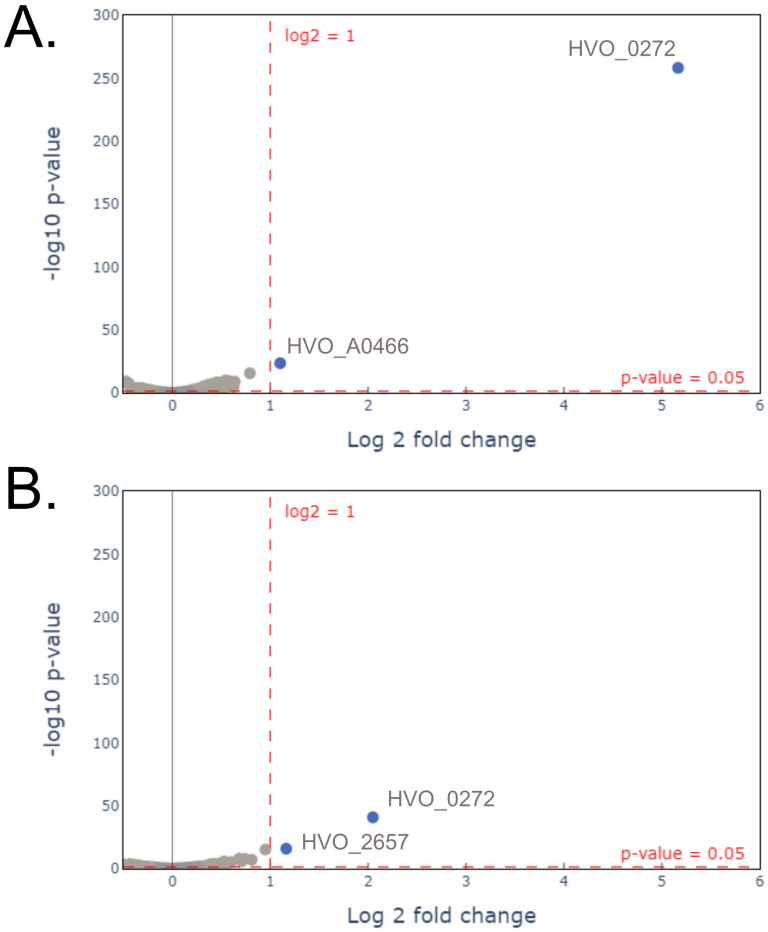

Supplementary Figure 6: Volcano plots of intracellular and EV-associated transcripts comparing cultures infected with HFPV-1 and uninfected control cultures. **(A)** Differential expression of transcripts in EVs from infected versus uninfected cultures. **(B)** Differential expression of intracellular transcripts from infected versus uninfected cultures. Cells and EVs were isolated at late stationary phase of growth. Volcano plots only depict transcripts that had an average TPM greater than 10 in either infected or uninfected samples.

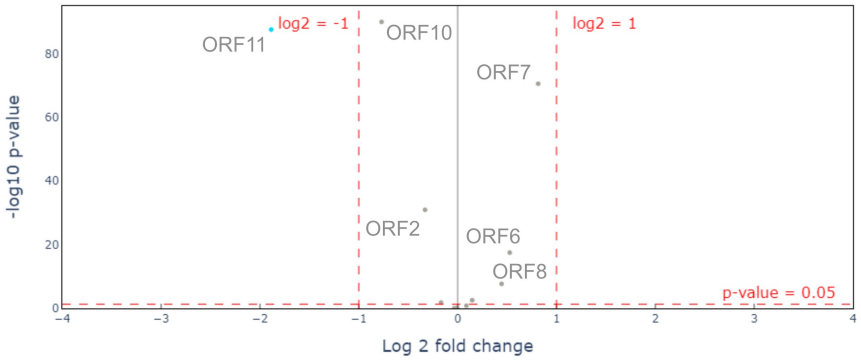

Supplementary Figure 7: Volcano plot comparing viral transcript abundance between EV-associated RNA and cellular RNA. RNA isolated from EVs and cells of cultures infected with HFPV-1 during late stationary phase.

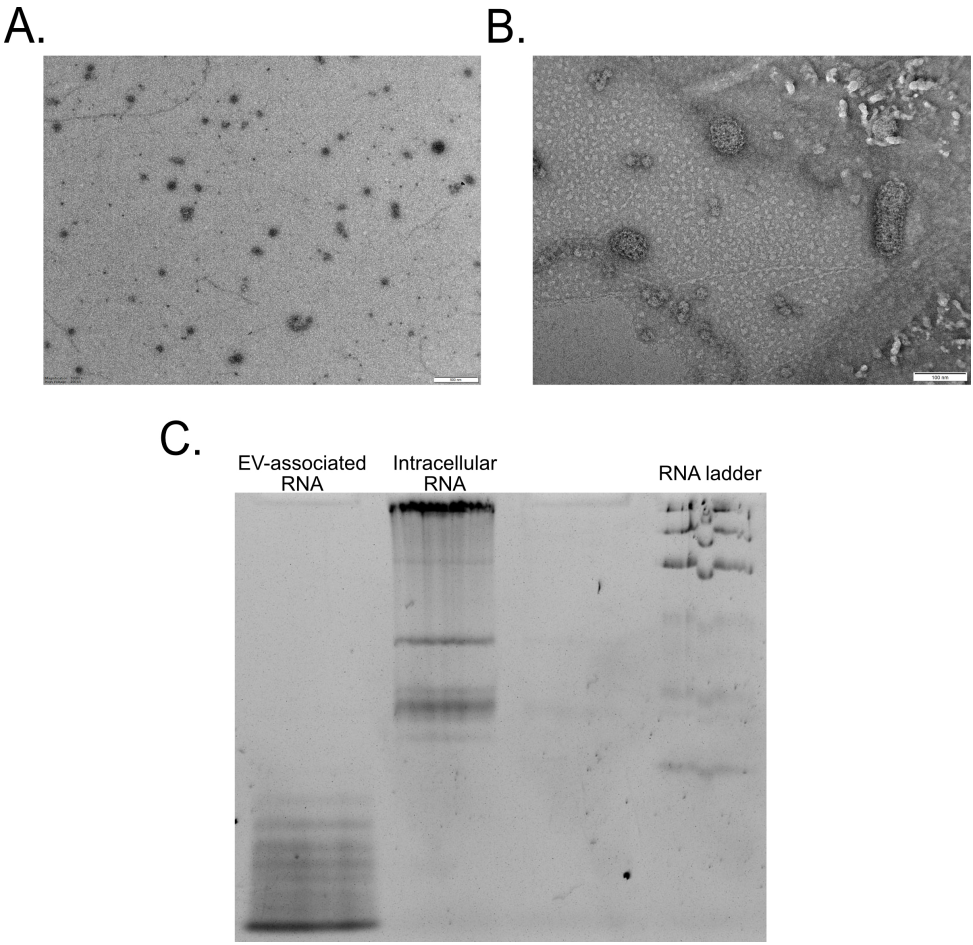

Supplementary Figure 8: EVs from other haloarchaea. (A) Transmission electron micrograph of purified EV from *Hbt. salinarum.* Scale bar: 500 nm. **(B)** Transmission electron micrograph of purified EVs from *Hrr. lacusprofundi.* Scale bar = 100 nm. **(C)** RNA extracted from gradient purified EVs and cells of *Hrr. lacusprofundi* on a 12.5% Urea-PAGE gel.

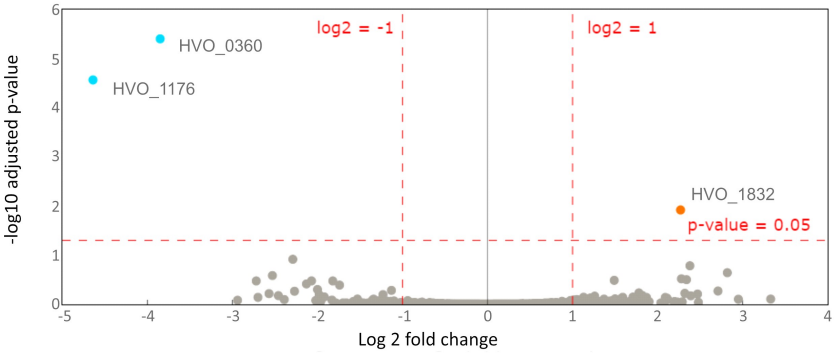

Supplementary Figure 9: Volcano plot comparing protein content from *H. volcanii* EVs isolated from upper and lower bands of Optiprep™ density gradient. EVs were isolated from three replicates at stationary phase of growth.

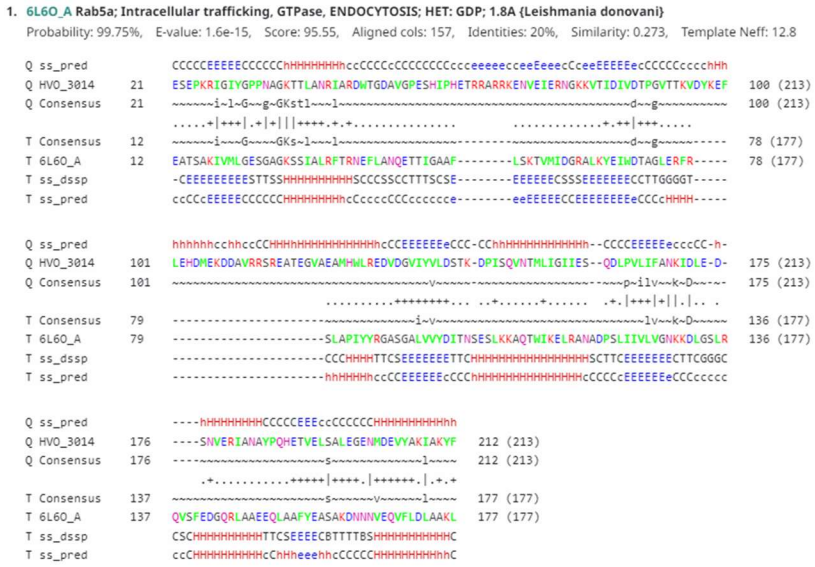

Supplementary Figure 10: HHpred alignment of HVO_3014 with Rab5a GTPase from *Leishmania donovani*. The protein sequence of HVO_3014 was analyzed using HHpred [1, 5] to identify domain-based homologous proteins using the default settings. Alignment with the best match to endosomal sorting protein, Rab5a GTPase, from unicellular Eukaryote, *Leishmania donovani*, is shown here.

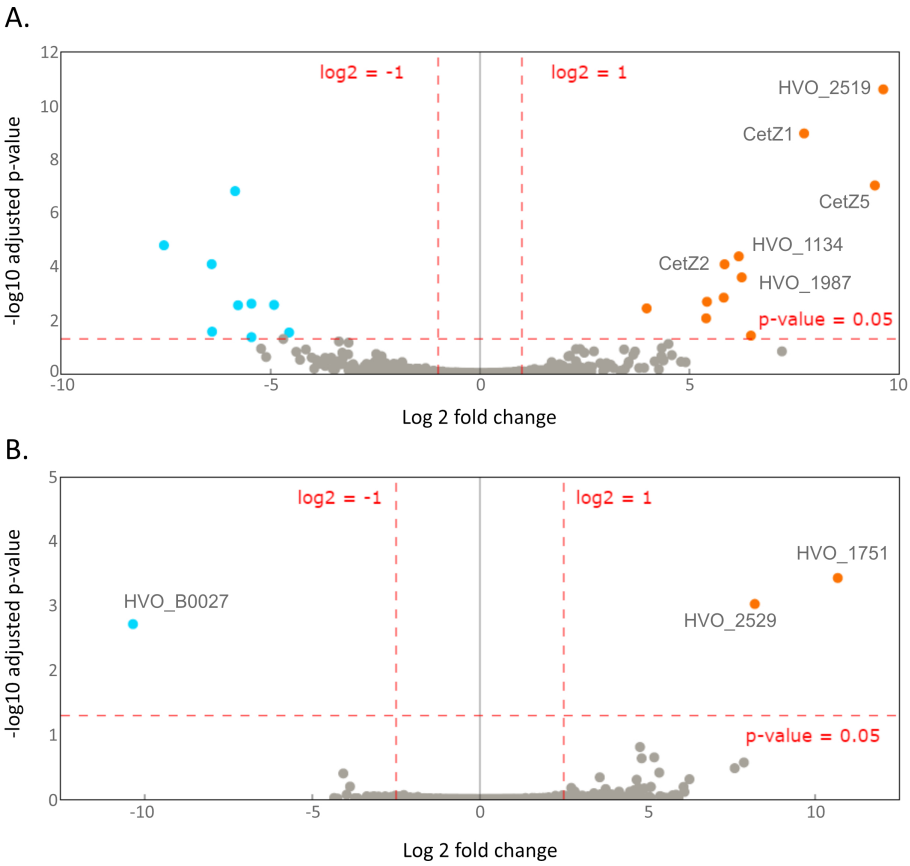

Supplementary Figure 11: Volcano plots depicting differences in protein abundance from UV-treated cultures. (A) Proteins isolated from EVs of UV-treated cultures are compared to their respective cell membrane protein content. **(B)** EV-associated proteins from UV-treated cultures are compared to EV-associated proteins from untreated cultures. Raw data found in Supplementary Table 11.

Supplementary Figure 12: Optiprep™ density gradient of OapA knock-out strain. EVs **(A)** before and **(B)** after ultracentrifugation. Red arrow indicates where particles concentrated. For comparison with parental strain, see Supplementary Figure 1A.

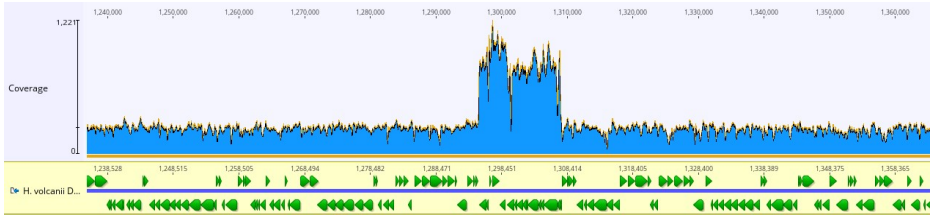

Supplementary Figure 13: Resequencing of OapA knockout strain shows activation of proviral region. Coverage blot of the genomic region including the provirus region. Image created in Geneious™.

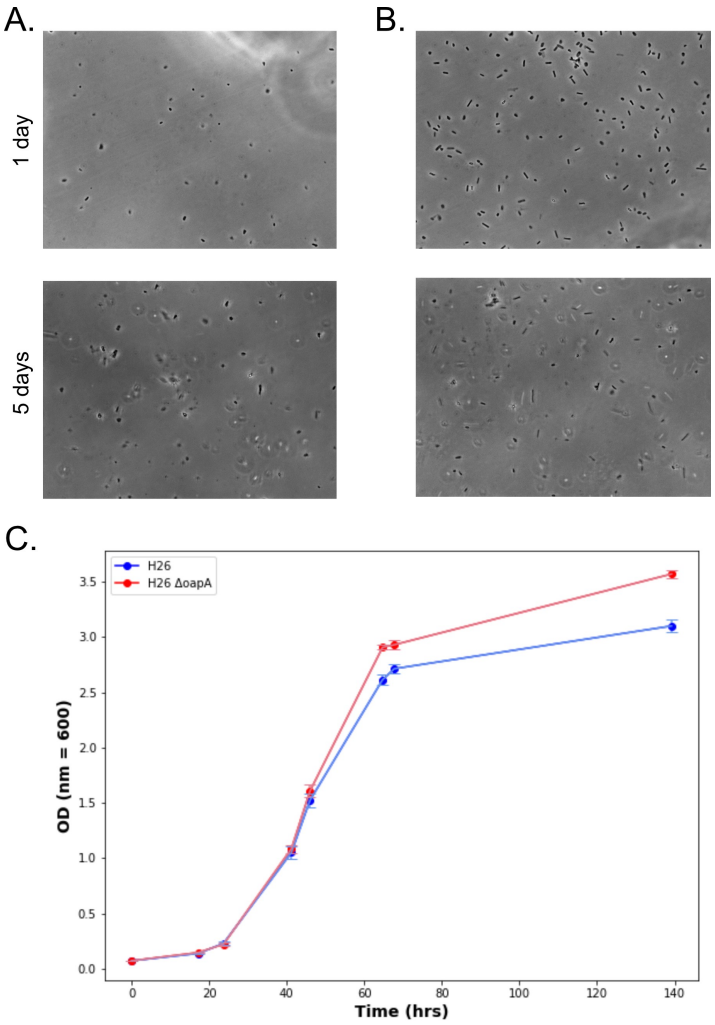

Supplementary Figure 14: Phenotypes of OapA knockout strain in comparison to parental strain. Phase contrast microscopy images of cells from OapA knockout strain **(A)** and parental strain **(B)** after 1 day (top) and 5 days (bottom) of growth. Samples were fixed with 1% glutaraldehyde and visualized with Axiophot Zeiss microscope. **(C)** Growth curve of parental strain (H26) and OapA knockout strain (H26 ΔoapA). Error bars represent standard deviation from three replicates.

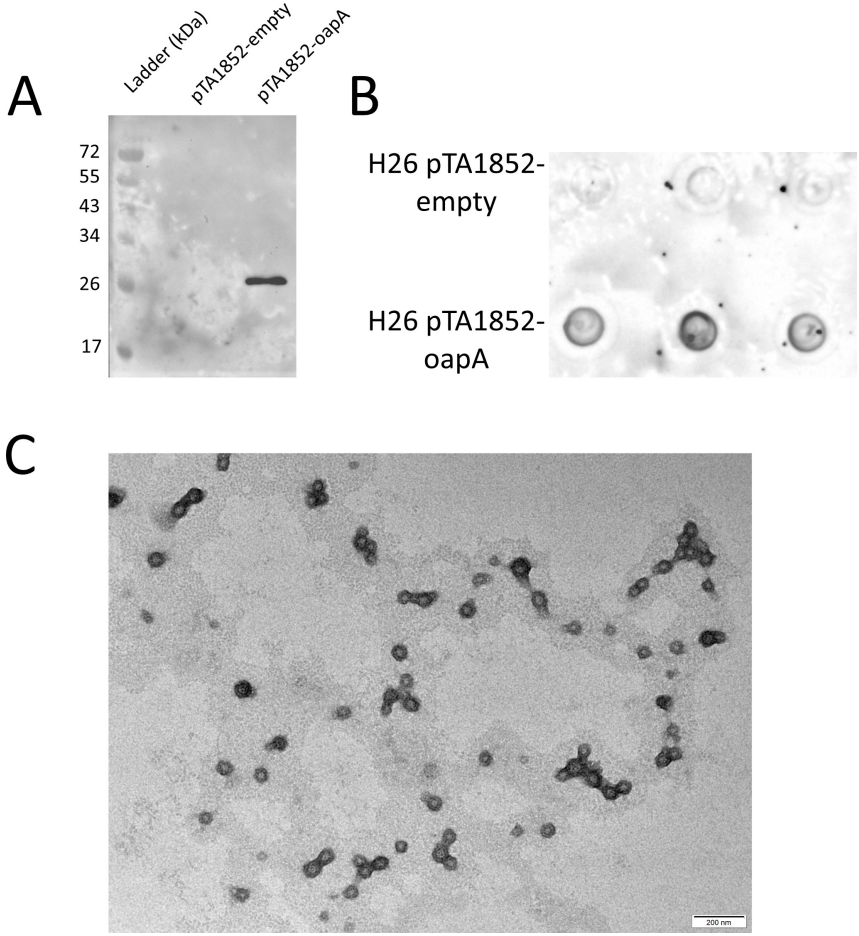

Supplementary Figure 15: EV production in strains overexpressing OapA. (A) Western blot with an anti-Strep tag antibody on affinity purified OapA expressed in H26, compared to an affinity purification from H26 with the empty vector (see methods). **(B)** Spot blot for quantification of EVs from cultures overexpressing OapA (Figure 5B). **(B)** Transmission electron micrographs of EVs isolated from strains overexpressing OapA. Scale bars denote 200 nm.

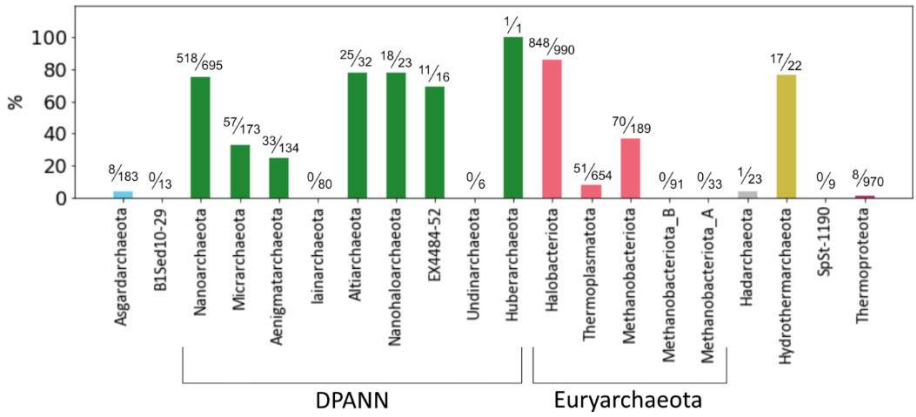

Supplementary Figure 16: Archaeal Ras-family GTPase homologs across the archaeal domain. Percentage of species identified containing a homolog for OapA within each phylum. Fraction above each bar denotes the number of species identified over the number of species surveyed.

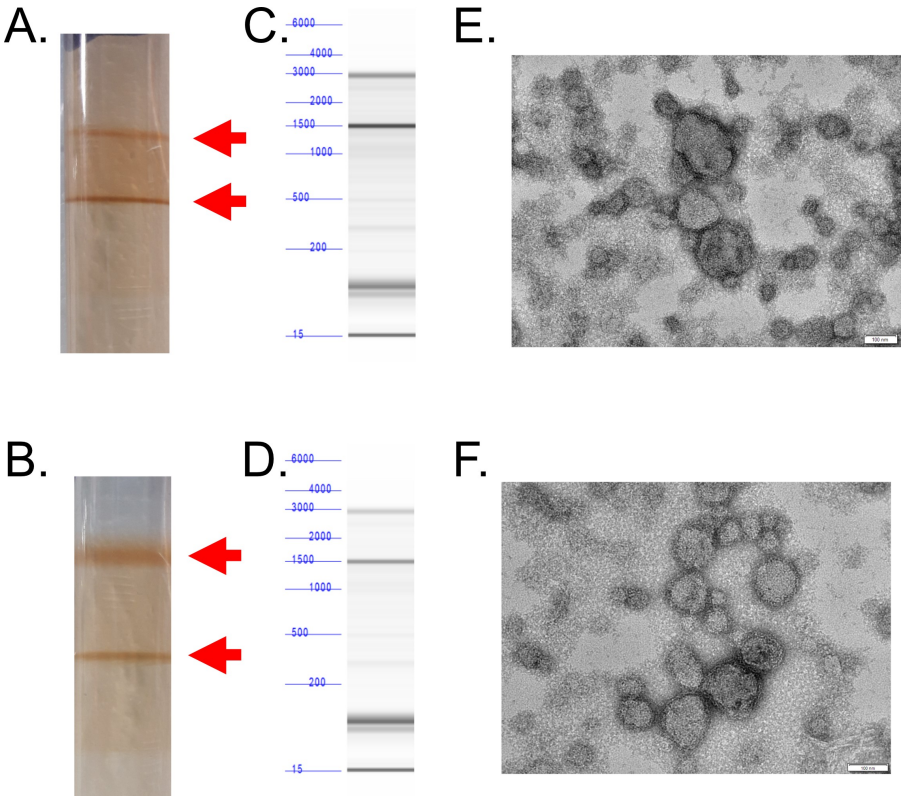

Supplementary Figure 17: EVs isolated from CetZ1 and CetZ2 knockout strains. Optiprep™ density gradients of EVs isolated from CetZ1 **(A)** and CetZ2 **(B)** knock out strains after ultracentrifugation. Red arrows indicate the upper and lower bands where particles had concentrated. **(C and D)** RNA was isolated from both strains and run on a fragment analyzer to observe the size distribution. For comparison to wild type, see Figure 2. **(E and F)** EVs could also be observed through TEM. Scale bars: 100 nm.

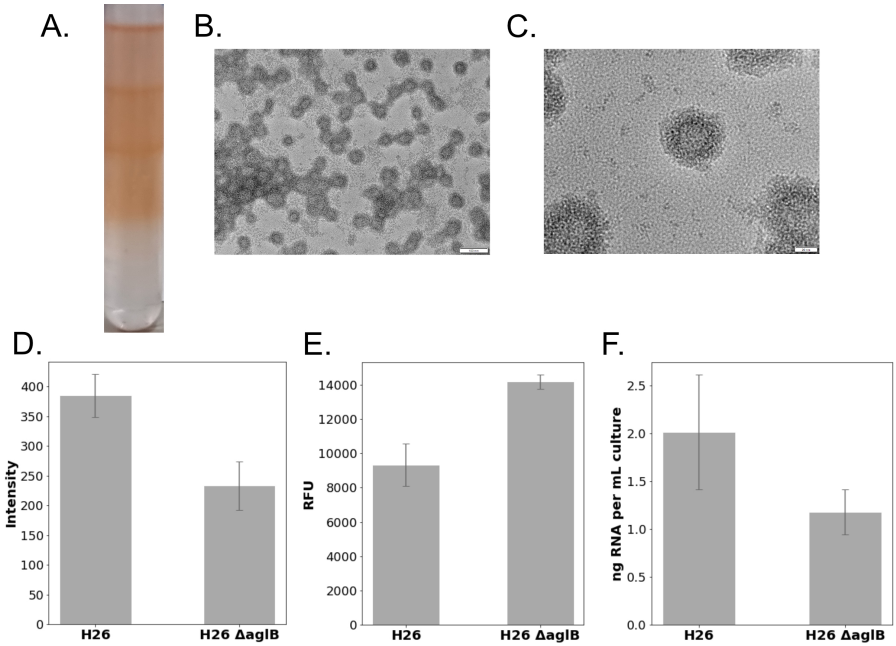

Supplementary Figure 18: Phenotypes of EVs from AglB knockout strain. (A) Bands of concentrated EVs after ultracentrifugation in Optiprep™ density gradient. Transmission electron microscopy of EVs isolated from AglB knockout strain with size bar 100 nm **(B)** and 20 nm **(C)**. Quantification of EV production of AglB knockout strain in comparison with parental strain by immunodetection **(D)** and fluorescence staining **(E)**. **(F)** Quantification of EV-associated RNA in culture supernatants of AglB knockout strain compared to parental strain normalized to OD (nm = 600). Error bars represent the standard deviation of three replicates. RFU = relative fluorescence unit.

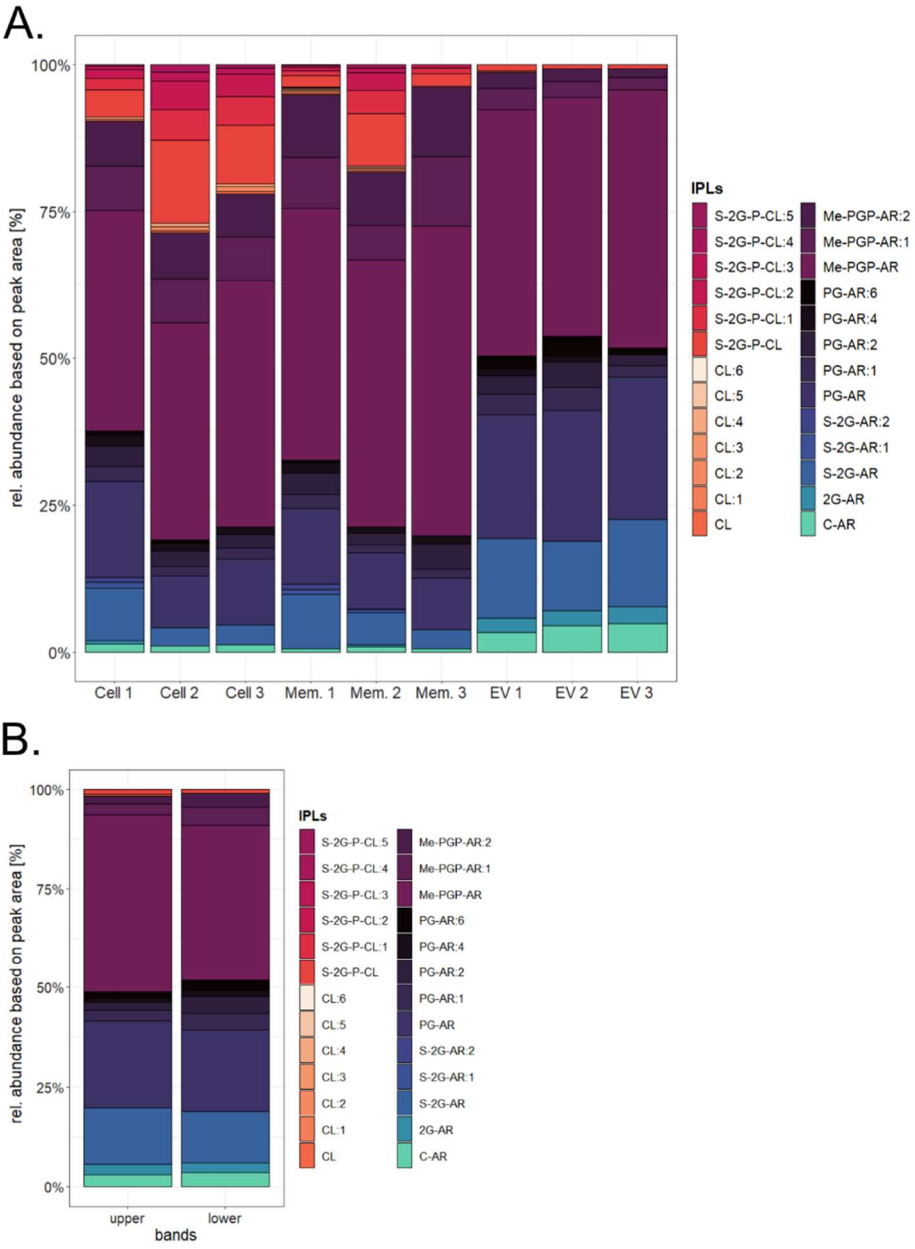
A.
100%
75%
50%
25%
0%
rel. abundance based on peak area [%]
Cell 1
Cell 2
Cell 3
Mem. 1
Mem. 2
Mem. 3
EV 1
EV 2
EV 3
IPLs
S-2G-P-CL:5
S-2G-P-CL:4
S-2G-P-CL:3
S-2G-P-CL:2
S-2G-P-CL:1
S-2G-P-CL
CL:6
CL:5
CL:4
CL:3
CL:2
CL:1
CL
Me-PGP-AR:2
Me-PGP-AR:1
Me-PGP-AR
PG-AR:6
PG-AR:4
PG-AR:2
PG-AR:1
PG-AR
S-2G-AR:2
S-2G-AR:1
S-2G-AR
2G-AR
C-AR
B.
100%
75%
50%
25%
0%
rel. abundance based on peak area [%]
upper
lower
bands
IPLs
S-2G-P-CL:5
S-2G-P-CL:4
S-2G-P-CL:3
S-2G-P-CL:2
S-2G-P-CL:1
S-2G-P-CL
CL:6
CL:5
CL:4
CL:3
CL:2
CL:1
CL
Me-PGP-AR:2
Me-PGP-AR:1
Me-PGP-AR
PG-AR:6
PG-AR:4
PG-AR:2
PG-AR:1
PG-AR
S-2G-AR:2
S-2G-AR:1
S-2G-AR
2G-AR
C-AR

Supplementary Figure 19: Distribution of lipid compounds comparing whole cells, cell membranes and EVs of H. volcanii. (A) Individual replicates used to calculate the average relative abundances in Figure 6. Cell 1-3: whole cells, Mem. 1-3: membrane fraction and EV 1-3: extracellular vesicles after ultracentrifugation in Optiprep™ density gradients and bands pooled together for each biological replicate. **(B)** The lipid distribution in the upper (left column) and lower band (right column) after ultracentrifugation from one biological replicate. Relative abundances were calculated based on the peak area of the most abundant adduct for each compound. Lipids were identified based on their retention time, fractionation pattern and exact mass.

Compound abbreviations: AR = archaeol (C20-C20 isoprenoidal chains), CL = cardiolipin, :nUS = lipid with n number of unsaturations, UK = unknown compound. Lipids with neutral headgroups: 1G = monoglycosyl, 2G = diglycosyl, C-AR = core-AR. Lipids with anionic headgroups: PGP-Me = phosphatidylglycerophosphate methyl esters, PG = phosphatidylglycerol, S-2G =sulfated diglycosyl, S-GP = sulfoglycophospho, S-2G-P = sulfated diglycosyl-phospho.

Supplementary Tables

Supplementary Table 1: Strains used in this study

Name	Reference	Organism	Description	Media	Supplement
H. volcanii DS2	[6]	*H. volcanii DS2*	Wild type strain	HV-cab/YPC	none
H26	[7]	*H. volcanii*	ΔpyrE2	HV-cab/YPC	uracil
H26 ΔoapA	[8]	*H. volcanii*	ΔpyrE2, ΔoapA	HV-cab/YPC	uracil
H26 ΔaglB	[9]	*H. volcanii*	ΔpyrE2, ΔaglB	HV-cab/YPC	uracil
H53	[7]	*H. volcanii*	ΔpyrE2, ΔtrpA	HV-cab/YPC	uracil, tryptophan
H53 ΔcetZ1	[10]	*H. volcanii*	ΔpyrE2, ΔtrpA, ΔcetZ1	HV-cab/YPC	uracil, tryptophan
H53 ΔcetZ2	[10]	*H. volcanii*	ΔpyrE2, ΔtrpA, ΔcetZ2	HV-cab/YPC	uracil, tryptophan
Halobacterium salinarum	[11]	*Halobacterium salinarum*	Wild type strain	HS-Media	none
Halorubrum lacusprofundi DL18	[12]	*Halorubrum lacusprofundi DL18*	Wild type strain	DBCM2	none

Supplementary Table 2: Primer Sequences

Name	Oligonucleotide sequence 5'-3'	Description
HFPV1F	CACGAACGAGAACACCGACC	Forward primer to test infection of HFPV-1
HFPV1R	TGATGACGAATCCAACGAGCAG	Reverse primer to test infection of HFPV-1
AglB_US_F	CCGGCCAAGCTTGGTTT-GCGAGCGACCCAGTCG	Forward primer for upstream flank of aglB with HindIII restriction sites
AglB_US_R	GAATTCGCCGCCCGAAGATCTT-GTGACCAACAACCGCCAAG	Reverse primer for upstream flank of aglB with EcoRI and BglII restriction sites
AglB_DS_F	AGATCTTCGGGCGGCGAATTCCAC-GAGCCGAGACGGCGACGA	Forward primer of downstream flank of aglB with BglII and EcoRI restriction sites
AglB_DS_R	CCGGCCG-GATCCGCGCGTCGCCGTGCTCG-GAC	Reverse primer for downstream flank of AglB with BamHI restriction sites
csg probe	GCTGTCAGCGTCGAGGTTTCC	Northern blot probe for the 5' end of S-layer mRNA

Supplementary Information

Supplementary Results, Supplementary Figures 1-19 and Supplementary Tables 1-2 were provided in the preceeding section
The remaining Supplementary Tables listed here are accessible online on *BioRxiv* under the following link: https://doi.org/10.1101/2023.03.03.530948

Abbreviated forms of Supplementary Tables 6, 9, 10 and 11 are included after this list; the choice of the specific subset is indicated in the legend of the respective table.

Supplementary Table 3: Differential expression calculated for transcripts from total vs small RNA libraries of EV associated RNA. One replicate of RNA associated with EVs isolated from the upper band of a density gradient was sequenced using a total RNA library and a small RNA library. Read mapping (90% minimum overlap identity, TPM) and differential expression (log2 ratio) performed with Geneious™ (2021.0.1). (Excel file)
Supplementary Table 4: Differential expression calculated for transcripts from EVs of upper versus lower band of a density gradient. One replicate of RNA associated with EVs isolated from the upper band and the lower band of a density gradient. Read mapping (90% minimum overlap identity, TPM) and differential expression (log2 ratio) performed with Geneious™ (2021.0.1). (Excel file)

Supplementary Table 5: Differential expression calculated for transcripts from EVs from untreated and UV treated cells. One replicate of RNA associated with EVs isolated from untreated and UV treated cells. Read mapping (99% minimum overlap identity, TPM) and differential expression (log2 ratio) performed with Geneious™ (2021.0.1). (Excel file)

Supplementary Table 6: Differential expression calculated for EV associated transcript normalized with intracellular levels. RNA was extracted from purified EVs and the respective cells in triplicates. Read mapping (99% minimum overlap identity, TPM) and differential expression (log2 ratio, p-value) were calculated with DESeq2 in Geneious™ (2021.0.1). (Excel file)
Supplementary Table 7: ncRNA enriched in EVs. List of the ncRNA that are highly expressed and with a high fold change in *H. volcanii* EVs. Data taken from Supplementary Table 6. (Excel file)

Supplementary Table 8: Differential expression calculated for transcripts from *Hbt. salinarum* EVs normalized to intracellular levels. RNA was extracted from purified EVs (duplicates) and the respective cells (one replicate). Read mapping (90% minimum overlap identity, TPM) and differential expression (log2 ratio) performed with Geneious™ (2021.0.1). (Excel file)

Supplementary Table 9: Proteins enriched in EVs after normalization with the protein content of cell membranes. Protein content of EVs was pooled from upper and lower bands in three replicates (total of 6 EV replicates) and quantities were compared with three replicates from host cell membrane preparations. Quantity was estimated using MaxQuant (v. 1.6.10.43) and differential expression analysis (log2 fold change, adjusted p-value) was calculated with DEP (v. 1.21.0) [79]. (Excel file)

Supplementary Table 10: Proteins enriched in EVs from UV-treated cells after normalization with the protein content of respective cell membranes. Protein content of EVs from UV treated cells was pooled from upper and lower bands in three replicates (total of 6 EV replicates) and quantities were compared with three replicates from respective host cell membrane preparations. Quantity was estimated using MaxQuant (v. 1.6.10.43) and differential expression analysis (log2 fold change, adjusted p-value) was calculated with DEP (v. 1.21.0) [79]. (Excel file)

Supplementary Table 11: Proteins identified as present in all EV samples. Protein content of EVs from untreated cells (3 replicates from upper and lower bands of density gradient each) and UV treated cells (3 replicates from upper and lower bands of density gradient each) was pooled (total of 12 EV replicates). Label-free quantities (LFQ) were calculated using MaxQuant (v. 1.6.10.43) and averaged over all replicates. Proteins were only considered present if peptide count was greater than or equal to 2 in all replicates and all replicates had a corresponding LFQ value. (Excel file)

Supplementary Table 12: Taxonomy of Archaea identified to contain Ras-superfamily small GTPase. 1,666 archaeal organisms out of 78,738 archaeal and bacterial genomes were identified to contain a homolog to Ras-superfamily small GTPase, OapA (see Methods). Taxonomy listed according to genome taxonomy database release (r207). (Excel file).

Supplementary Table 13: Mass spectrometry peak areas and relative abundances of lipid compounds extracted from whole cells, cell membranes and EVs of *H. volcanii*. Intact polar lipids were extracted from whole cells, cell membranes and vesicles of *H. volcanii* and measured with a Q-TOF MS (Bruker Daltonics). Output data were analyzed with the manufacturer's software (DataAnalysis 4.4.2, Bruker Daltonics) and lipid compounds were identified based on retention time, fractionation pattern and exact masses and quantified via mass spectrometry peak area. (Excel file)

Supplementary Table 6: Differential expression calculated for EV associated transcript normalized with intracellular levels. RNA was extracted from purified EVs and the respective cells in triplicates. Read mapping (99% minimum overlap identity, TPM) and differential expression (log2 ratio, p-value) were calculated with DESeq2 in Geneious™ (2021.0.1). Genes of High Expression and High Enrichment (EV TPM > 10, Log2 Fold Change > 2.0, p-value < 0.01) are displayed.

Name	Gene ID	Genome	Min	Max	RNA Type	EV TPM Average	Cell TPM Average	Differential Expression Log2 Ratio	Differential Expression p-value
HVO_2072	WP_013035656.1	CHR	1923913	1926396	mRNA	738.98	21.23	7.92	0
HVO_1988	WP_004041870.1	CHR	1834767	1835816	mRNA	14.59	1.98	5.67	2.29E-165
HVO_1987	WP_004041869.1	CHR	1833881	1834780	mRNA	14.82	2.40	5.45	2.13E-161
HVO_2755	WP_004043001.1	CHR	2594860	2595201	mRNA	22.46	5.31	4.85	2.10E-112
HVO_2804	#N/A	CHR	2636111	2636184	mRNA	620.57	194.30	4.47	1.48E-154
HVO_A0352	#N/A	pHV4	364513	364575	mRNA	1477.55	531.46	4.25	9.96E-141
HVO_A0134	N/A	pHV4	131940	132431	mRNA	13.07	5.10	4.15	3.03E-97
HVO_A0007_A	#N/A	pHV4	7920	9687	mRNA	37.97	14.88	4.06	8.70E-58
HVO_0381	WP_004044542.1	CHR	339904	340089	mRNA	50.25	29.64	3.60	1.10E-88
HVO_2777	WP_004043023.1	CHR	2616629	2617027	mRNA	30.36	17.93	3.56	2.40E-88
HVO_A0408	N/A	pHV4	413614	414760	mRNA	13.16	8.05	3.52	5.67E-93
HVO_A0008	WP_004043314.1	pHV4	8150	9448	mRNA	13.13	8.19	3.39	1.86E-45
HVO_2940	#N/A	CHR	2772189	2772305	mRNA	249.04	155.73	3.39	1.55E-48
HVO_C0080_A	#N/A	pHV1	80936	81022	mRNA	404.16	277.69	3.32	2.35E-78
HVO_2519	#N/A	CHR	2384839	2384987	mRNA	1503.78	1053.04	3.32	1.15E-102

HVO_2565	WP_004042620.1	CHR	2419453	2420295	mRNA	13.53	9.67	3.24	2.55E-57
HVO_2117	WP_004042001.1	CHR	1981148	1982068	mRNA	17.81	13.69	3.18	9.63E-71
HVO_2160	WP_004042044.1	CHR	2025177	2031950	mRNA	23.98	19.16	3.18	4.96E-75
HVO_0987	WP_004043956.1	CHR	896613	898142	mRNA	24.60	19.51	3.16	1.28E-98
HVO_0972	WP_004043971.1	CHR	882969	883490	mRNA	25.89	20.77	3.15	2.03E-78
HVO_0263	WP_013035611.1	CHR	235110	236276	mRNA	151.55	122.12	3.11	1.66E-86
HVO_0985	WP_004043958.1	CHR	894274	894576	mRNA	34.63	28.91	3.08	8.29E-77
HVO_2784	WP_004043029.1	CHR	2619760	2620263	mRNA	47.78	40.53	3.06	7.34E-80
HVO_0983	WP_004043960.1	CHR	893649	893909	mRNA	25.29	21.95	3.03	5.08E-58
HVO_2737	WP_004042964.1	CHR	2583344	2583706	mRNA	10.44	9.46	2.98	1.11E-50
HVO_0944	WP_004044001.1	CHR	855836	856375	mRNA	29.89	28.15	2.93	8.71E-68
HVO_2773	WP_004043019.1	CHR	2614266	2615048	mRNA	32.44	30.46	2.93	3.12E-81
HVO_2775	WP_004043021.1	CHR	2616249	2616425	mRNA	24.94	23.43	2.92	2.81E-46
HVO_0984	WP_004043959.1	CHR	893906	894274	mRNA	20.84	19.46	2.92	1.09E-62
HVO_C0065	N/A	pHV1	62797	63476	mRNA	11.12	10.28	2.89	1.09E-53
HVO_2776	WP_004043022.1	CHR	2616422	2616616	mRNA	35.60	34.86	2.87	5.07E-53
HVO_2073	WP_004041957.1	CHR	1926766	1927521	mRNA	11.16	10.93	2.84	6.60E-55
HVO_0986	WP_004043957.1	CHR	894580	896616	mRNA	19.71	19.51	2.84	7.95E-84
HVO_0196	WP_004045310.1	CHR	176934	177101	mRNA	105.87	105.43	2.83	9.62E-81
HVO_2778	WP_004043024.1	CHR	2617021	2617458	mRNA	41.75	40.99	2.83	2.26E-60
HVO_2116	WP_013035569.1	CHR	1980207	1981151	mRNA	15.70	15.73	2.82	1.04E-50
HVO_2782	WP_004043027.1	CHR	2618847	2619239	mRNA	34.30	34.63	2.81	2.96E-55

HVO_A0117	WP_013035143.1	pHV4	115728	116552	mRNA	10.02	9.95	2.81	8.62E-60
HVO_2783	WP_004043028.1	CHR	2619236	2619763	mRNA	33.72	34.08	2.81	1.92E-68
HVO_1518	#N/A	CHR	1382710	1385466	mRNA	70.10	68.40	2.79	3.58E-44
HVO_0275	WP_013035249.1	CHR	243876	245228	mRNA	71.79	73.16	2.73	1.04E-42
HVO_2774	WP_004043020.1	CHR	2615045	2616244	mRNA	19.80	21.63	2.71	8.75E-71
HVO_A0354	N/A	pHV4	365276	365704	mRNA	253.90	272.70	2.70	1.97E-65
HVO_0062	WP_004045090.1	CHR	61296	63134	mRNA	23.30	25.89	2.69	8.00E-71
HVO_2822	WP_013035380.1	CHR	2655111	2655413	mRNA	13.00	12.63	2.65	1.81E-08
HVO_0979	WP_004043964.1	CHR	889665	890366	mRNA	18.04	20.63	2.64	2.86E-61
HVO_0945	WP_004044000.1	CHR	856375	858144	mRNA	20.32	23.84	2.61	1.56E-61
HVO_2817	#N/A	CHR	2648777	2649943	mRNA	101.64	118.04	2.59	5.45E-64
HVO_2070	WP_049941511.1	CHR	1919938	1921572	mRNA	14.36	16.98	2.58	4.73E-65
HVO_1837	N/A	CHR	1697021	1698178	mRNA	46.67	55.45	2.57	4.19E-75
HVO_A0364	WP_013035046.1	pHV4	375384	376550	mRNA	46.18	55.39	2.56	5.55E-74
HVO_1276	#N/A	CHR	1165740	1165916	mRNA	671.75	781.02	2.56	2.41E-45
HVO_0946	WP_004043999.1	CHR	858141	858335	mRNA	29.10	34.84	2.55	2.43E-44
HVO_C0013	WP_013035120.1	pHV1	9798	11096	mRNA	53.72	64.91	2.55	6.38E-60
HVO_2757	WP_004043003.1	CHR	2596266	2596904	mRNA	17.13	20.99	2.50	2.62E-49
HVO_0982	WP_004043961.1	CHR	893082	893543	mRNA	25.94	33.35	2.46	3.45E-54
HVO_2779	WP_004043025.1	CHR	2617455	2617805	mRNA	52.08	66.85	2.45	3.90E-47
HVO_A0353	N/A	pHV4	364986	365228	mRNA	58.22	76.44	2.40	8.74E-47
HVO_0981	WP_004043962.1	CHR	892036	893085	mRNA	14.60	20.13	2.35	3.91E-50

HVO_2103	WP_004041986.1	CHR	1965879	1967369	mRNA	21.05	30.08	2.34	1.66E-53
HVO_2062	WP_004041947.1	CHR	1911379	1911816	mRNA	102.04	142.23	2.32	6.18E-44
HVO_0907	WP_004044032.1	CHR	824054	825853	mRNA	60.32	88.63	2.27	4.48E-56
HVO_0988	WP_004043955.1	CHR	898143	899663	mRNA	18.61	27.93	2.25	1.37E-54
HVO_2818	#N/A	CHR	2650123	2650398	mRNA	133.98	195.03	2.23	1.47E-31
HVO_0359	WP_004044564.1	CHR	327676	328941	mRNA	22.87	36.74	2.15	1.59E-44
HVO_0763	WP_049941502.1	CHR	684671	685198	mRNA	16.46	26.13	2.15	3.12E-34
HVO_0864	#N/A	CHR	781200	781303	mRNA	278.26	440.48	2.14	5.44E-45
HVO_C0037	WP_013035684.1	pHV1	30761	31930	mRNA	18.86	31.05	2.10	1.99E-45

Supplementary Table 9: Proteins enriched in EVs after normalization with the protein content of cell membranes. Protein content of EVs was pooled from upper and lower bands in three replicates (total of 6 EV replicates) and quantities were compared with three replicates from host cell membrane preparations. Quantity was estimated using MaxQuant (v. 1.6.10.43) and differential expression analysis (log2 fold change, adjusted p-value) was calculated with DEP (v. 1.21.0) [79]. The corresponding archaeal COG functional category (arCOG) and the description of archaeal COG functional category (arCOG description) are given for each protein. Proteins enriched with EVs when normalized to cell (log2 > 1, adjusted p-value < 0.05) are displayed.

Protein ID	HVO_XXXX	Description	arCOG	arCOG description	log2 fold change	adjusted p-value
WP_004041897.1	HVO_2013	CetZ5	D	Cell cycle control and mitosis	9.55	8.77E-07
WP_004042501.1	HVO_2519	hypothetical protein	S	Function Unknown	9.19	8.71E-09
ADE04578.1	HVO_2204	CetZ1	D	Cell cycle control and mitosis	8.69	3.51E-10
WP_004043803.1	HVO_1134	hypothetical protein	S	Function Unknown	7.25	4.84E-06
WP_004044352.1	HVO_0581	FtsZ2	D	Cell cycle control and mitosis	6.66	0.00153
WP_004041869.1	HVO_1987	proteinase IV-like protein	O	Post-translational modification, protein turnover, chaperone functions	6.29	0.00119
WP_004041843.1	HVO_1964	photosystem reaction center subunit H	R	General Functional Prediction only	5.89	0.00204
WP_004044192.1	HVO_0745	CetZ2	D	Cell cycle control and mitosis	5.31	0.00228
WP_004044872.1	HVO_2985	hypothetical protein	V	Defense mechanisms	5.2	0.0175
WP_004041076.1	HVO_B0079	ABC transporter ATP-binding protein	E	Amino Acid metabolis and transport	4.74	0.0011
WP_004044952.1	HVO_3014	GTP-binding protein	R	General Functional Prediction only	4.16	0.0133

Supplementary Table 10: Proteins enriched in EVs from UV-treated cells after normalization with the protein content of respective cell membranes. Protein content of EVs from UV treated cells was pooled from upper and lower bands in three replicates (total of 6 EV replicates) and quantities were compared with three replicates from respective host cell membrane preparations. Quantity was estimated using MaxQuant (v. 1.6.10.43) and differential expression analysis (log2 fold change, adjusted p-value) was calculated with DEP (v. 1.21.0) [79]. The corresponding archaeal COG functional category (arCOG) and the description of archaeal COG functional category (arCOG description) are given for each protein. Proteins enriched with Evs from UV-treated cells when normalized to cell (log2 > 1, adjusted p-value < 0.05) are displayed.

Protein ID	HVO_XXXX	Description	arCOG	arCOG description	Log2 fold change	adjusted p-value
WP_004042501.1	HVO_2519	hypothetical protein	S	Function unknown	9.63	2.39E-11
WP_004041897.1	HVO_2013	CetZ5	D	Cell cycle control and mitosis	9.43	9.28E-08
ADE04578.1	HVO_2204	CetZ1	D	Cell cycle control and mitosis	7.74	1.06E-09
WP_049914824.1	HVO_2399	ABC transporter permease	P	Inorganic ion transport and metabolism	6.47	0.0378
WP_004041869.1	HVO_1987	proteinase IV-like protein	O	Post-translational modification, protein turnover, chaperone functions	6.25	0.000252
WP_004043803.1	HVO_1134	hypothetical protein	S	Function unknown	6.18	4.14E-05
WP_004044192.1	HVO_0745	CetZ2	D	Cell cycle control and mitosis	5.84	8.17E-05
WP_004044872.1	HVO_2985	hypothetical protein	V	Defense mechanism	5.82	0.00144
WP_004041843.1	HVO_1964	photosystem reaction center subunit H	R	General Functional Prediction only	5.42	0.00205
WP_004044352.1	HVO_0581	FtsZ2	D	Cell cycle control and mitosis	5.4	0.00851
WP_004041076.1	HVO_B0079	ABC transporter ATP-binding protein	E	Amino Acid metabolis and transport	3.98	0.00362

Supplementary Table 11: Proteins identified as present in all EV samples. Protein content of EVs from untreated cells (3 replicates from upper and lower bands of density gradient each) and UV treated cells (3 replicates from upper and lower bands of density gradient each) was pooled (total of 12 EV replicates). Label-free quantities (LFQ) were calculated using MaxQuant (v. 1.6.10.43) and averaged over all replicates. Proteins were only considered present if peptide count was greater than or equal to 2 in all replicates and all replicates had a corresponding LFQ value. The corresponding archaeal COG functional category (arCOG) and the description of archaeal COG functional category (arCOG description) are given for each protein. The 100 most abundant proteins, with an average LFQ intensity > $3.4x10^{+7}$, are displayed.

Protein IDs	HVO_XXXX	Description	arCOG	arGOG description	Average LFQ intensity
ADE04578.1	HVO_2204	CetZ1	D	Cell cycle control and mitosis	1.93E+09
ELY33665.1	HVO_2072	major cell surface glycoprotein	T	Signal Transduction	1.75E+09
WP_004045090.1	HVO_0062	peptide ABC transporter substrate-binding protein	E	Amino Acid metabolis and transport	9.16E+08
ELY32287.1	HVO_2695	sugar ABC transporter substrate-binding protein	G	Carbohydrate metabolism and transport	6.38E+08
WP_004043971.1	HVO_0972	hypothetical protein	N	Cell motility	5.25E+08
WP_004043803.1	HVO_1134	hypothetical protein	S	Function Unknown	4.75E+08
WP_004044872.1	HVO_2985	hypothetical protein	V	Defense mechanisms	4.58E+08
ADE02586.1	HVO_2126	peptide ABC transporter substrate-binding protein	E	Amino Acid metabolis and transport	4.46E+08
WP_004044135.1	HVO_0801	phosphoesterase	O	Post-translational modification, protein turnover, chaperone functions	4.24E+08
WP_004041897.1	HVO_2013	CetZ5	D	Cell cycle control and mitosis	3.83E+08
WP_004043537.1	HVO_1401	BMP family ABC transporter substrate-binding protein	R	General Functional Prediction only	3.63E+08
WP_004044307.1	HVO_0628	ABC transporter substrate-binding protein	E	Amino Acid metabolis and transport	2.12E+08

WP_004042044.1	HVO_2160	PGF-CTERM sorting domain-containing protein	S	Function Unknown	2.02E+08
WP_004042501.1	HVO_2519	hypothetical protein	S	Function Unknown	1.98E+08
ADE03035.1	HVO_0763	quinol oxidase	S	Function Unknown	1.91E+08
WP_004041916.1	HVO_2031	BMP family ABC transporter substrate-binding protein	R	General Functional Prediction only	1.87E+08
WP_004041769.1	HVO_1888	molybdenum transporter	H	Coenzyme metabolis	1.77E+08
ADE01499.1	HVO_B0082	peptide ABC transporter substrate-binding protein	E	Amino Acid metabolis and transport	1.46E+08
WP_004041775.1	HVO_1894	hypothetical protein	S	Function Unknown	1.35E+08
WP_049941511.1	HVO_2070	sialidase	M	Cell wall/membrane/envelop biogenesis	1.26E+08
ELY32157.1	HVO_A0133	Tat (twin-arginine translocation) pathway signal sequence domain protein	S	Function Unknown	1.25E+08
WP_004043922.1	HVO_1020	PBS lyase HEAT-like repeat domain-containing protein	S	Function Unknown	1.19E+08
WP_004044607.1	HVO_0316	ATP synthase subunit A	C	Energy production and conversion	1.14E+08
WP_004042036.1	HVO_2153	membrane protein	Q	Secondary Structure	1.12E+08
WP_004044564.1	HVO_0359	elongation factor 1-alpha	J	Tranlsation	1.08E+08
WP_004042286.1	HVO_2397	adhesin	P	Inorganic ion transport and metabolism	1.07E+08
WP_004042262.1	HVO_2373	30S ribosomal protein S8e	J	Tranlsation	1.06E+08
WP_004041336.1	HVO_B0198	iron ABC transporter substrate-binding protein	P	Inorganic ion transport and metabolism	1.01E+08
WP_004044567.1	HVO_0356	elongation factor EF-2	J	Tranlsation	93035500
WP_004044823.1	HVO_2960	branched-chain alpha-keto acid dehydrogenase subunit E2	C	Energy production and conversion	90253333

WP_004044400.1	HVO_0530	sugar ABC transporter substrate-binding protein	G	Carbohydrate metabolism and transport	89559667
ADE01713.1	HVO_A0548	quinol oxidase	S	Function Unknown	87995000
WP_004045197.1	HVO_0106	hypothetical protein	S	Function Unknown	84348167
WP_004044192.1	HVO_0745	CetZ2	D	Cell cycle control and mitosis	79767833
WP_013035363.1	HVO_1530	MFS transporter	M	Cell wall/membrane/envelop biogenesis	75016917
WP_004044606.1	HVO_0317	V-type ATP synthase subunit B	C	Energy production and conversion	72820500
WP_004042940.1	HVO_2724	ribonuclease J	J	Tranlsation	71380500
WP_004041424.1	HVO_1546	dihydroxyacetone kinase subunit DhaK	G	Carbohydrate metabolism and transport	70506333
WP_004041481.1	HVO_1590	molecular chaperone DnaK	O	Post-translational modification, protein turnover, chaperone functions	70455500
WP_004044609.1	HVO_0314	ATP synthase subunit C	C	Energy production and conversion	70427417
ELY28087.1	HVO_1228	cytochrome Fbr	C	Energy production and conversion	70209917
WP_004043963.1	HVO_0980	NADH-quinone oxidoreductase subunit C	C	Energy production and conversion	69684500
WP_004043835.1	HVO_1103	hypothetical protein	S	Function Unknown	67152083
WP_004044718.1	HVO_2900	fumarase	C	Energy production and conversion	67080250
WP_004044820.1	HVO_2959	2-oxoisovalerate dehydrogenase subunit beta	C	Energy production and conversion	63911667
WP_004042273.1	HVO_2384	CBS domain-containing protein	R	General Functional Prediction only	63371000
WP_004044825.1	HVO_2961	dihydrolipoamide dehydrogenase	C	Energy production and conversion	61895000
WP_004042325.1	HVO_2432	basic amino acid ABC transporter substrate-binding protein	S	Function Unknown	60522000
ELY35686.1	HVO_1673	hypothetical protein	S	Function Unknown	57473083

WP_004043700.1	HVO_1241	photosynthetic protein synthase I	R	General Functional Prediction only	57030875
WP_004041107.1	HVO_B0047	iron ABC transporter substrate-binding protein	P	Inorganic ion transport and metabolism	56856500
WP_004044818.1	HVO_2958	pyruvate dehydrogenase (acetyl-transferring) E1 component subunit alpha	C	Energy production and conversion	55475833
WP_004042658.1	HVO_2588	isocitrate dehydrogenase (NADP(+))	C	Energy production and conversion	54533583
WP_004043964.1	HVO_0979	NADH dehydrogenase	C	Energy production and conversion	52595417
WP_004042268.1	HVO_2379	phosphate transport system regulatory protein PhoU	P	Inorganic ion transport and metabolism	51864333
WP_004044093.1	HVO_0843	hypothetical protein	S	Function Unknown	49737417
WP_004042616.1	HVO_2563	50S ribosomal protein L4	J	Tranlsation	49675083
WP_004042287.1	HVO_2398	ABC transporter ATP-binding protein	P	Inorganic ion transport and metabolism	48654833
WP_004045327.1	HVO_0213	rubrerythrin	R	General Functional Prediction only	47987500
WP_004041835.1	HVO_1955	aconitate hydratase	C	Energy production and conversion	47038167
ADE01609.1	HVO_B0135	hypothetical protein	S	Function Unknown	44420583
WP_004043050.1	HVO_2808	succinate dehydrogenase	C	Energy production and conversion	43540500
WP_004044952.1	HVO_3014	Era-like GTP binding protein, oapA	R	General Functional Prediction only	43503083
WP_013035331.1	HVO_2889	nuclease	L	Replication and repair	43181417
WP_004042006.1	HVO_2122	ABC transporter ATP-binding protein	E	Amino Acid metabolis and transport	41926675
WP_004043005.1	HVO_2758	50S ribosomal protein L11	J	Tranlsation	41821000
WP_004044604.1	HVO_0319	V-type ATP synthase subunit D	C	Energy production and conversion	41746750
WP_004043028.1	HVO_2783	30S ribosomal protein S4	J	Tranlsation	40564025

ELY33434.1	HVO_2205	NADH dehydrogenase	R	General Functional Prediction only	39342417
WP_004044569.1	HVO_0354	30S ribosomal protein S7	J	Tranlsation	39151833
WP_004044637.1	HVO_0285	metalloprotease	R	General Functional Prediction only	38823917
WP_004041171.1	HVO_B0363	dimethylsulfoxide reductase	C	Energy production and conversion	38244083
WP_004041062.1	HVO_B0093	peptide ABC transporter substrate-binding protein	E	Amino Acid metabolis and transport	37982833
WP_004044352.1	HVO_0581	FtsZ2	D	Cell cycle control and mitosis	37763667
WP_004043701.1	HVO_1240	Tat pathway signal protein	P	Inorganic ion transport and metabolism	37480250
WP_004042101.1	HVO_2209	2-oxo acid dehydrogenase	C	Energy production and conversion	35712000
WP_004041843.1	HVO_1964	photosystem reaction center subunit H	R	General Functional Prediction only	35670417
WP_004042542.1	HVO_2537	hypothetical protein	S	Function Unknown	34985850
WP_004041964.1	HVO_2081	hypothetical protein	S	Function Unknown	34952000
WP_004043696.1	HVO_1245	DSBA oxidoreductase	O	Post-translational modification, protein turnover, chaperone functions	34886083
WP_004045186.1	HVO_0102	zinc metalloprotease HtpX	O	Post-translational modification, protein turnover, chaperone functions	34727583
WP_004044965.1	HVO_0009	L-cysteine desulfhydrase	E	Amino Acid metabolis and transport	34348167

Supplementary References

1. Delmas S, Duggin IG, Allers T (2013) DNA damage induces nucleoid compaction via the Mre11-Rad50 complex in the archaeon Haloferax volcanii. Mol Microbiol 87:168–179. https://doi.org/10.1111/mmi.12091
2. Raden M, Ali SM, Alkhnbashi OS et al. (2018) Freiburg RNA tools: a central online resource for RNA-focused research and teaching. Nucleic Acids Res 46:W25-W29. https://doi.org/10.1093/nar/gky329
3. Will S, Joshi T, Hofacker IL et al. (2012) LocARNA-P: accurate boundary prediction and improved detection of structural RNAs. RNA 18:900–914. https://doi.org/10.1261/rna.029041.111
4. Will S, Reiche K, Hofacker IL et al. (2007) Inferring noncoding RNA families and classes by means of genome-scale structure-based clustering. PLoS Comput Biol 3:e65. https://doi.org/10.1371/journal.pcbi.0030065
5. Gabler F, Nam S-Z, Till S et al. (2020) Protein Sequence Analysis Using the MPI Bioinformatics Toolkit. Curr Protoc Bioinformatics 72:e108. https://doi.org/10.1002/cpbi.108
6. Hartman AL, Norais C, Badger JH et al. (2010) The complete genome sequence of Haloferax volcanii DS2, a model archaeon. PLoS One 5:e9605. https://doi.org/10.1371/journal.pone.0009605
7. Allers T, Ngo H-P, Mevarech M et al. (2004) Development of additional selectable markers for the halophilic archaeon Haloferax volcanii based on the leuB and trpA genes. Appl Environ Microbiol 70:943–953. https://doi.org/10.1128/AEM.70.2.943-953.2004
8. Wolters M, Borst A, Pfeiffer F et al. (2019) Bioinformatic and genetic characterization of three genes localized adjacent to the major replication origin of Haloferax volcanii. FEMS Microbiol Lett 366. https://doi.org/10.1093/femsle/fnz238
9. Abu-Qarn M, Yurist-Doutsch S, Giordano A et al. (2007) Haloferax volcanii AglB and AglD are involved in N-glycosylation of the S-layer glycoprotein and proper assembly of the surface layer. J Mol Biol 374:1224–1236. https://doi.org/10.1016/j.jmb.2007.10.042
10. Duggin IG, Aylett CHS, Walsh JC et al. (2015) CetZ tubulin-like proteins control archaeal cell shape. Nature 519:362–365. https://doi.org/10.1038/nature13983
11. Ng WV, Kennedy SP, Mahairas GG et al. (2000) Genome sequence of Halobacterium species NRC-1. Proc Natl Acad Sci U S A 97:12176–12181. https://doi.org/10.1073/pnas.190337797
12. Erdmann S, Tschitschko B, Zhong L et al. (2017) A plasmid from an Antarctic haloarchaeon uses specialized membrane vesicles to disseminate and infect plasmid-free cells. Nat Microbiol 2:1446–1455. https://doi.org/10.1038/s41564-017-0009-2

Supplementary Material for the Addendum

Extended Data: Selective enrichment of intact polar lipids in extracellular vesicles of halophilic *Euryarchaeota*

Supplementary Figures

Supplementary Figure 1: Distribution of lipid compounds comparing whole cells, cell membranes and EVs of *H. volcanii* with permission from Mills et al. (2023).

Supplementary Figure 2: PCR screening for pR1SE on pre-cultures of *Hrr. lacusprofundi* strains.

Supplementary Figure 3: Example profile showing the fragmentation of PG-AR Na^+ adducts in MS2 analysis with increasing unsaturation from 0 to 6 double bonds.

Supplementary Figure 4: Example profile showing the C-AR Na^+ adducts in MS2 analysis with increasing unsaturation from 0 to 6 double bonds.

Supplementary Figure 5: Distribution of lipid compounds comparing whole cells, cell membranes and vesicles of *Hrr. lacusprofundi* strains DL18 and R1S1.

Supplementary Figure 6: Distribution of lipid compounds comparing whole cells, cell membranes and extracellular vesicles of *Hrr. lacusprofundi* strains UNSW and DSMZ.

Supplementary Tables

Supplementary Table 1: Average relative abundance of intact polar lipids given as percentage of total population in the whole cell, cell membrane and extracellular (EV) fraction for *H. volcanii*.

The raw data from the lipid measurements of *Hrr. lacusprofundi* samples will be deposited in an appropriate data repository upon submission of the manuscript for peer-review. It is currently available upon request.

Supplementary References

Bale, N. J., Sorokin, D. Y., Hopmans, E. C., Koenen, M., Rijpstra, I. C. W., Villanueva, L., Wienk, H., & Sinninghe Damsté, J. S. (2019). New Insights Into the Polar Lipid Composition of Extremely Halo(alkali)philic Euryarchaea From Hypersaline Lakes. *Frontiers in microbiology, 10*. doi:10.3389/fmicb.2019.00377

Kellermann, M. Y., Yoshinaga, M. Y., Valentine, R. C., Wörmer, L., & Valentine, D. L. (2016). Important roles for membrane lipids in haloarchaeal bioenergetics. *Biochimica et Biophysica Acta (BBA)-Biomembranes, 1858*(11), 2940-2956. doi:10.1016/j.bbamem.2016.08.010

Mills, J., Gebhard, L. J., Schubotz, F., Shevchenko, A., Speth, D. R., Liao, Y., Duggin, I. G., Marchfelder, A., & Erdmann, S. (2023). Extracellular vesicles of *Euryarchaeida*: precursor to eukaryotic membrane trafficking. *bioRxiv*. doi:10.1101/2023.03.03.530948

Yoshinaga, M. Y., Kellermann, M. Y., Rossel, P. E., Schubotz, F., Lipp, J. S., & Hinrichs, K.-U. (2011). Systematic fragmentation patterns of archaeal intact polar lipids by high-performance liquid chromatography/electrospray ionization ion-trap mass spectrometry. *Rapid Communications in Mass Spectrometry, 25*(23), 3563-3574. doi:10.1002/rcm.5251

Supplementary Figures

A.

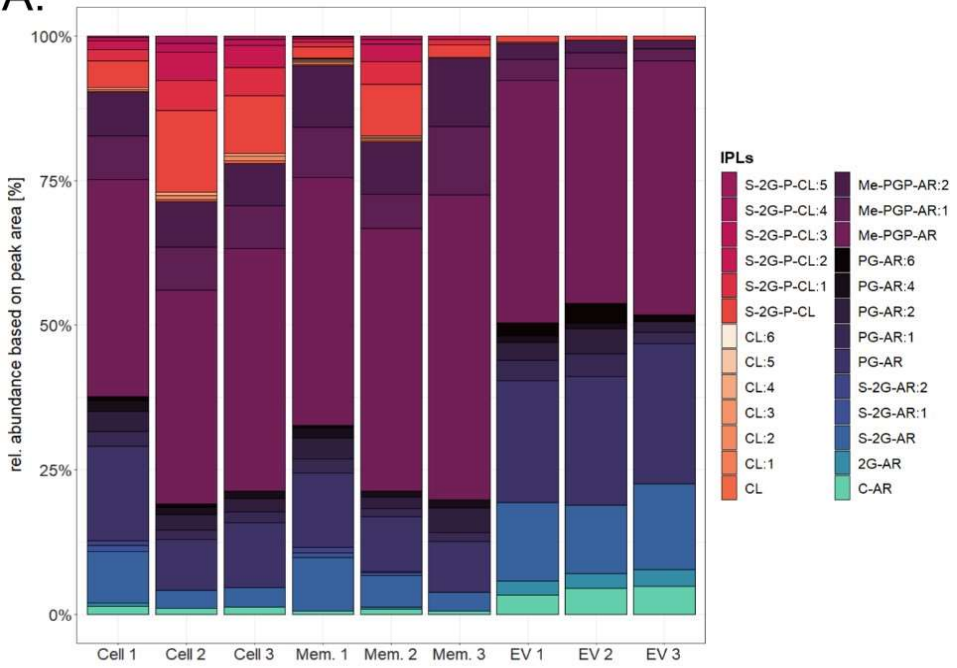

B.

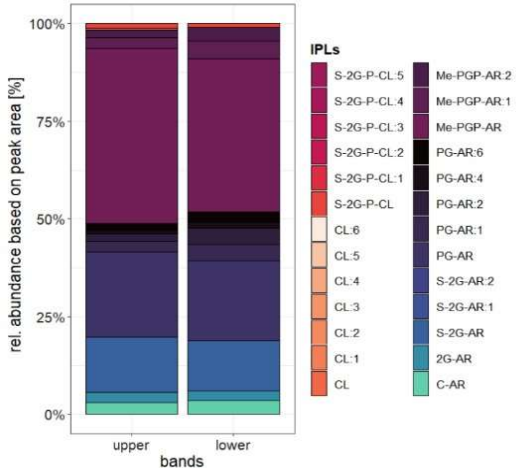

Supplementary Figure 1: Distribution of lipid compounds comparing whole cells, cell membranes and EVs of *H. volcanii* reproduced with permission from Mills *et al.* (2023). (A) Individual replicates used to calculate the average relative abundances in Figure 1. Cell 1-3: whole cells, Mem. 1-3: membrane fraction and EV 1-3: extracellular vesicles after ultracentrifugation in Optiprep™ density gradients and bands pooled together for each biological replicate. **(B)** The lipid distribution in the upper (left column) and lower band (right column) after ultracentrifugation from one biological replicate. Relative abundances were calculated based on the peak area of the most abundant adduct for each compound. Lipids were identified based on their retention time, fractionation pattern and exact mass Compound abbreviations: AR = archaeol (C_{20}-C_{20} isoprenoidal chains), CL = cardiolipin or dimeric phospholipid, :n = lipid with n number of unsaturations. Lipids with neutral headgroups: 1G = monoglycosyl, 2G = diglycosyl, C-AR = core-AR. Lipids with anionic headgroups: PGP-Me = phosphatidylglycerophosphate methyl esters, PG = phosphatidyl-glycerol, S-2G =sulfated diglycosyl, S-2G-P = sulfated diglycosyl-phospho.

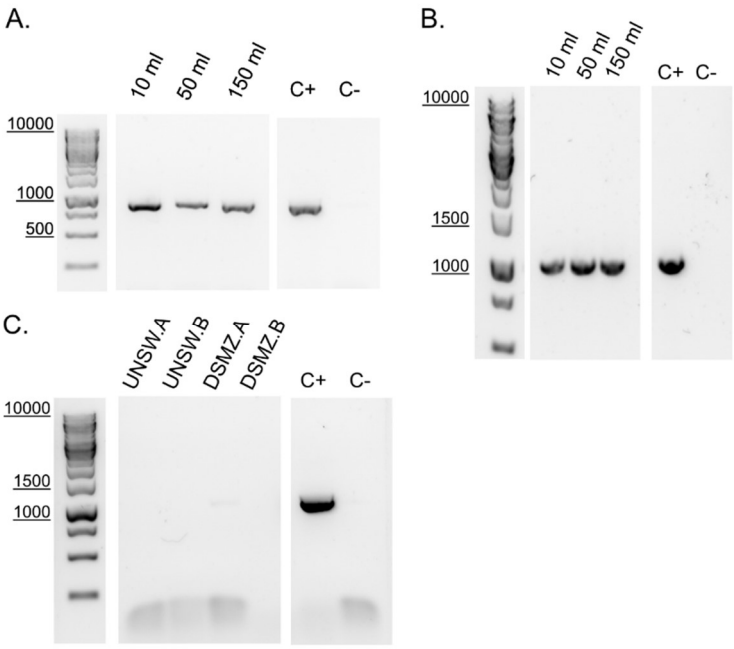

Supplementary Figure 2: PCR screening for pR1SE on pre-cultures of *Hrr. lacusprofundi* strains.

PCR with primers targeting a region of the pR1SE plasmid performed on aliquots of liquid cultures of *Hrr. lacusprofundi* DL18 **(A),** R1S1 **(B)** and ACAM34_UNSW and ACAM34_DSMZ **(C).** Samples were obtained from the first three pre-cultures for DL18 and R1S1 or from two 10 ml pre-cultures (A or B) for the two ACAM34 strains (C). Purified plasmid DNA (1 ng/µl) served as the positive control (C+), sterile ddH_2O served as the negative control (C-). First lane on the left: DNA Ladder (GeneRuler 1 kb Plus DNA Ladder, Thermo Scientific™), the DNA samples were separated on 1% agarose gels and stained with SYBR™ Safe.

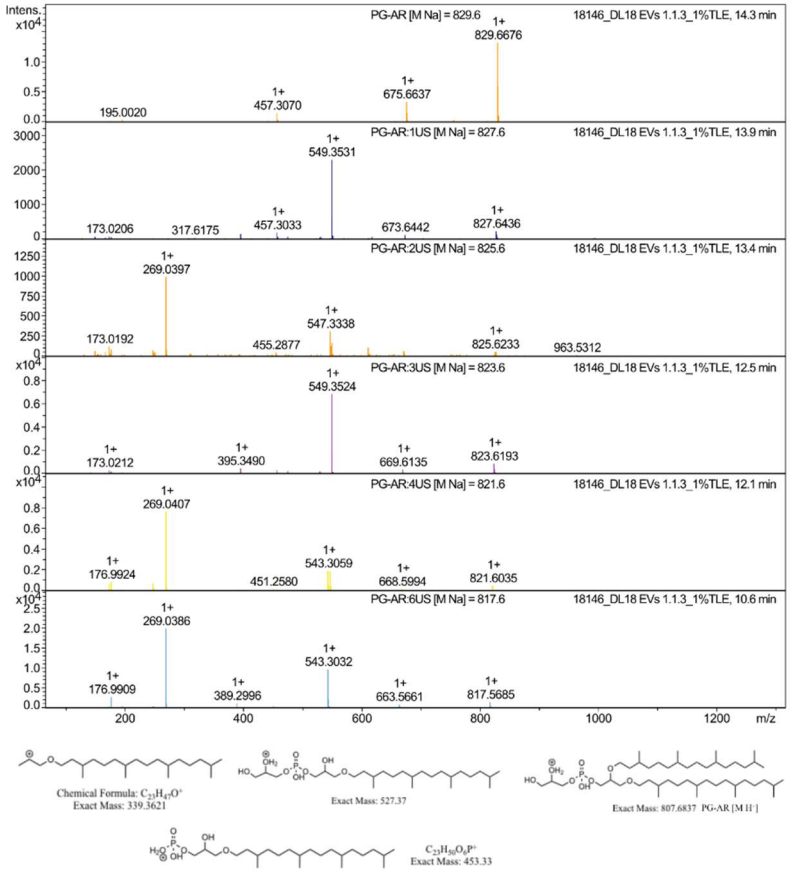

Supplementary Figure 3: Example profile showing the fragmentation of PG-AR Na^+ adducts in MS2 analysis with increasing unsaturation from 0 to 6 double bonds. Positive mode MS2 spectra (tandem mass spectrometry) are shown for PG-AR compounds obtained from the vesicle fraction of DL18 (sample EP 1.1.3, see Supplementary Figure 5). PG-AR Na^+ adducts are shown with increasing unsaturation going from the top to the bottom, with either 0, 1, 2, 3, 4 or 6 double bonds as indicated in their respective panels together with their predicted mass [M Na] and the retention time. Typical fragmentation products of the hydrogen adduct of PG-AR are shown at the bottom of the graph. Compounds were identified based on retention time, fractionation pattern and exact mass while accounting for the base adduct (Na^+ instead of H^+) and unsaturation state of the compound (Yoshinaga *et al.*, 2011; Kellermann *et al.*, 2016; Bale *et al.*, 2019). The mass to charge [m/z] of each fragment is indicated directly above it.

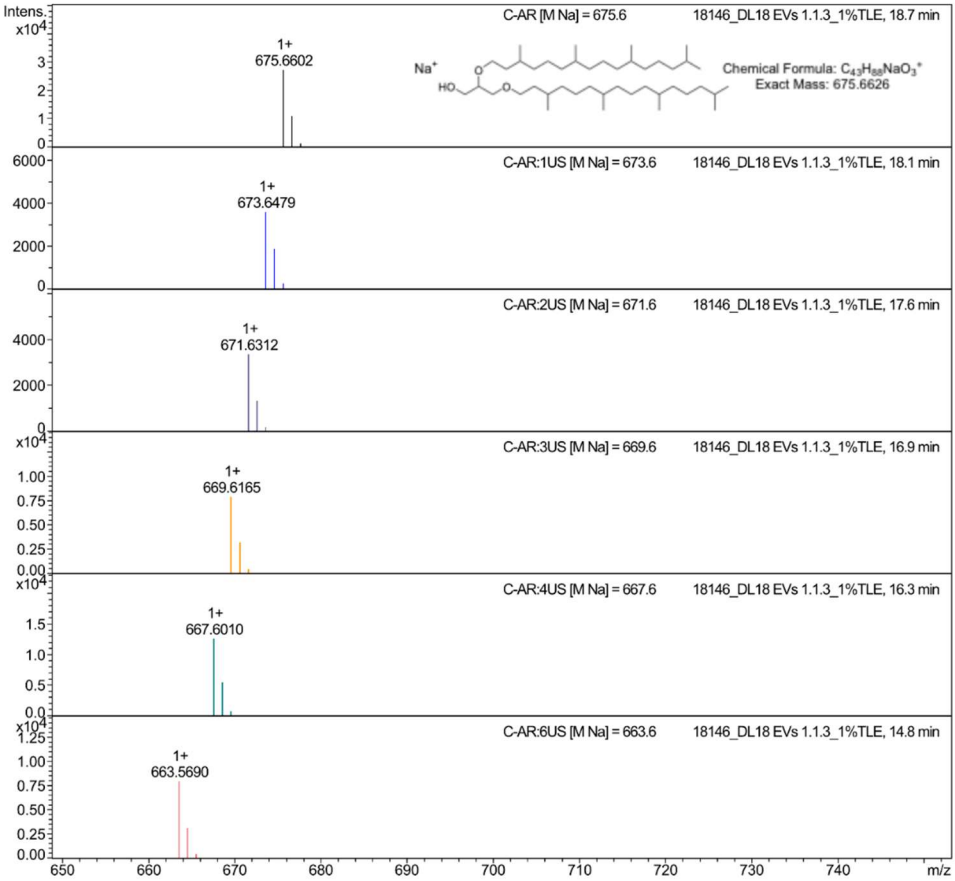

Supplementary Figure 4. Example profile showing the C-AR Na^+ adducts in MS2 analysis with increasing unsaturation from 0 to 6 double bonds. Positive mode MS2 spectra (tandem mass spectrometry) are shown for C-AR compounds obtained from the vesicle fraction of DL18 (sample EP 1.1.3, see Supplementary Figure 5). C-AR Na^+ adducts are shown with increasing unsaturation going from the top to the bottom, with either 0, 1, 2, 3, 4 or 6 double bonds as indicated in their respective panels together with the predicted mass [M Na] and the retention time. The structure of C-AR is shown in the first panel, Na^+ adducts of C-AR do not fragment. Compounds were identified based on retention time, and exact mass while accounting for the base adduct (Na^+ instead of H^+) and unsaturation state of the compound (Yoshinaga *et al.*, 2011; Kellermann *et al.*, 2016; Bale *et al.*, 2019). The mass to charge [m/z] of each fragment is indicated directly above it.

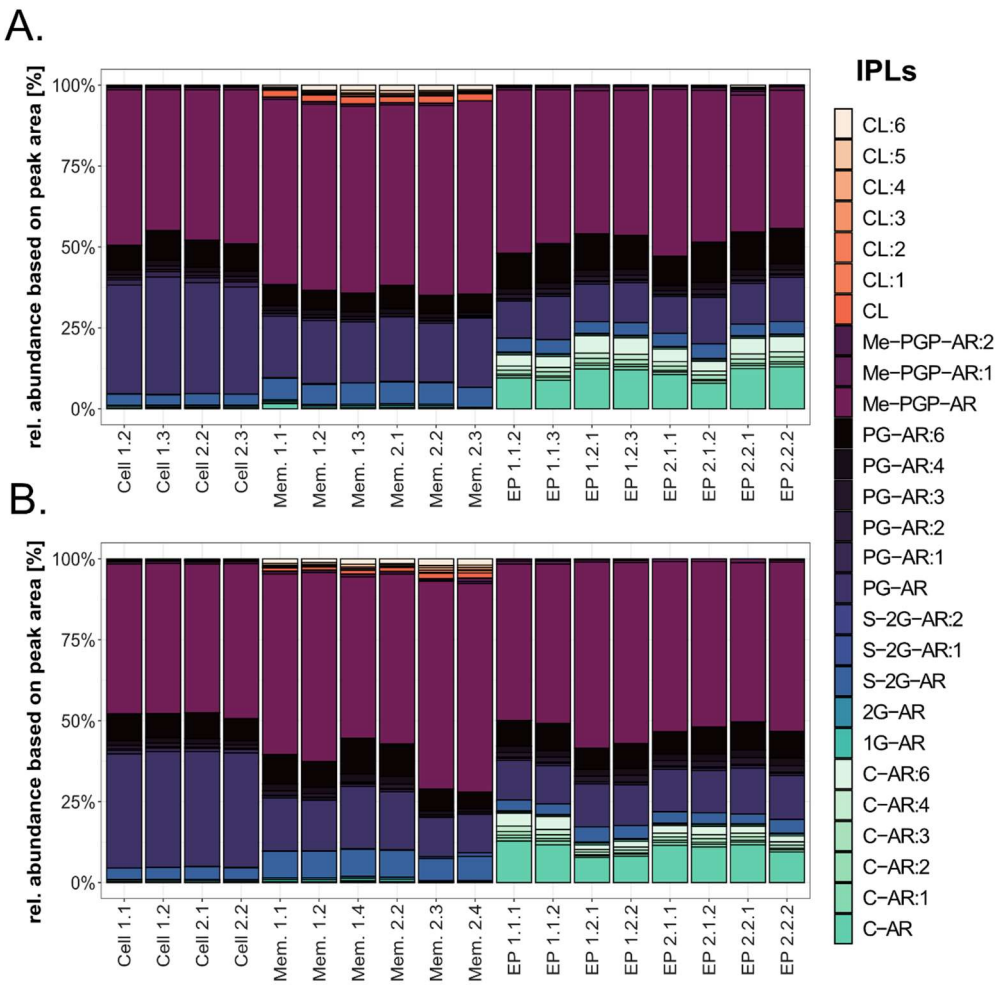

Supplementary Figure 5: Distribution of lipid compounds comparing whole cells, cell membranes and vesicles of *Hrr. lacusprofundi* strains DL18 and R1S1. Individual technical replicates of DL18 **(A)** and R1S1 **(B)** used to calculate the average relative abundances shown in Figure 2. For each biological replicate (n = 2, first number), several technical replicates were measured per fraction in order to calculate the average relative abundances. This included two technical replicates for lipid extraction for each biological repl. for the cellular fraction (Cell), and three technical repl. for the cell membrane samples (Mem.). The vesicle fraction (EP), containing both EVs and PVs, separated into two gradient bands after density gradient cen-

trifugation. However, as the overall lipid composition was very similar between samples obtained from different bands all vesicle samples were pooled for the calculation of average rel. abundances. The precise position is indicated by the number, where the first number indicates the biological repl. (1 or 2), the middle number the position in either the upper (1) or lower (2) gradient band, and the final number indicates the number of the technical repl. measured (1 or 2). Relative abundances were calculated based on the peak area of the most abundant adduct for each compound. Lipids were identified based on their retention time, fractionation pattern and exact mass. Compound abbreviations: AR = archaeol (C_{20}-C_{20} isoprenoidal chains), CL = cardiolipin or dimeric phospholipid, :n = lipid with n number of unsaturations. Lipids with neutral headgroups: 1G = monoglycosyl, 2G = diglycosyl, C-AR = core-AR. Lipids with anionic headgroups: PGP-Me = phosphatidylglycerophosphate methyl esters, PG = phosphatidyl-glycerol, S-2G =sulfated diglycosyl.

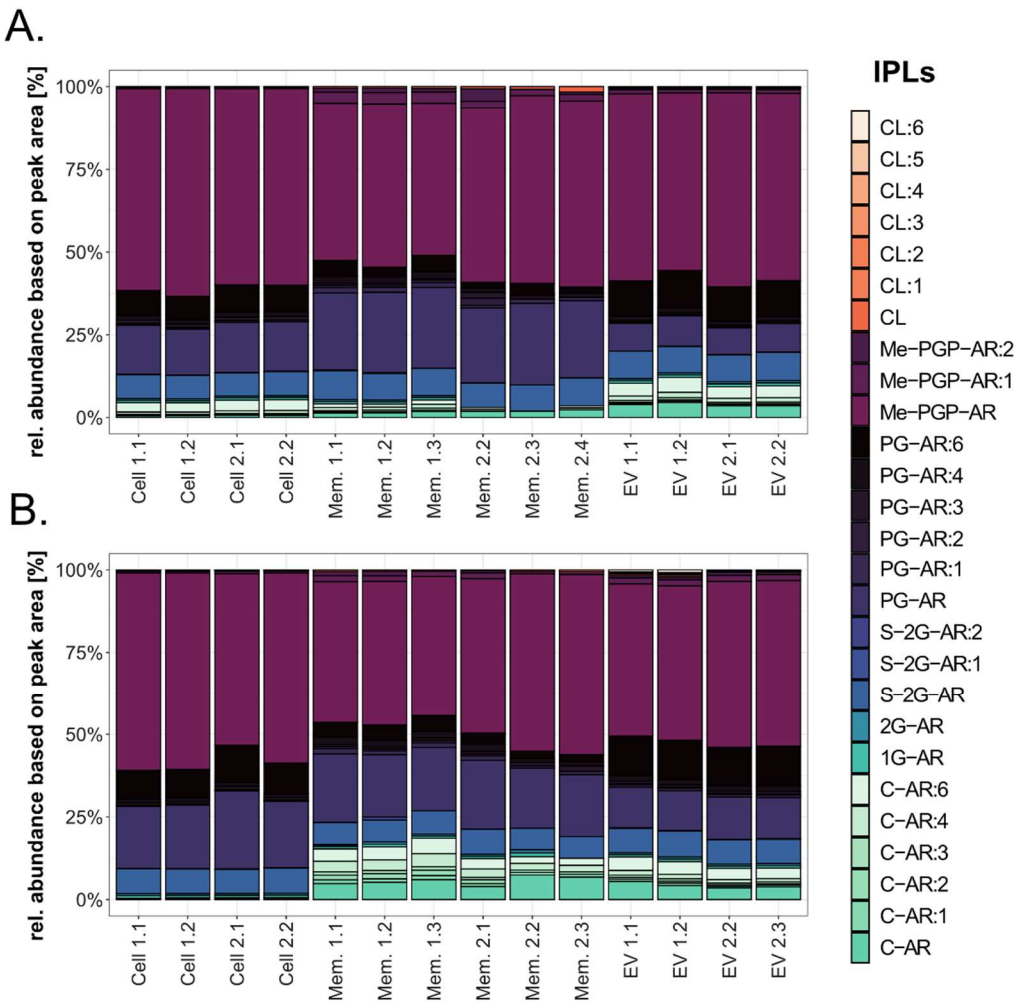

Supplementary Figure 6: Distribution of lipid compounds comparing whole cells, cell membranes and extracellular vesicles of *Hrr. lacusprofundi* strains UNSW and DSMZ. Individual technical replicates of UNSW **(A)** and DSMZ **(B)** used to calculate the average relative abundances shown in Figure 3. For each biological replicate (n = 2, first number), several technical replicates were measured per fraction in order to calculate the average relative abundances. This included two technical repl. for lipid extraction for each biological repl. for the cellular fraction (Cell), and three technical repl. for the cell membrane samples (Mem.). As no distinct bands were visible in the gradient after ultracentrifugation, samples from the vesicle fraction (EVs)

were pooled for the calculation of average rel. abundances with two technical repl. for each biological repl. Relative abundances were calculated based on the peak area of the most abundant adduct for each compound. Lipids were identified based on their retention time, fractionation pattern and exact mass. Compound abbreviations: AR = archaeol (C_{20}-C_{20} isoprenoidal chains), CL = cardiolipin or dimeric phospholipid, :n = lipid with n number of unsaturations. Lipids with neutral headgroups: 1G = monoglycosyl, 2G = diglycosyl, C-AR = core-AR. Lipids with anionic headgroups: PGP-Me = phosphatidylglycerophosphate methyl esters, PG = phosphatidyl-glycerol, S-2G =sulfated diglycosyl.

Supplementary Tables

Supplementary Table 1: Average relative abundance of intact polar lipids given as percentage of total population in the whole cell, cell membrane and extracellular (EV) fraction for *H. volcanii* see Mills *et al*. (2023). Average values were calculated from two independent biological replicates per fraction, per strain, with several technical replicates (see Supplementary Figure 1) and are given together with the standard deviation. Raw values are presented in Supplementary Table 13 of Mills *et al.* (2023), available at https://doi.org/10.1101/2023.03.03.530948. Compound abbreviations: AR = archaeol (C_{20}-C_{20} isoprenoidal chains), :US = unsaturated IPL. Lipids with neutral headgroups: 1G = monoglycosyl, 2G = diglycosyl, C-AR = core-AR. Lipids with anionic headgroups: CL = cardiolipin or dimeric phospholipid, Me-PGP = phosphatidylglycerophosphate methyl esters, PG = phosphatidylglycerol, S-2G = sulfated diglycosyl, S-2G-P = sulfated diglycosyl-phospho.

Compound	whole cell	cell membrane	EVs
Total unsaturated	32.5% ± 2.2%	31.3% ± 1.4%	15.6% ± 4.3%
Total saturated	67.5% ± 2.2%	68.7% ± 1.4%	84.4% ± 4.3%
PG-AR:US	6.7% ± 1.3%	6.7% ± 1.6%	10.4% ± 3.4%
PG-AR	12.1% ± 3.1%	10.4% ± 1.8%	22.2% ± 1.3%
Me-PGP-AR:US	15.1% ± 0.2%	19.4% ± 3.6%	5.2% ± 1.4%
Me-PGP-AR	38.8% ± 2.2%	47% ± 4.2%	41.6% ± 2.1%
S-2G-AR:US	0.6% ± 0.9%	0.8% ± 0.7%	0%
S-2G-AR	5.1% ± 2.7%	6% ± 2.5%	12.9% ± 1.4%
2G-AR	0.2% ± 0.25%	0.1% ± 0.15%	2.6% ± 0.2%
C-AR	1.2% ± 0.2%	0.6% ± 0.2%	4.1% ± 0.9%
CL:US	1% ± 0.5%	0.6% ± 0.4%	0%
CL	0.4% ± 0.05%	0.2% ± 0.1%	0.08% ± 0.2%
S-2G-P-CL:US	9.1% ± 3.6%	3.9% ± 3.1%	0%
S-2G-P-CL	9.6% ± 3.9%	4.4% ± 3.2%	0.8% ± 0.2%

Chapter IV

Plasmid vesicle formation is independent of the archaeal small vesiculating GTPase (ArcV) driven extracellular vesicle formation

Plasmid vesicle formation is independent of the archaeal small vesiculating GTPase (ArcV) driven extracellular vesicle formation

L. Johanna Gebhard[1], Lauren Queiss[1], Joshua Mills[1] &
Susanne Erdmann[1]

[1]Max Planck Institute for Marine Microbiology, Archaeal Virology, Celsiusstrasse 1, 28359, Bremen, Germany.

* The manuscript is in preparation and has not been revised by all authors

Author contributions: L.J.G. and S.E conceived the study, L.J.G. performed the majority of the experimental work, Analysis of the protein content and RNA content of EVs was performed by L.Q. and J.M. respectively, L.J.G drafted the manuscript with support from all authors, S.E. led the study.

Abstract

Plasmid vesicles (PVs) were first identified as packaging the pR1SE plasmid that infects the halophilic archaeon *Halorubrum lacusprofundi*. PVs are morphologically distinct from extracellular vesicles (EVs) produced by the host, and can disseminate the enclosed plasmid by infecting new host cells similar to a virus. However, it is still unclear whether PV formation is independent from the vesicle formation machinery of the host.

Recent studies indicate that EV formation in Euryarchaeota is dependent on initiation by a small GTPase (ArcV). Attempts of the deletion of the small archaeal vesiculating GTPase ArcV in *Halorubrum lacusprofundi* led to large genome re-organisation in three independent transformants, with a loss of ≥ 49 kb regions in the chromosome not adjacent to the targeted gene. Deletion of ArcV in *Hrr. lacusprofundi* did not prevent vesicle formation as previously described for a *Haloferax volcanii* ArcV mutant. Deletion mutants showed large irregular vesicles produced at approximately the same rate as the parental strain, that we attribute to the loss of one of two S-layer genes in the genome, leading to cell envelope instability. Lack of ArcV did not abolish PV particle release, but PV production and intracellular plasmid replication are negatively affected in the Δ*arcV* strain. We suggest that the loss of a *cdc6* protein in the deleted region on the host genome likely impacted pR1SE replication, indicating that the plasmid utilizes host replication proteins in addition to its own replication proteins. Nevertheless, since PV particle production is not prevented by the deletion of *arcV*, we conclude that PV production is independent of the host ArcV vesiculation machinery.

Introduction

Bacteria, Eukaryotes and Archaea all produce extracellular vesicles [EVs, Deatherage and Cookson (2012)] that may contain nucleic acids (Cai *et al.*, 2016; Koeppen *et al.*, 2016; Erdmann *et al.*, 2017; Moriano-Gutierrez *et al.*, 2020; Soler & Forterre, 2020; Mills *et al.*, 2023) in addition to other cellular components. They fulfil various roles as interaction vehicles between cells and their extracellular environment and have been linked to anti-viral defence (Manning & Kuehn, 2011), interactions of bacteria with multicellular organisms (Koeppen *et al.*, 2016; Moriano-Gutierrez *et al.*, 2020) as well as gene transfer in bacteria and archaea (Cai *et al.*, 2016; Erdmann *et al.*, 2017; Soler & Forterre, 2020). To date, the composition of EVs and the formation of EVs in Archaea has mainly been investigated for the *Sulfolobales,* (Ellen *et al.*, 2009; J. Liu *et al.*, 2021b) members of the *Thermoproteota* phylum [formerly known as *Crenarchaeota* Oren and Garrity (2021)]. The cell division machinery in *Sulfolobales* (Lindås *et al.*, 2008; Caspi & Dekker, 2018; Tarrason Risa *et al.*, 2020; Hurtig *et al.*, 2023) is homologous to the endosomal sorting complexes required for transport (ESCRT) system in eukaryotes (Henne *et al.*, 2011; McCullough *et al.*, 2018; Vietri *et al.*, 2020; J. Liu *et al.*, 2021b) and was shown to be involved in EV formation and the budding of viruses (J. Liu *et al.*, 2021a; J. Liu *et al.*, 2021b). Moreover, several studies have reported ESCRT homologues in metagenome-assembled genomes of the Asgard archaea superphylum (Spang *et al.*, 2015; Zaremba-Niedzwiedzka *et al.*, 2017; Lu *et al.*, 2020; Hatano *et al.*, 2022; Eme *et al.*, 2023) and in the genomes of the two cultured representatives so far (Imachi *et al.*, 2020; Rodrigues-Oliveira *et al.*, 2023).

A recent study indicates that EV formation in the major archaeal phyla *Euryarchaeota* and DPANN (Spang *et al.*, 2017) is likely driven by a different mechanism (Mills *et al.*, 2023). Mass spectrometry analysis of the composition of EVs produced by *H. volcanii* (*Euryarchaeota*) revealed eleven proteins

to be significantly enriched in EV preparations (Mills *et al.*, 2023). In addition to FtsZ2, which controls cell division (Liao *et al.*, 2018; Liao *et al.*, 2021), three CetZ proteins were identified, these tubulin-like proteins have been connected to cell shape, motility and cell-surface related functions (Duggin *et al.*, 2015; Brown & Duggin, 2023). Furthermore, other enriched proteins included transporters and many hypothetical proteins including a putative fusion protein (Mills *et al.*, 2023). Special focus was then paid to the enrichment of a small GTPase, *HVO_3014* (formerly known as OapA, re-named ArcV, see Wolters *et al.* (2019); Mills *et al.* (2023)) in *H. volcanii* EVs. OapA/Arc1 is a Rab-family-like GTPase, belonging to the Ras-superfamily of small GTPases (Mills *et al.*, 2023). A homologue of *HVO_3014* (Supplementary Figure 1), a Sar1-/Arf1-like small GTPase, likewise assigned to the Ras-superfamily, had previously been found in the vesicle samples of a variety of *Hrr. lacusprofundi* strains (Erdmann *et al.*, 2017). Knockout of *arcV* in *H. volcanii* led to impaired vesicle production [Mills *et al.* (2023), see Chapter III]. Ras-superfamily small GTPases were thus identified as drivers of EV formation in haloarchaea in addition to their regulatory functions in vesicle trafficking of eukaryotic cells by initiating vesicle coat formation (Kirchhausen, 2000; Nielsen *et al.*, 2008; Stenmark, 2009; Cui *et al.*, 2022). Eukaryotic viruses have been shown to exploit the cellular vesicle formation machinery at various stages of their life cycle including virus particle budding [(Votteler & Sundquist, 2013; Robinson *et al.*, 2018; Hassan *et al.*, 2021) and references therein]. Studies on hyperthermophilic archaea of the *Sulfolobus* genus have shown some of their viruses to be strictly dependent on the functional ESCRT machinery (Snyder *et al.*, 2013) or to down-regulate *escrt* genes to facilitate budding via asymmetric cell division (J. Liu *et al.*, 2021a). However, interactions of enveloped viruses with the GTPase-driven vesicle formation machinery of the *Euryarchaeota* remain to be identified.

The plasmid vesicles (PVs) that transfer the archaeal plasmid pR1SE between halophilic archaea (*Euryarchaeota*) show similarities to both host EVs

and enveloped viruses (Erdmann *et al.*, 2017; Gebhard *et al.*, 2023b). PVs are morphologically distinct from EVs produced by their host *Halorubrum lacusprofundi*, and can disseminate the enclosed plasmid by infecting new host cells similar to a virus. They are thought to use similar formation mechanisms as EVs, as the plasmid encodes pR1SE-specific proteins some of which include the same domains e.g. WD40 (Schapira *et al.*, 2017) as host proteins with predicted functions in EV formation (Erdmann *et al.*, 2017).
It is still unclear whether PV formation is dependent on the vesicle formation machinery of the host. Therefore, PVs represent an interesting model system to study vesicle formation as an 'intermediate' form with characteristics of both host EVs and membrane enveloped viruses.

Previous work on the composition of EVs produced by several *Hrr. lacusprofundi* strains also showed a number of host proteins which could play a role in EV and plasmid vesicle (PV) formation (Erdmann *et al.*, 2017). Notable among them was a CetZ-like protein, a BamB-like protein with a WD40 domain, showing similarities to the γ-subunit of the COPI complex which is involved in intracellular vesicle shuttling in eukaryotes (Faini *et al.*, 2013), and the aforementioned small GTPase (*Hlac_2746/arcV*). We generated a Δ*arcV* (*Hlac_2746)* mutant of *Hrr. lacusprofundi* to determine if the vesicle formation machinery is dependent on small Rab-family GTPases as was shown previously for the closely related *H. volcanii*. Analysis of the effect of ArcV deletion on the life-cycle of the specialized PVs (Erdmann *et al.*, 2017) could provide crucial new insights into their host dependency for cell entry and exit and determine their position between viruses, largely independent of the host machinery for cell exit, and extracellular vesicles produced by the host organism.

Methods

Strains and cultivation conditions

Halorubrum lacusprofundi ACAM34_UNSW [wild type, Mercier *et al.* (2022)] and its derivative strains ACAM34_UNSW_2.14 [escape mutant Mercier *et al.* (2022)], ACAM34_UNSWΔ*pyrE2* [parent, Gebhard *et al.* (2023a) see Chapter I], and ACAM34_UNSWΔ*pyrE2*Δ*Hlac_2746,* here referred to as UNSWΔpyrE2Δ*arcV* (Gebhard *et al.*, 2023a), were grown in rich DBCM2+ medium (Burns & Dyall-Smith, 2006). DBCM2+ contained per 1L: 180 g NaCl, 25 g MgCl, 29 g $MgSO_4 \cdot 7H_2O$, 5.8 g KCl, 1 g peptone (Oxoid, Basingstoke, United Kingdom), 0.5 g/l yeast extract (Oxoid) and 15 g agar for plates (Oxoid), dissolved in ddH_2O at pH 7.5. After autoclaving, 6 ml 1 M $CaCl_2$, 2 ml K_2HPO_4 buffer (Dyall-Smith, 2009), 4.4 ml 25 % (w/v) sodium pyruvate, 5 ml 1 M NH_4Cl, 1 ml SL10 trace elements solution and 3 ml vitamin 10 solution (Dyall-Smith, 2009) were added as supplements per litre of growth medium. Selection medium (DBCM2-), where peptone and yeast extract were replaced with 5 g/l casamino acids (Gebhard *et al.*, 2023a), was supplemented with pravastatin (with increasing concentrations) or 50 µg/ml uracil and 200 µg/ml 5-fluoroorotic acid as indicated. For growth on solid media, plates were incubated at 37 °C. Liquid cultures were incubated at 28 °C on orbital shakers at 120 rpm to delay biofilm formation in stationary phase.

Knockout of Hlac_2746 (arcV) in Hrr. lacusprofundi

The plasmid construction of pTA131_*hmgA_ΔHlac_2746* used to knock out the *arcV* equivalent *Hlac_2746* (Erdmann *et al.*, 2017) in *Hrr. lacusprofundi* ACAM34_UNSWΔ*pyrE2* was described in detail in a previous study [Gebhard *et al.* (2023a), see Chapter I]. Following passage through the *Escherichia coli dam*$^-$/*dcm*$^-$ de-methylation strain C2925 (New England Biolabs, Ipswich, MA, USA), plasmids were transformed into the haloarchaeal host following a polyethylene glycol (PEG) based protocol (Liao *et al.*, 2016;

Gebhard *et al.*, 2023a). Successful gene deletion required a double selection protocol with antibiotic and uracil auxotrophy selection pressures as established in Gebhard *et al*. (2023a), see Chapter I. Transformants were both plated on agar plates and transferred into liquid media (both DBCM2- with 7.5 µg/ml pravastatin) immediately following transformation. Sterile ddH_2O and a DNA aliquot of the methylated pTA131_*hmgA* vector were used as negative controls for transformation. After two successive dilutions into fresh medium, the third generation of liquid cultures was streaked onto agar plates (DBCM2- 7.5 µg/ml pravastatin) and successful pop-in of the vector was confirmed with colony PCR using forward and reverse primers prav_F & prav_R, respectively (see Supplementary Table 1) following a previously described PCR protocol [see Gebhard *et al.* (2023a) in Chapter I]. Two PCR-positive clones were selected for further cultivation and propagated over seven generations in liquid DBCM2- medium with increasing pravastatin concentrations (7.5, 2x 10, 2x 15 to 2x 20 µg/ml). Plasmid pop-out (Bitan-Banin *et al.*, 2003; Allers *et al.*, 2004) was initiated after eight generations by plating of diluted (10^{-2}-10^{-5}) liquid cultures onto agar plates (DBCM2- with 50 µg/ml uracil and 200 µg/ml 5-fluoroorotic acid).

Genome sequencing and analysis of mutants

Colonies were screened for successful gene deletion with genome sequencing primers (Hlac_2746KOF & KOR, see Supplementary Table 1) following a previously described PCR protocol (Gebhard *et al.*, 2023a). Identification of positive colonies was described in detail in a previous manuscript, see Gebhard *et al.* (2023a) in Chapter I. Partial deletion of *Hlac_2746*, hereafter referred to as *arcV*, was validated with in-house Sanger Sequencing using the same primer set on a ABI 3130xl Sequence Analyzer (Applied Biosystems, Foster City, United States). Deletion of the targeted region of *arcV* could be confirmed for three colonies: Δ*arcV*_2.1, Δ*arcV*_2.15, Δ*arcV*_2.19 which were selected for further analysis. Subsequently, library preparation

(FS DNA Library, NEBNext® Ultra™) and sequencing (Illumina HiSeq3000, 2 x 150 bp, 1 Gb per sample) were performed at the Max Planck-Genome-Centre Cologne (Germany). Read mapping of each clone to the reference genome of the wild type strain ACAM34_UNSW with 'geneious mapper' (Geneious Prime® 2023.1.2, Dotmatics, Boston, United States) with medium-low sensitivity and default settings confirmed gene deletion of *arcV* as no reads could be recruited for the targeted region. For genome comparison, the consensus of read recruitment to the reference genome was extracted, annotated with Prokka v1.14.5 (Seemann, 2014) and visualized with GenoVi 0.2.16 (Cumsille *et al.*, 2023). The amino acid sequences of ArcV from *H. volcanii* (*HVO_3014*), formerly known as OapA (Wolters *et al.*, 2019), and *Hrr. lacusprofundi* (*Hlac_2746*) were analysed and aligned with HHPred (Hildebrand *et al.*, 2009; Zimmermann *et al.*, 2018).

Production and purification of extracellular vesicles

EVs were isolated from the culture supernatant of different *Hrr. lacusprofundi* strains by centrifugation (45 min, 4,500 x *g*) and precipitated with 10% PEG_{6000} overnight at 4 °C. Vesicle preparations were resuspended in DBCM2 salt solution [DBCM2 without organic additives or supplements apart from $CaCl_2$, Mercier *et al.* (2022)] and subsequently filtered through 0.8, 0.45 and 2x 0.2 µm sized filters. For further purification, extracellular nucleic acids were removed from the samples with RNase A (NEB, 20 U/ml) and DNase I (NEB, 20 U/mL), following precipitation and resuspension in DBCM2 salt solution EVs were purified by ultracentrifugation (12 h at 150,920 x *g*) in OptiPrep™ density gradients (Sigma-Aldrich, St.Louis, United States). Images of parent and Δ*arcV*_2.1 EVs after OptiPrep™ density gradients were provided by Daniela Thies.

Electron microscopy

For Δ*arcV*_2.1, culture supernatant was directly used for electron microscopy after separation of cells and supernatant by centrifugation without further purification. EV preparations of other cultures were purified once with filtration after precipitation as described above. Micrographs were generated with transmission electron microscopy (TEM), after 5 min adsorption of EV aliquots to carbon-coated copper grids. Samples were stained with 2 % (w/v in ddH_2O) uranyl acetate for 1 min and imaged with a JEM2100 Plus TEM (at 200 kV).

Quantification of extracellular vesicle production

EVs were quantified from vesicle preparations with two methods previously described in Mills *et al*. (2023). For this purpose, EV production was compared between different strains of *Hrr. lacusprofundi,* firstly between parent and Δ*arcV* mutant and secondly between wild type ACAM34_UNSW and the escape mutant (ACAM34_UNSW_2.14). Vesicle preparations were purified by precipitation and filtration, as described above, from the supernatant of 50 ml liquid cultures in independent biological triplicates per strain. From these, half of the vesicle preparations were stained with 500 nM MitoTracker Green FM (Invitrogen, Waltham, United States) for 30 min, precipitated with 10 % PEG_{6000} and resuspended in DBCM2 salt solution (without organic additives). Relative fluorescence units (RFU) were measured in a DeNovix, DS-11 FX+ spectrophotometer with blue excitation at 470 nm and emission between 514 - 567 nm. For the parent and Δ*arcV*_2.1 strains, the remaining half was precipitated again using PEG_{6000} and resuspended in 100 µl 50 mM Tris-HCl pH 7.4. Subsequently, EVs were quantified with modified Western Blots, where 5 µl aliquots were spotted directly on nitrocellulose membranes (0.2 µm, Bio-Rad, Hercules, United States). After drying at RT for 90 min, membranes were incubated for 30 min in 3 % (w/v) skim milk powder in

1x TBS buffer (0.5 mM Tris-HCl pH 7.5, 15 mM NaCl in ddH_2O). The primary antibody against *Hrr. lacusprofundi* CetZ1 (*Hlac_1892),* custom-made order from Genosphere Biotechnologies (Boulogne-Billancourt, France), was diluted 1:1,000 into 3% milk powder in 1x TBS and incubated together with the membrane for 1 h, followed by two 10 min washing steps in 1x TBS-TT buffer (1x TBS with 0.05% Tween 20 and 0.05% Triton X, both v/v) and once with 1x TBS. The secondary antibody, HRP-conjugated anti-rabbit antibody (Promega), was also diluted 1:1,000 and let to bind over 1 h in 3% skim milk in 1x TBS. After two washing steps in 1x TBS-TT and 1x TBS respectively, the chemiluminescence reaction was initiated with Clarity Western ECL Substrate (Bio Rad) following the manufacturer's instructions. Relative chemiluminescence was measured with ImageJ (Schneider *et al.*, 2012) and averaged out of three technical replicates for every biological replicate, per strain.

Analysis of extracellular vesicles protein composition and RNA content

For protein analysis, EVs were isolated from the supernatant of 50 ml liquid cultures of *Hrr. lacusprofundi* parent and Δ*arcV*_2.1 strains (n = 3, each), purified and resuspended in 100 µl 50 mM Tris-HCl pH 7.4 as described above. Aliquots (10 µl) of each sample were mixed with 10 µl 8 M urea and 4 µl loading dye (0.2 g SDS, 1 mg Bromphenol Blue, 0.78 ml glycerol, 0.2 ml 0.5 M Tris pH 6.8 and 0.155 g DTT per 10 ml). Samples were cooked at 95 °C for 10 min, resolved by SDS-PAGE (8% acrylamide, Tris-HCl pH 8.8) and stained with Coomassie blue. For RNA analysis, EVs produced the parent and Δ*arcV_2.1* strain (n = 3, each) were purified in density gradients as described above. RNA extractions were performed following the protocol established in Mills *et al.* (2023), and the size distribution of small RNAs was determined in a Fragment Analyzer (Model 5300 from Agilent, Santa Clara, CA, USA) with the Agilent small RNA Kit (DNF-470) following the manufacturer's instructions.

Infection with pR1SE

Infection of the ACAM34_UNSWΔ*pyrE2*Δ*arcV*_2.1 strain with PVs containing the pR1SE plasmid was performed following an established protocol [see Gebhard, Vershinin *et al*., (2023), Chapter II]. The Δ*arcV*_2.1 mutant was compared to its parent strain in six biological replicates per strain including the uninfected controls ($n = 3$). For this purpose, PVs were isolated and purified from the supernatant *Hrr. lacusprofundi* strain DL18 (Erdmann *et al.*, 2017) as described above and mixed with host cells in a ratio of plasmid copy numbers (gcns) to receiving cells of 75 to 1. After 2 h, cell preparations were washed twice with sterile medium (10 min 10,000 x *g* centrifugation at RT) to remove unattached PVs and transferred into 50 ml of DBCM2+ medium containing 50 µg/ml uracil. A 2 ml aliquot was removed immediately from each culture for the 0 h.p.i. time point. Centrifugation (10 min at 14.000 x *g*) separated aliquots into supernatants and cell pellets, after which pellets were washed twice with sterile medium and snap-frozen with liquid nitrogen. Supernatant samples were precipitated with 10% PEG_{6000} and snap-frozen with liquid nitrogen. Growth of cultures was measured by optical density (OD) at 600 nm at 28 °C and 120 rpm over seven days. Additional samples for qPCR were removed during early infection (ca. 20 h.p.i.), early exponential growth (ca. 40 h.p.i.) and during late exponential growth (ca. 60 h.p.i.) and treated as described for above. Cultures were diluted into fresh medium once $OD_{600\,nm}$ reached approx. 1.5 in order to track PV infection over a longer timeframe as established for pR1SE infections [Gebhard *et al.* (2023b), see Chapter II]. Here samples were again taken during comparable stages of growth.

qPCR quantification

For qPCR quantification, DNA was extracted from cell pellets and supernatant samples with the Isolate II Genomic DNA Kit (Bioline, London, United

Kingdom) following the manufacturer's protocol. pR1SE gcns were quantified by qPCR following the protocol established in Gebhard, Vershinin *et al.*, (2023), primer sets and reaction conditions are listed in Supplementary Table 1. All reactions were performed in 10 µl reactions containing 1x SsoAdvanced Universal SYBR Green Supermix (Bio-Rad) in a CFX96 Touch Real-Time PCR machine (Bio-Rad Laboratories). The qPCR programme was set to 5 min at 95 °C followed by 30 s at 95 °C and 30 s at 61 °C or 67.8 °C for 35-40 cycles (see Supplementary Table 1). Only assays with efficiencies calculated to 95 - 105% and $R^2 \geq 0.98$ were included in the final analysis. All statistical analysis was performed with R version 4.1.2 (R. C. Team, 2021) and RStudio (R. Team, 2023). The effect of strain on titres and plasmid-host-ratios at each time point was determined by two-sided, unpaired Student's *t*-tests. Normal distribution and homogeneity of variances of sub-datasets were confirmed based on the consensus of Shapiro–Wilk's Test, F-Test, Bartlett's Test (Snedecor & Cochran, 1989), Levene's Test (Levene, 1960) and Fligner–Killeen's Test (Fligner & Killeen, 1976).

Results

Genome Sequencing reveals large genomic re-organisation in three ΔarcV clones

Knockout of ArcV was attempted with the pop-in pop-out method in the uracil auxotrophic mutant of *Hrr. lacusprofundi* (Gebhard *et al.*, 2023a). No growth was detected on plates after transformation, but growth was observed in liquid cultures with no apparent contamination in the two negative controls. After the forced plasmid excision from the prospective deletion mutants, three colonies were identified as deletion mutants after colony PCR (Supplementary Figure 2) were selected for further confirmation by genome sequencing.

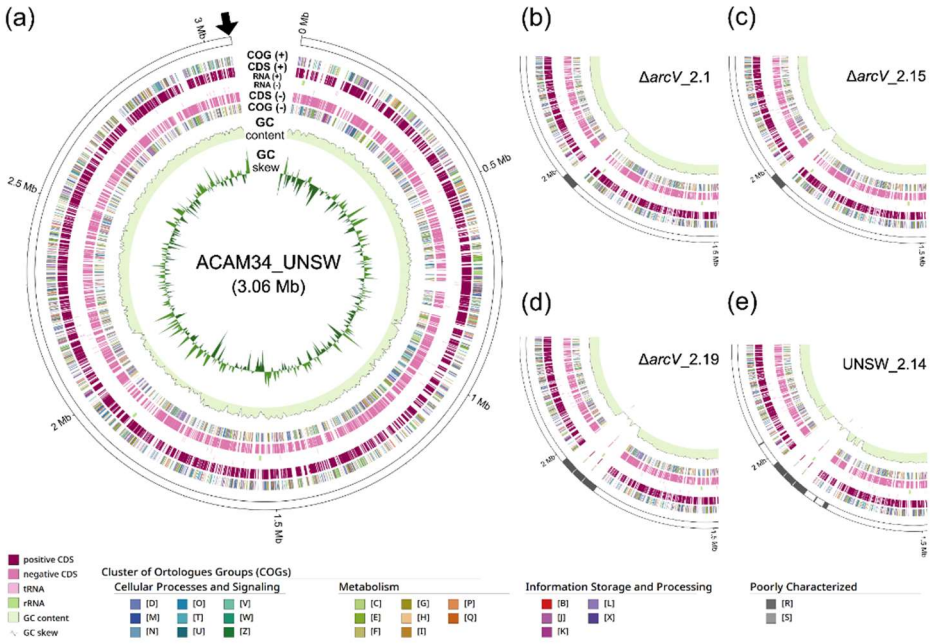

Figure 1: Genome comparison of the wild type strain ACAM34_UNSW with the three Δ*arcV* mutant strains and the virus resistant escape mutant UNSW_2.14. **(a)** Single replicon of the wild type strain ACAM34_UNSW (Mercier *et al.*, 2022) and relevant sections of the replicons of the daughter strains Δ*arcV*_2.1 **(b)**, Δ*arcV*_2.15 **(c)**, Δ*arcV*_2.19 **(d)** and UNSW_2.14 **(e)**. The genomic position is indicated on the outer white ring (Mb), the missing regions on the replicons of daughter strains are represented graphically in dark grey (approximation). The approximate position of *arcV* is indicated for the wild type replicon with a black arrow. The following circles represent respectively; the positions of clusters of orthologous groups (COGs) categories of coding sequences (CDSs) on the replicon with either forward (+) or negative (-) orientation, positions of tRNA-encoding genes (pink), rRNA-encoding genes (green), GC content (light green) and GC skew (dark green). The colour coding of COGs categories is indicated in the legend at the bottom. All genomes were annotated with Prokka (Seemann, 2014) and visualized with GenoVi (Cumsille *et al.*, 2023).

Read recruitment to the reference genome of the wild type ACAM34_UNSW strain [Mercier *et al.* (2022), see Figure 1A], revealed large ≥ 47 kb deletions at the position of approx. 1.9 Mb in addition to the expected in-frame deletion of *arcV* next to the origin of replication of the main host chromosome (Supplementary Figure 3). Two strains Δ*arcV*_2.1 (Figure 1B) and Δ*arcV*_2.15

(Figure 1C) show deletions of near identical size (approx. 49 kb) and position (1,933,408 bp to 1,982,442 bp and 1,933,417 bp to 1,982,419 bp). Both are flanked by two copies of the ISH3 family transposase ISHla1 (Siguier *et al.*, 2006; Filée *et al.*, 2007) with 100% identity (*ACAM34_UNSW01949* and *ACAM34_UNSW01989*). Two additional copies of the ISHla1 transposon (*ACAM34_UNSW01869* and *ACAM34_UNSW01984*) also enclose the larger deletion in Δ*arcV_2.19* (approx. 111 kb, positions 1,853,999 bp to 1,977,476 bp, Figure 1D). This mirrors the gene loss attributed to transposase activity previously observed in ACAM34_UNSW_2.14 after the strain acquired resistance to a lytic virus, HRTV-DL1, following infection over several generations (Mercier *et al.*, 2022). Here, the deleted region spans circa 200 kb with deleted sections from 1,781,187-1,806,805 bp, 1,853,999 bp to 1,977,375 bp and 2,054,778-2,047,260 bp (Figure 1E). In both cases a few coding sequences retain sequence coverage in the missing regions. These genes are predicted transposases (ISH3 family transposases) and likely represent an artefact from read mapping to multiple positions to the reference genome of the wild type. The missing regions in the three deletion mutants and the virus-resistant mutant cover a wide range of all major COG categories and notable genes include one of two surface (S-) layer proteins (*Hlac_2976*) and a Cdc6 protein (initiation of replication, *Hlac_2858*).

Characterization of the extracellular vesicles produced by the mutant.

The deletion of the *arcV* gene was previously shown to hinder extracellular vesicle (EV) formation in *H. volcanii* (Mills *et al.*, 2023). Therefore, EV production was compared between different strains of *Hrr. lacusprofundi,* namely between the parent strain and the newly generated Δ*arcV* mutant. Additionally, we compared EV production between wild type ACAM34_UNSW and a virus-resistant mutant (escape mutant ACAM34_UNSW_2.14) that lost the second S-layer gene, by a similar deletion as in the Δ*arcV*_2.1 mutant (see Figure 1E), to infer on the influence of

the S-layer gene deletion on EV production. Micrographs of EVs obtained directly from the culture supernatant of Δ*arcV_2.1* strain showed comparatively large and irregularly shaped EVs (Figure 2A-B). This kind of highly unusual EV morphology was not observed in purified preparations from the parent strain or the escape mutant (Supplementary Figure 4). Moreover, Δ*arcV* vesicle preparations behaved differently in gradient ultracentrifugation suggesting a different density distribution of the EV population of the parent strain (Supplementary Figure 4). Nevertheless, we could not detect a significant difference in EV quantity between parent and Δ*arcV* strain with either quantification method (Figure 2B, Supplementary Figure 5). In general, the parent, Δ*arcV_2.1* and wild type ACAM34_UNSW strains appear to show comparable rates of EV production, whereas the escape mutant UNSW_2.14 appears to produce noticeably fewer EVs.

Comparison of EV composition between parent and Δ*arcV_2.1* strains showed shifts in total protein content obtained from equal volumes of liquid culture (Supplementary Figure 6). Individual proteins were not identified yet, but the largest difference was observed in the size fraction between 95 – 250 kDa, likely containing components of the vesicle coat. Moreover, Δ*arcV_2.1* EVs contained significantly lower amounts of small RNAs with a narrower size distribution compared to the parent strain (Supplementary Figure 7). Small RNAs are generally enriched in the EVs of *Hrr. lacusprofundi* and other haloarchaea (Mills *et al.*, 2023) and may facilitate communication between cells in a population.

Infection with the pR1SE plasmid is inhibited in the ΔarcV strain.

In order to determine to which extent pR1SE reproduction is dependent on ArcV as well as the impact of the large-scale deletions including one of two host S-layer genes, we infected the Δ*arcV* mutant 2.1, with the pR1SE plasmid and tracked infection over time in comparison to the parent strain.

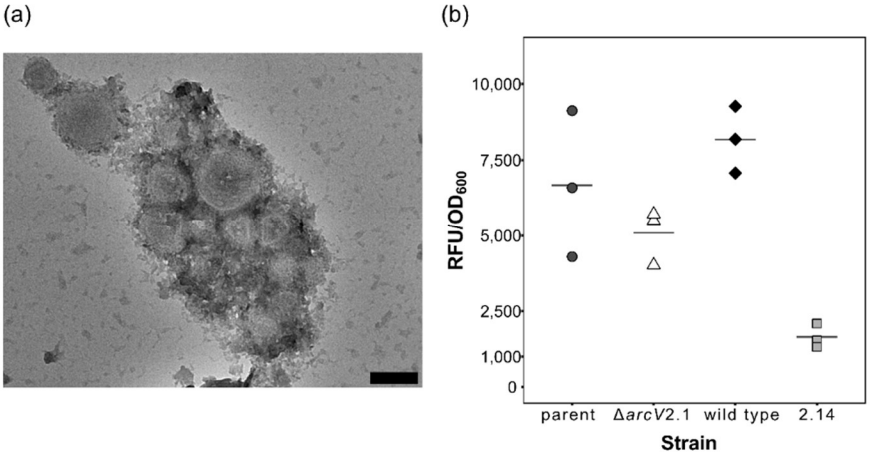

Figure 2: Unusual extracellular vesicle morphology in the Δ*arcV* mutant. Electron micrographs of EVs isolated directly from the culture supernatant of the Δ*arcV*_2.1 strain without further purification (a). The black scale bars represent 100 nm. (b) EV quantification from purified vesicle preparations from the parent (dark grey circles), Δ*arcV*_2.1 (white triangles), wild type (black diamonds) and escape mutant UNSW_2.14 strains (light grey squares). Relative fluorescence (RFU) normalized to OD_{600} is shown for three biological replicates per strain; the average is indicated by a grey line.

The infection efficiency after 2 hours of adsorption was noticeably higher in the Δ*arcV* mutant (10.56% ± 7.61%, $n = 3$) compared to the parent strain (3.45% ± 1.92%, $n = 3$).

Following the growth of cells over time, no notable difference in growth could be detected between the deletion mutant in comparison to the parental strain. Plasmid pR1SE genome copy numbers (gcns) were already detected in the supernatant of infected cultures at 20 hours post infection (h.p.i., Figure 3A). Titres reached maximal values of $6.33 \times 10^{+8}$ ($\pm 3.26 \times 10^{+8}$, $n = 3$) at 68 h.p.i. for the Δ*arcV*_2.1 strain and $7.87 \times 10^{+8}$ ($\pm 3.15 \times 10^{+8}$, $n = 3$) at 43 h.p.i. for the parent strain during the first part of the growth curve. The development of plasmid titres over time appeared to point towards a delayed

production of PVs in the deletion mutant. This observation was supported by the intracellular plasmid genome copies normalized to the main chromosome copies (plasmid-host-ratios, Figure 3B). Here, after initial increase in the Δ*arcV* mutant immediately post infection, which was reflected in the higher infection efficiency of pR1SE in the deletion mutant, plasmid-host-ratios decreased over time before rising again at 68 h.p.i..

Ratios increased in both strains after the dilution of cultures at 70 h.p.i, reaching their maximal values at 92 h.p.i. with 15.4 ± 1.1 ($n = 3$, parent) and 8.6 ± 0.6 ($n = 3$, Δ*arcV*) and either stagnated or declined slowly over the remaining incubation time. Nevertheless, plasmid-host-ratios in the Δ*arcV* mutant consistently stayed below the ratios recorded for the parent strain during the extended growth curve after 70 h.p.i. (Figure 3C) developments of plasmid titres again mirrored each other but showed a clear delay in the Δ*arcV* strain. While plasmid titres decreased over time after their initial peak at 91 h.p.i for the parent strain ($3.61 \times 10^{+9} \pm 3.8 \times 10^{+8}$, $n = 3$), plasmid titres in the Δ*arcV* strain reached their peak a day later at 115 h.p.i ($3.61 \times 10^{+9} \pm 3.8 \times 10^{+8}$, $n = 3$). Therefore, we conclude that all steps of the pR1SE life cycle are able to proceed despite the deletion of the *arcV* gene in the host. Uptake into the cell is increased while genome replication and particle release appear to be reduced in comparison to the control.

Discussion

PVs exhibit characteristics of both host EVs and membrane enveloped viruses yet it is still unclear to what degree PV formation is dependent on the EV formation machinery of the host. We deleted the *arcV* gene (*Hlac_2746*) in *Hrr. lacusprofundi* in order to determine the effect that this enzyme with a central function in EV formation would have on PV formation.

Genome sequencing revealed that all three clones of the Δ*arcV* deletion contained large genomic deletions in a region of the main chromosome, which is not adjacent to the targeted *arcV* gene. Therefore, these deletions are unlikely to have been caused by vector excision from the genome during pop-out as the final step of target gene deletion (Bitan-Banin *et al.*, 2003; Allers *et al.*, 2004). Moreover, as the deletions are located in the same region of the chromosome, but are not identical we consider the three strains to be distinct strains. Long-term cultivation of ACAM34 under laboratory conditions had led to the fusion of chromosome 1 and parts of chromosome 2 of the type strain (Anderson *et al.*, 2016) into one large chromosome found in the ACAM34_UNSW strain (Mercier *et al.*, 2022). Interestingly, the position on the genome and the size of the deleted regions closely mirror the genome re-organisation previously described for the virus resistant strain ACAM34_UNSW_2.14 (Mercier *et al.*, 2022).

This mutant acquired full resistance against the lytic virus HRTV-DL1 over long-term exposure at low multiplicity of infection at infection. The loss of approx. 200 kb was attributed to transposase activity in the region of the host chromosome containing parts of the former chromosome 2. This major re-organisation of the genome in the same region of the chromosome of ACAM34_UNSW has now been observed after two entirely different experiments; firstly, as a response to viral infection and secondly after the in-frame deletion of a gene located in a different region of the chromosome. Similar re-arrangements of genomes with large insertions into the main chromosome likely caused by transposase activity have also been described in other haloarchaea under laboratory conditions (Pfeiffer *et al.*, 2008; Hawkins *et al.*, 2013; Pfeiffer *et al.*, 2020). We propose that the region of the integrated former chromosome 2 flanked by several copies of the ISH3 family transposase ISHla1 (Siguier *et al.*, 2006; Mercier *et al.*, 2022) is vulnerable to transposase activity as a stress response of the host.

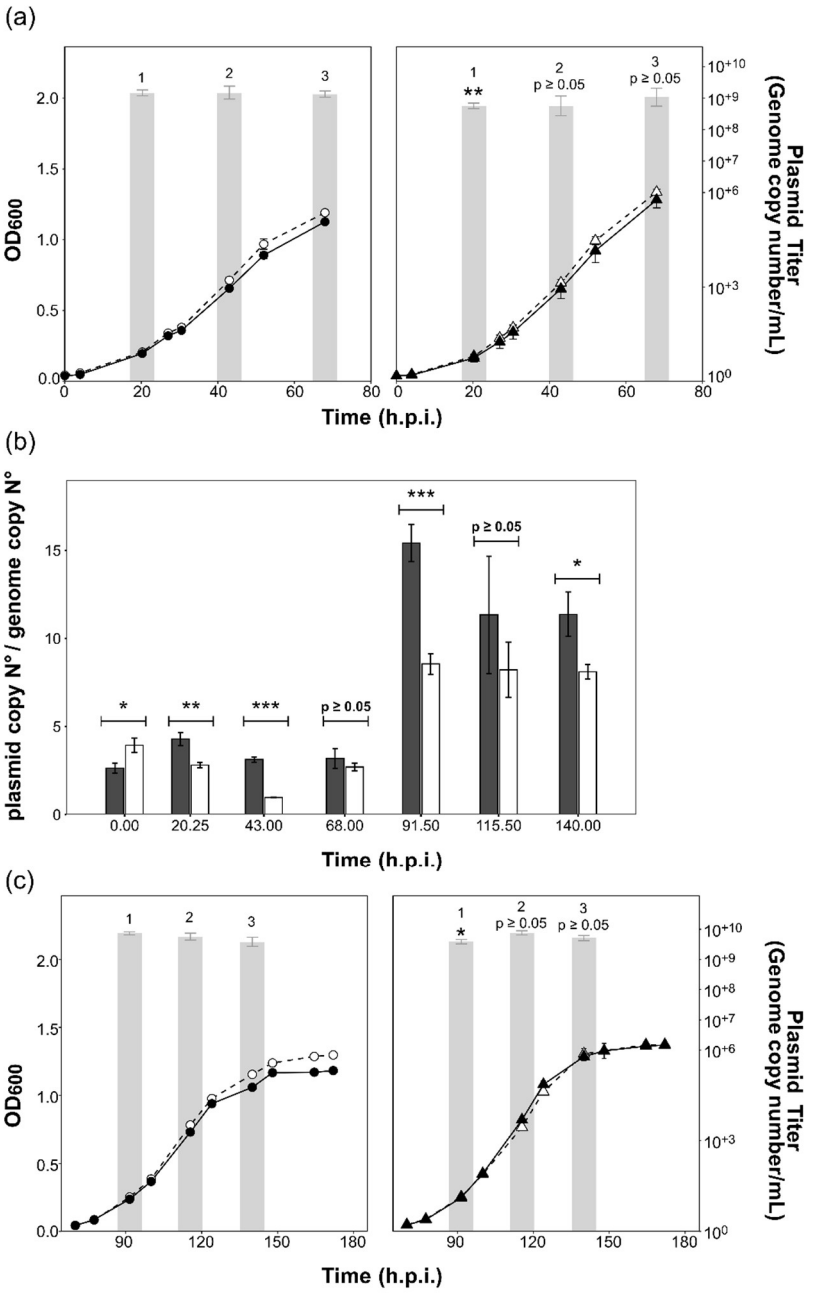
(a)
OD600
Plasmid Titer
(Genome copy number/mL)
Time (h.p.i.)
1
2
3
**
p ≥ 0.05
(b)
plasmid copy N° / genome copy N°
Time (h.p.i.)
*
**
***
p ≥ 0.05
0.00
20.25
43.00
68.00
91.50
115.50
140.00
(c)
OD600
Plasmid Titer
(Genome copy number/mL)
Time (h.p.i.)

Figure 3: Infection life cycle of the pR1SE plasmid is delayed in the Δ*arcV* strain. (a) Growth of *Hrr. lacusprofundi* parent (circles) and Δ*arcV*_2.1 (triangles) strains was monitored by OD_{600} (primary-axis) in biological triplicates (average of n = 3 ± standard deviation of the mean) for both uninfected controls (black, solid line) and pR1SE-infected (white, dashed line) cultures over time (hours post infection). Plasmid copy numbers per ml of infected cultures were quantified by qPCR and represented in logarithmic scale (to base 10) on the secondary y-axis (average of n = 3 ± standard deviation of the mean). Titers at each time point (numbered) were compared between strains with two-sided, unpaired student's t-tests, indicated in the graph on the right using the following significance codes: '***' for $p < 0.001$, '**' for $p < 0.01$, '*' for $p \leq 0.05$ and $p \geq 0.05$. **(b)** Plasmid to host ratios within cells are represented over time (h.p.i.) as pR1SE genome copy numbers to main host chromosome numbers per ng of DNA (average of n = 3 ± standard deviation of the mean) for the parent (dark grey) and Δ*arcV_2.1* (white) strains. Statistical significance is indicated in the graph using the same significance codes described above for (a). **(c)** Extended growth after dilution of the cultures shown in (a) at 68 h.p.i. with identical graphical representation and statistical analysis.

The deletion of the small vesiculating GTPase ArcV is not lethal in *Hrr. lacusprofundi* but leads to major restructuring of genome as the organism presumably struggles in the absence of *ArcV.* Screening of additional replicates after *arcV* deletion could solidify this hypothesis.

In the absence of unaffected mutants, we chose the Δ*arcV* clone 2.1, with the comparatively smallest genomic deletion, for further characterisation. In contrast to the previously reported deletion of *arcV* in *H. volcanii*, we observed extracellular vesicles (EVs) in the supernatant of Δ*arcV* cultures. EV quantification did not show a significant difference between the Δ*arcV* mutant and parent strain with either method. However, in contrast to EVs produced by the wild type ACAM34_UNSW or the ACAM34_UNSWΔ*pyrE2* parent strain EVs were noticeably larger and irregular in shape. We observed changes to the total protein content of EVs and a significant reduction in the small RNA content of Δ*arcV*_2.1 EVs. In our hypothesis, this could be the result of cell envelope instability expressed as over-vesiculation following the loss of one of two S-layer genes in conjunction with the deletion of *arcV* disrupting the regular formation of EVs and the packaging of small RNAs into EVs. Initial attempts to determine whether the deletion of the S-layer gene

indeed leads to hypervesiculation failed, because the UNSW_2.14 strain showed decreased EV production when compared to the parental strain. While we infer that the large deletion in the Δ*arcV* mutants is involved in causing instability of the cell envelope and vesicle formation in the Δ*arcV* mutants, it needs to be confirmed by targeted gene knockouts whether this morphology is indeed caused directly by the loss of the S-layer or other genes in the affected region. However, the changes in RNA and protein content of EVs produced by the Δ*arcV_2.1* strain strongly suggest that regular EV production is disrupted beyond what could be explained by cell envelope destabilization. Despite major genome re-organization and strange EV morphology, we did not observe major growth deficits in the deletion mutant. As for the escape mutant UNSW_2.14 (Mercier et al., 2022), one S-layer gene appears to be sufficient to retain cell integrity and growth under optimal conditions.

Haloferax Pleomorphic Virus-1 (Alarcón-Schumacher *et al.*, 2022) a membrane enveloped pleolipomorphic virus (Bamford *et al.*, 2017) was able to successfully infect and produce particles in the *H. volcanii* Δ*arcV* mutant despite the lack of EV production (J. Mills personal communication). Hence, we wanted to test whether the infectious pR1SE plasmid would likewise be able to successfully infect the *Hrr. lacusprofundi* Δ*arcV*_2.1 strain. Thus, our initial hypothesis had to be adjusted since the deletion of the small vesiculating GTPase did not have the same effect in *Hrr. lacusprofundi* as it did in *H. volcanii*. Nevertheless, we conclude that PV production is independent from ArcV-driven EV formation.

Initial infection efficiency and plasmid-to-host ratios were significantly higher in the mutant strain, suggesting that plasmid uptake into cells could have

potentially benefitted from a looser cell envelope due to irregular EV production in the mutant. However, over time both intracellular plasmid-to-host ratios and extracellular plasmid titres in the mutant were lower than those recorded for the parent strain, indicating that replication and particle release are delayed in the Δ*arcV* mutant. Since plasmid titres were recorded within the same order of magnitude for both strains, deletion of *arcV* does not appear to prevent pR1SE replication and PV formation and release. Furthermore, incidental packaging of pR1SE into EVs produced by the host would be expected to either produce a more irregular pattern or to be closely tied to the growth rate of the host. At this point, it is difficult to determine whether the delay in the pR1SE life cycle is directly caused by the deletion of *arcV*. The missing genomic region of the Δ*arcV* strain contains a Cdc6/Orc1 replication initiation protein (*Hlac_2958, ACAM34_UNSW01965*). pR1SE encodes a Cdc6/Orc1 protein (ORF29) adjacent to a predicted origin of replication additionally to the putative plasmid replication protein RepH [ORF1, Erdmann *et al.* (2017)]. The reduced pR1SE copy numbers in the mutant that has lost a Cdc6 protein could indicate that host Cdc6 proteins recognize the same origin leading to enhanced pR1SE replication.

This study expands and complements previous observations made on the PV life cycle (Gebhard *et al.*, 2023b), plasmid-host-ratios and extracellular titres of pR1SE both appear to increase during exponential growth of the host and plateau from early stationary phase onwards. The plasmid-to-host ratios recorded for pR1SE here also remain comparatively high for haloarchaeal plasmids. Haloarchaea (Breuert *et al.*, 2006; Soppa, 2013; Ludt & Soppa, 2019) often possess, in addition to the main chromosome, several mini-chromosomes, megaplasmids (> 100 kb), and plasmids. It has previously been suggested that the smaller sizes of rolling-circle replication plasmids in haloarchaea could be linked to higher copy numbers (S. Chen *et al.*, 2016),

a trend that appears to also extend to thermophilic *Euryarchaeota* (Erauso *et al.*, 1996; Gonnet *et al.*, 2011; Gorlas *et al.*, 2013). The minimal replication origin of plasmid pR1SE contains a putative RepH protein (Erdmann *et al.*, 2017), indicating that this plasmid may also replicate via rolling-circle replication. The copy numbers of megaplasmids have been reported as ≤ 2 for haloarchaea, including *Hrr. lacusprofundi*, when normalized to the main chromosome (Hawkins *et al.*, 2013; X. Liu *et al.*, 2013). Smaller plasmids (≤ 10 kb) generally exhibit copy numbers ranging from 6 - 15 (Charlebois *et al.*, 1987; Allers *et al.*, 2004; S. Chen *et al.*, 2016). Furthermore, lysogenic viral genomes in plasmid form are generally maintained intracellularly under stable copy number control and reach genomic virus-to-host ratios of 20 only when viral genes responsible for copy number control are deleted (Wang *et al.*, 2016; B. Chen *et al.*, 2020). Thus, the plasmid pR1SE (> 30 kb) plasmid-to-host ratios mirror values previously reported for much smaller plasmids or lysogenic viral genomes without copy number control.

Archaeal plasmids have also been extensively studied in the *Thermoproteota*, particularly in the *Sulfolobaceae*. Copy numbers of up to 50 per host chromosome have been reported for several large conjugative plasmids (~ 25 - 45 kb) immediately following conjugation into non-original host *Sulfolobus* strains (Schleper *et al.*, 1995; Prangishvili *et al.*, 1998; Erauso *et al.*, 2006). However, plasmid copy numbers declined over time and maintained stable low copy numbers in the long-term, similarly to the ratios observed in native hosts. To date no conjugative plasmids have been identified in haloarchaea, and for a long time conjugation was thought to be restricted to the *Sulfolobaceae* (Wagner et al., 2017) until a conjugative plasmid was recently identified in a thermophilic Euryarchaeon (Catchpole *et al.*, 2023). There however, the pT33-3 plasmid (103 kb) was maintained at approx. equal copy

numbers to the main host chromosome both in native hosts and after conjugation into a receiving host. The development of plasmid-to-host ratios in the native host strains of pR1SE, *Hrr. lacusprofundi* R1S1 and DL18 (Erdmann *et al.*, 2017) over time has not yet been analysed. However, in this and previous studies (Gebhard *et al.*, 2023b), infection with pR1SE had the opposite effect on the plasmid:host ratios of pR1SE with ratios increasing over time in successive generations. The additional data provided from the infection of the Δ*arcV* mutant of *Hrr. lacusprofundi* strengthens our previous observation that pR1SE dissemination has more resemblance to a viral infection than to the transmission of conjugative plasmids, while having seemingly no negative effect on the host organism. Moreover, PV particle production is not prevented by the deletion of *arcV* in the host, suggesting that PVs are at least independent of the host vesicle formation machinery that is driven by ArcV.

Author Contributions

L.J.G. and S.E conceived the study, L.J.G. performed the majority of the experimental work, analysis of the protein content and RNA content of EVs was performed by L.Q. and J.M. respectively, L.J.G drafted the manuscript with support from all authors, S.E. led the study.

Competing Interest Statement

The authors declare no competing interests.

Funding

Funding was provided by the Volkswagen Foundation (reference 98 190) to SE and the Max Planck Society (Munich, Germany) to SE.

Acknowledgements

We thank the Max Planck-Genome-Centre Cologne (Cologne, Germany) for assistance with DNA sequencing. We thank Daniela Thies (MPI for Marine Microbiology, Bremen, Germany) for assistance with the experiments and Guillermo Cera Ramirez (MPI for Marine Microbiology, Bremen, Germany) for his assistance as part of a MarMic Lab Rotation under the supervision of Lauren Queiss. Finally, we want to thank the Max-Planck-Institute for Marine Microbiology and the Max-Planck-Society for continuous support.

References

Alarcón-Schumacher, T., Naor, A., Gophna, U., & Erdmann, S. (2022). Isolation of a virus causing a chronic infection in the archaeal model organism *Haloferax volcanii* reveals antiviral activities of a provirus. *Proceedings of the National Academy of Sciences, 119*(35), e2205037119. doi:10.1073/pnas.2205037119

Allers, T., Ngo, H.-P., Mevarech, M., & Lloyd, R. G. (2004). Development of Additional Selectable Markers for the Halophilic Archaeon *Haloferax volcanii* Based on the *leuB* and *trpA* Genes. *Applied and Environmental Microbiology, 70*(2), 943-953. doi:10.1128/aem.70.2.943-953.2004

Anderson, I. J., DasSarma, P., Lucas, S., Copeland, A., Lapidus, A., Del Rio, T. G., Tice, H., Dalin, E., Bruce, D. C., & Goodwin, L. (2016). Complete genome sequence of the Antarctic *Halorubrum lacusprofundi* type strain ACAM 34. *Standards in genomic sciences, 11*(1), 70. doi:10.1186/s40793-016-0194-2

Bamford, D. H., Pietilä, M. K., Roine, E., Atanasova, N. S., Dienstbier, A., & Oksanen, H. M. (2017). ICTV virus taxonomy profile: *Pleolipoviridae*. *Journal of General Virology, 98*(12), 2916-2917. doi:10.1099/jgv.0.000972

Bitan-Banin, G., Ortenberg, R., & Mevarech, M. (2003). Development of a Gene Knockout System for the Halophilic Archaeon *Haloferax volcanii* by Use of the *pyrE* Gene. *Journal of bacteriology, 185*(3), 772-778. doi:10.1128/jb.185.3.772-778.2003

Breuert, S., Allers, T., Spohn, G., & Soppa, J. (2006). Regulated polyploidy in halophilic archaea. *PLOS ONE, 1*(1), e92. doi:10.1371/journal.pone.0000092

Brown, H. J., & Duggin, I. G. (2023). Diversity and Potential Multifunctionality of Archaeal CetZ Tubulin-like Cytoskeletal Proteins. *Biomolecules, 13*(1), 134. doi:10.3390/biom13010134

Burns, D., & Dyall-Smith, M. (2006). 22 Cultivation of haloarchaea. In *Methods in Microbiology* (Vol. 35, pp. 535-552): Elsevier.

Cai, J., Wu, G., Jose, P. A., & Zeng, C. (2016). Functional transferred DNA within extracellular vesicles. *Experimental Cell Research, 349*(1), 179-183. doi:10.1016/j.yexcr.2016.10.012

Caspi, Y., & Dekker, C. (2018). Dividing the Archaeal Way: The Ancient Cdv Cell-Division Machinery. *Frontiers in microbiology, 9*. doi:10.3389/fmicb.2018.00174

Catchpole, R. J., Barbe, V., Magdelenat, G., Marguet, E., Terns, M., Oberto, J., Forterre, P., & Da Cunha, V. (2023). A self-transmissible plasmid from a hyperthermophile that facilitates genetic modification of diverse Archaea. *Nature microbiology*. doi:10.1038/s41564-023-01387-x

Charlebois, R. L., Lam, W. L., Cline, S. W., & Doolittle, W. F. (1987). Characterization of pHV2 from *Halobacterium volcanii* and its use in demonstrating transformation of an archaebacterium. *Proceedings of the National Academy of Sciences, 84*(23), 8530-8534. doi:10.1073/pnas.84.23.8530

Chen, B., Chen, Z., Wang, Y., Gong, H., Sima, L., Wang, J., Ouyang, S., Gan, W., Krupovic, M., Chen, X., Du, S., & Sandri-Goldin, R. M. (2020). ORF4 of the Temperate Archaeal Virus SNJ1 Governs the Lysis-Lysogeny Switch and Superinfection Immunity. *Journal of virology, 94*(16), e00841-00820. doi:10.1128/JVI.00841-20

Chen, S., Wang, C., & Xiang, H. (2016). Sequence analysis and minimal replicon determination of a new haloarchaeal plasmid pHF2 isolated from *Haloferax sp*. strain Q22. *Plasmid, 83*, 1-7. doi:10.1016/j.plasmid.2015.11.001

Cui, L., Li, H., Xi, Y., Hu, Q., Liu, H., Fan, J., Xiang, Y., Zhang, X., Shui, W., & Lai, Y. (2022). Vesicle trafficking and vesicle fusion: mechanisms, biological functions, and their implications for potential disease therapy. *Molecular Biomedicine, 3*(1), 29. doi:10.1186/s43556-022-00090-3

Cumsille, A., Durán, R. E., Rodríguez-Delherbe, A., Saona-Urmeneta, V., Cámara, B., Seeger, M., Araya, M., Jara, N., & Buil-Aranda, C. (2023). GenoVi, an open-source automated circular genome visualizer for bacteria and archaea. *PLOS Computational Biology, 19*(4), e1010998. doi:10.1371/journal.pcbi.1010998

Deatherage, B. L., & Cookson, B. T. (2012). Membrane vesicle release in bacteria, eukaryotes, and archaea: a conserved yet underappreciated aspect of microbial life. *Infection and immunity, 80*(6), 1948-1957. doi:10.1128/iai.06014-11

Duggin, I. G., Aylett, C. H., Walsh, J. C., Michie, K. A., Wang, Q., Turnbull, L., Dawson, E. M., Harry, E. J., Whitchurch, C. B., & Amos, L. A. (2015). CetZ tubulin-like proteins control archaeal cell shape. *Nature, 519*(7543), 362. doi:10.1038/nature13983

Dyall-Smith, M. (2009). The halohandbook: protocols for halobacterial genetics, version 7.3. Retrieved from https://haloarchaea.com/wp-content/uploads/2018/10/Halohandbook_2009_v7.3mds.pdf

Ellen, A. F., Albers, S.-V., Huibers, W., Pitcher, A., Hobel, C. F., Schwarz, H., Folea, M., Schouten, S., Boekema, E. J., & Poolman, B. (2009). Proteomic analysis of secreted membrane vesicles of archaeal *Sulfolobus* species reveals the presence of endosome sorting complex components. *Extremophiles, 13*(1), 67. doi:10.1007/s00792-008-0199-x

Eme, L., Tamarit, D., Caceres, E. F., Stairs, C. W., De Anda, V., Schön, M. E., Seitz, K. W., Dombrowski, N., Lewis, W. H., Homa, F., Saw, J. H., Lombard, J., Nunoura, T., Li, W.-J., Hua, Z.-S., Chen, L.-X., Banfield, J. F., John, E. S., Reysenbach, A.-L., Stott, M. B., Schramm, A., Kjeldsen, K. U., Teske, A. P., Baker, B. J., & Ettema, T. J. G. (2023). Inference and reconstruction of the heimdallarchaeial ancestry of eukaryotes. *Nature*. doi:10.1038/s41586-023-06186-2

Erauso, G., Marsin, S., Benbouzid-Rollet, N., Baucher, M. F., Barbeyron, T., Zivanovic, Y., Prieur, D., & Forterre, P. (1996). Sequence of plasmid pGT5 from the archaeon *Pyrococcus abyssi:* evidence for rolling-circle replication in a hyperthermophile. *J Bacteriol, 178*(11), 3232-3237. doi:10.1128/jb.178.11.3232-3237.1996

Erauso, G., Stedman, K. M., van de Werken, H. J. G., Zillig, W., & van der Oost, J. (2006). Two novel conjugative plasmids from a single strain of *Sulfolobus*. *Microbiology, 152*(7), 1951-1968. doi:10.1099/mic.0.28861-0

Erdmann, S., Tschitschko, B., Zhong, L., Raftery, M. J., & Cavicchioli, R. (2017). A plasmid from an Antarctic haloarchaeon uses specialized membrane vesicles to disseminate and infect plasmid-free cells. *Nature microbiology, 2*(10), 1446. doi:10.1038/s41564-017-0009-2

Faini, M., Beck, R., Wieland, F. T., & Briggs, J. A. (2013). Vesicle coats: structure, function, and general principles of assembly. *Trends in cell biology, 23*(6), 279-288. doi:10.1016/j.tcb.2013.01.005

Filée, J., Siguier, P., & Chandler, M. (2007). Insertion sequence diversity in archaea. *Microbiol Mol Biol Rev, 71*(1), 121-157. doi:10.1128/mmbr.00031-06

Fligner, M. A., & Killeen, T. J. (1976). Distribution-Free Two-Sample Tests for Scale. *Journal of the American Statistical Association, 71*(353), 210-213. doi:10.1080/01621459.1976.10481517
Gebhard, L. J., Duggin, I. G., & Erdmann, S. (2023a). Improving the genetic system for *Halorubrum lacusprofundi* to allow in-frame deletions. *Frontiers in microbiology, 14*. doi:10.3389/fmicb.2023.1095621
Gebhard, L. J., Vershinin, Z., Alarcón-Schumacher, T., Eichler, J., & Erdmann, S. (2023b). Influence of N-Glycosylation on Virus-Host Interactions in *Halorubrum lacusprofundi*. *Viruses, 15*(7), 1469. doi:10.3390/v15071469
Gonnet, M., Erauso, G., Prieur, D., & Le Romancer, M. (2011). pAMT11, a novel plasmid isolated from a *Thermococcus sp.* strain closely related to the virus-like integrated element TKV1 of the *Thermococcus kodakaraensis* genome. *Research in Microbiology, 162*(2), 132-143. doi:10.1016/j.resmic.2010.11.003
Gorlas, A., Krupovič, M., Forterre, P., & Geslin, C. (2013). Living side by side with a virus: Characterization of two novel plasmids from *Thermococcus prieurii,* a host for the spindle-shaped virus TPV1. *Applied and Environmental Microbiology, 79*(12), 3822-3828. doi:10.1128/AEM.00525-13
Hassan, Z., Kumar, N. D., Reggiori, F., & Khan, G. (2021). How Viruses Hijack and Modify the Secretory Transport Pathway. *Cells, 10*(10). doi:10.3390/cells10102535
Hatano, T., Palani, S., Papatziamou, D., Salzer, R., Souza, D. P., Tamarit, D., Makwana, M., Potter, A., Haig, A., Xu, W., Townsend, D., Rochester, D., Bellini, D., Hussain, H. M. A., Ettema, T. J. G., Löwe, J., Baum, B., Robinson, N. P., & Balasubramanian, M. (2022). Asgard archaea shed light on the evolutionary origins of the eukaryotic ubiquitin-ESCRT machinery. *Nature communications, 13*(1), 3398. doi:10.1038/s41467-022-30656-2
Hawkins, M., Malla, S., Blythe, M. J., Nieduszynski, C. A., & Allers, T. (2013). Accelerated growth in the absence of DNA replication origins. *Nature, 503*(7477), 544-547. doi:10.1038/nature12650
Henne, William M., Buchkovich, Nicholas J., & Emr, Scott D. (2011). The ESCRT Pathway. *Developmental Cell, 21*(1), 77-91. doi:10.1016/j.devcel.2011.05.015
Hildebrand, A., Remmert, M., Biegert, A., & Söding, J. (2009). Fast and accurate automatic structure prediction with HHpred. *Proteins: Structure, Function, and Bioinformatics, 77*(S9), 128-132. doi:10.1002/prot.22499
Hurtig, F., Burgers, T. C. Q., Cezanne, A., Jiang, X., Mol, F. N., Traparić, J., Pulschen, A. A., Nierhaus, T., Tarrason-Risa, G., Harker-Kirschneck, L., Löwe, J., Šarić, A., Vlijm, R., & Baum, B. (2023). The patterned assembly and stepwise Vps4-mediated disassembly of composite ESCRT-III polymers drives archaeal cell division. *Science advances, 9*(11), eade5224. doi:10.1126/sciadv.ade5224
Imachi, H., Nobu, M. K., Nakahara, N., Morono, Y., Ogawara, M., Takaki, Y., Takano, Y., Uematsu, K., Ikuta, T., Ito, M., Matsui, Y., Miyazaki, M., Murata, K., Saito, Y., Sakai, S., Song, C., Tasumi, E., Yamanaka, Y., Yamaguchi, T., Kamagata, Y., Tamaki, H., & Takai, K. (2020). Isolation of an archaeon at the prokaryote–eukaryote interface. *Nature, 577*(7791), 519-525. doi:10.1038/s41586-019-1916-6
Kirchhausen, T. (2000). Three ways to make a vesicle. *Nature Reviews Molecular Cell Biology, 1*(3), 187-198. doi:10.1038/35043117
Koeppen, K., Hampton, T. H., Jarek, M., Scharfe, M., Gerber, S. A., Mielcarz, D. W., Demers, E. G., Dolben, E. L., Hammond, J. H., Hogan, D. A., & Stanton, B. A. (2016). A Novel Mechanism of Host-Pathogen Interaction through sRNA in Bacterial Outer Membrane Vesicles. *PLoS pathogens, 12*(6), e1005672. doi:10.1371/journal.ppat.1005672
Levene, H. (1960). Robust tests for equality of variances. In I. Olkin (Ed.), *Contributions to probability and statistics* (pp. 278-292). Palo Alto, California, USA: Stanford University Press.

Liao, Y., Ithurbide, S., de Silva, R. T., Erdmann, S., & Duggin, I. G. (2018). Archaeal cell biology: diverse functions of tubulin-like cytoskeletal proteins at the cell envelope. *Emerging Topics in Life Sciences, 2*(4), 547-559. doi:10.1042/etls20180026

Liao, Y., Ithurbide, S., Evenhuis, C., Löwe, J., & Duggin, I. G. (2021). Cell division in the archaeon *Haloferax volcanii* relies on two FtsZ proteins with distinct functions in division ring assembly and constriction. *Nature microbiology, 6*(5), 594-605. doi:10.1038/s41564-021-00894-z

Liao, Y., Williams, T. J., Walsh, J. C., Ji, M., Poljak, A., Curmi, P. M. G., Duggin, I. G., & Cavicchioli, R. (2016). Developing a genetic manipulation system for the Antarctic archaeon, *Halorubrum lacusprofundi*: investigating acetamidase gene function. *Scientific Reports, 6*, 34639. doi:10.1038/srep34639

Lindås, A.-C., Karlsson, E. A., Lindgren, M. T., Ettema, T. J. G., & Bernander, R. (2008). A unique cell division machinery in the Archaea. *Proceedings of the National Academy of Sciences, 105*(48), 18942-18946. doi:10.1073/pnas.0809467105

Liu, J., Cvirkaite-Krupovič, V., Baquero, D. P., Yang, Y., Zhang, Q., Shen, Y., & Krupovič, M. (2021a). Virus-induced cell gigantism and asymmetric cell division in archaea. *Proceedings of the National Academy of Sciences, 118*(15), e2022578118. doi:10.1073/pnas.2022578118

Liu, J., Cvirkaite-Krupovič, V., Commere, P.-H., Yang, Y., Zhou, F., Forterre, P., Shen, Y., & Krupovič, M. (2021b). Archaeal extracellular vesicles are produced in an ESCRT-dependent manner and promote gene transfer and nutrient cycling in extreme environments. *The ISME journal, 15*(10), 2892-2905. doi:10.1038/s41396-021-00984-0

Liu, X., Miao, D., Zhang, F., Wu, Z., Liu, J., & Xiang, H. (2013). Characterization of the minimal replicon of pHM300 and independent copy number control of major and minor chromosomes of *Haloferax mediterranei*. *FEMS microbiology letters, 339*(1), 66-74. doi:10.1111/1574-6968.12052

Lu, Z., Fu, T., Li, T., Liu, Y., Zhang, S., Li, J., Dai, J., Koonin, E. V., Li, G., Chu, H., & Li, M. (2020). Coevolution of Eukaryote-like Vps4 and ESCRT-III Subunits in the Asgard Archaea. *MBio, 11*(3), e00417-00420. doi:10.1128/mBio.00417-20

Ludt, K., & Soppa, J. (2019). Polyploidy in halophilic archaea: regulation, evolutionary advantages, and gene conversion. *Biochemical Society Transactions, 47*(3), 933-944. doi:10.1042/bst20190256

Manning, A. J., & Kuehn, M. J. (2011). Contribution of bacterial outer membrane vesicles to innate bacterial defense. *BMC microbiology, 11*(1), 258. doi:10.1186/1471-2180-11-258

McCullough, J., Frost, A., & Sundquist, W. I. (2018). Structures, Functions, and Dynamics of ESCRT-III/Vps4 Membrane Remodeling and Fission Complexes. *Annual Review of Cell and Developmental Biology, 34*(1), 85-109. doi:10.1146/annurev-cellbio-100616-060600

Mercier, C., Thies, D., Zhong, L., Raftery, M. J., Cavicchioli, R., & Erdmann, S. (2022). In depth characterization of an archaeal virus-host system reveals numerous virus exclusion mechanisms. *bioRxiv*. doi:10.1101/2022.10.18.512658

Mills, J., Gebhard, L. J., Schubotz, F., Shevchenko, A., Speth, D. R., Liao, Y., Duggin, I. G., Marchfelder, A., & Erdmann, S. (2023). Extracellular vesicles of *Euryarchaeida*: precursor to eukaryotic membrane trafficking. *bioRxiv*. doi:10.1101/2023.03.03.530948

Moriano-Gutierrez, S., Bongrand, C., Essock-Burns, T., Wu, L., McFall-Ngai, M. J., & Ruby, E. G. (2020). The noncoding small RNA SsrA is released by *Vibrio fischeri* and modulates critical host responses. *PLOS Biology, 18*(11), e3000934. doi:10.1371/journal.pbio.3000934

Nielsen, E., Cheung, A. Y., & Ueda, T. (2008). The Regulatory RAB and ARF GTPases for Vesicular Trafficking *Plant Physiology, 147*(4), 1516-1526. doi:10.1104/pp.108.121798

Oren, A., & Garrity, G. M. (2021). Valid publication of the names of forty-two phyla of prokaryotes. *International Journal of Systematic and Evolutionary Microbiology, 71*(10). doi:10.1099/ijsem.0.005056

Pfeiffer, F., Losensky, G., Marchfelder, A., Habermann, B., & Dyall-Smith, M. (2020). Whole-genome comparison between the type strain of *Halobacterium salinarum* (DSM 3754T) and the laboratory strains R1 and NRC-1. *MicrobiologyOpen, 9*(2), e974. doi:10.1002/mbo3.974

Pfeiffer, F., Schuster, S. C., Broicher, A., Falb, M., Palm, P., Rodewald, K., Ruepp, A., Soppa, J., Tittor, J., & Oesterhelt, D. (2008). Evolution in the laboratory: The genome of *Halobacterium salinarum* strain R1 compared to that of strain NRC-1. *Genomics, 91*(4), 335-346. doi:10.1016/j.ygeno.2008.01.001

Prangishvili, D., Albers, S.-V., Holz, I., Arnold, H. P., Stedman, K., Klein, T., Singh, H., Hiort, J., Schweier, A., Kristjansson, J. K., & Zillig, W. (1998). Conjugation in Archaea: Frequent Occurrence of Conjugative Plasmids in *Sulfolobus*. *Plasmid, 40*(3), 190-202. doi:10.1006/plas.1998.1363

Robinson, M., Schor, S., Barouch-Bentov, R., & Einav, S. (2018). Viral journeys on the intracellular highways. *Cellular and Molecular Life Sciences, 75*(20), 3693-3714. doi:10.1007/s00018-018-2882-0

Rodrigues-Oliveira, T., Wollweber, F., Ponce-Toledo, R. I., Xu, J., Rittmann, S. K. M. R., Klingl, A., Pilhofer, M., & Schleper, C. (2023). Actin cytoskeleton and complex cell architecture in an Asgard archaeon. *Nature, 613*(7943), 332-339. doi:10.1038/s41586-022-05550-y

Schapira, M., Tyers, M., Torrent, M., & Arrowsmith, C. H. (2017). WD40 repeat domain proteins: a novel target class? *Nature Reviews Drug Discovery, 16*(11), 773-786. doi:10.1038/nrd.2017.179

Schleper, C., Holz, I., Janekovic, D., Murphy, J., & Zillig, W. (1995). A multicopy plasmid of the extremely thermophilic archaeon *Sulfolobus* effects its transfer to recipients by mating. *Journal of bacteriology, 177*(15), 4417-4426. doi:10.1128/jb.177.15.4417-4426.1995

Schneider, C. A., Rasband, W. S., & Eliceiri, K. W. (2012). NIH Image to ImageJ: 25 years of image analysis. *Nature Methods, 9*(7), 671-675. doi:10.1038/nmeth.2089

Seemann, T. (2014). Prokka: rapid prokaryotic genome annotation. *Bioinformatics, 30*(14), 2068-2069. doi:10.1093/bioinformatics/btu153

Siguier, P., Pérochon, J., Lestrade, L., Mahillon, J., & Chandler, M. (2006). ISfinder: the reference centre for bacterial insertion sequences. *Nucleic acids research, 34*(suppl_1), D32-D36. doi:10.1093/nar/gkj014

Snedecor, G., & Cochran, W. (1989). Statistical methods 7th edition. *The Iowa State University*.

Snyder, J. C., Samson, R. Y., Brumfield, S. K., Bell, S. D., & Young, M. J. (2013). Functional interplay between a virus and the ESCRT machinery in Archaea. *Proceedings of the National Academy of Sciences, 110*(26), 10783-10787. doi:10.1073/pnas.1301605110

Soler, N., & Forterre, P. (2020). Vesiduction: the fourth way of HGT. *Environmental microbiology, 22*(7), 2457-2460. doi:10.1111/1462-2920.15056

Soppa, J. (2013). Evolutionary advantages of polyploidy in halophilic archaea. *Biochemical Society Transactions, 41*(1), 339-343. doi:10.1042/bst20120315

Spang, A., Caceres, E. F., & Ettema, T. J. G. (2017). Genomic exploration of the diversity, ecology, and evolution of the archaeal domain of life. *Science, 357*(6351), eaaf3883. doi:10.1126/science.aaf3883

Spang, A., Saw, J. H., Jørgensen, S. L., Zaremba-Niedzwiedzka, K., Martijn, J., Lind, A. E., van Eijk, R., Schleper, C., Guy, L., & Ettema, T. J. G. (2015). Complex archaea that bridge the gap between prokaryotes and eukaryotes. *Nature, 521*(7551), 173-179. doi:10.1038/nature14447

Stenmark, H. (2009). Rab GTPases as coordinators of vesicle traffic. *Nature Reviews Molecular Cell Biology, 10*(8), 513-525. doi:10.1038/nrm2728

Tarrason Risa, G., Hurtig, F., Bray, S., Hafner, A. E., Harker-Kirschneck, L., Faull, P., Davis, C., Papatziamou, D., Mutavchiev, D. R., Fan, C., Meneguello, L., Arashiro Pulschen, A., Dey, G., Culley, S., Kilkenny, M., Souza, D. P., Pellegrini, L., de Bruin, R. A. M., Henriques, R., Snijders, A. P., Šarić, A., Lindås, A.-C., Robinson, N. P., & Baum, B. (2020). The proteasome controls ESCRT-III–mediated cell division in an archaeon. *Science, 369*(6504), eaaz2532. doi:10.1126/science.aaz2532

Team, R. (2023). RStudio: Integrated Development Environment for R. (Version Version 2023.3.0.386). Boston, MA., United States: Posit Software, PBC. Retrieved from http://www.posit.co/.

Team, R. C. (2021). R: A language and environment for statistical computing. (Version Version 4.1.2). Vienna, Austria: R Foundation for Statistical Computing. Retrieved from https://www.R-project.org/.

Vietri, M., Radulovic, M., & Stenmark, H. (2020). The many functions of ESCRTs. *Nature Reviews Molecular Cell Biology, 21*(1), 25-42. doi:10.1038/s41580-019-0177-4

Votteler, J., & Sundquist, Wesley I. (2013). Virus Budding and the ESCRT Pathway. *Cell Host & Microbe, 14*(3), 232-241. doi:10.1016/j.chom.2013.08.012

Wagner, A., Whitaker, R. J., Krause, D. J., Heilers, J.-H., van Wolferen, M., van der Does, C., & Albers, S.-V. (2017). Mechanisms of gene flow in archaea. *Nature Reviews Microbiology, 15*(8), 492-501. doi:10.1038/nrmicro.2017.41

Wang, Y., Sima, L., Lv, J., Huang, S., Liu, Y., Wang, J., Krupovic, M., & Chen, X. (2016). Identification, Characterization, and Application of the Replicon Region of the Halophilic Temperate *Sphaerolipovirus* SNJ1. *Journal of bacteriology, 198*(14), 1952-1964. doi:10.1128/JB.00131-16

Wolters, M., Borst, A., Pfeiffer, F., & Soppa, J. (2019). Bioinformatic and genetic characterization of three genes localized adjacent to the major replication origin of *Haloferax volcanii*. *FEMS microbiology letters, 366*(21), fnz238. doi:10.1093/femsle/fnz238

Zaremba-Niedzwiedzka, K., Caceres, E. F., Saw, J. H., Bäckström, D., Juzokaite, L., Vancaester, E., Seitz, K. W., Anantharaman, K., Starnawski, P., Kjeldsen, K. U., Stott, M. B., Nunoura, T., Banfield, J. F., Schramm, A., Baker, B. J., Spang, A., & Ettema, T. J. G. (2017). Asgard archaea illuminate the origin of eukaryotic cellular complexity. *Nature, 541*, 353. doi:10.1038/nature21031

Zimmermann, L., Stephens, A., Nam, S.-Z., Rau, D., Kübler, J., Lozajic, M., Gabler, F., Söding, J., Lupas, A. N., & Alva, V. (2018). A Completely Reimplemented MPI Bioinformatics Toolkit with a New HHpred Server at its Core. *Journal of Molecular Biology, 430*(15), 2237-2243. doi:10.1016/j.jmb.2017.12.007

Supplementary Material

Plasmid vesicle formation is independent of the archaeal small vesiculating GTPase (ArcV) driven extracellular vesicle formation

Supplementary Figures

Supplementary Figure 1: Alignment of *Hrr. lacusprofundi* and *H. volcanii* ArcV with HHPred

Supplementary Figure 2: Screening of pTA131_*hmgA*_Δ*Hlac_2746* transformants of ACAM34_UNSWΔ*pyrE2* for successful gene deletion.

Supplementary Figure 3: Genomes of Δ*arcV* mutants _2.1, _2.15 and _2.19 showing the deletion of *arcV.*

Supplementary Figure 4: Gradient purification and micrographs of EVs from different *Hrr. lacusprofundi* strains.

Supplementary Figure 5: Quantification of EVs from *Hrr. lacusprofundi* ACAM34_UNSWΔ*arcV_2.1* and its parent strain.

Supplementary Figure 6: Comparison of the protein content of EVs produced by *Hrr. lacusprofundi* ACAM34_UNSWΔarcV_2.1 and its parent strain

Supplementary Figure 7: Comparison of the RNA content of EVs produced by *Hrr. lacusprofundi* ACAM34_UNSWΔ*arcV_2.1* and its parent strain.

Supplementary Tables

Supplementary Table 1: Primers used in this study

References

Gebhard, L. J., Duggin, I. G., & Erdmann, S. (2023). Improving the genetic system for *Halorubrum lacusprofundi* to allow in-frame deletions. *Frontiers in microbiology, 14*. doi:10.3389/fmicb.2023.1095621

Hildebrand, A., Remmert, M., Biegert, A., & Söding, J. (2009). Fast and accurate automatic structure prediction with HHpred. *Proteins: Structure, Function, and Bioinformatics, 77*(S9), 128-132. doi:10.1002/prot.22499

Zimmermann, L., Stephens, A., Nam, S.-Z., Rau, D., Kübler, J., Lozajic, M., Gabler, F., Söding, J., Lupas, A. N., & Alva, V. (2018). A Completely Reimplemented MPI Bioinformatics Toolkit with a New HHpred Server at its Core. *Journal of Molecular Biology, 430*(15), 2237-2243. doi:10.1016/j.jmb.2017.12.007

Supplementary Figures

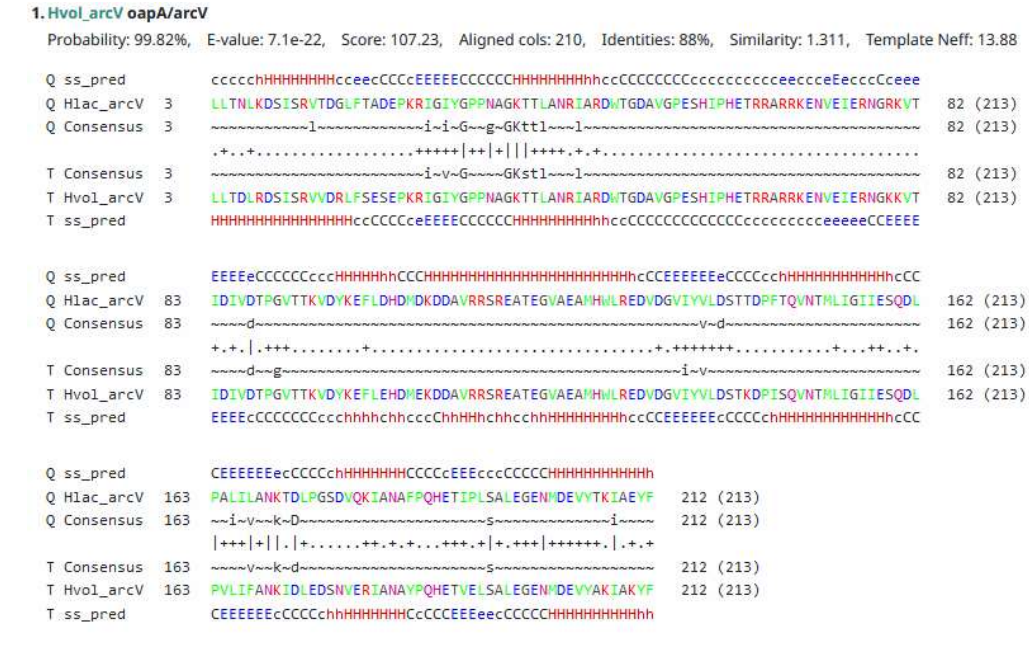

Supplementary Figure 1: Alignment of *Hrr. lacusprofundi* and *H. volcanii* ArcV with HHPred.

The protein sequences were aligned in HHPred (Hildebrand et al., 2009; Zimmermann et al., 2018) at default settings showing that *Hlac_2746* is indeed a homologue to *HVO_3014*.

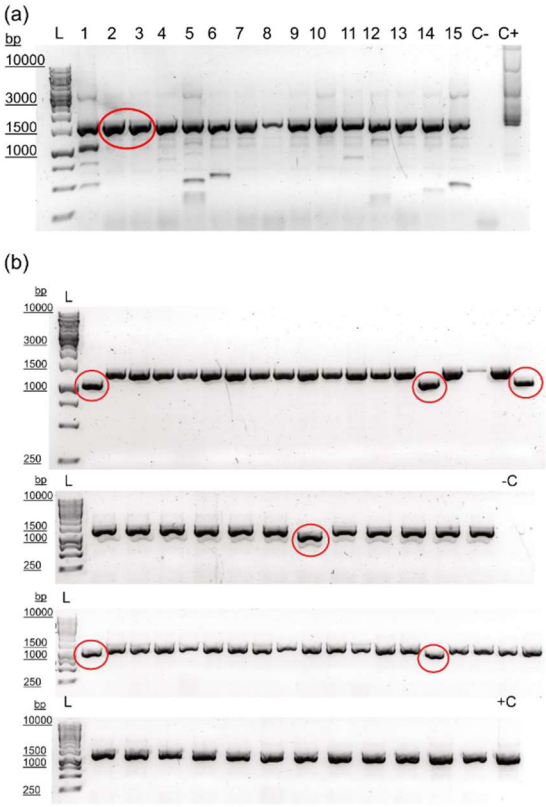

Supplementary Figure 2: Screening of pTA131_*hmgA*_Δ*arcV* transformants of ACAM34_UNSWΔ*pyrE2* for successful gene deletion. **(a)** PCR targeting the *hmgA* gene in order to confirm successful plasmid uptake into the genome under pop-in conditions on 15 ACAM34_UNSWΔ*pyrE2*Δ*arcV* clones after three generations. Clones that were selected for further cultivation are marked with a red circle. (-C) negative control with ddH_2O, (+C) positive control with purified pTA131_*hmgA* vector DNA. **(b)** reproduced with permission from Supplementary Figure 13 originally published in Gebhard *et al.* (2023). PCR targeting the predicted ArcV (*Hlac_2746*) on 62 potential ACAM34_UNSWΔ*pyrE2*Δ*arcV* clones after eight generations. Clones with PCR signals for mutated *arcV* are marked with red circles. (-C) negative control with ddH_2O, (+C) positive control with wild type ACAM34_UNSW genomic DNA. First lane from the left: DNA marker (GeneRuler 1 kb Plus DNA Ladder, Thermo Scientific™). DNA was separated on 1% agarose gels and stained with SYBR™ Safe.

(a)

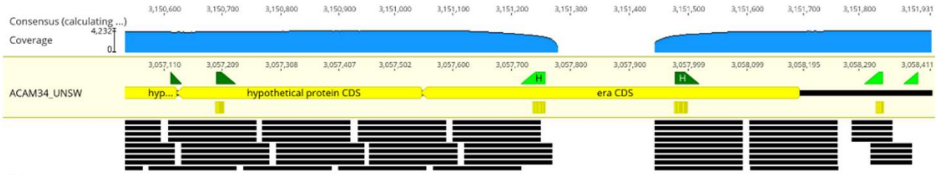
Consensus (calculating ...)
Coverage
ACAM34_UNSW
hyp...
hypothetical protein CDS
era CDS

(b)


Consensus (calculating ...)
Coverage
ACAM34_UNSW
Hlac_2746DF
Hlac_2746UR
era CDS

(c)

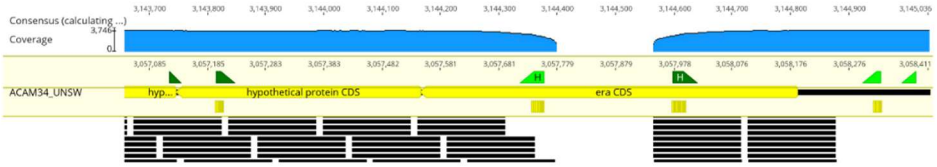
Consensus (calculating ...)
Coverage
ACAM34_UNSW
hyp...
hypothetical protein CDS
era CDS

(d)


Consensus (calculating ...)
Coverage
ACAM34_UNSW
Hlac_2746DF
Hlac_2746UR
era CDS

(e)

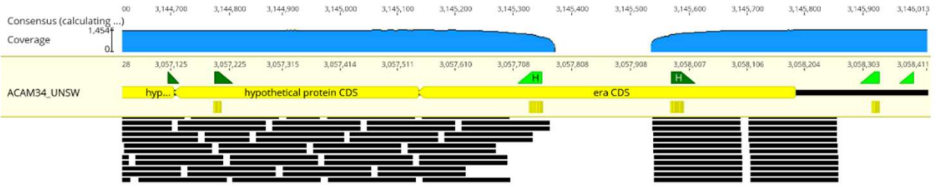
Consensus (calculating ...)
Coverage
ACAM34_UNSW
hyp...
hypothetical protein CDS
era CDS

(f)


Consensus (calculating ...)
Coverage
ACAM34_UNSW
Hlac_2746DF
Hlac_2746UR
era CDS

Supplementary Figure 3: Genomes of Δ*arcV* mutants _2.1, _2.15 and _2.19 showing the deletion of arcV. Read mapping of genome sequencing data of the mutant strains Δ*arcV*_2.1 **(a-b)**, Δ*arcV*_2.15 **(c-d)** and Δ*arcV*_2.19 (e-f) to the ACAM34_UNSW genome (log scale). Only the section with the deletion of *arcV* (*Hlac_2746*) is shown in two different magnifications, including the binding sites of forward (dark green) and reverse (light green) primers. Visualized using Geneious version 2023.1 created by Biomatters (www.geneious.com).

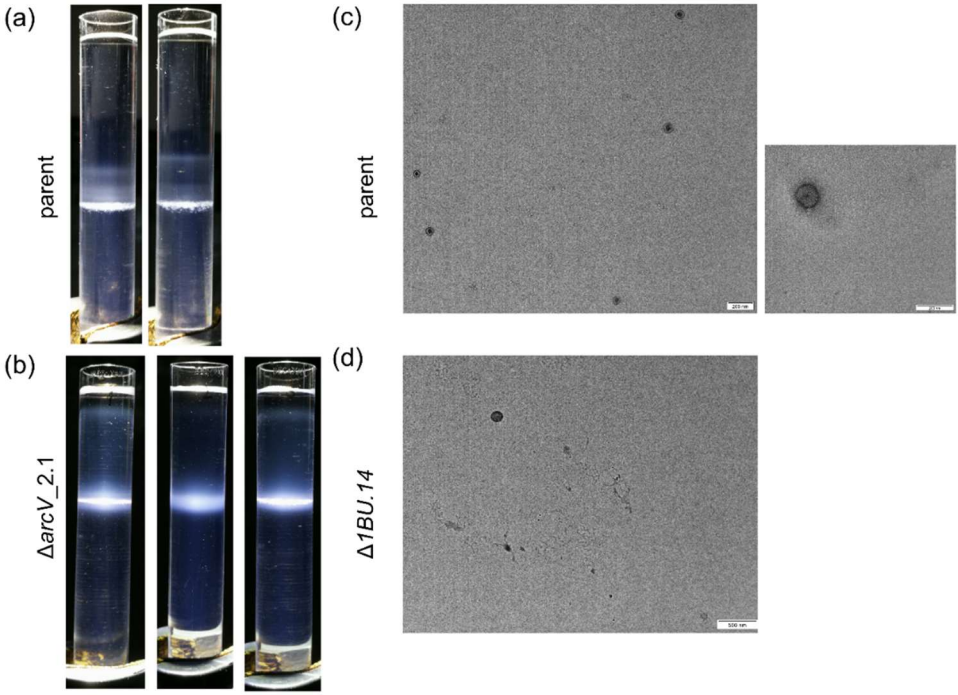

Supplementary Figure 4: Gradient purification and micrographs of EVs from different *Hrr. lacusprofundi* strains. Optiprep™ density gradient of parent **(a)** and Δ*arcV*_2.1 **(b)** EVs showing differences in the densities of the EVs produced by each strain (broad band(s) compared to two distinct bands). Transmission electron micrograph of purified (0.2 µm filtered) EV preparations from the parent strain **(c)** and the escape mutant ACAM34_UNSW_2.14 **(d)** which appears to produce fewer EVs in general, size bar indicates either 200 nm (for c) or 500 nm (for d).

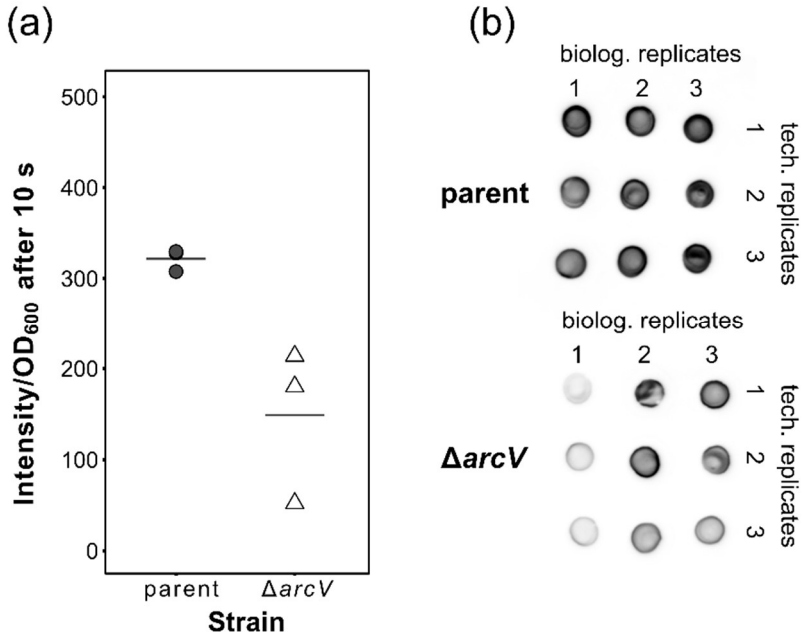

Supplementary Figure 5: Quantification of EVs from *Hrr. lacusprofundi* ACAM34_UNSWΔ*arcV_2.1* and its parent strain. (a) Quantification of EVs harvested from 25 ml of culture supernatant of the parent (dark grey circles) and Δ*arcV* (clone 2.1, white triangles) strains given as relative Intensity per unit of OD_{600} after 10 s of accumulation of chemiluminescent signal. Points represent the average of three technical replicates for every biological replicate; the average value per strain is represented with a grey line, **(b)** original spot blot.

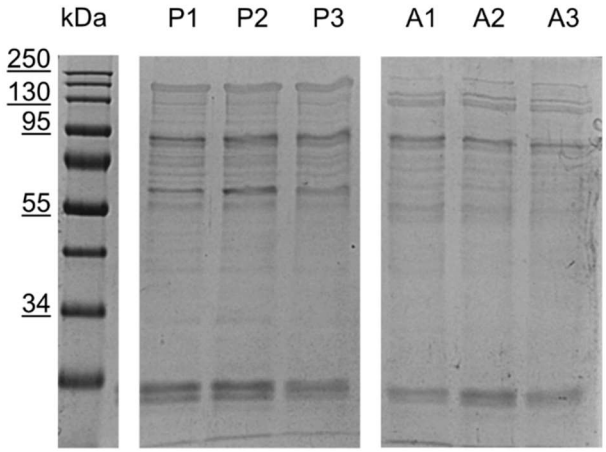

Supplementary Figure 6: Comparison of the protein content of EVs produced by *Hrr. lacusprofundi* ACAM34_UNSWΔ*arcV_2.1* and its parent strain. EVs samples (1-3) produced by the parent (P) and Δ*arcV_2.1* (A) strains were separated via SDS-PAGE (8% Acrylamide) and stained with Coomassie blue to visualize all proteins. Color Prestained Protein Standard (NEB) was added a as a size standard (kDa).

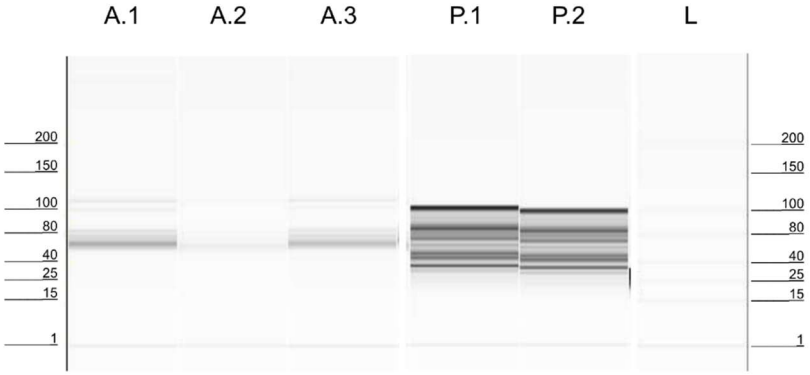

Supplementary Figure 7: Comparison of the RNA content of EVs produced by *Hrr. lacusprofundi* ACAM34_UNSWΔ*arcV_2.1* and its parent strain. The size distribution (nt) of small RNAs extracted from EVs (n = 3, or n = 2) produced by the Δ*arcV_2.1* (A) and parent (P) strain was analyzed on a fragment analyzer**.**

Supplementary Tables

Supplementary Table 1: Primers used in this study

Name	Sequence 5' -> 3'	Description	product length (bp)	annealing temperature for Q5 polymerase (°C) if applicable	qPCR conditions (primer concentration, annealing temperature) if applicable
prav_F	CTCATCTAGAGTGCCTAAT-GAGTGAGCTAAC	Forward genomic sequencing primer targeting *hmgA* gene insertion after plasmid uptake	1550	58	
prav_R	CTCAGCGGCCGCACTCTGAA-CCTATGAATCGAG	Reverse genomic sequencing primer targeting *hmgA* gene insertion after plasmid uptake	1550	58	
Hlac_2746KOF	CGAATAAGTAAACAACCGATATC	Forward genomic sequencing primer binding upstream of *Hrr. lacusprofundi arcV* gene *Hlac_2746*	1270	59	
Hlac_2746KOR	GGTGTGGCATTTACTTACG	Reverse genomic sequencing primer binding downstream of *Hrr. lacusprofundi arcV* gene *Hlac_2746*	1270	59	
qPMC2_F	GAGTTAGTGAAGTATCTTCG	Chromosome 1 of all *Hrr. lacusprofundi* strains for quantification (forward)	108		0.15 µM, 61 °C
qPMC2_R	GCTCTACATCCTCATAATAC	Chromosome 1 of all *Hrr. lacusprofundi* strains for quantification (reverse)	108		0.15 µM, 61 °C
qORF6F	ATCGACGACGCAGCCAACAC	ORF6 of pR1SE for quantification (forward)	179		0.125 µM, 67.8 °C
qORF6R	GTGATTGCGTCCGGGTTGAG	ORF6 of pR1SE for quantification (reverse)	179		0.125 µM, 67.8 °C

Discussion & Concluding Remarks

Over the course of this dissertation, I have described the successful improvement of the genetic system of *Halorubrum lacusprofundi* (Chapter I). This allowed us to create in-frame gene deletions in the host organism for pR1SE. We were then able to track the pR1SE infection cycle intracellularly and extracellularly (Chapter II) and compare it to two viruses, a lytic tailed virus and a membrane-enveloped chronic virus during infection of the wild-type (parental strain, *pyrE2* mutant) and an N-glycosylation deficient mutant of *Hrr. lacusprofundi.* By disrupting the N-glycosylation machinery of the host we were able to show that the stability of the two membrane enveloped particles, HFPV-1 virions and plasmid vesicles (PVs) was affected negatively. Comparing the lipid composition between host cells, host membranes and EVs (and PVs) identified selective enrichment of lipid species into the vesicle fraction for both *Hrr. lacusprofundi* and *H. volcanii* (Chapter III). Based on previous work showing that the *arcV* small GTPase is crucial for vesicle formation in *H. volcanii* (Chapter III) we created knock out mutants for the *arcV* homologue in *Hrr. lacusprofundi* (Chapter IV). The gene deletion led to wide-scale genomic re-arrangement of the host chromosome and altered the regular EV formation mechanism of *Hrr. lacus-profundi*. Nevertheless, we observed PV production after pR1SE infection indicating that PVs are independent from the host vesicle formation machinery that is driven by ArcV.

The main findings of this dissertation are presented and discussed in the respective chapters. In this general discussion, I will focus on the questions and hypotheses raised in those chapters, discuss our expanded knowledge of PVs in relation to comparable mobile genetic elements in prokaryotes, and provide suggestions future avenues for investigation.

Double selection is necessary for successful gene deletions in *Halorubrum*

As *Hrr. lacusprofundi* is currently the only known host of pR1SE and producer of PVs, we quickly ran into the hurdle of not being able to genetically manipulate the host organism. *Hrr. lacusprofundi* has posed a couple of challenges to the successful establishment of genetic systems. The genome contains many insertion sequences, and the secondary chromosome and the plasmid pHLAC01 are very flexible (Tschitschko *et al*., 2018; Harrison & Allers, 2022; Mercier *et al*., 2022). Liao and colleagues (2016) were unable to induce mutagenesis in the orotate phosphoribosyltransferase genes (*pyrE2*) in *Hrr. lacusprofundi*, but were able successfully establish a genetic system based on resistance to the antibiotic pravastatin.

As described in Chapter I, we have been able to induce spontaneous *pyrE2* gene deletions in two strains of *Hrr. lacusprofundi*. In the ACAM34_UNSW strain the gene deletion affected parts of a downstream gene but we did not identify growth defects in the mutant compared to the parent strain. While this is clearly not ideal, we observed identical deletions in two mutants generated in separate experiments suggesting that this was a spontaneous but targeted gene inactivation driven by the organism. Subsequently we demonstrated how a combination of selection pressures, uracil auxotrophy and pravastatin resistance, enabled in-frame deletions of multiple genes in the same strain with a pop-in pop-out system as is established in other haloarchaea (Dattani *et al.*, 2022; Harrison & Allers, 2022). The high ploidy of *Hrr. lacusprofundi* necessitated successive cultivation under increasing pravastatin concentrations to force cells to incorporate the vector plasmid into all copies of the chromosome, to increase the probability to recover mutants with the targeted gene deletions. While this considerably stretches out the

period between transformation and the recovery of deletion mutants, the protocol we have established now has been reliable in several gene deletions. This kind of double selection strategy is a promising approach to establish genetic systems in other genetically inaccessible cultivated archaea provided, that mutation in their *pyrE2* genes can be manipulated.

N-Glycosylation is crucial for the stability of budding viruses and PVs

Cell surface proteins of haloarchaea are highly glycosylated, which ensures protein folding, stability and function under hypersaline conditions (Yurist-Doutsch *et al*., 2010; Tamir & Eichler, 2017; Eichler, 2020; Vershinin *et al*., 2021a). Several PV proteins predicted to form parts of the vesicle coat contain N-glycosylation motifs, as do the capsid proteins of many haloarchaeal viruses (see Chapter II). For instance, the spike protein of the HRPV-1 virus is modified with N-linked glycans with an identical composition to the glycans attached to the S-layer glycoprotein of its host (Kandiba *et al*., 2012; Zaretsky *et al*., 2018).

Deletion of the archaeal oligosacharyltransferase (*aglB*) gene in *Hrr. lacusprofundi* allowed us to determine the effect N-glycosylation has on virus host interactions in this system Chapter II). Since *aglB* and its homologues are the central enzymes in the N-glycosylation pathway of prokaryotes and eukaryotes (Kohda, 2018), it naturally became the first target for our investigation. While N-glycosylation has been investigated extensively in *H. volcanii* [see Eichler (2020) and references therein], the only other studies directly describing the effect of N-glycosylation on virus host interactions in haloarchaea were performed with a host without a genetic system (Kandiba *et al*., 2012; Zaretsky *et al*., 2018).

Comparison of the effect of *aglB* deletion on the three infectious agents showed clear differences from one virus-host interaction to another. The lytic HRTV-DL1 virus (Mercier *et al*., 2022) was not affected by impaired

N-glycosylation in the host but the two membrane-enveloped particles, HFPV-1 (Alarcón-Schumacher *et al.*, 2022) and PVs, were both negatively affected. In both cases, particle production was clearly not prevented by the deletion of *aglB*, but particle stability and release were impacted. We observed increased HFPV-1 virion release in the *Hrr. lacusprofundi* Δ*aglB* mutant yet interestingly, in its preferred host *H. volcanii*, the HFPV-1 titers were significantly lower (ca. 2 orders of magnitude) in the Δ*aglB* mutant compared to the parent strain [personal communication by Tomás Alarcón-Schumacher, see Chapter 2 of Alarcón-Schumacher (2023)].

This contradicting result in two different host organisms is puzzling. Potentially HFPV-1 has optimized the budding release of virions in its preferred host and there, de-glycosylation would not be a benefit since the release mechanism is dependent on the normal conditions of S-layer stability. This could potentially explain our observations of lower viral production in the *H. volcanii* Δ*aglB* mutant but increased viral production in the *Hrr. lacusprofundi* Δ*aglB* mutant, where the less rigid S-layer could benefit the virus. In this case, HFPV-1 might be considered to employ a broad strategy for host takeover during infection in non-optimal hosts, which benefits from S-layer instability, but would be able to change its strategy to one uniquely suited to the conditions in its preferred host. In the latter case, infection and host takeover would be optimized for the most efficient replication in its preferred host, based on a delicate equilibrium in the host-virus arms race and which is vulnerable to strong changes in the host.
Impaired N-glycosylation of the host clearly did not prevent infection in any of the three infectious agents under the tested conditions. However, I assume the effect could be different outside of pure cultures, where at least HRTV-DL1 and PVs with their narrow host ranges would have to discriminate and recognize suitable hosts out of a mixed microbial population. In this case, impaired N-glycosylation of the host could affect infection efficiency if

the specific N-glycan modifications of the host are used by the infectious agents as unique markers to quickly recognize suitable hosts.

We expect HFPV-1, HRTV-DL1 and PV proteins to be glycosylated with the individual glycan modifications specific to *Hrr. lacusprofundi*, as was described previously for the spike protein of HRPV-1 and *Halorubrum* spp. PV6 (Kandiba *et al*., 2012; Zaretsky *et al*., 2018). Unfortunately, the specific N-linked glycans of *Hrr. lacusprofundi* have not been identified yet. Based on the previous work performed on the role of *agl* cluster enzymes in *H. volcanii* [see Jarrell *et al.* (2014), and references therein], and *Halobacterium salinarium* (Zaretsky *et al.,* 2019*;* Vershinin *et al*., 2021a; Vershinin *et al*., 2023), a wide area opens itself up for future investigations of the different impacts N-glycosylation has in *Hrr. lacusprofundi.*

Insights into vesicle formation in haloarchaea

The discovery of a predicted small Sar1/Arf-family GTPase protein in PV and EV preparations of *Hrr. lacusprofundi* (Erdmann *et al*., 2017) laid the groundwork for the eventual discovery of the crucial role that EV-associated Ras superfamily GTPases play for the vesicle formation of *Euryarchaeota* described in Chapter III (Mills *et al*., 2023). Already in 2017, the association of small GTPases and host and pR1SE-derived proteins with structural similarities to subunits of the eukaryotic COPI vesicle coat complex suggested COPI-like mechanism of vesicle formation. With the experimental work performed on *H. volcanii* EVs and identification of the spread of small Ras superfamily GTPases across archaea we can now propose that EV formation in *Euryarchaeota* is likely driven in a GTPase-dependent manner similar to intracellular vesicle trafficking in eukaryotes. Homologues of the eukaryotic ESCRT machinery of extracellular vesicle formation have been identified in archaea and their role in cell division and vesicle formation has been studied in the *Thermoproteota* (Lindås *et al*., 2008; Caspi & Dekker, 2018;

Liu *et al*., 2021b; Hurtig *et al*., 2023). Therefore, it seems plausible that both the intracellular and the extracellular vesicle trafficking machineries of eukaryotes could have been derived from the archaeal domain or from a common ancestor. PV formation is not inhibited by the deletion of the small GTPase in *Hrr. lacusprofundi*, which strongly suggests that PV formation is driven by a separate mechanism. pR1SE could of course also be exploiting vesicle formation machinery proteins in a virus-like manner as has been suggested for *Sulfolobus* viruses (Quemin *et al*., 2016; Liu *et al*., 2021a), and shown for eukaryotic viruses (Votteler & Sundquist, 2013; Kumari *et al*., 2022).

Deletion of the *arcV* gene in *Hrr. lacusprofundi* did not lead to the same vesicle formation deficient phenotype that was observed in the *H. volcanii*. Since the large-scale deletions in the genomes of the *Hrr. lacusprofundi arcV* mutants were not located adjacent to the successful in-frame deletion of *arcV*, and similar re-arrangements did not appear when other genes were deleted with the same method, we do not interpret this to be a direct result of the vector integration and excision the target site. We suggest the loss of the former regions of chromosome 2 to be due to transposase activity. We hypothesized that *arcV* is not an essential gene in *Hrr. lacusprofundi*, as mutants did not show any severe growth defects. However, the gene appears important enough to induce this large-scale re-arrangement of the genome as the organism tries to adjust to the deletion. Deletion of *arcV* clearly disrupted the regular ArcV-driven extracellular vesicle formation; therefore, an alternative process likely forms the large, irregular vesicles we observed in the *arcV* mutants. Repeating the gene deletion of *arcV* and screening of mutants could help us to determine for certain if this large-scale genome arrangement was a one-time occurrence or strongly tied to *arcV* deletion. Screening of genomes and phenotypes of multiple mutants could also help identify candidate proteins that could cause the formation of these irregular vesicles.

We were able to show that EVs of both *H. volcanii* and *Hrr. lacusprofundi* were selectively enriched in specific lipid species in a unique pattern for each species. Kasson *et al*. (2017) proposed that selective enrichment of lipids into budding viruses could be caused by local enrichment of lipid species at budding sites, by direct binding of lipids to capsid proteins or by physical properties of the viral/EV membrane that would cause lipids to separate during the budding process. If we follow the theory that the vesicle formation in *Euryarchaeota* is driven by a COPI-like mechanism, looking into the lipid composition of COPI vesicles could provide clues for potential mechanisms of enrichment. Indeed, COPI vesicles contain lower levels of sphingomyelin and cholesterol, which form liquid ordered phases in the membrane, compared to the Golgi apparatus from which they bud (Brügger *et al.*, 2000).

The formation of COPI vesicles begins with the recruitment of the Arf1 small GTPase to the Golgi membrane and GTP-bound Arf1 binds directly to the lipid bilayer (Antonny *et al.*, 1997). *In vitro* studies on membrane deformation showed that Arf1-GTP recruitment and COPI coat assembly occur preferentially on liquid-disordered regions of the membrane (Manneville *et al.*, 2008). Following a hypothesis by Pinot *et al.* (2010), in a homogeneous membrane with a mixed lipid composition, this process likely enriches liquid-disordered phase lipids in the region surrounding the budding vesicle. Then the positive curvature of the membrane during budding drives enrichment of lipids into the vesicle. Tension in the stem of the budding vesicle between EV enriched and Golgi-enriched lipids could then drive fission (Pinot *et al*., 2010). As far as I can tell this remains the most likely scenario for the selective enrichment of lipids into the COPI vesicles from a mixed membrane with small regions of local enrichment. Other eukaryotic intracellular vesicle types and viruses specifically use larger lipid rafts of liquid-ordered phases for budding [Sapoń *et al*. (2023) and references therein] which are not enriched in the COPI vesicles. In other studies, COPII vesicles were shown to be specifically enriched

with lipids with a conical shape *in vitro*, which likely facilitate vesicle formation based on their shape (Melero *et al.*, 2018).

Since archaea have a unique lipid chemistry, we are still far away from understanding how archaeal membranes are organized. Interest in 'archaeasomes', liposomes composed of archaeal lipids, is increasing (Chong *et al.*, 2022) and could provide answers to whether local enrichment of lipid species also occurs on archaeal membranes as it does in eukaryotes and bacteria. *H. volcanii* and other haloarchaea are pleomorphic, i.e., able to change their cell shapes, according to growth stage, nutrient availability and presence of specific proteins such as, e.g., CetZ-tubulin-like proteins (Duggin *et al.*, 2015; de Silva *et al.*, 2021; Schwarzer *et al.*, 2021; Schiller *et al.*, 2023). We do not know if changes in cell shape are also accompanied by shifts in the lipid composition of the cell membrane. Presumably, changes in curvature between e.g., rod-shaped cells and disk-shaped cells could also necessitate modifications in the lipids or localized enrichment in specific lipid species. This kind of shift in the available pool of lipids could then also affect selective enrichment of lipids into vesicles. We harvested both species for lipid extraction in early stationary phase, where *H. volcanii* cells were most likely disk-shaped and non-motile. Growth stage dependent pleomorphism has not yet been experimentally determined for *Hrr. lacusprofundi* but based on anecdotal evidence, assuming that it also exists in this organism, we might see differences in the lipid composition of cells and EVs at different stages of growth for both species.

Our results presented in Chapter III, along with previous studies e.g., Bamford *et al.* (2005); Ellen *et al.* (2009); Baquero *et al.* (2021), strongly suggest that selective enrichment of lipid species into lipid-containing particles such as vesicles and virions is common in archaea and could be driven by similar processes.

Expanding our knowledge about the pR1SE infection cycle

As proposed in the original publication (Erdmann *et al.*, 2017), we saw that pR1SE replication and PV production were tied to the growth rate of the host and stagnated once growth reached stationary phase (Chapter II & IV). This phenomenon is probably not caused by increases in host chromosome copy numbers shifting the plasmid-to-host ratios. *Hrr. lacusprofundi* like other haloarchaea has a genome composed of several replicons and is a highly polyploid organism (Breuert *et al.*, 2006; Ludt & Soppa, 2019). Polyploidy confers evolutionary advantages for life under extreme conditions e.g., increasing survival rates during desiccation and providing templates for efficient DNA repair (Zerulla *et al.*, 2014; Zerulla & Soppa, 2014; Ludt & Soppa, 2019). While the regulation of polyploidy has not been analysed for *Hrr. lacusprofundi*, in all other haloarchaea that have been described so far, regulation of polyploidy is coupled to the growth phase of the cell. Copy numbers increase during exponential growth and decrease during stationary phase (Breuert *et al.*, 2006; Jaakkola *et al.*, 2014; Ludt & Soppa, 2019).

In a multi-replicon genome not all components are present at the same copy numbers and secondary chromosomes/mini chromosomes can also be regulated outside of the main copy number control (Breuert *et al.*, 2006). pR1SE replication reaches a plateau during stationary phase likely caused by down-regulation of the host DNA replication machinery. From the infection of Δ*arcV* mutants (Chapter IV) we could infer that pR1SE may also encode targets for replication initiation proteins of the host in order to achieve its high intracellular copy numbers since replication was delayed in the mutants were one of the host replication initiation proteins was deleted.

While pR1SE is seemingly dependent on the host DNA replication machinery it does not appear to be subjected to strong copy number control by *Hrr. lacusprofundi* or is able to at least partially evade host control.

Plasmid-to-host ratios increased rapidly after infection and increased even further after dilution of the culture into a second generation. The development of intracellular high plasmid-to-host ratios is not accompanied by an additional increase in the extracellular PVs titres. Since we used comparatively high plasmid-to-host ratios for infection of the three strains (75:1), the resulting rapid plasmid replication could have quickly outpaced particle formation rates, leading to lagging PV formation. The high ratio did not prevent adsorption or pR1SE replication, indicating that adsorption and intracellular replication were not strongly constrained by receptor availability or the availability of resources for DNA replication.

These observations suggest several things about the pR1SE infection cycle. Firstly, that pR1SE replication is likely at least partially dependent on the replication initiation proteins of the host to achieve high plasmid-to-host ratios. Secondly, that pR1SE replication might be able to evade copy number control by the host to some degree, or does not compromise host fitness too much and will therefore not be subjected to strong copy number control. Thirdly, that under the conditions at which we performed the infection experiments, pR1SE replication occurs at high levels but PV production appears to be inhibited beyond a certain limit. This inhibition could be caused by a natural 'rate limit' for PV formation based on protein synthesis etc., or could theoretically be actively regulated by pR1SE in response to the environmental conditions and the fitness of the host. However, based on previous observations (Erdmann *et al*., 2017), it is likely that if we would track the plasmid-to-host ratios of pR1SE over an even longer time scale we would also eventually see plasmid integration into the host chromosome and lower PV yields.

pR1SE in the context of conjugative plasmids in archaea

Comparison of pR1SE to conjugative plasmids appears obvious, since conjugation, *i.e.* unidirectional dissemination through direct cell-to-cell contact,

is the main mechanism of plasmid self-transmission (Virolle *et al.*, 2020). Conjugative plasmids encode their own transfer mechanisms and are thus in a certain sense analogous to the pR1SE plasmid, although the mode is different. One of the proteins in the core region 2 of pR1SE, was predicted to have a similar structure as bacterial pilus proteins or vesicle associated proteins (Erdmann *et al.*, 2017). Pili-like proteins could potentially form part of the PV coat complex or be involved in attachment to the host cells during infection, but as PVs are clearly able to transmit independently of cell-to-cell contact this process would not be comparable to *bona fide* conjugation.

Until very recently archaeal conjugative plasmids had only been identified in the *Sulfolobales* of the *Thermoproteota* phylum (Schleper *et al*., 1995; Grogan, 1996; Prangishvili *et al.*, 1998; Wagner *et al.*, 2017), and not in any members of the major archaeal phylum *Euryarchaeota* which has comparatively many representatives in culture. The wide spread of homologues to the bacterial conjugation machinery across archaea (Krupovič *et al*., 2019b, Catchpole *et al.*, 2023) and predictions that archaea likely originally acquired conjugative plasmids via inter-domain transfer from bacteria in multiple instances (Guglielmini *et al*., 2012), strongly suggest that we have only scratched the surface of the diversity of archaeal conjugative plasmids so far. Catchpole and colleagues (2023) recently described the conjugative pT33-3 plasmid isolated from a hyperthermophilic Euryarchaeon *Thermococcus* sp. Conjugation is dependent on plasmid-encoded type IV secretion system-like genes and strictly requires cell to cell contact (Catchpole *et al.*, 2023). The pT33-3 plasmid appears to be conserved in size (~100 kB) and is present at approx. equal copy numbers to the host chromosome (Catchpole *et al.*, 2023).

In contrast, the pR1SE plasmid has exhibited large size range, the smallest known version of pR1SE that is still packaged into PVs is approx. 38 kB, but pR1SE can inflated up to at least 160 kB (Erdmann *et al.*, 2017). Lower PV

yields of inflated pR1SE are likely reflective of less efficient packaging of plasmid DNA into PVs and suggest that there is a upper size limit to the amount of DNA that can be packaged into PVs (Erdmann *et al.*, 2017). To the best of my knowledge, no universal upper size limit has ever been determined for conjugative plasmids, and conjugative megaplasmids with sizes above 200 kB have been identified in bacteria (Blanca-Ordóñez *et al.*, 2010; Smillie *et al*., 2010; Mindlin *et al*., 2021; Li *et al*., 2022). Since conjugative plasmids appear to be less limited in size compared to pR1SE we have to assume that the dissemination by PVs has other advantages that counter this effect or that pR1SE may be specifically evolving towards transmission with a streamlined plasmid.

We currently do not know whether pR1SE might have spread by inter-domain or inter-phylum transfers during its evolution as has been described for pT33-3 (Catchpole *et al.*, 2023). The phylogeny of pR1SE or pR1SE-encoded proteins has not been determined yet. pR1SE has a very narrow host-range, infection of other haloarchaea with PVs or transformation with pR1SE DNA have been unsuccessful so far (personal communication by S. Erdmann, and own unpublished work), and infection does not appear to trigger a strong immune response in *Hrr. lacusprofundi* strains. In contrast, pT33-3 can disseminate between different species and genera of *Thermococcales* in the laboratory and the spread of anti-pT33-3 CRISPR spacers among *Thermococcales* indicates both a wide host range and a strong immune response against this conjugative plasmid (Catchpole *et al.*, 2023). As described in Chapters II & IV, the increase in intracellular copy numbers of pR1SE over time shows an opposite development to the previously described behaviour of archaeal conjugative plasmids immediately after conjugation (Schleper *et al.*, 1995; Prangishvili *et al.*, 1998; Erauso *et al*., 2006;). Therefore, the intracellular replication of pR1SE is more similar to an actively replicating virus than to a conventional archaeal plasmid.

Interactions between viruses and plasmids across the borders of the virosphere

In the virosphere concept laid out by Koonin *et al.* (2021), viruses form a distinct group within the broader replicator space. However, the borders between the orthovirosphere, containing true viruses, the perivirosphere, of virus-like elements, and the outer space of non-viral mobile genetic elements (MGEs) are not rigid. Gene exchange and evolution across borders has shaped the virosphere we see today. Although plasmids also replicate independently, they are for the most part grouped firmly within the non-viral MGEs, although traces of large-scale recombination and gene-exchange clearly connect viruses and plasmids. The ancestry of some viral lineages can be traced to the replication initiation proteins of bacterial plasmids (Krupovič, 2013; Koonin *et al.*, 2015), and the opposite evolution from DNA viruses to plasmids in red algae and plant pathogens has also been demonstrated (Kazlauskas *et al.*, 2019). Increasing knowledge on the connections between plasmids and viruses will help us to better determine the position that pR1SE and PVs occupy within the broader replicator space.

The most famous example of direct plasmid and virus interaction is molecular piracy where satellite MGEs (including plasmids) hijack the capsid of a helper virus for their own dissemination (Briani *et al.*, 2001; Desnues *et al*., 2012; Lossouarn *et al.*, 2015; Dokland, 2019). In the case of phage-inducible chromosomal islands, the MGE is specifically integrated in the host genome but excises during the infection of the helper virus (Ruzin *et al.*, 2001; Penadés & Christie, 2015; Fillol-Salom *et al.*, 2018; Humphrey *et al.*, 2021). In *Vibrio cholerae* island-like elements have been incorporated into the host immune defence against phages (O'Hara *et al.*, 2017; O'Hara *et al.*, 2022). Recent work has shown that some phage-inducible chromosomal islands' encode

their own capsids but acquire the phage tails from helper phages with no apparent cost to the helper (Alqurainy *et al*., 2023).

In bacteria, temperate phages are able to recombine with plasmids into a hybrid form, sometimes called 'phage-plasmids' (Pfeifer *et al.*, 2021). The first P-Ps were isolated as either linear or circular free plasmids, which could transfer both horizontally and vertically (Łobocka *et al*., 2004; Gilcrease & Casjens, 2018; Ravin, 2011). Several characterized P-Ps encode both viral proteins incl. major capsid proteins and hallmark plasmid genes (Arbing *et al*., 2010; Hwang *et al*., 2013; Cruz *et al.*, 2014; Pfeifer *et al.*, 2022). Large-scale homologous recombination and transposon mediated gene transfer with plasmids and phages has shaped the composition of P-Ps (Pfeifer & Rocha, 2023). Some bacterial plasmids appear to have developed out of P-Ps (Kidgell *et al.*, 2002; Octavia *et al.*, 2015; Zhou *et al*., 2018) but the opposite evolution of a P-P into a functional phage by the loss of plasmid characteristics has not been described.

To the best of my knowledge, no virus-plasmids hybrids similar to the P-Ps of bacteria have been identified in archaea so far. Large-scale gene exchange between archaeal viruses and plasmids has been noted, mainly of putative replication or DNA binding proteins which connect archaeal viruses to closely related plasmids [see Iranzo *et al*. (2016) and references therein]. In archaea, the two viral satellites pSSVi and pSSVx are present either integrated or in plasmid form in their *Sulfolobales* hosts (Contursi *et al.*, 2014). They cannot disseminate themselves as they lack any structural protein genes and require infection with a fusellovirus, either SSV1 or SSV2, for dissemination in small spindle-shaped virions (Arnold *et al.*, 1999; Y. Wang *et al.*, 2007; Ren *et al*., 2013; Contursi *et al.*, 2014). As they encode their own distinct replication modules, Koonin *et al.* (2021) placed them at the outer border of the perivirosphere of virus-like elements. Defective proviruses in

plasmid form have also been identified in hyperthermophilic archaea (Bernick *et al.*, 2012; Gaudin *et al*., 2013; Gaudin *et al.*, 2014). Both plasmids contain viral proteins and the pTN3 plasmid from *Thermococcus* is transferred by vesiduction along with other regular plasmids (Soler *et al*., 2008, Gaudin *et al*., 2013; Gaudin *et al.*, 2014). Unlike PVs, these transporting EVs are morphologically indistinguishable from other EVs and do not contain any plasmid or provirus encoded proteins. Although these archaeal viruses clearly have some plasmid–like characteristics, they retain their virus identity much more than the P-Ps described in bacteria. It may be that archaeal P-Ps have simply not been discovered yet although the fact archaeal viruses form distinct groups separate from other viruses suggests the possibility that there might be a barrier to 'virus-plasmid' development in archaea.

The recently discovered 'Borgs', new archaeal MGEs identified based on sequences and associated with uncultivated anaerobic methane oxidizing archaea (Al-Shayeb *et al.*, 2022; Schoelmerich *et al.*, 2023a; Schoelmerich *et al.,* 2023b), could be candidates for such virus-plasmid fusions in archaea. Borgs are large (≤ 1 Mb) linear dsDNA MGEs with shared evolutionary origin but variable gene content including key metabolic genes of their *Methanoperedens* hosts which suggests a role for them as gene reservoirs and gene transfer agents for their hosts (Al-Shayeb *et al*., 2022; Schoelmerich *et al*., 2023a). No canonical plasmid genes have been identified in the published Borg sequences but many genes appear to have viral relatives or structural similarities to viral proteins (Schoelmerich *et al*., 2023a). It is not clear how these Borgs are associated with their *Methanoperedens* hosts, neither regarding host-specificity nor regarding possible modes of transfer between cells. There is no clear evidence that Borgs could exist in the extracellular space yet, apart from encoding individual proteins with structural similarity to viral capsid proteins. The authors speculate that Borgs might exist extracellularly, protected by some kind of encapsulating structure. Borgs showed

high copy numbers (average 8.8 to 1) compared to host genomes in the environment, which the authors state would be unusual for a stable intracellular interaction (Schoelmerich *et al*., 2023a). However, as previous work on conjugative plasmids in *Sulfolobus* strains (Schleper *et al*., 1995; Prangishvili *et al.,* 1998; Erauso *et al*., 2006), and our results for the pR1SE plasmid show, it is not unusual for large (~ 25 to 50 kB) archaeal plasmids to exist with copy numbers well above 10 intracellularly. Therefore, high intracellular copy numbers for Borgs should not be discounted as a possibility simply based on their size (~ 1 Mb), if they are highly mobile MGEs in the *Methanoperedens* population. We do not know yet know enough to clearly characterize the Borg and *Methano-peredens* interaction and to which way the evolution might be pointing, towards evolution into a more selfish virus-like MGE, or towards subjugation into the pangenome of the host.

In contrast to the Borgs, the pR1SE plasmid does not encode any homologues to known viral genes [Erdmann *et al.* (2017) and personal communication by D. Lücking] apart from its phage-like integrase. However, viral-like integrases have been identified in many archaeal plasmids (Peng, 2008; Forterre *et al*., 2015; H. Wang *et al*., 2015; Badel *et al*., 2021), and all archaeal tyrosine recombinases share a conserved Phage_integrase domain [Pfam PF00589, Badel *et al.* (2021)]. Therefore, this gene is not in itself an indicator for virus ancestry. It is possible that any viral ancestors of pR1SE have not yet been identified and that this plasmid might present a 'Frankenstein' hybrid of virus and plasmid-derived genes and an analogue to bacterial phage-plasmids after all. The life cycle of pR1SE is clearly virus-like and goes beyond what has been described for transfer of plasmids by vesiduction before (Soler & Forterre, 2020). In the absence of concrete evidence for any virus origin of pR1SE, the simplest explanation is that pR1SE has evolved out of archaeal plasmids.

pR1SE or its ancestors could originally have been helper plasmids that were incorporated into the anti-virus defence of their hosts, similar to the systems seen in *V. cholerae*. Since pR1SE or its ancestors would have closely interacted with viruses in this process, fusion or acquisition of virus genes might have started the evolution towards more selfish replication and dissemination that we see in pR1SE today. In the laboratory, established pR1SE infection does prevent infection with the known lytic tailed virus of *Hrr. lacusprofundi* (unpublished data) and co-infection assays with un-infected host cells might also show us exclusionary effects between pR1SE and viruses.

Scenarios for the future evolution of pR1SE & PVs in their native environment

Hypotheses for the origin of viruses can be divided into three distinct scenarios, which were recounted in detail in the Introduction of this thesis. Krupovič *et al*. (2019a) proposed a chimeric scenario in which primordial selfish replicons acquired cellular proteins to form their virions and state that new groups of viruses likely emerged repeatedly of the history of life. This seems to me currently as the most likely scenario for the evolution of viruses. In the original publication, the pR1SE mechanism of DNA transfer was described as a potential precursor to virus propagation (Erdmann *et al*., 2017), but is this the only path that pR1SE and PV evolution could follow?

We have not been able to infect other haloarchaea with PVs in the laboratory, but analysis of host-derived regions in the variable region 3 of the plasmid has identified regions with matches on genomes of other haloarchaea in different versions of the plasmid suggesting a broader host range for PVs in the environment (Erdmann *et al.*, 2017). Incorporation of host DNA into the pR1SE plasmid is likely facilitated through integration and excision from host chromosomes. Therefore, we can propose that pR1SE may play a role in horizontal gene transfer between *Hrr. lacusprofundi* and other haloarchaea.

We know that these Antarctic haloarchaea engage in large-scale gene exchange across species and genera and pR1SE could be one of the transfer agents along with viruses (DeMaere *et al.*, 2013; Williams *et al.*, 2014; Tschitschko *et al*., 2015; Erdmann *et al*., 2017; Tschitschko *et al.*, 2018). In that case, PVs would probably be advantageous for the transfer of larger genomic regions compared to virions since they are likely less limited in size. The same principle would apply to EVs but we do not see abundant packaging of cellular DNA into EVs of *Hrr. lacusprofundi*. This suggests that gene exchange via PVs could provide evolutionary advantages for the host organisms compared to classical vesiduction. However, the advantages of using PVs compared to large-scale DNA exchange by mating between cells are not clear yet, particularly considering the more 'selfish' replication and dissemination of PVs.

In pure cultures of *Hrr. lacusprofundi,* pR1SE would presumably be much less useful as a tool for gene transfer than it would be even in e.g., mixed incubations of different *Hrr. lacusprofundi* strains. Would we see a shutdown of PV production as pR1SE enters a 'lysogenic' state or even loss of the plasmid in incubations of pure cultures under optimal conditions for the host over evolutionary time-scales? Under these circumstances, we could image that pR1SE would be incorporated into the genome in a state similar to defective provirus. Individual genes or the entire plasmid could then be re-directed towards host functions in a similar process to virus exaptation *i.e.* the seizure of viruses and virus genes for host functions (Koonin & Krupovič, 2018). The most prominent examples for this phenomenon are the gene-transfer-agents that package and transmit host DNA in their capsids (Bertani & Baresi, 1987; Lang *et al*., 2012; Lang *et al.*, 2017).

Alternatively, the trajectory of pR1SE and PVs in their natural environment could point towards evolution into genuine viruses following previous patterns of virus evolution out of plasmids (Krupovič, 2013; Koonin *et al.,* 2015).

We think that pR1SE uses both its own replication proteins and likely directs the host DNA replication machinery towards itself. This provides the right conditions for more selfish re-direction of host resources towards pR1SE replication and PV production in a virus-like manner. Since PVs efficiently package the pR1SE with only low levels of host DNA, the plasmid DNA must be specifically recognized and packaged by proteins, although we do not currently know their identity. We know that pR1SE encodes proteins that likely form part of the PV coat although the structures and coat complex components have not been identified by e.g., cryo-electron microscopy yet. We also know that PVs contain a number of host proteins, whether by passive uptake of membrane proteins or through hijacking of/or dependence on the EV formation machinery. PVs are not virions per definition, since they do not contain viral genomes, but PVs may recruit other cellular proteins to modify their vesicle coat complex to increase infection efficiency over subsequent evolution. There is no certainty in predicting evolutionary outcomes in a complicated system with multiple factors the only thing that we can do is keep analysing PVs and their host interactions in their current state.

Concluding Remarks

Even with continued expansion of diversity in the archaeal MGE space, pR1SE and its transmission by PVs still exhibit a unique set of characteristics. The plasmid encodes its own putative transfer machinery like a conjugative plasmid but the mode of dissemination shows clear similarities to viruses. The interaction between pR1SE and its host *Hrr. lacusprofundi* appears to be commensal if not mutually beneficial for both partners. pR1SE likely expands the pan genome of *Hrr. lacusprofundi* and could facilitate horizontal gene transfer between haloarchaea. We have the rare opportunity to study the interactions of PVs with their host under laboratory conditions and put our results into context within broader conversations about the origin and evolution of viruses. We do not currently know of any other producers of

plasmid vesicles apart from pR1SE and its host *Hrr. lacusprofundi*, but identification is ongoing. Therefore, we do not yet know if this specific mechanism of DNA transfer has only arisen in a very specific ecological niche or could be found in microbial communities worldwide. Looking at recent advances in our understanding of virus evolution, I strongly suspect that pR1SE is not singular; other PV-like elements are most likely out there waiting to be identified.

Studying this system came with its own challenges. Outside of pre-established model systems in haloarchaea we had to overcome many obstacles in our characterization of PVs and their host interactions. I am sure that we have only scratched the surface on what there is to discover about this system. One major unknown is the composition of the PV coat complex and identification of the proteins that mediate attachment and fusion with the host across the S-layer barrier. We also had to make concessions to study the PV-host interactions in the laboratory mainly by using pure cultures of the host and growth of the host at much higher temperatures than would be naturally found in the hypersaline lakes from which they were isolated. Then again, this unique system would not have been discovered in the first place if we only stayed on well-trodden paths and extrapolated from model systems.

As we continue to explore the diversity of viruses and virus-like elements in all domains of life, it is becoming apparent that we cannot think of viruses simply as selfish parasites. The co-evolution between the virosphere and cellular life is complex and, in many ways, made current life on earth possible in the first place. Natural phenomena resist easy categorization; it is good for us as scientists to remember that and to look at the natural environment with an open mind.

References

Al-Shayeb, B., Schoelmerich, M. C., West-Roberts, J., Valentin-Alvarado, L. E., Sachdeva, R., Mullen, S., Crits-Christoph, A., Wilkins, M. J., Williams, K. H., Doudna, J. A., & Banfield, J. F. (2022). Borgs are giant genetic elements with potential to expand metabolic capacity. *Nature, 610*(7933), 731-736. doi:10.1038/s41586-022-05256-1

Alarcón-Schumacher, T. (2023). *Virus-host interactions during chronic infections & Diversity and evolution of Pleolipoviruses.* (Dr. rer. nat.). University of Bremen, Bremen.

Alarcón-Schumacher, T., Naor, A., Gophna, U., & Erdmann, S. (2022). Isolation of a virus causing a chronic infection in the archaeal model organism *Haloferax volcanii* reveals antiviral activities of a provirus. *Proceedings of the National Academy of Sciences, 119*(35), e2205037119. doi:10.1073/pnas.2205037119

Alqurainy, N., Miguel-Romero, L., Moura de Sousa, J., Chen, J., Rocha, E. P. C., Fillol-Salom, A., & Penadés, J. R. (2023). A widespread family of phage-inducible chromosomal islands only steals bacteriophage tails to spread in nature. *Cell Host & Microbe, 31*(1), 69-82.e65. doi:10.1016/j.chom.2022.12.001

Antonny, B., Beraud-Dufour, S., Chardin, P., & Chabre, M. (1997). N-Terminal Hydrophobic Residues of the G-Protein ADP-Ribosylation Factor-1 Insert into Membrane Phospholipids upon GDP to GTP Exchange. *Biochemistry, 36*(15), 4675-4684. doi:10.1021/bi962252b

Arbing, M. A., Handelman, S. K., Kuzin, A. P., Verdon, G., Wang, C., Su, M., Rothenbacher, F. P., Abashidze, M., Liu, M., Hurley, J. M., Xiao, R., Acton, T., Inouye, M., Montelione, G. T., Woychik, N. A., & Hunt, J. F. (2010). Crystal Structures of Phd-Doc, HigA, and YeeU Establish Multiple Evolutionary Links between Microbial Growth-Regulating Toxin-Antitoxin Systems. *Structure, 18*(8), 996-1010. doi:10.1016/j.str.2010.04.018

Arnold, H. P., She, Q., Phan, H., Stedman, K., Prangishvili, D., Holz, I., Kristjansson, J. K., Garrett, R., & Zillig, W. (1999). The genetic element pSSVx of the extremely thermophilic crenarchaeon *Sulfolobus* is a hybrid between a plasmid and a virus. *Molecular Microbiology, 34*(2), 217-226. doi:10.1046/j.1365-2958.1999.01573.x

Badel, C., Da Cunha, V., & Oberto, J. (2021). Archaeal tyrosine recombinases. *FEMS microbiology reviews, 45*(4). doi:10.1093/femsre/fuab004

Bamford, D. H., Ravantti, J. J., Rönnholm, G., Laurinavicius, S., Kukkaro, P., Dyall-Smith, M., Somerharju, P., Kalkkinen, N., & Bamford, J. K. (2005). Constituents of SH1, a novel lipid-containing virus infecting the halophilic euryarchaeon Haloarcula hispanica. *J Virol, 79*(14), 9097-9107. doi:10.1128/jvi.79.14.9097-9107.2005

Baquero, D. P., Gazi, A. D., Sachse, M., Liu, J., Schmitt, C., Moya-Nilges, M., Schouten, S., Prangishvili, D., & Krupovic, M. (2021). A filamentous archaeal virus is enveloped inside the cell and released through pyramidal portals. *Proceedings of the National Academy of Sciences, 118*(32), e2105540118. doi:10.1073/pnas.2105540118

Bernick, D. L., Karplus, K., Lui, L. M., Coker, J. K. C., Murphy, J. N., Chan, P. P., Cozen, A. E., & Lowe, T. M. (2012). Complete genome sequence of *Pyrobaculum oguniense*. *Standards in genomic sciences, 6*(3), 336-345. doi:10.4056/sigs.2645906

Bertani, G., & Baresi, L. (1987). Genetic transformation in the methanogen *Methanococcus voltae* PS. *Journal of bacteriology, 169*(6), 2730-2738. doi:10.1128/jb.169.6.2730-2738.1987

Blanca-Ordóñez, H., Oliva-García Juan, J., Pérez-Mendoza, D., Soto María, J., Olivares, J., Sanjuán, J., & Nogales, J. (2010). pSymA-Dependent Mobilization of the *Sinorhizobium meliloti* pSymB Megaplasmid. *Journal of bacteriology, 192*(23), 6309-6312. doi:10.1128/jb.00549-10

Breuert, S., Allers, T., Spohn, G., & Soppa, J. (2006). Regulated polyploidy in halophilic archaea. *PLOS ONE, 1*(1), e92. doi:10.1371/journal.pone.0000092

Briani, F., Dehò, G., Forti, F., & Ghisotti, D. (2001). The Plasmid Status of Satellite Bacteriophage P4. *Plasmid, 45*(1), 1-17. doi:10.1006/plas.2000.1497

Brügger, B., Sandhoff, R., Wegehingel, S., Gorgas, K., Malsam, J., Helms, J. B., Lehmann, W.-D., Nickel, W., & Wieland, F. T. (2000). Evidence for Segregation of Sphingomyelin

and Cholesterol during Formation of Copi-Coated Vesicles. *Journal of Cell Biology, 151*(3), 507-518. doi:10.1083/jcb.151.3.507
Caspi, Y., & Dekker, C. (2018). Dividing the Archaeal Way: The Ancient Cdv Cell-Division Machinery. *Frontiers in microbiology, 9*. doi:10.3389/fmicb.2018.00174
Catchpole, R. J., Barbe, V., Magdelenat, G., Marguet, E., Terns, M., Oberto, J., Forterre, P., & Da Cunha, V. (2023). A self-transmissible plasmid from a hyperthermophile that facilitates genetic modification of diverse Archaea. *Nature microbiology*. doi:10.1038/s41564-023-01387-x
Chong, P. L.-G., Chang, A., Yu, A., & Mammedova, A. (2022). Vesicular and Planar Membranes of Archaea Lipids: Unusual Physical Properties and Biomedical Applications. *International Journal of Molecular Sciences, 23*(14), 7616. doi:10.3390/ijms23147616
Contursi, P., Fusco, S., Cannio, R., & She, Q. (2014). Molecular biology of fuselloviruses and their satellites. *Extremophiles, 18*(3), 473-489. doi:10.1007/s00792-014-0634-0
Cruz, J. W., Rothenbacher, F. P., Maehigashi, T., Lane, W. S., Dunham, C. M., & Woychik, N. A. (2014). Doc toxin is a kinase that inactivates elongation factor Tu. *Journal of Biological Chemistry, 289*(11), 7788-7798. doi:10.1074/jbc.M113.544429
Dattani, A., Harrison, C., & Allers, T. (2022). Genetic Manipulation of *Haloferax* Species. In S. Ferreira-Cerca (Ed.), *Archaea: Methods and Protocols* (pp. 33-56). New York, NY: Springer US.
de Silva, R. T., Abdul-Halim, M. F., Pittrich, D. A., Brown, H. J., Pohlschroder, M., & Duggin, I. G. (2021). Improved growth and morphological plasticity of *Haloferax volcanii*. *Microbiology, 167*(2). doi:10.1099/mic.0.001012
DeMaere, M. Z., Williams, T. J., Allen, M. A., Brown, M. V., Gibson, J. A., Rich, J., Lauro, F. M., Dyall-Smith, M., Davenport, K. W., & Woyke, T. (2013). High level of intergenera gene exchange shapes the evolution of haloarchaea in an isolated Antarctic lake. *Proceedings of the National Academy of Sciences, 110*(42), 16939-16944. doi:10.1073/pnas.1307090110
Desnues, C., La Scola, B., Yutin, N., Fournous, G., Robert, C., Azza, S., Jardot, P., Monteil, S., Campocasso, A., Koonin, E. V., & Raoult, D. (2012). Provirophages and transpovirons as the diverse mobilome of giant viruses. *Proceedings of the National Academy of Sciences, 109*(44), 18078-18083. doi:10.1073/pnas.1208835109
Dokland, T. (2019). Molecular Piracy: Redirection of Bacteriophage Capsid Assembly by Mobile Genetic Elements. *Viruses, 11*(11), 1003. doi:10.3390/v11111003
Duggin, I. G., Aylett, C. H., Walsh, J. C., Michie, K. A., Wang, Q., Turnbull, L., Dawson, E. M., Harry, E. J., Whitchurch, C. B., & Amos, L. A. (2015). CetZ tubulin-like proteins control archaeal cell shape. *Nature, 519*(7543), 362. doi:10.1038/nature13983
Eichler, J. (2020). N-glycosylation in Archaea—New roles for an ancient posttranslational modification. *Molecular Microbiology, 114*(5), 735-741. doi:10.1111/mmi.14569
Ellen, A. F., Albers, S.-V., Huibers, W., Pitcher, A., Hobel, C. F., Schwarz, H., Folea, M., Schouten, S., Boekema, E. J., & Poolman, B. (2009). Proteomic analysis of secreted membrane vesicles of archaeal *Sulfolobus* species reveals the presence of endosome sorting complex components. *Extremophiles, 13*(1), 67. doi:10.1007/s00792-008-0199-x
Erauso, G., Stedman, K. M., van de Werken, H. J. G., Zillig, W., & van der Oost, J. (2006). Two novel conjugative plasmids from a single strain of *Sulfolobus*. *Microbiology, 152*(7), 1951-1968. doi:10.1099/mic.0.28861-0
Erdmann, S., Tschitschko, B., Zhong, L., Raftery, M. J., & Cavicchioli, R. (2017). A plasmid from an Antarctic haloarchaeon uses specialized membrane vesicles to disseminate and infect plasmid-free cells. *Nature microbiology, 2*(10), 1446. doi:10.1038/s41564-017-0009-2
Fillol-Salom, A., Martínez-Rubio, R., Abdulrahman, R. F., Chen, J., Davies, R., & Penadés, J. R. (2018). Phage-inducible chromosomal islands are ubiquitous within the bacterial universe. *The ISME journal, 12*(9), 2114-2128. doi:10.1038/s41396-018-0156-3

Forterre, P., Krupovič, M., Raymann, K., & Soler, N. (2015). Plasmids from euryarchaeota. In *Plasmids: Biology and Impact in Biotechnology and Discovery* (pp. 349-377): American Society of Microbiology.

Gaudin, M., Gauliard, E., Schouten, S., Houel-Renault, L., Lenormand, P., Marguet, E., & Forterre, P. (2013). Hyperthermophilic archaea produce membrane vesicles that can transfer DNA. *Environmental Microbiology Reports, 5*(1), 109-116. doi:10.1111/j.1758-2229.2012.00348.x

Gaudin, M., Krupovič, M., Marguet, E., Gauliard, E., Cvirkaite-Krupovič, V., Le Cam, E., Oberto, J., & Forterre, P. (2014). Extracellular membrane vesicles harbouring viral genomes. *Environmental microbiology, 16*(4), 1167-1175. doi:10.1111/1462-2920.12235

Gilcrease, E. B., & Casjens, S. R. (2018). The genome sequence of *Escherichia coli* tailed phage D6 and the diversity of *Enterobacteriales* circular plasmid prophages. *Virology, 515*, 203-214. doi:10.1016/j.virol.2017.12.019

Grogan, D. (1996). Exchange of genetic markers at extremely high temperatures in the archaeon *Sulfolobus acidocaldarius*. *Journal of bacteriology, 178*(11), 3207-3211. doi:10.1128/jb.178.11.3207-3211.1996

Guglielmini, J., de la Cruz, F., & Rocha, E. P. C. (2012). Evolution of Conjugation and Type IV Secretion Systems. *Molecular biology and evolution, 30*(2), 315-331. doi:10.1093/molbev/mss221

Harrison, C., & Allers, T. (2022). Progress and Challenges in Archaeal Genetic Manipulation. In S. Ferreira-Cerca (Ed.), *Archaea: Methods and Protocols* (pp. 25-31). New York, NY: Springer US.

Humphrey, S., San Millán, Á., Toll-Riera, M., Connolly, J., Flor-Duro, A., Chen, J., Ubeda, C., MacLean, R. C., & Penadés, J. R. (2021). Staphylococcal phages and pathogenicity islands drive plasmid evolution. *Nature communications, 12*(1), 5845. doi:10.1038/s41467-021-26101-5

Hurtig, F., Burgers, T. C. Q., Cezanne, A., Jiang, X., Mol, F. N., Traparić, J., Pulschen, A. A., Nierhaus, T., Tarrason-Risa, G., Harker-Kirschneck, L., Löwe, J., Šarić, A., Vlijm, R., & Baum, B. (2023). The patterned assembly and stepwise Vps4-mediated disassembly of composite ESCRT-III polymers drives archaeal cell division. *Science advances, 9*(11), eade5224. doi:10.1126/sciadv.ade5224

Hwang, L. C., Vecchiarelli, A. G., Han, Y.-W., Mizuuchi, M., Harada, Y., Funnell, B. E., & Mizuuchi, K. (2013). ParA-mediated plasmid partition driven by protein pattern self-organization. *The EMBO Journal, 32*(9), 1238-1249. doi:10.1038/emboj.2013.34

Iranzo, J., Koonin, E. V., Prangishvili, D., & Krupovic, M. (2016). Bipartite Network Analysis of the Archaeal Virosphere: Evolutionary Connections between Viruses and Capsidless Mobile Elements. *Journal of virology, 90*(24), 11043-11055. doi:10.1128/JVI.01622-16

Jaakkola, S. T., Zerulla, K., Guo, Q., Liu, Y., Ma, H., Yang, C., Bamford, D. H., Chen, X., Soppa, J., & Oksanen, H. M. (2014). Halophilic Archaea Cultivated from Surface Sterilized Middle-Late Eocene Rock Salt Are Polyploid. *PLOS ONE, 9*(10), e110533. doi:10.1371/journal.pone.0110533

Jarrell, K. F., Ding, Y., Meyer, B. H., Albers, S.-V., Kaminski, L., & Eichler, J. (2014). N-Linked Glycosylation in *Archaea*: a Structural, Functional, and Genetic Analysis. *Microbiology and Molecular Biology Reviews, 78*(2), 304-341. doi:10.1128/mmbr.00052-13

Kandiba, L., Aitio, O., Helin, J., Guan, Z., Permi, P., Bamford, D. H., Eichler, J., & Roine, E. (2012). Diversity in prokaryotic glycosylation: an archaeal-derived N-linked glycan contains legionaminic acid. *Molecular Microbiology, 84*(3), 578-593. doi:10.1111/j.1365-2958.2012.08045.x

Kasson, P., DiMaio, F., Yu, X., Lucas-Staat, S., Krupovič, M., Schouten, S., Prangishvili, D., & Egelman, E. H. (2017). Model for a novel membrane envelope in a filamentous hyperthermophilic virus. *eLife, 6*, e26268. doi:10.7554/eLife.26268

Kazlauskas, D., Varsani, A., Koonin, E. V., & Krupovič, M. (2019). Multiple origins of prokaryotic and eukaryotic single-stranded DNA viruses from bacterial and archaeal plasmids. *Nature communications, 10*(1), 3425. doi:10.1038/s41467-019-11433-0

Kidgell, C., Pickard, D., Wain, J., James, K., Diem Nga, L. T., Diep, T. S., Levine, M. M., O'Gaora, P., Prentice, M. B., Parkhill, J., Day, N., Farrar, J., & Dougan, G. (2002). Characterisation and distribution of a cryptic *Salmonella typhi* plasmid pHCM2. *Plasmid, 47*(3), 159-171. doi:10.1016/S0147-619X(02)00013-6

Kohda, D. (2018). Structural Basis of Protein Asn-Glycosylation by Oligosaccharyltransferases. In Y. Yamaguchi & K. Kato (Eds.), *Glycobiophysics* (pp. 171-199). Singapore: Springer Singapore.

Koonin, E. V., Dolja, V. V., Krupovič, M., & Kuhn, J. H. (2021). Viruses Defined by the Position of the Virosphere within the Replicator Space. *Microbiology and Molecular Biology Reviews, 85*(4), e00193-00120. doi:10.1128/MMBR.00193-20

Koonin, E. V., & Krupovič, M. (2018). The depths of virus exaptation. *Current opinion in virology, 31*, 1-8. doi:10.1016/j.coviro.2018.07.011

Koonin, E. V., Krupovič, M., & Yutin, N. (2015). Evolution of double-stranded DNA viruses of eukaryotes: from bacteriophages to transposons to giant viruses. *Annals of the New York Academy of Sciences, 1341*(1), 10-24. doi:10.1111/nyas.12728

Krupovič, M. (2013). Networks of evolutionary interactions underlying the polyphyletic origin of ssDNA viruses. *Curr Opin Virol, 3*(5), 578-586. doi:10.1016/j.coviro.2013.06.010

Krupovič, M., Dolja, V. V., & Koonin, E. V. (2019a). Origin of viruses: primordial replicators recruiting capsids from hosts. *Nature Reviews Microbiology, 17*(7), 449-458. doi:10.1038/s41579-019-0205-6

Krupovič, M., Makarova, K. S., Wolf, Y. I., Medvedeva, S., Prangishvili, D., Forterre, P., & Koonin, E. V. (2019b). Integrated mobile genetic elements in Thaumarchaeota. *Environmental microbiology, 21*(6), 2056-2078. doi:10.1111/1462-2920.14564

Kumari, S., Dash, P. K., Kumari, T., Guo, M.-L., Ghosh, J. K., Buch, S. J., & Tripathi, R. K. (2022). HIV-1 Nef hijacks both exocytic and endocytic pathways of host intracellular trafficking through differential regulation of Rab GTPases. *Biology of the Cell, 114*(10), 276-292. doi:10.1111/boc.202100027

Lang, A. S., Westbye, A. B., & Beatty, J. T. (2017). The Distribution, Evolution, and Roles of Gene Transfer Agents in Prokaryotic Genetic Exchange. *Annual review of virology, 4*(1), 87-104. doi:10.1146/annurev-virology-101416-041624

Lang, A. S., Zhaxybayeva, O., & Beatty, J. T. (2012). Gene transfer agents: phage-like elements of genetic exchange. *Nature Reviews Microbiology, 10*(7), 472-482. doi:10.1038/nrmicro2802

Li, M., Guan, C., Song, G., Gao, X., Yang, W., Wang, T., & Zhang, Y. (2022). Characterization of a Conjugative Multidrug Resistance IncP-2 Megaplasmid, pPAG5, from a Clinical *Pseudomonas aeruginosa* Isolate. *Microbiology Spectrum, 10*(1), e01992-01921. doi:10.1128/spectrum.01992-21

Liao, Y., Williams, T. J., Walsh, J. C., Ji, M., Poljak, A., Curmi, P. M. G., Duggin, I. G., & Cavicchioli, R. (2016). Developing a genetic manipulation system for the Antarctic archaeon, *Halorubrum lacusprofundi*: investigating acetamidase gene function. *Scientific Reports, 6*, 34639. doi:10.1038/srep34639

Lindås, A.-C., Karlsson, E. A., Lindgren, M. T., Ettema, T. J. G., & Bernander, R. (2008). A unique cell division machinery in the Archaea. *Proceedings of the National Academy of Sciences, 105*(48), 18942-18946. doi:10.1073/pnas.0809467105

Liu, J., Cvirkaite-Krupovič, V., Baquero, D. P., Yang, Y., Zhang, Q., Shen, Y., & Krupovič, M. (2021a). Virus-induced cell gigantism and asymmetric cell division in archaea. *Proceedings of the National Academy of Sciences, 118*(15), e2022578118. doi:10.1073/pnas.2022578118

Liu, J., Cvirkaite-Krupovič, V., Commere, P.-H., Yang, Y., Zhou, F., Forterre, P., Shen, Y., & Krupovič, M. (2021b). Archaeal extracellular vesicles are produced in an ESCRT-dependent manner and promote gene transfer and nutrient cycling in extreme

environments. *The ISME journal, 15*(10), 2892-2905. doi:10.1038/s41396-021-00984-0

Łobocka, M. B., Rose, D. J., Plunkett, G., Rusin, M., Samojedny, A., Lehnherr, H., Yarmolinsky, M. B., & Blattner, F. R. (2004). Genome of Bacteriophage P1. *Journal of bacteriology, 186*(21), 7032-7068. doi::10.1128/jb.186.21.7032-7068.2004

Lossouarn, J., Nesbø, C. L., Mercier, C., Zhaxybayeva, O., Johnson, M. S., Charchuck, R., Farasin, J., Bienvenu, N., Baudoux, A. C., & Michoud, G. (2015). 'Ménage à trois': a selfish genetic element uses a virus to propagate within *Thermotogales*. *Environmental microbiology, 17*(9), 3278-3288. doi:10.1111/1462-2920.12783

Ludt, K., & Soppa, J. (2019). Polyploidy in halophilic archaea: regulation, evolutionary advantages, and gene conversion. *Biochemical Society Transactions, 47*(3), 933-944. doi:10.1042/bst20190256

Manneville, J.-B., Casella, J.-F., Ambroggio, E., Gounon, P., Bertherat, J., Bassereau, P., Cartaud, J., Antonny, B., & Goud, B. (2008). COPI coat assembly occurs on liquid-disordered domains and the associated membrane deformations are limited by membrane tension. *Proceedings of the National Academy of Sciences, 105*(44), 16946-16951. doi:10.1073/pnas.0807102105

Melero, A., Chiaruttini, N., Karashima, T., Riezman, I., Funato, K., Barlowe, C., Riezman, H., & Roux, A. (2018). Lysophospholipids Facilitate COPII Vesicle Formation. *Current Biology, 28*(12), 1950-1958.e1956. doi:10.1016/j.cub.2018.04.076

Mercier, C., Thies, D., Zhong, L., Raftery, M. J., Cavicchioli, R., & Erdmann, S. (2022). In depth characterization of an archaeal virus-host system reveals numerous virus exclusion mechanisms. *bioRxiv*. doi:10.1101/2022.10.18.512658

Mills, J., Gebhard, L. J., Schubotz, F., Shevchenko, A., Speth, D. R., Liao, Y., Duggin, I. G., Marchfelder, A., & Erdmann, S. (2023). Extracellular vesicles of *Euryarchaeida*: precursor to eukaryotic membrane trafficking. *bioRxiv*. doi:10.1101/2023.03.03.530948

Mindlin, S., Maslova, O., Beletsky, A., Nurmukanova, V., Zong, Z., Mardanov, A., & Petrova, M. (2021). Ubiquitous Conjugative Mega-Plasmids of *Acinetobacter* Species and Their Role in Horizontal Transfer of Multi-Drug Resistance. *Frontiers in microbiology, 12*. doi:10.3389/fmicb.2021.728644

O'Hara, B. J., Barth, Z. K., McKitterick, A. C., & Seed, K. D. (2017). A highly specific phage defense system is a conserved feature of the *Vibrio cholerae* mobilome. *PLoS Genet, 13*(6), e1006838. doi:10.1371/journal.pgen.1006838

O'Hara, B. J., Alam, M., & Ng, W.-L. (2022). The *Vibrio cholerae* Seventh Pandemic Islands act in tandem to defend against a circulating phage. *PLoS Genet, 18*(8), e1010250. doi:10.1371/journal.pgen.1010250

Octavia, S., Sara, J., & Lan, R. (2015). Characterization of a large novel phage-like plasmid in *Salmonella enterica* serovar Typhimurium. *FEMS microbiology letters, 362*(8). doi:10.1093/femsle/fnv044

Penadés, J. R., & Christie, G. E. (2015). The Phage-Inducible Chromosomal Islands: A Family of Highly Evolved Molecular Parasites. *Annual review of virology, 2*(1), 181-201. doi:10.1146/annurev-virology-031413-085446

Peng, X. (2008). Evidence for the horizontal transfer of an integrase gene from a fusellovirus to a pRN-like plasmid within a single strain of Sulfolobus and the implications for plasmid survival. *Microbiology, 154*(2), 383-391. doi:10.1099/mic.0.2007/012963-0

Pfeifer, E., Bonnin, R. A., & Rocha, E. P. C. (2022). Phage-Plasmids Spread Antibiotic Resistance Genes through Infection and Lysogenic Conversion. *MBio, 13*(5), e01851-01822. doi:10.1128/mbio.01851-22

Pfeifer, E., Moura de Sousa, J. A., Touchon, M., & Rocha, E. P. C. (2021). Bacteria have numerous distinctive groups of phage–plasmids with conserved phage and variable plasmid gene repertoires. *Nucleic acids research, 49*(5), 2655-2673. doi:10.1093/nar/gkab064

Pfeifer, E., & Rocha, E. P. C. (2023). Phage-plasmids promote genetic exchanges between phages and plasmids and create novel ones. *bioRxiv*. doi:10.1101/2023.08.08.552325

Pinot, M., Goud, B., & Manneville, J.-B. (2010). Physical aspects of COPI vesicle formation. *Molecular Membrane Biology, 27*(8), 428-442. doi:10.3109/09687688.2010.510485

Prangishvili, D., Albers, S.-V., Holz, I., Arnold, H. P., Stedman, K., Klein, T., Singh, H., Hiort, J., Schweier, A., Kristjansson, J. K., & Zillig, W. (1998). Conjugation in Archaea: Frequent Occurrence of Conjugative Plasmids in *Sulfolobus*. *Plasmid, 40*(3), 190-202. doi:10.1006/plas.1998.1363

Quemin, E. R. J., Chlanda, P., Sachse, M., Forterre, P., Prangishvili, D., & Krupovič, M. (2016). Eukaryotic-Like Virus Budding in Archaea. *MBio, 7*(5), e01439-01416. doi:10.1128/mBio.01439-16

Ravin, N. V. (2011). N15: The linear phage–plasmid. *Plasmid, 65*(2), 102-109. doi:10.1016/j.plasmid.2010.12.004

Ren, Y., She, Q., & Huang, L. (2013). Transcriptomic analysis of the SSV2 infection of *Sulfolobus solfataricus* with and without the integrative plasmid pSSVi. *Virology, 441*(2), 126-134. doi:10.1016/j.virol.2013.03.012

Ruzin, A., Lindsay, J., & Novick, R. P. (2001). Molecular genetics of SaPI1 – a mobile pathogenicity island in *Staphylococcus aureus*. *Molecular Microbiology, 41*(2), 365-377. doi:10.1046/j.1365-2958.2001.02488.x

Sapoń, K., Mańka, R., Janas, T., & Janas, T. (2023). The role of lipid rafts in vesicle formation. *Journal of Cell Science, 136*(9). doi:10.1242/jcs.260887

Schiller, H., Kouassi, J., Hong, Y., Rados, T., Kwak, J., DiLucido, A., Safer, D., Marchfelder, A., Pfeiffer, F., Bisson-Filho, A., Schulze, S., & Pohlschroder, M. (2023). Identification and characterization of structural and regulatory cell-shape determinants in *Haloferax volcanii*. *bioRxiv*. doi:10.1101/2023.03.05.531186

Schleper, C., Holz, I., Janekovic, D., Murphy, J., & Zillig, W. (1995). A multicopy plasmid of the extremely thermophilic archaeon *Sulfolobus* effects its transfer to recipients by mating. *Journal of bacteriology, 177*(15), 4417-4426. doi:10.1128/jb.177.15.4417-4426.1995

Schoelmerich, M. C., Ly, L., West-Roberts, J., Shi, L.-D., Shen, C., Malvankar, N., Taib, N., Gribaldo, S., Woodcroft, B. J., Al-Shayeb, B., Dai, X., Mozsary, C., Hickey, S., He, C., Beaulaurier, J. A., Juul, S., Sachdeva, R., & Banfield, J. (2023a). Borg extrachromosomal elements of methane-oxidizing archaea have conserved and expressed genetic repertoires. *bioRxiv*. doi:10.1101/2023.08.01.549754

Schoelmerich, M. C., Sachdeva, R., West-Roberts, J., Waldburger, L., & Banfield, J. F. (2023b). Tandem repeats in giant archaeal Borg elements undergo rapid evolution and create new intrinsically disordered regions in proteins. *PLOS Biology, 21*(1), e3001980. doi:10.1371/journal.pbio.3001980

Schwarzer, S., Rodriguez-Franco, M., Oksanen, H. M., & Quax, T. E. F. (2021). Growth Phase Dependent Cell Shape of *Haloarcula*. *Microorganisms, 9*(2), 231. doi:10.3390/microorganisms9020231

Smillie, C., Garcillán-Barcia, M. P., Francia, M. V., Rocha, E. P. C., & Cruz, F. d. l. (2010). Mobility of Plasmids. *Microbiology and Molecular Biology Reviews, 74*(3), 434-452. doi:10.1128/mmbr.00020-10

Soler, N., & Forterre, P. (2020). Vesiduction: the fourth way of HGT. *Environmental microbiology, 22*(7), 2457-2460. doi:10.1111/1462-2920.15056

Soler, N., Marguet, E., Verbavatz, J.-M., & Forterre, P. (2008). Virus-like vesicles and extracellular DNA produced by hyperthermophilic archaea of the order *Thermococcales*. *Research in Microbiology, 159*(5), 390-399. doi:10.1016/j.resmic.2008.04.015

Tamir, A., & Eichler, J. (2017). N-Glycosylation Is Important for Proper *Haloferax volcanii* S-Layer Stability and Function. *Applied and Environmental Microbiology, 83*(6), e03152-03116. doi:10.1128/AEM.03152-16

Tschitschko, B., Erdmann, S., DeMaere, M. Z., Roux, S., Panwar, P., Allen, M. A., Williams, T. J., Brazendale, S., Hancock, A. M., Eloe-Fadrosh, E. A., & Cavicchioli, R. (2018). Genomic variation and biogeography of Antarctic haloarchaea. *Microbiome, 6*(1), 113. doi:10.1186/s40168-018-0495-3

Tschitschko, B., Williams, T. J., Allen, M. A., Páez-Espino, D., Kyrpides, N., Zhong, L., Raftery, M. J., & Cavicchioli, R. (2015). Antarctic archaea–virus interactions: metaproteome-led analysis of invasion, evasion and adaptation. *The ISME journal, 9*(9), 2094-2107. doi:10.1038/ismej.2015.110

Vershinin, Z., Zaretsky, M., Guan, Z., & Eichler, J. (2021). Identifying Components of a *Halobacterium salinarum* N-Glycosylation Pathway. *Front Microbiol, 12*, 779599. doi:10.3389/fmicb.2021.779599

Vershinin, Z., Zaretsky, M., Guan, Z., & Eichler, J. (2023). Agl28 and Agl29 are key components of a *Halobacterium salinarum* N-glycosylation pathway. *FEMS microbiology letters, 370*, fnad017. doi:10.1093/femsle/fnad017

Virolle, C., Goldlust, K., Djermoun, S., Bigot, S., & Lesterlin, C. (2020). Plasmid Transfer by Conjugation in Gram-Negative Bacteria: From the Cellular to the Community Level. *Genes, 11*(11), 1239. doi:10.3390/genes11111239

Votteler, J., & Sundquist, Wesley I. (2013). Virus Budding and the ESCRT Pathway. *Cell Host & Microbe, 14*(3), 232-241. doi:10.1016/j.chom.2013.08.012

Wagner, A., Whitaker, R. J., Krause, D. J., Heilers, J.-H., van Wolferen, M., van der Does, C., & Albers, S.-V. (2017). Mechanisms of gene flow in archaea. *Nature Reviews Microbiology, 15*(8), 492-501. doi:10.1038/nrmicro.2017.41

Wang, H., Peng, N., Shah, S. A., Huang, L., & She, Q. (2015). Archaeal extrachromosomal genetic elements. *Microbiol. Mol. Biol. Rev., 79*(1), 117-152. doi:10.1128/mmbr.00042-14

Wang, Y., Duan, Z., Zhu, H., Guo, X., Wang, Z., Zhou, J., She, Q., & Huang, L. (2007). A novel *Sulfolobus* non-conjugative extrachromosomal genetic element capable of integration into the host genome and spreading in the presence of a fusellovirus. *Virology, 363*(1), 124-133. doi:10.1016/j.virol.2007.01.035

Williams, T. J., Allen, M. A., DeMaere, M. Z., Kyrpides, N. C., Tringe, S. G., Woyke, T., & Cavicchioli, R. (2014). Microbial ecology of an Antarctic hypersaline lake: genomic assessment of ecophysiology among dominant haloarchaea. *The ISME journal, 8*(8), 1645. doi:10.1038/ismej.2014.18

Yurist-Doutsch, S., Magidovich, H., Ventura, V. V., Hitchen, P. G., Dell, A., & Eichler, J. (2010). N-glycosylation in Archaea: on the coordinated actions of *Haloferax volcanii* AglF and AglM. *Molecular Microbiology, 75*(4), 1047-1058. doi:10.1111/j.1365-2958.2009.07045.x

Zaretsky, M., Darnell, C. L., Schmid, A. K., & Eichler, J. (2019). N-Glycosylation Is Important for *Halobacterium salinarum* Archaellin Expression, Archaellum Assembly and Cell Motility. *Frontiers in microbiology, 10*. doi:10.3389/fmicb.2019.01367

Zaretsky, M., Roine, E., & Eichler, J. (2018). Sialic Acid-Like Sugars in Archaea: Legionaminic Acid Biosynthesis in the Halophile *Halorubrum* sp. PV6. *Frontiers in microbiology, 9*. doi:10.3389/fmicb.2018.02133

Zerulla, K., Chimileski, S., Näther, D., Gophna, U., Papke, R. T., & Soppa, J. (2014). DNA as a Phosphate Storage Polymer and the Alternative Advantages of Polyploidy for Growth or Survival. *PLOS ONE, 9*(4), e94819. doi:10.1371/journal.pone.0094819

Zerulla, K., & Soppa, J. (2014). Polyploidy in haloarchaea: advantages for growth and survival. *Frontiers in microbiology, 5*. doi:10.3389/fmicb.2014.00274

Zhou, W., Liu, L., Feng, Y., & Zong, Z. (2018). A P7 Phage-Like Plasmid Carrying mcr-1 in an ST15 *Klebsiella pneumoniae* Clinical Isolate. *Frontiers in microbiology, 9*. doi:10.3389/fmicb.2018.00011

Acknowledgements

I would like to start by thanking my supervisor and reviewer Susanne Erdmann. Thank you for offering me the opportunity to work in your group just after it was established. This PhD has been a winding road in many ways, but crucially not in terms of your continued support and encouragement. Thank you for the freedom you have given me to explore and develop my own ideas while also firmly telling me when you think I am headed the wrong way.

Secondly, I would like to thank Prof. Dr. Andreas Dotzauer for agreeing to review this thesis and to be part of my examination board. Additional thanks go to Prof. Dr. Michael Friedrich, Dr. Elina Roine, Dominik Lücking and Guillermo Cera Ramirez for agreeing to be members of my examination board. I want to thank Elina specifically for welcoming me in Helsinki during my stay at the University there and for teaching me all of the relevant science vocabulary in Finnish.

I would like to continue by thanking additional members of my thesis committee, Dr. Tristan Wagner, Prof. Dr. Jan-Hendrik Hehemann and Prof. Dr. Jerry Eichler for their support and advice along the way.

Thank you also to all of the co-authors and collaborators that I have had the privilege of working with during this time, and who have made the work assembled in this thesis possible.

Tomás and Jay, thank you for being the best office mates I could have wished for in these 4+ years, I have really enjoyed the laughs and problem-solving sessions along the way.

To the other past and present members of the Archaeal Virology group, thank you for creating such a wonderful working environment, it has truly been a pleasure to work together with you. I can honestly say that I have enjoyed every long, wandering discussion we have had in our lab meetings over the years. Special thanks go to Daniela and Ingrid for all of your invaluable help in the lab throughout my PhD.

My friends, thank you for all the laughs, cooking evenings, emotional support, and the great conversations over these past few years. I want to specifically thank Mara, Ula, Jan and Caro because we have been through so many highs and lows together ever since we met at the MPI as Baby MarMics in 2017, I am so grateful for our friendship

To my family, especially my parents who have promoted my curiosity from the beginning and have always encouraged me to pursue my goals and new challenges. I know that I haven't always made it easy for you, so I can only thank you for your unwavering support and even for half-jokingly explaining my work to other people by saying that I work with these weird things called archaea that nobody has heard of before.

Affirmation in lieu of oath

Universität Bremen | Fachbereich 02 | Postfach 33 04 40, 28334 Bremen

Universität Bremen
Fachbereich 2
Prüfungsamt Chemie
z. Hd. Frau Frauke Ernst
Leobener Straße

28359 Bremen
Deutschland

Prüfungsamt
Chemie

Frauke Ernst
Geschäftsstelle
Fachbereich 02
Leobener Str. / NW2
D-28359 Bremen

Verwaltungspavillon 06
Tel. 0421 218-62802
Fax 0421 218-9862802
frauke.ernst@uni-bremen.de
www.fb2.uni-bremen.de

Versicherung an Eides Statt

Name, Vorname	Gebhard, Laura Johanna
Matrikel-Nr.	4118888
Straße	
Ort, PLZ	

Ich, _____ (Vorname, Name)
versichere an Eides Statt durch meine Unterschrift, dass ich die vorstehende Arbeit selbständig und ohne fremde Hilfe angefertigt und alle Stellen, die ich wörtlich dem Sinne nach aus Veröffentlichungen entnommen habe, als solche kenntlich gemacht habe, mich auch keiner anderen als der angegebenen Literatur oder sonstiger Hilfsmittel bedient habe. Ich versichere an Eides Statt, dass ich die vorgenannten Angaben nach bestem Wissen und Gewissen gemacht habe und dass die Angaben der Wahrheit entsprechen und ich nichts verschwiegen habe.
Die Strafbarkeit einer falschen eidesstattlichen Versicherung ist mir bekannt, namentlich die Strafandrohung gemäß § 156 StGB bis zu drei Jahren Freiheitsstrafe oder Geldstrafe bei vorsätzlicher Begehung der Tat bzw. gemäß § 161 Abs. 1 StGB bis zu einem Jahr Freiheitsstrafe oder Geldstrafe bei fahrlässiger Begehung.

_____

Ort, Datum / Unterschrift

Declaration on the contribution of the candidate to a multi-author article/manuscript, which is included as a Chapter in the submitted doctoral thesis

Name of the candidate: Laura Johanna Gebhard

Title of the thesis: "Genetic and Biochemical Characterisation of Plasmid Vesicles and Other Virus-Like Elements in Archaea"

Contribution of the candidate in percentage of the total workload (up to 100% for each of the following categories):

Task	Chapter 1	Chapter 2	Chapter 3	Chapter 4
Experimental concept and design:	ca. 30%	ca. 50%	ca. 10%	ca. 90%
Experimental work and/or acquisition of (experimental) data	ca. 60%	ca. 80%	ca. 15%	ca. 90%
Data analysis and interpretation	ca. 70%	ca. 70%	ca. 15%	ca. 90%
Preparation of figures and tables	ca. 90%	ca. 80%	ca. 10%	ca. 95%
Drafting of the manuscript	ca. 70%	ca. 70%	ca. 15%	ca. 95%

We declare that all authors in this article/manuscript have been informed on and did not object to the listed contributions of the candidate as the author of this article/manuscript.

Date:

Signatures:

_____ _____

(Candidate) (Supervisor)